DETERMINATION OF TILT ANGLES OF SOLAR PANELS: A STUDY ON GAZİANTEP

Kadir BAKIRCI
Atatürk University
abakirci@atauni.edu.tr

Galip KALTAKKIRAN
Atatürk University
g.kaltakkiran@atauni.edu.tr

ABSTRACT: The intensity of the harmful emissions emitted from conventional energy sources and the high cost of these sources seriously affect the national economy. In this context, studies on new and renewable energy sources have been popular and encouraged around the world. Solar energy is one of the most important and prominent of these resources. In our country with a high potential for solar energy, using this clean energy source is very important in terms of environmental pollution and energy economy. In this study, optimum panel tilt angles are determined for Gaziantep province and model equations which gave optimum slope angles are developed. As a result, it is seen that the values obtained from the models and the calculated values are compatible.

Key words: solar energy, panel tilt angle, Gaziantep

INTRODUCTION

Developing technology has continuously increased the demand for energy needs. Thus, the necessary energy has been tried to be obtained from the sources easily from the nature and from the sources with high yield. Fossil fuels are one of the main sources of energy use. However, CO_2 and CO gases that are exposed as a result of the excessive use of fossil fuels negatively affect the atmosphere of our world. Therefore, solar energy is a non-hazardous source of energy without side effects. Geographical location of our country is quite good in terms of the amount of sunlight.

The demand for renewable energy sources has also expanded considerably. Being environmentally friendly and being a clean source is one of the main reasons for returning to the sun. Solar energy is used in most buildings to obtain heating, drying, cooling, air conditioning, electricity and hot water. Storage techniques should also increase rapidly in order to increase the use of solar energy in heating systems. The number of solar powered systems originating in Turkey is increasing with each passing day. In order to achieve maximum benefit from solar energy, solar panels must be placed at specific angles of inclination for months. However, when the inclination angles of the panel are impossible to change, the inclination angles of the panels remain constant. In this case, it is more appropriate to place the panels on the slope

equal to the latitude angle of the region. On the other hand, if the inclination angles of the panels can be changed seasonally twice a year, 15° should be added to the latitude angle of the region they are in during the winter and 15° in the latitude should be removed in summer.

In the literature, there are numerous studies conducted by the researchers about the calculation of the optimum inclination angles of solar panels for different purposes and locations [1-6]. In this study, the total solar irradiation on inclined surfaces ranging between 0-90 ° has calculated by MATLAB program and the optimum solar panel inclination angles for each month are calculated. Here, the total amount of solar energy gained is calculated as the fixed angle of the panels, seasonal or monthly changes. In addition, models have been developed to calculate the optimum angle of inclination based on the clearness index and the angle of declination.

METHODS

The average daily radiation on a tilted surface, HT, can be expressed by,

$$H_T = RH \tag{1}$$

The average daily radiation on a horizontal surface (H) and the ratio of the daily average radiation on a tilted surface to that on a horizontal surface for each month (R).

Lui and Jordan [7] have proposed that R can be expressed as:

$$R = \left(1 - \frac{H_d}{H}\right) R_b + H_d \left(\frac{1+\cos(s)}{2H}\right) + \rho\left(\frac{1-\cos(s)}{2}\right) \tag{2}$$

where Hd is the monthly-average daily diffuse radiation, Rb the ratio of the average beam radiation on the tilted surface to that on a horizontal surface for each month S the tilt of the surface from horizontal, and ρ=0.2 the ground reflectance.
Rb is a function of the transmittance of the atmosphere which depends upon the atmospheric cloudiness, water vapour and particulate concentration and Liu and Jordan [7] suggest that Rb can be estimated to be the ratio of extra-terrestrial.

$$R_b = \frac{\cos(\varphi - s)\cos(\delta)\sin(\omega_s^{'}) + \omega_s^{'}(\pi/180)\sin(\varphi - s)\sin(\delta)}{\cos(\varphi)\cos(\delta)\sin(\omega_s) + \omega_s(\pi/180)\sin(\varphi)\sin(\delta)} \tag{3}$$

where K_T clearness index, φ latitude, δ declination angle, ω is the hour angle and $\omega_s^{'}$ the sunset hour angle for the tilted surface [8]:

$$\delta = 23.45\sin\left[\frac{360(n+284)}{365}\right] \tag{4}$$

$$\omega_s = \arccos[-\tan(\varphi(\tan(\delta)] \tag{5}$$

$$\omega_s^{'} = \min\{\omega_s, \arccos[-\tan(\varphi - s)\tan(\delta)]\} \tag{6}$$

Page [9] suggest that H_d is the monthly-average daily diffuse.

$$H_d = H(1.00 - 1.13K_T) \quad (7)$$

$$K_T = H/H_o \quad (8)$$

where the fraction of the mean daily extra-terrestrial H_o, solar constant, I_{sc}, is 1353 W/m^2.

$$H_o = \frac{24}{\pi} I_{sc}\left(1 + 0.033\cos\frac{360n}{365}\right)\left(\cos\varphi\cos\delta\sin\omega_s + \frac{\pi\omega_s}{180}\sin\varphi\sin\delta\right) \quad (9)$$

RESULTS AND FINDINGS

In this study, monthly average daily total solar radiation values of different slopes of Gaziantep have calculated. MATLAB program has used to obtain the calculations in the study. Calculations are made for the values of the collector inclination angles between 0 and 90°.

Monthly-average daily extra-terrestrial, global and diffuse solar radiation on horizontal surfaces for Gaziantep province are given in Fig. 1. Monthly average daily total radiation values for different slope (0-90°) surfaces have calculated for January, February, March, April, May, June, July, August, September, October, November and December and variations in inclination angle are given in Figures 2 and 3, respectively.

According to Table 1, in Fig. 2, optimal tilt angle ($S_{opt.}$) in January 53°, in February 45°, in March 32°, in April 16°, in May 3°, in June 0° and in Fig. 3 in July 0°, in August 14°, in September 31°, in October 46°, in November 56°, in December 55°. However, if the inclination angles of the panels can be adjusted according to the fixed, seasonal and monthly optimum angles throughout the year, monthly and annual total solar energy potential values are given in Table 1. In Table 1, the annual total of the unit square meter is; 5215 MJ/m^2 when the panels are constant throughout the year with a latitude of approx. 37 °.

In seasonal applications, in summer (March-August) and winter (January, February, September, October, November and December), energy value is 5412 MJ/m^2. According to the optimum inclination angles, 5537 MJ/m^2 energy is obtained.

Table 1. Optimum Slope Angles and Solar Radiation Values for the Month of Gaziantep

Months	Sopt. [°]	H [MJm^{-2}-day]	$H_{T\,(sopt.)}$ [MJm^{-2}-day]	H_T (s=37°) [MJm^{-2}-day]	H_T (s=ϕ±15) [MJm^{-2}-day]	$H_{T\,(sopt.)}$ [MJm^{-2}-day]
January	53	5,8	8,14	245	252	252
February	45	8,46	10,58	294	294	296
March	32	12,02	13,40	414	411	415
April	16	15,59	15,99	460	478	480
May	3	18,8	18,82	525	565	583
June	0	21,63	21,63	559	613	649
July	0	21,69	21,69	592	644	672
August	14	19,68	20,05	587	617	622

September	31	16,34	18,26	546	521	548
October	46	11,57	15,09	463	466	468
November	56	7,51	11,21	323	336	336
December	55	4,84	6,94	208	215	215
Total	-	**164**	**182**	**5215**	**5412**	**5537**

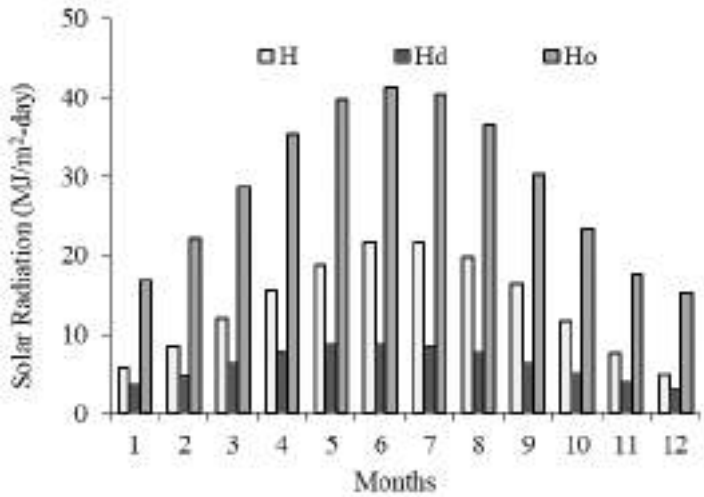

Figure 1. Monthly-Average Daily Extra-terrestrial, Global and Diffuse Solar Radiation On Horizontal Surfaces

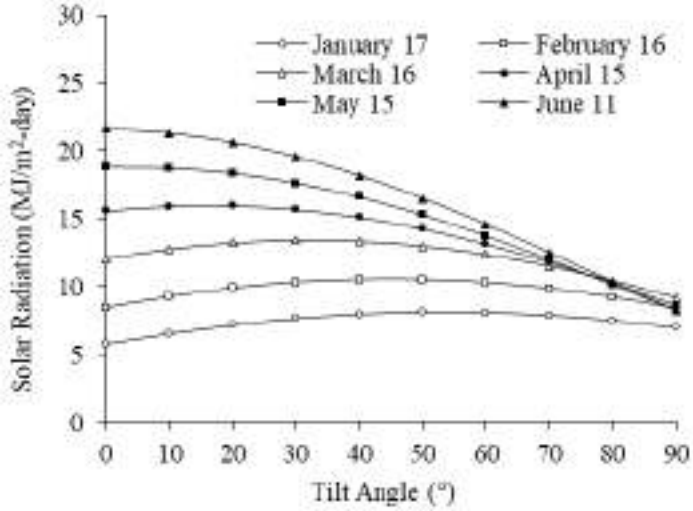

Figure 2. Monthly Average-Daily Solar Radiation Availability of Tilted Surfaces January - June

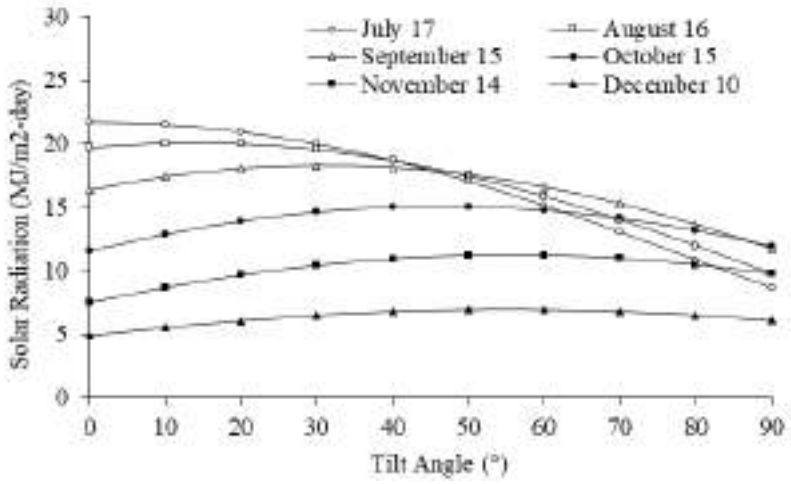

Figure 3. Monthly Average-Daily Solar Radiation Availability of Tilted Surfaces July - December

Table 2 shows the KT index, declination angle and optimum inclination angle values of Gaziantep province. Models have developed to calculate the optimum angle of inclination using KT index and declination angle values. The developed models are given as linear, second and third order polynomial equations with Equation 10, 11 and 12, respectively. In these equations, the letters in the a-g range are the correlation coefficients. The correlation coefficients for each equation are given in Table 3. The calculated optimum panel angle values and the optimum panel angle values obtained from the equations are given in Figure 4. Figure 4 shows that the values obtained from the models are consistent with the calculated values.

Table 2. Monthly KT, Declination and Optimal Tilt Angles for Gaziantep.

Months	January	February	March	April	May	June	July	August	September	October	November	December
K_T	0,34	0,38	0,42	0,44	0,47	0,52	0,54	0,54	0,54	0,49	0,43	0,32
d (δ) [°]	-20,68	-12,62	-2,02	10,15	19,26	23,39	21,18	13,12	1,41	-10,3	-19,6	-23,4
$S_{opt.}$ [°]	53	45	32	16	3	0	0	14	31	46	56	55

$$S_{opt} = a + b(K_T) + c(\delta) \quad (10)$$

$$S_{opt} = a + b(K_T) + c(\delta) + d(K_T^2) + e(\delta)^2 \quad (11)$$

$$S_{opt} = a + b(K_T) + c(\delta) + d(K_T^2) + e(\delta)^2 + f(K_T^3) + g(\delta)^3 \quad (12)$$

Table 3. Correlation Coefficients of Model Equations

City	**Correlation Coefficients**						
Gaziantep	**a**	**b**	**c**	**d**	**e**	**f**	**g**
Linear	10,4932	41,2938	-1,4057				
Second Degr.	-13,557	161,339	-1,397	-140,361	-0,003		
Third Degr.	54,248	-307,467	-1,425	928,750	-0,003	-802,778	0

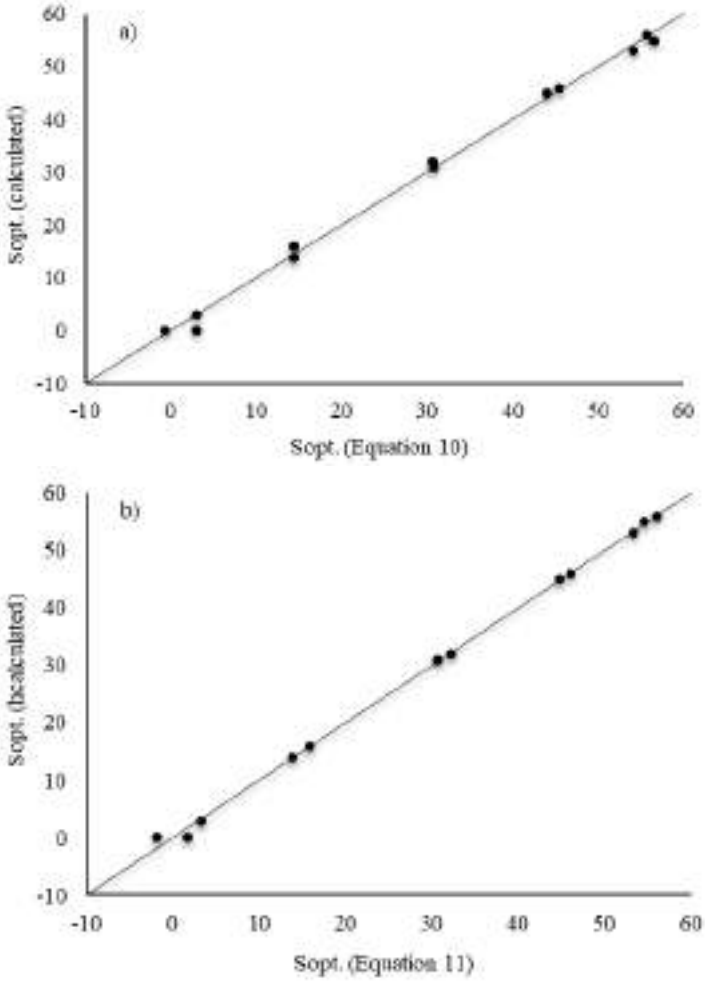

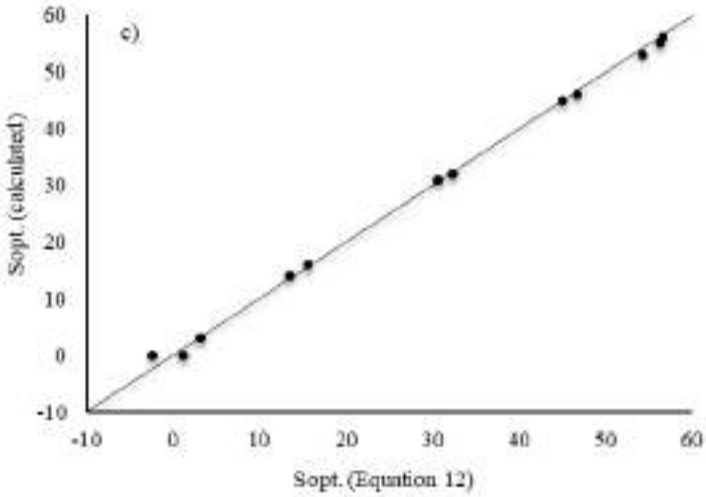

Figure 4. Comparison of Calculated Values and Obtained Values From Equations a) Eq. (10) b) Eq. (11)
c) Eq. (12)

In this study, models which provide the optimum angle of inclination depending on the clearness index and the angle of declination have developed. Thus, these models can be used to make the most of the solar energy at any time of the year.

ACKNOWLEDGEMENT

We would like to thank the General Directorate of State Meteorology for its contributions in the procurement of solar energy data

SYMBOLS

H	Monthly average daily global radiation (MJm^{-2}-day)
H_d	Monthly average daily diffuse radiation (MJm^{-2}-day)
H_o	Monthly average daily extra-terrestrial radiation (MJm^{-2}-day)
H_T	Monthly average daily global radiation on tilted surface (MJm^{-2}-day)
I_{sc}	Horizontal surface radiated solar radiation (Wm^{-2})
K_T	Clearness index
n	Number of days from January 1
s	Tilt of surface from horizontal (degree)

$s_{opt.}$ Optimum tilt angle (degree)

δ Declination angle ((degree)

φ Latitude (degrees)

ρ Ground reflectance

ω_s Hour angle (degree)

$\omega_s^{'}$ Sunset hour angle (degree)

REFERENCES

[1] Siraki, A. G., & Pillay P. (2012). Study of optimum tilt angles for solar panels in different latitudes for urban applications. Solar Energy, 6(86), 1920-1928.

[2] Tiris, M., & C. Tiris, C. (1998). Optimum collector slope and model evaluation: case study for Gebze, Turkey. Energy Conversion and Management, 39(3/4), 167–172.

[3] Gunerhan H., & Hepbasli, A. (2007). Determination of the optimum tilt angle of solar collectors for building applications. Building and Environment, 42, 779–783.

[4] Nfaoui, M., El-hami, K., & Besbes, M. (2018). Extracting the maximum energy from solar panels. Energy Reports, 4, 536-545.

[5] Ben-Othman, A., & Belkilani, K. (2018). Global solar radiation on tilted surfaces in Tunisia: Measurement, estimation and gained energy assessments. Energy Reports, 4, 101- 109.

[6] Bakirci, K. (2017). Investigation of solar energy potential to inclined surfaces. Environmental Progress & Sustainable Energy 36(5), 524-532.

[7] Liu, B. Y. H., & Jordan, R. C. (1960) "The interrelationship and characteristic distribution of direct, diffuse and total solar radiation", Solar Energy, 4(3), 1–19.

[8] Duffie, J. A., & Beckman, W. A. (1991). Solar Engineering of Thermal Processes. Wiley: New York.

[9] Page, J. K. (1961). The estimate of monthly mean values of daily total short-wave radiation on vertical and inclined surface from sunshine records for latitude 40°N to 40°S", Proc. UN Conference on New Sources of Energy, 4, 378–390.

MODELING AND CONTROL OF DOUBLY FED INDUCTION GENERATOR WITH BACK TO BACK MODULAR MULTILEVEL CONVERTERS

Assoc. Prof. Dr. AHMET METE VURAL
University Of Gaziantep, Department Of Electrical And Electronics Engineering
mete.vural@gaziantep.edu.tr.

Ahmed HACHIM
University Of Baghdad
elect.engineer83@gmail.com

ABSTRACT: This paper investigates the performance of the grid connected wind farm for high power transmission through the HVDC system. Multilevel converters are used to mitigate the harmonics and maintain the constant DC voltage in the line. Two closed loop controllers are used; one is on DFIG side and another one is on the grid side which takes the three phase line current and voltage with a reference DC voltage at the input to provide the appropriate on-off pulse time to maintain the required DC level. The wind farm, modular multilevel converter controller maintains the ripples whereas grid side modular multilevel converters take care of maintaining the constant DC voltage.
Key words: Doubly fed induction generator and back to back modular multilevel converters.

INTRODUCTION

Renewable energy Due to advancement in induction motor efficiency, wind farms is widely used nowadays, especially with doubly fed induction generator (DFIG). The technical applications and advantages are published in a number of papers (S. Muller 2002) and (Zhixin 2009) . The power generated from a wind farm is transmitted with grid since no distribution system can only rely on wind farm due to varying power generation due to wind speed. So the grid has to be connected and high voltage alternating current (HVAC) line is required to connect with the AC source. This HVAC transmission system has some drawbacks. One is that the long-range transmission cable leads to capacitive reactance which gives rise to losses and requires compensation. These drawbacks can be overcome by transmitting the generated power after converting it into DC which is suitable for long distance transmission with minimum losses (P. Bresesti 2007). The HVDC system can be categorized into two configurations: line commuted HVDC (LCC-HVDC) and voltage source converter based HVDC (VSC-HVDC). The VSC-HVDC is suitable for wind farm integration and presently the highest rated power (400 MW) wind plant is using HVDC system. For high power applications, modular multilevel converter (MMC) is preferred (M. Saeedifard 2010) . In this paper, we have integrated the wind farm with an HVDC line through the MMC. The wind farm and AC grid are asynchronous and can work independently. To make the frequency synchronization between these two, the DC voltage at coupling point is to be maintained as shown in Figure 1. The MMC is used here to convert back the DC to three phase AC. Controlling algorithm is required to maintain the constant DC at this point which may increase or sudden decrease in case

of fault or wind speed variation. We have investigated d-q controller for this purpose. References (X. I. Koutiva 2006) and (S. Muyeen 2010) suggested a VSC transmission for wind farm. The wind turbine was neither based on induction generator nor a permanent magnet synchronous generator (PMSG). The study in (C. Feltes 2007) proposed a variable frequency controller to reduce the converter capability of the DFIG wind plant. In (L. Xu, L. Yao 2007) and(C. Feltes 2007),the authors worked on the performance improvement in VSC-HVDC link in grid connected DFIG wind farm in case of a ride through fault. However, in (C. Feltes 2007) - (C. Feltes 2007), the author didn't discuss the start up control of wind farm rather focused only on the balanced and unbalanced condition of the system and based on two level VSC only. The MMC is introduced and discussed in the paper (M. Saeedifard 2010).Following in the similar line of action, the author in (J. Qin and M 2012) eliminates the circulating current while maintaining the DC voltage at the common point of coupling (PCC) using model predictive control strategy. Paper (M. Guan and Z 2012) focused on the operational characteristics of MMC and suggested an independent control over zero sequence components. In a further section of this paper, we discuss the system configuration of grid connected wind farm with MMC converter. In section III, the control mechanism described in detail along with a schematic block diagram and the results are discussed in section IV. Finally, a brief conclusion of this work is discussed in section V.

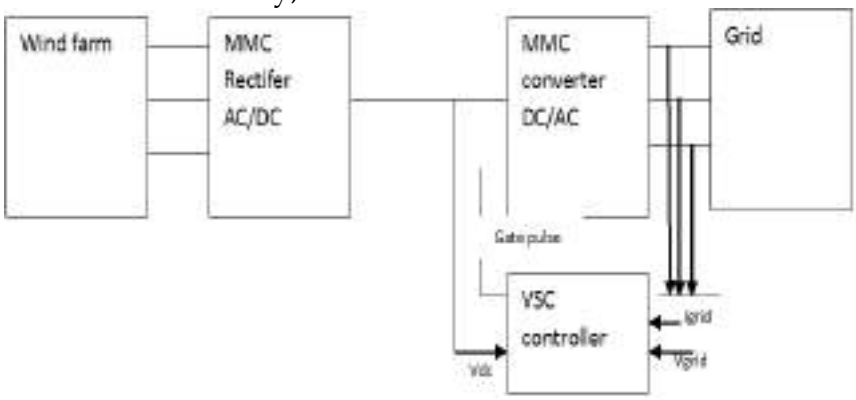

Figure. 1. Block diagram of connected DFIG with grid, though MMC converters.

SYSTEM CONFIGURATION

The sun The DFIG wind farm is connected with to the grid through VSC based transmission system with MMC rectifier at DFIG side (AC/DC) and another MMC converter being located (DC/AC) at grid side. The DFIG side MMC converter is used to avoid the ripples in the output and grid side MMC converter balances the DC at common coupling point. The related block diagrams are shown in Figures 2 and 3, respectively. We have designed a full bridge using 5 pairs of half MMC for each phase and a gating pulse is applied to them by the controller.

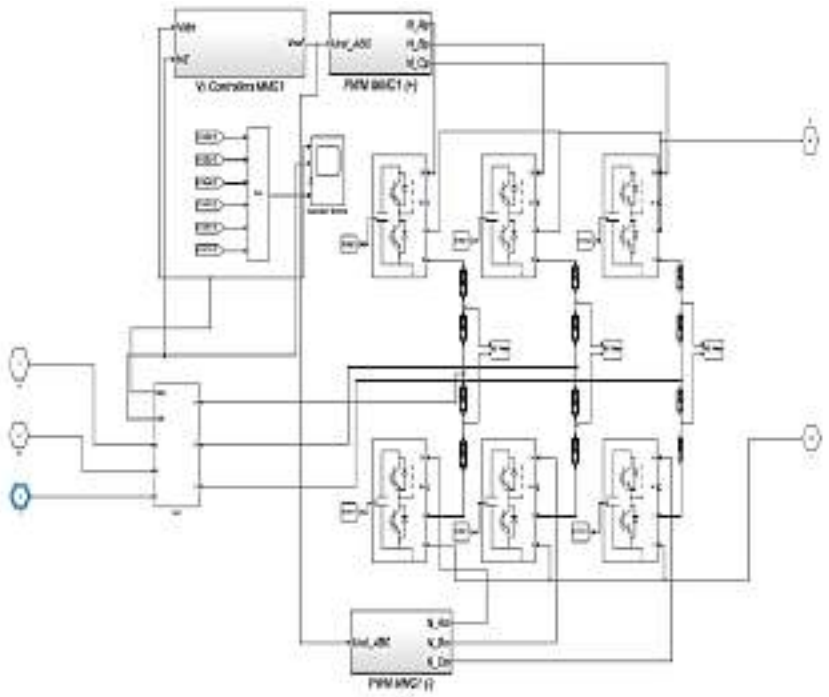

Figure. 2. Block diagram structures of MMC rectifier.

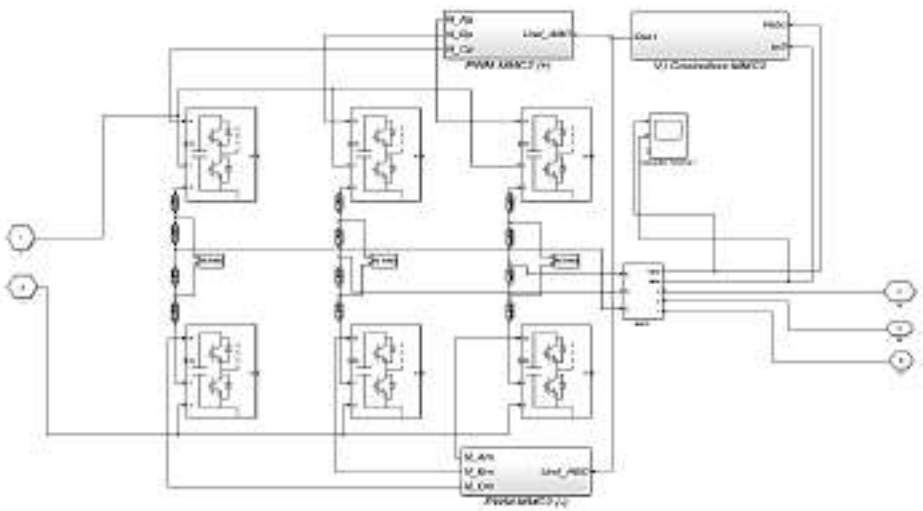

Figure. 3. Block diagram structures of MMC inverter.

The main motive of this work is to maintain a constant DC voltage at the common point of coupling (PCC). This is done with a grid side d-q controller, which takes three phase grid voltage and current into the input along with coupling DC voltage and controller.

CONTROLLER DESIGN

Our system needs two controllers: one is on DFIG side and another one is at the grid side for rectifier and converter respectively. Fortunately the d-q controller at both sides is enough to provide 5 level MMCs. The DFIG start-up controller is not discussed here as a lot of work is already published on it. We here focus only on MMC controllers as when DFIG plant is connected to the grid, then primary requirement is to transfer the maximum power from DFIG to PCC as shown in Figure 4, and to maintain it in case of load change. Similarly the MMC controller on the grid side has the responsibility to maintain the constant DC voltage between these two MMCs which are rectifier and converter. These two controllers for rectifier and the inverter are independent of each other and used to control
P & Q for the rectifier
Vdc and Q for the inverter
The block diagram for the controller is shown in Figure 4.

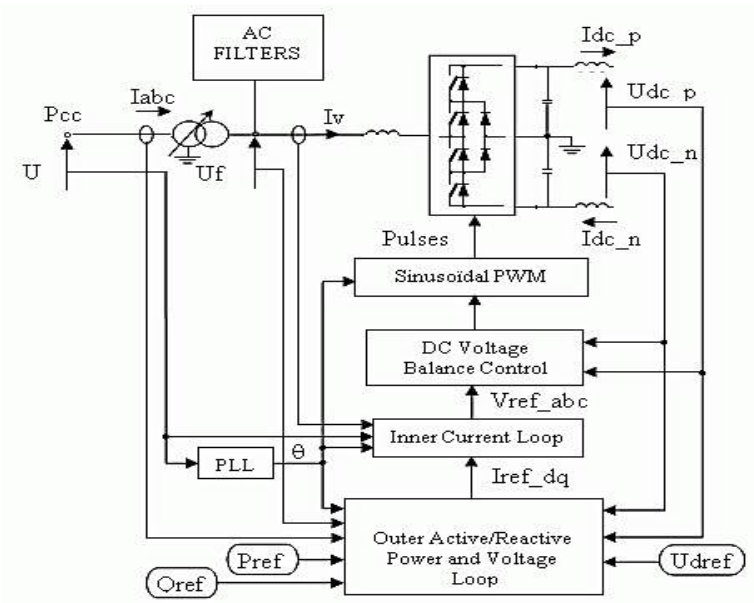

Figure. 4. Block diagram representation of MMC controller.

We have set the sampling time for this controller as 0.3 μs, which is ten times higher than simulation sample time. The sampling frequency in pulse width modulation (PWM) is chosen as 33 times the normal frequency to get the desired gate pulses. The controller is targeted to provide the reference signal as PWM generator and antialiasing filters are used in the bridge sub block. The controller is giving the reference signal to PWM and at the carrier frequency of 33 times of normal frequency. It generates the gating pulses. The unsynchronized PWM mode of operation is chosen for our model. The input feed to the controller is normalized sampled voltage and current. The three phase components are converted into real and imaginary part (space vector quantity) using Clark transformation. To match the orientation of signal due to transformer usage at the wind plant, the signal on the primary side of the transformer is rotated to ±pi/6. The real and imaginary components calculated by Clark transformation are now used to compute the direct axis 'd' and quadrature axis 'q'

which is done by dq transformation block. A controller needs active and reactive power, modulation index, DC current and voltage. These are calculated by the signal calculation blocks as shown in Figure 4.

3.1 Phase Locked Loop (PLL)
The PLL block is used to get the phase synchronous angle for dq transformation or more precisely the sin(Θ), cos(Θ). At steady state the sin(Θ) is in phase with fundamental real component and grid side phase (A) at the coupling point (Uabc).

3.2 Outer Active and Reactive Power and Voltage Loop
The loop is used to calculate the input Iref-dq current in an inner current loop. It operates into two controlling modes i.e. either use the active power flow of the PCC or pole to pole DC voltage. The active power flow is checked in the d-axis and reactive power flow is checked in the q-axis. The description of active and reactive power loop is described in Figure 5.

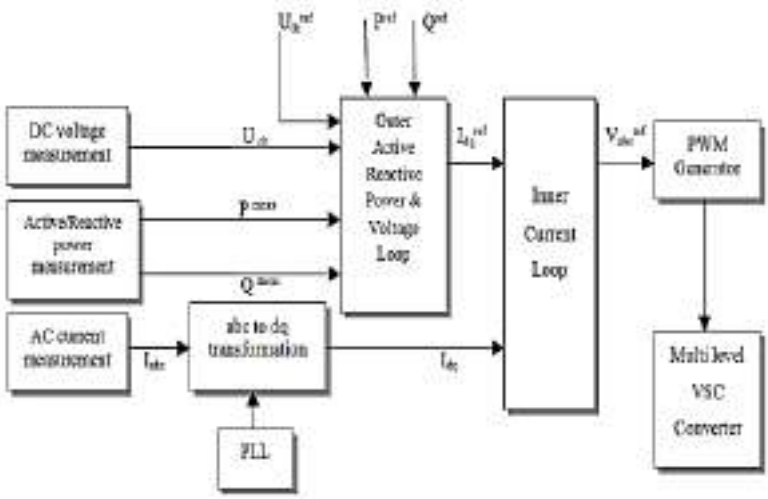

Figure. 5. Block diagram active and reactive power loop.

The reactive power controller inside this block uses a PI controller, used to increase the speed response. A regulator is also used to avoid the AC perturbation at the output of PI controller, which resets the PCC voltage to zero if it is less than a constant value. This regulated output is fed back to PI with a difference with the reference PCC DC voltage. The PCC AC voltage is controlled by two PI controllers which maintains the grid side AC within a secure range. The function of the active power controller is similar to the reactive power controller. The extra block used is ramp control, or which adjusts the power in order to get the desired value. During the fluctuation in AC system the DC controller takes the charge and override the active power regulator to maintain the PCC DC voltage. The DC control block is enabled only when the active power block is disabled. The output of this block is the reference value of the current reference regulator block. Since the input to the inner current loop is the dq reference current so active and reactive power input to this outer loop must be converted to current finally. This is done with the current reference calculation block. The current reference is estimated by dividing the power reference by the voltage (up to a minimum preset voltage value). The current limitation, block exerts the limit to scale

the active and reactive power equally. DC voltage control mode the priority is given to active power when limit is imposed.

3.3 Inner Current Loop

The inner current loop block is shown in Figure 6 and its main functions are described below.

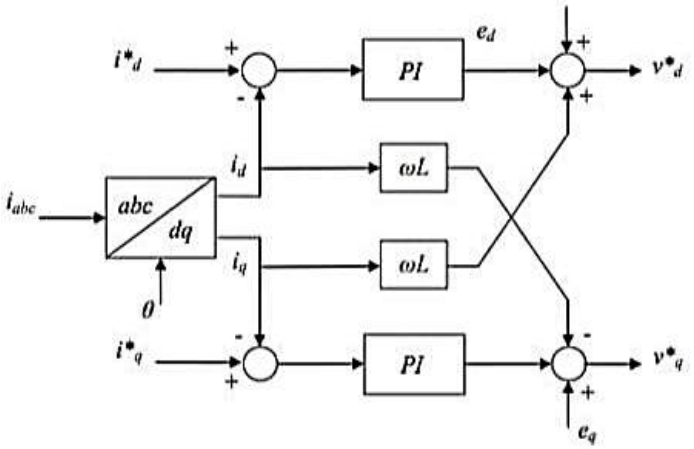

Figure. 6. Block diagram structure of inner current loop.

The AC current block uses a feed forward method to keep track of changing current reference vector which is d and q. This change in current can be due to short circuit faults. It adds the voltage across the impedance when the voltage drop is detected by computing the difference in U_dq voltage and what converter voltage should be. The state equations representing the dynamics of the VSC currents are used (an approximation is made by neglecting the AC filters). The "d" and "q" components are decoupled to obtain two independent first-order plant models. A PI controller is used to control the converter current in this block which reduces the error to zero in steady state. The output of the AC current control block is the unlimited reference voltage vector Vref_dq_tmp. The reference voltage limitation, block limits the reference voltage vector amplitude to 1.0, since over modulation is not desired. The Inverse dq and Inverse Clark transformation blocks are required to generate the three-phase voltage references to the PWM.

4. RESULTS

In this section we have carried the results of the study of grid connected DFIG with 5 level MMC transmission system which is controlled by d-q controller for both rectifiers and inverter. Results are simulated by the simulation program. The DFIG output is shown in Figure 7. The DC capacitor in DFIG starts charging after 0.05 Sec which is proved by the mechanical torque. When the capacitor starts charging it increase suddenly and slowly settle down and it started to provide the three phase voltage and current with power of 4 MW. We have designed MMC rectifier using 5 pairs of MMC in lower and upper arm of the bridge. The DC voltage output of MMC for each arm and each phase is shown in Figure 7. It proves that the controller settles down any changes in the load successfully and maintained the MMC output.

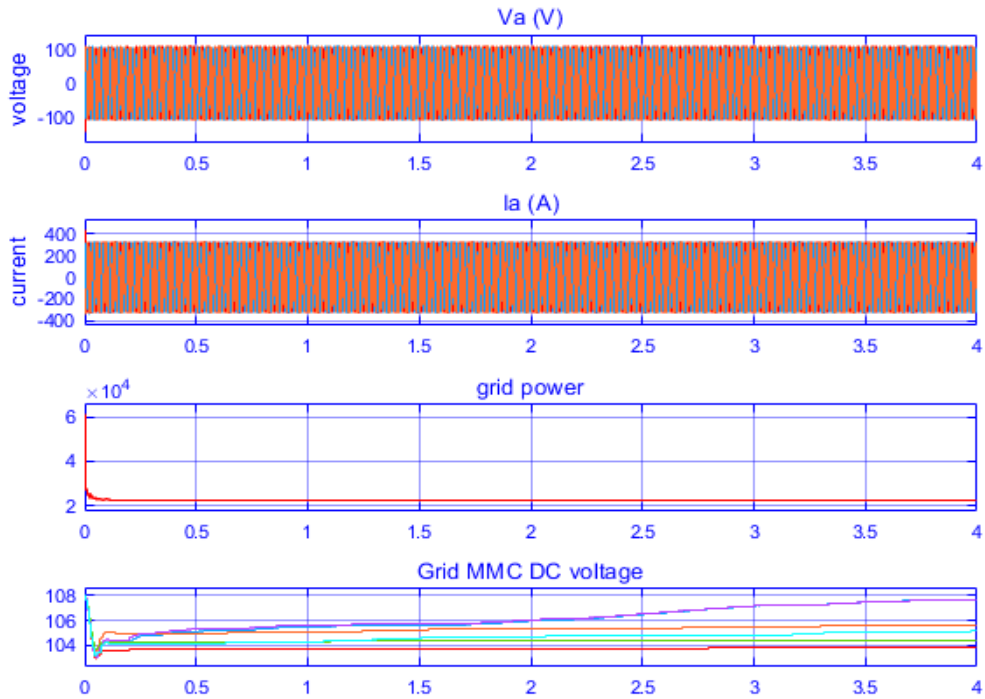

Figure. 7. DFIG output with charging of DFIG capacitors.

The disturbances in DFIG voltage graph are due to filter limitation which will be further tuned to fine parameters and smoother waveform will be generated. The gird side connected controller maintains the DC voltage (PCC), Initially, when DFIG started to generate power and supplied with grid, then it accumulates at PCC and coupling capacitor voltage at that time starts to rise and gird side MMC controller settles the PCC voltage near to a reference voltage by taking the grid voltage and current along with coupling capacitor voltage into the feedback input and generate the reference signal which is further feed to PWM to generate the gating pulses. The efficiency of the controller is analyzed if the coupling voltage is settled to reference DC voltage. In our case we have chosen 500 V DC voltage as a reference and our designed grid side MMC controller is able to manage the PCC voltage near to a reference voltage as shown in Figure 8 .

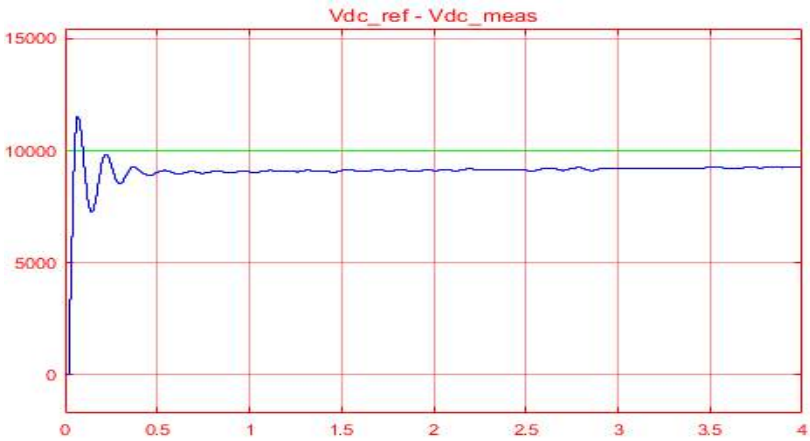

Figure. 8. DC coupling voltage in comparison with reference DC voltage.

The 1.6 MW grid generated output voltage and current is shown in Figure 9. The controlled MMC converter has the same configuration as the wind side controller, the MMC DC voltage for each arm and for each phase is also shown in Figure 9 which is also maintained at a constant level after cut in time.

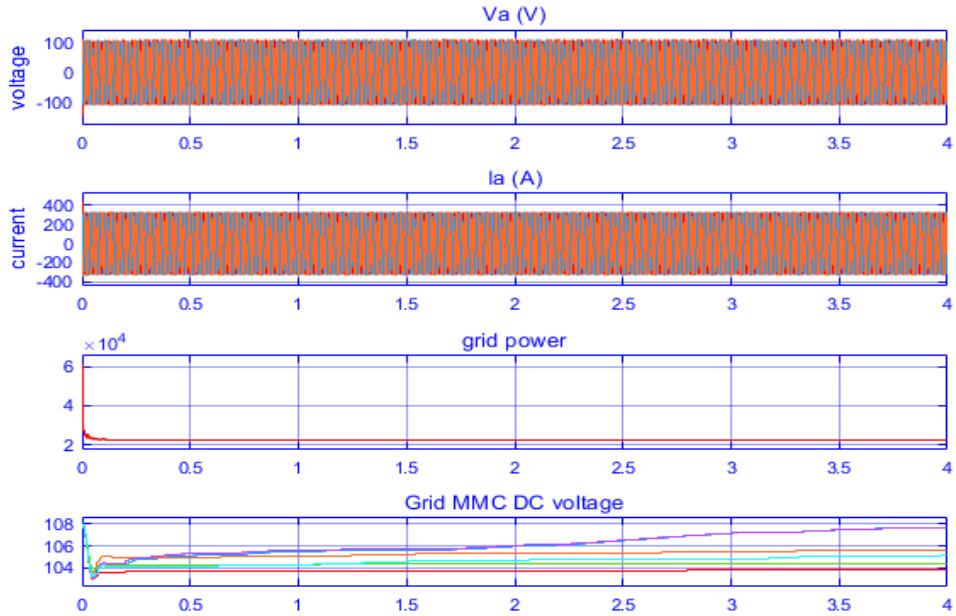

Figure. 9. Grid output voltage, current, power and MMC DC voltage output

CONCLUSION

In this paper DFIG based wind farm is integrated via the MMC-HVDC transmission system. To manage the changing load conditions at the wind farm side, a 5 level MMC rectifier controller is designed based on d-q theory. The DC thus generated is transmitted to the grid, which is further converted back to three phases again by using 5 level converter based on MMC with the same controller. The simulation is designed using the program and it has been analyzed that for high power transmission, MMC based transmission can be used and helps in integrating the wind farm and grid successfully and satisfactorily.

REFERENCES

A.Reidy and R. Watson, "Comparison of VSC based HVDC and HVAC interconnections to a large offshore wind farm," *in Proceedings of IEEE Power Engineering Society General Meeting*, Jun. 2005, vol. 1, pp. 1-8.

C. Feltes and I. Erlich, "Variable frequency operation of DFIG based wind farms connected to the grid through VSC-HVDC link," *in Proceedings of IEEE Power Engineering Society General Meeting*, Tampa, FL, 2007, pp. 1-8.

C. Du, M. Bollen, E. Agneholm, and A. Sannino, "A new control strategy of a VSC-HVDC system for high-quality supply of industrial plants," *IEEE Transactions on Power Delivery*, vol. 22, no. 4, pp. 2386-2394, Jul. 2007.

J. Peralta, H. Saad, S. Dennetière, J. Mahseredjian and S. Nguefeu, "Detailed and averaged models for a 401-level MMC-HVDC system," *IEEE Transactions on Power Delivery*, vol. 27, no. 3, pp.1501-1508, Jul. 2012.

J. Qin and M. Saeedifard, "Predictive control of a modular multilevel converter for a back-to-back HVDC System ," *IEEE Transactions onPower Delivery*, vol. 27, no. 3, pp. 1538-1547, July 2012.

JP da Costa, H. Pinheiro and T. Degner, "Robust controller for DFIGs of grid-connected wind turbines, " *IEEE Transactions on Industrial Electronics*, vol. 58, no. 29, pp. 4023-4038, Sep. 2011.

L. Xu, L. Yao, and C. Sasse, "Grid integration of large DFIG-based wind farms using VSC transmission," *IEEE Transactions on Power Systems*, vol. 22, no. 3, pp. 976-984, Aug. 2007.

M. Saeedifard and R. Iravani, "Dynamic performance of a modular multilevel back-to-back HVDC system," *IEEE Transactions on Power Delivery*, vol. 25, no. 4, pp. 2903-2912, Oct. 2010.

M. Guan and Z. Xu, "Modeling and control of a modular multilevel converter-based HVDC system under unbalanced grid conditions," *IEEE Transactions on Power Electronics,* vol. 22, no. 12, pp. 4858- 4867, Dec. 2012.

M. Saeedifard and R. Iravani, "Dynamic performance of a modular multilevel back-to-back HVDC system," *IEEE Transactions on Power Delivery*, vol. 25, no. 4, pp. 2903-2912, Oct. 2010.

P. Bresesti, W. Kling, R. Hendriks, and R. Vailati, "HVDC connection of offshore wind farms to the transmission system," *IEEE Transactions on Energy Conversion*, vol. 22, no. 1, pp. 37-43, Mar. 2007.

R.Pena, J.C.Clare and G.M.Asher, "Doubly fed induction generator using back-to-back PWM converters and its application to variable speed wind-energy generation," *in IEE Proceedings of Electric Power Applications*, 1996, 143(3): 231-241.

S. Muller, M. Deicke, and R. W. De Doncker, "Doubly fed inductiongenerator systems for wind turbines," *IEEE Industry Applications Magazine,* vol. 8, no. 3, pp. 26-33, May/Jun. 2002.

S. Muyeen, R. Takahashi, and J. Tamura, "Operation and control of HVDC-connected offshore wind farm," *IEEE Transactions on Sustainable Energy*, vol. 1, no. 1, pp. 30-37, Apr. 2010.

S. Li, T. Haskew, L. Xu, "Control of HVDC light system using conventional and direct vector control approaches", *IEEE Transactions on Power Electronics*, vol. 25, no. 12, pp. 3106-3118, Dec. 2010.

X. I. Koutiva, T. D. Vrionis, N. A. Vovos, and G. B. Giannakopoulos, "Optimal integration of an offshore wind farm to a weak grid," *IEEE Transactions on Power Delivery*, vol. 21, no. 2, pp. 987-994, Apr. 2006.

Zhixin Miao, Lingling Fang, D.Osborn, and S.Yuvarajan, "Control of DFIG-based wind generation to improve interarea oscillation damping," *IEEE Transactions on Energy Conversion*, vol. 24, no. 2, pp. 415-722, June. 2009.

REACTIVE POWER COMPENSATION IN THREE PHASE BALANCE LOADED SYSTEM BY USING STATCOM WITH DISPENSE OF THE INTERMEDIATE TRANSFORMER

Hamed SOODI, Electrical and Electronics Engineering Department, University of Gaziantep, hs45149@ mail2.gantep.edu.tr

Mete VURAL, Electrical and Electronics Engineering Department, University of Gaziantep, mete.vural@gaziantep.edu.tr

ABSTRACT: Power system with multi-phase and non-linear nature of consumers is being studied in term of performance and delivered efficiency constrains. Degradation of bus voltage and power factor is one of major dilemmas taking place due to non-linear load effects. For maintaining of power quality and shrinking the losses to the bearable limit in the power system, power compensator is proposed in order to compensate the extra quantity of power that is demanding by non-linear load and degrading the performance; so that performance will be maintained. This paper involves a potential solution to improve the power performance by adopting a three phase self-compensator based on multi-level cascade H-bridge converter. STATCOM is implemented to ensure the best possible DC link voltage of capacitor by performing of harmonic study so that THD is kept equal to 4.71%. decoupling method controller is implemented to control a phase shift pulse width modulator in which governing the multi-level H-bridge invertors. System is implemented in Simulink program and the results are found superior to improve voltage profile and power factor is approached to (0.99) at both inductive and capacitive load test.
Keywords: DQ, CHB, THD, FACTS, STATCOM.

INTRODUCTION

Power systems designers are always determined to implement a robust network ensures the delivery of power within equality constrains [1]. In order to accomplish the design criteria, it is necessary to look for the problems that come across while generation, transformation and distribution of power to the consumers [2]. Most of the studies were revealed that ninety present of power issues (quality related problems) are taking place on the distribution networks [3].
At [4], Arthur highlighted the (cause and effect) of power system quality disorder. Harmonics as described by previous researches as the ripples caused by overlapping of external or internal signals in the power grid which leads to distortion of the resultant signal (waveform) [5]. The assessment of distortion level due to harmonic is attributed to harmonics distortion study; however, the amount of damage/disorder can be monitored.
Power quality and efficiency issues as described at [4] are the low power factor, high consumption of reactive power (Q) is the main impact in power factor formula.

$$\text{p.f.} = \frac{\text{Active power}}{\text{Reactive power}} \qquad (1)$$

Form the concept of power factor it can be seen from the above equation that, the more reactive power, the less power factor. The presence of reactive loads (coils and

capacitors) is the main responsible of such issues. Due to non-desired and uneconomic effects which are arising due to reactive power, the efforts paid to find out a way to prevent such mess. Most of solutions that found in the literature are listed in [6], this paper is an continuation of the research conducted in [7]. In this paper, a three-phase power grid is used with STATCOM compensator to control reactive power demand by R-L and R-C load.

Harmonics mitigated by adopting multi-level cascade invertor (h-bridge); the reason behind using of H-bridge converter is the accuracy of resulted wave form and ripples minimization by the invertor's electronic switches.

Low power factor system consists of linear/non-linear reactive loads draw excessive reactive power which restricts the maximum active power transfer and moreover, adding losses to the power transmission and distribution systems therefor reactive power compensation is essential approach to maintain efficiency in distribution systems [6].

STATCOMMODE OF OPERATION

As far as the STATCOM is built up of DC invertors that taking the input voltages from the distribution components of power system and reforming the same into direct current DC signal, the resultant energy from the STATCOM observing mechanism is being stored into DC capacitors at the input which act as input signals to the said invertor in hereafter. In capacitive mode; STATCOM is consuming the energy i.e. reactive power from the power system at the point of connection and so converting it into DC from where it can be stored in capacitors. Figure 1 depicts the average voltage output at capacitor and inductive mode STATCOM that implemented with (n) levels of H-bridge invertors.

It is cleared in figure that waveform of DC voltage is found optimum at higher level invertor. In this project we used of (9, 13, 17, 21, 25) levels respectively to generate optimum result at both capacitive and inductive mode of STATCOM.

On the other hand, this stored energy is subjected for injection/ absorb in to/from bus bar where the compensator is connected; this mode is initiating for compensate the amount of reactive power that may demand by load.

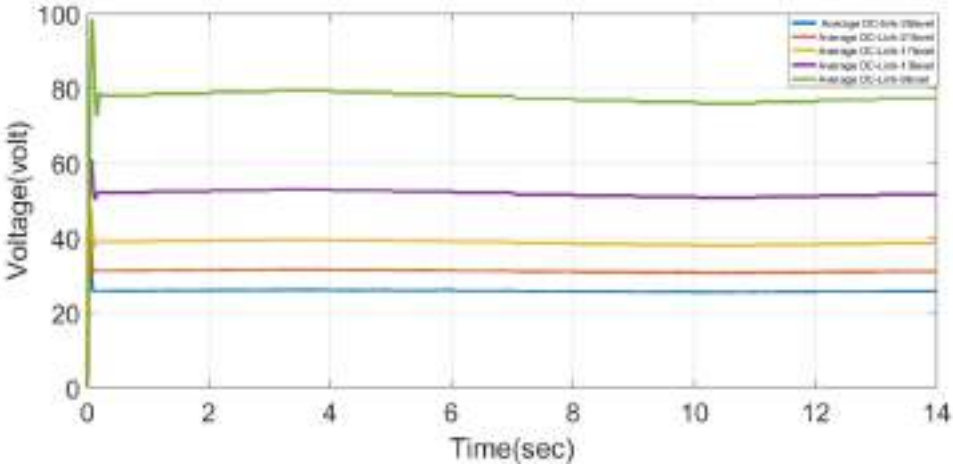

Figure 1. Voltage (average) at the output of capacitors.

In this stage of implementation, it is desired to ensure that converter will produce an AC voltage with lesser possible harmonic by converting the pre-stored energy to AC waveform. Again, maximizing the levels in waveform is affecting the resultant voltage. As mentioned above (9 to 25) levels are ensured across this work; levels of (m) may gain by using (N) of invertors as the following formula.

$$N = \frac{m - 1}{2} \qquad (2)$$

Where (N) is the number of DC invertors and in our case H-bridge is used.
Five case studies are started to investigate the harmonics at the resultant waveform at the output of invertor, the numerical results are proved that twelve unites of H- bridge can generate the optimum output with twenty-five level and minimum total harmonic distortion of 4.71 present. The Figure 2 is demonstrating the resulted voltage of convertor at all five conducted experiments.

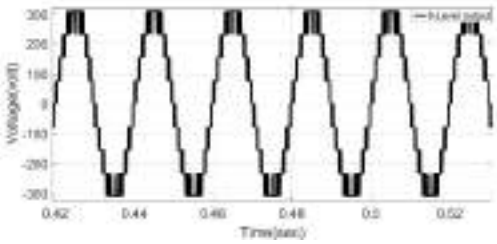

Figure (2, A): 9 levels, THD= 13.3 %.

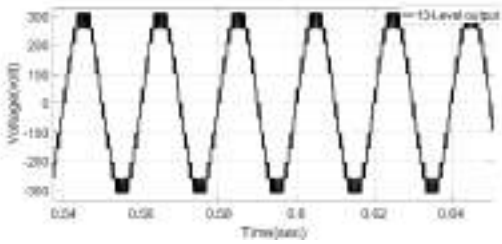

Figure (2, B): 13 levels, THD= 9.89 %.

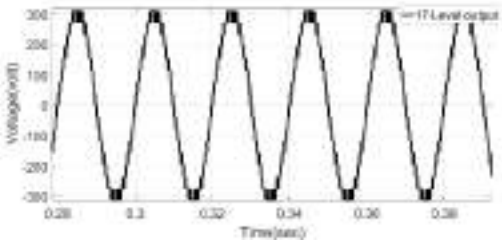

Figure (2, C): 17 levels, THD= 7.27 %.

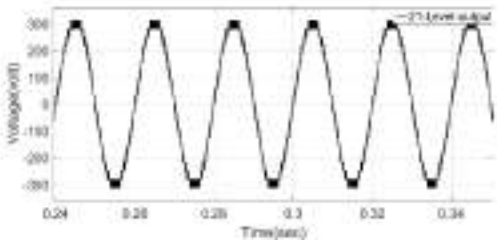

Figure (2, D): 21 levels, THD=6 %.

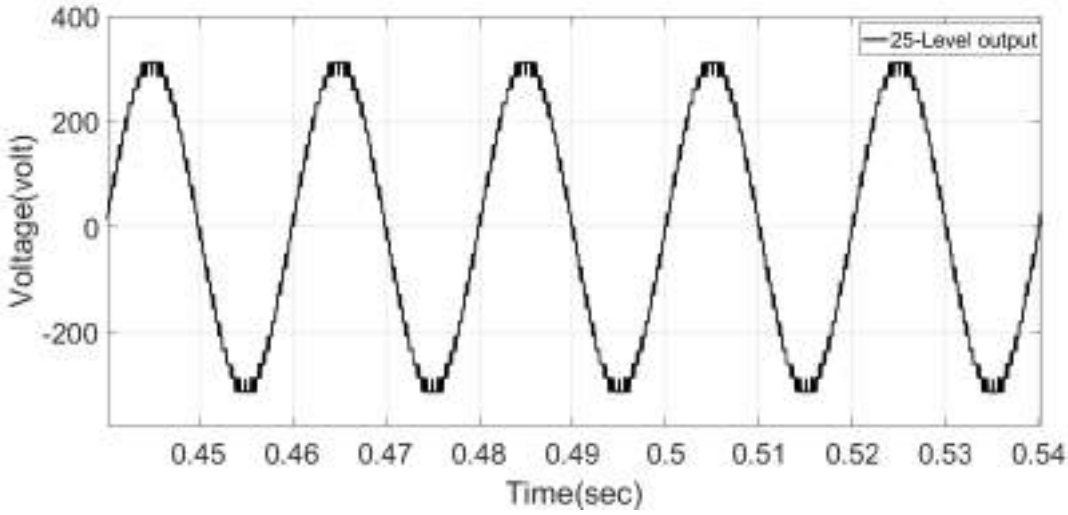

Figure (2, E): 25 levels, THD= 4.71%.

Figure 2. Depicts of convertor output as respect to harmonics within five case studies.

SINUSOIDAL PWM MODULATION SCHEME (SPWM)

The efficiency of multilevel converter is directly dependent upon the modulation schemes used for switching of converter. The efficiency is measured in terms of switching losses and harmonics present in the converters output. SPWM is the most popular and commonly used technique for controlling of multilevel converters. As demonstrated in [12], phase shift pulse width modulator (PS_PWM) was being used to generate a number of signals that used to trigger each arm in the H-bridge, hence there are two arms at every unit of invertor so four signals are required to trigger the switches (four IGBTs/ diode are mounted on every invertor). Upon each signal existence, the said switch (transistor(s) that mounted in both arms of invertor) will be open and close for pre-evaluated duration of time to break of DC stored energy of condenser and form the final AC waveform. The gate signal is needed to be in rectangular pulse and this task is expected to be performed at triggering circuit. Phase shifting pulse width modulator is taking couple of inputs called carrier and reference respectively. The carrier must be high frequency triangular wave which will get compared with fifty Hz reference sign wave. The same is producing of rectangular pulse to operate the inverter switches.

COMPENSATOR IMPLEMENTATION

Because of load nature fluctuations and the undesired incident which may exist due to reactive power (Q), compensators are proposed to control the reactive power demand at non-linear load. STATCOM is one of best solutions to compensate the reactive power, Figure 3 depicts the infrastructure of STATCOM, it does the same by adopting an effective control and power electronic approaches. The structure of implemented compensator is explained below.

Back-to-back converter

H-bridge multi-level converter is determined to perform the bidirectional operations in STATCOM compensator. As per the demand STATCOM may absorb reactive power from the system or may inject that to maintain the overall performance and power quality. as explained earlier STATCOM may begin with absorbing an amount of reactive power the same is drawing AC signal that will propagate backward to the condensers, at this stage converter will act as rectifier and convert the signal into DC form, the best results from this stage will take place with twenty-five levels converter. On the other hand, when reactive power is needed to inject in any bus bar (depending upon the point of connection with between the power grid and compensator), converter will perform conversion of DC waveform into AC signal hence it will work as invertor and depend on triggering circuit the transistors will be operated to perform the same.

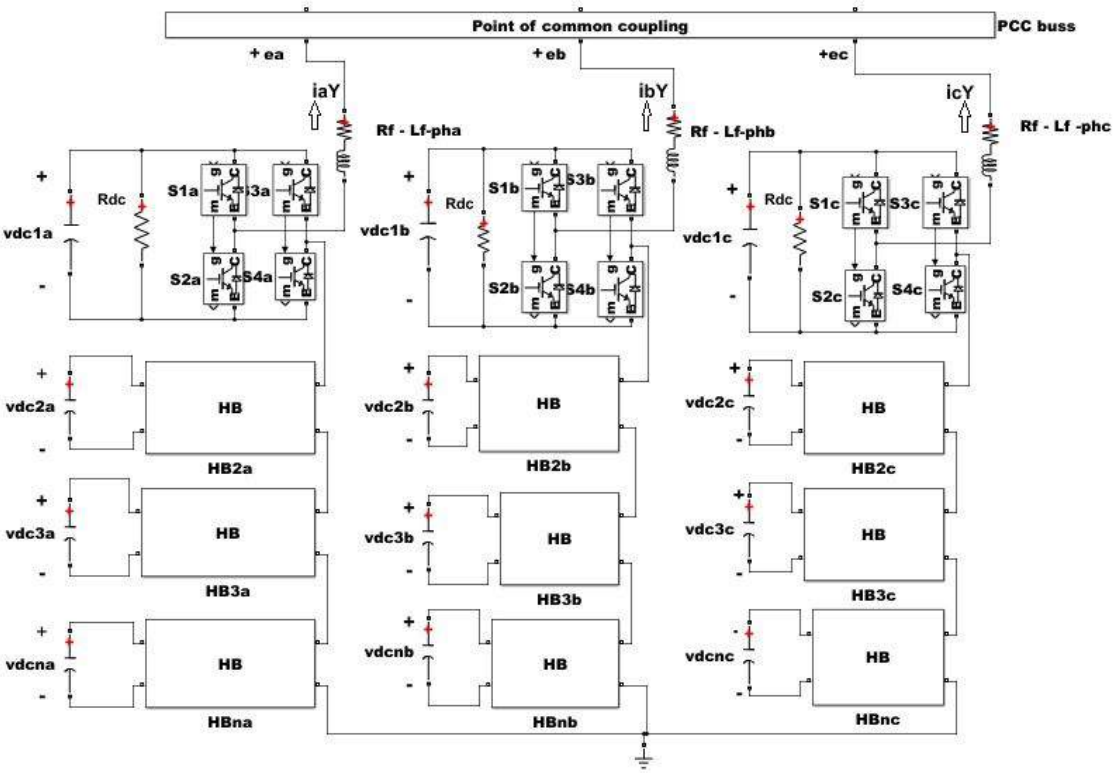

Figure 3. STATCOM basic structure.

Trigger circuit

PSPWM is used in this project to generate gate signals which allow the transistor to perform the switching operation. One of the important facts is to generate rectangular waveforms that make the invertor to produce an AC voltage signal of 50 Hz, 380 volts and in-phase with bus bar voltage (high voltage side); hence synchronization is required and it was attributed to the controller circuit. Phase lock loop (PLL) block is employed from Simulink library and integrated with the PI controller. However, PSPWM is comparing a reference signal of 50 Hz (sign wave) with carrier signal of triangular shape and 1.8 KHz. Ultimately rectangular pulses will be generated and diverted into the inverters.

Condensers

As depicted in the figure (3) for each H bridge there is one capacitor that used to store the rectified signal absorbed from the power grid, in our case twelve H-bridges are used so that same number of capacitors is connected at the input; each capacitor is having a capacity of (3000 μF). The same is connected across the inverter arms and expected to store a per-defined mount of energy.

Controller

The alternative current and voltage at STATCOM's output are being controlled by employing the current decopuling method. The control stratigy of this paradigm is began with decomposing of signal into real and imaginary components and hence resourcing results into phase locked loop block so as to unify the phase variation. One the preporcessing part is overed; resultant compontes are directed into DQ transformation block. The STATCOM capacitors are being controlled using the PI

controlled output, the last is producing Iqref and Idref, the compination is used to set the level of DC voltage of those capacitors and the reactive power reulation as well; as depicted in Figure4.

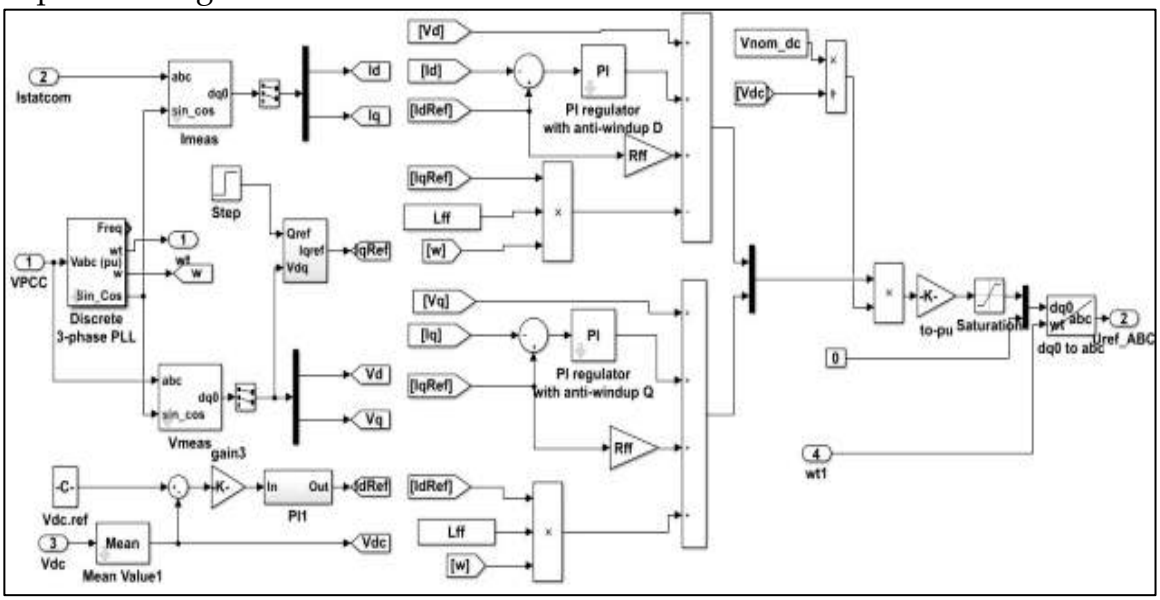

Figure 4. The fundemental structure of P-I controller.

Two loops can be observed in PI circuit, outer and inner loops are used to produce (I_{dref} and I_{qref}). DC voltage of the capacitors is limited by comparation circuit to set the upper limit of capacitor avarage voltage, this proccess are managed by I_{dref}, whereas I_{qref} is used to regulate the reactive power. Real and reactive components of the internal and external currents respectively, are being used to generate Ed* and Eq* as depicted in Figure 4, the comparation of Id and Iq with internal and external current referances is yeilding both Ed* and Eq* respactively. Modulation index of PWM is generated by normalizing the Alpha-Beta cooardinations in which producd by transforming the Ed* and Ed* into the corcerned coorainatio. At the point of common connection between the STATCOM and power lines, the set of space vector components are generated as V_{dq}, I_{dq} and $V_{dq\text{-}inv}$.

$$V_{dq}=R_f\times i_{dq}+L_f\frac{d}{dt}i_{dq}+j\omega_s L_f\times i_{dq}+v_{dqinv} \quad (3)$$

A new experssion dervied from above quation can be existed at steady state conditions as below:

$$V_{dq}=R_f\times i_{dq}+j\omega_s L_f\times i_{dq}+v_{dqinv} \quad (4)$$

In here, knowing that Vq is equal to zero and Vd is constant; the power that imegrate from AC lines into STATCOM paradigm an be written as:

$$p(t)=\frac{Vd*Id+Vq*Iq}{2}=\frac{VdId}{2} \quad (5)$$

$$q(t)=\frac{VqId-VdIq}{2}=-\frac{VdIq}{2} \quad (6)$$

However, Direct and qaderate comonents are being monitered and Figured on plot (5) and (6).

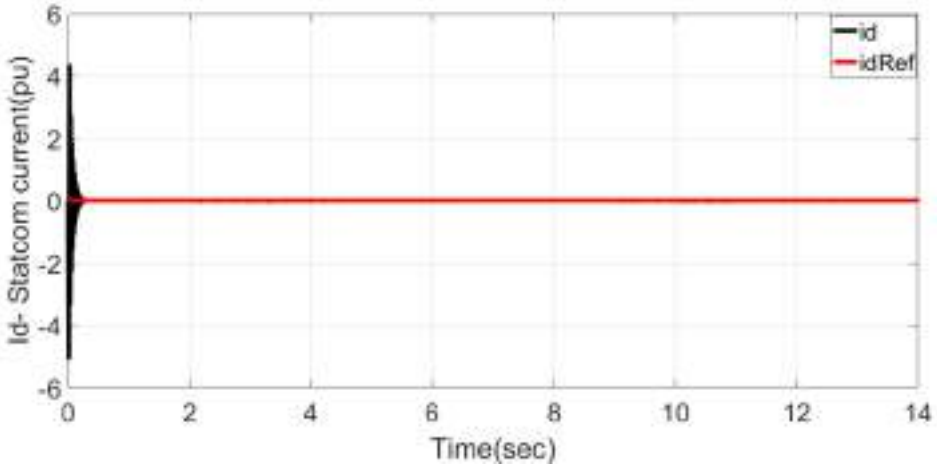

Figure 5.Direct axis current of controller.

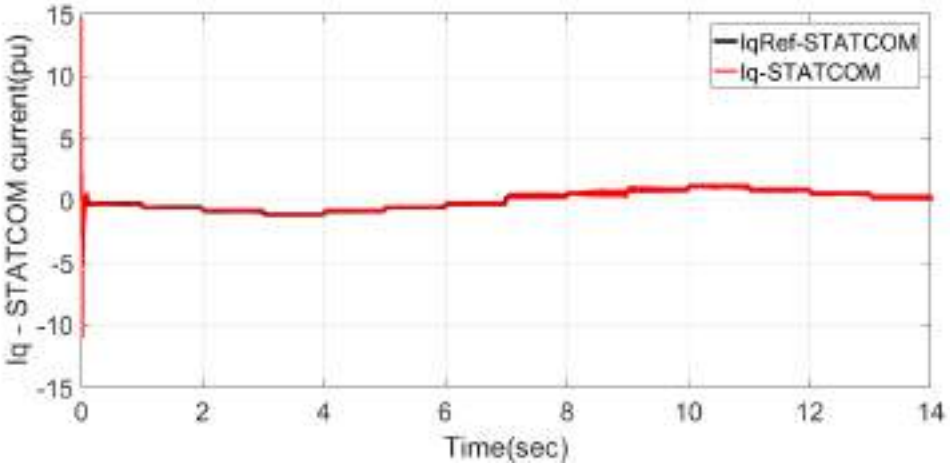

Figure 6. Quaderate axis current in PI controller.

SYSTEM IMPLEMENTATION

Mathematical model

The STATCOM equivalent circuit is shown in the Figure 7, consist of a converter within series inductance in three-line connection to the transmission line and DC-side capacitor.

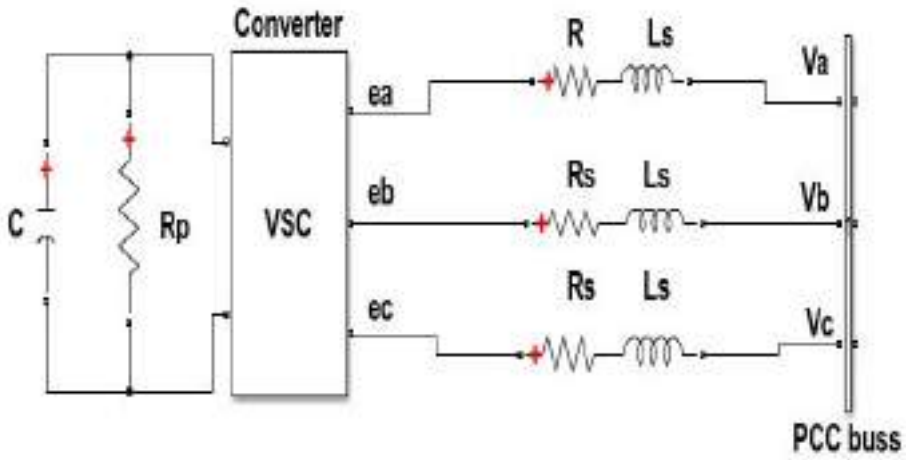

Figure 7. Voltage source convertor equivalent circuit.

Three-phase voltage equations of CHB-STATCOM can be written as in Equations (7-9).

$$L_s \frac{dia}{dt} + R_s ia + va = ea = ns_a v_{dc} \quad (7)$$

$$L_s \frac{dib}{dt} + R_s ib + vb = eb = ns_b v_{dc} \quad (8)$$

$$L_s \frac{dic}{dt} + R_s ic + vc = ec = ns_c v_{dc} \quad (9)$$

Where:

Where ia, ib, and ic are the current in phase a, b, and c, va, vb, and vc are -phase line-to-neutral voltages in phase a, b, and c, R_s and L_s are the accounts for the leakage of the actual power transformers, n is the total number of cells/phase, $s_a, s_b, and\ s_c$ are the switching function (which can be$+1, -1\ and\ 0$).

The AC-side circuit three phase equations in matrix can be written as

$$\frac{d}{dt}\begin{bmatrix} ia' \\ ib' \\ ic' \end{bmatrix} = \begin{bmatrix} -\frac{Rs'\ Wb}{L'} & 0 & 0 \\ 0 & \frac{-Rs'\ Wb}{L'} & 0 \\ 0 & 0 & \frac{-Rs'\ Wb}{L'} \end{bmatrix} \begin{bmatrix} ia' \\ ib' \\ ic' \end{bmatrix} + \frac{Wb}{L'} \begin{bmatrix} ea' - va' \\ eb' - vb' \\ ec' - vc' \end{bmatrix} \quad (10)$$

The " ' " is used for the indication of the per-unit quantities,Where a per-unit system has been adopted according to the following definitions.

$$ix' = \frac{i_x}{i_{base}}\ ,\ \ vx' = \frac{v_x}{v_{base}}\ ,\ z_{base} = \frac{v_{base}}{i_{base}}$$

The parking transformation is then applied as following:

$$Tr = 2/3 \begin{bmatrix} \cos(\theta) & \cos(\theta\text{-}2pi/3\ ) & \cos(\theta\text{+}2\ pi/3) \\ \text{-}\sin(\theta) & \text{-}\sin(\theta\text{-}2/3\ pi) & \text{-}\sin(\theta\text{+}2/3\ pi) \\ 1/\sqrt{2} & 1/\sqrt{2} & 1/\sqrt{2} \end{bmatrix} \quad (11)$$

With assuming that $W = \frac{d\theta}{dt}$, the terms below will produce:

$$\frac{d}{dt}\begin{bmatrix} i\ d' \\ i\ q' \end{bmatrix} = \begin{bmatrix} -\frac{Rs'\ Wb}{L'} & W \\ -W & -\frac{Rs'\ Wb}{L'} \end{bmatrix} \begin{bmatrix} id' \\ iq' \end{bmatrix} + \frac{Wb}{L'} \begin{bmatrix} Ed' - |V'| \\ Eq' \end{bmatrix} \quad (12)$$

By neglecting of the harmonics voltages will be written as:

$$E\ d' = M * V'dc * \cos(\propto) \quad (13)$$

$$E\ q' = M * V'dc * \sin(\propto) \quad (14)$$

Knowing that, M is the relation of invertor's DC side voltage to the AC side voltages which forms the amplification factor is called modulation signal. In order to achieve the decoupling currents, the following equations can be written.

Simulink Model

A three-phase power system was implemented in Simulink/program, it consists of a three-phase generator and transmission lines that serve a non-linear load; simulation is set for fourteen seconds. However, the first test is beginning with inductive load (R-L) and it lasted for seven seconds, hereafter load was switched to be capacitive load (R-C) and the same load was remained till the simulation end (lasted for seven seconds as well). Data of system parameters are listed in the Table 1.

Table 1. System parameters

Quantity	Value

Simulation time	14 sec.
Supplied voltage(L-L)	380 RMS
Operating frequency	50 Hz
Load reactive power (inductive load)	450 VAR
Load active power (inductive load)	450 Watt
Reactive power (capacitive load)	450 VAR
Active power (capacitive load)	450 Watt

Experiment is begun after conducting a harmonic test for assuring a best possible output with minimum distortion level. However, system is operated at normal condition without involving the compensator and so, load consumption is calculated and power factor is found. Hereafter, compensator is integrated with the grid and aiming to enhance the power quality. Table 2 is listing the parameter settings of the STATCOM compensator.

Table 2. Structure of STATCOM compensator

Subject	**Value/sort**	**Number of units**
Capacitors	3000 µF	12 per phase
H-Bridge	-----	12 per phase
Low pass filter	R=0.2Ω, L=10 mH	1
Trigger circuit	PS-PWM	12

RESULTS AND DISCUSSION

At the situation is power system running without STATCOM, Simulation was conducted for 14 sec (s) and began with reactive load at the duration occurs in (0 sec to 7 sec). Similarly, capacitive load is integrated as soon as the first half of simulation time is over. During this stage of experiment, the power factor, voltage profile and the load consumption of reactive power are calculated; Figure 8 is depicting the voltage profile at the monitoring bus bar.

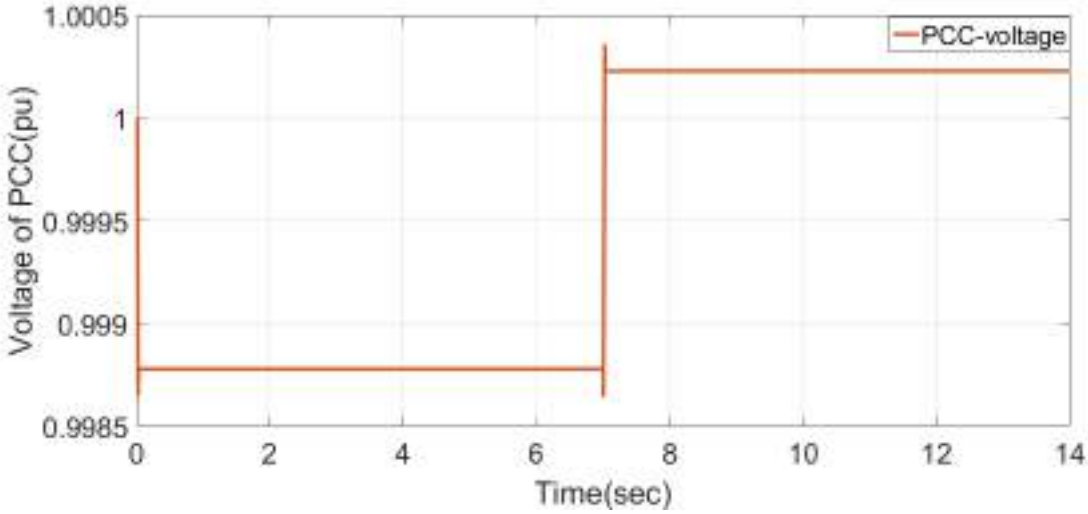

Figure 8. Voltage profile without STATCOM.

The per unit voltage as provided from the generator is equal to unity (1pu), the conducted test shows that voltage is dropped while system serves an inductive load. At time (7 sec) of the simulation, load was switched into capacitive and voltage was found jumped above the rated value. Another quantity has been monitored such as reactive power and power factor, Figure 9, Figure 10, is describing the behaviours of system that running with reactive load and capacitive load without STATCOM interface.

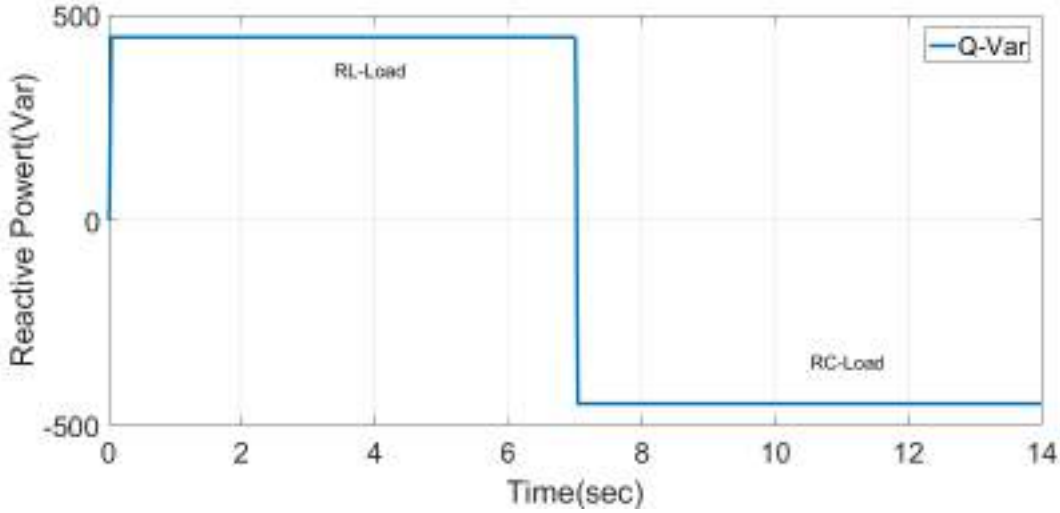

Figure 9. Reactive power (Q) without STATCOM.

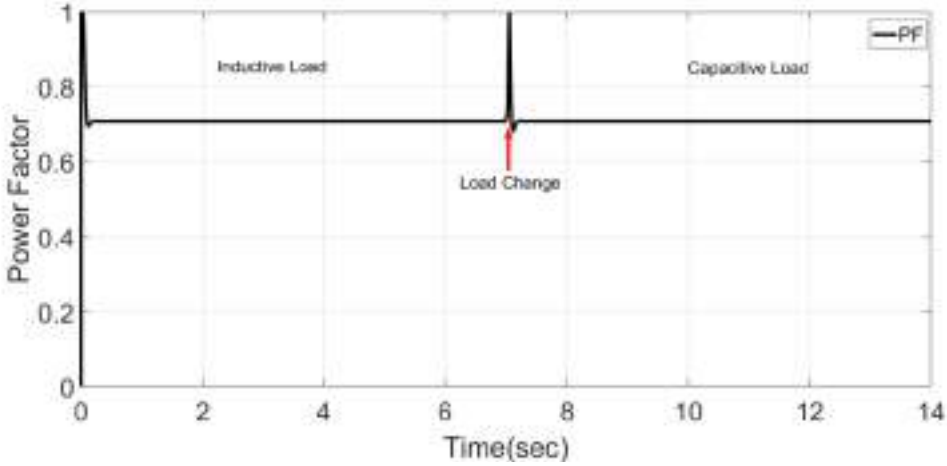

Figure 10. Power factor without STATCOM

To improve the quality of power system, the phase angle between the voltage and current must be minimized and for doing so, the extra demand of reactive power must be compensated from another device. STATCOM is used to compensate the reactive power by injecting or absorbing the required amount of the same.
Now, STATCOM is interfaced near to the load and hence started to compensate the reactive power. In this project, two scenarios were conducted that absorbing the reactive power from the bus bar and injecting the same into bus bar; injection and absorption can be happen base of system requirement which mostly attributed to the load nature. Therefor, the system plotted in figure (7) was implemented where the STATCOM is connected in shut with the test bas bar. Experiment is begun with injecting a 100 VAR of reactive power into the system followed by another injection of 200 VAR however; the same was conducted when the load is (R-L) and the upcoming steps are listed in table (3).

Table 3. STATCOM modes of operation

Time period	Load nature	STATCOM (Q) injected/absorbed
0-1	R-L	100 VAR (inj.)
1-2	R-L	200 VAR (inj.)
2-3	R-L	300 VAR (inj.)
3-4	R-L	400 VAR (inj.)
4-5	R-L	300 VAR (inj.)
5-6	R-L	200 VAR (inj.)
6-7	R-L	100 VAR (inj.)
7-8	R-C	-100 VAR (abs.)
8-9	R-C	-200 VAR (abs.)
9-10	R-C	-300 VAR (abs.)
10-11	R-C	-400 VAR (abs.)
11-12	R-C	-300 VAR (abs.)
12-13	R-C	-200 VAR (abs.)
13-14	R-C	-100 VAR (abs.)

Upon injection of any amount of reactive power, it leads to supply the same into the load and reduce (mince) the injected amount from the generator supplied amount

therefor the reactive power supplied (demanded) from the generator will be reduced and so the phase

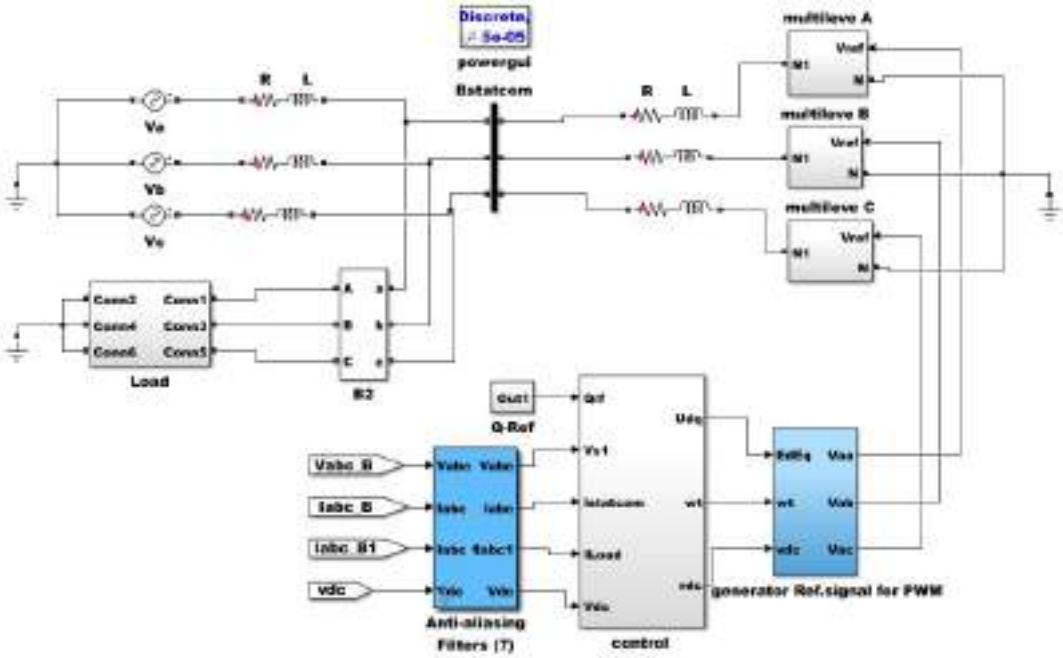

Figure 11. Picturing the power system as it implemented in Simulink as well as the compensator (STATCOM).

Angle will be minimized; the phase angle is in reverse proportion with reactive power quantity (VAR). it is cleared from the table (3) that 100 VAR is injected till the end of first second and 200 VAR is injected hereafter and each injection or absorption lasts for one second only. At the moment when injection of reactive power is increased till 400 VAR (around 95% from the total reactive power demand) process will be reversed by absorbing multiplications of 100 VAR as declared in table (3), Figure 11 is depicting reactive power compensation as revealed by table (3), so, 100 VAR is injected at the starting and similarly 200 VAR is injected after that. Ultimately, the system will return to its initial conditions by absorbing the pre-injected amounts of reactive power. In table (3) it is noted that negative values of reactive power are presented, the STATCOM operate in inductive mode on post 7 seconds from the simulation time. Otherwise, the STATCOM is operate in capacitive mode.

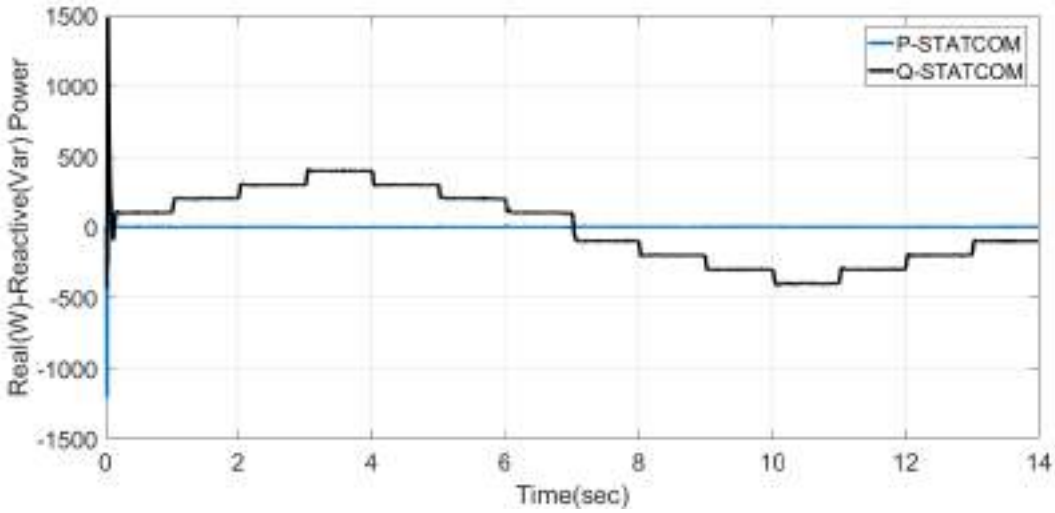

Figure 12. Reactive power compensation as revealed by table (3)

At the end of this(14 seconds), the bus voltage at PCC is improve when the STATCOM operate in capacitive/inductive mode was recorded in each iteration with respect to simulation time and depicted in the Figure 13.

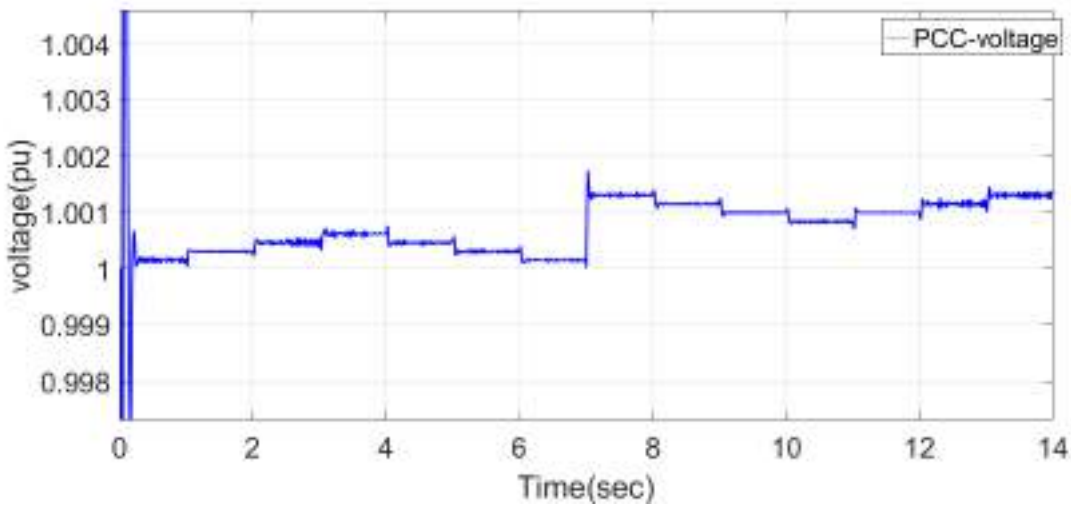

Figure 13. Bus voltage recorded in presence of STATCOM entire the simulation time

Figure 14 shows that power factor is optimized when the STATCOM was injecting a 400 VAR at R-L load and absorbed -400 VAR at R-C load, so; 0.99 is much closed to unity.

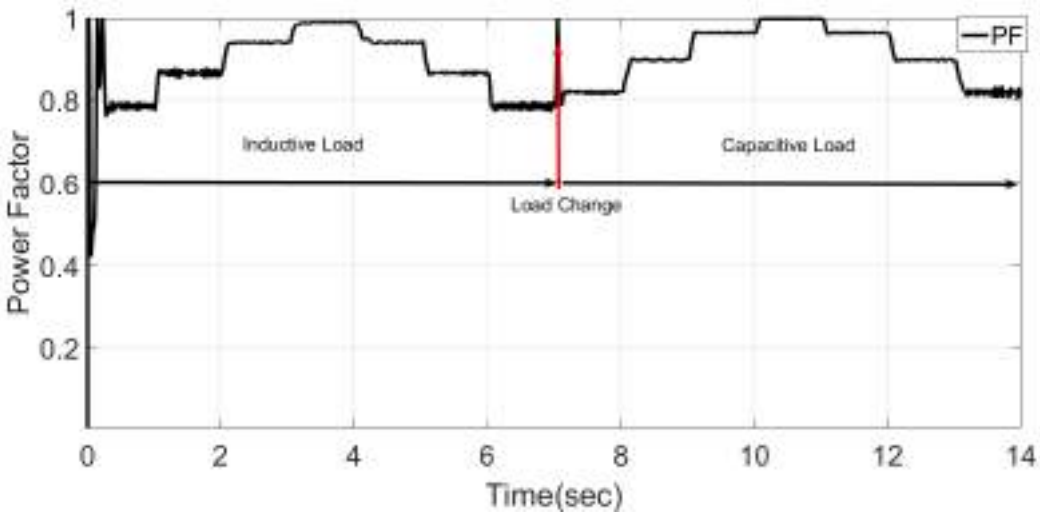

Figure 14. Power factor recorded in presence of STATCOM entire the simulation time

CONCLUSION

Three phase voltage source convertors are used to construct a STATCOM to compensate of reactive power in three phase distribution system. The compensator is implemented with three phase balanced load system so that reactive power can be injected and absorbed respectively. Reactive load in both inductive and capacitive natures was used to examine the power quality fluctuations under such environments. However, system was implemented as three sections entity that involving the power grid, STATCOM compensator and the controller circuit. The procedure above is clarified that power transformer has dispensed in this experiment and the required arrangements are done on PI controller so that STATCOM can work in both reactive mode and capacitive mode. Performance of this model is examined by monitoring the system response of reactive power exchanging between the compensator and power grid; however, reactive power (Q) is injected while simulation first half (inductive load) and absorbed in hereafter; the portion of Q exchanged between system terminals is relative to reactive power amount that supplied by mother system. 20% of load demand from reactive power is began to produce by STATCOM, this percentage was increased later as 50%, 70% and 95% when inductive load is been on demand; otherwise the same reactive power is being absorbed with the similar percentage. Results have shown that harmonics are eliminated by 96% and power factor is enhanced to be 0.999.

REFERENCES

IEEE Project 1346 Working Group. (1994, May). Electric power system compatibility with industrial process equipment. Part 1. Voltage sags. In Industrial and Commercial Power Systems Technical Conference (pp. 261-266).

Edris, A. A. (1997). Proposed terms and definitions for flexible AC transmission system (FACTS). IEEE Transactions on Power Delivery.

Hingorani, N. G., Gyugyi, L., & El-Hawary, M. (2000). Understanding FACTS: concepts and technology of flexible AC transmission systems (Vol. 1). New York: IEEE press.

Morán, L. A., Dixon, J. W., Espinoza, J. R., & Wallace, R. R. (1999, September). Using active power filters to improve power quality. In 5th Brazilian Power Electronics Conference (pp. 501-511).

Singh, B., Saha, R., Chandra, A., & Al-Haddad, K. (2009). Static synchronous compensators (STATCOM): a review. IET Power Electronics, 2(4), 297-324.

Colak, I., Kabalci, E., & Bayindir, R. (2011). Review of multilevel voltage source inverter topologies and control schemes. Energy conversion and management, 52(2), 1114-1128.

Rodríguez, J., Bernet, S., Wu, B., Pontt, J. O., & Kouro, S. (2007). Multilevel voltage-source-converter topologies for industrial medium-voltage drives. IEEE Transactions on industrial electronics, 54(6), 2930-2945.

Rodriguez, J., Lai, J. S., & Peng, F. Z. (2002). Multilevel inverters: a survey of topologies, controls, and applications. IEEE Transactions on industrial electronics, 49(4), 724-738.

Rao, P., Crow, M. L., & Yang, Z. (2000). STATCOM control for power system voltage control applications. IEEE Transactions on power delivery, 15(4), 1311-1317.

Peng, F. Z., & Lai, J. S. (1996, October). Dynamic performance and control of a static var generator using cascade multilevel inverters. In Industry Applications Conference, 1996. Thirty-First IAS Annual Meeting, IAS'96., Conference Record of the 1996 IEEE (Vol. 2, pp. 1009-1015). IEEE.

Prasad, K. N. V., Kumar, G. R., Kiran, T. V., & Narayana, G. S. (2013, January). Comparison of different topologies of cascaded H-Bridge multilevel inverter. In Computer Communication and Informatics (ICCCI), 2013 International Conference on (pp. 1-6). IEEE.

Xu, L., Agelidis, V. G., & Acha, E. (2001). Development considerations of DSP-controlled PWM VSC-based STATCOM. IEE Proceedings-Electric Power Applications, 148(5), 449-455.

Bashi, S. A., Mailah, N. F., Kadir, M. Z., & Leong, K. H. (2008). Generation of triggering signals for multilevel converter. European Journal of Scientific Research, 24(4), 548-555.

Radan, A., Shahirinia, A. H., & Falahi, M. (2007, June). Evaluation of carrier-based PWM methods for multi-level inverters. In Industrial Electronics, 2007. ISIE 2007. IEEE International Symposium on (pp. 389-394). IEEE.

TRIBOLOGICAL EFFECT OF BORIC ACID

Şerafettin EKİNCİ
Selçuk University, Technology Faculty, Department of Mechanical Engineering
sekinci@selcuk.edu.tr

ABSTRACT: A lot of study has been done on the lubrication systems in order to minimize the wear in friction-driven mechanical systems. With the increasing demand for multifunctional, environmentally friendly lubricants with high tribological performance, various lubricants have been developed that can be used in engineering systems. One of these lubricants is boric acid. Surface roughness, wear ratio and friction coefficient values were used in order to determine tribological properties of boric acid as an environment friendly additive and mineral oil mixture in the present study. Wear experiments were conducted with a ball on disc experimental setup immersed in an oil reservoir at room temperature. The evolution of both the friction coefficient and wear behavior were determined under 10N load, at 2 m/s sliding velocity and a total sliding distance of 9000 m. Surface roughness was determined using AFM. Wear rate was calculated utilizing SEM visuals and data. The test results showed that friction coefficient decreased due to the presence of boric acid additive.

Key words: boric acid, lubricant, surface roughness, wear.

EFFECT OF CONNECTING ROD BODY LENGTH, WIDTH AND WALL THICKNESS ON DESIGN PARAMETERS

Ahmet SAYRUGAÇ
Celikel Agriculture Machinery Industry and Ltd. Sti.
ahmetsayrugac@gmail.com

Mahmut ÜNALDI
Selcuk University, Cihanbeyli Vocational School
munaldi@selcuk.edu.tr (Corresponding author)

Murat CİNİVİZ
Selcuk University, Faculty of Technology
mciniviz@selcuk.edu.tr

ABSTRACT: The connecting rod, which used for convert linear motion into circular motion in the Internal Combustion Engines, is a part that is exposed to the sudden changing loads. As a result of R&D studies, in order to produce engines with low volume and high powered, the following results appear in connection with connecting rods; should be more sensitive, light, durable and economical. At the beginning of this study, design parameters and the forces which are exposed of the connecting rods were examined in depth. During the computer analysis changes in temperature and weather conditions have been ignored and it is assumed that the load distribution is homogeneous. Body length and body width, and inner-outer wall thicknesses of the connecting rod were determined as independent variables. The effects of the three-level design of the four factors on the dependent variables were examined statistically related to Experimental Design Analysis (DOE).

Key words: Analysis, Connecting rod, Internal Combustion Engine.

OPTIMIZATION OF FATIGUE OF THE CNT REINFORCED GRP PIPES

Mustafa TAŞYÜREK
Selcuk University, School of Civil Aviation, Department of Airframe and Powerplant Maintenance, Konya
mtasyurek@selcuk.edu.tr

Necmettin TARAKÇIOĞLU
Selcuk University, Faculty of Technology, Department of Metallurgical and Materials Engineering 42075, Konya
ntarakcioglu@selcuk.edu.tr

ABSTRACT: This study focuses on the estimated approach of fatigue results of layered nano-composite pipes. The study deals with the evaluation of the production conditions of the composite pipe currently used in industry. In this context, the active working conditions of the produced pipe samples, the rate of strengthening and the change of surface due to different reasons were investigated. The artificially created conditions were investigated through the Taguchi program and the dominance of the input parameters on the outcome was revealed. According to the results, it was determined that working conditions were the most effective parameter on the results. It has been observed that the content and shape change have become more effective from a certain level.

Key words: Fatigue, Layered Pipe, Optimization.

NUMERICAL MODEL OF THE PRESSURE DISTRBUTION IN REINFORCED CONCRETE ELEVATED (RCE) FLUMES

Fardous N. Al Eqabi
Civil Engineering Department- Wasit University
fardosn227@uowasit.edu.iq

Faisal A. Al Tabatabaie
Civil Engineering Department- Wasit University

Thaar S. Al Gasham
Civil Engineering Department- Wasit University
thaar@uowasit.edu.iq

Baqir M. Al Qutby
Civil Engineering Department- Wasit University
Kutbyb@gmail.com

ABSTRACT: Reinforced concrete flumes are elevated hydraulic structures which transport water through an intersection of a channel with a canal, roads, valley, and depressions. In general, they are fabricated with various shapes such as rectangular, semicircular, elliptical, etc. However, the flow of water in reinforced concrete elevated (RCE) flume is governed by the conservation equations of mass, momentum, and energy. In addition, the value and distribution of the water pressure are the critical parameter in the structural designing of RCE flumes. Moreover, the distribution of flexural and shear stresses in these structures are complex, leading to a tedious design process. This paper aims at understanding numerically the distribution of water pressure in these structures and indicating zones where the pressure maximum values occur. The FLOW3D package was utilized to perform the numerical analysis and the adopted models were compared with a previous experimental study. The results of the finite volume were excellently traced the experimental results with a percentage of error did not exceed 9%. Additionally, the maximum pressure occurred in the bottom of the structure and minimum pressure of water occurred in the surface. Moreover, water pressure was distributed hydrostatic with a depth in the longitudinal and transverse directions.

Keyword-Hydraulic structure, Reinforced concrete elevated (RCE) flume, CFD, distribution pressure, FLOW3D program, VOF.

INTRODUCTION

In hydraulic structures, RCE flumes are thin-walled elevated hydraulic structures conveying water over an obstruction such as canals, valley, road barriers, and ravine [1,2]. They are considered as one of the most important and complex hydraulic structures. They consist of a flume body, a support, a bearing, and other parts, as illustrated in Figure (1) [3, 4]. In normal situations, the RCE flumes are designed depending on two types of loading; structural loading (self-weight, pre-stressed, live

load, etc.), and non-structural loading (dry shrinkage temperature, water load, wind load, ice load etc.) [5]. The literatures are very poor and limited in the subject of RCE flume. The previous studies focused on the structural analysis for different shapes and under various cases of water level of the RCE flume. Hong et al. [6] were performed a numerical analysis on an elevated flume with semicircular section, supported simply. It was subjected to a different water levels. The results illustrated that the stresses and deformations proportional directly with water depth. Moreover, the maximum value of these stresses occurred in the middle span of the flume body. Tan [7] explored numerically the variations in the stresses and the corresponding strains in Enzitan elevated flume during the construction and operation processes. The Enzitan flume is U shape located in the shimen city (China), and it is simply supported. A study was introduced by Tan et al [8] on a rectangular section reinforced concrete masonry arch elevated flume (Xuechuan flume) to carry out the force analysis considering self weight ,water pressure and earthquake effect. In this investigation, the distribution of stresses and deformation were inspected under four cases (dead weight only, dead weight and design water level, dead weight and maximum water level and dead weight, design water level and earthquake effect). Results showed that the water pressure is the main factor affecting on the flume structure.

In this paper, a numerical study using Flow3D package was presented. The simulated models were validated versus an experimental ones AL- Adili [9], then the water pressure distribution on the walls of the Baochuan rectangular flume and the Sunjiagon semicircular flume was studied [10,11].

A.Installing a Flume Body on The Pier B. Connection of Flume in Expansion Joint

C. Complement Flume Installation
Fig. (1) Stage of Field Installation of an Elevated Flume Structure[4]

COMPUTATIONAL FLUID DYNAMIC

The computational fluid dynamic is a computer software which can solve the governing equations of fluid flow (partial differential equation of conservation momentum, energy , and mass) using 3D finite volume of fluid FOV, thus enables the understanding and study of the behavior of fluid dynamics.

FLOW3D package is one of the programs used to simulate fluid dynamics. This program can model and solve different fluid-related problems and eliminate the need for experimental measurements and attempts. There are six turbulent models in FLOW3D program which are " Prandtl mixing length model, One-equation turbulent energy model", "The two-equation k-e model", "Renormalized group(RNG) model", "Two-equation (k-w) model" and "Large eddy simulation model.

GOVERNING EQUATIONS

In the FLOW3D package, problems can be solved based on the momentum and continuity governing equations (known as Navier-Stock equations). The Cartesian coordinates (X, Y, and Z) or cylindrical coordinates, (r, θ, and z) are used to write differential equations in the program to be solved. The additional term should be added to Change from Cartesian coordinates to cylindrical geometry. This term is involved a coefficient ξ representing a cylindrical geometry when its value is 1.0 while ξ=0 for Cartesian coordinate. The continuity and momentum equations of incompressible flow are presented below [12].

$$\frac{Vf}{\rho} c2 \frac{\partial P}{\partial t} + \frac{\partial}{\partial x} u\, Ax + R \frac{\partial}{\partial y} v\, Ay + \frac{\partial}{\partial z} w\, Az + \xi \frac{u\, Ax}{x} = RSOR/\rho \qquad (1)$$

Where:

Vf is the fractional volume open to flow, RSOR is the mass source, ρ is the density of the fluid, (U,V, and W) are represented velocities in the directions of (x,y, z), or (r, θ, z). A_x, A_y, and A_z are represented fractional areas open to flow in those directions, P is the pressure, C2 is the square of the sound and R is a coefficient of coordinates-dependent.

$$\frac{\partial u}{\partial t} + \frac{1}{VF}\left(u\, Ax \frac{\partial u}{\partial x} + v\, Ay\, R \frac{\partial u}{\partial y} + w\, Az \frac{\partial u}{\partial z}\right) - \frac{\xi AY\, v2}{xVF} = -\frac{1}{\rho} \times \frac{\partial P}{\partial X} + GX + fx + bx - \frac{RS0R}{\rho VF}(u - uw - \delta us) \qquad (2)$$

$$\frac{\partial v}{\partial t} + \frac{1}{VF}\left(u\,Ax\frac{\partial v}{\partial x} + v\,Ay\,R\frac{\partial v}{\partial y} + w\,Az\frac{\partial v}{\partial z}\right) - \frac{\xi\,AY\,uv}{xVF} = -\frac{1}{\rho}\frac{\partial P}{\partial Y} + Gy + fy + by - \frac{RS0R}{\rho VF}(v - vw - \delta vs) \quad \textbf{(3)}$$

$$\frac{\partial w}{\partial t} + \frac{1}{VF}\left(u\,Ax\frac{\partial w}{\partial x} + v\,Ay\,R\frac{\partial w}{\partial y} + w\,Az\frac{\partial w}{\partial z}\right) = -\frac{1}{\rho}\frac{\partial P}{\partial z} + Gz + fz + bz - \frac{RS0R}{\rho VF}(w - ww - \delta ws) \quad \textbf{(4)}$$

Where; Gx, Gy,and Gz represent of acceleration of the body in three dimensions. "Fx, Fy, and Fz are the accelerations" of viscous. "bx,by, and bz are the flow losses in porous media or across" the porous baffle plate.

THE TURBULENT MODEL (NUMERICAL MODEL)

AutoCAD 3D modeling tools were used to draw the flume channels in 3D solid geometry and exported to the FLOW3D package as a stereolithographic file. The proposed model was used by AL-Adili [9]. The laboratory flume had dimensions of 0.9 m width, 0.6 m height, and 20 m length with a slope of 0.0005 as shown in Figure (2). While, the modeling of the laboratory flume in the FLOW3D model was illustrated in Figure (3). For the channel modeling in this application, the general conditions, including the systems simulation, the geometry, physical conditions, and out puts adjustments and its related options need to be defined. In physical terms, and according to the physical principle governing the phenomenon, the software allows the selection of the relevant conditions. This study is governed by the physical conditions gravity, turbulence, and viscosity. The two-equation k-e model was adopted in this study for validating the velocities at different depths in experimental work with velocities at different depths that will obtain from numerical work.

Fig. (2) Laboratory Open Channel According AL- Adili [9].

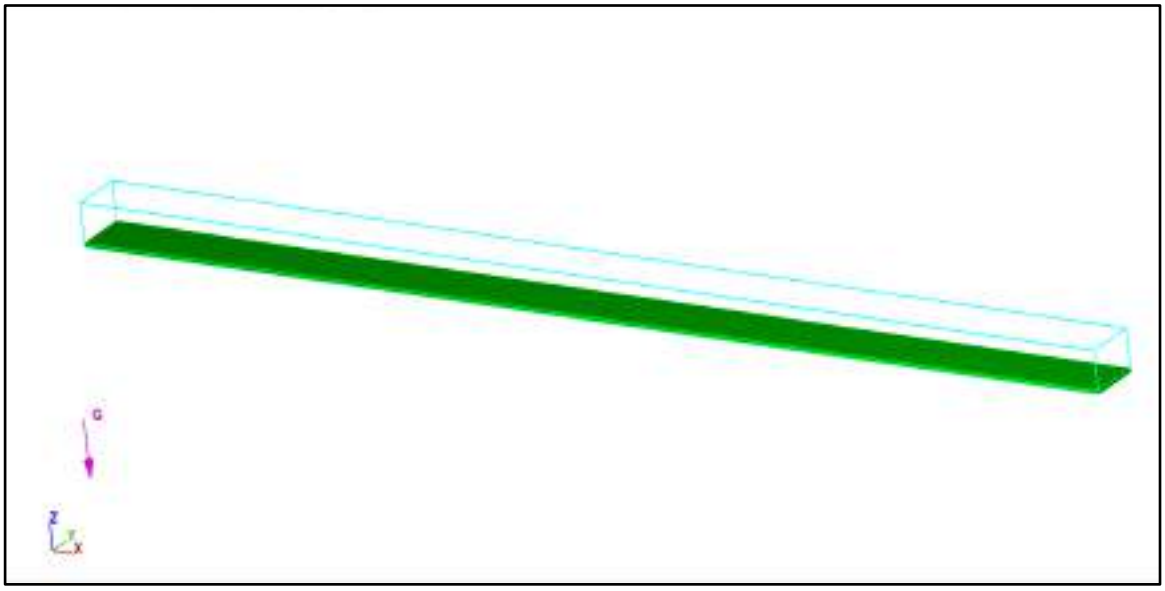

Fig. (3) Modeling of Flume Laboratory in FLOW3D package

Grid generation is one of the most significant issues in a FLOW3D package to obtain an exact solution of the defined problem. The suitable mesh size with good domain is considered a critical portion for "any numerical simulation". Hence, the accuracy of results affected by the grid and cell size. Increasing the number of cells give results with high accuracy, yet the computational time is increased. Thus, the optimum cells amount and size should be assigned . We used FAVOR to obtain the best number of cells. Thus, "getting of "accurate geometric shapes"". The cell size that adopted in this study is 0.039m. The meshing of the flume is shown in Figure (4).

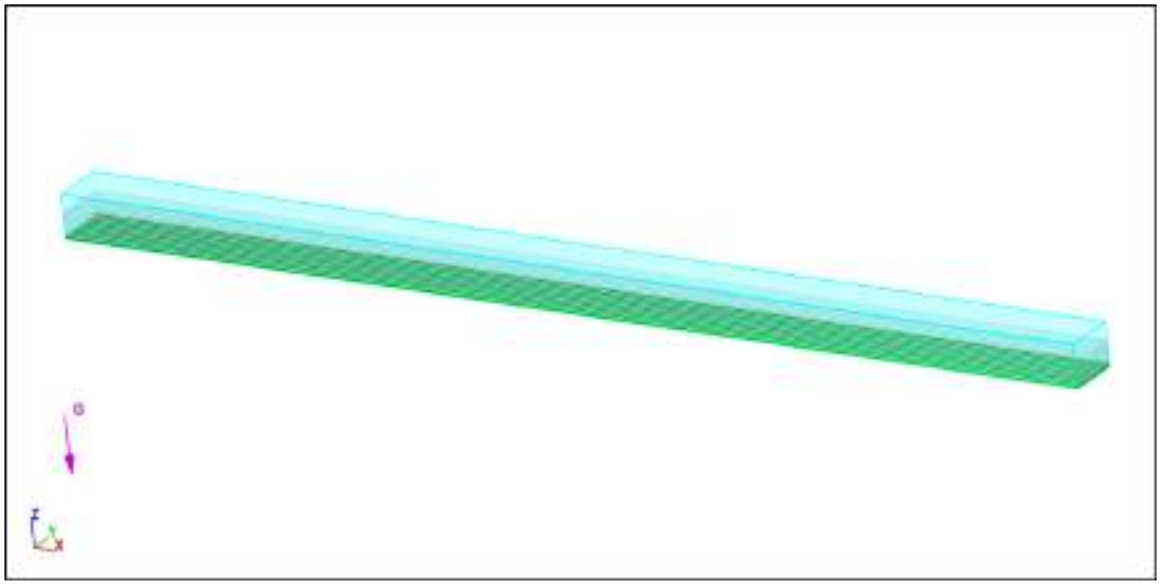

Fig.(4) Meshing Generation of the Model

BOUNDRAY AND INITIAL CONDITION

To get the solution of the governing equation, the initial boundary conditions and the boundary condition of the problem must be defined. The initial boundary condition is the starting condition in the simulation. Finding the solution of the problem depends on the initial state of the simulation. The initial condition is assumed as an approximate

true state at time t = 0. The initial condition includes the global and fluid regions. The boundary conditions used in this study are detailed and shown in Figure (5).

Inlet and Outlet Boundary Condition

Inlet and outlet flow boundary conditions (in X min and X max) are the volume flow rate specified over the whole inlet plane and the outlet flow specified as a boundary condition of outlet flow.

Wall

On a channel wall, the bottom and side walls (Y min, Y max, and Z min) are specified with no slip wall condition. This boundary condition is implemented in the wall and it prescribes that the fluid next to the wall assumes the velocity at the wall, which is zero i.e. U = V = W = 0

Free Surface

Here, the boundary condition (Z max) used for the free surface is the specified pressure. This signifies that the fluid elevation is also specified and follows a hydrostatic distribution.

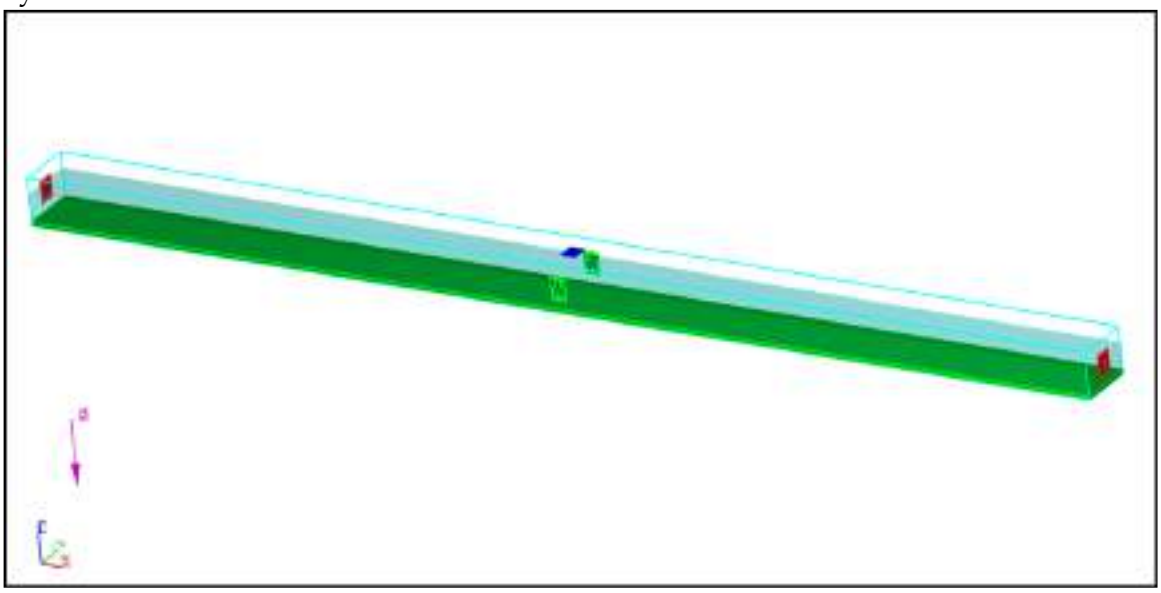

Fig. (5) Boundary Conditions of The Laboratory Flume

VERIFEICATION OF LABORATORY FLUME MODEL

As indicated previously, the verification of the numerical model was based on the study introduced by Al-Adili [9] on Laboratory Open Channel flume. Therefore, the values of the velocities at different heights from the water surface for different discharges and the numerical results of the velocities were compared as illustrated in Table(1) and Figure (6). Moreover, Figures (7) to (10) showed the velocities in 3D for different discharges. Figure (6) clearly showed that the results of the numerical velocities agreed well with the experimental results with an acceptable error range of 3.97 to 8.4 % (Table 1).

Table (1) Comparison Between the Experimental and Numerical Velocities for the Model

Discharge m^3/Sec	Vertical distance from top (m)	Experimental work of velocity (m/Sec)	Numerical work of velocity (m/Sec)	Error %
0.03238	0.13	0.078	0.081	3.97

0.03118	0.2	0.078	0.0832	6.66
0.02194	0.25	0.067	0.0715	6.72
0.01255	0.27	0.025	0.0271	8.4

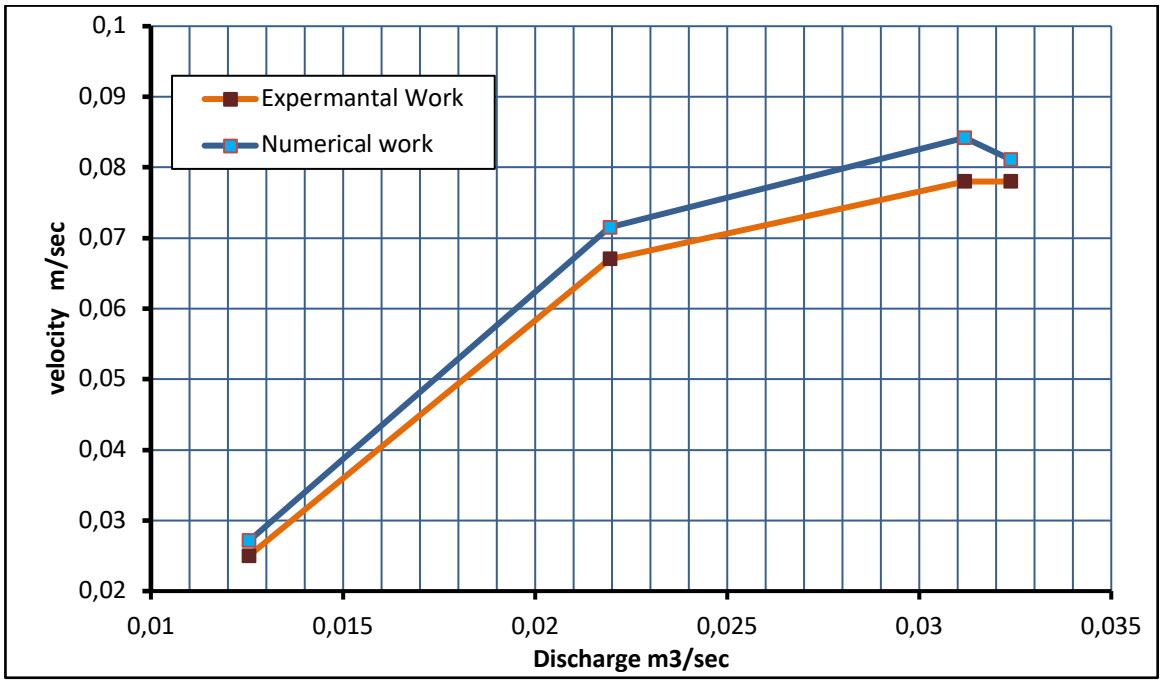

Fig (6) Verification Between the Numerical and Experimental Velocities at Different Discharge

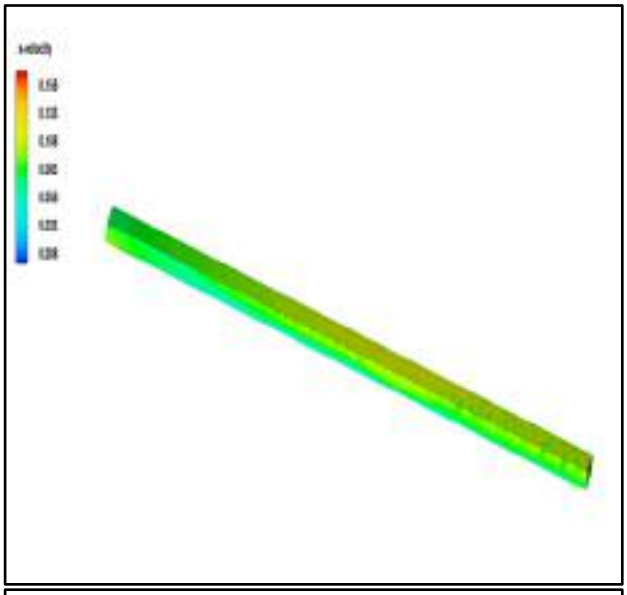

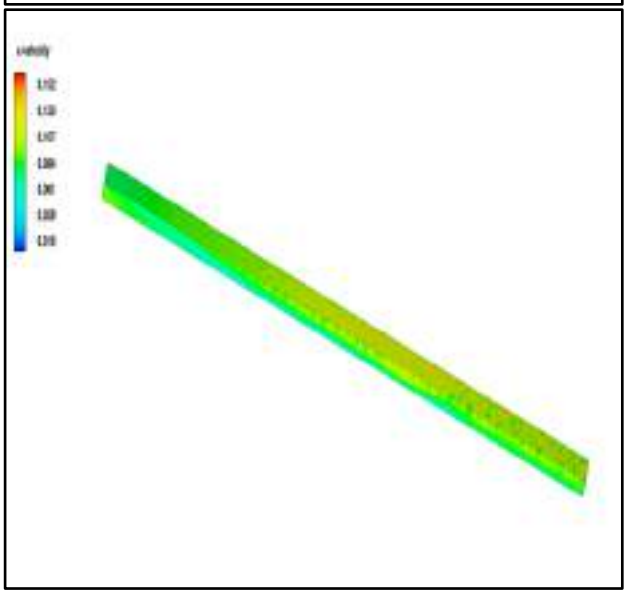

Fig. (7) Velocity at Discharge 0.03238m³/Sec

Fig. (8) Velocity at Discharge 0.031180m³/Sec

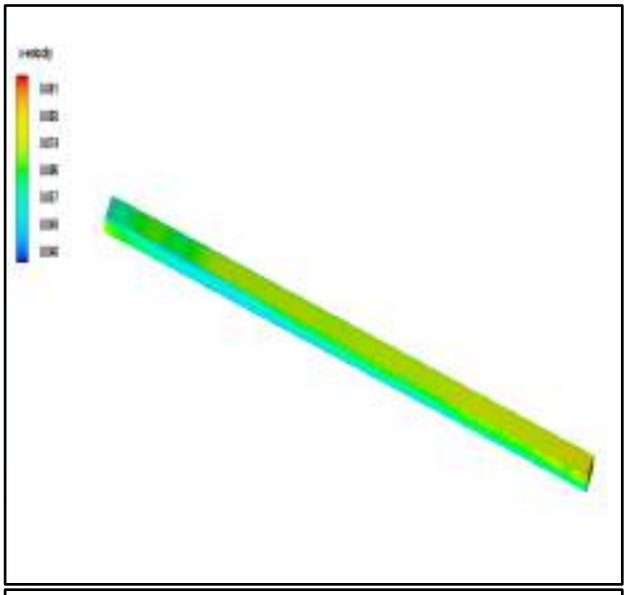

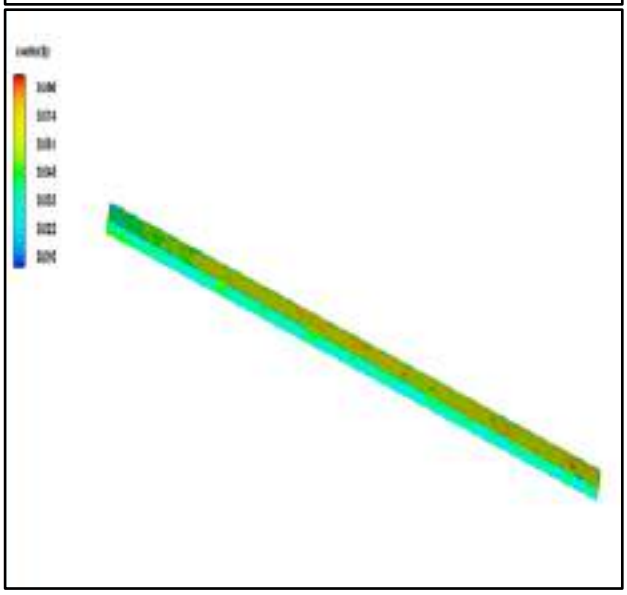

Fig.(9) Velocity at Discharge 0.02194 cm³/Sec **Fig.(10) Velocity at Discharge 0.01255cm³/Sec**

BAOCHUAN AND SUNJIAGOU ELEVATED FLUME (CASE STUDY)

The Baochuan rectangular flume is a structure located in Huangshan city at Auhni province and it is crossed with Hanghui highway. Baochuan flume which has a flow rate design is 0.52 m3/Sec, the design and maximum of water level are 0.5m and 0.58m respectively, longitudinal slope of 0.002 and total length of 120m. Moreover, it has 0.68m height and width of 0.8m [10].

At Miyun county in Beijing, the Sunjiagon semicircular flume was built. It has a design flow rate 4m3/Sec, design and maximum of water level are1.24m and 1.4 respectively, longitudinal slope of 0.00172 and total length of 72m. Dimensions of sunjiagon flume are inner radius of 1m and clear height of 1.4m[11]. The modeling, meshing and boundary condition of the Baochuan flume structure and the Sunjiagon flume structure in FLOW3D package are illustrated in figure (11)and (12).

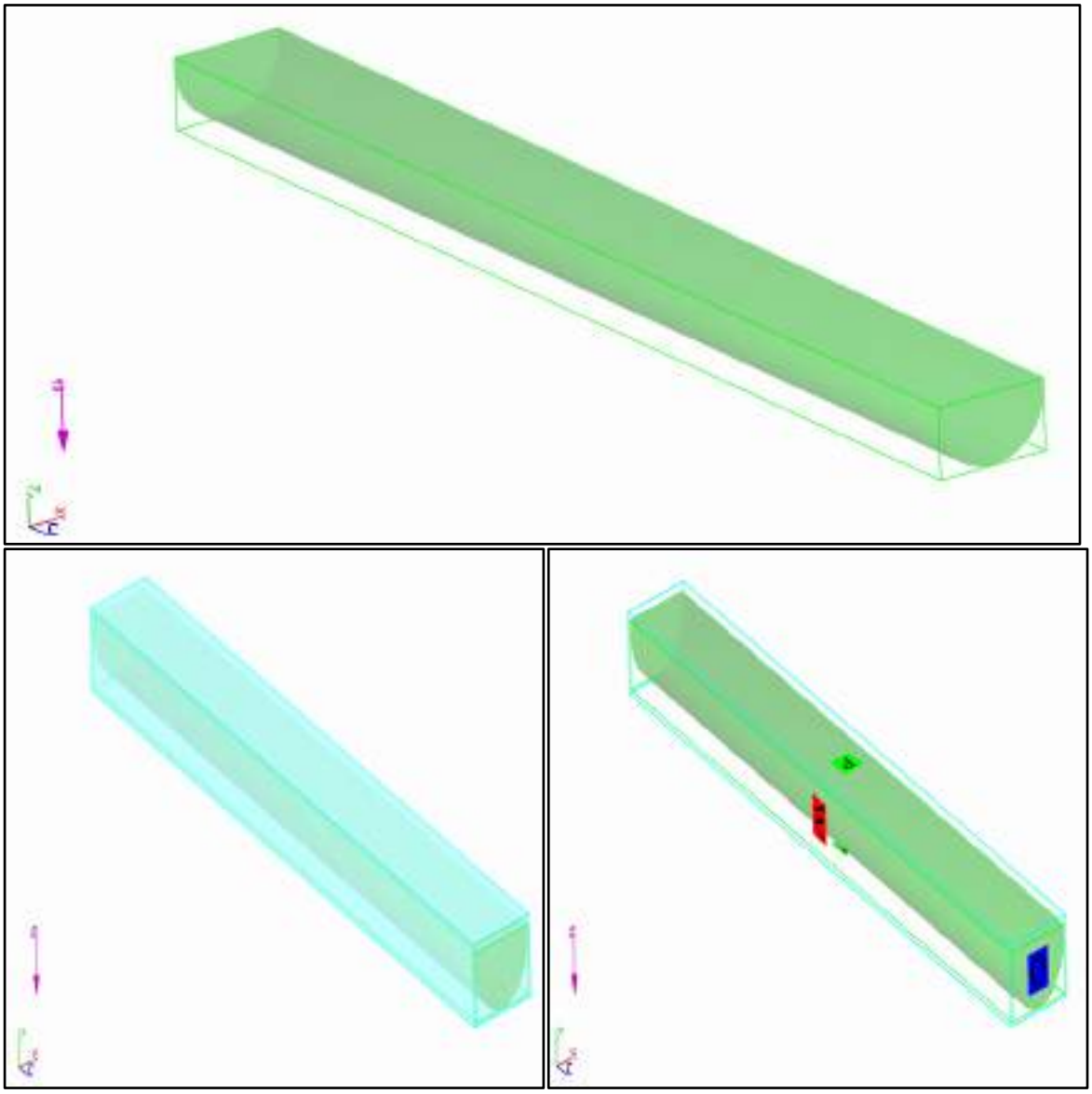

Fig. (11) Modeling, Meshing and Boundary Condition of the Sunjiagou Flume Structure in FLOW3D Package

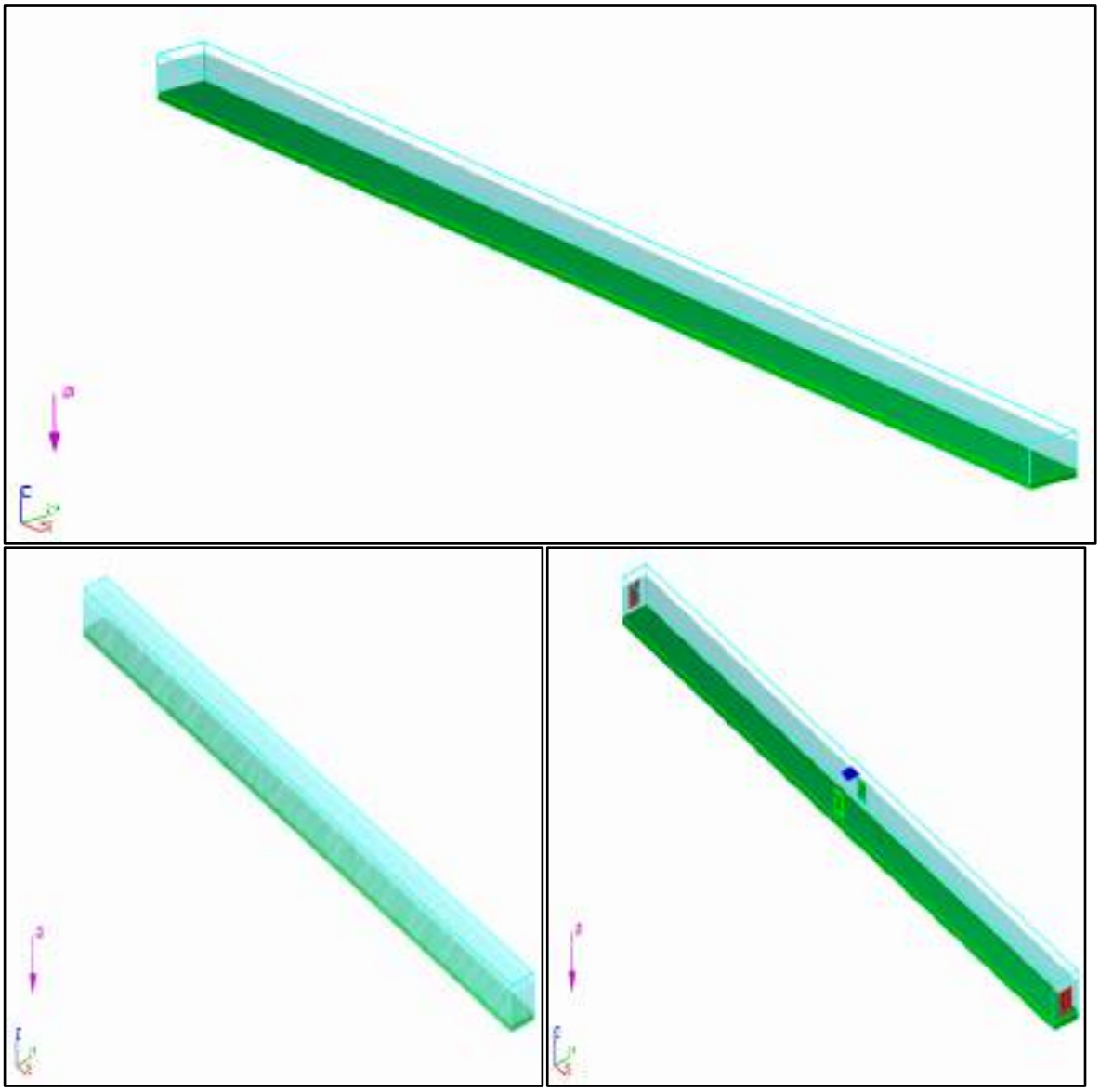

Fig. (12) Modeling, Meshing and Boundary Condition of Baochuan Flume Structure in FLOW3D package

DISCUTION AND RESULT OF FLOW3D SOFTWARE

The aim of numerical work is to study the pressure distribution in the elevated flume hydraulic structure. It is important to locate the maximum value of the water pressure, which considered the main factor act on the elevated channel construction and the base design [9,11]. After applying the geometry condition, hydrodynamic condition, and boundary condition of flume structure, and executing the program the results of the 3D simulation were obtained**: -** Figure (13) shows the water pressure distribution in rectangular and semicircular elevated flume. Figure (14) and (15) illustrates that the pressure is distributed hydrostatically with the water depth in two different cross sections, and maximum water pressure appeared at the lower point of the bottom. Hydrostatic pressure was proportional directly with the depth of water where, the hydrostatic pressure increased with the increase of water depth. It should be noted that the depth of hydrostatic pressure of the flow in the other directions was similar to

those in figure (14) and (15). Figure (16) and (17) show the transverse water pressure distribution near to the bottom of flume in two dimensional and a one dimensional views. Figure (13)and (16) illustrates that the lower value of pressure for semicircular and rectangular shapes in longitudinal and transverse direction occurred on the surface. Moreover, the figure (17) shows that the pressure did not change in the transverse direction and distributed linearly for both shapes.

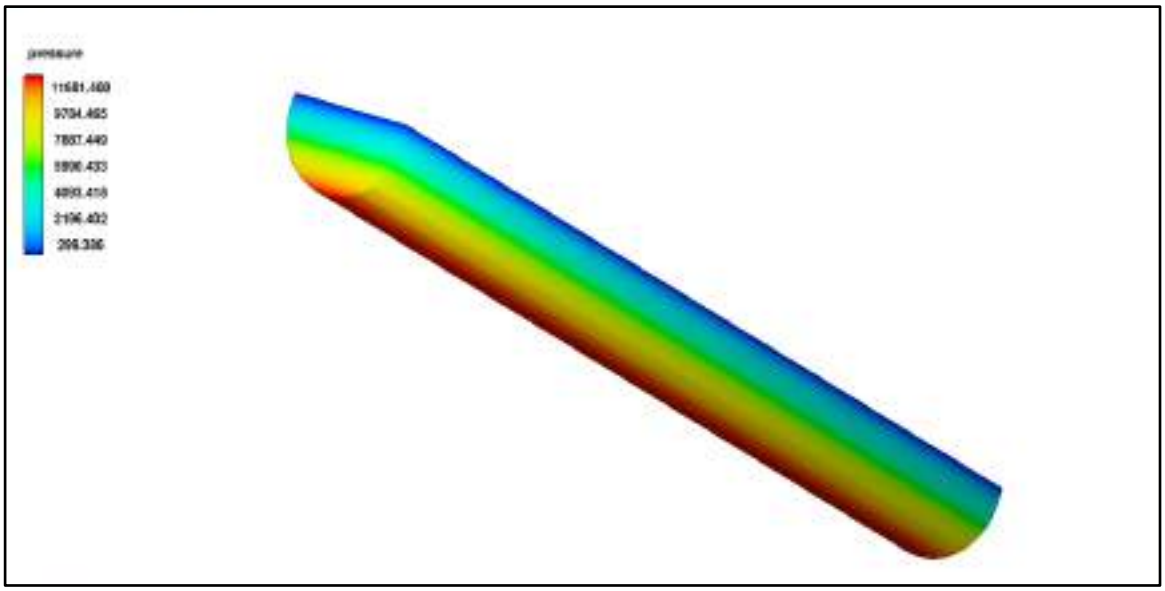

.

Semicircular section

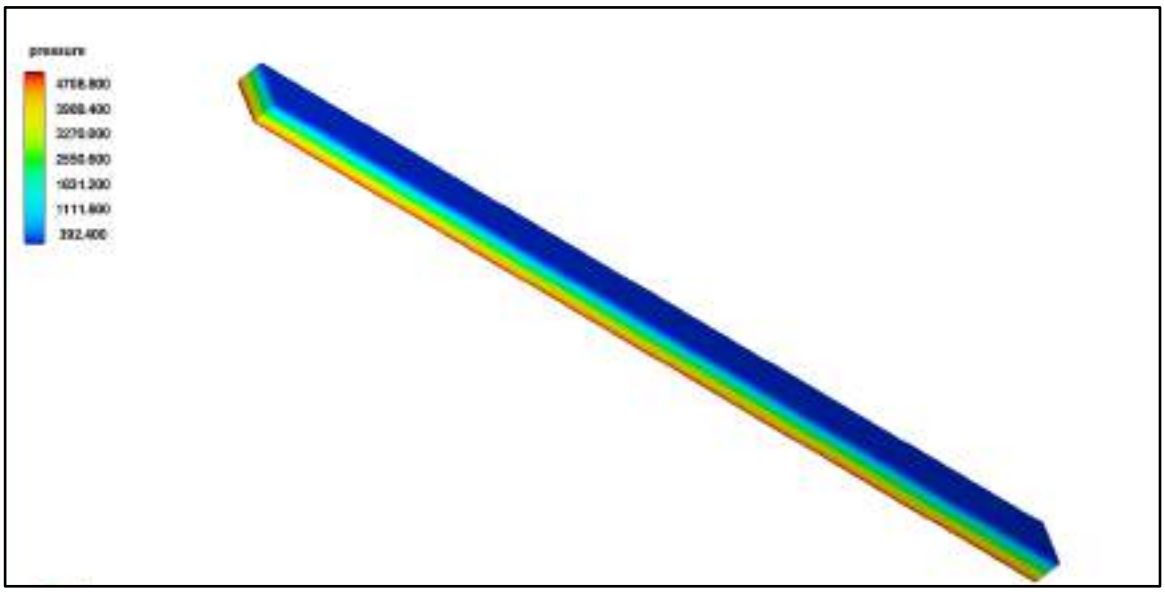

Rectangular section

Fig. (13)Distribution Pressure of Semicircular and Rectangular Elevated Flume in 3D

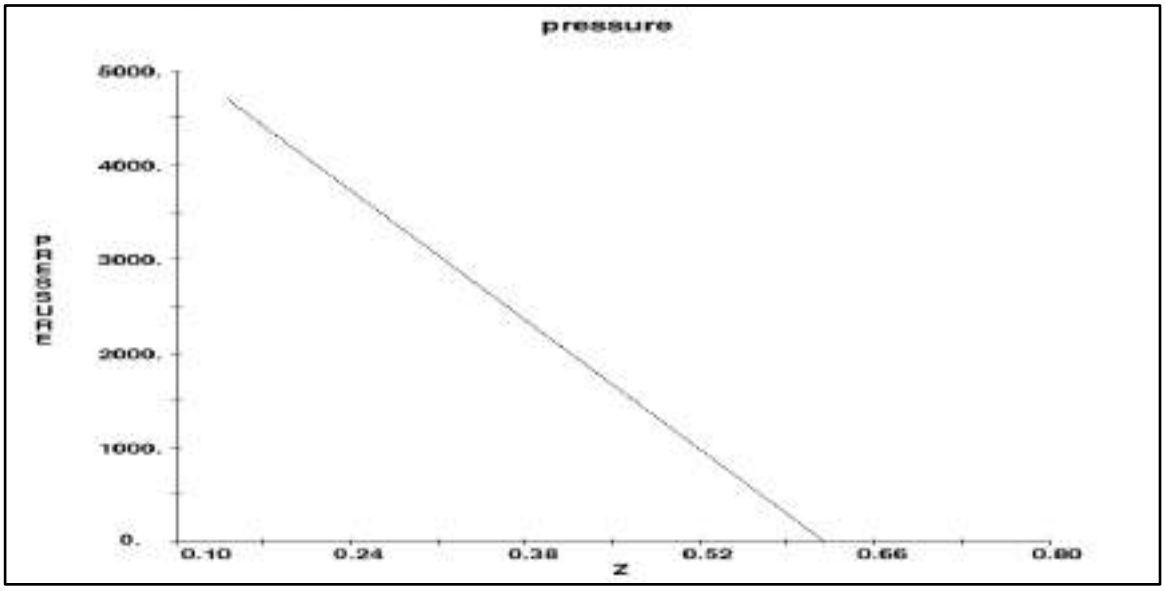

Fig. (14) Pressure Distribution in the 1D of the Rectangular Elevated Flume

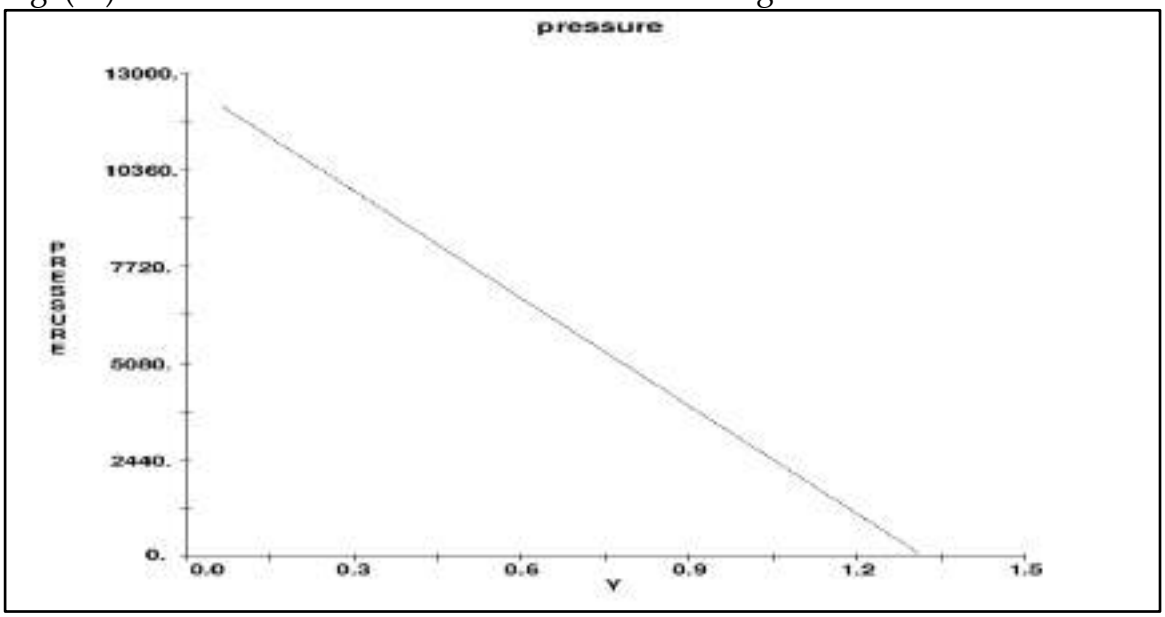

Fig. (15) Pressure Distribution in the 1D of the Semicircular Elevated Flume

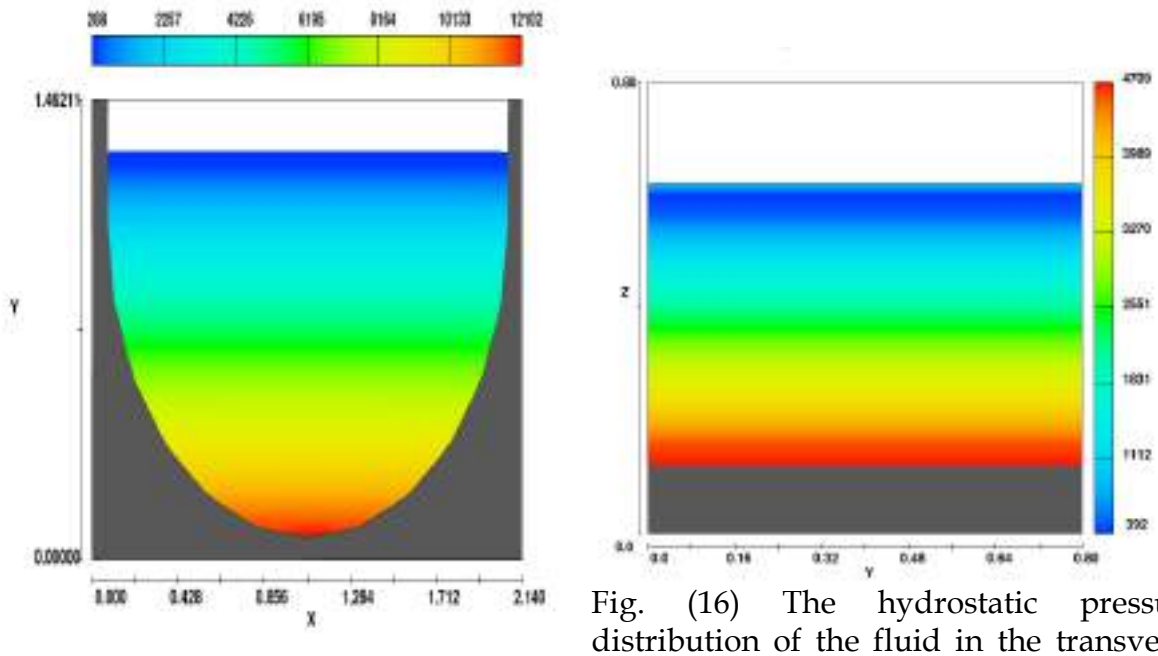

Fig. (16) The hydrostatic pressure distribution of the fluid in the transverse direction, by the Flow 3D numerical model of rectangular and semicircular.

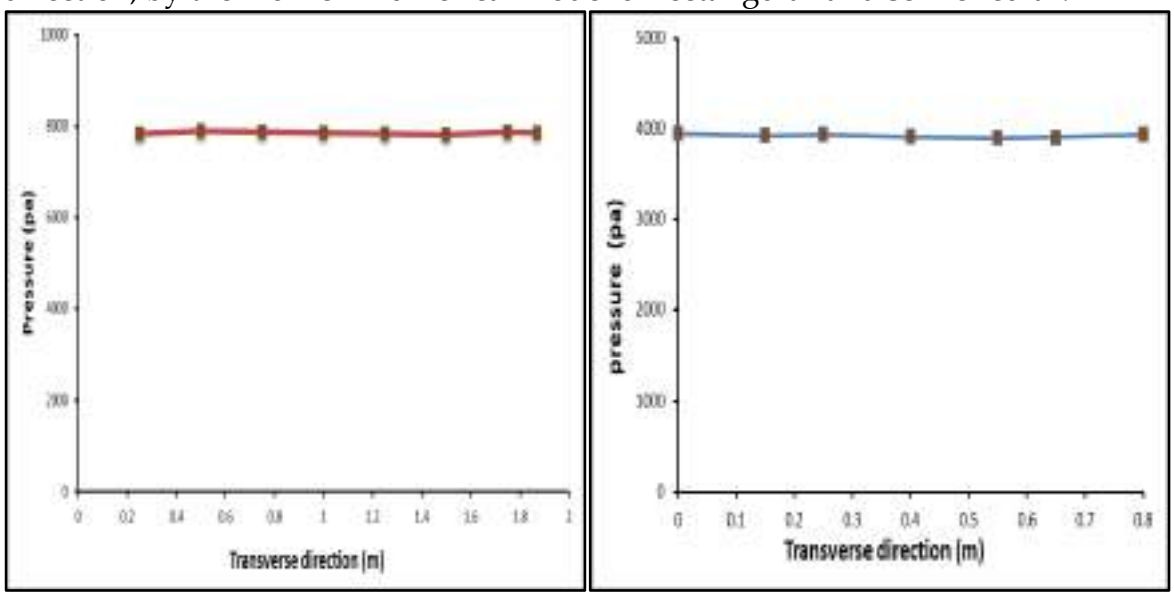

Fig.(17) The Distribution of Water Pressure in the Transverse Direction Close to the Bottom of Flume Structure.

REFERENCES

[1] Hong, D., & Kelun, W. (2014). Finite Element Analysis of Reinforced Concrete Aqueduct During Operation Period. In International Conference on Electronic, Industrial and Control Engineering.

[2] Duan, Q. H., Zeng, D. D., Yang, L. F., & Luo, Y. J. (2013). Review on the Ultimate Bearing Capacity of the Aqueduct's Supporting Structure. In Applied Mechanics and Materials (Vol. 368, pp. 1468-1471). Trans Tech Publications.

[3] Ri-Chen, J., Yan, T., & Jun, H. (2010, October). The study on force characteristics of large rectangle aqueduct with longitudinal beams. In Intelligent System Design and Engineering Application (ISDEA), 2010 International Conference on (Vol. 2, pp. 753-757). IEEE.

[4] Yeon, K. S., Hwang, J. Y., Kim, C. Y., & Yeon, J. H. (2015). Longitudinal Thermal Movement of Polymer Concrete Irrigation Aqueducts. In Advanced Materials Research (Vol. 1129, pp. 586-592). Trans Tech Publications.

[5] Deng, H. F., Wang, Y., Zhu, M., Cheng, Z., & Xu, X. L. (2011). In Situ Load Experimental Research on the Stress Characteristics of Large Span Aqueduct. In Applied Mechanics and Materials(Vol. 71, pp. 4949-4952). Trans Tech Publications.

[6]Hong, D., &Kelun,W. (2014) "Finite Element Analysis of Reinforced Concrete Aqueduct During Operation Period." International Conference on Mechatronics, Electronic, Industrial and Control Engineering (MEIC-14). 1251-1255.

[7]Tan, M. (2013). Simulation Analysis Reinforced Concrete U-Shaped Aqueduct. In Applied Mechanics and Materials (Vol. 394, pp. 345-348). Trans Tech Publications.

[8]Tan, M., & Wei, K. (2013, December). Force calculation and study of reinforced concrete rectangular-sectioned aqueduct. In Instrumentation and Measurement, Sensor Network and Automation (IMSNA), 2nd International Symposium on (pp. 326-329). IEEE.

[9] Al Adili, A. (2016). Investigation of the Effect of Manning Roughness on Froude Number in Subcritical Flow. Journal of Construction and Building Materials, 1(1).

[10] Ji, D., & Zhang, X. (2012, September). Force Analysis of Reinforced Concrete Rectangular-sectioned Beam-supported Aqueduct. In 2nd International Conference on Electronic & Mechanical Engineering and Information Technology. Atlantis Press.

[11] Liu, K. D. (2013). Force Analysis of Reinforced Concrete U-Shaped Beam-Supported Aqueduct. In Applied Mechanics and Materials (Vol. 394, pp. 381-384). Trans Tech Publications.

[12] Flow Science, 2014, "FLOW 3D version 11 user manual".

[13] Xiangzan, X.(2014). Finite Element Calculation of Reinforced Concrete Rib Arch Aqueduct. In International Conference on Electronic ,Industrial and Control Engineering.

INVESTIGATION OF SIMULTANEOUS EEG-fMRI ANALYSIS METHODS

Zülfikar ASLAN
Gaziantep Üniversitesi Teknik Bilimler Meslek Yüksekokulu
zulfikaraslan@gantep.edu.tr

Mehmet AKIN
Dicle Üniversitesi Elektrik-Elektronik Mühendisliği
makin @dicle.edu.tr

ABSTRACT: Electroencephalography (EEG) and Functional Magnetic Resonance Imaging (fMRI) are two effective methods to investigate human brain functions. A combination of EEG and fMRI data is used because these two are complementary to each other in their basic aspects: EEG is a direct measurement of neural mass activity and provides high temporal resolution while fMRI, is an indirect measurement of neural activity, which is based on hemodynamic changes (i.e., changes in the blood flow) and provides high spatial resolution. Therefore, simultaneous snapshots of EEG and fMRI is expected to be capable of presenting both temporal and spatial characteristics of a brain activity. The significance and potential of multimodal brain imaging has been increasingly reported by recent studies many of which focused on the use of simultaneous EEG and fMRI. In this study, the methods that utilize simultaneous EEG and fMRI to investigate brain activities are presented and compared to discuss and reveal potential benefits of these methods.

Key words: simultaneous EEG-fMRI , neuroimaging, functional magnetic resonance imaging

EŞZAMANLI EEG-fMRI ANALİZ METOTLARININ İNCELENMESİ

ÖZET: Elektroensefalografi (EEG) ve fonksiyonel manyetik rezonans görüntüleme (fMRI), insan beyin fonksiyonunun değerlendirilmesinde kullanılan son derece etkili yöntemlerdir. EEG ve fMRI verilerinin kombinasyonun birlikte kullanılmasının nedeni, her iki veri türünün temel yönleri açısından birbirini tamamlayıcı olması ile ilgilidir: EEG, nöral kitle aktivitesinin doğrudan ölçümüdür ve yüksek zamansal çözünürlük sağlar. fMRI, nöral aktivitenin dolaylı bir ölçümüdür ve hemodinamik (kan dolaşımı ile ilgili hareketleri içeren durumlar) değişikliklere dayanır ve yüksek mekansal çözünürlük sunar. Her iki yöntem sinaptik aktivitenin değişimlerine çok duyarlıdır, bu da eş zamanlı EEG ve fMRI ile aynı nöral olayların hem yüksek zamansal hem de mekansal çözünürlük ile karakterize olabileceğini düşündürmektedir. Multimodal beyin görüntülemenin önemi, insan beyni işlevinin hem yüksek zamansal hem de mekansal çözünürlüğünü elde etmeyi amaçlayan eşzamanlı EEG-fMRI'yi kullanarak giderek artan sayıda çalışma tarafından belgelenmiştir. Bu çalışmada, eşzamanlı EEG-fMRI verilerinin analizi için kullanılan analiz metotları tanıtılarak ve karşılaştırılarak, her bir yaklaşımla sağlanan faydalar belirtilmektedir.

Anahtar sözcükler: eşzamanlı EEG- fMRI , nörogörüntüleme, fonksiyonel manyetik rezonans görüntüleme

GİRİŞ

Nörobilim, mühendislik, bilgisayar bilimi, kimya, felsefe, psikoloji, matematik ve tıp gibi diğer disiplinlerle yakından çalışan disiplinler arası bir bilimdir. Nörobilimciler, sinir sisteminin hücresel, işlevsel, davranışsal, evrimsel, hesaplamalı, moleküler, hücresel ve tıbbi yönlerini inceler. Farklı yönlere odaklanan çeşitli alanlar vardır, ancak ortak yönleri bulunmaktadır [1]. Nörogörüntüleme teknikleri kullanılarak ölçülen serebral aktivitenin farklı doğası, uzun zaman önce fark edilmiştir. Karmaşık doğasını yakalamak söz konusu olduğunda tek modalite kayıtlarının kullanılmasının sınırlı olabileceği açıktır. Dolayısıyla, multimodal bir yaklaşıma geçmenin nörobilimcilerin bu aktivitenin dinamiklerini ve yapısını daha iyi anlamalarına izin vereceği tartışılmıştır. Bu, elektroensefalografi (EEG) ve fonksiyonel manyetik rezonans görüntüleme (fMRI) ile kaydedilen kan oksijenli seviye bağımlı (BOLD) sinyali gibi farklı tekniklerden gelen bilgilerin birleştirilmesinin önemli bir metodolojik zorluğu temsil ettiği anlamına gelir [2].

Fonksiyonel ayrışma ve entegrasyon beyin işlevinin organizasyonunda temel ilkeler olduğundan, [3] beyin ağlarındaki bağlantı mekanizmalarının anlaşılması insan nöro biliminde önemli bir amaçtır [4]. Aynı zamanda, bağlantı bozukluğunun, şizofreni gibi majör nöropsikiyatrik bozuklukların tespitinde son derece önemli olduğuna inanılmaktadır [5]. Fonksiyonel manyetik rezonans görüntüleme (fMRI), beynin ağ yapısını anlama da oldukça etkili bir modelitedir. Örneğin belirli bir bilişsel görevde yer alan beyin bölgelerini karakterize etmede son derece yararlıdır. fMRI verilerine dayanarak, beyin bölgelerinin etkileşimi ile ilgili farklı anlayışlar, bir korelasyon ilişkisinin (işlevsel bağlantı), daha kolay olarak anlaşılmasını sağlayabilir [6].
EEG-fMRI, ağ yapısını, örneğin bilişsel işlem sırasında ve gama salınımları gibi ilgili bağlama mekanizmalarını tanımlamak için kullanılabilir. Buna göre, hem ağ yapısının hem de nörofizyolojik mekanizmaların karakterizasyonu belirlemek için eş zamanlı EEG-fMRI kullanımı bu hedef için metodolojik temeli sağlamaktadır [7,8].
Beyin ağlarının tanımlanmasında, BOLD (Blood-oxygen-level dependent) sinyallerinin dinlenme durumunda oldukça güvenilir bir şekilde tanımlanmış korelasyonlu zaman serilerinin mekansal örüntülerine dayanarak, varsayılan mod ağı (DMN), dorsal dikkat ağı (DAN) veya salience ağı (SN) gibi birkaç beyin ağı tanımlanmıştır. Örneğin, dinlenme halindeki ağlarda değişiklikler Alzheimer hastalığı gibi çeşitli nöropsikiyatrik durumlarda bulunur [9].
Dinlenme durumu için eş zamanlı EEG-fMRI ile yapılan ilk çalışmalar, alfa osilasyonları gibi spesifik frekans örüntülerinin BOLD korelasyonlarını tanımlamaya çalışmıştır [10-12]. Bununla birlikte, ağ dinamiklerini karakterize etmek için, EEG sinyalinin, ağlar içinde ve arasında fonksiyonel bağlantıya bağlanması fikri ortaya çıkmıştır. Örneğin, Hlinka ve ark., Fonksiyonel bağlantının DMN varyansının % 70' inin delta ve beta salınımları ile açıklandığını göstermiştir [13]. Scheeringa ve arkadaşları alfa gücü arttığında, primer görme korteksi ve oksipital bölgeler

arasındaki BOLD bağlantısının yanı sıra DMN' nin görsel alanları ve bölgeleri arasındaki negatif bağlanma azaldığını göstermiştir [14]. Chang ve arkadaşları, DMN, DAN ve SN arasındaki fonksiyonel bağlantıyı araştırmıştır. Alfa gücü ile DMN ve DAN arasındaki bağlantıların gücü arasında ters bir ilişki bulmuşlardır. Dahası, alfa gücü, DMN ve DAN arasındaki anti-korelasyonun mekansal boyutuyla ilişkili olduğunu gözlemlemişlerdir [15].

Hem EEG hem de fMRI' ın eş zamanlı olarak kullanılmasının en önemli yönü, sinaptik işleme duyarlılıklarında örtüşmesi ve buna bağlı olarak beyin fonksiyonunun yüksek zamansal ve yüksek mekansal çözünürlükle değerlendirilmesidir. Bugün EEG-fMRI için en umut verici uygulamalardan biri, beyin ağ yapısının ve dinamiklerinin karakterizasyonudur. Eşzamanlı EEG-fMRI'nin uygulanabilirliğini araştırmaya yönelik motivasyonun çoğu, iki kayıt modalitesinin ayrı olarak sağladığı beyin işlevinin seçici görünümünden gelmektedir. fMRI kötü bir zamansal ters problemden muzdariptir, yani, bölgesel aktivasyonlara sahip bir harita, "ne zaman" ve bu aktivasyonların hangi sırada gerçekleştiği ile ilgili çıkarımlara kolayca izin vermemektedir [16].

Bu, EEG'de iyi bilinen mekansal ters problem ile benzerlik göstermektedir, bu durumda, beyindeki kaynakların mekansal lokalizasyonunun kafa derisindeki elektriksel potansiyellerden kesinlik kazanması mümkün değildir [17,18]. Bununla birlikte, EEG ve fMRI' nin güçlü ve zayıf yönleri tamamlayıcı olduğu için, eş zamanlı EEG-fMRI, büyük ölçüde imkansız gibi görünen şeylere ulaşabilir, yani insan beyni aktivitesinin hem yüksek mekansal hem de yüksek zamansal çözünürlükle kaydedilebilir.

EEG-fMRI' nin ilk uygulamaları, epileptojenik EEG aktivitesinin nöral kaynaklarının tanısal ve ön-cerrahi planlamaya yönelik lokalizasyonunda klinik bir ilgiden doğmuştur [19]. Patolojik beyin aktivitesinin başlangıcı, EEG ölçümlerinden açıkça anlaşılmasına rağmen, bu patojenik nöral olayların yayıldığı korteksteki konumlar, tek başına EEG' den net olarak anlaşılamamaktadır. Epilepsinin cerrahi öncesi değerlendirilmesinde EEG ve fMRI' nin eşzamanlı ölçümü ve eş zamanlı analizi, ayrı kayıt protokolleri ile mümkün olanın ötesinde kavrayış sağlar [20,21]. Bu klinik araştırma çizgisine dayanarak, bilişsel varsayılan modları yansıtan içsel beyin durumları, rastgele EEG salınımları ve dinlenme durumunda fMRI sinyalinin dalgalanmaları arasındaki ilişkilerin değerlendirilmesi ile tanımlanmıştır [22,23].

Eşzamanlı EEG-fMRI ile önemli bir zorluk, her iki modelde de potansiyel olarak görülen azalmış sinyal kalitesidir. Manyetik rezonans sistemi ortamında EEG kayıtları için iletken materyallerin kullanılmasının gerekliliği, görüntü elde edilmesini engelleyebilir [24] ve elektromanyetik akımların indüksiyonuna bağlı olarak EEG sinyal kalitesini ciddi ölçüde bozmaktadır [25-27].

Teknik zorlukların çoğu, son zamanlardaki teknolojik gelişmelerle çözülmüş bulunmaktadır. Bununla birlikte, araştırılan araştırma sorusuna ve birleşik analizler için kullanılan metotlara bağlı olarak, eşzamanlı EEG-fMRI, her bir kayıt modalitesinin özelliklerinin tek başına verilmesi durumunda arzu edilebilecek mekansal ve zamansal çözünürlüğü elde edilmesini mümkün kılmayabilir. Seçilen analiz yönteminin içsel özellikleri, varsayımsal sonucu kuvvetli bir şekilde etkilediğinden, veri entegrasyonu için kullanılan yöntemin seçimi çok önemlidir. Bu nedenle bu çalışmada, eşzamanlı EEG-fMRI verileri üzerinde analiz için en sık hangi metotların kullanıldığı üzerinde durulmuştur [54,55].

MATERYAL

Elektroensefalogram (EEG)

Bir elektroensefalogram (EEG) beyindeki elektriksel aktiviteyi değerlendirmek için kullanılan bir testtir. Beyin hücreleri elektriksel impulslarla birbirleriyle iletişim kurar. Bu etkinlikle ilişkili olası problemleri tespit etmek için EEG kullanılabilir. Bir EEG kaydındaki elektriksel dürtüler, zirveleri ve vadileri olan dalgalı çizgiler gibi görünür. Bu çizgiler, doktorların anormal kalıpların olup olmadığını hızlı bir şekilde değerlendirmesini sağlar. Herhangi bir düzensizlik nöbet veya diğer beyin bozukluklarının bir işareti olabilir. Beyin bir elektrik sistemidir - tüm düşüncelerimiz (bilinçli ya da başka türlü), elektrik akımları yardımıyla birbirlerine sinyaller gönderen bir nöron ağından üretilir. Daha fazla elektrik sinyali, daha fazla beyin aktivitesine karşılık gelen, nöral iletişimi göstermektedir. Bir EEG kulaklığının elektrotları, az sayıdaki nöronlardaki değişiklikleri algılayamaz, bunun yerine aynı anda sinyal veren binlerce nöronun elektriksel değişimlerini tespit eder. Elektrotlardan gelen sinyal daha sonra bir amplifikatöre gönderilir, burada sinyali güçlendirir. Bir bilgisayar daha sonra bu sinyali alır ve hızlı bir zamansal çözünürlükle çeşitli beyin aktivitesi haritaları oluşturabilir. EEG'nin bir dezavantajı mekansal çözünürlüktür - elektrotlar beynin yüzeyindeki elektriksel aktiviteyi ölçtüğünden, sinyalin yüzeye yakın bir yerde mi (kortekste) mi yoksa daha derin bir bölgede mi üretildiğini bilmek zordur. Bu sınırlamayı aşma girişiminde bulunabilecek hesaplamalar bulunmaktadır, ancak EEG araştırması için bir sorun olmaya devam etmektedir [28].

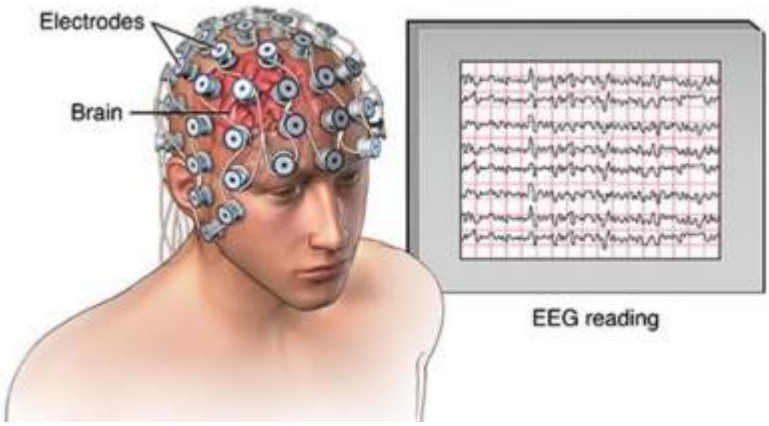

Şekil 1. EEG elektrotları ve sinyalinin bir örneği [30]

Functional magnetic resonance imaging (fMRI)

Bir kişi çeşitli aktiviteleri yaparken beyinde birkaç şey olması gerekmektedir. Örneğin Sağ kol hareket ettirilmek istendiğinde, beynin belirli bir kısmı, bu eylemi tamamlamak için mesaj göndermek için aktivitesini arttıracak ve beynin bu alanı biraz daha fazla oksijen bakımından zengin kan akacaktır. fMRI, MRI ile benzemekle birlikte, hesaplamalar oksijenli kan akışının miktarının nasıl değiştiğini belirlemeye yöneliktir. Beynin bir bölümünde diğerlerine göre daha fazla oksijenli kan varsa, o zaman bu beyin bölgesinin daha aktif olma ihtimali vardır. Bu kan Oksijenasyon Seviye Bağımlı yanıt olarak bilinir (BOLD). fMRI en önemli dezavantajı zamansal çözünürlüktür. Kan akışının değişmesi birkaç saniye sürdüğü için ve gerçek kayıt hesaplama faktörleriyle sınırlı olduğundan, veri toplama yavaşlar. Bu genellikle, katılımcıların bir uyarana birden çok kez maruz kaldıkları ve her defasında beyin

tepkisinin farklı zaman noktalarının kaydedildiği anlamına gelir (örneğin, uyaranın başlangıcında uyaranın başlangıcında, ikinci kez uyaranın başlangıcından 10ms sonra, vb. Yanıt kaydedilir). Bu elbette ki yeni bir cevabın kaydedilmesinin doğruluğunu zayıflatabilir, ancak tam bir beyin yanıtı aralığı sağlar [29].

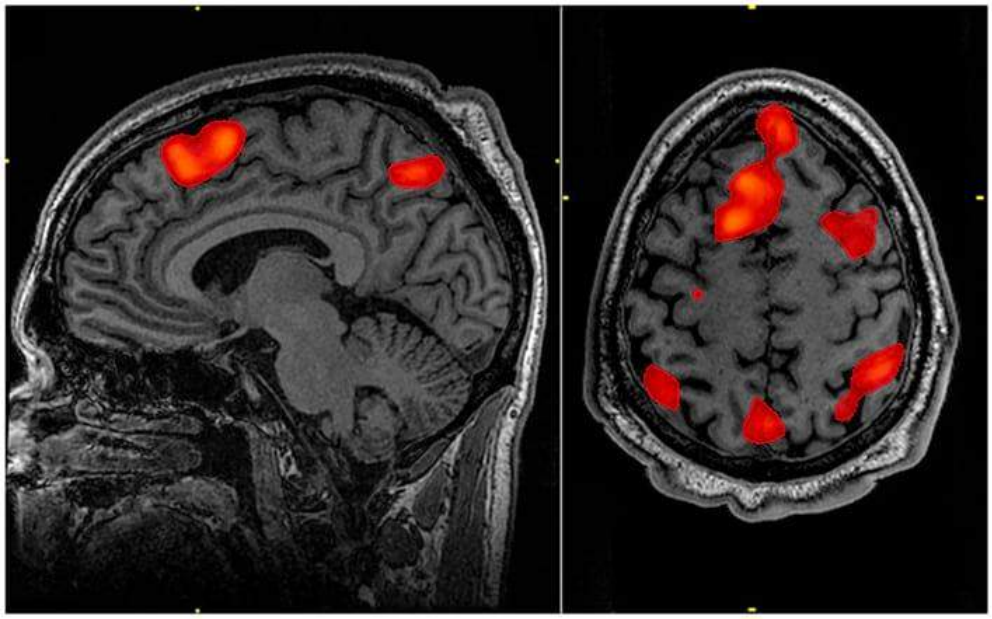

Şekil 2. Örnek bir fMRI görüntüsü [29]

METOT

Asimetrik Veri Entegrasyonu

EEG-fMRI entegrasyonu için asimetrik yaklaşımlar, diğerinin analizini yönlendirmek için bir modaliteden elde edilen bilgiler kullanılarak diğer modalitenin ağırlığı karakterize edilir. Bu yaklaşımlardan en etkili olanları, fMRI bilgili EEG ve EEG bilgili fMRI olmuştur [54].

fMRI Bilgili EEG

fMRI tarafından bilgilendirilmiş EEG, fMRI' den elde edilen sonuçları kullanarak elektromanyetik kaynak görüntülenmesine rehberlik ederek, mekansal EEG ters problemini hafifletmeyi amaçlamaktadır [31-33]. Bunu yapmak için, kafa geometrisi ve beynin en ilgili biyofiziksel özellikleri (örneğin, doku iletkenliği) ilk olarak, simüle edilerek göz önüne alınmış ve saç derisinde akıntıların yollarının hesaplanabileceği bir ileri model oluşturulmaya çalışılmıştır [34]. fMRI' dan elde edilen bilgiler kullanılarak, kafa derisinden eş zamanlı olarak kaydedilmiş EEG' den, mekânsal-zamansal bilgi elde etmek için, fMRI haritalarındaki aktivasyon örüntüleri kullanılabilir [35].

Bu bağlamda, fMRI sonucunun istatistiksel haritaları, elektrofizyolojik sinyalin kaynağı olan belirli bir bölgenin olasılığını sağlayarak varsayılan kaynak alanını sınırlamak için kullanılabilir [36,37]. Dolayısıyla, bu kombinasyonlardan hangisi seçilirse seçilsin, fMRI verileri yerlerin ortaya çıkarılmasına yardımcı olurken, EEG' den türetilen bilgiler milisaniye kararında nöral olayların zaman dilimlerini sağlar [38-40].

Bledowski ve arkadaşları, örneğin; Ayrı oturumlar sırasında da olsa EEG ve fMRI verilerini toplarken, denekler görsel çalışma belleği görevi gerçekleştirmişlerdir. fMRI' den türetilen kaynak model kullanılarak, ilgili beyin bölgelerinin zaman periyotları

yüksek zamansal çözünürlük ile türetilebilmektedir. Böylece, çalışma hafızası alımı sırasında nöral işlem aşamaları gerçekleştirilerek hem mekansal hem de zamansal ölçek te, eş zamanlı olarak çalışılabilinir [41].
Dolayısıyla, eş zamanlı olarak ölçülen veriler üzerinde fMRI ile oluşturulmuş EEG için yaklaşımlar kullanılmasına rağmen, güçlü yönleri ayrı kayıtlar bağlamında daha belirgindir. Tek denemelerden elde edilen bilgiler dikkate alınmadığı için karşılaştırılabilmekte dir, ancak zorunlu olarak aynı deney koşulları altında elde edilen EEG ve fMRI verileri ile çalışmak oldukça mümkündür. Bu, her modalite için, örneğin fMRI ile eşzamanlı olarak ölçüldüğü zaman, EEG'deki kaçınılmaz gürültülerin önüne geçerek, deneysel koşulların optimizasyonuna izin verir [40].
Birçok durumda, elektrofizyolojik ve nöral aktivitenin fMRI belirteçleri arasında sıkı bir ilişki olduğuna dair önemli kanıtlar olsa da , bu varsayımları ihlal eden durumlar söz konusu olabilmektedir. Örneğin, bir fMRI cevabı gösteren bölgeler kafa derisinde elektriksel olarak sessiz kaldığında, akım akışının iptal edilmesine yol açan kaynakların bir araya gelmesi ya da nöral aktivitenin uyarıcı-tetiklemeli bir senkronizasyonu, herhangi bir metabolik maliyet olmaksızın saptanabilir bir elektrofizyolojik tepkiye yol açması gibi durumlarda gerçekleşebilir. İlk durum, fMRI ağırlıklı bir kaynak yeniden yapılanması için sorun teşkil etmese de, ikincisinde bunu söylemek mümkün değildir: fMRI tabanlı bir ağırlıklandırma, net fMRI aktivasyonlarından yoksun olan beyin bölgelerindeki kaynakların yeniden yapılandırılmasını olumsuz etkileyecek ve sonuçta brüt lokalizasyon hatalarına yol açacaktır. Ancak, EEG kaynak analizleri için farklı yöntemleri dikkatli bir şekilde birleştirerek, bu belirsiz durumları tanımlamak mümkün olabilir [54].

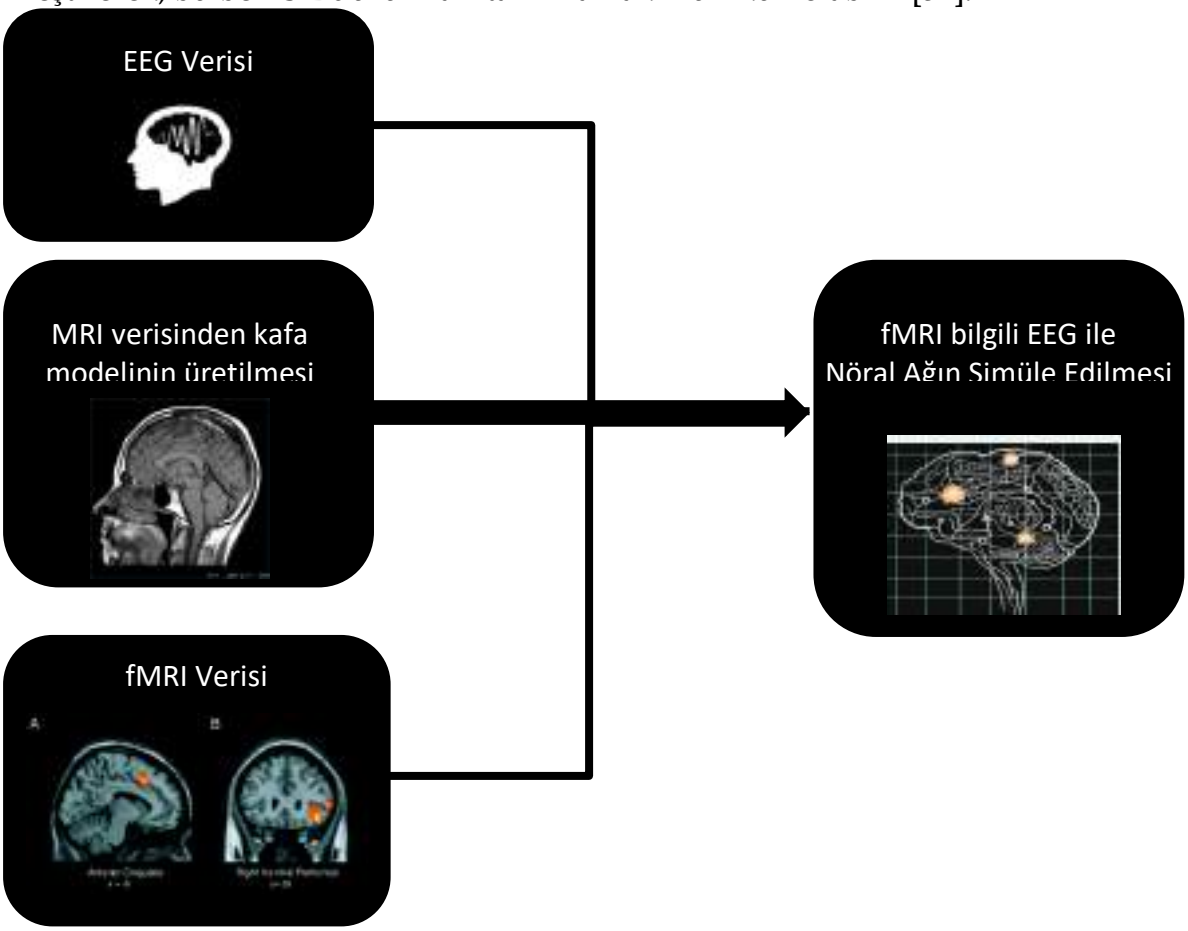

Şekil 3. fMRI bilgili EEG Modeli [54]

Şekil 3'de fMRI bilgili EEG modelinin yapısı gösterilmektedir. fMRI bilgili EEG modelinde, beyindeki aktif EEG sinyal değişikliklerine yol açan aktif kortikal bölgelerin yerini ve aktivitesini tahmin etmek için, ileri veya kafa modelleri bireysel MR görüntülerinden oluşturulmuştur. Burada cilt, kafatası ve beyin dokusunu temsil eden hacimler çıkartılmıştır. Böyle bir modele ve EEG zaman ve ilgili kafa derisi topografilerine (bir katılımcının kafasına kaydedilen EEG aktivitesinin örüntüsüne) dayanarak, EEG kaynakları çıkarılabilir.

EEG Bilgili fMRI

EEG ve fMRI arasında doğrudan ilişki varsayıldığında, hem EEG ve hem fMRI sinyallerinin zaman içindeki değişikliklerinin eş zamanlı olduğu beklenecektir [8]. İlgili EEG sinyaline ait, belirli bir özellik çıkarılarak, sinyalin incelenen olaya ait kısmı izole edilerek kullanılabileceği gibi, ERP (Event Related Potential) genliği, ERP gecikmesi, faz bağdaşımı veya çeşitli EEG bantları içindeki güç miktarı da özellik olarak kullanılabilir.

Hangi EEG-türevli özellik kullanılırsa kullanılsın, temel varsayım, bu özelliklerin zaman içinde gösterdiği dalgalanmaların fMRI sinyalinde görülen dalgalanmalarla orantılı olmasıdır. Bu yaklaşımda, fMRI verilerinin işlenmesi, dilim-zaman düzeltme, mekansal yeniden hizalama, mekansal normalleşme ve yumuşatma gibi temel işlemleri içerir [42]. Bu işlemler sırasında normal bir fMRI verisi modellemeye göre en önemli fark, fMRI verisine ait sinyal sadece hemodinamik değişiklikleri değil, EEG verisinden çıkarılan özellikleri de kullanır. Böylece, üretilen modele ait sinyal, EEG' den çıkarılan özelliklere göre zamandaki bazı noktalar için parametrik olarak güçlendirilir. Yani, ilgilenilen olayın olduğu anların EEG ve fMRI sinyallerinde örtüştüğü noktalar belirlenir. Bu durum Şekil 4.'de gösterilmektedir [54].

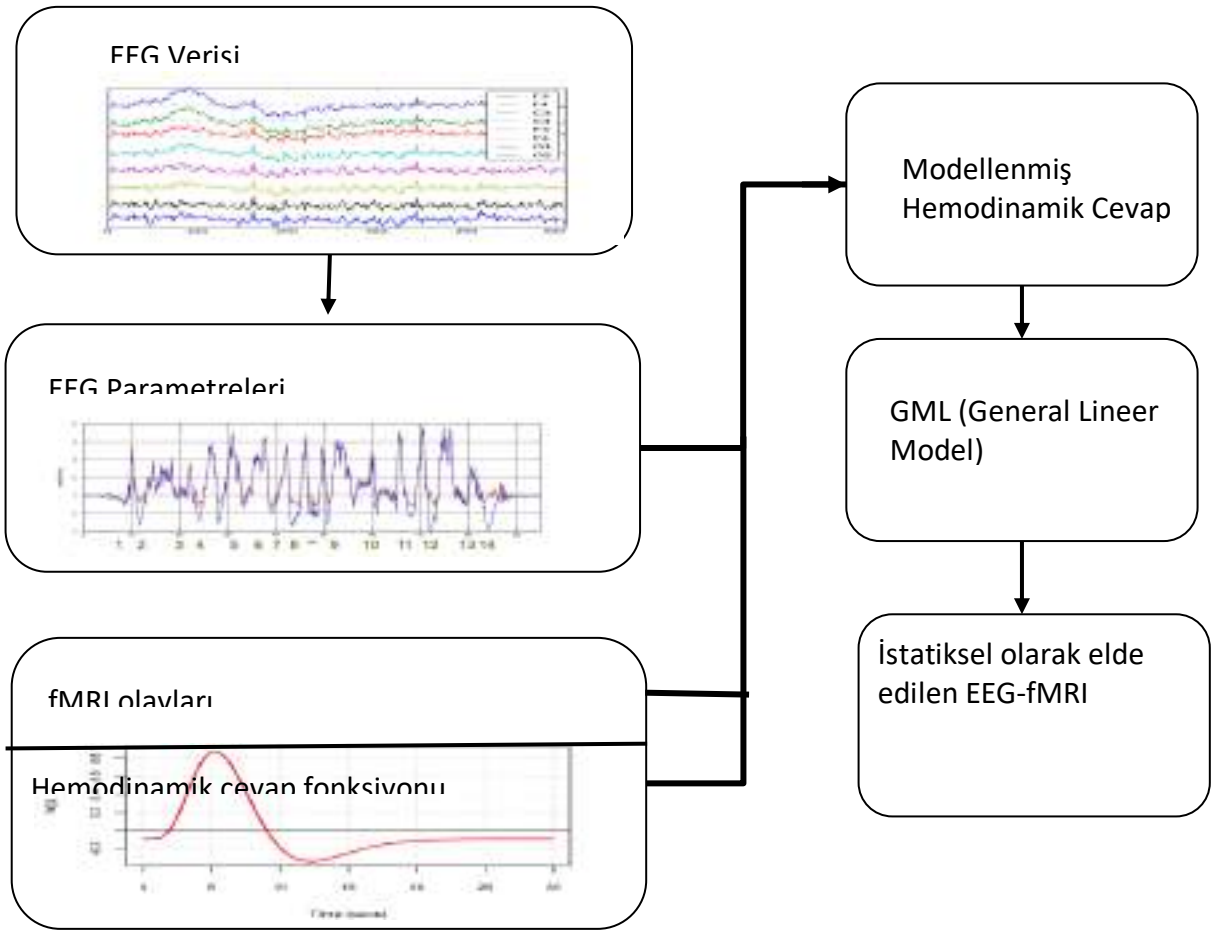

Şekil 4. EEG bilgili fMRI Modeli [54]

Üretilen bu model, daha sonra incelenen deneklerin hepsinde test edilir. Test sırasında, aynı durum veya başka durumlara (dinlenme gibi) ait veriler kullanılabilir. Böylece, üretilen modelin, elektropsikolojik ve hemodinamik değişiklikler arasındaki ilişkiyi doğru modelleyip modellemediği anlaşılır.

Debener ve arkadaşları, performans izleme amaçlı takip edilen deneklerdeki EEG sinyal değişikliklerinin, orta singulat beyin bölgesindeki fMRI değişiklikleri ile örtüşüp örtüşmediğini test etmişlerdir. Deneklerin görev performansı sırasında kaydedilen hatalı yanıtlarını EEG sinyalinde belirlemişlerdir [43]. Bu bilgi daha sonra fMRI verilerinin parametreli bir analizi için kullanılmıştır. Gerçekten de, bu analiz EEG sinyalindeki hatalı yanıtları gösteren anlardaki genlik değerlerinin orta singulat aktivasyonlarıyla ilişkisini kanıtlamıştır. Dahası, ilk denemedeki genlik değerlerine bağlı parametre değerleri, sonraki denemelerdeki görev davranışını tahmin ederek, ilgili dalgalanmalarının rastgele gürültü olmadığını, ancak işlevsel bilgileri taşıdığını göstermektedir. Benzer bir analiz tekniği Eichele ve arkadaşları tarafından geliştirilmiştir [44].

EEG tarafından bilgilendirilen fMRI, her iki modalite tarafından yakalanan sinyallere katkıda bulunan nöral özelliklerin, kısmen çakıştığını ve doğrusal bir ilişki sergilediğini varsaymaktadır. fMRI tarafından bilgilendirilmiş EEG'nin aksine, aktivasyon örüntülerinin mekansal organizasyonu hakkında özel bir varsayım yoktur. Bu stratejinin, kafa derisinde kaydedilen ERP' nin biyofiziksel jeneratörleri olmayan beyin yapıları veya ağlarında etkilere neden olabileceğini ima etmektedir [43,45].

Ayrıca, tek EEG dönemlerinin yüksek düzeyde gürültü içerdiğini ve tek denemeli EEG analizlerinin bireysel denemelerin sinyal-gürültü oranını arttıran tekniklere dayanması gerektiğini de unutmamak gerekir.

Alternatif olarak, öznitelik çıkarmadan önce mekansal-zamansal olarak örtüşen EEG sinyallerinin karışmamasını sağlayan ve en sık kullanılan algoritma, bağımsız bileşen analizi (ICA) algoritmasıdır [46,47]. Her durumda, devam eden beyin aktivitesinin sadece bir kısmı, bir seferde EEG tarafından bilgilendirilmiş bir fMRI analizi için kullanılabilir ve ilgili özelliğin seçimi, genellikle, ele alınan araştırma sorusu tarafından belirlenir. [48].

Nörogeneratif Modelleme

Nörogeneratif model, ilk olarak, EEG ve fMRI sinyallerine neden olan fizyolojik süreçleri belirler. Bu model, beyin aktiviteleri sırasında elde edilen eş zamanlı EEG-fMRI kayıtlarını kullanarak nöron ağını yeniden oluşturulabilir. Böyle bir çerçevede, veri entegrasyonu, elektrofizyolojik ve hemodinamik sinyal üretiminin biyofiziksel süreçlerini simüle etme yeteneğine dayanmaktadır.

Çok önemli veriler için ileriye dönük bir model (generatif model), elektrofizyolojik ve hemodinamik aktivitelerin yanı sıra nörovasküler bağlanma akışı arasındaki bağlantı hakkında varsayımlar içermektedir [49,50]. Nöral olayların dizisi, serebral kan akışındaki değişikliklere neden olur ve bu da fMRI sinyallerinde değişikliklere neden olur. Bu nedenle Nörogeneratif modelleme, ayrıntı zenginliğine bağlı olarak, nörovasküler bağlantılara aracılık eden hücresel mekanizmalardan, morfolojik düzeyde bağlantı modellerine kadar değişen farklı tanımlama seviyelerini içerebilmektedir [54].

Bu yaklaşım, nöral toplulukların dinamiklerini, bağlantı desenlerinden hücresel olaylara kadar çeşitli ölçeklerde matematiksel olarak modellemeye dayanır. Ek olarak, biyofiziksel ileri modeller, nöral olayların ölçülen EEG ve fMRI sinyallerine dönüşümünü belirtmelidir. Bu verilere dayanarak, önceden tanımlanmış bir nöral aktivite örüntüsünün sonucu simüle edilebilir (ileri modelleme) veya eşzamanlı EEG-fMRI veri kümesi verildiğinde, en olası nöral olaylar, gözlemlenen EEG-fMRI sinyal özelliklerine dayanarak çıkarılabilir.

Gerçek veriler verildiğinde, prosedürün ikinci basamağı, ters modelleme içerir: eşzamanlı EEG-fMRI gözlemlerinden nöral aktivite tahmin edilebilmektedir. Bojak ve arkadaşları, eş zamanlı EEG-fMRI analizi ve nöral popülasyon modelinin uygunluğunu araştırmak için simüle edilmiş verileri kullanarak nörojeneratif modellerin uygulanmasını gerçekleştirmişlerdir. Her ne kadar korteksteki sadece birkaç bölgeyle sınırlı olsa da, görsel sistemdeki bağlantı değişikliklerinin etkilerini eşzamanlı EEG-fMRI verilerinin aktivite modeline göre belirleyebilmişlerdir. Bu çalışma, bu modellerin, EEG ve fMRI sinyal üretiminin temel mekanizmalarına ilişkin sorular için uygunluğunu etkili bir şekilde ortaya koymaktadır [51].

Multimodal Veri Füzyonu

Makine öğrenme algoritmaları hem EEG hem de fMRI verilerine başarıyla uygulanmaktadır. Gözetimsiz öğrenme yaklaşımları, veri kümelerini işleyerek verilerin içinde gruplar ve özellikler otomatik olarak çıkarılabilmektedir. EEG ile gürültü düzeltme/temizleme veya fMRI'daki işlevsel ağların tanımlanması için, ise daha çok gözetimli öğrenme yaklaşımları tercih edilmektedir [52]. Örnek olarak, beyin aktivitelerine bakarak, beyni uyaran durumun kategorisinin tahmini gözetimli

öğrenme yaklaşımı (örneğin sınıflandırma) ile yapılabilmektedir. Veri füzyonu yaklaşımları, EEG-fMRI verilerine uygulandığında, eldeki tüm verileri ortak veya simetrik olarak kullanarak, çok değişkenli istatistiksel bir model ortaya koyar. Daha önce bahsedilen modeller ise (ör: EEG bilgili fMRI gibi) daha çok bir modaliteyi baz alarak, diğer modaliteden gelen veriyi yardımcı olarak kullanırlar [54].
Multimodal veri füzyonu yöntemleri, fizyolojik varsayımlara dayanma, ön bilgi gerektirme veya yukarıda tartışılan yaklaşımlarla diğer benzerlikleri paylaşma derecesine göre büyük ölçüde farklıdır. Örneğin ICA, verideki tüm değişkenleri inceleyerek, istatistiksel olarak bağımsız olanları çıkarabilen gözetimsiz bir öğrenme yöntemidir. Çok modlu veri füzyonu için ICA'yi kullanmak üzere çok sayıda model önerilmiştir. Örnek olarak EEG ve fMRI sinyalleri önce ayrı ayrı işlenir ve daha sonra veri tipleri arasındaki ilişkileri incelemek için ICA uygulanır. Tek modalite kullanılan durumlarda (örneğin sadece EEG veya sadece fMRI) ya zamansal olarak (EEG) ya da mekansal (fMRI) bağımsız bileşenler açığa çıkarılırken, bu çok modlu yaklaşımda iki kategorideki bağımsız bileşenler aynı anda ortaya çıkarılabilir. Bu tekniği kullanarak Calhoun ve arkadaşları işitsel oddball cevabının mekansal dinamiklerini incelemeyi başarmışlardır [53].
Burada uygulanan algoritmaların çoğunluğunun bilgisayar bilimlerinde uzun bir geçmişi olmasına rağmen, nörobilimsel problemlere uygulanmaları oldukça yeni bir gelişmedir. Bununla birlikte, bu yöntemlerin eş zamanlı EEG-fMRI için çok değişkenli analiz şemaları sağlayarak yüksek fayda sağladığı kanıtlanmıştır. Öte yandan, çok modlu veri füzyonu için çeşitli matematiksel yaklaşımlar olduğu için, belirli bir konu için uyarlanmış bir füzyon modelinin seçilmesi bazen zor olabilir. Dahası, mevcut yaklaşımların bazıları hala, hemodinamik ya da diğer fizyolojik varsayımları içermektedir, bu nedenle henüz bu algoritmaların tam gücünün tüm avantajlarından yararlanmamaktadır [54].

SONUÇ

Son yıllardaki teknolojik gelişmelerden sonra, eşzamanlı EEG-fMRI verisi eskiye göre daha kolay, daha yüksek sinyal kalitesine sahip olarak elde edilebilmektedir. Bu yöntemlerin kombinasyonunun avantajlı yönü, hem EEG hem de fMRI'nin sinaptik işleme duyarlılıklarında örtüşmesi ve buna bağlı olarak beyin fonksiyonunun yüksek zamansal ve yüksek mekansal çözünürlüğe sahip olarak değerlendirilmesidir. Bugün EEG-fMRI için en umut verici uygulamalardan biri, beyin ağ yapısının ve dinamiklerinin karakterizasyonudur [55].
EEG ve fMRI verilerinin eş zamanlı analizi için çeşitli farklı yöntemler önerilmiştir. Bu çalışma, bu tür analiz yaklaşımlarının potansiyel avantajlarını ve sınırlamalarını sunmayı amaçlamaktadır. Örneğin kafa derisi EEG nöral yapısı ile ilgilendiğinde, fMRI tarafından bilgilendirilmiş EEG tercih edilen yöntemdir. Bu yaklaşım, yüksek ve iyi tanımlanmış mekansal olarak çözünürlüğe sahiptir. Öte yandan, EEG tarafından bilgilendirilmiş fMRI' ye dayanan analizler, tek deneme seviyesinde tanımlanan çapraz-modal aktivite örüntülerinin doğrusal bir ilişkisi ile karakterize edilen fonksiyonel ağları ortaya çıkarmak için en uygun görünmektedir.
Nörojeneratif modeller, EEG ve fMRI sinyal üretiminin altında yatan fizyolojik mekanizmalar ve biyofiziksel özellikler hakkındaki hipotezleri test etmek için

güçlüdür ve bunların karşılıklı etkileşimleri, bu modelleri teorik nörobiyoloji alanında güçlü araçlar haline getirmektedir.
Son olarak, eşzamanlı EEG-fMRI için çok değişkenli füzyon yöntemlerinin uygulanmasından bahsedecek olursak, bu alanla ilişkili yaklaşımlar, örneğin, modaliteler arasındaki bağlantıların tanımlanması, EEG ve fMRI' den ortaklaşa davranışın tahmin edilmesi ya da her iki modalite için ortak olan değişkenlerin ortaya çıkması gibi problemleri ele almak için çok uygundur.

KAYNAKLAR

[1] https://www.medicalnewstoday.com/articles/248680.php , 29.08.2018

[2] Rosa, M. J., Daunizeau, J., & Friston, K. J. (2010). EEG-fMRI integration: a critical review of biophysical modeling and data analysis approaches. Journal of integrative neuroscience, 9(04), 453-476.

[3] Friston, K. J. (2009). Modalities, modes, and models in functional neuroimaging. Science, 326(5951), 399-403.

[4]Fox, P. T., & Friston, K. J. (2012). Distributed processing; distributed functions?. Neuroimage, 61(2), 407-426.

[5] Schmitt, A., Hasan, A., Gruber, O., & Falkai, P. (2011). Schizophrenia as a disorder of disconnectivity. European archives of psychiatry and clinical neuroscience, 261(2), 150.

[6] Friston, K. J., Li, B., Daunizeau, J., & Stephan, K. E. (2011). Network discovery with DCM. Neuroimage, 56(3), 1202-1221.

[7] Mulert, C., & Lemieux, L. (Eds.). (2009). EEG-fMRI: physiological basis, technique, and applications. Springer Science & Business Media.

[8] Ullsperger, M., & Debener, S. (2010). Simultaneous EEG and fMRI: recording, analysis, and application. Oxford University Press.

[9] Franciotti, R., Falasca, N. W., Bonanni, L., Anzellotti, F., Maruotti, V., Comani, S., ... & Onofrj, M. (2013). Default network is not hypoactive in dementia with fluctuating cognition: an Alzheimer disease/dementia with Lewy bodies comparison. Neurobiology of aging, 34(4), 1148-1158.

[10] Goldman, R. I., Stern, J. M., Engel Jr, J., & Cohen, M. S. (2002). Simultaneous EEG and fMRI of the alpha rhythm. Neuroreport, 13(18), 2487.

[11] Moosmann, M., Ritter, P., Krastel, I., Brink, A., Thees, S., Blankenburg, F., ... & Villringer, A. (2003). Correlates of alpha rhythm in functional magnetic resonance imaging and near infrared spectroscopy. Neuroimage, 20(1), 145-158.

[12] Laufs, H., Kleinschmidt, A., Beyerle, A., Eger, E., Salek-Haddadi, A., Preibisch, C., & Krakow, K. (2003). EEG-correlated fMRI of human alpha activity. Neuroimage, 19(4), 1463-1476.

[13] Hlinka, J., Alexakis, C., Diukova, A., Liddle, P. F., & Auer, D. P. (2010). Slow EEG pattern predicts reduced intrinsic functional connectivity in the default mode network: an inter-subject analysis. Neuroimage, 53(1), 239-246.

[14] Scheeringa, R., Petersson, K. M., Kleinschmidt, A., Jensen, O., & Bastiaansen, M. C. (2012). EEG alpha power modulation of fMRI resting-state connectivity. Brain connectivity, 2(5), 254-264.

[15] Chang, C., Liu, Z., Chen, M. C., Liu, X., & Duyn, J. H. (2013). EEG correlates of time-varying BOLD functional connectivity. Neuroimage, 72, 227-236.

[16] Logothetis, N. K. (2008). What we can do and what we cannot do with fMRI. Nature, 453(7197), 869.

[17] Michel, C. M., Murray, M. M., Lantz, G., Gonzalez, S., Spinelli, L., & de Peralta, R. G. (2004). EEG source imaging. Clinical neurophysiology, 115(10), 2195-2222.

[18] Grech, R., Cassar, T., Muscat, J., Camilleri, K. P., Fabri, S. G., Zervakis, M., ... & Vanrumste, B. (2008). Review on solving the inverse problem in EEG source analysis. Journal of neuroengineering and rehabilitation, 5(1), 25.

[19] Ives, J. R., Warach, S., Schmitt, F., Edelman, R. R., & Schomer, D. L. (1993). Monitoring the patient's EEG during echo planar MRI. Electroencephalography and clinical neurophysiology, 87(6), 417-420.

[20] Mulert, C., Pogarell, O., & Hegerl, U. (2008). Simultaneous EEG-fMRI: perspectives in psychiatry. Clinical EEG and neuroscience, 39(2), 61-64.

[21] Gotman, J., & Pittau, F. (2011). Combining EEG and fMRI in the study of epileptic discharges. Epilepsia, 52, 38-42.

[22] Laufs, H., Krakow, K., Sterzer, P., Eger, E., Beyerle, A., Salek-Haddadi, A., & Kleinschmidt, A. (2003). Electroencephalographic signatures of attentional and cognitive default modes in spontaneous brain activity fluctuations at rest. Proceedings of the national academy of sciences, 100(19), 11053-11058.

[23] Laufs, H. (2008). Endogenous brain oscillations and related networks detected by surface EEG-combined fMRI. Human brain mapping, 29(7), 762-769.

[24] Mullinger, K., Debener, S., Coxon, R., & Bowtell, R. (2008). Effects of simultaneous EEG recording on MRI data quality at 1.5, 3 and 7 tesla. International Journal of Psychophysiology, 67(3), 178-188.

[25] Kruggel, F., Wiggins, C. J., Herrmann, C. S., & von Cramon, D. Y. (2000). Recording of the event-related potentials during functional MRI at 3.0 Tesla field strength. Magnetic Resonance in Medicine: An Official Journal of the International Society for Magnetic Resonance in Medicine, 44(2), 277-282.

[26] Debener, S., Mullinger, K. J., Niazy, R. K., & Bowtell, R. W. (2008). Properties of the ballistocardiogram artefact as revealed by EEG recordings at 1.5, 3 and 7 T static magnetic field strength. International Journal of Psychophysiology, 67(3), 189-199.

[27] Yan, W. X., Mullinger, K. J., Brookes, M. J., & Bowtell, R. (2009). Understanding gradient artefacts in simultaneous EEG/fMRI. Neuroimage, 46(2), 459-471.

[28] https://www.healthline.com/health/eeg, 29.08.2018

[29] https://imotions.com/blog/eeg-vs-mri-vs-fmri-differences/ , 29.08.2018

[30]Cheema, M. A., Zhang, W., & Chang, L. (Eds.). (2016). Databases Theory and Applications: 27th Australasian Database Conference, ADC 2016, Sydney, NSW, September 28-29, 2016, Proceedings (Vol. 9877). Springer.

[31] Heinze, H. J., Mangun, G. R., Burchert, W., Hinrichs, H., Scholz, M., Münte, T. F., ... & Gazzaniga, M. S. (1994). Combined spatial and temporal imaging of brain activity during visual selective attention in humans. Nature, 372(6506), 543-546.

[32] Babiloni, F., Carducci, F., Cincotti, F., Del Gratta, C., Roberti, G. M., Romani, G. L., ... & Babiloni, C. (2000). Integration of high resolution EEG and functional magnetic resonance in the study of human movement-related potentials. Methods of information in medicine, 39(02), 179-182.

[33] Babiloni, F., Babiloni, C., Carducci, F., Gratta, D. C., Romani, G. L., Rossini, P. M., & Cincotti, F. (2002). Cortical source estimate of combined high resolution EEG and fMRI data related to voluntary movements. Methods of information in medicine, 41(05), 443-450.

[34] Hallez, H., Vanrumste, B., Grech, R., Muscat, J., De Clercq, W., Vergult, A., ... & Lemahieu, I. (2007). Review on solving the forward problem in EEG source analysis. Journal of neuroengineering and rehabilitation, 4(1), 46.

[35] Hämäläinen, M. S., & Ilmoniemi, R. J. (1994). Interpreting magnetic fields of the brain: minimum norm estimates. Medical & biological engineering & computing, 32(1), 35-42.

[36] Dale, A. M., Liu, A. K., Fischl, B. R., Buckner, R. L., Belliveau, J. W., Lewine, J. D., & Halgren, E. (2000). Dynamic statistical parametric mapping: combining fMRI and MEG for high-resolution imaging of cortical activity. Neuron, 26(1), 55-67.

[37] Ou, W., Nummenmaa, A., Ahveninen, J., Belliveau, J. W., Hämäläinen, M. S., & Golland, P. (2010). Multimodal functional imaging using fMRI-informed regional EEG/MEG source estimation. Neuroimage, 52(1), 97-108.

[38] Vanni, S., Warnking, J., Dojat, M., Delon-Martin, C., Bullier, J., & Segebarth, C. (2004). Sequence of pattern onset responses in the human visual areas: an fMRI constrained VEP source analysis. Neuroimage, 21(3), 801-817.

[39] Wibral, M., Bledowski, C., Kohler, A., Singer, W., & Muckli, L. (2008). The timing of feedback to early visual cortex in the perception of long-range apparent motion. Cerebral cortex, 19(7), 1567-1582.

[40] Wibral, M., Bledowski, C., & Turi, G. (2010). Integration of separately recorded EEG/MEG and fMRI data. Simultaneous EEG and fMRI: recording, analysis, and application (Ullsperger M, Debener S, eds), 209-234.

[41] Bledowski, C., Kadosh, K. C., Wibral, M., Rahm, B., Bittner, R. A., Hoechstetter, K., ... & Linden, D. E. (2006). Mental chronometry of working memory retrieval: a combined functional magnetic resonance imaging and event-related potentials approach. Journal of Neuroscience, 26(3), 821-829.

[42] Strother, S. C. (2006). Evaluating fMRI preprocessing pipelines. IEEE Engineering in Medicine and Biology Magazine, 25(2), 27-41.
[43] Debener, S., Ullsperger, M., Siegel, M., Fiehler, K., Von Cramon, D. Y., & Engel, A. K. (2005). Trial-by-trial coupling of concurrent electroencephalogram and functional magnetic resonance imaging identifies the dynamics of performance monitoring. Journal of Neuroscience, 25(50), 11730-11737.
[44] Eichele, T., Specht, K., Moosmann, M., Jongsma, M. L., Quiroga, R. Q., Nordby, H., & Hugdahl, K. (2005). Assessing the spatiotemporal evolution of neuronal activation with single-trial event-related potentials and functional MRI. Proceedings of the National Academy of Sciences, 102(49), 17798-17803.
[45] Minati, L., Rosazza, C., Zucca, I., D'Incerti, L., Scaioli, V., & Bruzzone, M. G. (2008). Spatial correspondence between functional MRI (fMRI) activations and cortical current density maps of event-related potentials (ERP): a study with four tasks. Brain topography, 21(2), 112-127.
[46] James, C. J., & Hesse, C. W. (2004). Independent component analysis for biomedical signals. Physiological measurement, 26(1), R15.
[47] Onton, J., Westerfield, M., Townsend, J., & Makeig, S. (2006). Imaging human EEG dynamics using independent component analysis. Neuroscience & Biobehavioral Reviews, 30(6), 808-822.
[48] Bénar, C. G., Schön, D., Grimault, S., Nazarian, B., Burle, B., Roth, M., ... & Anton, J. L. (2007). Single-trial analysis of oddball event-related potentials in simultaneous EEG-fMRI. Human brain mapping, 28(7), 602-613.
[49] Logothetis, N. K., & Wandell, B. A. (2004). Interpreting the BOLD signal. Annu. Rev. Physiol., 66, 735-769.
[50] Stephan, K. E., Harrison, L. M., Penny, W. D., & Friston, K. J. (2004). Biophysical models of fMRI responses. Current opinion in neurobiology, 14(5), 629-635.
[51] Bojak, I., Oostendorp, T. F., Reid, A. T., & Kötter, R. (2011). Towards a model-based integration of co-registered electroencephalography/functional magnetic resonance imaging data with realistic neural population meshes. Philosophical Transactions of the Royal Society of London A: Mathematical, Physical and Engineering Sciences, 369(1952), 3785-3801.
[52] Mennes, M., Wouters, H., Vanrumste, B., Lagae, L., & Stiers, P. (2010). Validation of ICA as a tool to remove eye movement artifacts from EEG/ERP. Psychophysiology, 47(6), 1142-1150.
[53] Calhoun, V. D., Adali, T., Pearlson, G. D., & Kiehl, K. A. (2006). Neuronal chronometry of target detection: fusion of hemodynamic and event-related potential data. Neuroimage, 30(2), 544-553.
[54] Huster, R. J., Debener, S., Eichele, T., & Herrmann, C. S. (2012). Methods for simultaneous EEG-fMRI: an introductory review. Journal of Neuroscience, 32(18), 6053-6060.
[55] Mulert, C. (2013). Simultaneous EEG and fMRI: towards the characterization of structure and dynamics of brain networks. Dialogues in clinical neuroscience, 15(3), 381.

EFFECT OF SOIL LAYER INCLINATION AND HYDRAULIC CONDUCTIVITY RATIO ON PRESSURE HEAD ALONG SHEET PILE FACE

Manal A. Muhammed*, Ali N. Hillo, Thaar S. Al-Gasham
Civil Department, Engineering College/ Wasit University, Kut, Iraq
manala277@uowasit.edu.iq, dralinasser@uowasit.edu.iq ,thaar@uowasit.edu.iq

ABSTRACT: This paper deals with numerical investigation on the effect of soil inclination on pressure head along sheet pile face, when the sheet pile is placed at the up-stream or at the down-stream with angles of inclination of the soil layer (0°, 30°, 60°, and 90°) and the hydraulic conductivity ratio (kmax/kmin) is (2, 3, and 4). The finite element method is used to solve this problem by using Geo-Studio Seep/W 2007 software. The feasibility of applying the program with some available research has been validated by conducting a study of a simple hydraulic structure using single sheet pile immersed in anisotropic, homogeneous soil to find the exit gradient at the inclination angle 180 and the ratio of hydraulic conductivity (kmax/kmin = 4), where the difference ratio AE=15%. This indicates a good consensus with previous research. It was concluded that the effect of soil layer inclination on the pressure head along sheet pile face at up-stream is greater than when the sheet pile at down-stream.

Keywords: Seepage, finite elements, uplift pressure, Seep/W 2007.

INTRODUCTION

Dams are rarely constructed on an impregnable soil, so when designing these structures, consideration must be given to safety (safety of the structure, loss of water through seepage, ease of operation and maintenance, etc.). Hydraulic structures generally are constructed on permeable soil. Therefore, engineers face many problems, especially in the implementation of one of these problems (Mohammed-Ali). The problem of seepage of water through the soil under the structure, which affects the correct performance of the functions of the dam and ultimately to failure and this is due to differences in water level at the up-stream and the down-stream of the structure. Where the force of the flow of water seepage under resulting uplift pressure which in turn leads to the withdrawal of soil particles with the flow of water seepage, and formation of irregular paths similar to the pipes, when the exit gradient approaches the critical gradient at the down-stream. This phenomenon is known as piping phenomenon, Therefore preventive measures were taken using (sheet pile, cutoff walls, drainages, reflected filters, curtains and wells) to ensure the safety of structure. In designing any structure against seepage problem, two important points must be considered (Obead, 2013):

Safety against uplift pressure.

Safety against piping phenomenon.

Many researchers have provided solution for the problem of seepage under hydraulic structures (experimental, process, analytical, graphical, numerical and analog electricity).

Reddy et al., (1971) used the principle of transverse transformations and conformal mapping and presented a solution for the flow confined to the steady state, around sheet pile, immersed in an isotropic and homogeneous soil of finite depth.

Punmia, (1981) studied mathematical solutions by Khosla for calculation of the exit gradient and uplift pressure under the hydraulic structures where the solutions gave quick and accurate results by using a set of curves applied to any form of structure that contains one or more lines of cutoff.

Al-Damluji et al., (2004) presented a solution of two-dimensional steady state field problems by the boundary element method. A typical problem of steady state seepage beneath an impermeable sheet pile wall was solved. It was concluded that an acceptable agreement can be obtained between the boundary element method and the finite element method or closed form solution.

Khassaf et al., (2011) used ANSYS11.0 program to find the optimal location and the angle of inclination of the cutting walls where the numerical investigations of the effect of the angle of deflection of the cut-off to control exit gradient and uplift pressure head under the hydraulic structures. It was concluded that the deviation of the walls of the cutoff towards the downstream D/S side with a deviation angle less than 120° is the best and best to increase the safety coefficient against the piping phenomenon.

Zainal, (2011) used Geo-studio Seep/W 2007 program to study the effect of changing the angle of the cutoff wall from 0 to 180 degrees. The results obtained that the lowest possible values for the exit gradient, uplift pressure and water flow, with two cutoff walls were used one with angle 60° , the other with an angle 120°.

Alghazali and Alnealy, (2015) used Slide program to analyze seepage under hydraulic structures through single and multi-layer soil and the effect of hydraulic structures by inclination the cut-off at downstream, upstream and at both of them. The results obtained that given decreasing in uplift pressure, exit gradient, seepage and

increasing in safety factor against piping phenomenon, when using double cutoff at U/S at angle =45° and D/S with angle =120°.

OBJECTIVES OF THE STUDY

The main objectives of this research can be illustrated in the following points:

Studying the effect of soil inclination layer at different angles of inclination and different hydraulic conductivity ratios on pressure head along sheet pile face.

Finding the angle of inclination and the optimum hydraulic conductivity ratio to minimize the seepage pressure head on sheet pile face.

GENERAL CASE OF STUDY

Finite element method is used here to analyze the general case of study by Geo-studio Seep/W 2007 program. The dam section is shown in Fig. 1. The porous medium under the structure is anisotropic soil foundation, where the ratio of max. to min. hydraulic condutivity (kmax/kmin) is taken as 2, 3 and 4. They are most commonly used and degree of layer inclination is (0°, 30°, 60°, and 90°).

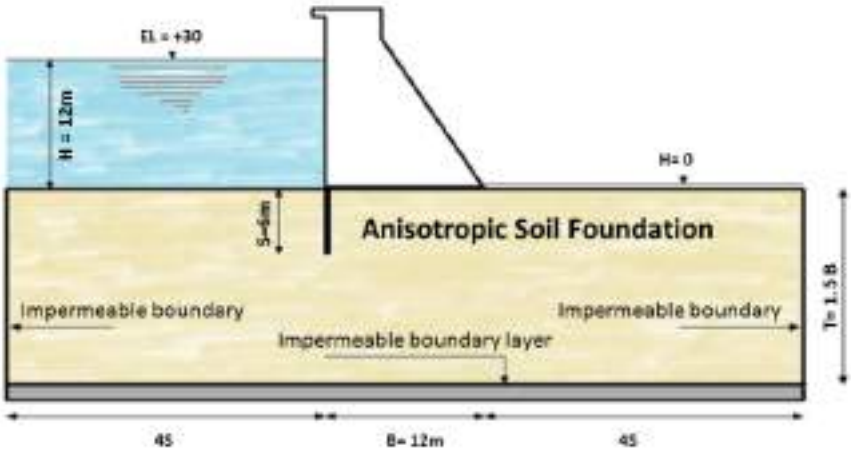

Sheet Pile at Up-Stream.

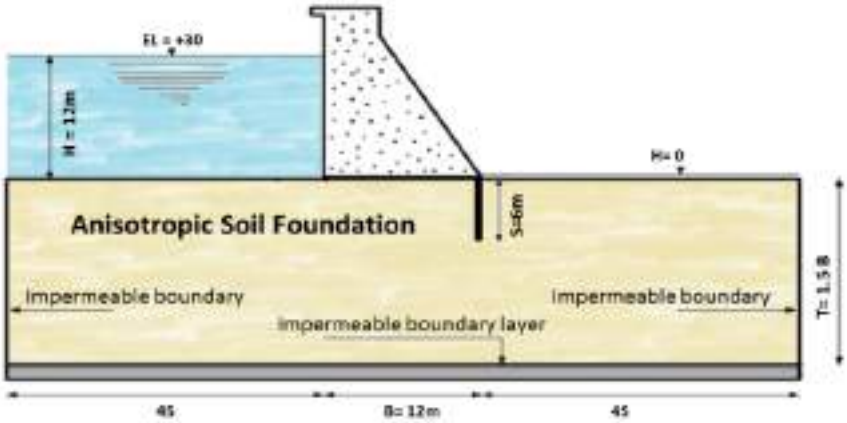

Sheet Pile at Down-Stream.

Figure 1:General Case of Study and Boundary Conditions With a- Sheet Pile at Up-Stream and b- Sheet Pile at Down- Stream.

BOUNDARY CONDITIONS

Before starting the solution, the boundary conditions should be specified for steady state of a confined flow as follows:

**Reservoir Boundary*: The height of the water above these boundaries has always a known value, so that the pressure on any point of these boundaries is also known; so, the pressure (p) at any point for boundary equals to

$P = \gamma_w H_o$ (1)

where: γ is density gravity of water, and $H_\circ$ is piezometric head.

Piezometric head distribution along the reservoir boundaries is constant that is:

$H = H_\circ = P/\gamma_w + z$ (2)

**Impervious Boundary*: Impervious boundary has the perpendicular velocity function on the surface equal to zero ($\partial h/\partial n=0$).

Application of Finite Element in the Seepage under Hydraulic Structure

The application of finite element techniques in hydraulic structures constructed on an anisotropic pours medium is solving the governing equation of flow. The finite element method solves the question by dividing it in to smaller areas or finite element. These finite elements are connected to each other by nodes located on the limits of the element boundaries, Fig. 2. The node is a part of the finite elements.

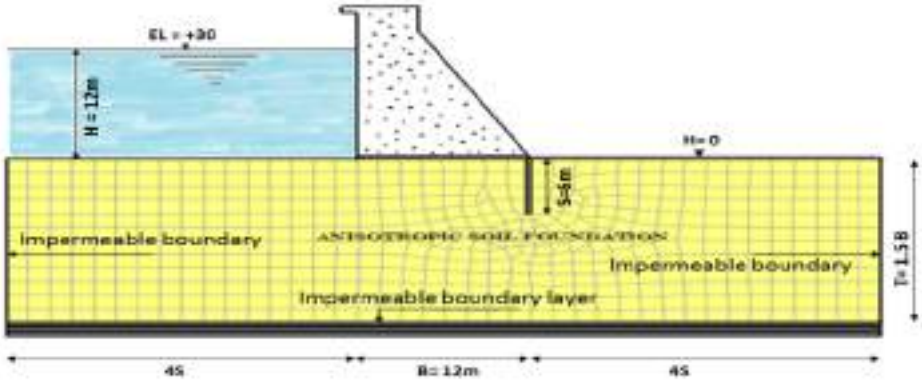

Figure 2: Finite Element With Mesh Discretization.

The partial differential equation and of the boundary line S_1 that represents the boundaries of reservoirs :

$$K_x \frac{\partial h}{\partial x} I_x + K_y \frac{\partial h}{\partial y} I_y = 0 \quad (3)$$

This is the equivalent of the boundary line S_2 that represents impermeable surface. The piezometeric head (H) through finite element is represented by the following equation:

$$H^e = \sum_{i=1}^{n} N_i H_i \quad (4)$$

where:

n: the number of nodes in one finite element,

Ni: shape function in the node I,

Hi: piezometeric head value in the node I, and

H^e: approximate solution for piezometeric head distribution in the finite element (e).

By substitution equation (4) in equation (3) to obtain:

$$\frac{\partial}{\partial x}\left(Kx \frac{\partial}{\partial x} \sum_1^n N_i H_i \right) + \frac{\partial}{\partial y}\left(Ky \frac{\partial}{\partial y} \sum_1^n N_i H_i \right) = R \neq 0 \quad (5)$$

where R represents (Residual). The weighting residual works to find the values of the variables in the nodes so that the residual (R) is as small as possible so that the residual is close to zero.

The element matrix can be written as follows:

$$K_{ij} = \int_{Ae} \left(\frac{\partial N_j}{\partial x} K_x \frac{\partial Nj}{\partial x} + \frac{\partial Nj}{\partial y} K_y \frac{\partial Nj}{\partial y} \right) dxdy \quad (6)$$

$$\int_{Se1} \left(Kx\, Ix\, Nj \frac{\partial Ni}{\partial x} + Ky\, Iy\, Nj \frac{\partial Ni}{\partial y} \right) ds \quad (7)$$

Because the linearly integrated limit is not involved in the composition of the specified segment matrix, it is easy to delete the linear integration limit from equation (7), for

not being actively involved in the configuration of the element matrix and thus the equation becomes as follows:

$$Kij = \int_{Ae}\left(\frac{\partial Nj}{\partial x}\, Kx\, \frac{\partial Ni}{\partial x} + \frac{\partial Nj}{\partial y} Ky \frac{\partial Ni}{\partial y}\right) dx\, dy = 0 \qquad (8)$$

K^e can take the matrix shape as follows:

$$[K^e] = \int_{Ae} [B^e]^T\, [D^e]\, [B^e]\, dx\, dy = 0 \qquad (9)$$

whereas:

$$[B^e] = \begin{bmatrix} \frac{\partial N1^e}{\partial x} & \frac{\partial N2^e}{\partial x} & \dots\dots\dots\dots\dots & \frac{\partial Nn^e}{\partial x} \\ \frac{\partial N1^e}{\partial y} & \frac{\partial N2^e}{\partial y} & \dots\dots\dots\dots\dots & \frac{\partial Nn^e}{\partial y} \end{bmatrix} \qquad (10)$$

$$[D^e] = \begin{bmatrix} K^e x & 0 \\ 0 & K^e y \end{bmatrix}$$

From assembly process we get the equation

$$[K]\,[H] = 0 \qquad (11)$$

where [K] is the global matrix $=\sum[K^e]$

VERIFICATION OF THE MODEL

In this section, the Geo- Studio Seep/W 2007 program has been applied to verify the work capacity of the program properly and that the purpose is to present some analysis of the common problems and provide a standard reference used to verify the possibility of working the program. Mishra and Reddy, (1983) provided analytical procedure to the exit gradient for steady confined flow in an anisotropic porous medium to find exit gradient of the corresponding fictitious isotropic flow domain. It was concluded that the region was exposed to the risk of piping at the down-stream side of vertical sheet pile is larger for the case of horizontal layer than for vertical layer to finite element results to a simple hydraulic structure with a single sheet pile are presented to the exit gradient distribution along the down-stream side . Figure 3 shows a domain of mathematical model. The hydraulic conductivity considered for kmax / kmin to be 4, when the major axis of the hydraulic conductivity makes an angle with the horizontal axis comparative analysis was performed, which shows that the highest percentage difference as in Table 1, and this confirms the validity work of program of the new finite element formulations for seepage flow in anisotropic porous media.

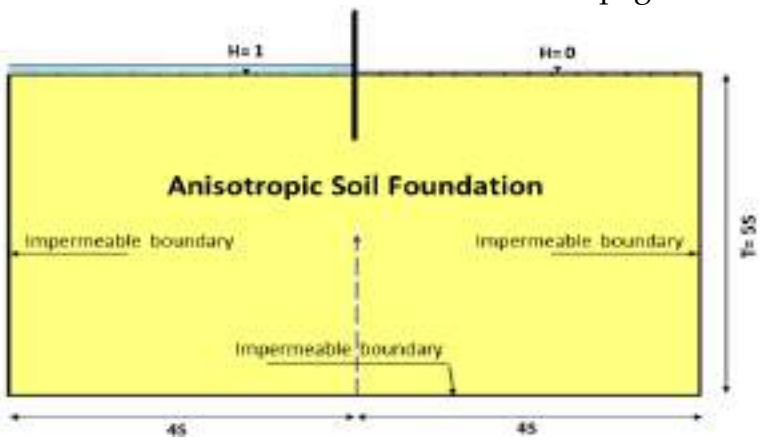

Figure 3: Single Sheet Pile Embedded in Anisotropic Soil Foundation, Boundary Conditions.

Table 3: Comparison Between Analytical Solution By Mishra and Reddy and Finite Element Solution By Geo- Studio Seep/W 2007 Program For Single Sheet Pile Embedded in Anisotropic Porous Media For kmax/kmin = 4.

Ie.S/H / X ̄/S	$\theta = 0$ and $180°$			$\theta = 30°$		
	analytic	F.E.M	Err.%	analytic	F.E.M	Err.%
0.00	0.320	0.352	-10	0.00	0.002	-------
0.25	0.310	0.331	-6.77	0.120	0.132	-10
0.50	0.305	0.322	-5.57	0.160	0.183	-14.3
0.75	0.300	0.310	-3.33	0.20	0.210	-5.00
1.00	0.290	0.299	-3.1	0.232	0.200	13.79
1.25	0.270	0.291	-7.77	0.210	0.191	9.0
1.50	0.260	0.285	-9.61	0.200	0.188	6.0
1.75	0.230	0.261	-13.4	0.190	0.176	7.36
2.00	0.220	0.244	-10.90	0.180	0.165	8.33
2.25	0.210	0.234	-11.428	0.165	0.150	7.87
2.50	0.200	0.205	-2.5	0.152	0.152	0
2.75	0.190	0.180	5.26	0.140	0.140	0
3.00	0.180	0.172	4.44	0.130	0.131	-0.769
3.25	0.170	0.161	5.29	0.120	0.130	-8.33
3.50	0.160	0.150	6.25	0.120	0.130	-8.33
3.75	0.150	0.143	4.67	0.105	0.121	-15.23
4.00	0.140	0.135	3.57	0.100	0.090	10

RESULTS AND DISCUSSION

The problem of the effect of soil inclination layer on pressure head along sheet pile has been investigated for each:

LOCATION OF SHEET PILE AT DOWN-STREAM

It is noted that when the angle of the soil inclination is changed and the ratio of the hydraulic conductivity is (2, 3 and 4), the pressure head increased by increasing the angle of the soil inclination, and the values increase between (24.5 -24.9) at 0 ≤θ≤30.

When 60 ≤θ≤90, the results are close or have identical values, especially when the hydraulic conductivity ratio equals 2 as shown in Figure 4, 5 and 6.

In the case of change in the hydraulic conductivity ratio of the soil angle of the soil, it is also noticed that there is an increase in pressure head by increasing the change in the hydraulic conductivity ratio, where the highest value is 27.0 by increasing pressure head at θ= 90° as shown in Figure 10, and the rate of increase will be 1.5% at 60≤θ≤90 for kmax/kmin= 4, while the highest value to increase pressure head to 24.9 is when 0≤θ≤30 for kmax/kmin=2, by the rate 2,8% as illustrated in Figure 7, 8 and 9.

LOCATION OF SHEET PILE AT UP-STREAM

It is noted that the increase in the angle of the soil inclination on the pressure is constant. There is no change for 0≤θ≤90 at the point of contact of the sheet pile with the hydraulic structure, where the value 30 represents the highest value of the pressure for all case kmax/kmin equal (2, 3, and 4), as in Figure 11, 12, and 13. The values gradually started to decrease with the pressure head at the end of the sheet pile between (24.7- 29.7) at a rate 16.8% this is for all cases, in the case of hydraulic conductivity is constant and there is a difference in the angle of soil inclination. When the angle of the soil inclination is proved with the difference in the ratio of hydraulic conductivity, the percentage of difference in the pressure head values at the end of the sheet pile equals 4% for kmax/kmin =4 at 0 ≤ θ ≤90, while in Figure 17, the highest pressure head value was found for kmax/kmin=2.

CONCLUSION

Finite element method has been used in many researches for the purpose of analysing the seepage flow through the soil foundation which is under the hydraulic structure as well as the seepage control. Using the Geo-studio Seep/W 2007 program based on the theoretical application of models, the following points could be concluded:

When the sheet pile is at up-stream, the pressure head gradually begins to decrease if the angle of soil inclination changes or in case of change in the hydraulic conductivity ratio, so that the degree of variation with a small percentage of all cases and therefore obtained the lowest value of pressure head at the angle of soil inclination in the region to the end of the sheet pile for kmax/kmin =2 at θ=90.

When the sheet pile is at down-stream, there is no effect on the pressure head in the case of soil inclination or in case of change in the ratio of hydraulic conductivity, although there is a difference when the percentage of difference is not indicated on the sheet pile and also shows that the greater the angle of soil inclination, identical values were obtained.

The safety of the structure against failure by piping and the safety factor against the piping phenomenon is increased, when the location of the sheet piles are in the area of the down-stream, especially at the angle of soil inclination 60≤ θ ≤90.

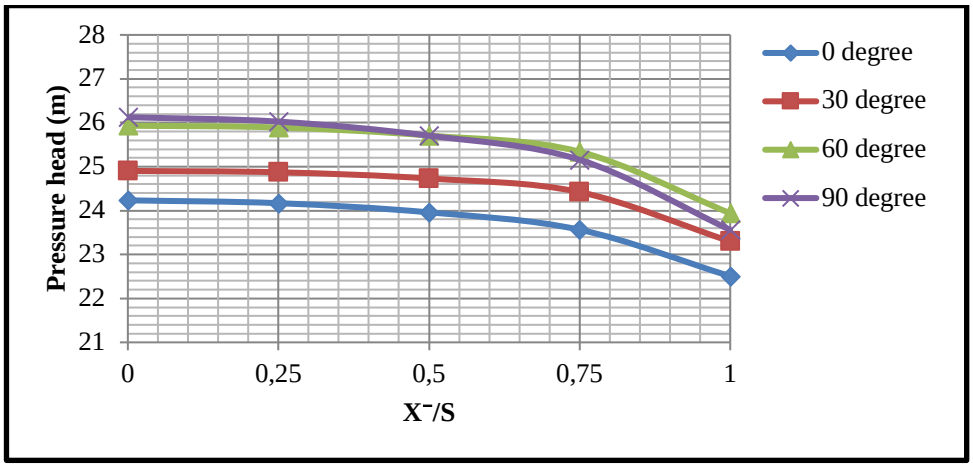

Figure 4: Variation of Pressure Head Along Sheet Pile For kmax/kmin=2 at Down-Stream.

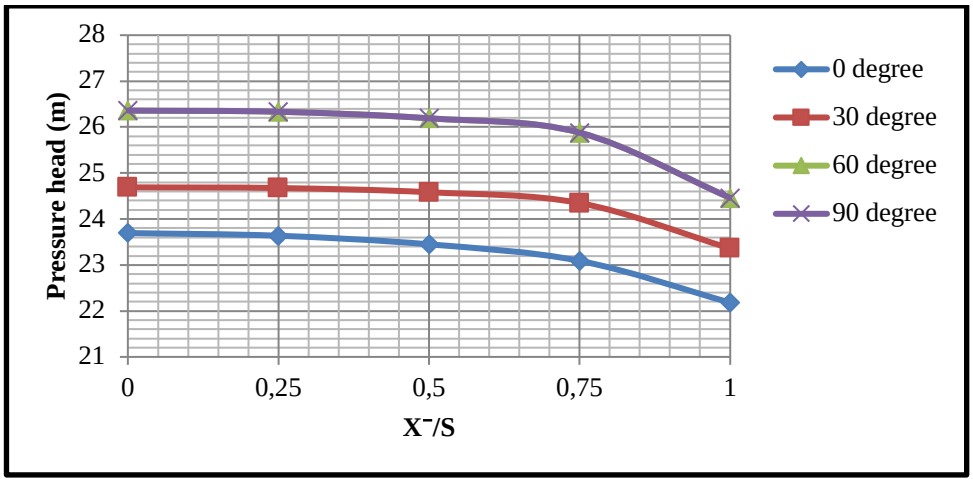

Figure 5: Variation of Pressure Head Along Sheet Pile For kmax/kmin=3 at Down-Stream.

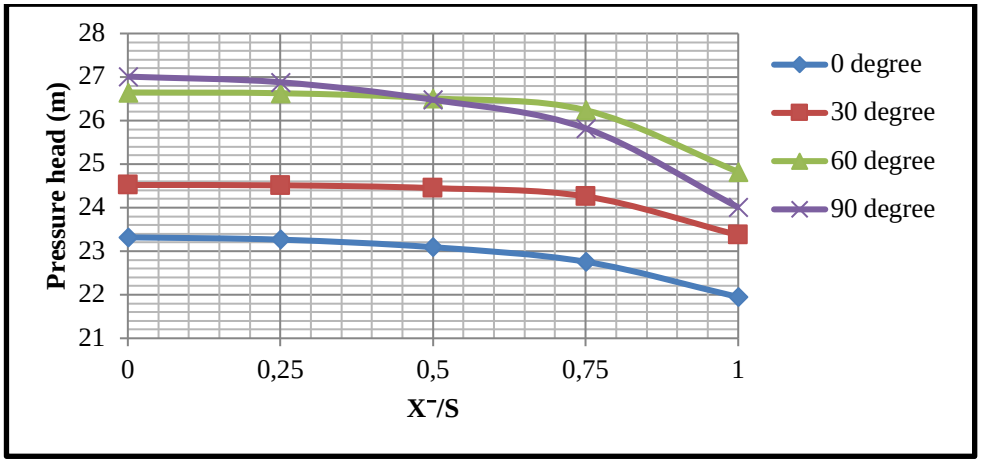

Figure 6: Variation of Pressure Head Along Sheet Pile For kmax/kmin=4 at Down-Stream.

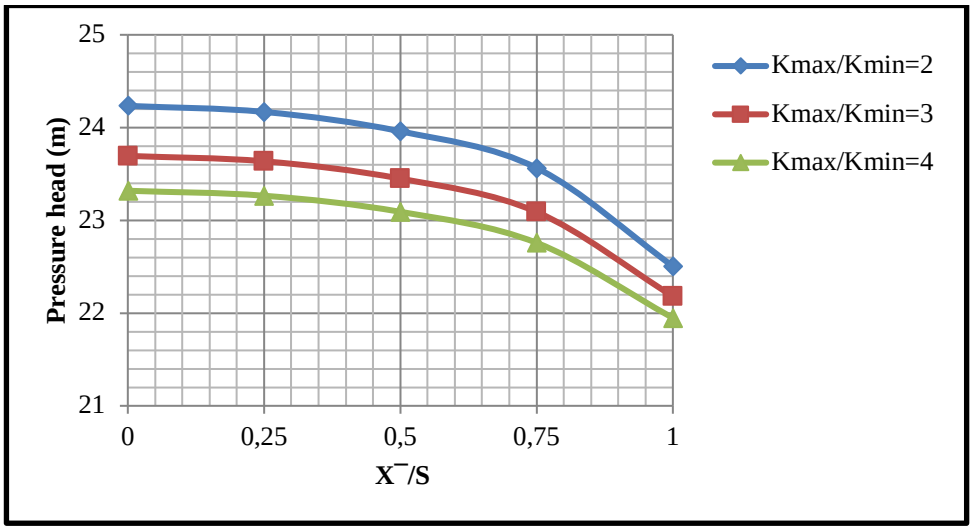

Figure 7: variation of pressure head along sheet pile for θ= 0 at Down-Stream.

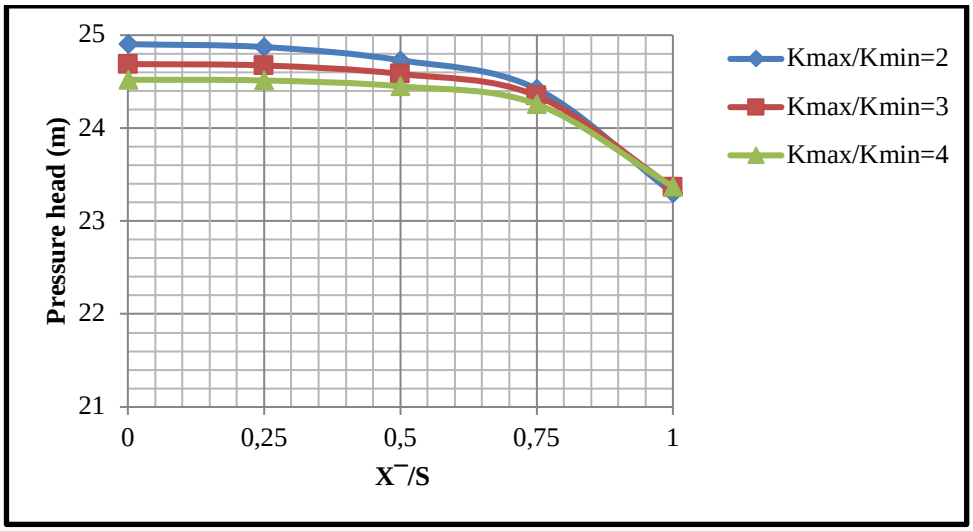

Figure 8: Variation of Pressure Head Along Sheet Pile For θ=30 at Down-Stream

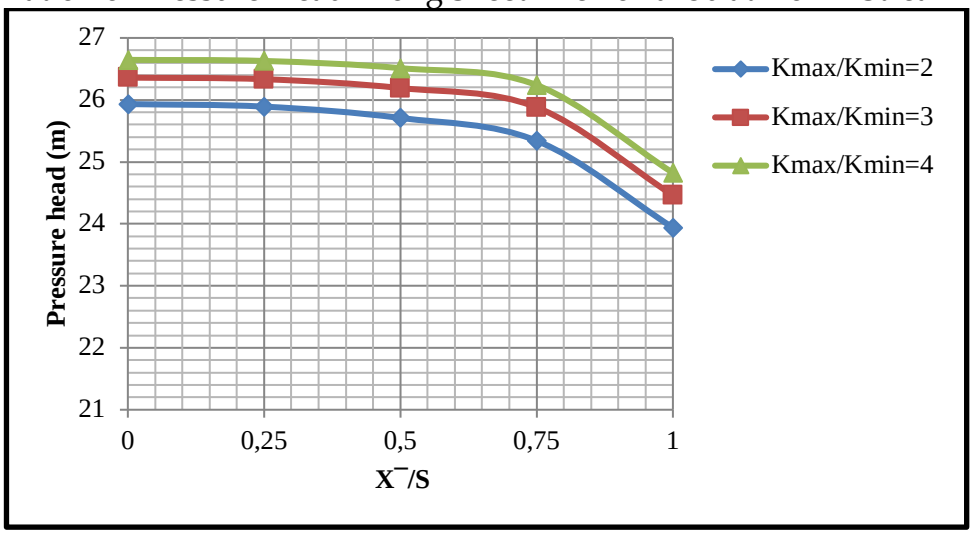

Figure 9: Variation of Uplift Head Along Sheet Pile For θ= 60 at Down-Stream.

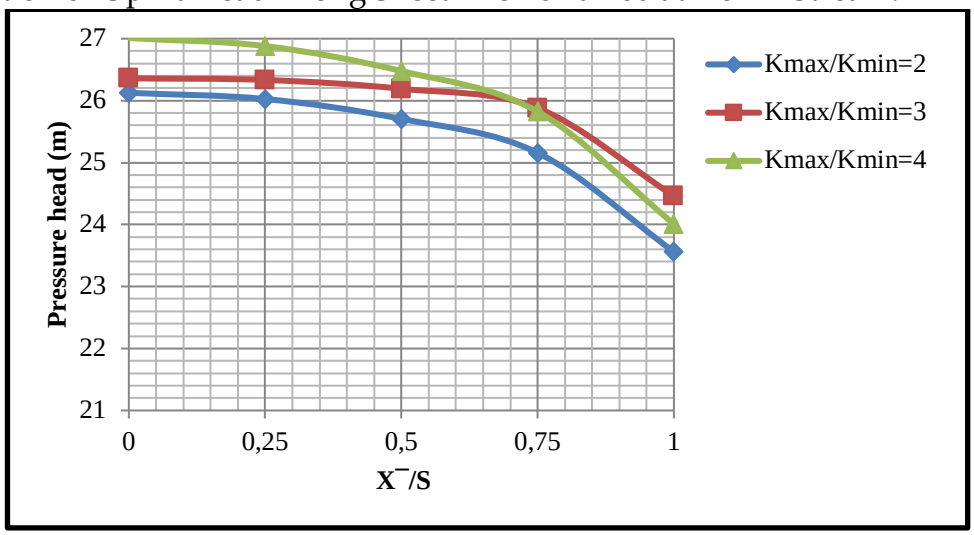

Figure 10: Variation of Uplift Head Along Sheet Pile For θ= 90 at Down-Stream.

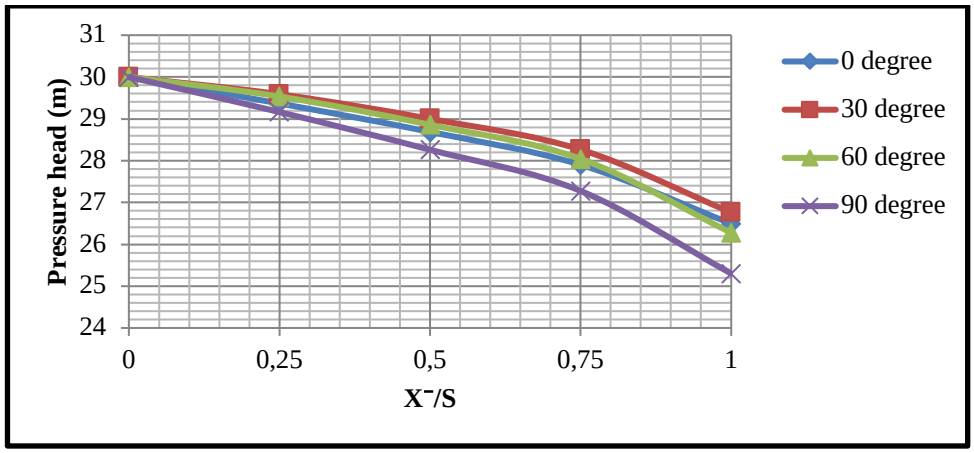

Figure 11: Variation of Pressure Head Along Sheet Pile For kmax/kmin=2 at Up-Stream.

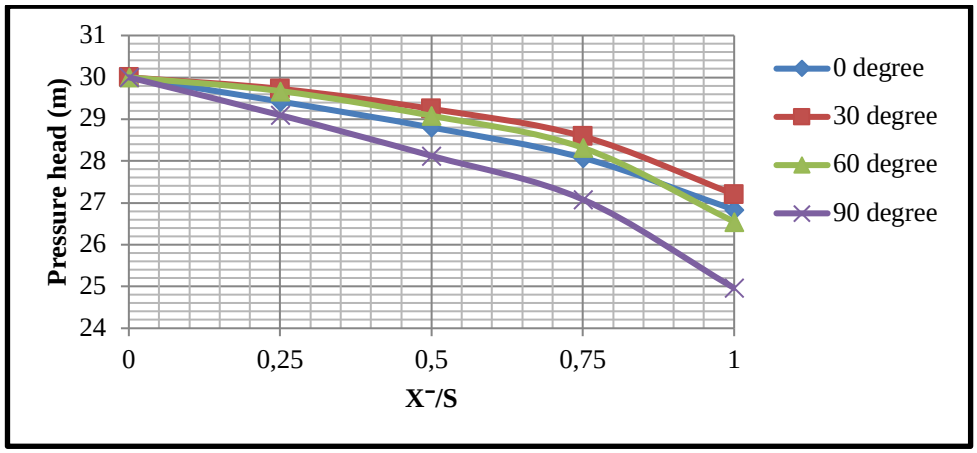

Figure 12: Variation of Pressure head along sheet pile for kmax/kmin=3 at Up-Stream.

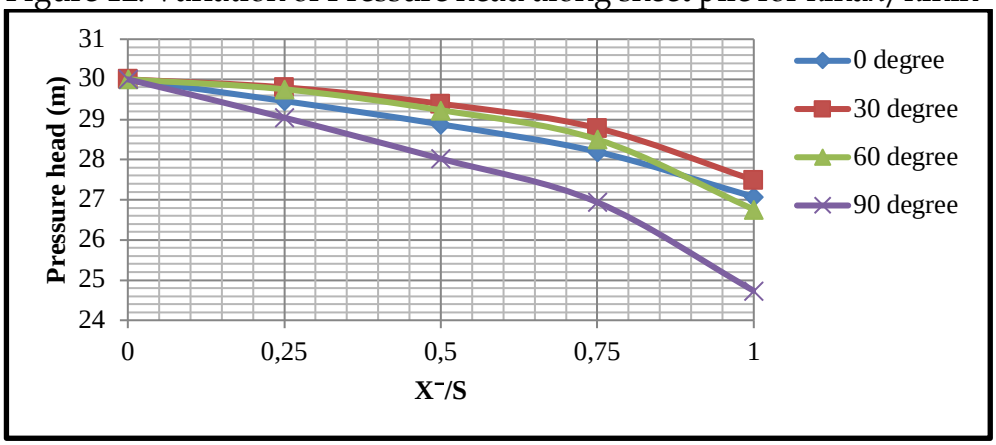

Figure 13: Variation of Pressure Head Along Sheet Pile For kmax/kmin=4 at Up-Stream.

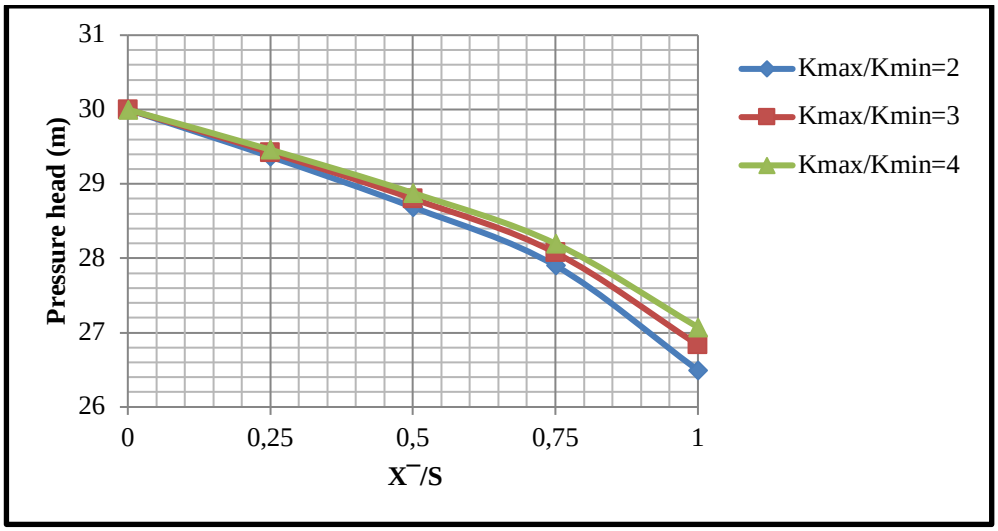

Figure 14: Variation of Pressure Head Along Sheet Pile For θ= 0 at Up-Stream

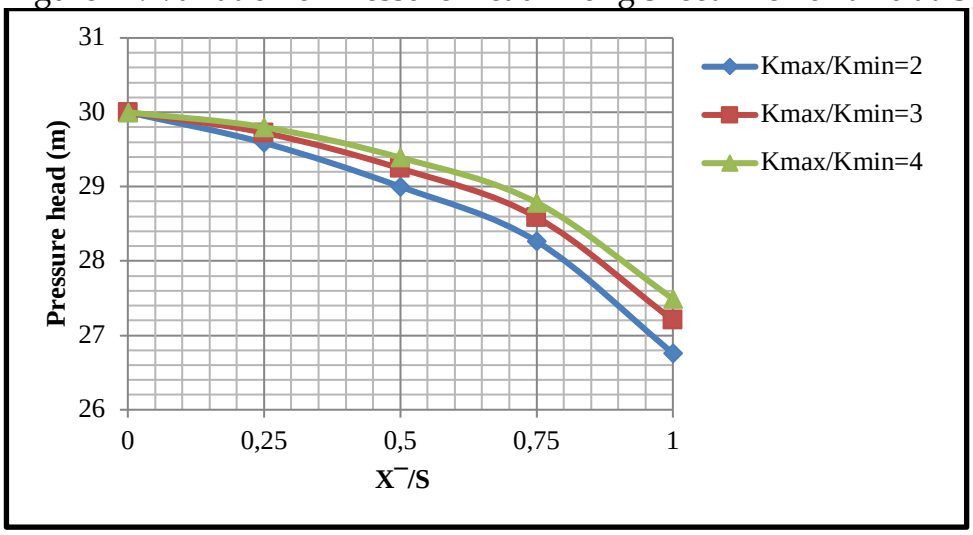

Figure 15: Variation of Pressure Head Along Sheet Pile For θ= 30 at Up-Stream.

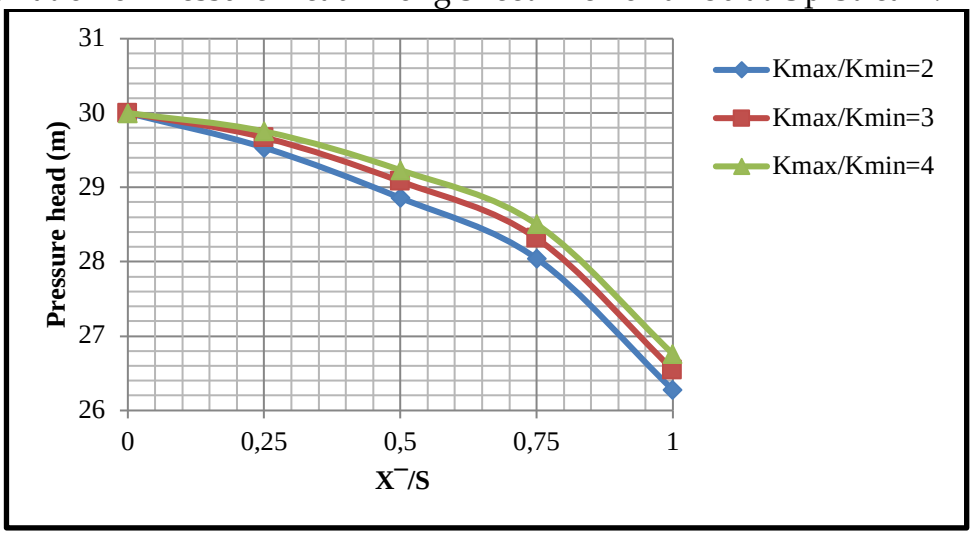

Figure 16: Variation of Pressure Head Along Sheet Pile For θ= 60 at Up-Stream

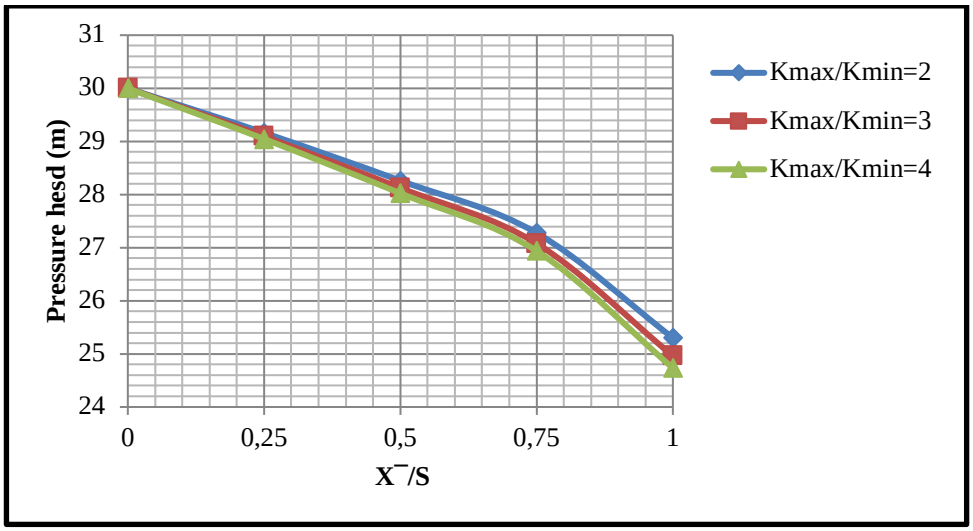

Figure 17: Variation of Pressure Head Along Sheet Pile For $\boldsymbol{\theta}$ = 90 aT Up-Stream

REFERENCES

Al–Damluji, O. F., Fattah, M. Y., and Adthami, R. A. J., (2004). "Solution of Two-Dimensional Steady-State Flow Field Problems by the Boundary Element Method", Engineering and Technology Journal, University of Technology, Vol. 23, No. 12.

Alghazali N. O. S. and Alnealy H. K. T., (2015)."Analysis of Seepage Under Hydraulic Structure Using Slide Program", American Journal Of Civil Engineering, Vol. 3, No. 4, 2015.

Hillo, A.N.,(1993) "Finite Elements For Seepage Below Hydraulic Structures on Anisotropic Soil Foundation" .M.Sc. Thesis Department of Civil Engineeing. College of Engineering. University of Basrah.

Khassaf, S. I., Al-Damarchi H. T. N., and Al-Zrejawi H. Ch. D., (2011). "Optimum Location and Angle of Inclination of Cut-off to Control Exit Gradient and Uplift Pressure Head under Hydraulic Structure", Jordan Journal of Civil Engineering, Vol. 5, No. 3.

Mishra G. C. and Reddy A. S., (1983). "Exit Gradient in Anisotropic Porous Medium" Journal of Hydraulic Engi neering, Vol. 109, No. 6.

Mohammed-A. W. , (2011). ”The Effect of Middle Sheet Pile on Uplift Pressure under Hydraulic Structures”, European Journal of Scientific Research, ISSN 1450-216X Vol. 65, No.3.

Obead, I. H., (2013). ”Effect of Position and Inclination Angle of Cutoff Wall on Seepage Control in the Foundation oF Dam”, Journal of Karbala University, Vol. 11 No. 4, pp. 17-32.

Punmia B.C., (1981). “Design of Hydraulic Structure with Intermediate Filters”, Journal Hydraulic Engineering Division, ASCE, Vol. 102, No.1.

Reddy, A. S., Mishra. G.C. and Seetharamiah, K.,(1971). “Flow Around Inclined Sheet Pile”. ASCE,.J.Hyd. Div. Vol. 97.No.HY7, 1971.

Zainal, A. K. E., (2011). ”The Effect of Cutoff Wall Angle on Seepage under Dams”, Journal of Engineering, Vol. 17.

MAGNESIUM OXIDE ADDING TO AL2024 ALLOYS

Engin ERGÜL
Teknik Programlar Bölümü, İzmir Meslek Yüksekokulu, Dokuz Eylül Üniversitesi, İzmir, Türkiye
engin.ergul@deu.edu.tr

Halil İbrahim KURT
Makine ve Metal Teknolojileri Bölümü, Teknik Bilimler MYO, Gaziantep Üniversitesi, Gaziantep, Türkiye
hikurt@gantep.edu.tr

Murat ODUNCUOĞLU
Fizik Bölümü, Yıldız Teknik Üniversitesi, İstanbul, Türkiye
oduncuoglu@gantep.edu.tr

Necip Fazıl YILMAZ
Mühendislik Fakültesi, Makine Mühendisliği Bölümü, Gaziantep Üniversitesi, Gaziantep, Türkiye nfyilmaz@gantep.edu.tr

Serdar SALMAN
Metalurji ve Malzeme Mühendisliği, Teknoloji Fakültesi, Marmara Üniversitesi, İstanbul, Türkiye
ssalman@marmara.edu.tr

Ferhat GÜL
Metalürji ve Malzeme Mühendisliği, Teknoloji Fakültesi, Gazi Üniversitesi, Ankara, Türkiye
fgul@gazi.edu.tr

ABSTRACT: One of the most important physical properties in metal and its alloys, metal matrix composites and materials science and technology are the density and porosity content. These two concepts have a significant effect on the microstructure and hence the mechanical properties of the materials produced. The aim of this course is to provide advanced engineering materials which are produced or developed especially in engineering applications with low density and high mechanical properties. Therefore, the density and density-related porosity content is extremely important. In this study, nano-scale magnesium oxide particles were added to the Al2024 alloy and the density analysis of the produced aluminum matrix composites were analyzed according to the Archimedes principle and the porosity content was investigated by comparing theoretical and measured densities. The effect of reinforcing content on the physical properties of the produced composites was studied to determine.
Key words: composite, nano, density, porosity, magnesium oxide.

AL2024 ALAŞIMINA MAGNEZYUM OKSİT İLAVESİ

ÖZET: Metal ve alaşımları, metal matrisli kompozitler, malzeme bilimi ve teknolojilerinde en önemli fiziksel özelliklerden biri yoğunluk ve porozite içeriğidir. Bu iki kavram üretilen malzemelerin mikroyapı ve dolayısıyla mekanik özellikleri üzerinde önemli bir etkiye sahiptir. Özellikle mühendislik uygulamalarında üretilen veya geliştirilen yeni ve ileri teknoloji ürünü olan gelişmiş mühendislik mazemelerinin düşük yoğunluklu ve yüksek mekanik özellikler göstermesi amaçlanmaktadır. Bu nedenle yoğunluk ve yoğunlukla ilişkili porozite içeriği son derece önem arz etmektedir. Bu çalışmada nano magnezyum oksit partiküller Al2024 alaşımına ilave edilmiş ve üretilen alüminyum matrisli kompozitlerin yoğunluk analizleri Arşimet prensibine göre, prozite içeriği ise teorik ve ölçülen yoğunlukların kıyaslanması sonucu araştırılmıştır. Güçlendirici içeriğinin üretilen kompozitlerin fiziksel özelliğine etkisi belirlenmeye çalışılmıştır.

Anahtar sözcükler: kompozit, nano, yoğunluk, porozite, magnezyum oksit

GİRİŞ

Metal matrisli kompozitler, istenen ve gerekli özellikleri sağlamak üzere en az biri metal olan iki veya daha fazla farklı malzemenin bileşimiyle elde edilen yeni ve ileri mühendislik malzemelerdir. Belirli bir uygulama alanı için en uygun bileşimli kompozit malzemenin üretilebilmesi için matris, güçlendirici türü, şekli, boyutu, dağılımı ve homojenliği gibi kompozitin bileşenleri hakkında detaylı bilgiye sahip olmak gerekmektedir. Gelişmiş mekanik ve kimyasal özelliklere sahip hibrit kompozit, havacılık ve otomotiv uygulamalarında yaygın olarak kullanılmaktadır. Çok yüksek mukavemet - ağırlık oranı, alüminyum hibrit metal matris kompozitlerinin yaygın olarak üretilmesinin ve düşük maliyet nedeniyle yapısal uygulamada kullanılmasının temel nedenidir (Kumaraswamy, Bharat, & Krishna Rao, 2018). Alüminyum alaşımlı kompozit malzemeler üstün mekanik ve tribolojik özellikleri nedeniyle geleneksel malzemelerin yerini alma eğilimindedir (Venkatesan & Xavior, 2018). MgO (magnezyum oksit), iyi dökme yeteneği, iyi kaynaklanabilir özelliği, geri dönüştürülebilirlik özelliğine sahip ve doğada bol miktarda bulunan hafiftir bir bileşiktir (ME, Bhaskar, & Kiran). MgO gibi güçlendirici parçacıklar, yüksek mekanik özellikleri nedeniyle geleneksel alüminyum bazlı kompozitler için potansiyel bir alternatif olarak kullanılmaktadır (Franco-Madrid et al., 2017). Genellikle, üretilen tüm malzemelerde düşük yoğunluk ve yüksek mekanik özelliklerin elde edilmesi amaçlanır. Bununla birlikte porozite içeriği malzemelerin mekanik özelliklerini olumsuz yönde etkiler. Bu çalışmada ise, üretilen kompzitlerin yoğunluk değerlerinin belirlenmesi ve porozite içeriğinin değişimi belirlenmeye çalışılmıştır.

YÖNTEM

Bu çalışmada, <45 nm küçük çaplarda magnezyum oksit partikül güçlendirici olarak Al2024 alaşımı matris olarak kullanılmıştır. Üretim öncesi güçlendiriciler ıslatılabilirliği arttırmak için nikel-fosfor ile kaplanmıştır. Ergitilen matris malzemesi 640°C sıcaklığa indirilmiş bu sıcaklıkta farklı ağırlık oranlarında nano magnezyum

oksit partiküller erigiye ilave edilerek 10 dk 500 rpm hızında karıştırılmıştır. Devamında 800°C hızlı ısıtılmış 18x200 çapındaki kalıba dökülmüştür. Üretime boyunca sistem yüksek saflıkta argon atmosferi koruyucu gaz olarak kullanılmış, curuf alma ve gaz giderme işlemleri uygulanmıştır.
Üretilen kompozitlerin yoğunlukları Arşimet prensibine göre belirlenmiştir. Teorik ve ölçülen yoğunluk kullanılarak relatif yoğunluk değerleri ve porozite içeriği tespit edilmiştir (Fakhraei, Emamy, & Farhangi, 2013).
dt =[(%n)1*δ1] + [(%n)2*δ2] + … + [(%n)n*δn] Burada; dt: Kompozitin teorik yoğunluğu, (%n)n: Her bir takviyenin karışım içindeki ağırlıkça yüzdesi, δn: Her bir takviyenin yoğunluğudur.
Deneysel yoğunluk (dm)= [da/(da – dw)] Burada; da: Numunenin havadaki ağırlığı ve dw: Numunenin sudaki ağırlığıdır.
Relatif yoğunluklar dm/dt formülü kullanılarak ve porozite içeriği ise % porozite = 100((dt / dm)-1) formülü kullanılarak hesaplanmıştır.
BULGULAR

Şekil 1'de nikel-fosfor ile kaplanmış nano magnezyum oksit güçlendiriciler ilave edilerek üretilen alüminyum matrisli kompozitlere ait teorik ve ölçülen yoğunluk değerleri verilmiştir. %0.2 MgO içeren kompozitin teorik yoğunluğu 2.781 gr/cm^3 %0.5 MgO içeren kompozitin teorik yoğunluğu 2.784 gr/cm^3 %1.0 MgO içeren kompozitin teorik yoğunluğu 2.788 gr/cm^3 ve %1.5 MgO içeren kompozitin teorik yoğunluğu 2.792 gr/cm$^{3'}$ tür. Artan güçlendirici içeriğiyle kompozitlerin teorik yoğunluk değerleri artmaktadır. %0.2 MgO içeren kompozitin ölçülen yoğunluğu 2.686 gr/cm^3 %0.5 MgO içeren kompozitin ölçülen yoğunluğu 2.704 gr/cm^3 %1.0 MgO içeren kompozitin ölçülen yoğunluğu 2.759 gr/cm^3 ve %1.5 MgO içeren kompozitin ölçülen yoğunluğu 2.768 gr/cm$^{3'}$ tür. Aynı şekilde artan güçlendirici içeriğiyle de kompozitlerin ölçülen yoğunluk değerleri artmaktadır. %0.2 magnezyum oksit ilave edilen bölgede teorik ve ölçülen yoğunluk farkları maksimumdur ve bu fark % 1.5 magnezyum oksit oranına doğru lineer olarak azalmaktadır. Minimum teorik ve ölçülen yoğunluk farkları %1.5 MgO içeriğiyle elde edilmiştir. Elde edilen sonuçlar literatür ile karşılaştırıldığında uyum içerisinde olduğu görülmektedir (Annigeri & Kumar, 2018; Kumar, Rao, Selvaraj, & Bhagyashekar, 2010; Sharma, 2003).

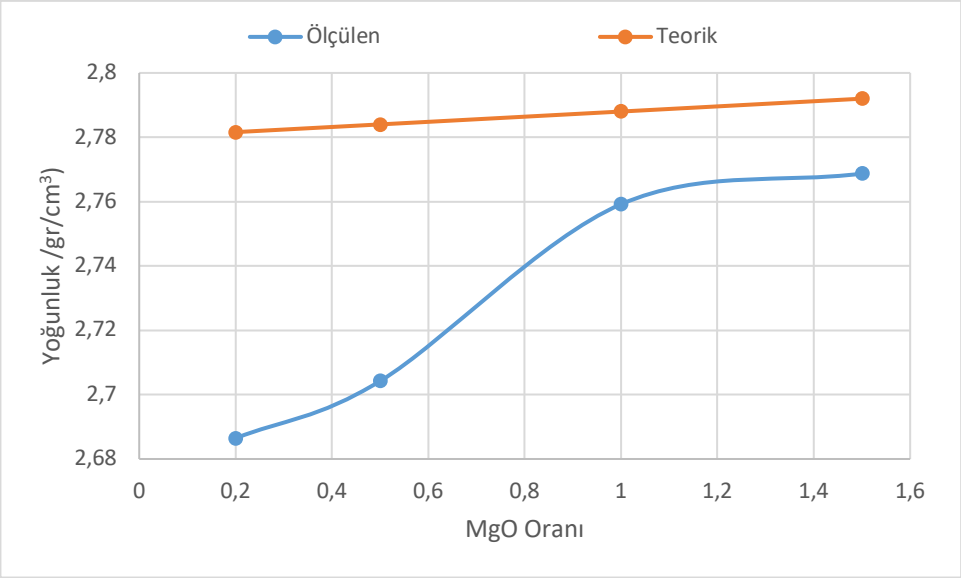

Şekil 1. Kompozitlerin Teorik ve Ölçülen Yoğunlukları

Şekil 2'de üretilen alüminyum matrisli kompozitlere ait relatif yoğunluk değerleri verilmiştir. %0.2 MgO içeren kompozitin relatif yoğunluğu %96.578, %0.5 MgO içeren kompozitin relatif yoğunluğu %97.134, %1.0 MgO içeren kompozitin relatif yoğunluğu %98.966 ve %1.5 MgO içeren kompozitin relatif yoğunluğu %99.166 olarak belirlenmiştir. Magnezyum oksit artış oranına bağlı olarak üretilen kompozitlerin relatif yoğunluk değerleri artmaktadır. Minimum relatif yoğunluk ağırlıkça %0.2 MgO içeren kompozitte, maksimum relatif yoğunluk değeri ağırlıkça %1.5 MgO içeren kompozitte elde edilmiştir. Yüksek relatif yoğunluk değerleri daha az porozite anlamı ve daha düşük relatif porozite değeri daha yüksek porozite içeriğidir. (Aldoshan & Khanna, 2017).

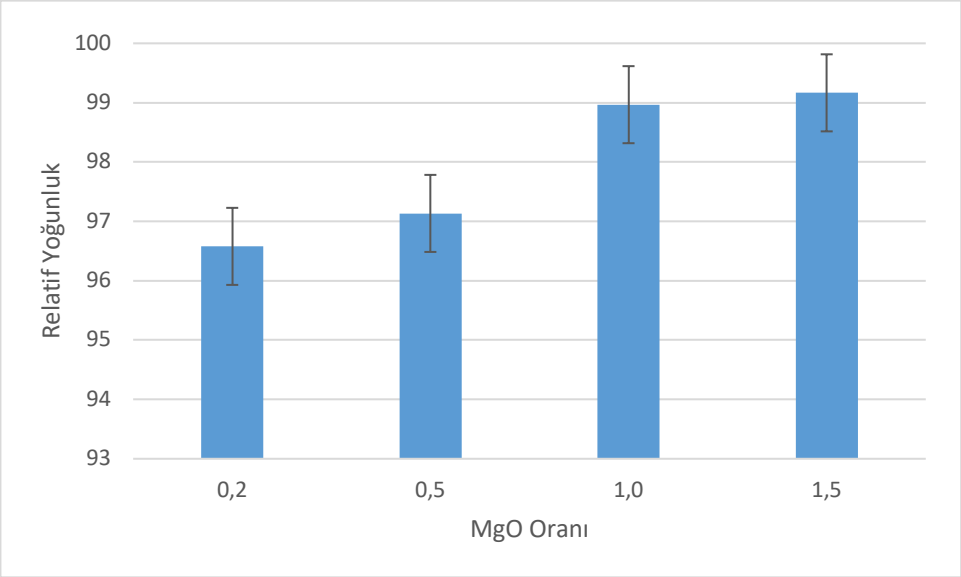

Şekil 2. Kompozitlerin Relatif Yoğunlukları

Şekil 3, kompozitlerde porozite içeriğinin değişmini göstermektedir. %0.2 MgO içeren kompozitin porozite içeriği %3.542, %0.5 MgO içeren kompozitin porozite içeriği

%2.865, %1.0 MgO içeren kompozitin porozite içeriği %1.033 ve %1.5 MgO içeren kompozitin porozite içeriği %0.833 olarak gerçekleşmiştir. Artan güçlendirici içeriğiyle kompozitlerin yüzde porozite oranı liner olarak azalmakta, minimum pozoite ağırlıkça %1.5 MgO içeren kompozitte ve maksimum pozite oranı %0.2 MgO içieren kompozitte görülmüştür. Porozite içeriğinin artması kompozitlerde mekanik özelliklerinin kötüleşmesine neden olmaktadır (Aqida, Ghazali, & Hashim, 2004). Genellikle artan güçlendirici içeriğiyle kompozitlerde porozite oranının artması beklenir (Hossein Abdizadeh, Ebrahimifard, & Baghchesara, 2014; H Abdizadeh, Vajargah, & Baghchesara, 2015; Baghchesara, Abdizadeh, & Baharvandi, 2012). Ancak, seramik partiküllerin nikel ile kaplama sonucu ve yüksek sıcaklık vasıtasıyla artan ıstatılabilirlik nedeniyle porozite oranında azalma görülmektedir.

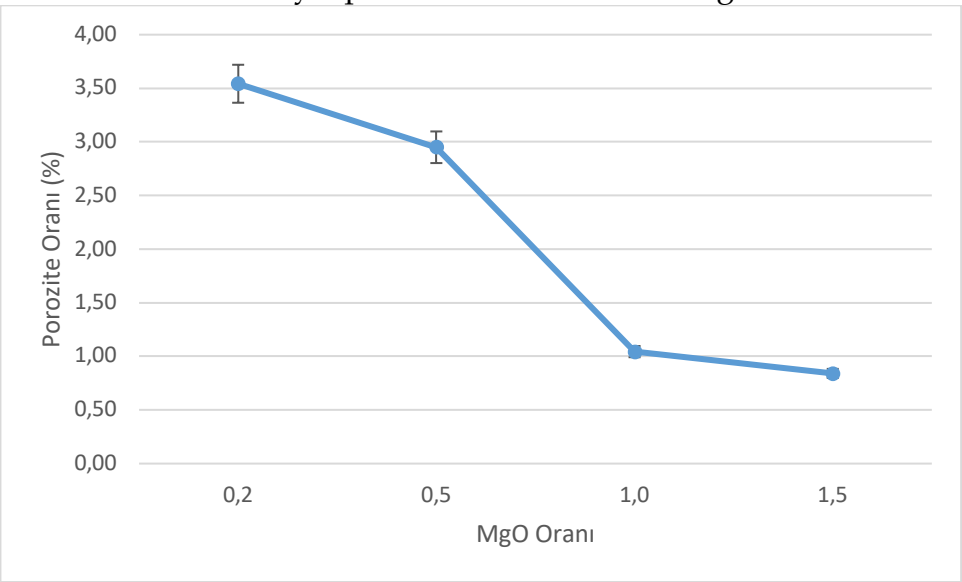

Şekil 3. Kompozitlerin Porozite Oranı

SONUÇ

Bu çalışmada, Al2024 matris malzemesi olarak kullanılmış olup matris içerisine ağırlıkça farklı oranlarda nano magnezyum oksit partiküller ilave edilerek alüminyum matrisli kompozit malzemeler yarı-katı karıştırma yöntemiyle dökülerek üretilmiştir. Üretilen kompozitlerin teorik, deneysel, relatif yoğunlukları ve porozite analizleri yapılmıştır. Bu çalışmadan aşağıda belirtilen sonuçlar elde edilmiştir.

- Magnezyum oksit artış oranıyla malzemelerin teorik ve ölçülen yoğunluklarında artış gözlenmiştir.
- Maksimum teorik ve deneysel yoğunluk ağırlıkça %1.5 magnezyum oksit içeriğiyle elde dilmiştir. Teorik ve ölçülen yoğunluk değerleri arasındaki minimum ve maksimum fark %1.5 ve %0.2 MgO partikül içeren kompozitlerde elde edilmiştir.
- Relatif yoğunluk değerleri lineer olarak artmakta ve maksimum relatif yoğunluk ağırlıkça %1.5 MgO içeren kompozitte meydan gelmiştir.
- Üretilen kompozitlerde porozite içeriği lineer olarak azalmakta, minimum porozite oranı Al2024/1.5MgO kompozitte gerçekleşmektedir.

TEŞEKKÜR

Bu çalışmada destekleri için TÜBİTAK'a (Proje No: 217M084) teşekkür ederiz.

KAYNAKLAR

Abdizadeh, H., Ebrahimifard, R., & Baghchesara, M. A. (2014). Investigation of microstructure and mechanical properties of nano MgO reinforced Al composites manufactured by stir casting and powder metallurgy methods: A comparative study. *Composites Part B: Engineering, 56*, 217-221. doi: https://doi.org/10.1016/j.compositesb.2013.08.023

Abdizadeh, H., Vajargah, P., & Baghchesara, M. (2015). Fabrication of MgO nanoparticulates reinforced aluminum matrix composites using stir-casting method. *KOVOVE MATERIALY-METALLIC MATERIALS, 53*(5), 319-326.

Aldoshan, A., & Khanna, S. (2017). Effect of relative density on the dynamic compressive behavior of carbon nanotube reinforced aluminum foam. *Materials Science and Engineering: A, 689*, 17-24. doi: https://doi.org/10.1016/j.msea.2017.01.100

Annigeri, U. K., & Kumar, G. V. (2018). Effect of Reinforcement on Density, Hardness and Wear Behavior of Aluminum Metal Matrix Composites: A Review. *Materials Today: Proceedings, 5*(5), 11233-11237.

Aqida, S., Ghazali, M., & Hashim, J. (2004). Effects of porosity on mechanical properties of metal matrix composite: an overview. *Jurnal Teknologi, 40*(A), 17-32.

Baghchesara, M. A., Abdizadeh, H., & Baharvandi, H. R. (2012). *Effects of MgO nano particles on microstructural and mechanical properties of aluminum matrix composite prepared via powder metallurgy route.* Paper presented at the International Journal of Modern Physics: Conference Series.

Fakhraei, O., Emamy, M., & Farhangi, H. (2013). The effect of Al–5Ti–1B grain refiner on the structure and tensile properties of Al–20%Mg alloy. *Materials Science and Engineering: A, 560*(0), 148-153. doi: http://dx.doi.org/10.1016/j.msea.2012.09.050

Franco-Madrid, J., Garay-Reyes, C., Estrada-Guel, I., Nava-Dino, C., Maldonado-Orozco, M., & Martínez-Sánchez, R. (2017). Microstructural and Mechanical Behavior in the Al 2024 Alloy Modified With Addition of CeO 2. *Microscopy and Microanalysis, 23*(S1), 1650-1651.

Kumar, G. V., Rao, C., Selvaraj, N., & Bhagyashekar, M. (2010). Studies on Al6061-SiC and Al7075-Al2O3 metal matrix composites. *Journal of Minerals and Materials Characterization and Engineering, 9*(01), 43.

Kumaraswamy, H. S., Bharat, V., & Krishna Rao, T. (2018). Influence Of Mechanical &Tribological BehaviourOf Al 2024 MMC Fabricated By Stir Casting Technique- A Review. *Materials Today: Proceedings, 5*(5, Part 2), 11962-11970. doi: https://doi.org/10.1016/j.matpr.2018.02.170

ME, N. K., Bhaskar, H., & Kiran, T. Characterization of Za-27 Alloy Reinforced with MgO Particles by Stir Casting Technique.

Sharma, S. (2003). Equation for the density of particle-reinforced metal matrix composites: A new approach. *Journal of Materials Engineering and Performance, 12*(3), 324-330.

Venkatesan, S., & Xavior, M. A. (2018). Analysis of Mechanical Properties of Aluminum Alloy Metal Matrix Composite by Squeeze Casting – A Review. *Materials*

Today: Proceedings, 5(5, Part 2), 11175-11184. doi: https://doi.org/10.1016/j.matpr.2018.01.141

COBALT COATING OF CARBON NANOTUBE

Necip Fazıl YILMAZ
Mühendislik Fakültesi, Makine Mühendisliği Bölümü, Gaziantep Üniversitesi, Gaziantep, Türkiye nfyilmaz@gantep.edu.tr

Engin ERGÜL
Teknik Programlar Bölümü, İzmir Meslek Yüksekokulu, Dokuz Eylül Üniversitesi, İzmir, Türkiye
engin.ergul@deu.edu.tr

Halil İbrahim KURT
Makine ve Metal Teknolojileri Bölümü, Teknik Bilimler MYO, Gaziantep Üniversitesi, Gaziantep, Türkiye
hikurt@gantep.edu.tr

Murat ODUNCUOĞLU
Fizik Bölümü, Yıldız Teknik Üniversitesi, İstanbul, Türkiye
oduncuoglu@gantep.edu.tr

Ferhat GÜL
Metalürji ve Malzeme Mühendisliği, Teknoloji Fakültesi, Gazi Üniversitesi, Ankara, Türkiye
fgul@gazi.edu.tr

Serdar SALMAN
Metalürji ve Malzeme Mühendisliği, Teknoloji Fakültesi, Marmara Üniversitesi, İstanbul, Türkiye
ssalman@marmara.edu.tr

ABSTRACT: Carbon nanotubes are expensively attracting scientific and technological interest by means of their important advantages on materials. Some researches have shown that carbon nanotubes possess remarkable mechanical properties like exceptionally high elastic modulus and large elastic strain etc. Electroless coating is one of the most important methods for manufacturing composites of metallic. Coatings containing solid particles such as MgO, TiB_2, B_4C and TiC etc. have been developed for better mechanical properties such as wear resistance or dispersion hardening. One important way of producing composite coatings is co-deposition of particles into a metal matrix from an electroless bath. Cobalt–phosphorous can be one of the most popular electroless coatings, and because of its good properties, corrosion resistance, uniform coating thickness and applicability for a variety of materials and surfaces. In this work aims to investigate the effect of cobalt coating on multi-wall carbon nanotubes and reveal the interactions between the bath and CNTs.

Key words: cobalt, nano, coating, cnt.

KARBON NANO TÜPE KOBALT KAPLAMANIN UYGULANMASI

ÖZET: Karbon nanotüpler, malzemeler üzerindeki önemli avantajları sayesinde bilimsel ve teknolojik ilgiyi yoğun bir şekilde çekmektedir. Bazı araştırmalar, karbon nanotüplerin yüksek elastiklik modülü ve büyük elastik gerilme gibi olağanüstü mekanik özelliklere sahip olduğunu göstermiştir. Akımsız kaplama, metalik kompozitlerin üretimi için en önemli yöntemlerden biridir. MgO, TiB_2, B_4C ve TiC gibi katı partikülleri içeren kaplamalar, aşınma direnci veya dispersiyon sertleştirmesi gibi daha iyi mekanik özellikler için geliştirilmiştir. Kompozit kaplamaların üretilmesinin en önemli yollarından biri parçacıkların banyodan bir metal matris üzerine çökeltilmesidir. Kobalt-fosfor kaplama iyi özellikleri, korozyon direnci, düzgün kaplama kalınlığı ve çeşitli malzeme ve yüzeyler için uygulanabilirliği nedeniyle en popüler kaplamalarından biri olabilir. Bu çalışmada, kobalt kaplamanın çoğul duvarlı karbon nanotüpler üzerindeki etkisini araştırma ve banyo ile CNT'ler arasındaki etkileşimleri ortaya çıkarma amaçlanmıştır.
Anahtar sözcükler: kobalt, nano, kaplama, cnt.

GİRİŞ

Karbon nanotüpler (CNT'ler), polimerik, seramik ve metalik malzemelerdeki mekanik özellikleri geliştirmek için ideal bir takviye malzemesi olarak kullanılmaktadır. CNT'ler, hafif ve yüksek mukavemetli kompozitler için güçlü takviyelerdir (Isaza Merino, Ledezma Sillas, Meza, & Herrera Ramirez, 2017). Karbon nanotüpler, kompozit materyallerin nano boyutlu takviyeleri olarak kullanılmaktadır. Nano boyutlu takviyeler geliştirilmiş malzeme özellikleri sağlayabilir. Ayrıca, tek duvarlı karbon nanotüpler (SWNT) ve çoğul duvarlı karbon nanotüpler, yüksek mekanik mukavemet, sertlik, esneklik, termal ve elektrik iletkenliği gibi önemli malzeme özellikleri sergiler (Kim et al., 2009; Shim, Starkovich, & Kotov, 2006). Karbon nano tüpler çeşitli kaplama yöntemleri ile kaplanabilmektedir. Bunlardan biri parçacıkların bir banyodan bir metal matris üzerine çökeltilmesidir. Yapılan araştırmalar sonucunda, kobalt gibi bazı metallerin eklenmesi ile tek katmanlı mükemmel tüpler elde edilmiştir. Kobaltın seçimi, manyetik bir metal olması gerçeğine dayanır. Kobalt kaplı karbon nanotüpler, çok farklı elektrik ve manyetik özelliklere sahiptir. Ayrıca karbon nano tüpler, süper yoğun, hafif kompozit malzemelerde nano ölçekli fiberler olarak düşük yoğunlukları ile birleştikleri yüksek sertlik ve esneklik artırıcı malzeme olarak kullanılabilir (Chen, Xia, Peng, Li, & Xie, 2000). Karbon nantüpün kompozit üretiminde saf kullanımı Al_4C_3 bileşiğinin oluşumu ve bu bileşiğin üretilen kompozitin özelliklerinin olumsuz yönde etkilemesidir (Li, Qiu, Luan, & Li, 2017). Bu çalışmanın amacı, çoğul duvarlı karbon nanotüpün kobalt ile kaplanabilirliğinin araştırılması ve kompozit üretiminde kobalt kaplanmış karbon nantüpün bir alternatif hale getirilmesidir.

YÖNTEM

Güçlendirici parçacıklarının kaplanması, olumsuz/istenmeyen ara yüzey reaksiyonunu önlemek ve matris ile güçlendirici arasında daha iyi bağ oluşumun yani ıslatılabilirliği arttırmak için benimsenen başarılı tekniklerden biridir (Mallory, Hajdu, Electroplaters, & Society, 1990). Kaplama teknikleri, takviye özelliklerinin bozulmadan daha iyi, homojen ve ince bir tabaka kaplamasına ulaşmayı amaçlamaktadır. Bu çalışmada, kompozit malzemelerde takviye olarak kullanılan çoğul duvarlı karbon nanotüpün yüzey özelliklerini iyileştirmek amacıyla kobalt ile kaplanması üzerinedir (Pantano, 2012). Kullanılan karbon nano tüpün dış çapı 8-10 nm iç çapı 5-8 nm, uzunluğu 1-3 µm, gerçek yoğunluğu 2,4 gr/cm3, spesifik yüzey alanı 240 m^2/gr ve saflığı > %92 üzerinde olup siyah renklidir.
Yüzey kimyasını değiştirmek için karbon nantüpler akımsız kaplama öncesi 15 saat asit işleme (HNO_3 :H_2SO_4 = 1 : 3) maruz bırakılmışlardır. Akımsız kaplama işleminde, partiküllerin yüzeyleri hassaslaştırma, aktivasyon işlemlerine tabi tutuluş ve devamında kobalt kaplama banyosuna alınarak kaplama işlemi gerçekleştirilmiştir (Kilicarslan, Toptan, & Kerti, 2012). Hassaslaştırma işlemi 1 litre saf su içerisinde 25.5 gr $SnCl_2.2H_2O$+8.3ml HCI 0.25 gr çözeltisinde 15 dk karıştırılarak, aktivasyon işlemi 1 litre saf su içerisinde $PdCl_2$ + 20.8 HCl çözeltisinde 15 dk karıştırılarak gerçekleştirilmiştir. Her iki aşamada sıcaklık 90±2^oC olarak ayarlanmıştır. Hassaslaştırılan ve aktifleştirilen partiküller Tablo 1'de gösterilen kaplama banyosuna alınmış ve 30 dk süreye 90±2^oC sıcaklıkta kaplama işlemine maruz bırakılmıştır. Akımsız kaplama banyosunun pH ölçümleri pH metre ile tartım işlemi ise 0,0001 g hassasiyetli terazi ile gerçekleştirilmiştir. Kaplama banyosu manyetik karıştırıcı ile karıştırılmıştır. Yapılan kaplamalar 8,5±0,5 pH değeri belirlenmiştir (Firoozbakht, Monirvaghefi, & Niroumand, 2011).

Tablo 1. Akımsız kaplama işlemi sırasında banyoda kullanılan solüsyonlar ve bileşimleri

Amaç	İsim	Kompozisyonu
Kobalt kaynağı	Kobalt Sülfat	$CoSO_4$. $7H_2O$
İndirgeyici	Sodyum hipfosfat	$NaH_2PO_2.H_2O$
Kompleks Ajan	Trisodyum sitrat	$C_6H_5Na_3O_7.2H_2O$
Ph Düzenleyici	Sodyum hidroksit	NaOH

BULGULAR

Şekil 1'de akımsız kobalt kaplanmış numuneye ait taramalı elektron mikroskobu görüntüsü ve bu numuneye ait elektron dağılım spektroskopisi verilmiştir. Akımsız kobalt-fosfor kaplanmış çoğul duvarlı karbon nantüpün çapı ortalama 15.53 nm'dir. Partiküllerin yüzeyi kobalt-fosfor ile başarılı bir şekilde kaplanabilmiştir. Bu, spektrometre aracılığıyla açık bir şekilde numunenin kobalt içerdiği ile de görülebilir. Kaplama kalınlığı her bölgede aynı kalınlıkta elde edilemeyebilir. Kaplama sonrası maksimum dış çap genişliği 20.43 nm olduğu görülmüştür. Bununla birlikte, sıcaklık, banyonun konsantrasyonu ve zaman kontrol edilerek kaplama genişliği kontrol altına alınabilir (Koppad, Ram, & Kashyap, 2013).

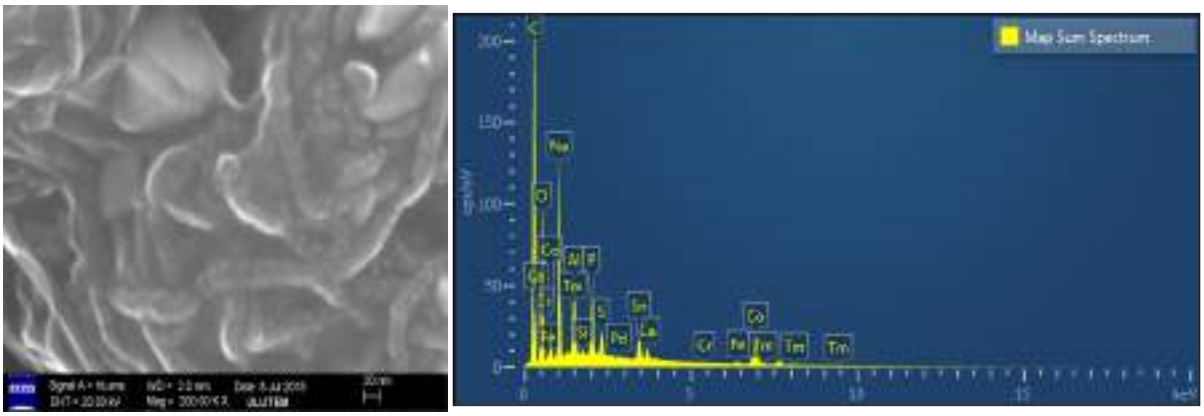

Şeki 1. Akımsız Kobalt Kaplanmış CNT

Şekil 2'de kobalt-fosfor kaplanmış numuneye ait elektron dağılım spektrumu ve elementel kompozisyon dağılımı verilmiştir. Bu grafikten numunelere ait kimyasal element içerikleri ve özellikle kobalt içeriği belirlenebilir. Bu da yapılan kaplama işleminin başarılı olduğunu göstermektedir. Özellikle ifa etmek gerekir ki, hassaslaştırma ve aktifleştirme işlemi kaplama öncesi son derece önemli olup başarılı bir kaplamanın gerçekleştirilebilmesi bu aşamalardaki işlemin kalitesiyle doğru orantılıdır. Elektron dağılım spektrumunda kalayın (Sn) görülmesi ve paladyumun (Pd) görülmemesi bu olayı açıklamaktadır. Kalay elementinin üzerine paladyumun depozite olması ve paladyumun üzerine kobaltın difüze olması gerekmektedir. Eğer paladyum kalay üzerine uygun şekilde yerleşmezse kobalt kalay ile iyi bağ kuramamaktadır. Bu nedenle paladyum ve kobalt elementi daha iyi şekilde bağ kurabildiği söylenebilir.

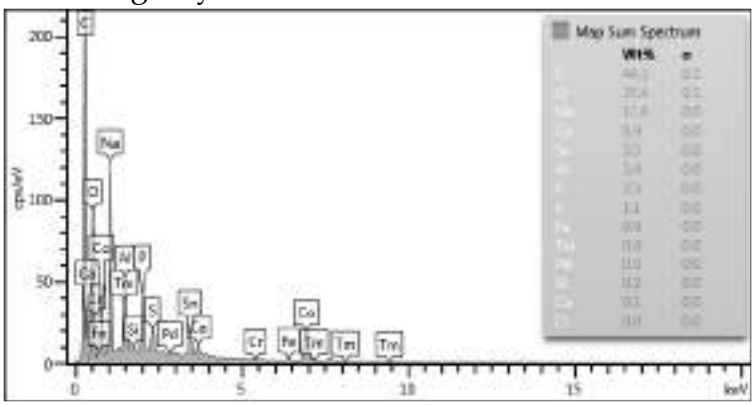

Şeki 2. Akımsız Kobalt Kaplanmış CNT'e ait EDS Spektrumu

Şekil 3 akımsız kobalt kaplanmış numunelere ait elementel haritalama görüntüsü verilmiştir. Fosfor ve kobalt içeriklerinin dağılımı ve verilen taramalı elektron mikroskobu görüntüsünde içeriği görülebilir. Bu nedenle kobalt ve fosfor elementleri dağılımının homojen olduğu belirlenmiştir.

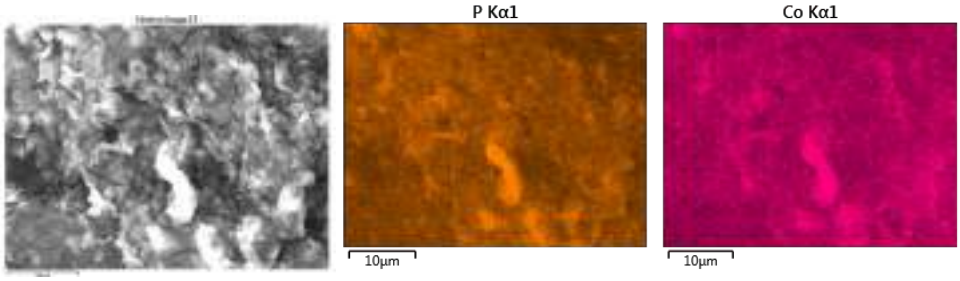

Şekil 3. Akımsız Kobalt Kaplanmış CNT'e ait Elementel Haritalama Görüntüsü

SONUÇ

Bu çalışmada, çoğul duvarlı karbon nanotüpün akımsız kaplama yöntemiyle kobalt ile kaplanabilirliği araştırılmıştır. Kaplama öncesi karbon nanotüpler asit işlemine tabi tutularak kaplama işleminin amacına uygun hale getirilmiştir. Devamında karbon nantüpler hassaslaştırma, aktifleştirme ve kobalt banyosuna iletilerek kaplama işlemi gerçekleştirilmiştir. Kaplama sıcaklığı yaklaşık olarak 90°C olarak ve PH 8.5 olarak belirlenmiştir. Uygulanan yöntemle kobalt işlemi başarılı bir şekilde gerçekleştirilmiştir. Nano boyutlu partikülleri akımsız yöntemle kaplama işleminde karşılaşılan en büyük problemlerden biri olan nano boyuttan mikro boyuta geçme görülmemesidir. Ortalama kaplama kalınlığı 15.53 nm ve maksimum kaplama kalınlığı 20.43 nm olarak tespit edilmiştir. Kobalt ve fosfor içeriği elementel haritalama ve elektron dağılım spektrumu aracılığıyla belirlenmiş ve homojen dağılım meydana geldiği tespit edilmiştir.

TEŞEKKÜR

Bu çalışmada destekleri için TÜBİTAK'a (Proje No: 217M084) teşekkür ederiz.

KAYNAKLAR

Chen, X., Xia, J., Peng, J., Li, W., & Xie, S. (2000). Carbon-nanotube metal-matrix composites prepared by electroless plating. *Composites Science and Technology, 60*(2), 301-306. doi: https://doi.org/10.1016/S0266-3538(99)00127-X

Firoozbakht, M., Monirvaghefi, S. M., & Niroumand, B. (2011). Electroless composite coating of Ni–P–carbon nanotubes on magnesium powder. *Journal of Alloys and Compounds, 509*, S496-S502.

Isaza Merino, C. A., Ledezma Sillas, J. E., Meza, J. M., & Herrera Ramirez, J. M. (2017). Metal matrix composites reinforced with carbon nanotubes by an alternative technique. *Journal of Alloys and Compounds, 707*, 257-263. doi: https://doi.org/10.1016/j.jallcom.2016.11.348

Kilicarslan, A., Toptan, F., & Kerti, I. (2012). Electroless nickel–phosphorus coating on boron carbide particles. *Materials Letters, 76*, 11-14.

Kim, C., Lim, B., Kim, B., Shim, U., Oh, S., Sung, B., . . . Baik, S. (2009). Strengthening of copper matrix composites by nickel-coated single-walled carbon nanotube reinforcements. *Synthetic Metals, 159*(5), 424-429. doi: https://doi.org/10.1016/j.synthmet.2008.10.017

Koppad, P. G., Ram, H. A., & Kashyap, K. (2013). On shear-lag and thermal mismatch model in multiwalled carbon nanotube/copper matrix nanocomposites. *Journal of Alloys and Compounds, 549*, 82-87.

Li, C., Qiu, R., Luan, B., & Li, Z. (2017). Effect of carbon nanotubes and high temperature extrusion on the microstructure evolution of Al-Cu alloy. *Materials Science and Engineering: A, 704*, 38-44. doi: https://doi.org/10.1016/j.msea.2017.06.055

Mallory, G. O., Hajdu, J. B., Electroplaters, A., & Society, S. F. (1990). *Electroless Plating: Fundamentals and Applications*: The Society.
Pantano, A. (2012). *Carbon Nanotube Based Composites: Processing, Properties, Modelling and Application*: Smithers Information Limited.
Shim, B. S., Starkovich, J., & Kotov, N. (2006). Multilayer composites from vapor-grown carbon nano-fibers. *Composites Science and Technology, 66*(9), 1174-1181. doi: http://dx.doi.org/10.1016/j.compscitech.2005.11.004.

SYNTHESIS AND CHARACTERIZATION OF $Ce_{1-x-y}Sm_xHo_yO_2$ CERAMIC ELECTROLYTES BY SOL-GEL METHOD

Ahmet Hamdi BAKIR
Kahramanmaraş Sütçü İmam Üniversitesi Fen Bilimleri Enstitüsü
ahmethamdibakir@gmail.com

Handan Özlü TORUN
Kahramanmaraş Sütçü İmam Üniversitesi Fen Bilimleri Enstitüsü
handanozlu@gmail.com

ABSTRACT: In the last few years, the decline in lignite sources has led to the search for new energy and the invention of Solid Oxide Fuel Cell has been realized. Solid oxide fuel cells are those that have high efficiency at high temperature in the fuel cell technology. Due to this feature, it can be used in many areas such as constant power generation systems, cogeneration units, military works. The main components of a solid oxide fuel cell are anode, cathode and electrolyte. The most important component for solid oxide fuel cells; These are ceramic electrolytes having oxygen ionic conductivity. The efficiency of the solid oxide fuel cell depends on the type of electrolyte used. Electrolytes with high conductivity and high efficiency between 550-700°C reduce system cost for installation and operation, increase applicability. Nowadays, zirconium based electrolytes are most commonly used as ceramic electrolytes in solid oxide fuel cells. However, these electrolytes have a high conductivity value of 1000°C and above. Cerium (IV) Oxide and Bismuth (III) oxide-based electrolytes have high conductivity at lower temperature.
In this study, CeO_2-based triple system sample materials were synthesized by sol-gel reaction and subjected to heat treatment. The structural properties of these solid ceramic electrolytes produced for solid oxide fuel cell (SOFC) are characterized by X-Ray Diffractometry (XRD), Differential Thermal Analysis - Thermo-weight meter (DTA-TG). The surface properties of solid ceramic electrolytes produced were investigated by Scanning Electron Microscope (SEM). The electrical properties are characterized by a four-point electrical conductivity method. The results of XRD measurements showed that $Ce_{1-x-y}Sm_xHo_yO_{2\ y}$ (x = 5, 10, 15, y = 5, 10, 15) samples had cubic crystallographic structure. Phase stability With DTA measurements, control and comparison of most samples has been shown to be the stable of CeO_2. The highest electrical conductivity
$Ce_{0.80}Sm_{0.10}Ho_{0.10}$ system is $6.92x10^{-3}$ $(\Omega.cm)^{-1}$ at 655 ° C.
It was found that the compound obtained as a result of the evaluations could be used in medium temperature solid oxide fuel cells.
This study was supported by KSU-BAP unit with 2018 / 2-26 coded project.

Key words: Sol-Gel Method, Solid Oxide Fuel Pilot, Ce-based ceramic electrolyte

$Ce_{1-x-y}Sm_xHo_yO_2$ SERAMİK ELEKTROLİTLERİN SOL-JEL YÖNTEMİ İLE SENTEZ VE KARAKTERİZASYONU

Ahmet Hamdi BAKIR
Kahramanmaraş Sütçü İmam Üniversitesi Fen Bilimleri Enstitüsü
ahmethamdibakir@gmail.com

Handan Özlü TORUN
Kahramanmaraş Sütçü İmam Üniversitesi Fen Bilimleri Enstitüsü
handanozlu@gmail.com

ÖZET: Son yıllarda giderek azalan linyit kaynakları yeni enerji arayışlarını doğurmasıyla birlikte Katı Oksit Yakıt Pili buluşu gerçekleşmiştir. Katı oksit yakıt pilleri, yakıt pili teknolojisi içerisinde yüksek sıcaklıkta yüksek verimliliğe sahip olandır. Bu özelliğinden dolayı sabit güç üretim sistemlerinde, kojenerasyon ünitelerinde, askeri çalışmalar gibi birçok alanda kullanılabilmektedir. Bir katı oksit yakıt pilinin temel bileşenleri anot, katot ve elektrolittir. Katı oksit yakıt hücreleri için en önemli bileşen; oksijen iyonik iletkenliğine sahip olan seramik elektrolitlerdir. Katı oksit yakıt hücresinin verimliliği kullanılan elektrolitin çeşidine bağlıdır. 550-700 ^oC arasında yüksek iletkenlik ve yüksek verim özellikleri gösteren elektrolitler kurulum ve işletme için sistem maliyetini azaltır, uygulanabilirliği artırır. Günümüzde katı oksit yakıt pillerinde seramik elektrolit olarak en çok bilinen kullanılan zirkonyum tabanlı elektrolitlerdir. Ancak bu elektrolitler 1000 C ve üstünde yüksek iletkenlik değerine sahiptir. Seryum(IV) Oksit ve Bismuth(III) oxide tabanlı elektrolitler ise daha düşük sıcaklıkta yüksek iletkenliğe sahiptir.
Bu çalışmada CeO_2 tabanlı üçlü sistem örnek materyalleri sol jel metodu ve sonrasında her biri ısıl işleme tabi tutularak sentezlenmiştir. Katı oksit yakıt pili (KOYP) için üretilen bu katı seramik elektrolitlerin yapısal özellikleri X-Işınları Difraktometresi (XRD), Diferansiyel Termal Analiz - Termo ağırlık ölçer (DTA -TG) ile karakterize edilmiştir. Üretilen katı seramik elektrolitlerin yüzey özellikleri Taramalı Elektron Mikroskobu (SEM) ile incelenmiştir. Elektriksel özellikleri ise dört nokta elektriksel iletkenlik yöntemi yoluyla karakterize edilmiştir. XRD ölçümleri sonuçları, $Ce_{1-x-y}Sm_xHo_yO_2$ (x=5, 10, 15, y=5, 10, 15) örneklerinin florit yapıda olduğunu göstermiştir. Sıcaklığa bağlı elektriksel iyonik iletkenlik ölçümleri sonucunda en yüksek elektriksel iletkenlik $Ce_{0.80}Sm_{0.10}Ho_{0.10}$ sistemi için 655°C'de 6.92x10-3 (Ω.cm)-1'dir.
Değerlendirmeler sonucunda elde edilen bileşiğin orta sıcaklık katı oksit yakıt hücrelerinde kullanılabileceği bulgulandı.
Bu çalışma, KSÜ-BAP birimi tarafından 2018/2-26 kodlu proje ile desteklenmiştir.

Anahtar sözcükler: Sol-Jel Yöntemi, Katı Oksit Yakıt Pili, Ce- tabanlı seramik elektrolit

QUALITY OF FRESH-CUT SULTANA TABLE GRAPE COATED WITH SODIUM ALGINATE DURING STORAGE

Ayşe Tülin OZ[1], Büşra ERYOL[1]
Osmaniye Korkut Ata University,Engineering Faculty,Food Engineering Department
Karacaoğlan Campus,80000 Osmaniye, Turkey

ABSTRACT: This study was carried out to investigate the effect of different sodium alginate concentrations on storage time and quality of fresh-cut Sultani seedless grape varieties. It was stored at 1 ° C and 90% relative humidity for 25 days. The results of the present research could also be used to reduce the risks of microbial decay. The effect of the fruit on other quality parameters has produced noticeable differences. The treated fruits showed less weight loss and microbial decay,; however, there was no significant difference between the fruits treated with 0.75% and 1.5% sodium alginate (Na-Alg). The changes in the total phenolic and antioxidant capacities of the grapes covered with sodium alginate were obtained higher than the control fruit. In general, it has been found that it has more external competence than fruits coated with Sodium Alginate (Na-Alg).
Keywords:Grape,Sodium Alginate, Post-harvest preservation,Quality

SODYUM ALJİNAT İLE KAPLANAN AZ İŞLENMİŞ SOFRALIK SULTANİ ÇEKİRDEKSİZ ÜZÜM ÇEŞİDİNİN DEPOLAMA SIRASINDA KALİTESİNE ETKİSİ

Ayşe Tülin ÖZ[1] , Büşra ERYOL[1]
Osmaniye Korkut Ata Üniversitesi,Mühendislik Fakültesi,Gıda Mühendisliği Bölümü
Karacaoğlan Kampüsü,80000 Osmaniye, Türkiye

ÖZET: Bu çalışma, az işlenmiş taze sofralık Sultani çekirdeksiz üzüm çeşidinde Sodyum Aljinat uygulamasının depolama süresine ve kalitesine etkisini belirlemek amacı ile yürütülmüştür. Yeme olumu döneminde hasat edilen Sultani Çekirdeksiz üzümü sap kısımları üzüm tanesi üzerinde kalacak şekilde tanelenerek üç farklı Sodyum Aljinat konsantrasyonlarına daldırma işlemi uygulanarak kaplama yapıldıktan sonra polipropilen kaplarda 1 °C ve % 90-95 oransal nemde 25 gün süreyle depolanmıştır. Az işlenmiş sofralık Sultani çekirdeksiz üzüm tanelerinin yenilebilir sodyum aljinat kaplama uygulamasının meyvenin mikrobiyolojik kalitesini ve mikrobiyal bozulma risklerini azaltmak için de kullanılabileceğini araştırma sonucu elde edilmiştir. Meyvenin diğer kalite parametreleri üzerindeki etkisi gözle görülür farklar meydana geldiği belirlenmiştir. Muamele edilen meyvelerin ağırlık kaybı ve mikrobiyal bozulma miktarı kontrol grubuna göre daha sınırlı kalmıştır. Toplam çözünebilir kuru madde (TSS), titre edilebilir asitlik (TA) gibi lezzetle ilişkili faktörler, muamele edilmiş meyvelerde daha yüksek olduğu, bununla birlikte,% 0.75 ve % 1.5 sodyum aljinat (Na-Alg) ile muamele edilen meyveler arasında önemli bir fark olmadığı belirlenmiştir. Sodyum Aljinat ile kaplı üzümlerin toplam fenolik madde ve

antioksidan kapasiteleri kontrol meyvesinden daha yüksek olduğu belirlenmiştir. Kontrol uygulamalarında depolama süresi sonunda görülen mikrobiyal bozulmanın önemli düzeyde arttığı ve pazarlanamaz seviyeye ulaştığı belirlenmiştir. Genel olarak, Sodyum Aljinat (Na-Alg) ile kaplanmış meyvelerin görsel ve pazarlama kalitesinin daha olduğu saptanmıştır.

Anahtar Kelime: Üzüm, Sodyum Aljinat, Hasat Sonrası Muhafaza, Kalite

1.Introduction

Grape is a non-climatic type of fruit with low physiological activity.The table grape (Vitis vinifera) is one of the most perishable fruits and is often subject to postharvest disorders such as stem (rachis) browning, weight loss, berry drop, and fungal decay (Sousa et al., 2013). These effects are mainly caused by pathogenic fungi such as B. cinerea. Low temperature combined with sulfur dioxide fumigation has been routinely used to treat table grapes for storage. However, this method has been increasingly challenged, due to the phytotoxicity of this chemical preservative, development of antimicrobial resistance, and food safety concerns regarding effects of chemical residues on human health and the environment (Taylor, 1993). Therefore, development of safer, more effective, economical, and convenient storage methods are needed in order to control postharvest fungal decay and maintain food quality and safety of table grapes.
The use of various eco-friendly applications has been gaining importance in recent years in order to increase the strength and prevent rotting during the preservation of fresh fruits and vegetables.
Healthy eating and healthy lifestyle is on high demand currently at the global level. This concept has raised the need for better preservation of the perishables such as fruits and vegetables, as they are an abundant source of bioactive compounds, vitamins and minerals (Diaz-Mula, Serrano, & Valero, 2012). Edible coatings have been used to enhance the shelf life of whole as well as fresh-cut fruits and vegetables. They have been proven to retard physiological processes such as respiration, degradation of cell wall, transpiration and also restrict microbial action; thereby preserving the quality of the fruit and vegetable (Ali, Muhammad, Sijam, & Siddiqui, 2011). In recent years, a lot of research work has been carried out on application of various kinds of edible coatings. Generally, they are based on polysaccharides, proteins and lipids for extending the shelf life of various horticultural commodities (Chen et al., 2016; Gardesh et al., 2016; Khaliq, Mohamed, Ali, Ding, & Ghazali, 2015; Suseno, Savitri, Sapei, & Padmawijaya, 2014; Synowiec et al., 2014). Out of these coating materials, polysaccharide based edible coatings such as alginate are gaining popularity in recent times.
Alginate is obtained from the brown seaweed belonging to the family *Phaeophyceae*. It has been proven to be a potential coating material for causing delay in the ripening process and its effectiveness enhances on incorporation of any antioxidant or antimicrobial agents. Alginate comprises of colloidal properties such as thickening, stabilizing etc and therefore, it could be effectively used in coating and film preparation (Benavides, Villalobos-Carvajal, & Reyes, 2012). Studies on the application

of alginate coating on whole fruits have demonstrated the enhancement of shelf-life of strawberry (Peretto et al., 2017), mandarin (Chen et al., 2016), carambola (Gol et al., 2015), sweet cherry fruit (Diaz-Mula et al., 2012).
Edible coatings could also be enriched with certain additives such as antibrowning and antimicrobial agents, which in turn enhance the performance of the native edible coating material (Dhall, 2013). However, enriching the edible coatings with natural plant extracts and its application on various fruits and vegetables is gaining popularity over the use of chemical preservatives. Use of chitosan coating enriched with moringa leaf extract on avocado (Tesfay & Magwaza, 2017) and alginate coating enriched with grape seed extract on grapes (Aloui et al., 2014), have demonstrated improvement in their overall quality. The study, was carried out to determine the effects of different sodium alginate concentrations on the pathological and physiological disorders and quality changes in the storage of Sultani seedless grapes.

2. Materials and methods

2.1. Fruit material and experimental design

In the 2018 product year, Sultani Seedless grape varieties, which were harvested from a producer vineyard in Sarıgöl district in Manisa province, were used. Grape berries were packed and then they were brought to Osmaniye Korkut Ata University, Department of Food Engineering. Sultana table grape fruits were harvested at fully ripe at harvest stage.Sultana table grape were washed with distilled water, then berries were removed from cluster with 1-2 mm stem by scissors manually. Sodium Alginate coatings were prepared following the protocol of Rojas-Grau et al. (2008). Film forming solution was prepared by dissolving alginate powder (0%,0.75% and 1.5% in distilled water and heated at 75°C with continuous stirring until the clear solution formed. Excess water removed from grape berries.The arils were divided into three groups for the treatments.The grape berries were dipped in the corresponding solutions for 2min., then left to dry. After coating, residue of coating solution was removed on to sterilized sieved trays at 20 °C. After coating, grape berries (250 g) were transferred in polypropylene boxes (280 mL) .The boxes were stored for 20 days at 1 °C and 90% relative humidity.

2.2. Analytical determinations

2.2.1.Weight loss percentage

The weight loss during storage was measured by monitoring the weight changes of the fruit. The weight loss was considered the difference between the initial and final weight of coated and uncoated fruit. The results are expressed as the percentage loss from the initial weight, according to the method described by Meng et al. (2008). Weight loss was expressed as percentage of initial weight.

2.2.2 Decay rate of grapes

The grapes were examined for any microorganism infection during storage. Thirty grapes were used for each measurement. The decay percentage of coated and uncoated fruit was calculated as the number of decayed fruit divided by the initial number of all grapes multiplied by 100 (Gol et al., 2013).

2.2.3 Colour

Surface colour of the samples was determined using Labscan XE colorimeter (HunterLab, Inc., Reston, VA, USA) to assess the L-(lightness), a-(greenness) and b-(yellowness) values at 400–700 nm range spectral resolution of 10 nm and a wavelength accuracy of 1 nm under CIE Illumination D65 and d/10° illumination. Standardization was done using a black tile followed by a white tile. Total colour difference (TCD) was calculated using L, a, b-values as per Eq. (1): TCD = $(\Delta L)2 + (\Delta a)2 + (\Delta b)2$ (1) where ΔL, Δa and Δb represents the difference in L, a, b-values at a particular interval from the respective initial values.

2.2.4 Sensory Analyis

One hundred untrained tasters responded to questions regarding their acceptance and purchase intention. For acceptability of appearance, flavour, colour, taste, aftertaste, texture and overall assessment, a nine-point hedonic scale was used (1: extremely poor; 5: excellent). The intent to purchase was assessed on a five-point structured hedonic scale (1: certainly would not buy, 5: certainly would buy) (Santos et al., 2012).

2.2.5 Statistical analyses

Each result was expressed as the mean value ± standard deviation. All statistical analyses were performed using SPSS version 13.0 (SPSS,Inc., Chicago, IL). One-way ANOVA and the least significant difference (LSD) test were used to determine the significance of mean differences among treatments and storage times. Differences at $P < 0.05$ were considered significant and are indicated using different letter designations.

2.2.6. Total phenolics concent and Scavengig

Total phenolics content in the fresh sample was determined according to the Folin-Ciocalteau procedure (Singleton, Orthofer, & Lamuela-Ranventos, 1999). Briefly, 5 g of sample was extracted with 80% ethanol. To 0.1 mL aliquot of the sample, 2.9 mL distilled water, 0.5 mL of 1 N Folin-Ciocalteau reagent and 2 mL Na_2CO_3 (20%) was added. After an incubation period of 60 min, the absorbance of the mixture was measured at 760 nm using a UV–visible spectrophotometer (Varian, Cary 50, Varian, USA). The results were expressed in terms of mg of gallic acid equivalent per 100 g fresh weight of the sample using gallic acid as a standard.

2.2.7 Measurement of total soluble solids (TSS), titratable acidity (TA), and total phenolic content (TPC)

Measurement of total soluble solids (TSS), titratable acidity (TA), and total phenolic content (TPC)

Replicate fresh juice samples (5 mL) made using 15 berries per replicate were used to determine TSS and TA. TSS was measured using a digital refractometer (PR-101 Palette, Atago, Tokyo, Japan) and expressed as percent soluble solids. Titratable acidity (TA) was determined by titration with 0.05 mol/L NaOH to pH 8.2 and expressed as grams of tartaric acid equivalents per liter of juice. Ten grapes from each replicate cluster were cut into small slices and mixed; five grams of each mixture was extracted using an ultrasonic cleaner (KQ-500DE, Kunshan Ultrasonic Instruments Co. Ltd.) for 30 min in 25 mL methanol acidified with 0.05% HCl. Each extract was centrifuged at 12,000 × g for 20 min and supernatants were analyzed for total phenolic content (TPC). TPC was determined according to the method by Kähkönen et al. (1999). Samples (600 µL, three replicates) were introduced into test tubes; 3.0 mL of Folin-Ciocalteu's reagent and 2.4 mL of sodium carbonate (7.5%) were added. The tubes were mixed and allowed to stand for 30 min in the dark. Absorption at 765 nm was measured (shimadzu-2450 UV–vis spectrophotometer). Results are expressed as mg gallic acid equivalent (GAE) kg^{-1} FW (where FW designates fresh weight).

3.RESULT AND DISCUSSION

The treatments of coatings on fruits provides a semi-permeable membrane on fruit to movement of water. Thus reducing moisture loss from fruit surface and also a modified atmosphere between the fruit and environment. The rateof weight loss increased with the storage timeat1°C. Treat ments significantly ($P<0.0001$) retarded the loss in weight and the weight loss values of these treatments were lover than control. Such delay in weight loss may be attribu ted to the effect of NaAlg on decreasing the respiration rateof fruits.Studies revealed that aminimum loss in water content may sharply affect berry appearance of table gr apes, leading to browning, wilting and shrivelling.In deed, the highest changes in ber ry appearance were observed in control.

3.1. Weight Loss(%)

There were statistically significant differences between control and coating treatments throughout the storage. At the end of storage, 12.7% weight loss was measured in the control group, 8,5% in NaAlg (0.75%) coating itself, while it was 5.4% in NaAlg (1.5%). The percentage of weight loss was mostly observed in the control fruit. The least change was observed in the coating fruit of 1.5%. As a result, the coating material positively affected the weight loss percentage in the grape.

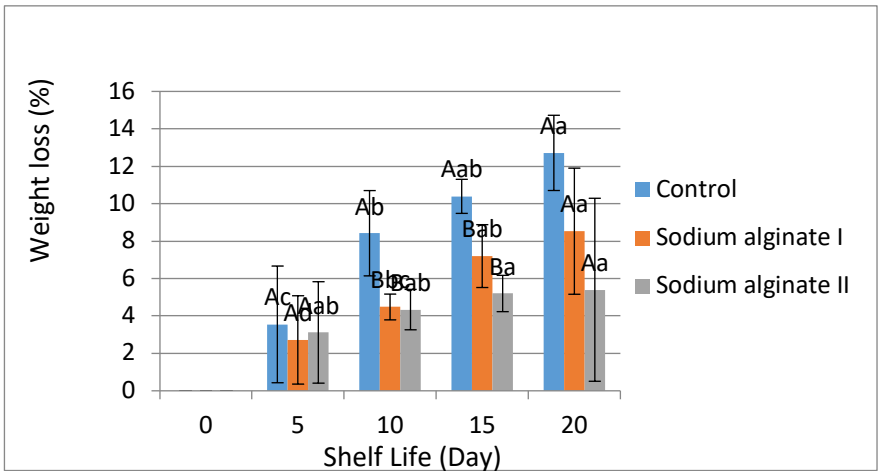

Fig.1.Sodium alginate activity in grape versus mass loss. Values are the mean (± SD) of three enzymatic analyses of three lots of grapes from different bunches. Values with different letters are significantly different ($p < 0.05$).

3.2.Firmness(N)

Fruit firmness has been accepted as one of the most important factors that affect the quality of fruit commodities during postharvest storage. At the begining of storage, grape firmness were around 2 N while it decreased to 1.68 control 1.7 (NaAlg I), and 1.96 for (NaAlgII), coating did not affect firmness loss as control during the 20 days of storage. The firmness did not show much change on the 5th and 10th day analyzes. However, a significant decrease was observed in the control group fruits at the end of the storage period. The tightness of the control grapes decreased sharply with increasing storage time in all varieties. The coating application provided the grape tightness during storage.ANOVA results also showed that the fruit deformation force (N) was expressed as the fruit hardness of grapes. The reduction in firmness loss by alginate coating can be explained by minimizing weight losses through coating application that has been reported in table grapes (Sánchez González et al., 2011), plum (Liu, Wang, & Young, 2014),and apples (Olivas et al., 2007) by different edible coatings.

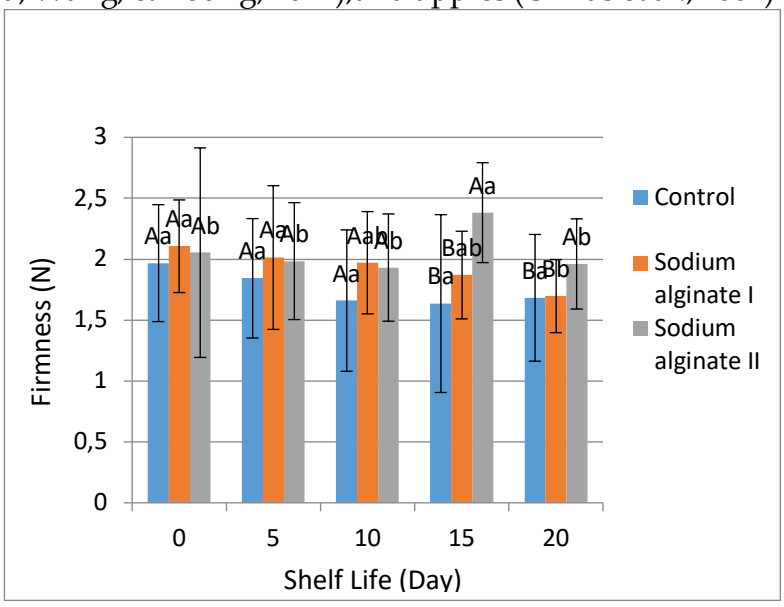

Fig.2.Sodium alginate activity in grape versus firmness. Values are the mean (± SD) of three enzymatic analyses of three lots of grapes from different bunches. Values with different letters are significantly different ($p < 0.05$).

3.3.Decay and Browning Indeks

Occurs during the storage period from physiological and fungal disorders were determined and calculated according to scale 0-5. In the experiment, the highest rot development was observed in the control group. It was observed in sodium alginate coated grapes at a concentration of 0.75%.Pathogenic and physiological losses in grape cluster during storage increased.

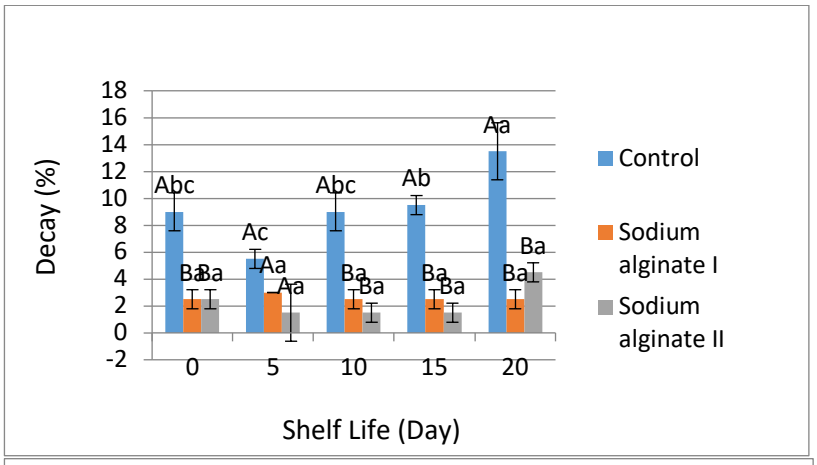

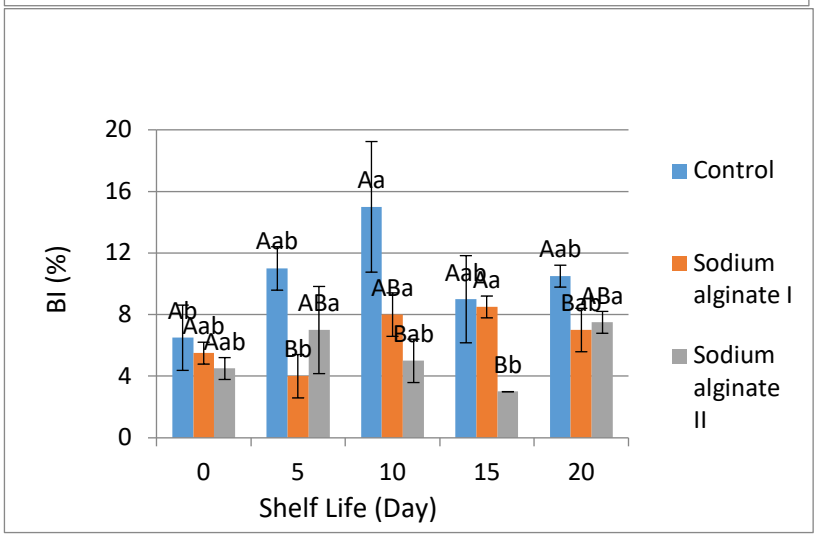

Fig.3,4.Sodium alginate activity in grape versus decay and browning indeks.. Values are the mean (± SD) of three enzymatic analyses of three lots of grapes from different bunches. Values with different letters are significantly different ($p < 0.05$).

3.4.Sensory Evulatıon

Changes in sensory characteristics of various grape samples are shown. However, visual quality, browning indeks, flavor, and texture of all samples underwent significant ($P < 0.05$) changes with storage time. All sensory quality attributes of the control became unacceptable after only of storage.Postharvest coating of grapes with this treatment decreased respiration rate,decreased water loss, and conferred higher resistance to gray mold.

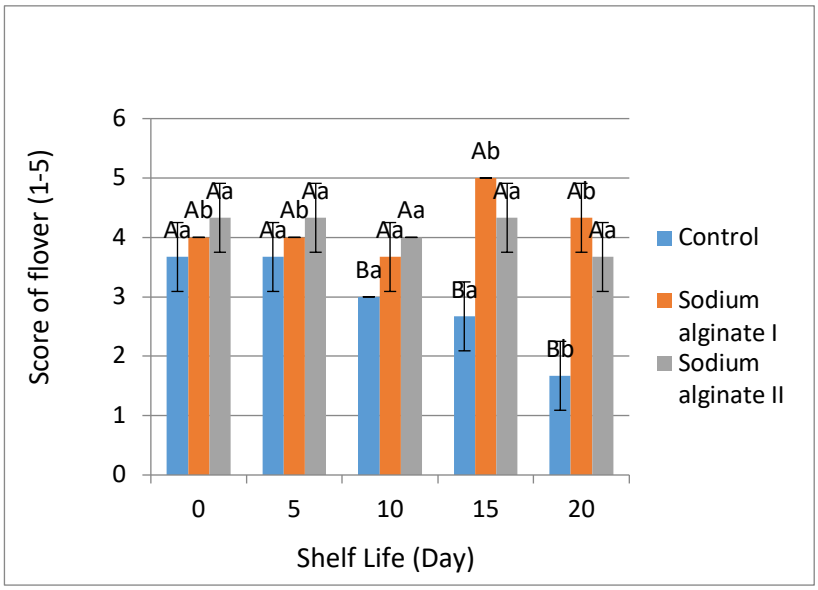

Fig.5.Sodium alginate activity in grape versus sensory score.Values are the mean (± SD) of three enzymatic analyses of three lots of grapes from different bunches. Values with different letters are significantly different ($p < 0.05$).

3.5.TSS(%)

After firmness determination, the fruit from each replicate were manually peeled and the flesh tissue was cut in small pieces and used to determine total soluble solids concentration (TSS) and titratable acidity (TA) in duplicate.While obtained no significant differences among coating treatments in regard to soluable solid content (TSS), the highest TSS was observed in (NaAlgII). Although it was not important, TSS caused a change in the grape fruits at the end of the 20th day. The effects of different coating applications on the TSS of grapes showed no stable change. Changes in the amount of TSS were limited with the advancement of storage time. Investigation of the Effectiveness of Different Coating Materials in the Storage of Seedless Sultana Grape Varieties It is important that the storage temperature is low and the breathing effect of coating application is important (Wills et al., 1998; Thompson et al., 2002; Karaçalı, 2012).

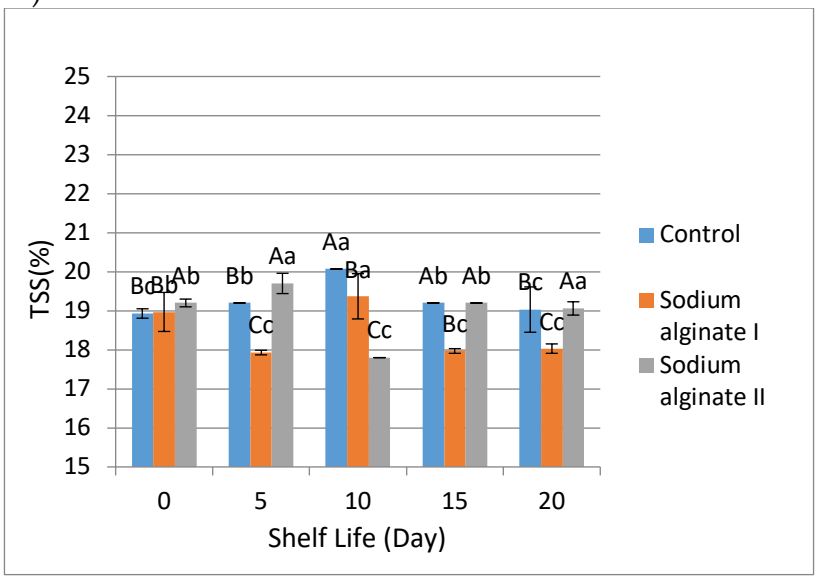

Fig.6.The effect of different coating concentrations on the brix value in grapes. Values are the mean (± SD) value of the three enzymatic analyzes obtained from three groups of grapes. Values with different letters are significantly different ($p <0.05$).

3.6.Color

The colour of the grapes was measured at three different equatorial positions of the fruit with the CIELab system. Colour parameters a*, b*and L* were measured in a CR-300 colorimeter (MINOLTA Co., Osaka, Japan), as recommended by the International Commission on Illumination (CIE,1986).
L color ValueofSultana Table grape between 30.89 to 38.43at the begining of storage. However there is some fluctating during storage. Na-
Alg treatmented groups L color value higher than control group.
L color value did not observe a stable change in table fruit grape. However, at least L color change occurs in grapes coated with sodium alginate II concentration.

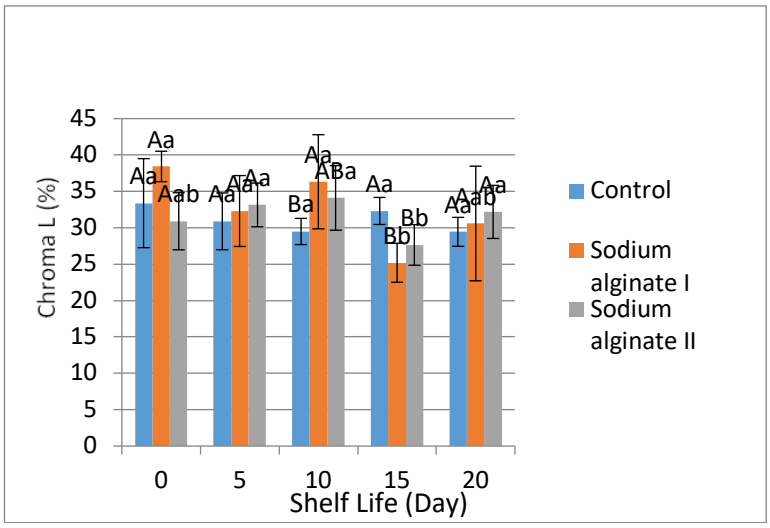

Fig.7.The effect of different coating concentrations on the L color value in grapes. Values are the mean (± SD) value of the three enzymatic analyzes obtained from three groups of grapes. Values with different letters are not significantly different. (p <0.05).

Table shows the changes in Hunter L-, a- and b-values of samples during the storage. Peel colour is a very important aspect which determines the quality of a fruit in terms of maturity and harvest time. Consumer preference is also greatly influenced by the colour of the fruit peel. A decrease in L-value indicates browning of the tissues. There were non-significant (P > 0.05) differences in the L-values of all the coated samples on the however the difference was significant (P < 0.05) when compared to control. Overall, significant (P < 0.05) differences were observed in the L-values of control with respect to coated samples during the storage period of 20 days. A decline in a-values was observed in case of control as well as coated samples during the storage. The samples were non-significantly (P > 0.05) different from each other.

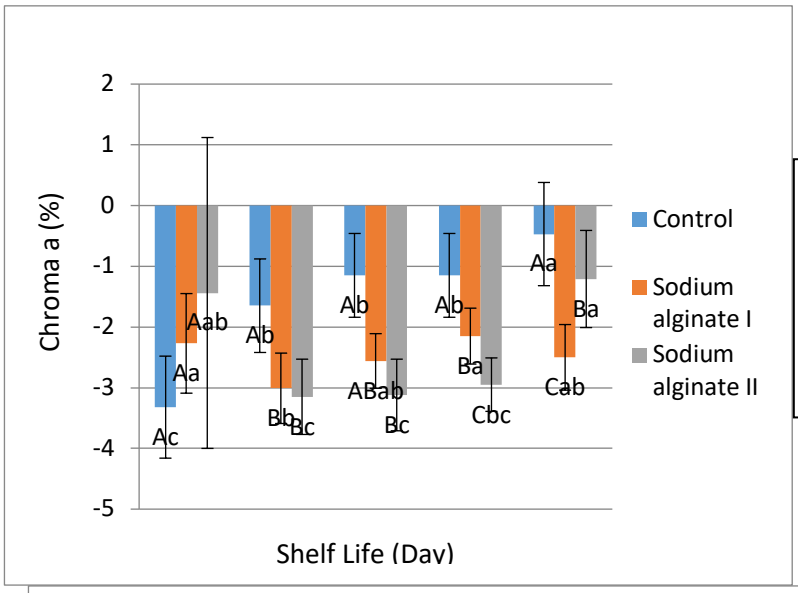

Fig.8.The effect of different coating concentrations on the color value in grapes. The values are the mean (± SD) value of the three enzymatic assays obtained from three groups of grapes. ($p < 0.05$).

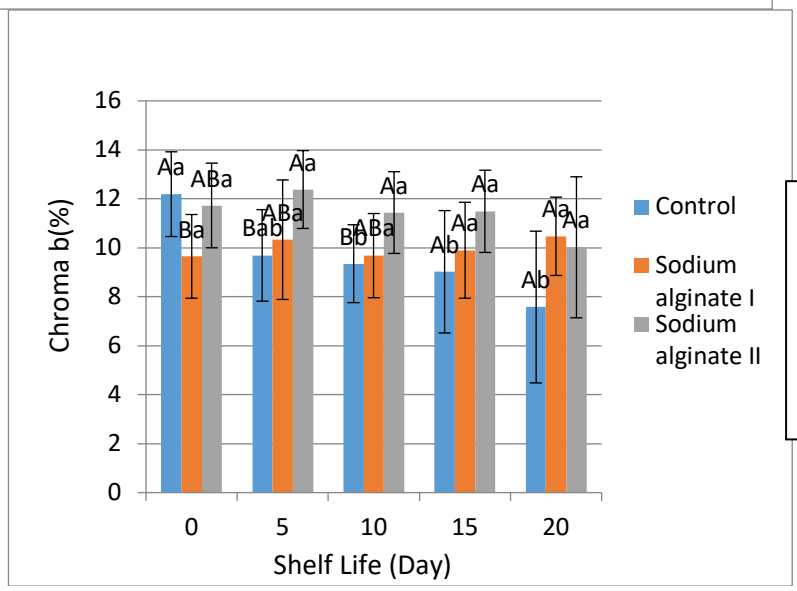

Fig.9.Effect of different coating concentrations on the color value of b in grapes. The values are the mean (± SD) value of the three enzymatic assays obtained from three groups of grapes. ($p < 0.05$)

Following H values, b values showed a reduction in control in the case of coated samples over a 20 day storage period. Total colour difference was determined to understand the effect of coatings on the colour of the samples.

3.7.pH and T.A

The value of pH did not significantly change and nearly remained constant throughout storage in coated and uncoated grape samples.

The amount of grape TA is a low fruit and decreases during storage. According to the results of the study, TA values did not show a stable decrease according to the initial values at the end of the 20 day storage period. At the end of the storage period, it was found that the amount of TA was higher in some dayscompared to the control group in some applications and these applications decreased the acid decrease relatively.

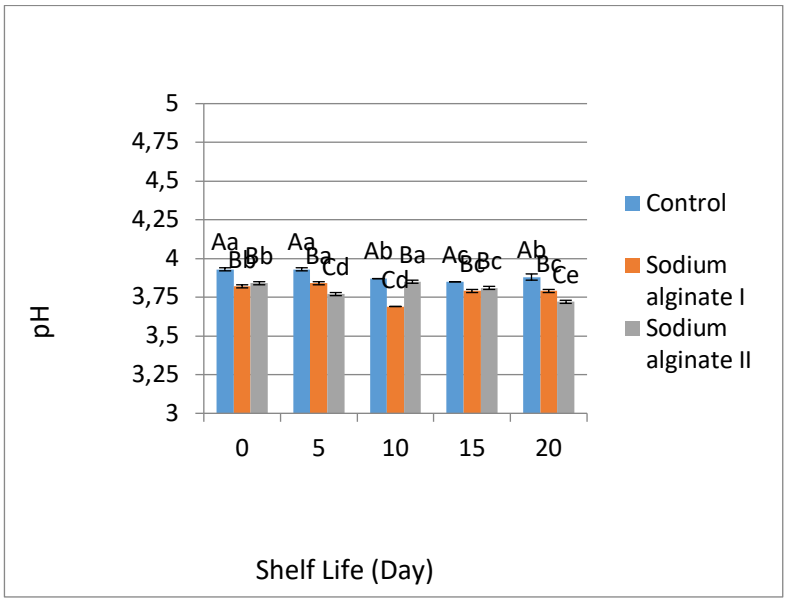

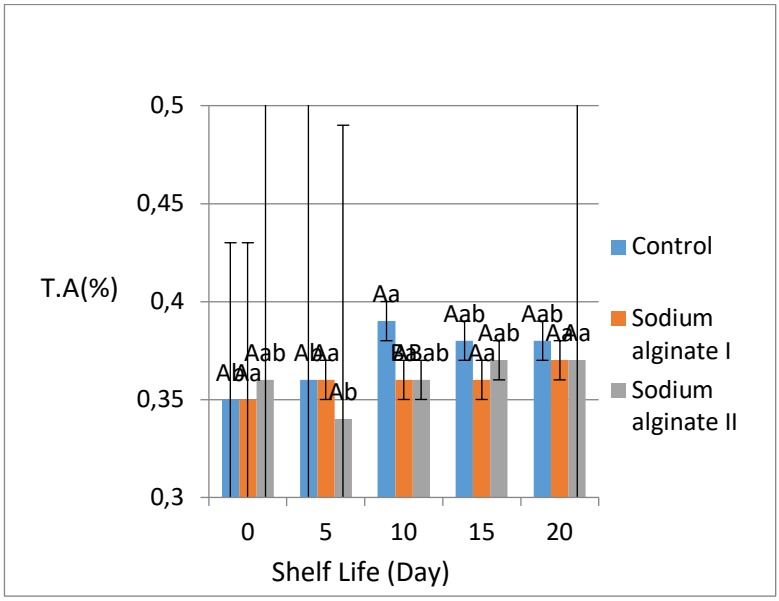

Fig.10,11.pH and T.Avalues of sodium alginate coated grapes. Vertical bars represent the standard deviation of the vehicles. The least significant difference (LSD) was calculated in P = 0.05 to compare the differences between means. There was no significant difference.

3.6 Total phenolics

Phenolic compounds play an important role especially in the color, taste and aroma characteristics of grapes, and the phenol content of the grapes may vary depending on , climate and storage temperatures (Kök et al., 2017). Phenolics are the secondary metabolites present in fruits and vegetables that possess antioxidant activity by capturing free radicals, produced during oxidative stress (Peretto et al., 2017). They are also capable in promoting auto-oxidation, chelation of metal ions and could cause modulation in the activity of some enzymes (Howard, Clark, & Brownmiller, 2003). In terms of these characteristics changes depending on applications increased or decreased at the end of retention. Fig. 12 represents the changes in the total phenol (TP) content in grape subjected to different coating treatments during storage period. The maximum retention of TP was found in sodium alginate II coated samples

(60%),sodium alginate I coated sample (58%), and control fruits (30%) at the end of 20th day. In control sample, the TP content showed a sharp decline after 20th day of storage which reached.

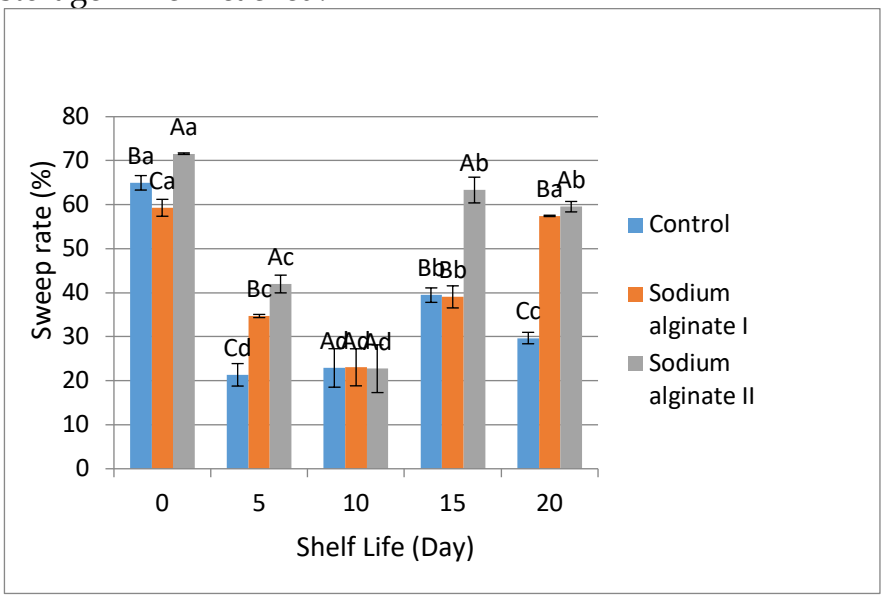

Fig.20.

Conclusion

Edible coatings and films containing natural extracts are being used widely to enhance the overall quality of fruits and vegetables with extended shelf life. The present study confirmed that the use of sodium alginate could enhance the quality of the grape fruit. Alginate based coatings not only improved the visual attributes of grape but also efficiently retained the nutritional parameters by retarding the respiration rate and the reby delaying senescence. Also, its effect on different fruits and vegetables needs to be introspected.

The results of this study indicate that edible sodium alginate coatings were effective in maintaining the physicochemical, sensory and microbiological qualities of table grapes. The sodium alginate were responsible for delaying the ripening process of the grapes resulting in decreased weight loss, soluble solids and increased moisture retention and preservation of the titratable acidity values. The flavour was the only sensory attribute in which the control group obtained a significantly better score than the samples. Based on these results, edible coatings with can be used to improve the post-harvest quality of grapes.

REFERENCES

Li, S., Zhang, L., Liu, M., Wang, X., Zhao, G., & Zong, W. (2017). Effect of poly-ε-lysine incorporated into alginate-based edible coatings on microbial and physicochemical properties of fresh-cut kiwifruit. Postharvest Biology and Technology, 134, 114–121. doi:10.1016/j.postharvbio.2017.08.01.

Konuk Takma, D., & Korel, F. (2017). Impact of preharvest and postharvest alginate treatments enriched with vanillin on postharvest decay, biochemical properties, quality and sensory attributes of table grapes. Food Chemistry, 221, 187–195. doi:10.1016/j.foodchem.2016.09.195

Shen, Y., & Yang, H. (2017). Effect of preharvest chitosan- g -salicylic acid treatment on postharvest table grape quality, shelf life, and resistance to Botrytis cinerea -induced spoilage. Scientia Horticulturae, 224, 367–373. doi:10.1016/j.scienta.2017.06.046

Nair, M. S., Saxena, A., & Kaur, C. (2018). Effect of chitosan and alginate based coatings enriched with pomegranate peel extract to extend the postharvest quality of guava (Psidium guajava L.). Food Chemistry, 240, 245–252. doi:10.1016/j.foodchem.2017.07.122

Karaçalı, İ. 2002. Bahçe Ürünlerinin Muhafaza ve Pazarlanması. Ege Üniversitesi Ziraat Fak. Yayınları No:494, İzmir.

Lurie, S., E. Pesis, O. Gadiyeva, O. Feygenberg, R. Ben-Arie, T. Kaplunov, Y. Zutahy and A. Lichter, 2006. Modified ethanol atmosphere to control decay of table grapes during storage. Postharvest Biol.Tech. 42(3): 222-227

Çoban, H., Yuvarlak çekirdeksiz üzüm çe idinde potasyum nitrat uygulamalar n n verim ve baz kalite kriterlerine etkisi üzerinde ara t rmalar , ANADOLU, J of AARI 12(2):65-72, (2002).

Altındişli, A., S. Kara, H. Çoban ve E. lter, Erken sofralık olarak hasat edilen yuvarlak çekirdeksiz üzümlerde baz olgunluk durumlar n n belirlenmesi üzerinde bir ara t rma , Bahçe ürünlerinde muhafaza ve pazarlama sempozyumu, 61- 65, Yalova, (1997)

Keskin, N., Keskin, S., Çavuşoğlu, Ş., Şevgin, N., Kunter, B., Karadoğan, B., Kalkan, N.N., 2015. Karaerik (Cimin) üzüm çeşidinde hasat sonrası uv-c ve sıcak su uygulamalarının meyve kalitesi ve soğukta muhafaza üzerine etkileri. GAP VII. Tarım Kongresi Bildiri Kitabı, s:34-40.

Kök, D., Bal, E., Bahar, E., 2017. Physical and biochemical traits of selected grape varieties cultivated in Tekirdağ, Turkey. Int. J. Sustainable Agricultural Management and Informatics, 3(3): 215-223.

Martinez-Romero, D., Guillen, F., Castillo, S., Valero, D., Serrano, M., 2003. Modified atmosphere packaging maintains quality of table grapes. J. Food Sci., 68: 1838-1843.

Tozlu, C., 2001. Sofralık üzüm çeşitlerinin muhafazası ve pazarlanması aşamalarında kükürt dioksit (SO2) kalıntı düzeylerinin belirlenmesi. Yüksek Lisans Tezi, Ankara Üniv. Fen Bilimleri Enst. Bahçe Bitkileri Anabilim Dalı, Ankara. 47s.

in vitro PHYTOCHEMICAL and ANTIBACTERIAL PROPERTIES *of Peganum harmala* L.

Filiz UCAN TURKMEN
Kilis 7 Aralık University
ucanfiliz@gmail.com

Hatice Aysun MERCIMEK TAKCI
Kilis 7 Aralık University
mersimek@hotmail.com

Fatma Esen SARIGULLU ONALAN
Kilis 7 Aralık University
esenefesari@hotmail.com

ABSTRACT: Phytocehmical properties and antibacterial activity against *E. coli*, *Klebsiella* spp and MRSA in seed extracts of *Peganum harmala* L. (harmal) obtained from Gazıantep herbalist and used by folk medicine were investigated. The highest phenolic and flavonoid content in seed extracts prepared used by solvents with different polarity, were detected in distiled water extract with 11.60±0.02 mg GAE/g and metanolic extract with 0.859±0.08 mg RE/g, respectively. According to antioxidant activity results, the highest DPPH inhibition was determined as %85.12±0.44 in metanol extract. Metanolic harmal seed extract showed the highest antibacterial activity against MRSA, *E. coli* and *Klebsiella* spp. bacteria, with 12, 11 and 13 mm inhibition zone, respectively. Results of our study are showed that bioactive substances in methanolic extract are able to use at medicinal preparate following chemical, biological, pharmacological, and toxic analyzes of theirs.
,

Key words: harmal seed, MRSA, antioxidant, phytochemical properties

Peganum harmala L. (ÜZERLİK TOHUMU)'NUN *in vitro* FİTOKİMYASAL VE ANTİBAKTERİYEL ÖZELİKLERİNİN İNCELENEMESİ

ÖZET: Bu çalışmada Gaziantep aktarlarından temin edilen ve halk hekimliğinde kullanılan *Peganum harmala* L. (üzerlik) tohum özütlerinde fitokimyasal özellikler ve *E. coli*, *Klebsiella* spp ve MRSA'ya karşı antibakteriyel aktivitesi incelenmiştir. Farklı polariteye sahip çözücüler kullanılarak hazırlanan özütlerde en yüksek fenolik madde içeriği 11.60±0.02 mg GAE/g ile saf suda; flavonoid içerik ise 0.859±0.08 mg RE/g ile metanolik özütte rastlanmıştır. Antioksidan aktivite sonuçlarına göre en yüksek DPPH inhibisyonu %85.12±0.44 olarak metanol özütünde tespit edilmiştir. Metanolik üzerlik tohumu özütü MRSA, *E. coli* ve *Klebsiella* spp. test bakterilerine karşı 12, 11 ve 13 mm inhibisyon zonu ile en yüksek antibakteriyel aktiviteyi göstermiştir. Çalışmamızın sonuçları, metanolik özütteki biyoaktif maddelerin kimyasal, biyolojik, farmakolojik ve toksik analizlerini takiben tıbbi preparatlarda kullanılabileceğini göstermektedir.

Anahtar sözcükler: üzerlik tohumu, MRSA, antioksidan, fitokimyasal özellikler

GİRİŞ

Zygophyllaceae familyasına ait *Peganum harmala* L. (üzerlik tohumu) genel olarak Suriye Rue olarak da bilinmektedir. Tıbbi olarak kullanılan bu bitki geleneksel İran tıbbında 'Esfand', 'Espand' ve 'Harmal' olarak da tanımlanmaktadır. *Peganum harmala*'nın asıl kökeni Orta Asya'dır. Fakat günümüzde Avusturalya'da, Afrika'nın kuzeyinde ve Amerika'nın güney batısında yetişmektedir (Niroumand ve ark., 2015; Kırıcı ve ark., 2018).

Habitatı yarı kurak, bozkır ve kumlu topraklardır (Mahmoudian ve ark., 2002). Çok yıllık, otsu, tüysüz, 30 ila 50 cm boylarında büyüyen, sürücü köklere sahiptir (Mahmoudian ve ark., 2002; Niroumand ve ark., 2015;). Yaprakları dar, etli, parlak yeşil ve sert yapılıdır. Çiçekler yalnız, küçük, soluk sarı veya beyaz ve taç yapraklar 5 tanedir (Niroumand ve ark., 2015). Mayıs-Temmuz aylarında çiçek açan üzerlik bitkisi daha sonra tohum oluşturur. Meyveler üçgen 50'den fazla siyahımsı tohumları içeren 3 odacıklı küresel kapsüllerden oluşmaktadır (Mahmoudian ve ark., 2002). Olgunlaşmamış meyveler yeşil, olgunlaştıklarında turuncu-kahverengidir (Niroumand ve ark., 2015).

Tohumlarından elde edilen "Türk Kırmızı" olarak da bilinen kırmızı renkteki boyar madde Batı Asya'da halıların ve yünlerin boyanmasında kullanılmaktadır. Tohumların yanı sıra dalları ve kökleri mürekkep, boya ve dövme yapımında kullanılmaktadır Endüstriyel kullanımına ek olarak, halk hekimliğinde tıbbi olarak da değerlendirilmektedir. Boğaz ve karın ağrılarına karşı, bağırsak rahatsızlıklarına, siğilin tedavisinde, akciğer/karaciğer hastalıklarının tedavisinde, ağrı kesici ve ateş düşürücü olarak kullanımı XV. yüzyıl tıp kitabı olan Yadigar'da yer almıştır (Kırıcı ve ark., 2018).

P. harmala'nın farmakolojik aktif bileşenleri, tohumlarda ve köklerde yer alan çeşitli alkoloidlerdir (Koçak ve Şahin, 2009). Bu alkoloitler β-karbolin (trisiklik pyrido[3,4-b]indol) halka yapısı taşımaktadır ve harmin, harmalin (harmadin), harmol ve harman olarak tanımlanmıştır (Kartal ve ark., 2004). Quinazolin türevleri olarak da vasisin ve vasisinon bulundurmaktadır (Mahmoudian ve ark., 2002). Aynı zamanda peganin, isopeganin, dipeganin, deoxypeganin, harmalidin ve pegamin alkaloidleri de tanımlanmıştır (Mahmoudian ve ark., 2002; Kartal ve ark., 2004). Beta-karbolin alkaloidler, monoamin oksidazın geri dönüşümlü inhibitörleri olup, hipotermi, titreme ve düşük tansiyon aktivitesi gibi çeşitli farmakolojik etkilere sahiptirler (Kartal ve ark., 2004). Bu etkilerin yanı sıra harmala alkaloidlerinin kardiyovasküler etkileri bildirilmiştir (Koçak ve Şahin, 2009). Ülkemizde halk arasında meyvelerinden nazarlık, tohumları ise nazara karşı tütsü olarak kullanılmaktadır (Kartal ve ark., 2004).

Çalışmamızda Gaziantep aktarlarından temin edilen üzerlik tohumundan farklı çözücüler kullanarak hazırlanan özütlerinin *in vitro* fitokimyasal ve antibakteriyel özellikleri araştırılmıştır.

YÖNTEM

Gaziantep aktarlarından temin edilen üzerlik tohumları distile su, aseton, metanol ve hekzan çözücüleri (1:10 (w/v)) ile 72 saat oda sıcaklığında çalkalamalı koşullarda ekstrakte edilmiştir. Ekstraksiyon işlemi tamamlanan örnekler filtre kağıdından (Whatman filter paper No.1) süzülmüştür. Çözücüler her bir çözücünün kaynama sıcaklığına göre evaparatörde uçurulmuştur. Evaporasyon sonrası örneklerin son konsantrasyonu 100 mg/mL olacak şekilde metanol içerisinde süspanse edilmiştir. Örnekler kullanılana kadar +4ºC'de depolanmıştır. Fitokimyasal ve antibakteriyel özelliklerin belirlenmesi için 10-100 mg/ml konsantrasyonlarda özütler test edilmiştir.

Toplam fenolik madde miktarı

Bitki özütlerindeki çözünebilen toplam fenolik madde içeriği Folin-Ciocalteu ayıracı kullanılarak belirlenmiştir. Özütlerin 0.5 mL'sine 2.5 mL Folin-Ciocalteu reaktifi (%10) ve 2.5 mL $NaHCO_3$ (%7.5) çözeltisi eklenerek 45°C'de 45 dakika su banyosunda inkübe edilmiştir. Karışımların absorbansı 765 nm'de spektrofotometrik olarak ölçülmüştür. Standart olarak gallik asitin kullanıldığı kalibrasyon grafiğine göre, toplam fenolik içerik gram başına mg gallik asit eşdeğerleri (mg GAE/g) olarak ifade edilmiştir (Stankovic, 2011).

Toplam flavonoid madde miktarı

Sharm ve Vig (2013) tarafından bildirilen yönteme göre, özütler 1:5 metanol ile seyreltilmiştir. Örneklere 0.3 mL $NaNO_2$ (%5) eklenmiş ve 5 dk oda sıcaklığında inkübe edilmiştir. Karışıma 0.6 mL $AlCl_3.6H_2O$ (%10) eklenmiş ve aynı koşullarda inkübasyonu takiben, 2 mL 1M NaOH eklenerek son hacim saf su ile 10 mL'ye tamamlanmıştır. Hazırlanan karışımların absorbansı 510 nm'de spektrofotometrik olarak belirlenmiştir. Toplam flavonoid içerik, gram başına mg rutin eşdeğerleri (mg RE/g) olarak ifade edilmiştir (Sharm ve Vig, 2013).

Antioksidan aktivite tayini

Özütlerin serbest radikalleri yakalama etkinliği olarak ifade edilen antioksidan aktiviteleri, DPPH (2,2-diphenyl 1-picrylhydrazyl) radikali kullanılarak Uçan Türkmen ve arkadaşlarının (2016) metoduna göre belirlenmiştir. Özütlerin 100 µL'sine, 3.9 mL metanol içerisinde hazırlanmış DPPH radikali (0.025 g/l) eklenmiştir. Karışım 2 saat oda sıcaklığında karanlıkta bekletilmiştir. DPPH çözeltisinin mor renginin açılması esasına dayanan bu analizde, arta kalan DPPH miktarı 515 nm'de spektrofotometrede ölçülmüştür. % olarak belirlenen DPPH inhibisyonu aşağıdaki formüle göre hesaplanmıştır (Ucan ve ark., 2016). Analiz sonuçları, SPSS 22.0 paket programı kullanılarak varyans analizine tabi tutulmuş ve önemli bulunan farklılıklar Tukey çoklu karşılaştırma testine göre belirlenmiştir ($p<0.05$).
%İnhibisyon= [(Akontrol−Aörnek)/Akontrol]×100.

Antibakteriyel Aktivitenin Belirlenmesi

Yaprak özütlerinin antimikrobiyal aktivitesi *E. coli*, *Klebsiella* spp ve *S. aureus*, bakterilerine karşı Kirby-Bauer disk difüzyon yöntemi kullanılarak araştırılmıştır.

Patojen mikroorganizmalar Kilis Devlet Hastanesi Mikrobiyoloji Bölümü'nden temin edilmiştir. Negatif kontrol olarak saf metanol kullanılmıştır. Pozitif kontrol olarak *S. aureus*'a karşı metisilin (Himedia SD019-1CT 5 mcg/disk); diğer suşlar için tetrasiklin (Himedia SD037-1CT 30 mcg/disk) kullanılmıştır. 30 µL özütlerden emdirilerek hazırlanan boş steril diskler, 0,5 MacFarland bulanıklığına ayarlanmış bakteri kültürlerinin eküvyon çubuğu ile yayıldığı Mueller Hinton Agar (MHA) besiyerlerine aktarılmıştır. 37°C'de 12-24 saat inkübe edilen petri plaklarında, disklerin etrafında bakterilerin üremediği inhibisyon zonları ölçülerek, antibakteriyel aktivite mm cinsinden hesaplanmıştır.

BULGULAR

Çözücülerin polaritelerine bağlı olarak ekstraksiyon verimi değişmekle birlikte çalışmada en etkili çözücünün verimi ile metanol (%24.5) olduğu belirlenmiştir. Polaritesi yüksek saf su %23 verimle metanolü izlemiş, aseton ve hekzan çözücüleri için % ekstraksiyon verimi sırasıyla %18 ve 14 olarak saptanmıştır.
10-100 mg/ml konsantrasyonlarda test edilen üzerlik özütlerinin toplam fenolik içerikleri Tablo 1'de verilmiştir. Üzerlik tohumlarındaki toplam fenolik madde içeriği 1.55±0.01 ve 11.60±0.02 mg GAE/g arasında hesaplanmıştır. Bu sonuçlara göre, en yüksek fenolik madde içerikleri 100 mg/mL konsantrasyonda metanol ve saf su özütlerinde 9.54±0.50 ve 11.60±0.02 mg GAE/g olarak belirlenmiştir. 10 mg/mL konsantrasyonda ki hekzan ve saf su özütlerinde ise en düşük fenolik içeriğe rastlanmıştır (1.55±0.01; 1.55±0.02 mg GAE/g). Test edilen tüm çözücüler için madde konsantrasyonu arttıkça toplam fenolik madde içeriğinin de arttığı gözlenmiştir.

Tablo 1. Üzerlik Özütlerinin Toplam Fenolik İçerikleri (mg GAE/g)

	Metanol	**Hekzan**	**Saf su**	**Aseton**
10 mg/mL	3.66±0.01^{e}	1.55±0.01^{d}	1.55±0.02^{e}	3.82±0.3^{c}
25 mg/mL	4.80±0.02^{d}	2.07±0.17^{c}	5.00±0.24^{d}	4.07±0.08^{c}
50 mg/mL	6.65±0.26^{c}	2.48±0.08^{c}	7.07±0.32^{c}	4.15±0.16^{c}
75 mg/mL	8.26±0.49^{b}	4.15±0.23^{b}	8.61±0.61^{b}	4.89±0.09^{b}
100 mg/mL	9.54±0.50^{a}	5.24±0.22^{a}	11.60±0.02^{a}	5.43±0.22^{a}

***(Gösterilen veriler n=3'ün ortalama değerleridir. Grafikte farklı simgeler ($^{a-e}$, $^{a-d}$ ve $^{a-c}$) ile ifade edilen değerler arasındaki fark önemli bulunmuştur ($p<0.05$)).**

Üzerlik tohumlarının fenolik madde içeriklerinin araştırıldığı çalışmada, en yüksek fenolik içerik aseton, etil asetat, etil asetat-metanol ve saf su-aseton çözücülerinde sırasıyla 116.01, 80.52, 73.53 ve 70.96 µg GAE/mg olarak bildirilmiştir (Kanwal ve ark., 2016). Farklı bir çalışmada, çalışmamıza benzer şekilde yürütülen ekstraksiyon metodu sonucu üzerlik tohumlarında en yüksek fenolik içerik sulu özütlerde 19.68±1.56 mg GAE/100 mg olarak tespit edilmiştir (Khadhr ve ark., 2017).

10-100 mg/mL konsantrasyonlarda hazırlanan üzerlik özütlerinin toplam flavonoid içerikleri Tablo 2'de verilmiştir. Üzerlik özütlerindeki en yüksek toplam flavonoid içerik metanol özütlerinde belirlenmiş olup 100 mg/mL konsantrasyonda 0.859±0.08 mg RE/g'dir. Toplam fenolik içerikteki sonuçlara benzer şekilde en düşük flavonoid içerik hekzan ve saf su özütlerinde 0.098±0.00 ve 0.097±0.00 mg RE/g olarak saptanmıştır.

Tablo 2. Üzerlik Özütlerinin Toplam Flavonoid İçerikleri (mg RE/g)

	Metanol	**Hekzan**	**Saf su**	**Aseton**
10 mg/mL	0.134±0.00^{e}	0.098±0.00^{d}	0.097±0.00^{e}	0.123±0.00^{d}
25 mg/mL	0.244±0.02^{d}	0.210±0.01^{c}	0.162±0.01^{d}	0.251±0.02^{c}
50 mg/mL	0.390±0.04^{c}	0.251±0.02^{bc}	0.276±0.01^{c}	0.319±0.01^{b}
75 mg/mL	0.597±0.00^{b}	0.312±0.01^{ab}	0.344±0.01b^{a}	0.348±0.03^{d}
100 mg/mL	0.859±0.08^{a}	0.350±0.05^{a}	0.444±0.03^{a}	0.406±0.03^{a}

*(Gösterilen veriler n=3'ün ortalama değerleridir. Grafikte farklı simgeler ($^{a-e}$ ve $^{a-d}$) ile ifade edilen değerler arasındaki fark önemli bulunmuştur ($p<0.05$)).

Khadhr ve ark., (2017) tarafından yapılan çalışmada en yüksek fenolik madde içeriği sulu üzerlik tohumunda rastlanmasına karşın (19.68±1.56 mg GAE/100 mg), çalışmamıza benzer şekilde en yüksek flavonoid madde içeriği 134.34± 3.56 ile metanolik özütte hesaplanmıştır.

10-100 mg/ml konsantrasyonlarda hazırlanan üzerlik özütlerinin antioksidan aktivitesi Tablo 3'de verilmiştir.

Tablo 3. Üzerlik Özütlerinin Antioksidan Aktivitesi (% DPPH inhibisyonu)

	Metanol	**Hekzan**	**Saf su**	**Aseton**
10 mg/mL	69.46±0.67^{d}	8.72±0.44^{d}	35.48±9.11^{d}	23.38±1.67^{c}
25 mg/mL	73.57±2.00^{c}	17.38±0.89^{c}	57.91±5.89^{c}	47.42±3.50^{b}
50 mg/mL	80.34±0.78^{b}	30.48±1.33^{b}	66.46±1.33^{bc}	82.18±2.50^{a}
75 mg/mL	85.01±1.44^{a}	45.42±2.1^{a}	79.01±1.00^{ab}	83.73±0.50^{a}
100 mg/mL	85.12±0.44^{a}	49.42±2.05^{a}	80.29±2.94^{a}	83.23±0.33^{a}

*(Gösterilen veriler n=3'ün ortalama değerleridir. Grafikte farklı simgeler ($^{a-d}$ ve $^{a-c}$) ile ifade edilen değerler arasındaki fark önemli bulunmuştur ($p<0.05$)).

DPPH radikali giderme antioksidan aktivitesi %8.72±0.44 ve 85.12±0.44 değerleri arasında belirlenmiş olup, en yüksek metanol yaprak özütlerinde 100 mg/mL konsantrasyonda %85.12±0.44'tür. En düşük flavonoid içerikler 10 ve 25 mg/mL konsantrasyonlarda hekzan özütlerinde sırasıyla %8.72±0.44 ve 17.38±0.89 olarak

belirlenmiştir. Yüksek toplam fenolik ve flavonoid içeriklerine paralel olarak metanolik üzerlik özütünde antioksidan aktivite yüksektir. En yüksek madde konsantrasyonunda hekzan özütlerinde antioksidan aktivite %49.42±2.05 olarak hesaplanmıştır. Bitki özütlerinin içerdiği fenolik ve flavonoid içerik incelendiğinde, en aktif doğal antioksidanlardan fenolik bileşiklerin yüksek olduğu metanolik özütlerde antioksidan aktivite de yüksek bulunmuştur.
Diğer özütlerle karşılaştırıldığında aseton özütünde düşük fenolik (5.43±0.22 mg GAE/g) ve flavonoid (0.406±0.03 mg RE/g) içeriğe karşın yüksek antioksidan (83.23±0.33) aktivite gözlenmesi, antioksidan aktivitenin sadece fenolik madde içeriğine bağımlı olmadığını, başka faktörlerinde göz önünde bulundurulması gerektiğini göstermektedir. Fitokimyasal analiz sonuçlarına göre, çözücüler için test edilen tüm konsantrasyonlar arasındaki farklar önemli bulunmuştur.
100 mg/mL konsantrasyonda özütlerden antibakteriyel çalışmaları sürdürülmüştür (Tablo 4). Test edilen bakterilere karşı en yüksek inhibisyon metanolik üzerlik tohumu özütlerinde rastlanmıştır. Aseton özütü test bakterilerinin tümüne karşı, hekzan özütleri ise *Klebsiella* spp. ve *E. coli*'ye karşı inhibitör etki gösterememiştir.

Tablo 4. Üzerlik Özütlerinin Antibakteriyel Aktivitesi (mm cinsinden)

	S. aureus	*E. coli*	*Klebsiella* spp.
Hekzan tohum özütü	7	-*	-*
Aseton tohum özütü	-*	-*	-*
Saf su tohum özütü	10	8	8
Metanol tohum özütü	12	11	13
Tetrasiklin		15	16
Metisilin	-*		

*Agar plaklarında inhibisyonu zonu gözlenmemiştir.
Metanol özütünün en yüksek inhibisyon etkisi 13 mm inhibisyon zonu ile *Klebsiella* spp. üzerinde belirlenmiştir. Metanol özütünün *E. coli* ve *Klebsiella* spp.'ye karşı gösterdiği inhibitör etki (11 ve 13 mm) standart antibiyotik ile kıyaslandığında (15 ve 16 mm), özütlerin daha az aktivite gösterdiği saptanmıştır (Şekil 1). Ancak bu aktivite antibakteriyel etki gösteren biyoaktif maddenin özütten saflaştırılması sonucu arttırılabilir. Böylece söz konusu molekül bu bakterilere yönelik tedaviler için hazırlanacak bitkisel preparatlarda yer alabilecektir.

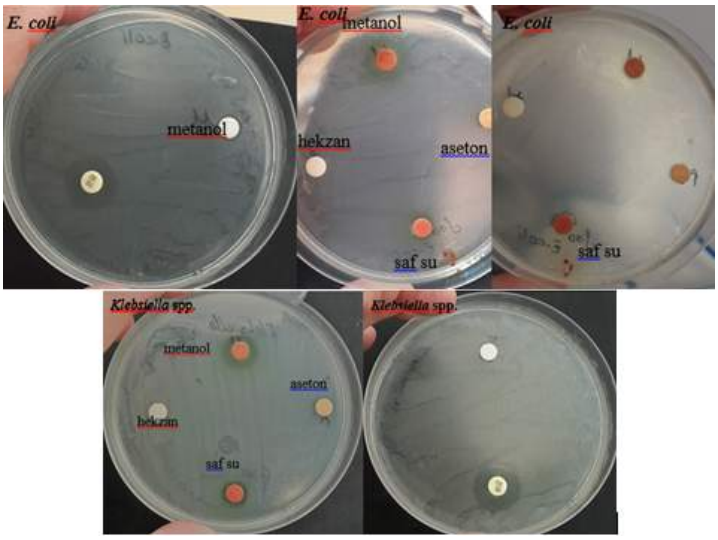

Şekil 1. *E. coli* ve *Klebsiella* spp.'ye karşı üzerlik özütlerinin inhibitör etkisi

Çalışmamızda en ilginç sonuçlar *S. aureus*'a karşı elde edilmiştir. Söz konusu bakteri, hastane kaynaklı ve toplum enfeksiyonlarına yol açmaktadır. Özellikle nozokomiyal enfeksiyonlarda pnömonin en yaygını, bakteriyeminin 3. en yaygın etkenleri arasında yer almaktadır. *S. aureus*'un yoğun bakım ünitelerinde enfeksiyon etkeni olan suşlarının %80'ni metisilin dirençlidir. Bu sebeple çalışmamız da *S. aureus*'a karşı diğer suşlardan farklı metisilin antibiyotiği pozitif kontrol olarak kullanılmıştır.

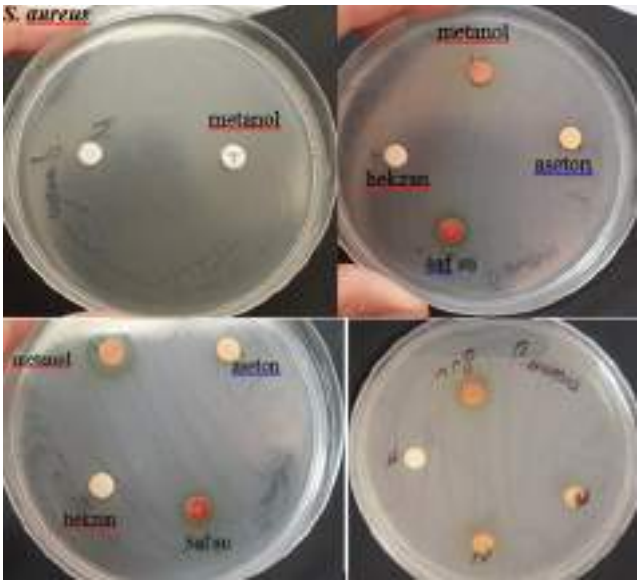

Şekil 2. *S. aureus'a* karşı üzerlik özütlerinin inhibitör etkisi

Tablo 4 ve Şekil 2'de gözlendiği gibi klinik suş metisilin dirençlidir (MRSA). Aseton hariç tüm üzerlik özütlerinin suş üzerindeki antibakteriyel aktivitesi kaydedeğer bir sonuçtur. Bu bulgulara göre tohum özütünde özellikle *S. aureus'*a karşı inhibitör etkili molekülün tanımlanması ile tıbbi ilaçlarda hammadde olarak kullanılması mümkün olacaktır.

Tüm test bakterilerine karşı en yüksek inhibitör etki metanol ve saf su özütlerinde gözlenmiştir. Bitkilerde antioksidan ve antibakteriyel aktivite gösteren fenolik

bileşiklerin hidrofobik karakterlerinden dolayı metanol ve su gibi polaritesi yüksek çözücülerde daha verimli ekstrakte edilmektedir. Bu literatür bilgisi, en yüksek aktiviteleri metanol ve su özütlerinde gözlemlediğimiz sonuçlarımızı destekler niteliktedir.

SONUÇ

Bu çalışmada *Peganum harmala* L.'nın fitokimyasal özellikleri ve antibakteriyel aktivitesi araştırılmıştır. Farklı çözücüler kullanılarak sürdürülen analizlerde, çözücülerin polaritesine bağlı olarak en yüksek ekstraksiyon verimi %24.5 ve 23 ile metanol ve saf suda belirlenmiştir. Ekstraksiyon verimine paralel olarak en yüksek fenolik içeriğe 9.54±0.50 ve 11.60±0.02 mg GAE/g; flavonoid içeriğe ise 0.859±0.08 ve 0.444±0.03 mg RE/g ile metanol ve saf suda rastlanmıştır. Antioksidan aktivite göz önünde bulundurulduğunda, aseton hariç en yüksek aktivite %85.12±0.44 ve 80.29±2.94 ile metanol ve saf suda hesaplanmıştır. Antibakteriyel aktivite analizleri sonucu metanol ve saf su özütlerinin tüm test bakterilerine karşı inhibitör etki gösterdiği saptanmıştır. Üzerlik tohumlarındaki etken biyoaktif moleküllerin ekstrakte edilmesi için en uygun çözücülerin metanol ve saf su olduğu tespit edilmiştir. Çalışmamızda ki incelenen hastane enfeksiyonu etkeni test bakterisi MRSA'ya karşı saf su ve metanol özütlerinde gözlenen inhibitör etki ileriki analizler için ümit vericidir.

ÖNERİLER

Çalışmamızın sonuçlarına dayanarak üzerlik tohumlarının metanol ve saf su özütlerindeki biyoaktif maddenin izolasyonu ve saflaştırılması, kimyasal analizleri, biyolojik, farmakolojik ve toksik etkilerinin belirlenmesi *Peganum harmala* L.'nın tıbbi preparatlarda kullanımına olanak sağlayacaktır.

KAYNAKLAR

Kanwal1, Z. G., Hafeez, A., Ul Haq, I., Ur-Rehman, T., Aun Muhammad, S., Shazadi, I., Fatima, N., Ur Rehman, N., (2016). Antioxidant, Antimicrobial and Antileishmanial Study of Different Parts of *Peganum harmala*. International Journal of Biosciences, *9*(1), 45-48.

Kartal, M., Altun, M. L., & Kurucu, S. (2004). *Peganum harmala* L. (Üzerlik) Tohumlarında Harmol, Harmalol, Harmin Ve Harmalin Alkaloitlerinin Ybsk Yöntemi İle Analizi. 14. Bitkisel İlaç Hammaddeleri Toplantısı, Bildiriler, Eskişehir, Eds. K.H.C.Başer ve N.Kırımer.

Kırıcı, S., Kayırani S. D., & Tokuz, G. (2018). Doğu Akdeniz Bölgesinde Üzerlik (*Peganum harmala* L.) Bitkisinin Tütsü Olarak Kullanımı. Lokman Hekim Dergisi, *8*(1), 01-12.

Koçak, Y., & Şahin, A., (2009). *Peganum harmala* L. (Üzerlik) Tohum Ekstresinin Analjezik Aktivitesi ve Akut Toksisitesinin Fareler Üzerinde Belirlenmesi, Y.Y.U. Veteriner Fakultesi Dergisi, *20*(1), 27-30

Mahmoudian, M., Jalilpour, H., & Salehian, P., (2002). Toxicity of *Peganum harmala*: Review and a Case Report. Iranian Journal of Pharmacology & Therapeutics, *1*(1), 1-4.

Maroua Khadhr, M., Bousta, D., El Hajaji, H., Lachkar, M., Barkai, H., Ibnsouda-Koraichi, S., & Boukhchina, S., (2017). Phytochemical Screening, Total Phenolics and

Biological Activities of Tunisian *Peganum harmala* Seed Extracts. Journal of Chemical and Pharmaceutical Research, *9*(2):32-39.

Niroumand, M. C., Farzaei, H. M., & Amin, G. (2015). Medicinal properties of Peganum harmala L. in traditional Iranian medicine and modern phytotherapy: a review. J Tradit Chin Med., *35*(1), 104-109

Sharm, S., & Vig P.A., (2013). Evaluation of in Vitro Antioxidant Properties of Methanol and Aqueous Extracts of Parkinsoniaaculeata L. Leaves, The Scientific World Journal, 1-7.

Stankovic, M.S., (2011). Total phenolic content, flavonoid concentration and antioxidant activity of Marrubium peregrinum L. Extracts. Kragujevac J. Sci., *33*, 63-72.

Ucan Turkmen, F., Mercimek Takcı, H. A., & Sekeroglu, N., (2016). Total Phenolic Content, Antioxidant and Antimicrobial Activities of Homemade and Industrial Samples of Breakfast Zahter, Herbal Mixture, Akademik Gıda, *14*(3), 253-257.

ENERGY DEMAND AND CLEAN ENVIRONMENT CHALLENGES: CHINA AS A SETTER OF BELT AND ROAD INITIATIVE

*[1] Corresponding Author:
Abdul Rauf
School of Economics and Management, Southeast University, Nanjing 210096, China (phone: 0086-13770641422; e-mail: abdulrauf@seu.edu.cn)
[1]Xiaoxing Liu:
School of Economics and Management, Southeast University, Nanjing 210096, China; (e-mail: *starsunmoon198@163.com*)
[2]Waqas Amin
School of Economics, Shandong University, 27-Shanda Nan lu, Jinan. Shandong, China (e-mail: waqas.amin97@yahoo.com)

ABSTRACT: The topical research study is the investigation to gauge the relationship among renewable energy, energy consumption, growth, industrial production, population growth and environmental degradation (CO2) in China, since the inauguration of Belt and Road Initiative (BRI) scenario. The current study strings the period from 1978 to 2017, where the intent of time consideration is based on the Chinese economic reforms that initiated in 1978.Sustainable development Goals (SDG) entice to every nation, to chance on for 17 goals accomplishment in real-world frame. Primarily, the unit root test employed to check the stationary of on-hand variables, where some variables show at level and others at first difference. The retrieving situation is a fine position to utilize the Autoregressive Distributed Lags (ARDL) bound testing model for disclosing the short-run and long-run association between the variables. In the long run, a negative parameter of ECM expression and its significance endorse the long run cointegration linkage subsisted among the variables. At long-run relationship agriculture value added, industrial value added, energy consumption and economic growth have an adverse effect on the environment, while rest variables have insignificant for environmental degradation. On contrary, in short-run population, economic growth and also have the alarming effect on ecological setting but the renewable energy effectual for the environment at all. In a word, the concentrating study will be a directing indication for Chinese government and policymakers to command the procedures in presence of (BRI) projects for energy demand by especially fixing the renewable energy source (hydro, wind, biomass and solar etc.). Furthermore, water treatment plants adjacent to industries should be imbedded for clear-out the polluted water that may harmful to the adjoining societies. Hence, the study implications may helpful for the success of BRI projects in term of "in time accomplishment and target gains realized.

Key words: ARDL, Belt and Road Initiative, China, Combats, Environmental degradation, Economic growth.

DESIGN AND IMPLEMENTATION of A SMART CNC PLOTTER CONTROLLED BY MICROCONTROLLER

Mustafa ALJANABI
Gaziantep University – Electrical and Electronics Engineering Department
soofeto@gmail.com

ABSTRACT: This project is designing and implementing a low cost plotter system works with three dimension (CNC) plotter machine. The main function of this microcontroller based system is writing and sketching images. This process can be happen through communication between the system machine (CNC) and the personal computer (PC). The system used low cost microcontroller Arduino UNO as a backbone, as well as used two stepper motors for x-axis and y-axis and servo motor for z-axis. All motors controlled by the Arduino Uno. The result of the system is designed mechanical system along with the embedded system resulting in accuracy. The system used C# for Arduino programing, as well used the inkscape portable for images analysis and G-Code sender for user interface.

Key words: CNC plotter, smart CNC.

INTRODUCTION

There are many kinds of CNC robotic machines these are [1, 2]: 1) laser cutting CNC machine, 2) printed circuit board CNC machines (drill machine) 3) CNC writing and sketching machine. CNC writing and sketching machines are widely used nowadays. It is used in many applications such as: 1) writing text, 2) sketching images [3-5] the basic circuits CNC plotter writing and sketching machine is shown in Fig.1. In this circuit, the output result may be a texting, or sketching depends on the input variables. In many applications, there is a need to be the output texting or sketching. Therefore two stages of writing and sketching must be used to achieve adjustable output regardless input variables. The first and second stages are used stepper motors for x-axis and y-axis as well the system used servo motor for z-axis.

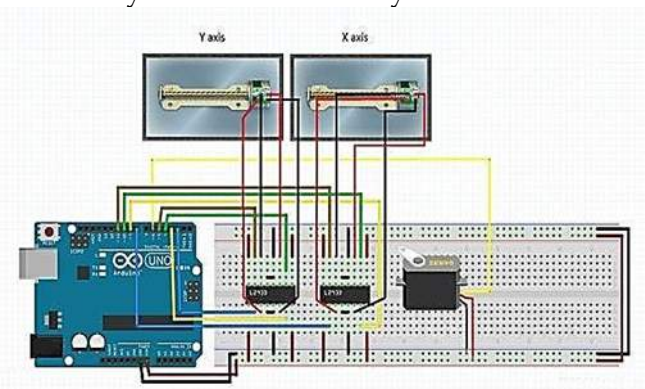

Figure.1 (CNC) circuit design system of CNC plotter writing and sketching machine

OBJECTIVES OF THE STUDY

The aims of this study are to develop and design smart CNC robotic machine based on Arduino UNO and together with stepper and servo motors. Specifically, this study aims:

• design and implement a control system that can control the motors to do the main aim planned for.

• ***evaluating and testing the functionality, accuracy and reliability of the manufacturing prototype.***

THE PROJECT COMPONENTS

This project used different components to achieve the last design of CNC.

Arduino UNO

Stepper motors

Servo motor

The Arduino UNO

The Arduino UNO is the backbone of this project. The Arduino UNO is a smart microcontroller board that depends on the ATmege328 (datasheet) (which can be generate a pulse- width modulation PWM outputs), The Arduino Uno used USB to connected to a computer through cable and it can be powered by this USB cable or with an external power sup as shown in figure 2.

Figure. 2 Arduino UNO model

The main advantages of Arduino UNO:

Cheap and have large libraries

Open source microcontroller.

High response for signal processing.

Wide range of input and output.

The Stepper Motors

The stepper motors are the engine of this project. This kind of motors used in small projects that need accurately control so that why it is used in this project. In figure 3 the stepper motor is shown.

Figure. 3 Stepper motor model.

The stepper motor has 4 input wires. All these wires are connected to the L298N motor controller.
The main aim for using L298N motor controller module is to control the stepper motor. The L298N is a controller used to change the polarity of the stepper motors. Figure 4 is shown the L298N dual motor controller.

Figure 4 L298N dual motor controller.
This project used two steppers motors for x-axis and y-axis because of this reason two L298N motor controllers are used. The connection of stepper motors to the L298N motor controller is shown in figure 5.

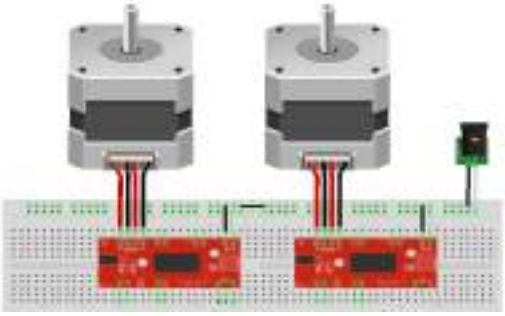

Figure.5 The connection of stepper motors to the dual motor controller.

The Servo Motor

In this project the servo motor is used to control the z- axis the servo motor consist of three main components as shown in figure 6. These components are:
Control circuit unit (microcontroller).
Motor take the signal from control circuit.
Gear train.

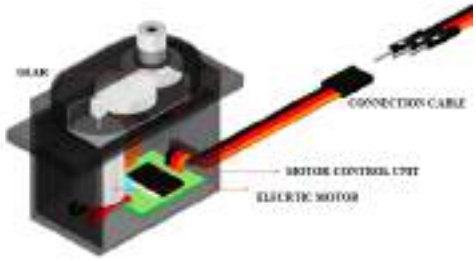

Figure. 6 The servo motor main components

As well as the servo motor has three wires as shown in figure7. These wires are:

GND wire. This pin response for connecting the motor to the ground.

Vin wire. This pin is response for connecting servo motor to 5 volt input.

Control wire. This pin is response about the control signal (PWM) pulse - width modulation that produced from Arduino UNO.

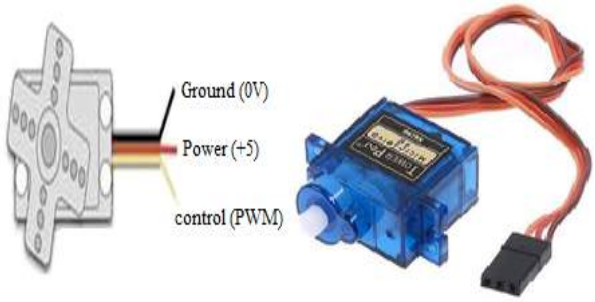

Figure 7 the servo motor wires

As well as in this project a DVD / CD driver used for x-axis movement and y-axis movement. As shown in figure 8.

Figure 8 the DVD / CD driver

3. Design and Implementation of CNC Machine

This part will talk about how connected all the project components together and programed to get a CNC machine as shown in figure 9 A, B, C and D.

First step steeper motors are connected to the Arduino through the L298N motor controller to control the x-axis and y-axis movements. The L298N motor controller used to change the polarity of the stepper motors. That is means changing the motor rotation from right to left and vice versa.

Second step is connected the servo motor to Arduino. The servo motor is responsible about pen movement (z- direction). The aim of this motor is to control pen movement from top to bottom through specific time period called (PWM) pulse-width modulation. The (PWM) it is generated by the Arduino.

The project used C# program language to program all components that used in project.

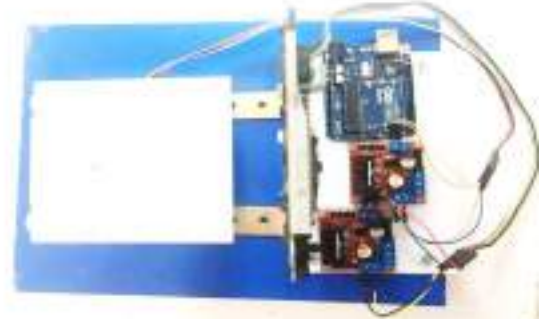

A

B

C

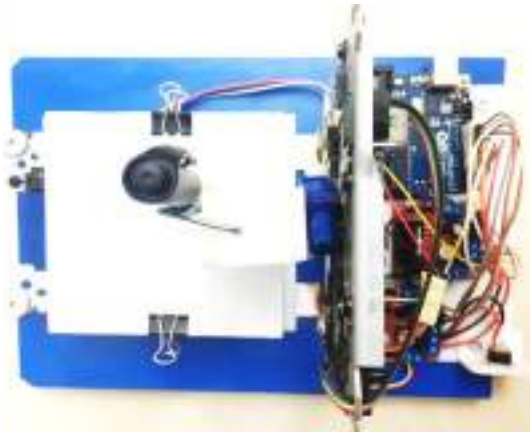

D

Figure 9 a prototype Smart CNC robotic machine.

EXPERIMENTAL RESULTS

The circuit shown in Fig.1 is practically implemented as shown in Fig.9 and Fig 10. The implemented prototype operates at a both side writing text as shown in Fig.10 A and B and sketching images as shown in Fig.11.

CONCLUSION

From this work the following conclusions have been reported:
1. The experimental results show good agreement.
2. The prototype has the capability to control the output regardless input variables.
3. Because of using Arduino microcontroller, stepper and servo motors the circuit has high accuracy.

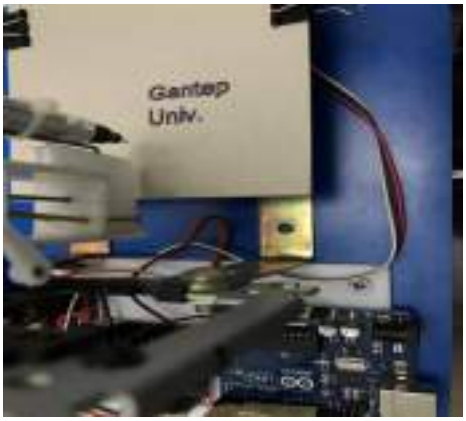

A
Figure 10 prototype operates at writing text side.

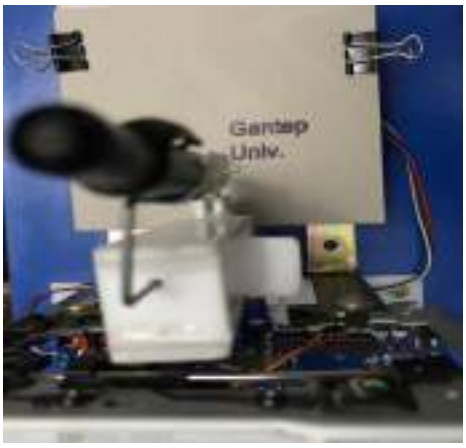

B
Figure 10 prototype operates at writing text side.

Figure 11 prototype operates at sketching images side

References

[1] Calabrese, F., & Celentano, G. (2007, September). Design and realization of a STEP-NC compliant CNC embedded controller. In Emerging Technologies and Factory Automation, 2007. ETFA. IEEE Conference on (pp. 1010-1017). IEEE

[2] Wu, H., Zhang, C., Li, G., & Wang, B. (2006, August). Windows XP embedded based open architecture computer numerical control system. In Mechatronic and Embedded Systems and Applications, Proceedings of the 2nd IEEE/ASME International Conference on (pp. 1-6). IEEE.

[3] Patel, N. A., Pradhan, S. N., & Shah, K. D. (2009, February). Two legged robot design, simulation and realization. In Autonomous Robots and Agents, 2009. ICARA 2009. 4th International Conference on (pp. 426-429). IEEE

[4] Shin, Y. C., Chin, H., & Brink, M. J. (1991). Characterization of CNC machining centers. Journal of Manufacturing Systems, 10(5), 407-421..

[5] Heisel, U., & Gringel, M. (1996). Machine tool design requirements for high-speed machining. CIRP Annals-Manufacturing Technology, 45(1), 389-392.

[6] Kumar, M., & Puttige, V. (2009). low cost automation for CNC machining center‖, IJMET, Vol. 3. I. Pahole, L. Rataj, M. Ficko, S. Klancnik, S. Brezovnik, M. Brezocnik, and J. Balic," Construction and evaluation of low-cost tableCNC milling machine.

[7] Pabolu, V. K., & Srinivas, S. K. N. H. (2010). Design and implementation of a three dimensional CNC machine. International Journal on Computer Science and Engineering, 2(8), 2567-2570.

[8] Andrei, T., & Nae, I. (2010). Practical Applications Performed by a Stepper Motor CNC Router. Petroleum-Gas University of Ploiesti Bulletin, Technical Series, 62(1).

[9] da Rocha, P. A. S., e Souza, R. D. D. S., & de Lima Tostes, M. E. (2010, November). Prototype CNC machine design. In Industry Applications (INDUSCON), 2010 9th IEEE/IAS International Conference on (pp. 1-5). IEEE.
Chicago

[10] Xu, X. M., Li, Y., Sun, J. H., & Wang, S. G. (2012). Research and development of open CNC system based on PC and motion controller. Procedia Engineering, 29, 1845-1850.

[11] andian, S., & Pandian, S. R. (2014). A low-cost build-your-own three axis CNC mill prototype. Int. J. Mechanical Engineering and Robotics, 2(1), 6-11

NEW TOPOLOGY OF ASYMMETRICAL CASCADE H-BRIDGE MULTI-LEVEL INVERTER

Omar AL-BASRI
Department of Electric and Electronic Engineering, Gaziantep University, Gaziantep 27310, Turkey
Omarsat84@yahoo.com

Ergun ERÇELEBİ
Department of Electric and Electronic Engineering, Gaziantep University, Gaziantep 27310, Turkey
ercelebi@gantep.edu.tr

ABSTRACT: The cascade H-bridge inverter utilization has been swelled since the last decennium. These inverters are suitable in various high voltage & power application due to their ability to combine waveforms with better harmonic series and accurate output. This paper displays a cascade H-bridge multilevel inverter model which is designed with a conventional H-bridge unit. The inverter can produce a better sinusoidal waveform by increasing the number of output voltage levels. The cardinal modification in this paper is to use asymmetric voltage distribution between the H-bridge cells instead of symmetric method and the control method which is used is the charge balance control method so as to balance the power drawn from each H-bridge and that leads to increase the life cycle of the connected batteries to the inverter

Key words: Multilevel inverter, cascade H-Bridge, charge balance control method, symmetric voltage distribution; Asymmetric voltage distribution.

INTRODUCTION

Currently, renewable powers sources (RPSs) have obtained senior solicitude in worldwide to find vital solutions for world power squeeze and pollution lessening problem. RPS can solve the problems of the rising electrical demand on the utility grid and providing energy for outlying areas as well. The increasing number of RPSs and distributed generations (DGs) need new techniques for running and administering of the electrical power transferred between RPSs and clients, in order to preserve and enhance the power-supply reliability and quality that match the universal standard requirements. [1], [2].

One of the fundamental evolutions in the RPS systems is the improvement in the power converters, which play the pivotal role to convert the produced energy to the loads/utility grid. Consequently, the classical inverters like DC-DC converters, and DC-AC converters are represented by more motivated topologies that aim to increase system efficiency, reliability, life time, and to customize system size and cost [3] , [4].

Between the approved converters topologies, multi-level inverters (MLIs) have been characterized by many features such as reduced output filter size, low dv/dt, low electromagnetic interference (EMI), generating output voltage with extremely low THD, and increased system efficiency due to its operation with fundamental switching

frequencies. Moreover, using MLIs lead to eliminate the boosting step on the input side of the inverter and the power transformer at the output AC side [2], [5] – [13].
The various topologies of MLIs can be classified into three main groups named as diode clamped multi-level inverter and flying capacitor multi-level inverter and cascade H-bridge multi-level inverter. These main categories are also classified as single dc-voltage source MLIs and multi dc-voltage sources MLIs. Single dc-voltage source has only one dc-voltage source, and many capacitors and diodes. It has No.t the capability of voltage boosting since the output peak AC voltage has to be the same as the input dc-voltage source value [14]. Furthermore, the control algorithm of single dc-voltage source meets many difficulties than multi-sources type as it needs capacitors voltage balancing techniques. On the contrary, multi-dc voltage sources MLIs have many dc-voltage sources and reduced number of capacitors and clamped diodes. It features several merits such as high modularity degree, simple cell structure and reduced manufacturing costs. In addition, when a fault is occurred in one of these cells, the faulty cell can be replaced easily without affecting the faultless unit. Diode clamped mli and flying capacitor are considered as single dc- voltage source mli while cascade H-bridge consider as multi dc-voltage source converter. Due to the method in which the sources distributed, cascade multilevel inverter are also divided into symmetrical and asymmetrical inverters. If one of the input dc sources is grotesque then we can recognize that inverter as asymmetrical inverter[2-5] , which can produce more numbers of output levels and amplitude than symmetrical type[6] .The most distinct feature of cascade multilevel inverter is that it need separate dc sources as input , so it is considered as the most suitable way to use with renewable energy sources such as pv panels which increase in interest because of the global increasing demand and reducing the negative impact of the power generations on the environment In the literature, there are many different topologies of MLIs are addressed. In [15], the authors presented multilevel dc link topology (MLDCL). It was constructed by connecting half H-bridge cells in series configuration, and a main cascaded H-bridge stage was connected across them to change the produced voltage polarity. However, this MLI topology needs an in-creased components compared to the basic topologies, besides there is a high voltage stresses across switches.
While, in [16], the authors presented three phases asymmetrical multilevel cascaded inverter, where the output voltage of different levels were generated by connected cells in series. It used the phase-shift between the inverter three legs to produce the line voltage instead of using H-bridge to get the AC-voltage different polarities as in [15]. And so on, this topology needs to increase the number of dc-voltage sources and power switches to generate higher number of voltage levels.
It is clear from the above aforementioned works that all trends aim to develop and improve the MLIs power and/or control stages need to be done, as almost all of them need large number of the components count, dc-voltage sources, and electrolytic capacitors. In this paper present a new cascade h-bridge MLI topology that represent reduction in the components count compared to the mentioned literature topologies, and with increasing the output voltage levels number. Furthermore, the proposed topology with the feature of its switches has reduced stresses with unheeding to output voltage levels.
The basic structure of this paper is as follows: the operation principles of the proposed cascade H-bridge inverter is introduced in the next section. After that control

techniques for multilevel inverter will be explained. while in the third section simulation results will be viewed

CASCADE H- BRIDGE MULTI-LEVEL INVERTER STRUCTURE AND OPERATION

The H-bridge unit is considered the heart of the cascade multilevel inverter by series connection of these H-bridges. Single-phase full-bridge or H-bridge inverter unit can produce three level output waveforms as (vdc ,0,-vdc).And the series connection of these units bridge converters can exceed the number of output levels, for example to five or seven dependents to the number of the connected cells. Fig. 1 shows a single-phase structure of the H-bridge unit it is clear from this schematic that each H-bridge consists of two arms each arm involves two switches and the load connected the two arms and due to this configuration looks like h letter in English language and it is called by this appellation. The four switches (power electronic switches) connected with anti-parallel diodes to ensure the bidirectional current flow when the converter connect to passive loads. The other important point in H-bridge operation principle is that the switches of the same arm must work alternatively to avoid the short circuit across the dc source. Figure 2 shows the schematic of single-phase cascade inverter with multi dc sources MDCSs [11]. Each DC source is connected to a single-phase full-bridge inverter. Each inverter level can generate three different voltage outputs. The main duty of this multilevel inverter is to compose the required voltage from several separate dc sources, which may be obtained from batteries, fuel cells, or ultra-capacitors in an HEV. Where v(an) represents the output voltage of the cascaded inverter and it can be calculated by adding the amounts of va1(t),va2(t),vaN(t), Where N is the number of the cascaded bridges. The produced voltage levels from this inverter in symmetrical voltage distribution is directly proportional with the number of the connected h bridge, according to this equation.

$$n = 1 + 2N \tag{1}$$

Where N is the number of the cascaded h bridge.

The maximum vo also can give as the dc sources that cascaded .as:

$$V_{omax} = NV_{dc} \tag{2}$$

From the literature review presented above in this paper it is obvious that the main concerns in order to improve the quality of the produced voltage from the inverter so that it meet the international standards is to increase the produced output levels which lead to decrease the harmonics content but at the same time in symmetrical distribution of DC voltages and from the above two equation it is clear that if we aim to produce more level at the output voltage we have to use more number of DC sources and H-bridges, consequently the cost and the number of the power electronic switches and the size will increase and that is the most constrains or disadvantage related to symmetrical inverters .

In order to overcome this point of symmetric distributions of voltages, asymmetrical topology was introduced in this method voltage distributions between the bridge cells

will be No.t equal for example if we give vdc to the first H-bridge the second cell H-bridge will be supplied by 2vdc. By binary progress distribution of voltages , we will gain an increment in the number of levels produced in the output voltage with the same number of dc sources and switches in the symmetric method .Equation three gives the relation between the produced output labels and the connected H-bridge cells

$$V_{omax} = 2^{(N+1)-1} \tag{3}$$

Equation (3) binary progress ratio

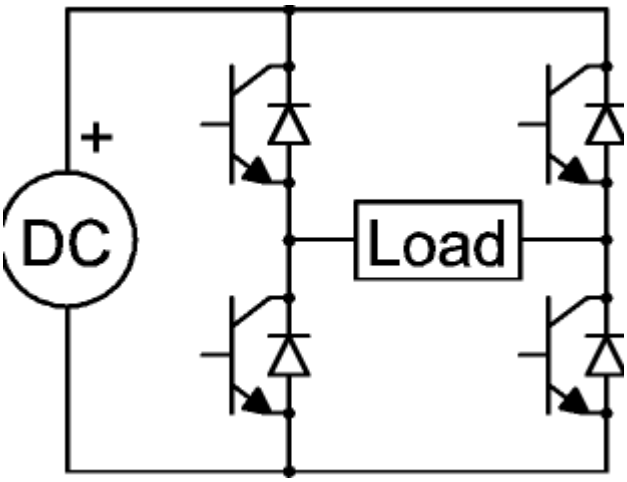

Figure. 1 Single Phase H-bridge Inverter (Three Level Output)

While if we use the ternary progress distribution of voltages between the bridges for example the first cell will be fed with vdc the second will be fed with 3vdc and so on, the equation for the output levels as function with the number of dc sources is given in the following equation,

$$n = 3^n \tag{4}$$

Equation (3) in ternary progress ratio

By comparing the equations (3)-(4) by (1) it is clear that the output levels increased in the asymmetrical topology at the same time by comparing with asymmetric topology. This is just an example to show the difference between symmetric and asymmetric inverter topologies .The way for adjustment of the values of dc sources in this paper is also based in asymmetrical configurations and selected to be as follow [12].

$$V_{dc} = V_{dc1} \tag{5}$$

$$V_{dc\,m} = 2V_{dc1} \tag{6}$$

M=2, 3, N and the output levels number is given as:

$$n = 4N - 1 \tag{7}$$

Where N is the number of the series connected H bridges. The reason behind the selection of this manner is according to the fact that we canNo.t use the charge balance control method in [9] and [10], because of different voltages of batteries.

The main advantages of this method over the fundamental frequency control method is to equalize the amount of power which is drawn from different batteries as results battery life will equalized and reduced the maintence cost. Several modulation patterns can be used to implement the charge balance control method in full wave pattern the angles will route continuously after one cycle while in half-wave pattern the rotating angle will rotate after half cycle. If any pattern is used we will make all the dc sources get charges and balanced after specific time of operation except the battery which use in the first h bridges so the amount of power will be given as:

$$P_{DC}, k = \frac{1}{T}\int_0^T vo_k \ .idc_k \, dt \tag{8}$$

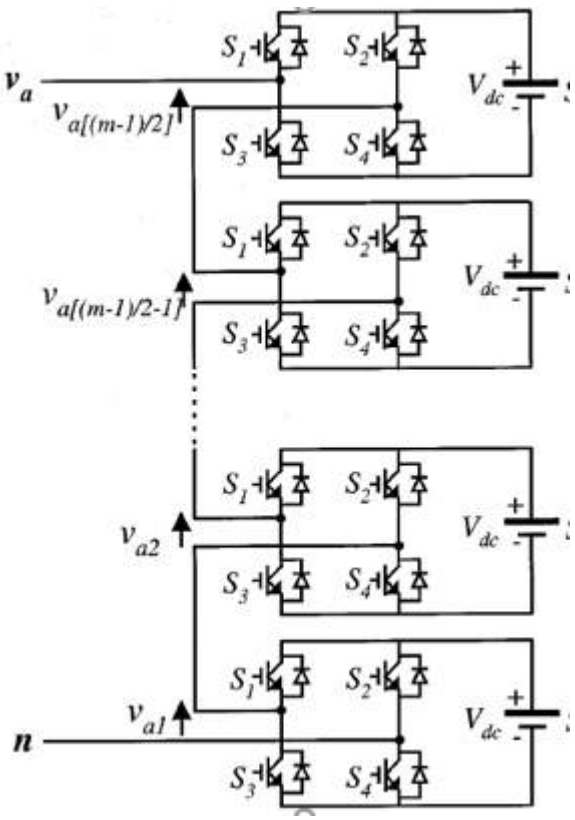

Figure 2. Single Phase Scheme of Cascaded H-bridge Inverter

METHODOLOGY AND CONTROL TECHNIQUES FOR MULTILEVEL INVERTER

There are diverse techniques available for a CHB MLI [13, 15]. Such as Sinusoidal pulse with modulation, space vector pulse with modulation, third-harmonic pwm and fundamental frequency control method Among all those techniques, fundamental frequency control technique (FFCT) which produces less total harmonic distortion (THD) values is most preferable. In this method every semiconductor device is turned on one time per fundamental cycle and that leads to reduce the conduction losses and the electromagnetic interference [6]. on the other hand, it has the drawback related to the amount of power which drawn from one dc source is different from the other sources, so the battery life will be different from each other and that leads to high maintenance cost [2] .In order to overcome this disadvantage of these method, the

charge balance control method is proposed in this work to equalize the amount of power which drawn from each dc source. Figure 3 shows a schematic cooperation between fundamental frequency control method and the charge balance control method. This figure consists of three patterns and it is labelled from up as follows the first pattern depict the fundamental frequency control method and it is clear that there is a difference between the duty cycles of each h bridge cell in this pattern the first H-bridge conduct for very tiny time while the second and third H-bridge conduct for a long period comparing with the first cell and that shows the drawback of this method .In order to overcome this point the charge balance control method take its place in the second and third patterns if we focus in these patterns we will notice that the duty cycle equalized in each H-bridge cells by using charge balance method that means every switches will conduct with equal period which means the avoidance of excessive heat of switches which conduct for long period in fundamental method ,related to pattern three it represent also a charge balance control method but with half wave swap instead of full wave which shown in pattern two and that's why it is called as half wave charge balance control method .

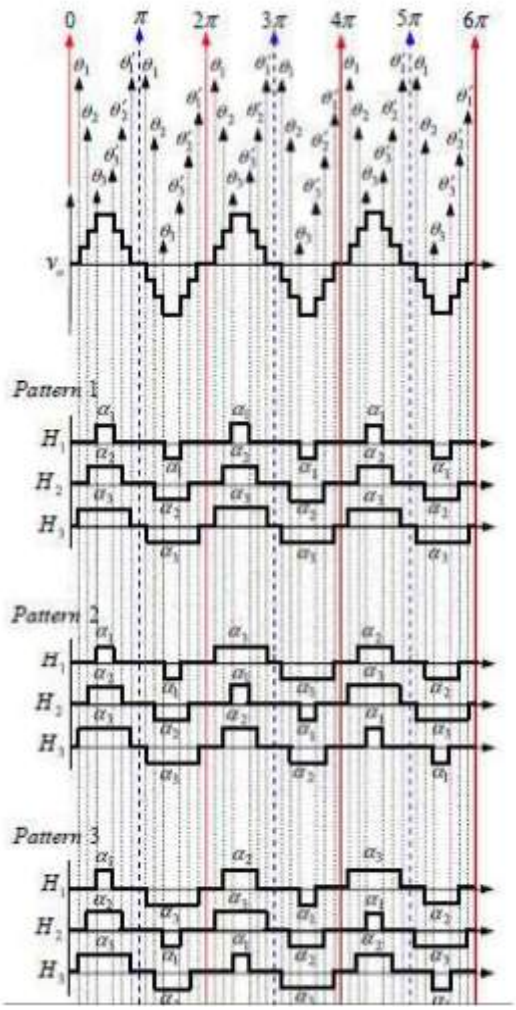

Figure 3. Pattern 1 Fundamental Frequency Control Method

Pattern 2 Full Wave Charge Balance Control Method
Pattern 3 Half Wave Charge Balance Control Method

From figure 3 it is clear that with the charge balance control technique the duty cycle of each H-bridge will equitize so the amount of power that drawn from each cell will be the same on the other hand this method related to symmetric distributing of voltages which have the drawback of less No. of output levels so to solve this problem and to increase the produced No. of levels at the output voltage wave form, so to solve this problem this paper implements asymmetric inverter as well as it uses charge balance control method. The charge balance will be implemented to all cells except the first one. The distribution of voltages will be as follows: the first H-bridge cell will be fed with vdc while the proceedings cells will be fed with 2vdc (binary manner distribution) and will earn fifteen levels by using four H-bridge cells at the output terminals of the inverter instead of 9 level related to the slandered symmetrical topology .

RESULTS AND FINDINGS

Simulation results in MATLAB 2017b are used to prove the operation of the proposed inverter two experiments are done one by using fundamental frequency control method while the other uses the charge balance control method the aim of these two experiment is to show clearly the difference between the two methods furthermore to verify the advantage of the proposed method in the following subsection we put the results of the inverter by using fundamental frequency control method while the results which related to charge balance control method take its place in the after the next division .

Results by Using Fundamental Frequency Control Method

It is clear from the figure 2 shown above that the proposed inverter formed from four H-bridge cell. Each block cell contains four terminals: two of them represent the output of cell while the other represent the input for the gates. Figure four shows the H-bridge block in details.

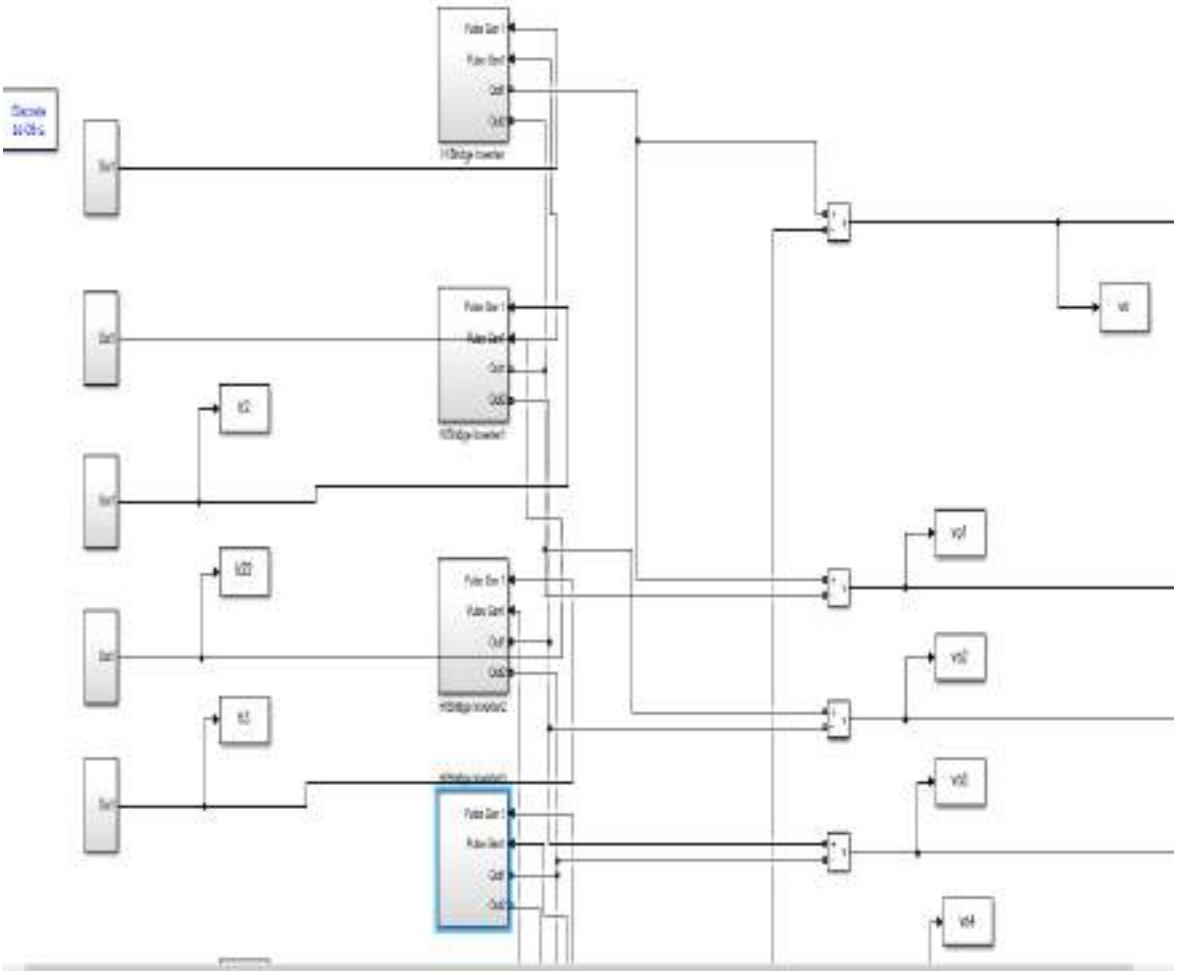

Figure 4. Simulink Block of the Proposed Inverter.

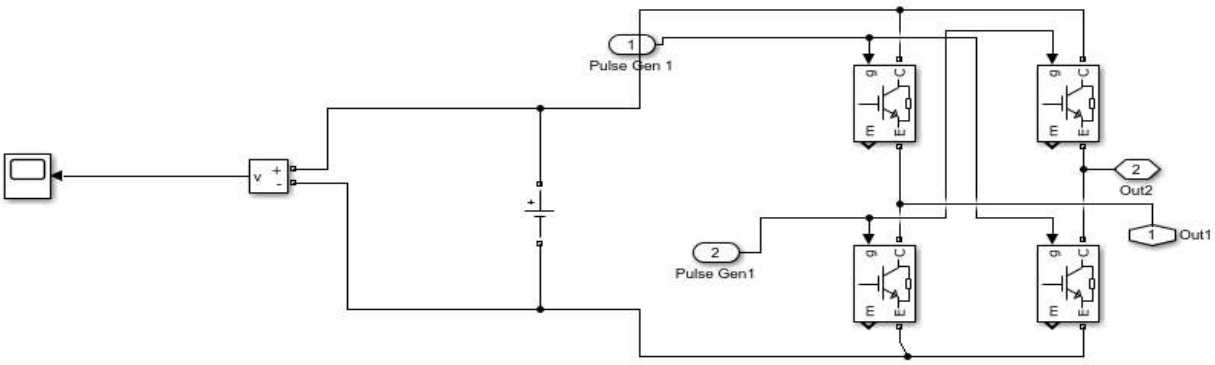

Figure 5. H-bridge Block in Details.

The following figures shows the output of each cell and it is clear that by using this method of control we can achieve e more No. of levels but the duty cycle of each H-bridge unit is different from the other and that means the amount of power drawn from each cell is different from the amount of power of the adjacent cell.

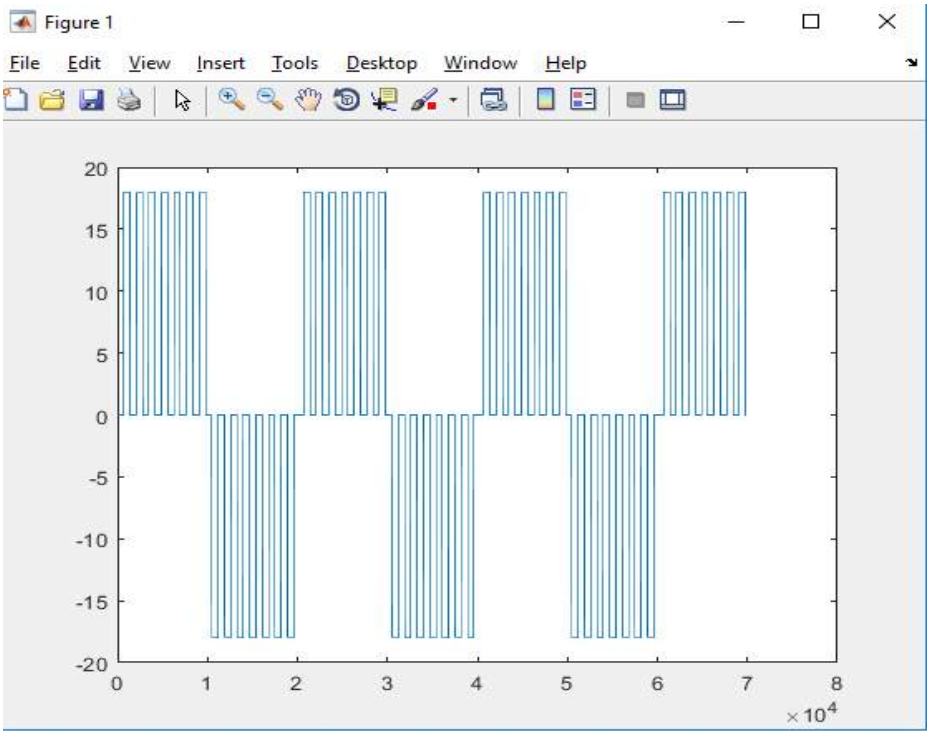

Figure 6. First H-bridge Output Waveform

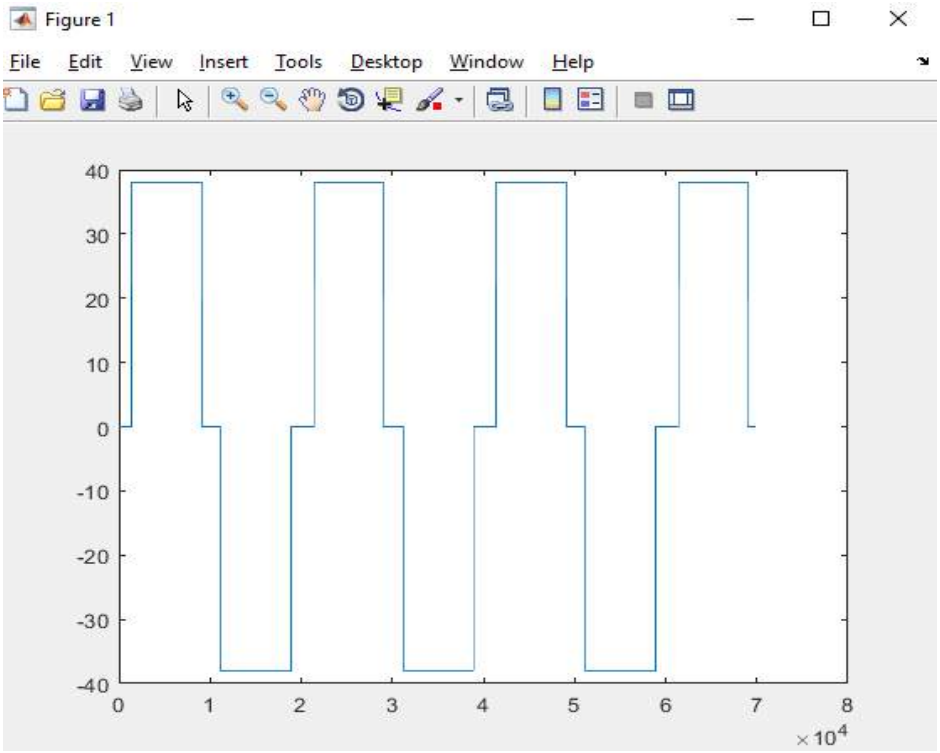

Figure 7. Second H-bridge Output Waveform

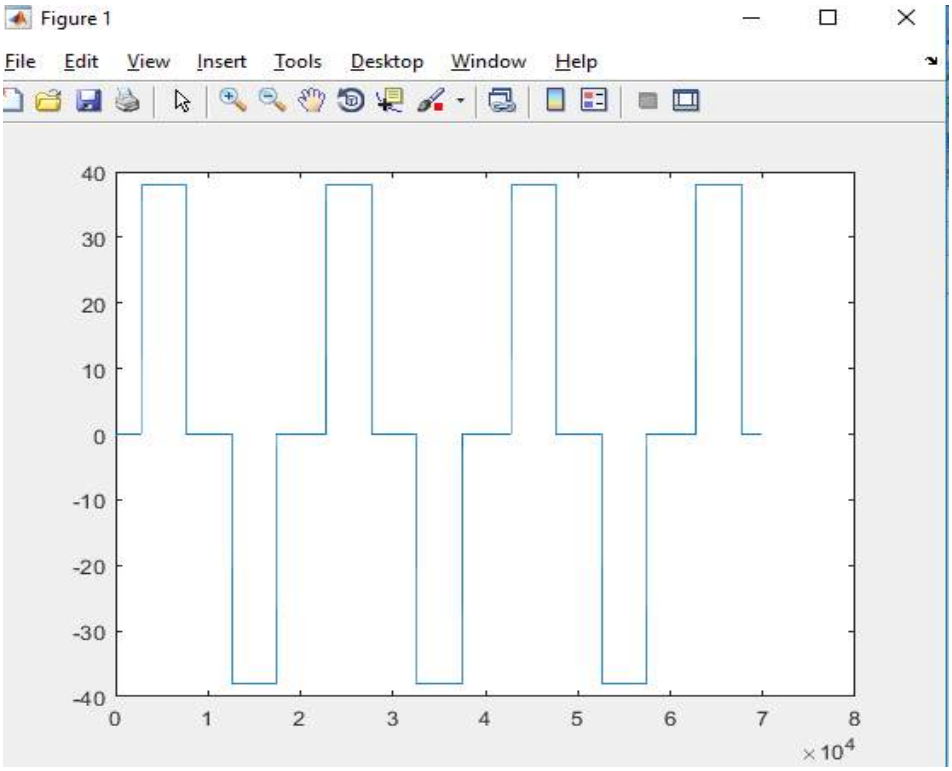

Figure 8. Third H-bridge Output Waveform

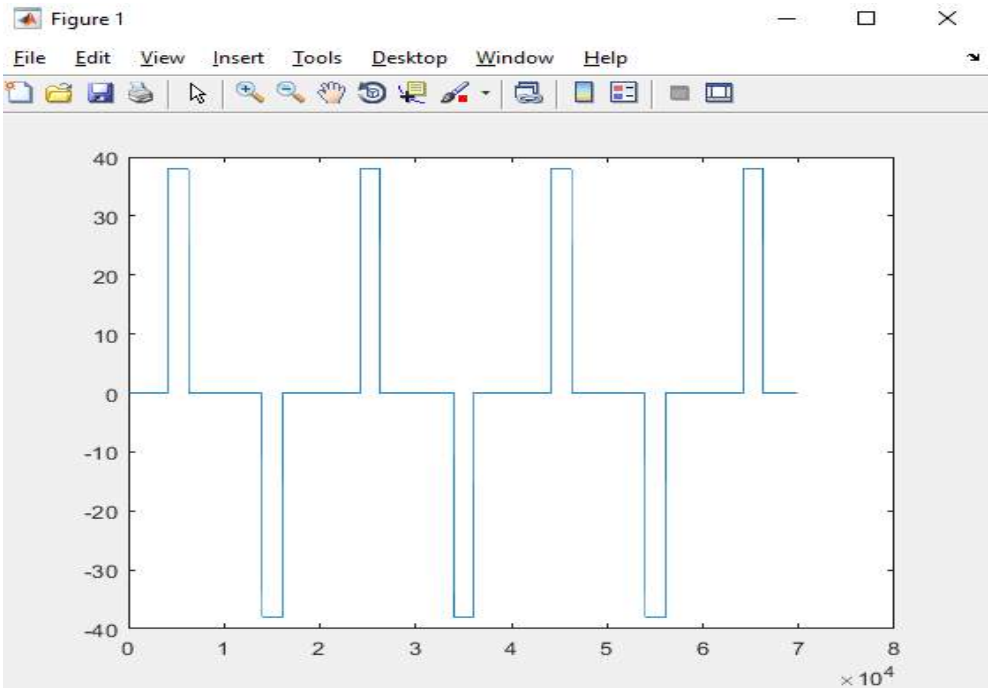

Figure 9. Fourth H-bridge Output Waveform

Results by Using Full Wave Charge Balance Control Method

This experiment uses full wave charge balance control method. The following figures shows the output of each H-bridge and it is clear that by using this method the on duration or the duty cycle of each H-bridge will be equalize.

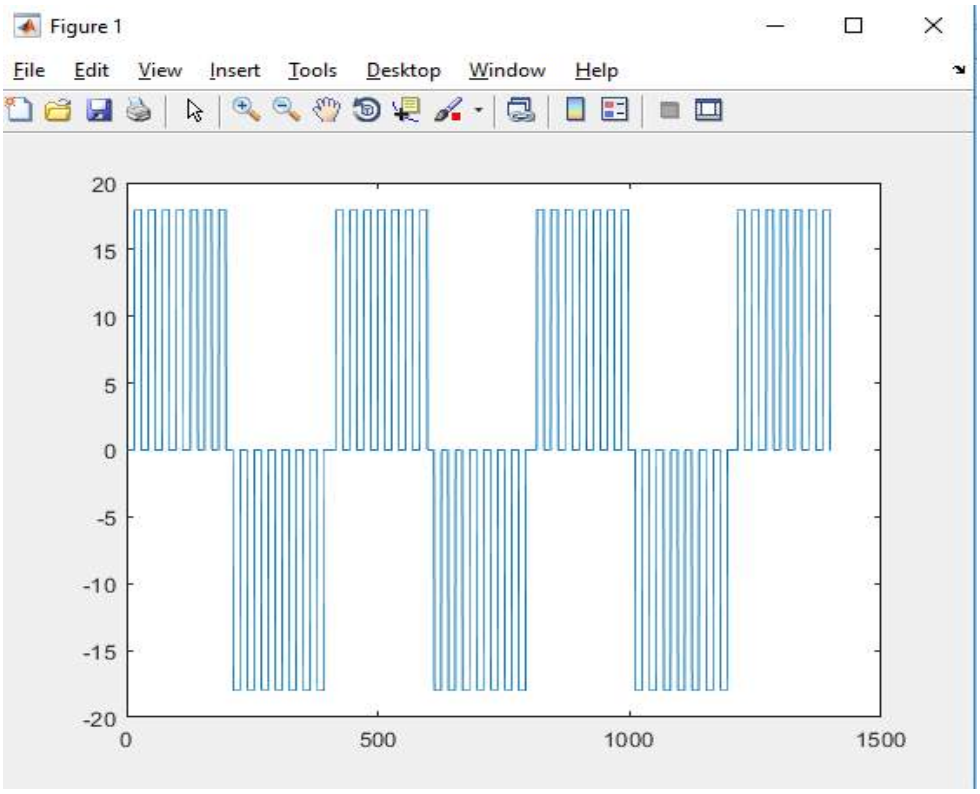

Figure 10. First H-bridge Output Waveform by Full Wave Charge Balance Control Method

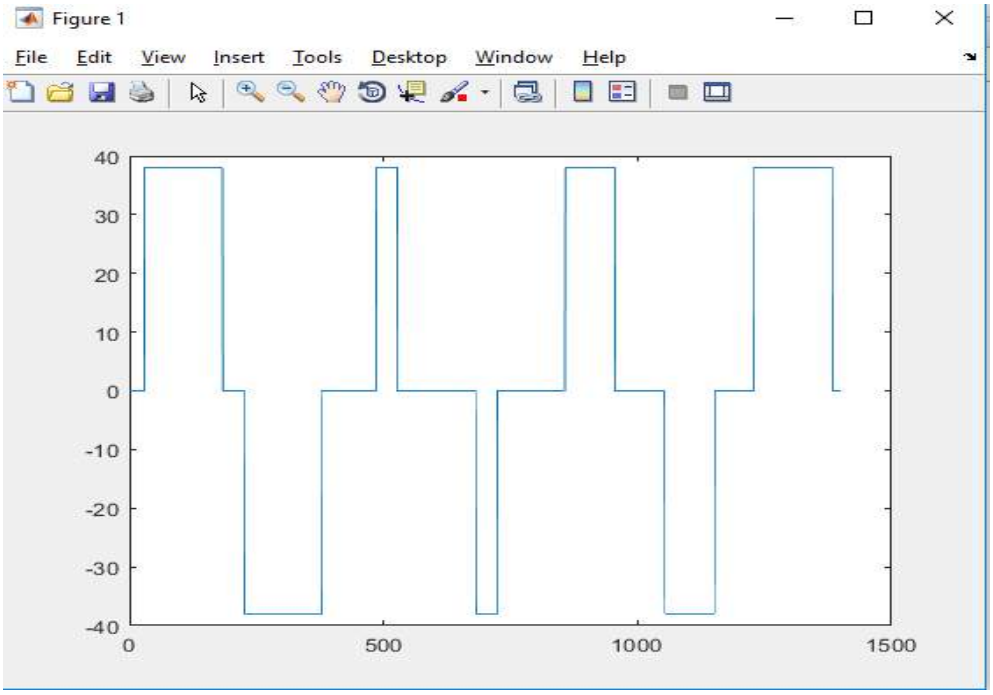

Figure 11. Second H-bridge Output Waveform by Full Wave Charge Balance Control Method

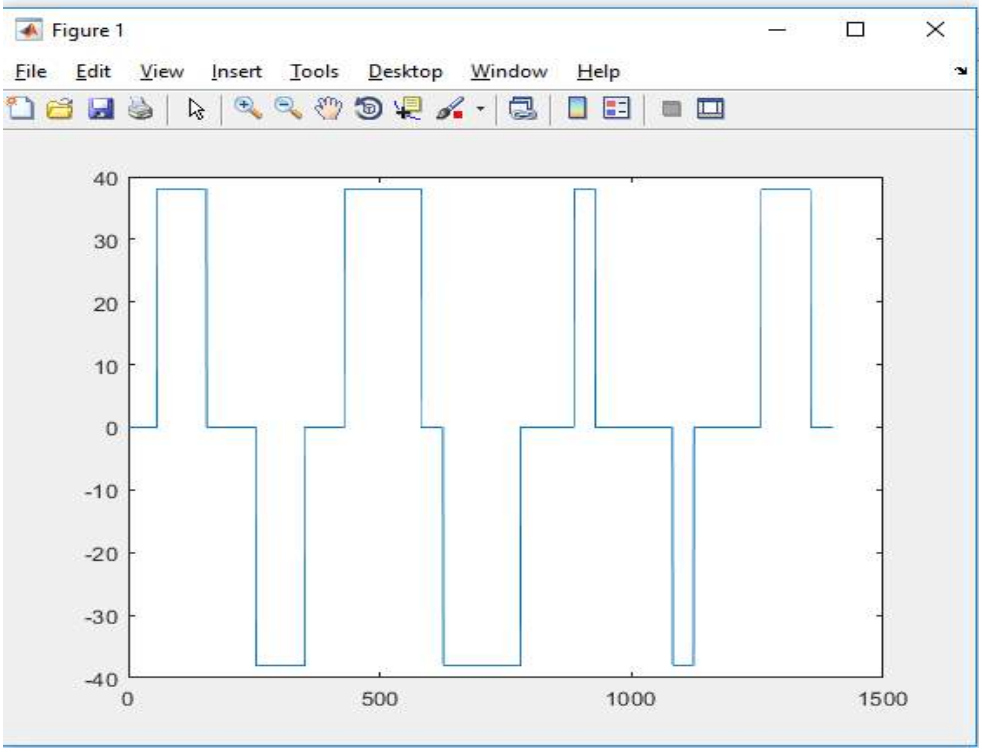

Figure 12. Third H-bridge Output Waveform by Full Wave Charge Balance Control Method

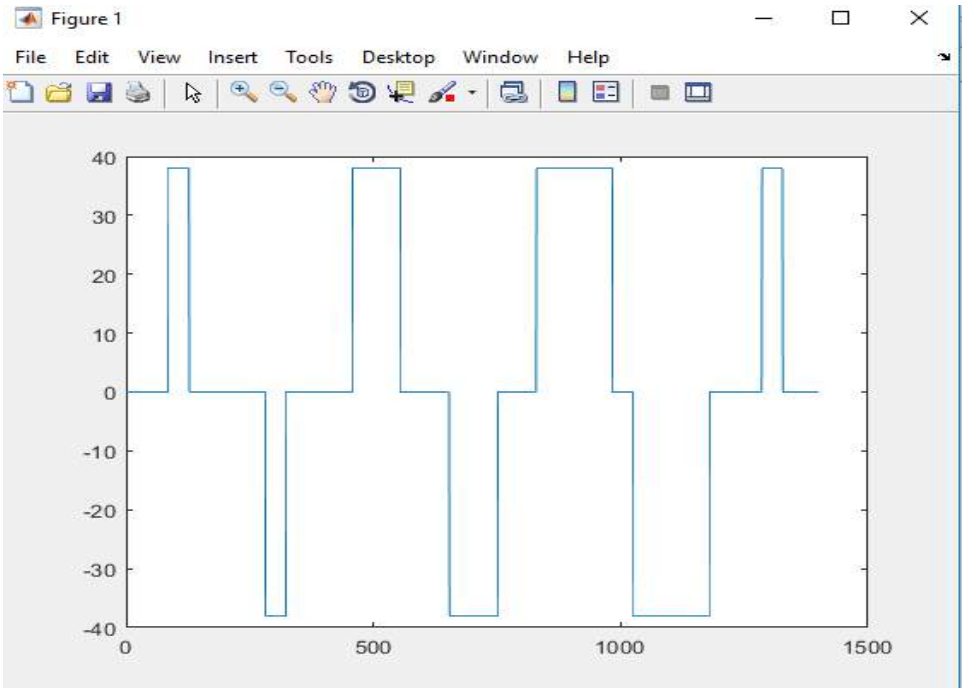

Figure 13. Fourth H-bridge Output Waveform by Full Wave Charge Balance Control Method

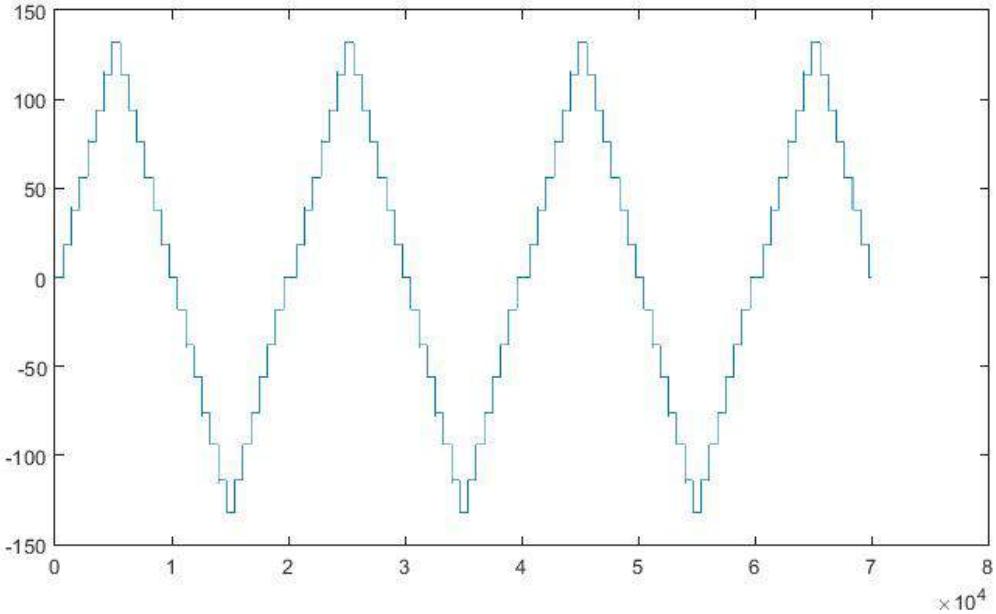

Figure 14. Final Output Wave Form

CONCLUSION

In this work an improvement in the cascade inverter is done this improvement includes two points: the first is related to the number of the output levels witch increased by using the asymmetrical topology with minimum number of dc sources and semiconductor switches and the second concern with the amount of power which drawn from each DC source (except the first source) is equalized by using the charge balance control method this inverter
is working perfectly as shown in the simulation result .

REFERENCES

[1] Adam, G. P., & Williams, B. W. (2014). New emerging voltage source converter for high-voltage application: hybrid multilevel converter with dc side H-bridge chain links. *IET Generation, Transmission & Distribution*, *8*(4), 765-773. doi:10.1049/iet-gtd.2013.0076

[2] Agelidis, V., Baker, D., Lawrance, W., & Nayar, C. (n.d.). A multilevel PWM inverter topology for photovoltaic applications. *ISIE '97 Proceeding of the IEEE International Symposium on Industrial Electronics*. doi:10.1109/isie.1997.649027

[3] Babaei, E. (2011). Charge Balance Control Methods for a Class of Fundamental Frequency Modulated Asymmetric Cascaded Multilevel Inverters. *Journal of Power Electronics*, *11*(6), 811-818. doi:10.6113/jpe.2011.11.6.811

[4] Bahravar, S., Babaei, E., & Hosseini, S. H. (2012). New cascaded multilevel inverter topology with reduced variety of magnitudes of dc voltage sources. *2012 IEEE 5th India International Conference on Power Electronics (IICPE)*. doi:10.1109/iicpe.2012.6450408

[5] Calais, M., Borle, L., & Agelidis, V. (n.d.). Analysis of multicarrier PWM methods for a single-phase five level inverter. *2001 IEEE 32nd Annual Power Electronics Specialists Conference (IEEE Cat. No..01CH37230)*. doi:10.1109/pesc.2001.954308

[6] Cintron-Rivera, J. G., Li, Y., Jiang, S., & Peng, F. Z. (2011). Quasi-Z-Source inverter with energy storage for Photovoltaic power generation systems. *2011 Twenty-Sixth Annual IEEE Applied Power Electronics Conference and Exposition (APEC)*. doi:10.1109/apec.2011.5744628

[7] Ding, K., Cheng, K., & Zou, Y. (2012). Analysis of an asymmetric modulation method for cascaded multilevel inverters. *IET Power Electronics*, *5*(1), 74. doi:10.1049/iet-pel.2010.0370

[8] Farokhnia, N., Fathi, S., Yousefpoor, N., & Bakhshizadeh, M. (2012). Minimisation of total harmonic distortion in a cascaded multilevel inverter by regulating voltages of DC sources. *IET Power Electronics*, *5*(1), 106. doi:10.1049/iet-pel.2011.0092

[9] Hossain, M. K., & Ali, M. H. (2014). Low voltage ride through capability enhancement of grid connected PV system by SDBR. *2014 IEEE PES T&D Conference and Exposition*. doi:10.1109/tdc.2014.6863248

[10] Kouro, S., Leon, J. I., Vinnikov, D., & Franquelo, L. G. (2015). Grid-Connected Photovoltaic Systems: An Overview of Recent Research and Emerging PV Converter TechNo.logy. *IEEE Industrial Electronics Magazine*, *9*(1), 47-61. doi:10.1109/mie.2014.2376976

[11] Linus, R. M., & Damodharan, P. (2015). Maximum power point tracking method using a modified perturb and observe algorithm for grid connected wind energy conversion systems. *IET Renewable Power Generation*, *9*(6), 682-689. doi:10.1049/iet-rpg.2014.0070

[12] Manjrekar, M., & Lipo, T. (n.d.). A hybrid multilevel inverter topology for drive applications. *APEC '98 Thirteenth Annual Applied Power Electronics Conference and Exposition*. doi:10.1109/apec.1998.653825

[13] Osborn, D. (2013). Wind Power Grid Integration wind power grid integration : Transmission Planning wind power grid integration transmission planning. *Renewable Energy Systems*, 1740-1768. doi:10.1007/978-1-4614-5820-3_90

[14] Sung-Jun Park, Feel-Soon Kang, Man Hyung Lee, & Kim, C. (2003). A new single-phase five-level PWM inverter employing a deadbeat control scheme. *IEEE Transactions on Power Electronics*, *18*(3), 831-843. doi:10.1109/tpel.2003.810837

[15] Rao, S. N., Kumar, D. V., & Babu, C. S. (2013). New multilevel inverter topology with reduced number of switches using advanced modulation strategies. 2013

International Conference on Power, Energy and Control (ICPEC). doi:10.1109/icpec.2013.6527745.

EFFECT OF LED TEMPERATURES ON DRYING TIME OF HAZELNUT (CORYLUS AVELLANA L.) AT NATURAL CIRCULATION DRYING SYSTEMS

Mithat AKGÜN
Makine ve Metal Teknolojileri Bölümü, Teknik Bilimler MYO, Ordu Üniversitesi
mithatakgun@gmail.com

Özer ŞENYURT
Elektrik ve Enerji Bölümü, Teknik Bilimler MYO, Ordu Üniversitesi
ozersenyurt@hotmail.com

Levent KANDEMİR
Yenilenebilir Enerji, FBE, Ordu Üniversitesi
leventkandemir52@gmail.com

ABSTRACT: Much of the world hazelnut (Corylus Avellana L.) production is planted in the provinces on the coastal cities in the Black Sea region of Turkey. That region is rainy and quite humidity during hazelnut harvest season. A well-designed mechanical drying system can be a reasonable solution for drying the hazelnuts in a short period of time by protecting their quality.
In this experimental work, a natural circulating drying system with LED's was used with three different color temperatures of 3000 K, 4000 K and 6500 K to show mechanical drying of the hazelnuts in a short time with less energy and preserving food properties. Within the established system, the hazelnut has been tested in three different range of diameters (Ø14-15 mm, Ø16-17 mm, Ø18 mm and above). The distance between the LED and the nut was 10 cm and the lumens (10,000 lumens) were constant.
According to the results, hazelnut drying time increases by about 10% as hazelnut size increases. As the LED color temperature increases, the hazelnut dries up longer. Compared with solar drying, the drying time of the LED is 75% shorter on average. The hazelnut internal temperature is about 10% higher than the inside temperature of the oven depending on the hazelnut size and LED color temperature. LED's of 6500 K are comply with optimum drying temperature. Also, LED's with 3000 K value are comply with optimum drying time.

Key words: hazelnut drying, drying curve, LED color temperature, mass transfer.

DOĞAL DOLAŞIMLI KURUTMA SİSTEMLERİNDE LED SICAKLIKLARININ FINDIĞIN (CORYLUS AVELLANA L.) KURUMA SÜRESİNE ETKİSİ

ÖZET: Dünya fındık (Corylus Avellana L.) üretiminin büyük miktarı Türkiye'nin Karadeniz kenarında olan illerde gerçekleştirilmektedir. Fındık hasat zamanında bölge yağışlı ve oldukça nemlidir. Bu delenle fındığın güneşte kurutularak neminin %6' ya düşürülmesi oldukça zaman almakta, fındıkta istenmeyen kalite kayıplarına ve bozulmalara sebep olmaktadır. Fındığın kalitesinin koruyarak kısa sürede, daha az

maliyetle ve hem sanayicinin hem de üreticinin kullanabileceği bir mekanik kurutma sistemine ihtiyaç duyulmaktadır.
Bu deneysel çalışmada, daha az enerji ile kısa sürede ve gıda özelliklerini koruyacak şekilde fındığın mekanik kurutulmasını sağlayacak üç farklı renk sıcaklığına (3000 K, 4000 K, 6500 K) sahip LED'li doğal dolaşımlı kurutma sistemi kullanılmıştır. Kurulan sistem içerisinde fındık üç farklı çap aralığında (14-15 mm, 16-17 mm, 18 mm ve üstü) denenmiştir. LED ile fındık arasındaki mesafe 10 cm ve lümen değerleri (10.000 lümen) sabit tutulmuştur.
Fındık kuruma süresi fındık boyutu arttıkça yaklaşık %10 artmaktadır. LED renk sıcaklığı arttıkça fındık daha uzun sürede kurumaktadır. Güneşte kurutma ile karşılaştırıldığında LED' li kurutma süresi ortalama %75 daha kısadır. Fındık iç sıcaklığı fırın içi sıcaklığından (fındık boyutu ve LED renk sıcaklığına bağlı olarak değişir) yaklaşık % 10 daha fazladır. Doğal dolaşımlı LED'li kurutma sistemlerinde 10 cm mesafe için fındık iç sıcaklığı ve ortam sıcaklığı dikkate alındığında en uygun kurutma ortam sıcaklığını 6500 K değerindeki LED'ler sağlarken, en kısa sürede kurutmayı da 3000 K değerindeki LED'ler sağlamıştır.

Anahtar kelimeler: fındık kurutma, kuruma eğrisi, led renk sıcaklığı.

GİRİŞ

Karadeniz bölgesi sahil kesiminde bulunan illerde (Düzce, Sakarya, Samsun, Ordu, Giresun Trabzon, Rize) fındık tarımı yapılmakta ve çoğunlukla halkın geçim kaynağını oluşturmaktadır. Dünya fındık üretiminin yaklaşık %70 bu bölgede üretilmektedir. Fındık yurt içerisinde ve büyük oranda da ihraç edilerek tüketilmektedir.

Bölgede fındık hasadı, fındık türü ve arazinin yüksekliğine bağlı olarak Ağustos başı Eylül sonu arasında yapılmaktadır. Fındık olgunlaşmadan (ilk nem %26 - %36) dalından koparılmakta veya olgunlaşmış fındık (ilk nem %22 - %28) yerden toplanmaktadır. Genellikle bir zülüf içerisindeki fındık toplandıktan sonra bir süre yere serili olarak güneşte kurutulmakta ve fındık nemi yaklaşık %16-20 olduğunda fındık patozlanarak zurufundan fındık ayrılmaktadır. Zurufundan arılan kabuklu fındık bir örtü üzerine serilerek güneşte iç fındık nemi max. %6'a düşene kadar kurutulmaktadır. Fındık hasat döneminde bölge genellikle oldukça yağışlı ve nemli olduğu için yere serili olarak kurutulan fındıkta kalite kayıpları oluşmakta ve zaman zamanda fındık çürüyerek ziyan olmaktadır. Ayrıca toplam fındık kuruma süresi (zuruflu ve zurufsuz) hava şartlarına bağlı olarak 7 gün ila 20 gün arasında değişmekte bu da işçilik maliyetini artırmakta ve zaman kayıplarına neden olmaktadır. Fındık kurutma problemlerini en aza indirmek için çok az miktarda kabuklu fındık mekanik kurutucularda kurutulmaktadır.

Mekanik fındık kurutucuları genelde silindirik bir deponun içerisindeki helezonla karıştırılan fındığın üzerinden ısıtılmış hava sevk edilmesi ile fındığın kurutulması şeklinde çalışmaktadır. Bu sistemlerde yakıt olarak ya mazot ya da fındık dalları ve kabukları kullanılmaktadır. Mazot fiyatının artması, sistemin hantal olması ve kurutma süresinin de nispeten uzun olması dolayısıyla sistem sadece fındık

fabrikalarında kullanılmakta ve fındık üreticileri tarafından tercih edilmemektedir. Çok azda olsa fındık raflı sistemlerde üzerinden ısıtılmış hava geçirilerek mekanik olarak kurutulmaktadır. Bu sistemlerde fındık kuruma süresini ve kalitesini etkileyen fındık türü, boyutu, hava hızı, hava sıcaklığı ve nemi üzerinde bir kontrol yoktur.

Üründen şartlandırılmış havaya olan kütle transferi parametrelerini ve kuruma sırasında fındıkta oluşan fiziksel ve kimyasal değişimleri belirlemek için çok farklı teorik ve deneysel çalışmalar yapılmıştır.

Kurutma prosesinde, nemli malzemelerin ısı ve kütle transferini tanımlayan ilk teorik model 1973 yılında Luikov tarafından önerilmiştir.

Demirtaş C. (1996), dalından koparılmış nem oranı yüksek fındığın mekanik kurutma davranışını incelemiştir. Kurutma havasının dört farklı bağıl nemi (%0,45 - 0,70), üç farklı hava hızı (0,2 - 0,6 m/s)ve dört farklı hava sıcaklığında (25 - 50°C) çalışılmış ve tombul fındığın 3 günde (72 saat) kuruduğunu tespit etmiştir.

Demirtaş C. ve ark. (1998) kabuklu fındıkların (tekne, hava boşluğu ve çekirdek) tek tabakalı kurumasını modellemek için difüzyon tabanlı bir kurutma modeli kullanılmışlar. Kabuklu fındıklardan elde edilen deneysel sonuçlar teorik sonuçlarla korelasyon göstermiştir. Fındık için yayılma kuvveti ifadesi kullanıldığında, tüm fındığın nem içeriğinin ve sıcaklığının difüzivitesini açıklayan bir korelasyon belirlenmiştir. Kabuklu fındık difüzivitesi, 25 - 45°C ortam sıcaklığı, 0,2 - 0,3 - 1 m/s hava hızı ve havaya göre %60 bağıl nemdeki verilere en uygun teorik eğriler kullanılarak belirlenmiştir. Kabuklu fındığın difüzivitesi, kurutma havası sıcaklığının ve hızının bir fonksiyonu olarak belirlenmiştir.

Çetin M. ve Erişen A.(2011), yaptıkları çalışmada, suni kurutmanın Türk fındığı kalitesine etkisini yatay silindirik tip bir kurutucu kullanarak araştırmışlar. Geleneksel kurutma yönteminin aksine bir girdap akışı ile çalkalanmış ısıtılmış havada (1,0m/s ve 40-55°C) fındık kurutulmuştur. Taze fındıkların yapay bir kurutucuda kurutulmasındaki en uygun koşullar, uzun süreli depolamayı kolaylaştırmak için maksimum nem içeriğine (%5-6) sahip olarak belirlenmiştir. Sıcak hava ile en kısa kuruma süresi 10,5 saat olarak ölçülmüştür.

Krokida ve ark. (2003), kurutucu hava şartlarının (hızı, sıcaklığı ve nemi) ve ürünün karakteristik boyutunun kuruma kinetiğine olan etkisi incelemişlerdir. Kurutmada seçilen ürünler; patates, havuç, sarımsak, mantar, soğan, pırasa, mısır, bezelye, kereviz, balkabağı ve domatestir. Nem transferinin hesaplanmasında logaritmik model kullanılmıştır. Kurutulan ürünlerin denge nemi %10 olarak belirlenmiştir. Çalışma, havanın farklı iki sıcaklığında yapılmıştır (30°C ve 70°C). Kısmen sıcaklıkla kurutma sabitlerinin arttığı denge nem bileşeninin de azaldığı belirtilmiştir.

Kaya ve ark. (2011) yaptıkları deneysel çalışmada; hava parametrelerinin çeşitli değerleri (25°C, 35°C, 45°C ve 55°C sıcaklık; 0,3, 0,6 ve 0,9 m/s hızlar; %20, %40, %60 ve %80 bağıl nem) için fındığın kurutma özelliklerini tespit etmişlerdir.

López ve ark. (1998), farklı sıcaklıklarda (30°C - 80°C) İspanyol fındığı (Corylus avellana L.) için denge nem içeriği izotermlerini statik gravimetrik yöntem kullanılarak belirlemişler. İnce tabaka kurutma deneyleri, fındığın kurutma özelliklerini belirlemek için zorlanmış hava sirkülasyonu ve farklı çalışma koşullarında yapılmıştır. Hava sıcaklığı (30°C - 70°C), hava hızı (0,5 m/s - 2 m/s) ve kuruma yatağı yükleme yoğunluğunun (50 kg/m^2 - 150 kg/m^2) etkisinde, kabuksuz ve kabuklu fındık incelendi. G.A.B.'nin deneysel denge nem içeriği verilerine uyacak altı matematiksel model kullanılmış ve modelin en uygun olduğu görülmüştür. Fick'in difüzyon modeline deneysel ince tabakalı kurutma eğrileri yerleştirilerek difüzyon katsayıları belirlenmiş. Etkin difüzyon katsayısının sıcaklıkla değişimi Arrhenius tipinde olduğunu ve kurutma parametreleri k ve n'nin hava sıcaklığı ve bağıl nem ile ilişkili olduğunu ortaya koymuşlardır.

Karadeniz bölgesindeki uygun olmayan fındık kurutma şartlarından doğan olumsuzlukları gidermek için çok farklı çalışmalar yapılmış fakat fındığın kalitesini koruyarak daha az enerji ile kısa sürede ve gıda özelliklerini koruyacak şekilde fındığın mekanik kurutulmasını sağlayacak, hem üreticilerin hem de fındık fabrikalarının kullanabileceği bir fındık kurutma sistemine ihtiyaç vardır. Bu açığın kapatılması için daha düşük enerji maliyetli ve uzun ömürlü (sürekli çalışma halinde 15 yıl) üç farklı renk sıcaklığına (3000 K, 4000 K, 6500 K) sahip LED'li doğal dolaşımlı kurutma sistemi tasarlanmış ve bu sistem içerisinde kabuklu fındık kurutma deneyleri yapılmıştır.

Deneysel Çalışma

Bu deneysel çalışma için, uzun kullanım ömürlü ve düşük enerji maliyetli Şekil 1'de verilen LED'li fındık kurutma sistemi tasarlanmış ve sistemin imalatı gerçekleştirilerek kurutma deneyleri yapılmıştır. Bu sistemde ısıtıcı olarak LED renk sıcaklık skalasının farklı bölgelerinden olmak üzere üç farklı renk sıcaklığına (3000K, 4000K, 6500K) sahip LED'ler kullanılmıştır. Üç farklı renk sıcaklığı için ortam ışık akısı yaklaşık 10.000 Lümen olarak sabit tutulmuştur. Sistem içerisinde fındık ile LED arasındaki mesafe 10 cm olarak sabit tutulmuştur. LED'li kurutmanın fotoğrafı Şekil 2'de verilmiştir.

LED'li kurutma ile karşılaştırma yapabilmek için yaş fındık, geleneksel yöntem (güneşte kurutma) ve mekanik yöntem (etüvde 44°C) ile de kurutulmuştur. Güneşte kurutmada gündüz gölge sıcaklığı maksimum 32°C ve gece minimum 26°C, güneş altında ortam sıcaklığı maksimum 38,7°C ve fındık iç sıcaklığı 62,3°C olarak ölçülmüştür. Güneşte kurutmanın fotoğrafı Şekil 3'de verilmiştir.

Deneylerde Giresun ilinden hasat edilen Tombul fındık (Corylus Avellana L.) kullanılmış fındık içinin ilk nemi infrared nem tayin cihazı ile ortalama %34 ölçülmüştür. Kurutma işlemi üç farklı çap aralığındaki (Ø14-15 mm, Ø16-7 mm, Ø18 mm ve üstü) kabuklu fındık ile yapılmıştır.

Kurutucu içerisinde ışınım ve doğal dolaşımla ısı transferi gerçekleşmiş ve fırın içerisindeki hava hızı sıfır kabul edilmiştir. Kurutma sisteminin dış ortamı deneyler

boyunca 30°C'de sabit tutulmuştur. Işınımın fırın ve fındık iç sıcaklığına etkisini belirlemek için, fındık içi sıcaklığı ve kurutma fırının iç sıcaklığı thermo elemanlarla sürekli olarak ölçülmüştür.

Deneyler sırasında fındığın zamana bağlı kütle kaybı, ortam sıcaklığı, fırın iç sıcaklığı ve fındık iç sıcaklığı ölçülmüştür. Tüm deneyler iç fındık nemi %6'ya düştüğünde sonlandırılmıştır.

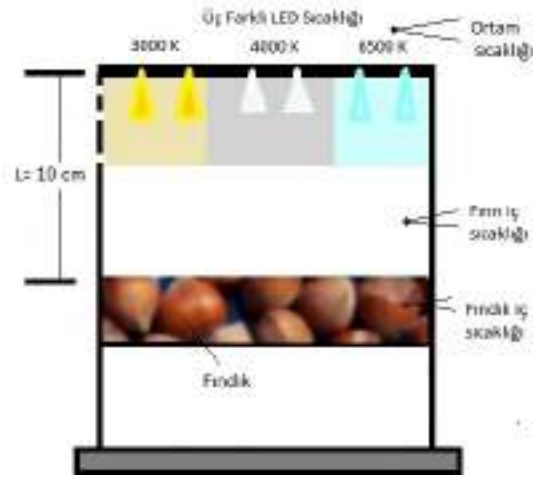

Şekil 1. LED'li fındık kurutma sisteminin şematik görünüşü

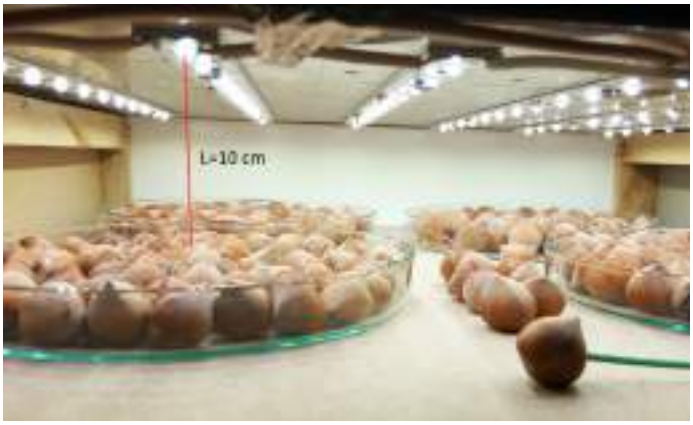

Şekil 2. LED'li fındık kurutma sistemi

Şekil 3. Güneşte fındık kurutma

BULGULAR VE TARTIŞMA

Fındığın mekanik kurutulmasını sağlamak için 3000 K, 4000 K ve 6500 K renk sıcaklıklı LED'li kurutma, etüv (44°C= sabit) ve güneşte kurutma sistemlerinde sıcaklık değişimleri ve kütle kayıpları ölçülmüştür.

Kurulan sistem içerisinde fındık, üç farklı çap aralığında 14-15 mm, 16-17 mm, 18 mm ve üstü olmak üzere 5 farklı yöntemde kurutulmuştur.

Kurutma sıcaklığının fındığın kalitesini etkilemesi dolayısıyla hem zamana bağlı sıcaklık değişimleri hem de zaman bağlı fındık kütle kaybı grafikleri elde edilse de burada tüm parametreleri ortaya koymaya yetecek kadar grafik verilmiştir.

Şekil 4'de LED renk sıcaklığına bağlı olarak fındık iç sıcaklığının zamana bağlı değişimi verilmiştir. Grafikte görüldüğü gibi ortam sıcaklığı 30°C iken LED ile ısıtılan fındık iç sıcaklığı (max. 49 - 56°C) her bir LED değeri için zamanla yaklaşık sabit kalmaktadır. LED renk sıcaklığı arttıkça fındık iç sıcaklığı ters orantılı olarak düşmektedir. Uzun süreli fındık iç sıcaklığının 50°C üzerde olması fındık kalitesini (fındıkta peroksit ve serbest yağ asit miktarında artış görülmektedir) bozmaktadır. Bu nedenle, verilen geometri için doğal dolaşımlı fındık kurutmada 6500 K renk sıcaklığı daha uygundur.

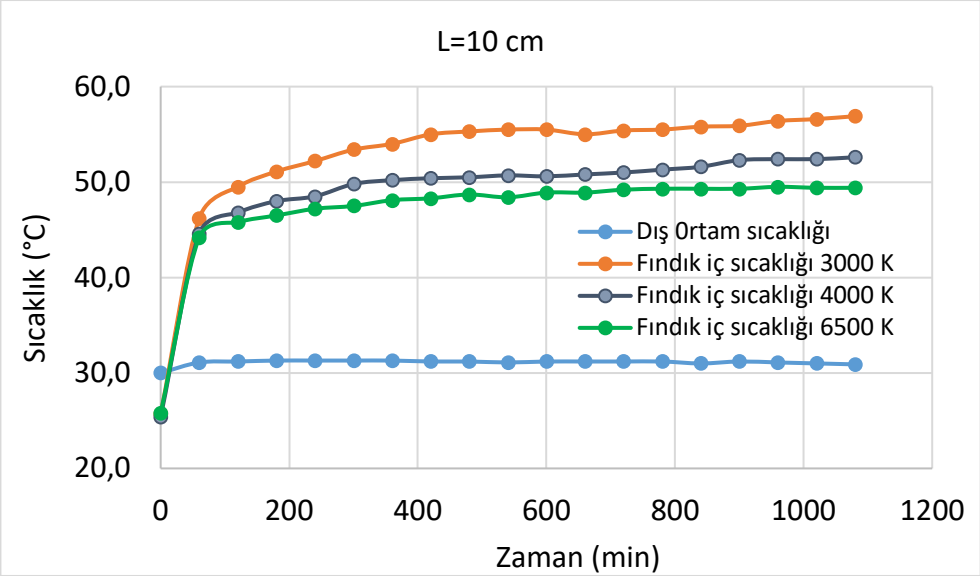

Şekil 4. LED renk sıcaklığına bağlı olarak fındık iç sıcaklığının zamana bağlı değişimi

Şekil 5'de LED renk sıcaklığına bağlı olarak fırın iç sıcaklığının zamana bağlı değişimi verilmiştir. LED renk sıcaklığı artarken fırın iç sıcaklığı ters orantılı olarak düşmektedir.

Verilen fırın geometrisinde üç farklı LED sıcaklığı için zamana bağlı fırın iç sıcaklıkları optimum sıcaklık aralığında (44,9°C - 47,7°C) kalmıştır.

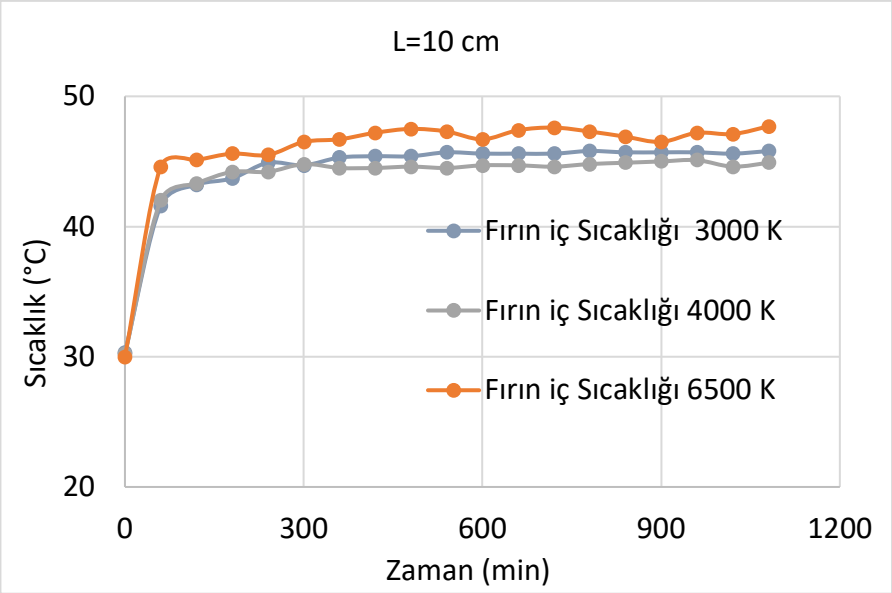

Şekil 5. LED renk sıcaklığına bağlı olarak fırın iç sıcaklığının zamana bağlı değişimi

LED renk sıcaklığının (3000 K) fırın sıcaklığı ve fındık iç sıcaklığına etkisi Şekil 6'da verilmiştir. Işınım etkisi ile fındık iç sıcaklığı fırın içi sıcaklığından LED renk sıcaklığına bağlı olarak değişse de ortalama %10 daha fazla olup, 3000 K için bu artış maksimum %24 olmuştur.

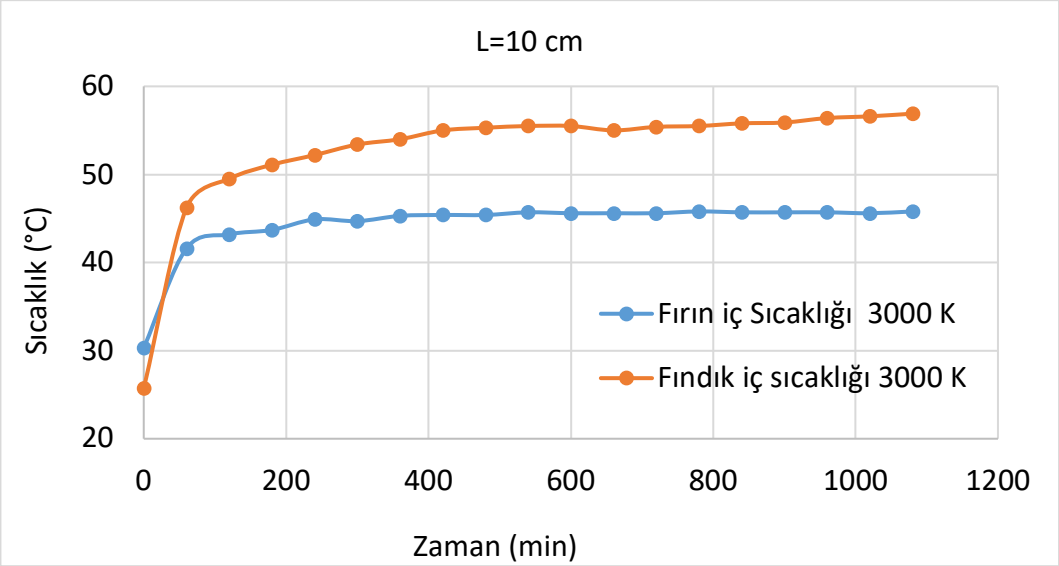

Şekil 6. LED renk sıcaklığının (3000 K) fırın sıcaklığı ve fındık iç sıcaklığına etkisi

LED renk sıcaklığına bağlı olarak fındık kütle- zaman değişimi Şekil 7'de verilmiştir. Fındık çapının 14-15 mm olarak seçildiği kurutma şartlarında LED renk sıcaklığı attıkça kuruma süresi de artmaktadır. Fındık %6 nem değerine 17 h (3000 K), 18 h (4000K) ve 22 h (6500 K)'de ulaşmaktadır. 3000 K'ne göre sırasıyla %5,8 ve %29,4 daha uzun sürede kuruma gerçekleşmiştir.

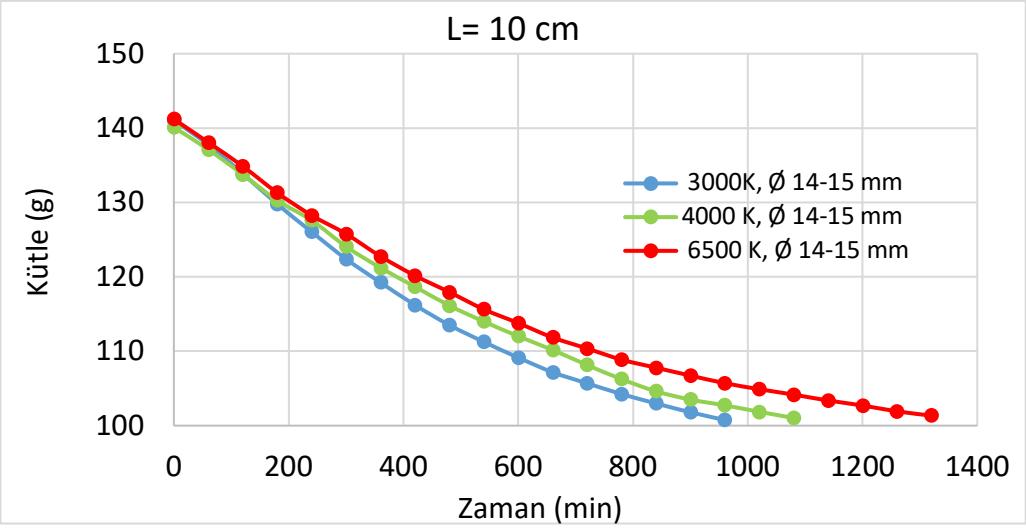

Şekil 7. LED renk sıcaklığına bağlı olarak fındık kütle kaybının zamanla değişimi

Şekil 8'de fındık çapının (Ø14-15 mm, Ø16-17 mm, Ø18 mm ve üstü) zamana bağlı kütle kaybına etkisi verilmiştir. Burada en kısa sürede kurutmanın gerçekleştiği renk sıcaklığı olan 3000 K için fındık boyutunun kütle kaybına etkisi grafiği verilmiştir. Fındık boyutu arttıkça kuruma süresi de artmakta olup, Ø14-15 mm çapa göre bu artış sırasıyla %6,25 ve %25'dir.

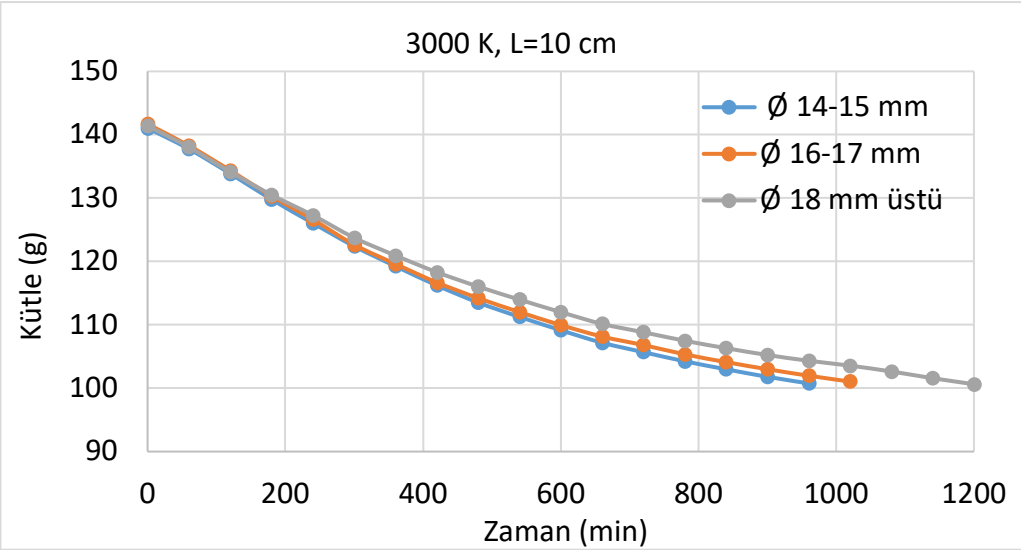

Şekil 8. Fındık boyutunun zamana bağlı kütle kaybına etkisi

LED'li kurutma ile Güneş ve etüvde (43°C) fındık kurutmada kütle kaybının zamanla değişimi Şekil 9'da verilmiştir. Bölgede hasat edilen Tombul fındık boyutu yüzde olarak en fazla 16-17 mm çap olduğu için karşılaştırma grafiği olarak bu boyut

seçilmiştir. Nemi %34 olarak hasat edilen fındığın neminin %6'ya en kısa sürede (15 saat) düştüğü 3000 K renk sıcaklıklı LED'li kurutmadır. Ancak bu kurutma şartları için 3000 K renk sıcaklıklı fındık kurutma fırın sıcaklığı (47°C) ve fındık iç sıcaklığı (57°C) dikkate alındığında uygun bir kurutma renk sıcaklığı olmadığı görülmektedir. Güneşte kurutma (67 saat) ile kıyaslandığında etüvde kurutma (33 saat) %51, 6500 K LED'li kurutma (21 saat) %69, 4000 K LED'li kurutma (16 saat) %76, 3000 K LED'li kurutma (15 saat) %77,4 daha kısa sürede kurutma işlemi gerçekleşmiştir.

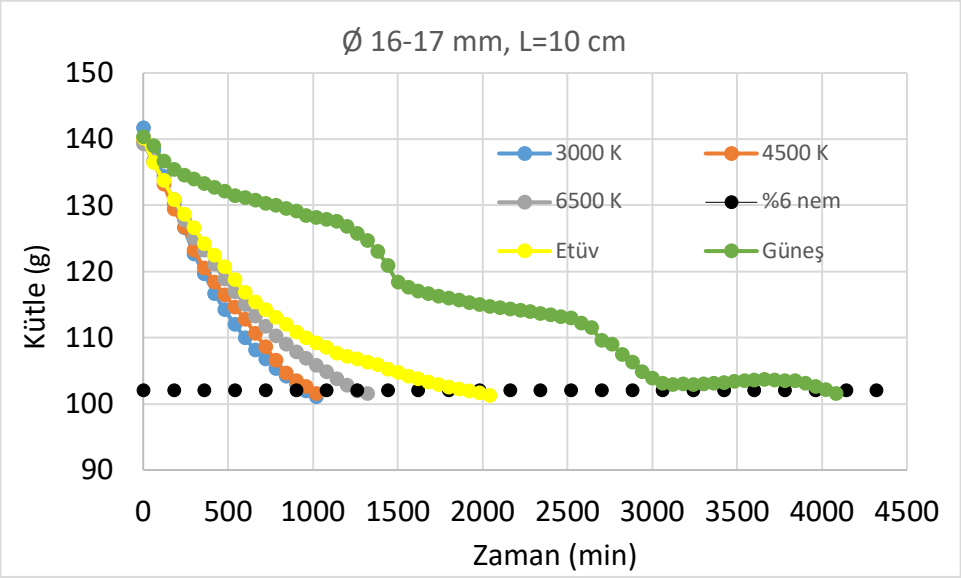

Şekil 9. Fındık kütle kaybının zamanla değişimi

Güneşte yapılan geleneksel kurutmada gündüz nem kaybı hızlı artmış, gece nem kaybı oldukça yavaşlamış veya tersine artmıştır.

Mekanik kurutma sistemlerinde kurutma süresinin kısalması (LED kullanımı) hem zaman hem de enerji verimliliği açısından uygun olması yanında, makinaların rantabl kullanımı ve daha fazla üreticiye hitap etmesi açısından çok önemlidir.

SONUÇLAR

Doğal dolaşımlı LED'li fındık kurutma sistemleri hem geleneksel kurutma (Güneş) hem de diğer mekanik kurutuculardan hem zaman hem de kurutma maliyeti açısından daha avantajlıdır.

Verilen geometri için sıcak beyaz (sarı) renkli (3000 K) LED ile yapılan doğal dolaşımlı fındık kurutma en kısa süre olmasına rağmen gıda özelliklerinin korunması açısında uygun sıcaklık aralığına sahip değildir. En uygun sıcaklık aralığı 6500 K renk sıcaklığındaki LED'de sağlanmıştır.

LED'li kurutma sistemlerinde kabin sıcaklığı fındığın bozulma sıcaklığını geçmeyecek şekilde akışkan hava hızı ve kabin geometrisi değiştirerek ayarlanmalıdır. Bu durumda sıcak beyaz renkli (3000 K) LED kullanımı daha avantajlı olacaktır.

Kaliteli LED kullanımı (sürekli kullanımda 15 yıl ömür) ve LED'lerin doğru yerleştirilmesi sayesinde tesis ilk yatırım ve işletme maliyeti oldukça düşüktür.

LED'li kurutma sistemleri yenilenebilir enerji kaynaklarından (Güneş panelleri) beslenmesi nedeniyle enerji maliyeti düşük ve çevreye olumsuz bir etki yapmamaktadır.

Kurulan bu sistem, fındık kurutma (max. 2 ay) yanında bölgede bulunan ve yağıştan dolayı kurutulması mümkün olmayan diğer meyve ve sebzelerin kurutulmasında da kullanılacağından sadece bir ürüne yönelik kurutma sistemi olmayacaktır.

KAYNAKLAR

Lukov A.V., (1973) *Systems of Differantial Equation of Heat and Mass Transfer in Capillary Porous*, Int. Journal of Heat and Mass Transfer, 18, 1-14.

Demirtaş C., (1996) *Fındık Kurutma Şartlarının Belirlenmesi*, KTÜ Fen Bilimleri Enstitüsü Dotora Tezi, Trabzon.

Demirtaş C.,Ayhan T., Kaygusuz K., (1998), *Drying Behaviour of Hazelnuts*, Food Agric, 76, 559-564.

Krokida M.K., Karathanos V.T., Maroulis Z.B. And Kouris D.M., (2003), *Drying Kinetics of Some Vegatables*, J. Food Engineering, 59: 391-403.

A.Kaya, O. Aydın, M. Akgün, (2011) "*Driying kinetics and moisture transfer parameters of hazelnut*", Journal of Food Processing and Preservation(ISI), 35 714–721.

Çetin M., Erişen A., (2011), *Artificial drying of newly harvested Turkish hazelnuts*, Natural Products An Indian Journal, 7(4), 181-186.

López A., Piqué M.T. , Boatella J., Ferrán A., Garcia J., Romero A., (1998), *Drying Characteristics of The Hazelnut*, Drying Technology, 16 (3-5):627-649.

Turan A., İslam A., (2016), *Çakıldak Fındık Çeşidinde Kurutma Ortamları ve Muhafaza Süresine Bağlı Olarak Meydana Gelen Değişimler*, Ordu Üniv. Bil. Tek. Derg., 6:2, 272-285.

STRUCTURAL PERFORMANCE OF REINFORCED CONCRETE CORBELS EXPOSED TO HIGH FIRE FLAME

Hussain A. Jabir
Civil Engineering Department, College of Engineering, University of Wasit, Iraq
haskar@uowasit.edu.iq

Thaar S. Al-Gasham
Civil Engineering Department, College of Engineering, University of Wasit, Iraq
thaar@uowasit.eudu.iq

Jasim M. Mhalhal
Civil Engineering Department, College of Engineering, University of Wasit, Iraq
jmahmood@uowasit.edu.iq

ABSTRACT: This paper presents and investigated the behavior and strength of reinforced concrete corbels exposed to high fire flame experimentally. The experimental program consists of testing five corbel specimens. The corbel dimensions were (150×250×250) mm. All specimens were casted with normal weight concrete of an approximately 30 MPa cylindrical compressive strength. Four specimens were burnt using a furnace and one specimen was kept without burning as a control specimen.

The test parameter was the fire flame temperature (300, 500, 700 and 900 ^{o}C), the cooling method is processed gradually by left the corbels in the free air, the exposure time is (1 hour). After cooling, the specimens were tested statically by applying a concentrated load on the column segment to distributed the load inversely to the two parts of corbel gradually till the specimen failure with the constant shear span to effective depth ratio of unity. The specimens were tested using 1000 kN testing machine. The specimens were positioned in the machine so that the deflection at center of the specimen was measured at each load step.

The test result shows that the mode of failure of fire-exposed specimens is different than that of control specimen, and the stiffness of the specimens exposed to the temperature greater than 500 ^{o}C is significantly effected compared with those exposed to temperature less than 500 ^{o}C. Additionally, the strength of specimens decreased from 13.3% to 46.7% with increasing the fire flame temperature from 300 to 900 ^{o}C and exposure time of 1 hour with respect to the control specimen.

Keywords: Corbels, Reinforced concrete, Fire flame, Temperature, Burning.

İNTRODUCTION

In reinforced concrete buildings, the exposure to a fire is considered as the most dangerous problem, facing these constructions. Therefore, the reinforced concrete buildings must be designed to have an efficient fire resistance, and thus avoiding a collapse or at least providing a sufficient time to allow people for escaping[1].

In the past, many studies were conducted on the reinforced concrete members exposed to high temperature. Most of these studies addressed the behavior of reinforced

concrete columns under fire[2–5], these investigations concluded that the reinforced columns declined more of their strength when they exposed to fire, especially for temperature exceeded 300° .
The reinforced concrete slabs subjected to fire were investigate by many researches[6–9]. However, the behavior of reinforced concrete corbels under fire is limited or lost; therefore, this study aims at inspecting the structural response of reinforced concrete corbels exposed to high temperature.

TEST SPECIMENS AND BURNING PROCESSES

The experimental program included of testing five corbels. Tested specimens details are illustrated in Figure (1) and Plate (1). For all specimens, the overall dimensions and the all reinforcement details were kept constants. The corbel length and width were 250mm and 150mm, respectively. Their depth was 250 at the end contacting with the column and 125mm at the free end. The dimensions of the column supporting two corbels were (150×200×450) mm. The column was reinforced with (4ϕ12 mm) longitudinal bars, at its corners, and 6 mm diameter closed ties spaced longitudinally at (163mm) center to center. All specimens were reinforced with (3ϕ12 mm) deformed steel bars, on the tension side (as main reinforcement). Deformed bars of (ϕ 6 mm) diameter were used as shear reinforcement and framing bars of the tested corbels. One specimens for each bar size were tested according to ASTM A 615M- 02P. Properties of the reinforcing bars are presented in Table (1).

Normal weight concrete with target compressive strength of 30 MPa at 28 days were used to casting the tested specimens, the procedure of ACI 211.1-97 was employed to design the mixture, where obtained the ratios as (1 cement: 2.6 sand: 2.8 gravel, by weight) with water/cement ratio about 0.55, The average cylindrical compressive strength of 28-day obtaining was 31.16 MPa. After a day casting, the specimens were covered with sheets and after 3 days they lifted from the moulds and placed in curing pit to complete the curing duration and then burned.

The corbel specimens were designated using a code composed of two parts separated by (-) symbol, each one has capital letter followed by number. The letter of first part is (C) meaning that the specimen is corbel, this letter is followed by a number referring to the fire temperature divided by 100. The second part is (0G) for the reference specimen refers to the specimen not exposure to fire flame, (1G) for the others and kept same for all corbels, it means that specimens burned for one hour and then cooled gradually by leaving them in free air. Table (2) lists the full details of the test specimens.

The burning processes were carried out in a workshop of the College of Engineering at Wasit University. A diesel furnace, with dimensions of 80 cm length, 55cm width, and 50cm height, was used. The furnace has a digital recorder to monitoring the degree of temperature inside it as shown in Plate (2).

The fire-exposed specimens experienced tiny cracks distributed in a random configuration. These fire cracks increased in number and in density as the exposure temperature increased.

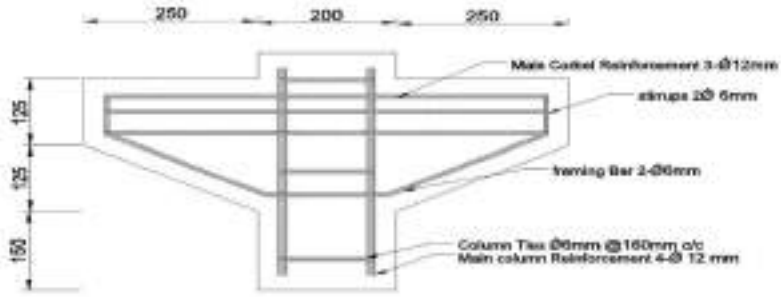

Figure (1) Typical Details of Tested Corbel.

Plate (1) Details of Steel Reinforcement.

Table (1) Properties of the Reinforcing Bars.

Nominal Diamete	Measured Diameter	Surface Texture	Area (mm2)	Measured Diameter	Yield Stress fy MPa	Ultimate Strength f_u MPa
6	5.83	deformed	29.3	5.83	598	657
12	11.87	deformed	126.7	11.87	648	721

Table (2) Details of Specimens.

Specimen Designation	Exposure Temperature(°C)	Exposure Duration (hr)	Concrete Cylinder Compressive Strength (MPa)
C0-0G	0	0	32.16
C3-0G	300	1	33.68
C5-0G	500	1	30.96
C7-0G	700	1	29.1
C9-0G	900	1	29.9

Plate (2) Burning a Corbel Specimen.

TESTİNG PROCEDURE

After completing the burning, the specimens were tested statically by applying a concentrated loading gradually till the specimen failure. The tests were carried out at the concrete laboratory of engineering College of Wasit University. The corbel specimens were tested in configuration opposite to that in the real site as shown in Plate (3). The loading was subjected throughout the column stubs using a hydraulic jack with 1000 kN capacity. A load cell was inserted between the jack and the specimen to record the loading value. At each load increments, the deflection at the center of the

column stub was measured by a dial gauge placed under the column as well as the crack propagation was carefully marked.

Plate (3) Test Setup.

TEST RESULTS AND DISCUSSION

Failure Modes

The control specimen **C0-0G** (without burning) showed first crack at loads of 48 kN at the lower reentrant corner of the corbel, as the external loading increased this cracks propagated toward the upper reentrant corner in nearly vertical direction. At load of 90 kN, diagonal cracks started to developed at the point of support and extended to the upper reentrant corbel corner with increasing the applied loading. Finally, the control specimen failed due to the formation of two inclined splitting cracks in both sides, plate (4). The high compressive struts, developed between the points of support and applied loading, resulted in these diagonal splitting cracks.

For 300 ^{o}C-exposed specimen, the first flexural crack occurred at approximately 40 KN, and then, at 70 KN, additional diagonal crack initiated at the supporting points and turned into upper internal corner of corbels. However, these inclined cracks did not reach the upper corners as case of control specimen. This specimen failed because of formation cracks in both sides, developed from the supporting point and to the

upward in direction parallel to the external corbel edges, as shown in Plate (5). The other exposed specimens failed in mode similar to that of C3-1G specimen, except that the cracks causing failure developed at one side which was closer to the fire resource in the furnace as shown in Plates (6 to 8). The failure of burned specimens in this configuration can be attributed to the following reasons; first, the concrete exposed to high temperature lost ability to develop compressive strut between loading points. Second, the these specimens have a rough surface due to spalling off the concrete cover leading to initiate high friction force at supporting points, and it increased with increasing the rotation at support. Finally, the friction force causes the corbel to fail in direct tension especially in the zones where the concrete confinement is weak as in supporting points.

Plate (4) Failure Mode of C0-0G Specimen.

Plate (5) Failure Mode of C3-1G Specimen.

Plate (6) Failure Mode of C5-1G Specimen.

Plate (7) Failure Mode of C7-1G Specimen.

Plate (8) Failure Mode of C9-1G Specimen.

Cracking and Ultimate Loadings

The cracking and ultimate loading for all specimens are listed in Table (3). The specimens, exposed to temperature of 300 °C and 500 °C, cracked at loads 16.7 % and 58.3% lesser than that of control specimen. The specimens, exposed to fire flame exceeding to 500 °C, showed first crack at same loading that was 79.2% smaller than control specimen cracking load. The drop in the cracking load of exposed specimens resulted from decreasing the concrete compressive strength due to fire flame exposure.

Finally, the failure loads dropped with rising exposure temperature as illustrated in Figure (2). The specimens, subjected to 300 °C, 500 °C, 700 °C, and 900 °C, collapsed at load 13.3%, 36.7%, 46%, and 46.7% smaller than that of unexposed specimen, in other words the residual strength were 86.7%, 63.3%, 54%, and 53.3% for specimens exposed to fire flame temperature 300 °C, 500 °C, 700 °C and 900 °C, respectively as shown in Figure (3), the reduction in the residual strength of the corbels can be assigned to the two main factors, the first factor is the cracks formation and propagation increased as the degree of temperature increased because of evaporate the moisture in the concrete. The second factor is the steel reinforcement more elongate as the temperature increased. In contrast, the shrinkage of concrete occurs [10].

As shown above the specimens, burned at temperature exceeding 500 °C, showed approximately similar cracking and collapse loads, this phenomena due to losing the concrete its structural function at temperature greater than 600 °C as explained by earlier studies.

Table (3) Cracking and Failure Loads of Specimens.

Specimen Designation	Cracking Load (kN)	Failure Load (kN)	Residual Strength %
C0-0G	48	150	100

C3-0G	40	130	86.7 63
C5-0G	20	95	63.3
C7-0G	10	81	54
C9-0G	10	80	53.3

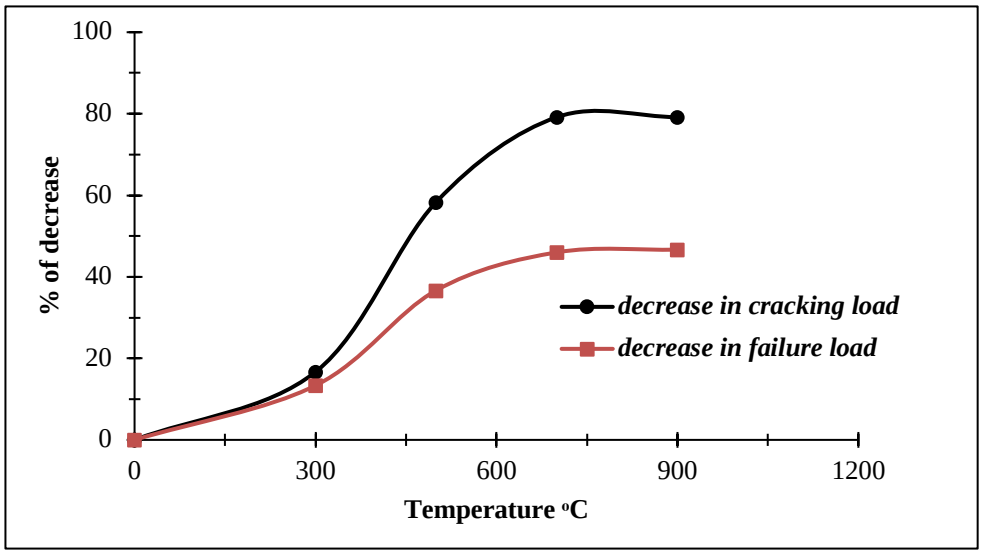

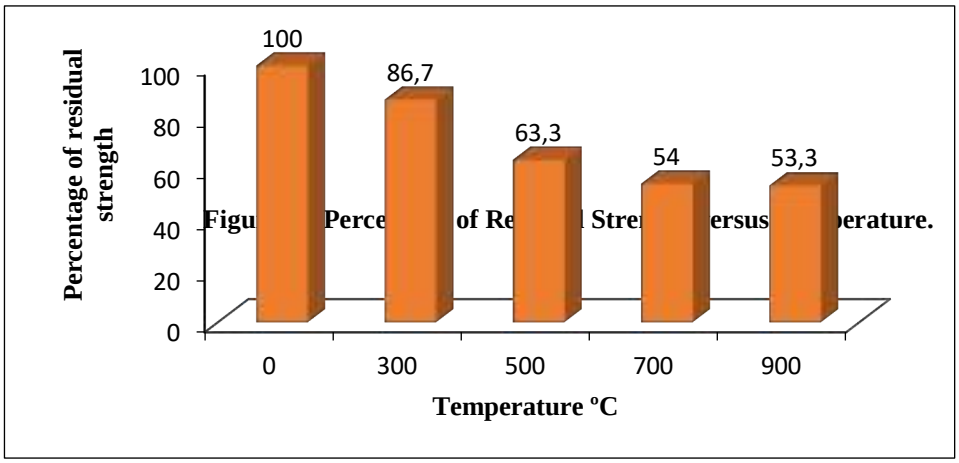

Figure (2) Percentage of Decrease in Cracking and Failure Load.

Load -Deflection Response

The load-deflection responses for the five corbel specimens are illustrated in Figure (4). It is obvious from this figure that the corbel stiffness reduced with augmented the exposure temperature. This due to reductions in both concrete modulus of elasticity

and the inertia moment of corbels as a result of dropping in the concrete strength and existing fire cracks, respectively. The specimens C0-0G and C3-1G show approximately identical responses, where the central deflection increased linearly with applying loading until first crack occurred, then the responses sloped at greater rate and continued in this slope till yielding the flexural steels (second point of deviation). Beyond this, the central deflection rising severally with applied load till the specimen failure. The other exposed specimens behaved nearly linearly, without clear change in the slope of their responses after occurring the first crack, since the bond strength between concrete and steel bars damaged.

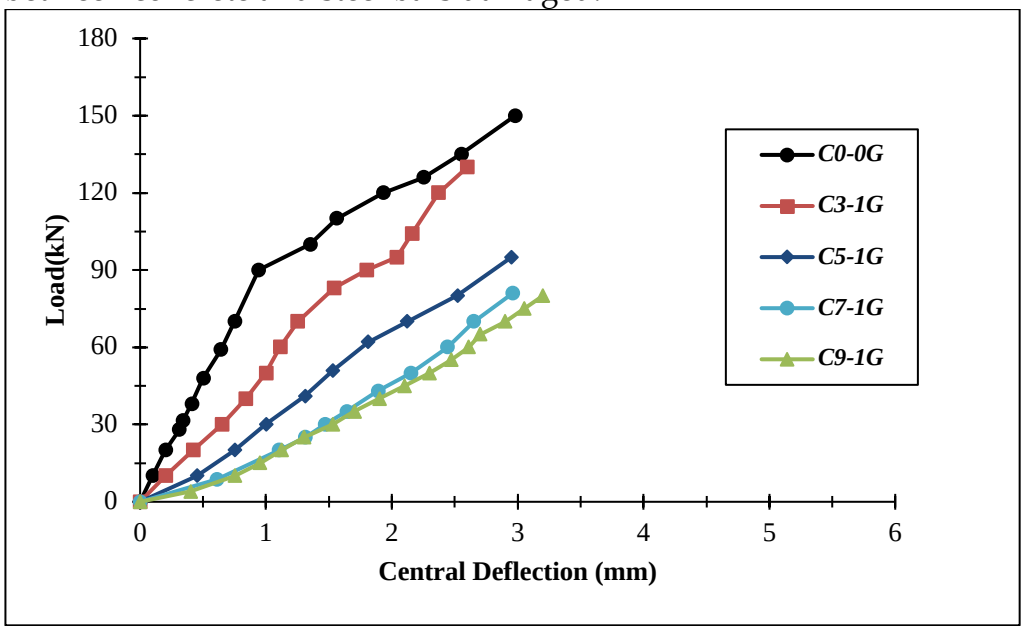

Figure (4) Load-Deflection Responses for Corbel Specimens.

CONCLUSIONS

In this paper, experimental test was carried out to investigate the behavior and the residual strength of reinforced concrete corbels exposed to fire flame temperatures ranging from 300 to 900 °C for a burning duration of 1 hour. The main conclusions of this paper can be listed as follow:

The fire-exposed specimens failed at mode different than that of unexposed specimen. The control specimen failed due to diagonal splitting cracks and the exposed specimens failed by formation vertical crack developed at supporting points and propagated toward the top of corbels.

There is clear dropped in first crack load for the specimens exposed to fire flame temperature exceeded 500 °C, as a result of the diminution in concrete compressive strength with compare to the specimens exposed to temperature equal or less than 500 °C.

The corbel strengths were significantly affected by fire. The strength of specimen burned at 300 °C dropped about 13.3% and the 900 °C exposed- specimen lost 46.7% from its strength.

The corbel stiffness decreased significantly with increasing the exposure temperature especially for those exposed to fire greater than 500 ^{o}C.
As expected the central deflection increased as the temperature increased for the specimens exposed to the fire flame compared with the control specimen.
The corbel specimens, burned at temperature exceeding 500 ^{o}C, showed approximately linear behavior without evident change in load-deflection response till failure.

REFERENCES

[1] K. Sakai, S.A. Sheikh, What do we know about confinement in reinforced concrete columns?(A critical review of previous work and code provisions), ACI Struct. J. 86 (1989) 192–207.
[2] T.S.S. Al-Gasham, EXPERIMENTAL PERFORMANCE OF REINFORCED CONCRETE HOLLOW COLUMNS EXPOSED TO FIRE, Al-Qadisiyah J. Eng. Sci. 9 (2016) 211–224.
[3] M.M. Bikhiet, N.F. El-Shafey, H.M. El-Hashimy, Behavior of reinforced concrete short columns exposed to fire, Alexandria Eng. J. 53 (2014) 643–653.
[4] A. Echevarria, A.E. Zaghi, R. Christenson, R. Plank, Residual axial capacity comparison of CFFT and RC bridge columns after fire, Polymers (Basel). 7 (2015) 876–895.
[5] M.A.A. El-Shaer, STRUCTURAL ANALYSIS FOR CONCRETE COLUMNS SUBJECTED TO TEMPERATURE., Acta Tech. Corvininesis-Bulletin Eng. 7 (2014).
[6] E. Omer, B.A. Izzuddin, A.Y. Elghazouli, Failure of lightly reinforced concrete floor slabs with planar edge restraints under fire, J. Struct. Eng. 135 (2009) 1068–1080.
[7] V.K.R. Kodur, L.A. Bisby, S.H.C. Foo, Thermal behavior of fire-exposed concrete slabs reinforced with fiber-reinforced polymer bars, ACI Struct. J. 102 (2005) 799.
[8] A.S. Usmani, N.J.K. Cameron, Limit capacity of laterally restrained reinforced concrete floor slabs in fire, Cem. Concr. Compos. 26 (2004) 127–140.
[9] A.Y. Elghazouli, B.A. Izzuddin, Failure of lightly reinforced concrete members under fire. II: Parametric studies and design considerations, J. Struct. Eng. 130 (2004) 18–31.
[10] S. Yehia, G. Kashwani, Performance of Structures Exposed to Extreme High Temperature—An Overview, Open J. Civ. Eng. 3 (2013) 154.

COMPRESSIVE STRENGTH OF CONCRETES PRODUCED WITH ANALCIME BLENDED CEMENTS

Yasemin AKGÜN
Ordu University
yakgun@odu.edu.tr

Ömer Fatih YAZICIOĞLU
Civil Engineer
omerfatihyazicioglu@gmail.com

ABSTRACT: Cement that is one of the concrete components is responsible for intensive energy consumption and also for 5-8% of world CO_2 emissions. Therefore, pozzolanic blended cement production is one of the easiest solutions to support the energy saving policies by reducing the amount of clinker and to minimize of damage to environment caused during the production. This solution also corresponds to the improvement of performance of concrete that is end product. The aim of this study is to investigate the developments of compressive strength of concretes produced with blended cements containing analcime that is natural zeolite mineral. In the study, ıt was produced concrete samples produced with blended cements obtained by replacing analcime with cement in ratios 0%, 10%, 30% and 50% by weight of cement. On the test series, 1, 2, 7, 14 and 28 days compressive strength tests were carried out. According to the results obtained from the tests, it has been determined that analcime can be an alternative up to 30% replacement ratio to another zeolite minerals which is used as a pozzolan in sustainable concrete productions.

Key words: analcime, concrete, compressive strength, zeolite.

INTRODUCTION

Due to the decreasing natural energy resources and increasing environmental pollution in the world, the use of pozzolanic natural mineral additive in cement and construction industry has increased. Natural pozzolans are generally preferred to artificial pozzolans as a result of economic and reserve comparisons. The blended cement is obtained by replacing clinker with natural pozzolans (Erdoğan, 2013). This situation leads to energy-efficient, economic and environmental cement productions. In mortar/concrete produced with cements containing pozzolan, besides high strength, permeability is decreased, (Güçlüer 2016, Oymael, 2010, Karakurt, 2010, Yıldız, 2010, Albayrak 2007, Atlıhan 2007, Turanlı et al., 2007, 2005, 2004 and Gürkan, 2006,), resistance against acidity is provided (Bilim, 2011), alkali-aggregate reaction is prevented (Yıldırım, 2007), heat of hydration is decreased and durability is also increased (Akgün, 2016, 2017, Ahmadi, 2010 and Jonatka, 2008).

The performance improvement of mortar/concrete varies depending on activity of pozzolan which can be determined by various methods (Uzal, 2007). Pozzolanic activity can be defined as reaction ability with $Ca(OH)_2$ of the active-amorphous silica

in pozzolan. At the end of this reaction, the amount of portlandite ($Ca(OH)_2$) decreases, the amount of calcium silicate hydrate (CSH) increases (Erdoğdu, 2007).

Zeolite minerals that are natural pozzolan has been used in cement productions for these purposes. The natural zeolites formed by the alteration of vitric proclastic beds are more reactive materials than fly ash and furnace slags which are pozzolanic materials (Chan, 1999). Zeolites. as mentioned above, contributes to the formation of cement-like hydrated products (CSH) during the hydration of the cement and to $Ca(OH)_2$ consumption which occurs during the hydration process (Trnı'k 2015). Thus, zeolites improve the performance of mortars/concretes.

Analcime is a natural pozzolan and is one of the valuable minerals of zeolite group. Analcime is a feldspathite mineral with a very large amount of hydrated sodium aluminosilicate ($Na(AlSi_2O_6).H_2O$) in its structure. (Colella 2001).

The aim of this study is to investigate how will affected to compressive strength of concretes when used analcime which is natural zeolite added to Portland cement at different ratios.

MATERIALS AND METHODS

The specific surface area (Blaine fineness), density, chemical composition and mineralogical structure of materials used as pozzolan in blended cements have important effects on strength. Therefore, these parameters were determined by using materials and methods given below.
The natural zeolite mineral, analcime, was replaced by cement. The analcime (A) which is from natural zeolite species was obtained from Ordu/Perşembe regions of Turkey. The cement used in the experiments was CEM I 42.5 R type of portland cement (PC) produced in accordance with TS EN 197-1 (TSI, 2012). In pozzolanic activity tests, CEN standard sand was used. In lime-pozzolan mixtures, slaked lime ($Ca(OH)_2$) was used as specified in TS 25 (TSI, 2008). In the concrete mixtures, the naturally formed aggregate with the maximum grain size of 16 mm was used. Aggregates used in this study were provided from the Harşit valley, Giresun Province of Turkey. It was used superplasticizer (at 1.5%, 1.75% and 2.0% ratios) complying with TS EN 934-2 (TSI, 2013) by adding to mixture water to recover of adverse effect caused of natural zeolite in blended cements.. In production of all samples, water that does not contain organic substances and mineral salts that may be harmful is used.

Density and specific surface (Blaine) of natural zeolite was determined according to TS EN 197-1 (TSI, 2012) and TS EN 196-6 (TSI, 2010), respectively. The pozzolanic activities of zeolite was determined by the compressive strengths of lime-pozzolan mortars according to TS 25 (TSI, 2008). X-Rays Fluorescence Spectrometer (XRF) analysis was performed to determine the chemical composition of natural zeolite. X-Ray Diffraction (XRD) analysis was performed to determine the mineralogical composition. Some views were also obtained using a Scanning Electron Microscope (SEM). Tests for compressive strength developments were carried out on concretes that were prepared by using portland cement (PC) and zeolite according to TS 12390-

2 (TSI, 2010). The results obtained from the test series were compared amongst themselves and with each other.

Pozzolanic Activity Tests and Preparation of Samples

In TS 25, the pozzolanic activity test is defined as a characteristic determined in terms of compressive strength of the mortar obtained by mixing natural pozzolan, water, standard sand and calcium hydroxide ($Ca(OH)_2$). The amounts of materials required to prepare three test samples for tests on pozzolanic activity are given in Table 1. The moulds of the prepared samples were covered with a glass plate to prevent evaporation. The samples were allowed to stand at room temperature for 24 hours (23 ± 2) °C. And then, they were left for 6 days in drying oven at 55 ± 2 °C without removing the moulds. The samples removed from the oven were left to cool at room temperature. Finally, the compressive strengths of samples were performed in accordance with TS EN 196-1.

Table 1. The Amounts of Materials for Tests on Pozzolanic Activity

Materials	TS 25	The amounts for tests
Slaked lime ($CaOH_2$)	150g	150g
Pozzolan	2x150x(density of pozzolan /density of $CaOH_2$) (g)	2x150x(2.28/2.15) = 318.14g
Standard sand	1350g	1350g
Water	0.5x (150+pozzolan) (g)	0.5x(150+318.14) = 234.07g

Compressive Strength Tests and Preparation of Concretes

Samples was prepared in laboratory environment where temperatures are 20±2°C and relative humidity is 60±5%. The amounts of zeolite used in blended cements were 0%, 10%, 30% and 50% of the cement weight. The mixtures were produced with the labels PC, A10, A30 and A50. The absolute volume method given in TS 802 (TSI, 2016) was used in mixture calculation of concretes. The water-to-cement ratio of concrete samples is 0.5. The slump of concretes is 7-8 cm. The amounts of materials required to prepare concrete samples for tests on compressive strength are given in Table 2. The samples taken from molds after 24 hours from their productions were kept in the curing tank at a temperature of 21 ± 1°C up to 28 days. Concrete samples were prepared by applying the standard mixing, molding and curing procedures stated in TS 12390-2 (TSI, 2010). The compressive strength developments of concretes were carried out in accordance with the TS EN 12390-3/AC (TSI, 2012). The compressive strengths of 150 mm cube concrete specimens were determined at 1, 2, 7, 14 and 28 days of age.

Table 2. The Amounts of Materials for Tests on Compressive Strength

Components	PC	A10	A30	A50
Portland Cement (kg/m^3)	350	315	245	175
Natural Zeolite (kg/m^3)	-	35	105	175
Water (kg/m^3)	175	175	175	175
Water / Cement	0.50	0.50	0.50	0.50
0-4 mm Aggregate (kg/m^3)	789.99	787.99	783.99	778.31
4-8 mm Aggregate (kg/m^3)	351.11	350.22	348.44	345.91
8-16 mm Aggregate (kg/m^3)	614.44	612.88	609.77	605.35
Plasticizer (kg/m^3)	-	5.25	6.13	7.00

RESULTS AND DISCUSSIONS

Some Properties of Portland Cement, Analcime, Blended Cements and Aggregates

Some properties of portland cement (PC), analcime (A), blended cements (A10, A30, A50) and aggregates are presented in Table 3, 4, 5 and 6. Density of analcime is 26.92% lower than PC. Specific surface area of analcime is 48.91% higher than PC. This situation depends on mineral structure, porosity and fragilement properties of zeolite. Cumulative passing (%) of 45 µm sieve for Portland cement and analcime are 67.11% and 70.80%, respectively. Density of blended cements has decreased with increasing of zeolite ratios. Fineness of blended cements containing zeolite has increased with

increasing of zeolite ratios. Aggregates used in this study are standard aggregates for concretes complying with TS 706 EN 12620 (TSI, 2009).

Table 3. Properties of Portland Cement (PC).

Chemical composition	(wt.%)	Physical and mechanical properties of portland cement			
SiO_2	19.53	Density, (g/cm^3)	3.12		
Al_2O_3	5.33	Initial set, (h)	2.50		
Fe_2O_3	3.56	Final set, (h)	4.15		
CaO	62.26	Volume expansion, mm	2.00		
MgO	0.99	Specific surface (Blaine) (cm^2/g)	3210		
SO_3	3.02	The compressive strengths (MPa)	2 days	7 days	28 days
Loss of ignition	3.06		32.30	44.60	53.00
		Over sieve (%)	45µm	90 µm	200 µm
			32.89	12.15	2.73

Table 4. Properties of Analcime

Chemical composition	Analcime (wt.%)	Physical properties	
SiO_2	46.71		Analcime
Al_2O_3	17.24	Density, (g/cm^3)	2.28
Fe_2O_3	9.21	Blaine fineness (cm^2/g)	4780
CaO	3.03		
MgO	5.29	Over sieve (%)	
Na_2O	4.84	45µm	29.20
K_2O	4.08	90 µm	9.80
Loss of ignition	7.00	200 µm	2.15

Table 5. Properties of Blended Cements

Physical properties	PC	A10	A30	A50
Specific surface (cm^2/g) (Blaine fineness)	3210	3752	3918	4449
Density (g/cm^3)	3.12	2.79	2.75	2.71

Table 6. Density and Water Absorption Ratios of Aggregates

Aggregates	Dry density	Saturated	Visible density	Water
Coarse (≥4mm)	2.50	2.55	2.65	2.20
Fine (≤4mm)	2.55	2.60	2.69	1.96

Pozzolanic Activity of Analcime

Pozzolanic activity of analcime are given in Table 7. According to Table 7, in TS 25, one of the conformity criterias for pozzolans is the 7 day compressive strength of samples prepared with lime-natural pozzolan mixture. The limit value of the compressive strength is at least 4 MPa. In test study performed for analcime, the average compressive strength value for the lime-zeolite (pozzolan) mixture samples was determined as 6.30MPa. It has also been emphasized that the sum of SiO_2 + Al_2O_3 + Fe_2O_3 in TS 25 should be at least 70% by mass. The value of this total was found to be 73.16% for analcime. At the same time, the specific surfaces of the pozzolans should be greater than 3000 cm^2/g. The specific surface of pozzolan which is used in this study were found to be 4780 cm^2/g for analcime. In pozzolanic activity tests. Because of the specific surface of natural zeolite were below of portland cement fineness, the reaction which is between pozzolan and lime was increased. It is thought that, this situation was lead to an increment at value of pozzolanic activity. These value show that the zeolite used in study have an usability potential as a pozzolan.

Table 7. Pozzolanic Activity of Analcime

TS 25 limit values	Analcime
Lime-pozzolan mixture 7 days compressive strength > 4MPa	6.30MPa
SiO_2+Al_2O_3+Fe_2O_3 wt. content >%70	%73.16
Specific surface area > 3000cm^2/g	4780 cm^2/g

Mineralogical Composition of Analcime

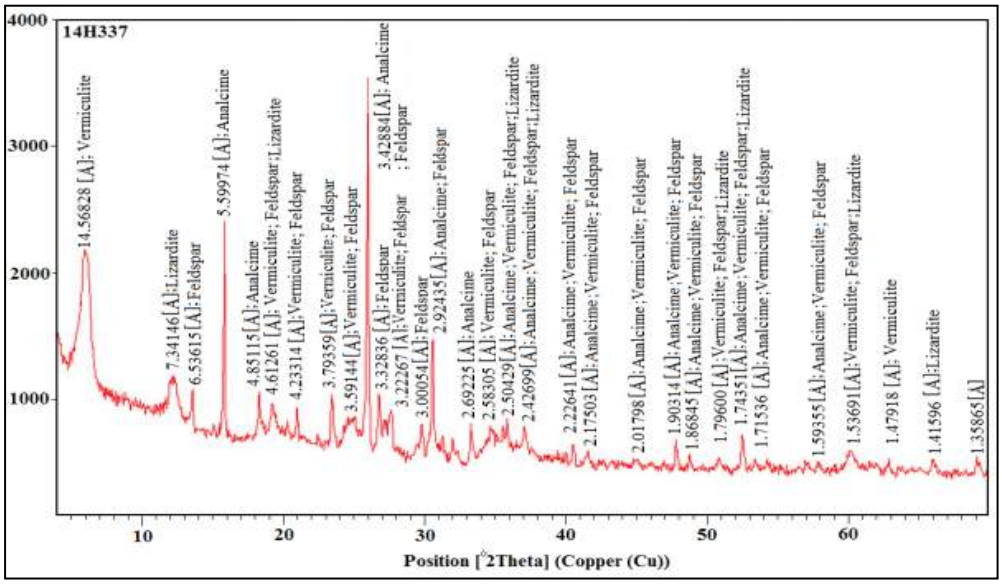

Figure 1. XRD Diffraction Patterns of Analcime

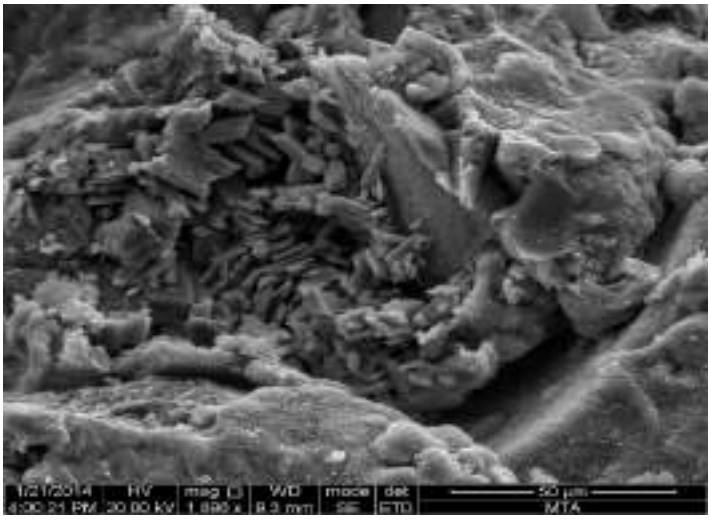
Figure 2. SEM View of Analcime

XRD diffraction patterns and SEM views are presented in Figs. 1 and 2. According to the mineral modal ratios at the mineralogical composition results determined by the X-ray diffraction analysis (XRD) of analcime sample, the analcime rock is a vitric tuff and consists of glass splinters and crystal components. Glass splinters are converted to zeolite and chlorite, which are heavily altered. The analcime samples confirm the requirements of national and international standards for zeolite applications.

Compressive Strength of Concretes

The average cube compressive strength developments (MPa) and density (g/cm3) at 1, 2, 7, 14 and 28 days of concretes produced by blended cements containing analcime are given in Table 8. The relations of specific surface area and density of

cements/concretes are given Figure 3. The variations of average compressive strength for concretes are given Figure 4.

Table 8. The Average Compressive Strength and Density of Concretes

Concretes		PC	A10	A30	A50
Density (g/cm^3)	Ages	2.42	2.40	2.38	2.32
Compressive Strength (MPa)	1 days	33.71	23.72	19.67	8.81
	2 days	47.57	42.91	30.25	17.12
	7 days	54.98	45.86	34.22	19.40
	14 days	58.90	53.48	41.05	23.50
	28 days	64.38	55.84	44.29	26.83

According to Table 8, 2 days compressive strength of concretes containing analcime blended cement (A10, A30, A50) is 10%, 36% and 64% lower than that of traditional concrete, respectively. 28 days compressive strength of that is 13%, 30% and 58% lower. This decrease is directly proportional with analcime replacement ratio. It is seen that, the concretes containing analcime blended cement have structural concrete class characteristic up to 30% replacement ratio at both early and 28 days of age. Also, the densities of blended cements and concretes slightly decreased with increasing of replacement ratio due to the low density of analcime.

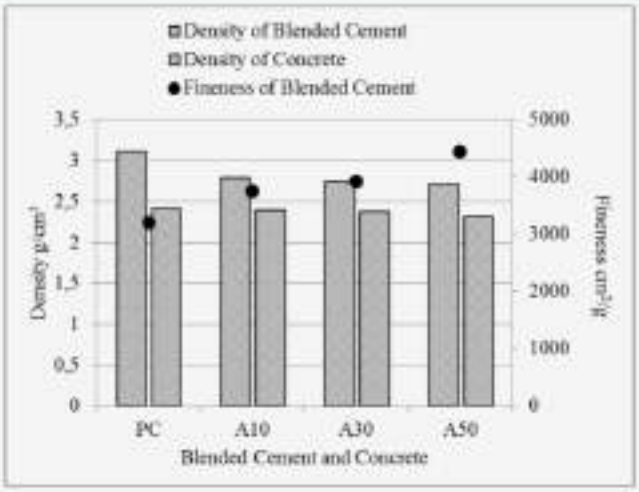

Figure 3. The Relations of Specific Surface Area and Density of Cements/Concretes

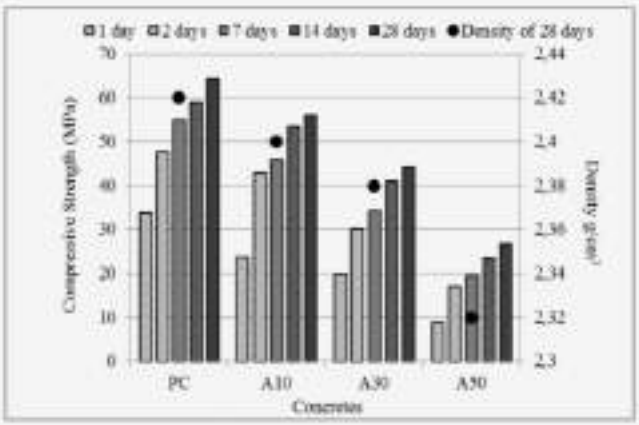

Figure 4. The Variations of Average Compressive Strength with Density for Concretes

CONCLUSIONS

It is known that, the reducing at amount of clinker by using replacement material leads to efficient-using of energy sources in the cement productions. Therefore, in the production of concrete, the use of blended cement provides energy-saving, economic and eco-friendly solutions without compromising from product performance.
The natural zeolite analcime investigated in this study has a appropriate potential as pozzolan for sustainable blended cement productions due to its properties such as high silica-alumina content, mineralogical structure and pozzolanic activity.
The density of blended cements/concretes slightly decreased with increasing of replacement ratio due to the low density of analcime.

The concretes containing analcime blended cement have structural concrete class characteristic up to 30% replacement ratio at both early and 28 days of age in terms of compressive strength. Analcime can be an alternative up to 30% replacement ratio to

another zeolite minerals which is used as a pozzolan in sustainable concrete productions.
It should be specified that this assessment made here is valid only for zeolite type subject to this study and for the production under these operating conditions. It is also thought that it would be appropriate to make the studies on the analcimes obtained from different regions.

ACKNOWLEDGEMENT

This study was funded by the Scientific Research Project Unit of Ordu University under Project No: TF-1521. Also, we would like to thanks to Laboratories of General Directorate of Mineral Research And Explorations and Votorantim Cement companies.

REFERENCES

Ahmadi, B., and Sherkarchi, M. (2010). Use of natural zeolite as a supplementary cementitious material. *Cement and Concrete Composites*, *32*, 134-141.
Akgün, Y., ve Yazıcıoğlu, Ö.F. (2016). İki farklı doğal zeolit katkısının çimento harç aşınma dayanımına etkisi. *Ordu Üniversitesi, ODÜ Bilim ve Teknoloji Dergisi*, *Cilt:6, No: 1*, 94-104.
Akgün, Y., ve Yazıcıoğlu, Ö.F. (2017). İki farklı doğal zeolitin Portland çimentosu hidratasyon ısısına etkileri. *Uluslararası Yapılarda Kimyasal Katkılar 5. Sempozyumu ve Sergisi, Bildiriler Kitabı,* 391-404.
Albayrak, M., Yörükoğlu, A., Karahan, S., Atlıhan, S., Aruntaş, H. Y., and Girgin, İ. (2007). Influence of zeolite additive on properties of autoclaved aerated concrete. *Building and Environment, 42 (9)*, 3161-3165.
Atlıhan,S., Aruntaş, H. Y., and Girgin, İ. (2007). Influence of zeolite additive on properties of autoclaved aerated concrete. *Building and Environment, 42 (9):* 3161-3165.
Bilim, C. (2011). Properties of cement mortars containing clinoptilolite as a supplementary cementitious material. *Construction and Building Materials, 25,* 3175-3180.
Chan SYN, Ji X. (1999). Comparative study of the initial surface absorption and chloride diffusion of high performance zeolite, silica fume and PFA concretes. *Cem Concr Compos., 21*, 293–300.
Colella, C., Gennaro, M. de', and Aiello, R., (2001). Use of zeolitic tuff in building industry , Reviews in Mineralogy and Geochemistry; Natural Zeolites, ed: D.L. Bish, D.W. Ming, *Mineralogical Society of America, Vol. 45,* Chapter 16, pp:551-587.
Erdoğan T. Y., (2013). Beton. *ODTÜ Yayını*. Ankara
Erdoğdu. K., Tokyay. M., ve Türker. P. (2007). Traslar ve Traslı Çimentolar. *TÇMB. AR-GE. Y99-2.* Ankara
Güçlüer, K., (2016). Zeolit ve Metakaolinin Gazbeton Üretiminde Kullanılabilirliğinin Araştırılması. *Afyon Kocatepe Üniversitesi Fen ve Mühendislik Bilimleri Dergisi, vol: 16* pp: 338-343.

Gürkan, A., (2006). Pomza ve Zeolitin Alkali Silika Reaksiyonu Üzerine Etkisi, *Doktora Tezi, Dokuz Eylül Üniversitesi Fen Bilimleri Enstitüsü*, İzmir 100-115.
Janotka, I., and Krajci, L. (2008) Sulfate resistance and passivation ability of the mortar made from pozzolan cement with zeolite. *Journal of Thermal Analysis and Calorimetry, 94*, pp. 7-14.
Karakurt C., Kurama H., and Topçu İ., B. (2010). Utilization of natural zeolite in aerated concrete production. *Cement and Concrete Composites, 32*, 1-8.
Oymael, S., (2010). Examinations of the internal structure of zeolite-blended cements. *Trakya Univ. J. Sci. 11(1)*, 29-39.
Trnı´k, A., Scheinherrova´, L., Medved, I., and Cerny, R., (2015). Simultaneous DSC and TG analysis of high-performance concrete containing natural zeolite as a supplementary cementitious material. *J Therm. Anal. Calorim., 121*, 67–73.
Turanli, L., Yücel, H., GÖNCÜOĞLU, M. C., Çulfaz, A., ve Uzal, B., (2007). Doğal Zeolitlerin İnşaat Endüstrisinde Kullanımı. *Proje No: 104M393*, Ankara
Turanli, L., Uzal, B., and Bektas, F., (2005). Effect of large amounts of natural pozzolan addition on properties of blended cements. *Cement and Concrete Research, Vol.35*, No.6, pp.1106-1111.
Turanli, L., Uzal, B., and Bektas, F., (2004). Effect of material characteristics on the properties of blended cements containing high volumes of natural pozzolans. *Cement and Concrete Research, Vol.34*, No.12, pp.2272-2282.
Uzal B., (2007). Properties And Hydration Of Cementitious Systems Containing Low, Moderate And High Amounts Of Natural Zeolites. *Doktora Tezi, Orta Doğu Teknik Üniversitesi Fen Bilimleri Enstitüsü*, Ankara, 40-45.
Yıldırım, Fen, S., (2007). Puzolanik zeolitin çimentoda katkı uygunluğunun araştırılması. *Mustafa Kemal Üniversitesi, Fen Bilimleri Enstitüsü. Yüksek Lisans Tezi.*
Yıldız, K., Dorum, A., ve Koçak, Yılmz., (2010). Pomza zeolit ve CEM I çimentosunun minerolojik moleküler elektrokinetik ve termal uyumunun yüksek dayanımlı betona etkisinin araştırılması. *Gazi Üniv. Müh. Mim. Fak. Der. J. Fac. Eng. Arch. Gazi Univ., Cilt 25*, No 4, 867-879.
TS EN 934-2 (2013). Admixtures for concrete, mortar and grout - Part 2: Concrete admixtures - Definitions, requirements, conformity, marking and labelling. Turkish Standards Institue, Ankara, Turkey.
TS 25, (2008). Natural pozzolan (Trass) for use in cement and concrete - Definitions, requirements and conformity criteria. Turkish Standards Institue, Ankara, Turkey .
TS EN 197-1 (2012). Cement – Part 1: Composition, specification and conformity criteria for common cements. Turkish Standards Institue, Ankara, Turkey.
TS 196-6 (2010). Methods of testing cement - Part 6: Determination of fineness. Turkish Standards Institue, Ankara, Turkey.
TS 802 (2016). Design of concrete mixes, Turkish Standards Institue, Ankara, Turkey.
TS EN 196-1. (2009). Methods of testing cement - Part 1: Determination of strength. Turkish Standarts Institute, Ankara, Turkey.
TS 12390-2 (2010). Testing hardened concrete - Part 2: Making and curing specimens for strength tests, Turkish Standarts Institute, Ankara, Turkey.
TS 706 EN 12620 (TSI, 2009). Aggregates for concrete. Turkish Standarts Institute, Ankara, Turkey.
TS 12390-3/AC (2012). Testing hardened concrete - Part 3 : Compressive strength of test specimens, Turkish Standarts Institute, Ankara, Turkey.

THERMAL PERFORMANCE OF ZEOLITE AS AN INSULATION MATERIAL FOR EXTERNAL WALLS

Adem ATMACA
Gaziantep University
aatmaca@gantep.edu.tr

Elif TELEFONCU
Gaziantep University
elif.telefoncu@gmail.com

Abdulkadir ÇEVİK
Gaziantep University
akcevik@gantep.edu.tr

ABSTRACT: The building sector has noteworthy influence over the energy consumption, emissions released and total natural resource consumption. Buildings consume two kinds of energies during their lifetime; direct and indirect. Direct energy is used for construction, operation, repair, and demolition; while indirect energy is consumed for the production of materials used in its construction. The materials used in these building designs also have a great importance. Zeolite, which is a lightweight material with a micro porous crystal structure, high water absorption and large surface area, draws attention. For this reason, in this study, the thermal conductivity of zeolite, its usability as an external thermal insulation material and its energy efficient performance have been investigated. These designs require different areas of expertise and technology. BIM systems (Building Information Modeling), which has an important place in this regard, is a database that enables designs to be realized in a short time and at a lower cost. By providing architects and engineers work on the same building model simultaneously, it helps to prevent errors caused by lack of coordination. In this study, Autodesk Revit program developed for BIM has been used. Revit, along with analysis solutions, allows the user to predict the impact of the building which they design on their surroundings. It enables to calculate energy expenditure of a building. The design developed in this program have been evaluated within the framework of the criteria determined by simulation tools of Autodesk Revit software. As a result, in this study, it is aimed to make proposals about the future of Zeolite used as building material, its properties and relationship of its usage with the environment.

Key words: Zeolite, building energy analysis, thermal insulation, Autodesk Revit

INTRODUCTION

Due to the increase in the world population, complex and multi-storey buildings have become widespread in recent years. As the building height and the number of storeys increase, the quality of the material used becomes important (Erdem vd., 1997).

Providing thermal quality in today's building is proportional to the thermal conductivity values of the material used as building element or component in the building. The thermal conductivity value of the material is a value which changes depending on the structural characteristic of the material and the specific heat capacity (Gündüz, 2007).

Rapid growth of the world population and developing technology increase the need for energy increasingly. The limited energy resources in the face of increasing need lead us to save energy. For this reason, in construction industry high heat and sound insulation, light, high pressure strength, easy to obtain and use, heat resistant and economical materials draws attention. As a result of the researches, it has been discovered that materials which can carry such properties can be produced from zeolites. The zeolite can be defined as an aqueous alumina silicate containing alkali and earth alkaline cations. With the use of zeolites in industrial areas revealed in the 1940s, rapid development of usage area of zeolite was observed that discovering to contain zeolite in marine and lacustrine tuffs after the 1950s (Sarıkaya, 2006).

Lightweight building materials obtained with the use of natural zeolites will provide significant savings in energy expenditures resulting from both the initial investments of heating and cooling systems as well as the energy consumption during the use of structures with its high thermal insulation property (Bektaş vd.,2003).

Usage Area of Zeolite

Zeolites have lots of physical and chemical properties. The main physical and chemical properties are ion exchange, adsorption and related molecular sieve structure, silica content, also light colored in sedimentary zeolites, lightness pore structure of small crystals. This kind of properties have led to the use of zeolites in a wide range of industrial areas.
This ındustrial areas can be collected in five main sections: pollution control, energy, agriculture, animal husbandry, mine-metallurgy and other fields (DPT, 2001).

Pollution Control

Zeolites are widely used in pollution control because of their ion exchange and adsorption properties. For this purpose, zeolites are used for the retention of radioactive wastes in water, for keeping metal ions and nitrogen compounds in waste water, for cleaning flue gases, for cleaning oil spills, for waste storage and for oxygen production.

Energy

The increasing energy demand increases the tendency towards resources that are being developed, such as nuclear and solar energy, as well as coal and oil. Synthetic and natural zeolites play an important role in converting these sources into energy. In this sector zeolites can be used to product oxygen need for coal gasification and energy conversion and cleaning of the explosive gases which occurs in combustion.
Zeolites are also used to remove carbon dioxide for the purification of natural gases. Depending on the water-giving properties of zeolites with temperature, heating and cooling of the structure, same meaning of solar heat transfer can be used as a heat exchanger. It can also be used as a catalyst in the production of petroleum products.

Agriculture & Livestock

Zeolite tuffs are used to remove the bad smell of fertilizers and to increase the ph value of acid volcanic soils. Natural zeolites are used as fertilizer carrier in fertilization and soil preparation. Also it is used as a drug carrier in the fight against agriculture.

Mining and Metallurgy

Zeolites are used in mining, searching of mine deposits. It is used to hold some heavy metals in metallurgy.

Other Uses

Apart from the above-mentioned areas, zeolites are used in many areas such as paper sector, construction sector, health sector and detergent sector. Zeolites are used as an additive in paper production, as a concrete additive in construction sector, in toothpaste and medicine production in the health sector, and in the detergent sector in place of phosphates (DPT, 2001).

METHODS

The building which is the subject of the study is located within the borders of Gaziantep. In this direction, applications (architectural, static, mechanical, electrical) projects, site plans, images taken on-site and the reports prepared about the structures are utilized. Computer Aided Design software is used for editing the photographs and creating maps. The sample structure is drawn using the Autodesk Revit Program and analyzed the impact with the environment. In this study, it is aimed to decrease the energy expenditures in the usage process of buildings. At this point, efficient use of energy has come to the fore. Within the scope of the thesis, the design parameters and systems which are effective in reducing the energy expenditures are examined and the effects of these parameters on the building energy expenditures are determined by means of numerical comparison with the energy simulation program (simulation tools of Revit) and appropriate alternatives are developed to reduce the energy expenditures. Other materials used in the study are the sources obtained from

libraries, related articles and theses, data obtained from the internet, regulations and conferences.

RESULTS AND FINDINGS

Zeolites are a good energy storage material and can be used in heating and cooling processes. For this purpose, particle size, air flow and time are important factors.
Since zeolitic tuffs have almost the same thermal conductivity coefficient of asbestos as the insulation material, it can be used as thermal insulation material in construction.
As a result of the researches, it has been stated that zeolite has more energy efficient density than conventional storage materials.

CONCLUSION

The main aim of this study is to investigate the thermal performance of zeolite which will be used as exterior material and to determine the advantage of this material compared to other materials.

Thanks to water giving properties, zeolite can be used for heating and climatization of small structures, in other words, it is possible that zeolites can be used as heat exchangers in the transfer of solar energy.

Zeolites regulate the moisture content of the building when used as a building block, thanks to its cation exchange properties.

As a result, the properties of zeolite, its usage areas and its relationship with energy have been investigated extensively by literature review.

RECOMMENDATIONS

In this study, zeolite was examined as external wall's material. Although some researches are reliable, additional researches can be done to examine the properties of the material in order to reach to the full scale characterization.

Natural zeolites have started to gain new acceptance in many market areas despite the presence of widespread usage areas and big market potential. Until now, there has not been sufficient search and development in our country, which has significant reserve potential. It is necessary to investigate the reserves, usage areas and technological properties of the mines determined. In this way, when the natural zeolite potential has been determined, it will be great benefit to our country.

Projects and researches on the use of natural zeolites should be supported and research institutions such as the university should be encouraged to carry out projects with abroad to follow the abroad developments.

REFERENCES

Bektaş F.,Uzal B., Turanlı L. (2003). *Öğütülmüş Doğal Zeolitin Doğal Alkali-Silika Reaksiyonu ve Sülfat Etkisi ile Genleşmesinin incelenmesi.* . 5. Ulusal Beton Kongresi, İnsaat Mühendisleri Odası İstanbul Subesi, 1-3 Ekim 2003, İstanbul, 403-409

DPT, (2001). Sekizinci Beş Yıllık Kalkınma Planı, *Madencilik Özel İhtisas Komisyonu Raporu, Endüstriyel Hammaddeler Alt Komisyonu Genel Endüstri Mineralleri II (Mika-Zeolit-Lületaşı) Çalışma Grubu Raporu,* DPT, Ankara

Erdem, E., Donat R., Çetisli, H. (1997). *Hydration and Mechanical Properties of Cement Containing Zeolite. 1. International Symposium on Mineral Admixtures in Cement,* 6-9 November 1997, Istanbul-Turkey, 216-220.

Gündüz, L. (2007). *Bimsblok ve Binalarda Isı Yalıtımı Değerlendirmesi.* Yapı Malzeme İhtisas Dergisi, 115, 36-38.

Sarıkaya, H. (2006). *Zeolit Katkılı Betonların Fiziksel ve Mekanik Özelliklerinin Arastırılması.* Yüksek Lisans Tezi, SDÜ Fen Bilimleri Enstitüsü, Isparta, 73s.

LIFE CYCLE ASSESSMENT OF MUNICIPAL SOLID WASTE INCINERATION POWER PLANT

Akif TAŞKIN
Graduate School of Natural and Applied Sciences, Erciyes University, 38039 Kayseri, Turkey
taskinakif@gmail.com

Nesrin KAYATAŞ DEMİR
Department of Energy Systems Engineering, Erciyes University, 38039 Kayseri, Turkey
nkayatas@erciyes.edu.tr

ABSTRACT: Increasing demand on clean energy and waste management problems have forced the authorities to find out new technologies to provide sustainability. These matters have merged under the name of incineration, which is one of the developing waste to energy technologies. This paper presents the environmental impacts of an incineration plant assumed to be operated on Kayseri municipal solid waste landfill area by using life cycle assessment methodology. Functional unit is selected as 1 kWh electricity generated by incineration power plant and system boundary consists of incineration process. SimaPro software is used for calculations and CML-IA baseline methodology is used for impact assessments of plant. Lifetime of the plant is assumed to be 20 years and energy production during the lifetime is considered. The results show that steel, cement and pitch are main contributors for all environmental impact categories. Moreover, global warming potential of this power plant is calculated as 3.06E-02 kg CO_2 eq/kWh for whole lifetime of the plant.

Key words: Incineration, life cycle assessment, sustainability, waste to energy.

INTRODUCTION

Municipal solid waste management (MSWM) is crucial issue for municipalities and governments. Collection, transportation, landfilling and waste to energy are the main subject areas of MSWM. In a MSWM system waste hierarchy is defined as prevention, minimization, reuse, recycling, energy conversion and disposal (Pennog Business Process Excellence, 2013). Wastes are accepted as resource of energy so, energy conversion from waste (WtE) is conformed as both part of energy and waste sectors. Waste to energy is developing matter due to the increased energy demand of the world. Incineration, pyrolysis, combined heat and power (CHP) and landfilling are the major energy conversion technologies from wastes. Type of the energy conversion technology depends on the regional parameters and authorities must analyze the regional requirements and must apply the most feasible solution (World Energy Council, 2016). Capital investments costs of WtE technologies for 15 MW output power plants are compared and it is proven that incineration technology has lower capital

investment cost than others (Renewable Energy World, 2014). Moreover, capital costs of energy generation from waste is still higher than conventional energy generation technologies for the same amount of energy output (U.S. Energy Information Administration (EIA), 2013). Incineration is developing technology due to the economic and thermal advantages among the other WtE technologies. Incineration is useful process to reduce the amount of municipal solid wastes besides the energy conversion from wastes. Also, incineration ashes provide to reduce the required area for dumping of wastes (World Bank, 2016). From an environmental point of view WtE technologies must be analyzed to provide sustainability. Life cycle assessment is useful method to reveal the environmental impacts of a WtE power plant.

However, even though many studies have published on the thermal analysis of incineration plants (Lino & Ismail, 2017), (Hwang, Choi, Kim, Heo, & Zoh, 2017), (Wang, et al., 2018), (Dong, et al., 2018), (Makarichi & Techato, 2018), there has been very little research on the environmental impacts of them (Beylot, Muller, Descat, Ménard, & Villeneuve, 2018), (Silva & Lopes, 2017). The present study identifies the environmental impacts of a municipal solid waste incineration plant assumed to be operating on Kayseri landfill area. For this purpose, waste management system of Kayseri is considered, and life cycle assessment methodology is used for impact calculations. SimaPro LCA software package is used for creating models and impact analysis. Ecoinvent and European Reference Life Cycle Database (ELCD) are used for inventory evaluations.

METHODS

In the present study, life cycle assessment procedure of municipal solid waste incineration plant is performed depending on the ISO standards (ISO, 1997), (ISO, 2006). ISO standards suggest that a LCA process is performed under following steps;
Goal and scope definition
Life cycle inventory
Impact assessment
Interpretation

Goal of this work is to analyze the environmental impacts of an incineration plant assumed to be operating on Kayseri landfill area. We are neglected the waste collection, transportation, landfill area and other sub-processes of municipal solid waste management system of Kayseri. We only considered the incineration plant with waste bunker, grate incinerator, steam boiler, electrostatic precipitator and wet scrubber. 1 kWh energy generation by incineration plant is selected as functional unit and lifetime of the plant is assumed as 20 years. It is assumed that municipal solid waste contains nearly 93 % combustible composition and 7 %, incombustible composition. Electrical efficiency is accepted as 30 %. Municipal solid waste capacity is 1000 ton/day and Kocasinan, Melikgazi, Talas, İncesu and Hacılar districts' wastes are collecting and dumping to Kayseri landfill area. One kg of municipal solid waste contains 1.39 MJ (0.4 kWh) of electrical and 2.85 MJ thermal energy (Ecoinvent, 2018). Waste flow is continuous and stable throughout the year and 500 ton/day waste is assumed to be incinerated. So, overall electricity generation for 20 years is calculated

as nearly 540 GWh by considering efficiency, waste flow and day off times according to regional parameters.

Life cycle inventory is collected from literature, Ecoinvent and ELCD databases, Kayseri Metropolitan Municipality and other district municipalities. Accuracy of these data significantly affect the life cycle impact assessment results. Life cycle impacts evaluations are carried out by using CML-IA characterization methods as follows (PRe-Sustainability, 2018);

Depletion of abiotic resources
Climate change
Stratospheric Ozone depletion
Human toxicity
Fresh-water aquatic eco-toxicity
Marine ecotoxicity
Terrestrial ecotoxicity
Photo-oxidant formation
Acidification
Eutrophication

CML-IA approach is determined for midpoint processes. Moreover, in this study we have not used normalization approach which is used for reference comparisons.

RESULTS AND FINDINGS

Results of this work mainly depend on the data which are gathered in life cycle inventory phase. We have compiled the collected data on SimaPro software and total impact values of incineration plant are given on the Table 1. According to the Table 1, this plant is responsible from 1.65E+07 kg CO2- equivalent global warming on the earth throughout its lifetime.

Table 1. Impact Categories of Incineration WtE Plant

Impact category	**Unit**	**Total**
Abiotic depletion	kg Sb eq	6.02E+01
Abiotic depletion (fossil fuels)	kWh	4.58 E+07
Global warming	kg CO2 eq	1.65E+07
Ozone layer depletion	kg CFC-11 eq	1.34E+00
Human toxicity	kg 1,4-DB eq	2.03E+07
Fresh water aquatic ecotoxicity	kg 1,4-DB eq	8.89E+06
Marine aquatic ecotoxicity	kg 1,4-DB eq	1.63E+10
Terrestrial ecotoxicity	kg 1,4-DB eq	7.79E+04
Photochemical oxidation	kg C2H4 eq	5.80E+03
Acidification	kg SO2 eq	6.08E+04
Eutrophication	kg PO4 eq	2.33E+04

Table 2 and Figure 1 give information on the percentage impact values of the incineration plant components which are gravel, reinforcing steel, chromium steel, pitch, sand, cement and wastes. As can be seen from the Table 2 and Figure 1, steel extensively shares all impacts effects by percentage.

Table 2. Impact Categories of Incineration WtE Plant Components (%)

Impact category	**Gravel, round**	**Reinforcing steel**	**Steel, chromium steel 18/8**	**Pitch**	**Sand**	**Cement, unspecified**	**Waste bitumen sheet**	**Waste concrete**
Abiotic depletion	2.47	64.81	16.39	0.42	0.70	13.70	0.15	1.36
Abiotic depletion (fossil fuels)	3.63	49.44	2.44	24.15	1.03	11.93	0.27	7.11
Global warming	2.56	50.48	2.36	2.25	0.73	26.19	11.44	4.00
Ozone layer depletion	4.60	34.93	1.52	36.06	1.32	11.05	0.61	9.91
Human toxicity	0.81	63.14	29.69	0.54	0.23	2.28	2.20	1.10
Fresh water aquatic ecotoxicity	0.89	66.50	12.56	0.63	0.25	3.29	13.91	1.97
Marine aquatic ecotoxicity	1.79	72.82	7.57	1.28	0.51	6.85	7.28	1.91
Terrestrial ecotoxicity	1.02	78.58	9.40	2.29	0.29	7.08	0.19	1.15
Photochemical oxidation	2.36	80.65	2.39	4.12	0.67	6.89	0.32	2.60
Acidification	4.39	60.25	3.78	6.43	1.25	15.92	0.95	7.05
Eutrophication	2.74	75.60	2.85	2.47	0.78	10.31	0.89	4.34

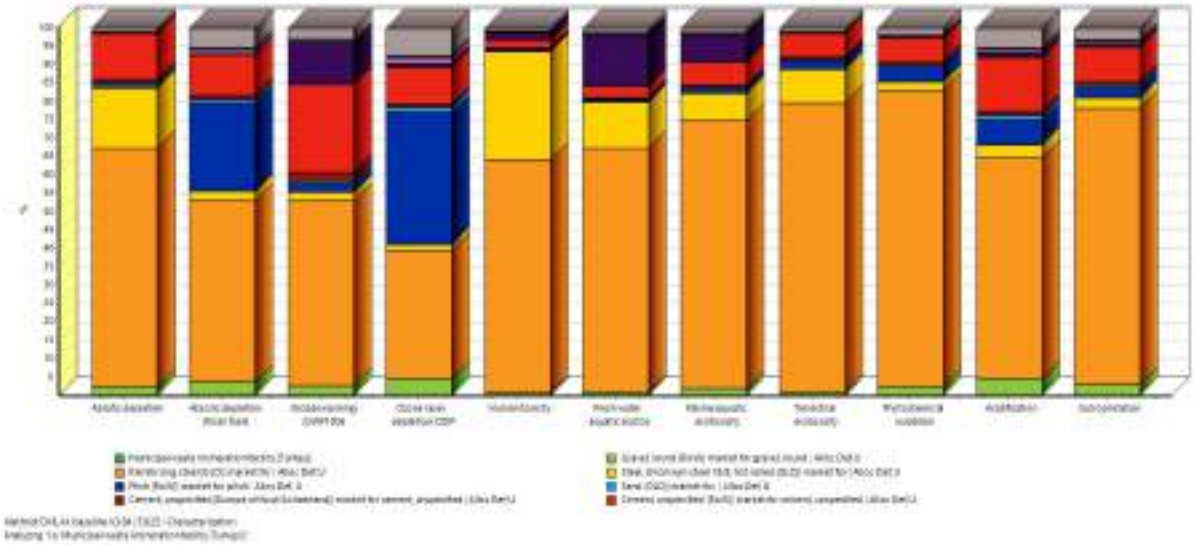

Figure 1. Impact Categories of Incineration WtE Plant Components (%)

Impact category values are divided the electricity output of the incineration plant for the 20 years lifetime and results are given on the Table 3. According to the Table 3, global warming potential of this power plant is 3.06E-02 kg CO_2 eq per kWh. Figure 3 demonstrates the flow diagram of the GWP of incineration plant by %.

Table 3. Impact Categories of Incineration WtE Plant per kWh

Impact category	**Unit**	**Total**
Abiotic depletion	kg Sb eq/kWh	1.11E-07
Abiotic depletion (fossil fuels)		3.06E-01
Global warming	kg CO2 eq/kWh	3.06E-02
Ozone layer depletion	kg CFC-11 eq/ kWh	2.48E-09
Human toxicity	kg 1,4-DB eq/kWh	3.76E-02
Fresh water aquatic ecotoxicity	kg 1,4-DB eq/kWh	1.65E-02
Marine aquatic ecotoxicity	kg 1,4-DB eq/kWh	3.02E+01
Terrestrial ecotoxicity	kg 1,4-DB eq/kWh	1.44E-04
Photochemical oxidation	kg C2H4 eq/kWh	1.07E-05
Acidification	kg SO2 eq/kWh	1.13E-04
Eutrophication	kg PO4 eq/kWh	4.32E-05

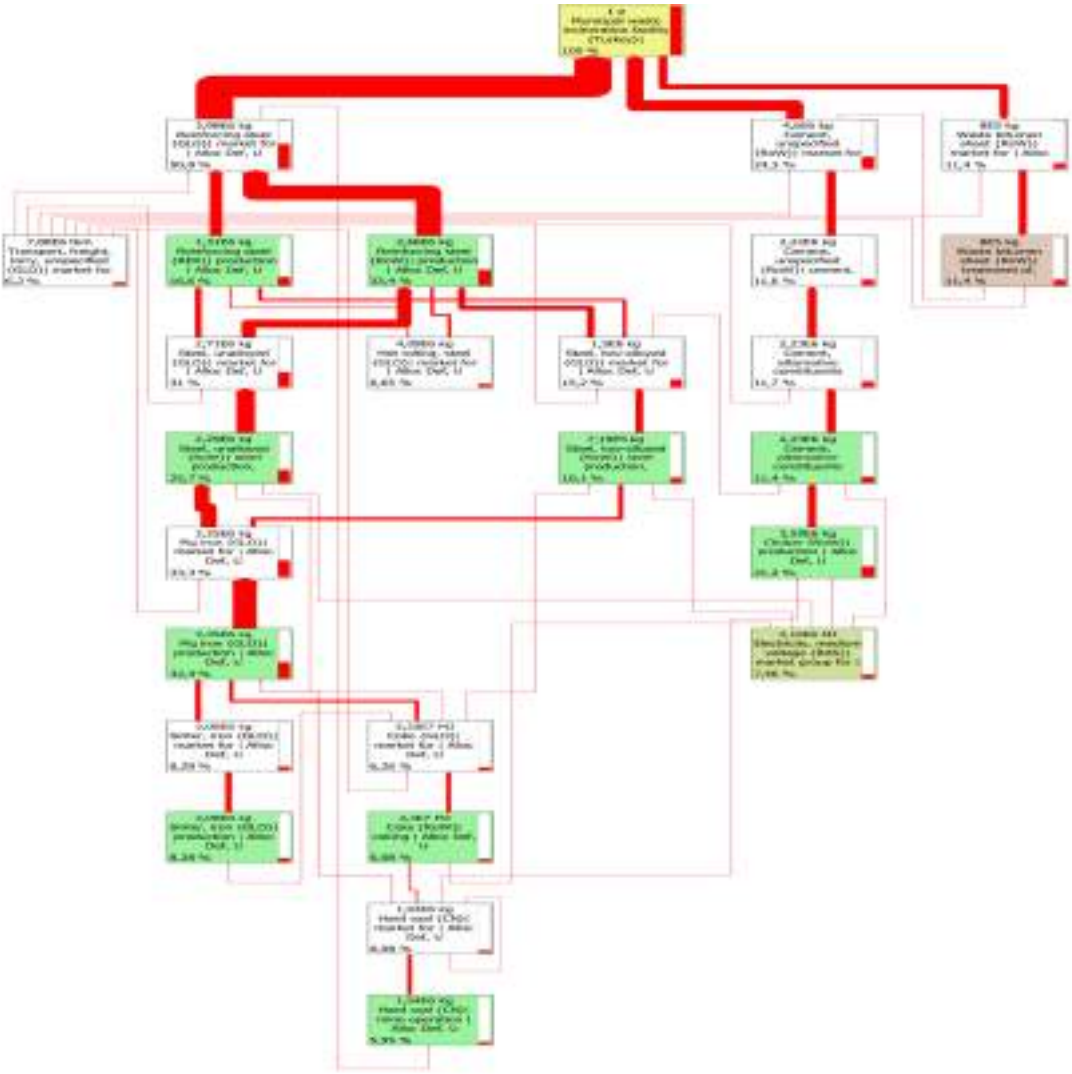

Figure 2. Global Warming Potential Impact Analysis of Incineration WtE Plant (%)

CONCLUSIONS

Municipal solid waste management is significant problem for municipalities due to the complexity of processes such as waste to energy, soil and water pollution, odor effects and volume of the wastes. Incineration is playing an important role in the waste management systems of cities. The present paper reveals the environmental impacts of an incineration power plant from the life cycle assessment perspective. Results show that incineration is one of the feasible ways to generate energy from wastes, to diminish the environmental impacts and to reduce the volume of the wastes approximately 90 %. Moreover, incineration ashes can be used in cement industry as raw material, this outcomes as an additional advantage of incineration. Results also show that steel has considerable effect on all impact categories. Additionally, cement and pitch are other significant effective components of impacts.

Consequently, WtE is an optional way to produce electricity by means of energy security, foreign source dependency and environmental aspects. Incineration is developing WtE technology and it can be more feasible by decreasing investment costs and increasing plant energy efficiency. Furthermore, total environmental impacts of incineration plant can be reduced by using alternative materials instead of steel.

ACKNOWLEDGEMENTS

The authors gratefully acknowledge Erciyes University Scientific Research Projects Funding Department (ERU-BAP) for supporting this work financially (Grant No: FDK-2016-6871). Authors also thank to Metropolitan Municipality of Kayseri for their collaboration.

REFERENCES

An Independent Engineering Evaluation of Waste-to-Energy Technologies. (2014). Retrieved 2018, from https://www.renewableenergyworld.com/articles/2014/01/an-independent-engineering-evaluation-of-waste-to-energy-technologies.html.

Beylot, A., Muller, S., Descat, M., Ménard, Y., & Villeneuve, J. (2018). Life cycle assessment of the French municipal solid waste incineration sector. *Waste Management,80*, 144-153. doi:10.1016/j.wasman.2018.08.037.

Dong, J., Tang, Y., Nzihou, A., Chi, Y., Weiss-Hortala, E., Ni, M., & Zhou, Z. (2018). Comparison of waste-to-energy technologies of gasification and incineration using life cycle assessment: Case studies in Finland, France and China. Journal of Cleaner Production,203, 287-300. doi:10.1016/j.jclepro.2018.08.139.

Ecoinvent Database. (2018). Retrieved 2018, from https://www.ecoinvent.org/.

Hwang, K., Choi, S., Kim, M., Heo, J., & Zoh, K. (2017). Emission of greenhouse gases from waste incineration in Korea. *Journal of Environmental Management,196*, 710-718. doi:10.1016/j.jenvman.2017.03.071.

ISO 14040: Environmental management - life cycle assessment - principles and framework. (1997). Geneve (Switzerland): ISO.

ISO 14044: Environmental management, life cycle assessment, requirements and guidelines. (2006). Geneve (Switzerland): ISO.

Lino, F., & Ismail, K. (2017). Incineration and recycling for MSW treatment: Case study of Campinas, Brazil. *Sustainable Cities and Society,35*, 752-757. doi:10.1016/j.scs.2017.09.028.

Makarichi, L., Jutidamrongphan, W., & Techato, K. A. (2018). The evolution of waste-to-energy incineration: A review. Renewable and Sustainable Energy Reviews, 91, 812-821. https://doi.org/10.1016/j.rser.2018.04.088.

Silva, S., & Lopes, A. M. (2017). Environmental aspects and impacts of a waste incineration plant. *Energy Procedia,136*, 239-244. doi:10.1016/j.egypro.2017.10.250.

Small Scale Environmental Solutions – A New Market Opportunity. (2013). Retrieved 2018, from http://www.pennog.com/small-scale-environmental-solutions-a-new-market-opportunity/.

SimaPro Database Manual Methods Library. (2018). Retrieved 2018, from https://www.pre-sustainability.com/download/manuals/DatabaseManualMethods.pdf.

The Annual Energy Outlook 2013, With Projections to 2040. (2013). Retrieved 2018, from https://www.eia.gov/outlooks/aeo/pdf/0383(2013).pdf.

Wang, Y., Zhang, X., Liao, W., Wu, J., Yang, X., Shui, W., Peng, H. (2018). Investigating impact of waste reuse on the sustainability of municipal solid waste (MSW) incineration industry using emergy approach: A case study from Sichuan province, China. *Waste Management,77*, 252-267. doi: 10.1016/j.wasman. 2018.04.003.

World Bank Technıcal Guidance Report, Municipal Solid Waste Incineration. (1999). Retrieved 2018, from http://web.mit.edu/urbanupgrading/urbanenvironment/resources/references/pdfs/MunicipalSWIncin.pdf.

World Energy Resources, Waste to Energy. (2016). Retrieved 2018, from https://www.worldenergy.org/wp-content/uploads/2017/03/WEResources_Waste_to_Energy_2016.pdf.

INVESTIGATION ON THE TRACKING SPEED OF DC MOTOR UNDER DIFFERENT EXTERNAL TORQUE

Mustafa HASAN
Department of Electrical and Electronics Engineering, **Gaziantep University, Gaziantep, TURKEY** eng.mustafa.lateef@gmail.com

Ergun ERÇELEBİ
Department of Electrical and Electronics Engineering, **Gaziantep University, Gaziantep, TURKEY** ergun.ercelebi@gmail.com

ABSTRACT: This paper investigates the closed loop speed control of DC motor fed from a buck step-down converter device. The dynamic system (DC motor driven by buck step-down converter) is derived in the form of transfer function and state-space. The detailed account of the simulation environment presented through frequency and time domain, respectively. The buck converter is driven by a PWM signal with a high fixed frequency. Adjusting the PWM duty cycle is equivalent to the adjusting in the voltage applied to the terminal of the motor, this, in turn, controls directly on the motor speed. Finally, performances of the Proportional-Integral (PI) controller technique is presented and discussed in terms of duty cycle, angular velocity and motor input voltage. The main objective is to achieve a constant speed under different load condition based on the smooth trajectory tracking.

Key words: Step down buck converter, DC motor, Proportional Integral controller.

INTRODUCTION

Recently, DC machines have been extensively used in many industrial applications because they are cheap, have simple control structure and wide range of speed and torque. Although AC power supply is simpler to use, the devising of high-efficiency DC power converters has made the implementation of DC machine even more practical and economical.

Nowadays all DC motor drivers use semiconductor devices such as MOSFET which is used for high-speed switching of the output voltage and to provide high current with less dissipation of heat. They are relatively cheap, small in size and operate with high efficiency providing practical and efficient control ways of the DC motor.

Kirchhoff's law led to $N = k(V - I_a R_a)/\Phi$,Where k is constant, N- speed of the motor, Φ- magnetic flux, R_a-armature resistance and I_a-is the armature current. So, the above formula denotes three facts: The Speed of the DC motor is directly proportional to the applied voltage and inversely proportional to both of armature voltage drop ($I_a R_a$) and the flux due to the field windings.

Due to power loss dissipated from armature resistor in armature resistance control method and the failure of providing precise speed control with the desirable scope in the field flux control method, both of these methods are undesirable, so the best solution for this dilemma is to drive Dc motors by Pulse-width modulation (PWM) signals in regard to the applied voltage on the motor.

Modification of the duty cycle and the operating frequency of the switch-mode power supplies (SMPS) circuit lead to change the voltage level that applies to the motor, by either elevating or decreasing according to the speed and torque control requirements. However, the switching strategy leads to unaccecptable dynamic behavior and forming a very noisy shaped trajectories which result in vast forces applying on the DC motor so a large current is consumed by the motor, the final result is a harmful effect on both of the electronic components and the power supply **Geçersiz kaynak belirtildi.** .

A component with a power supply (MOSFET) is usually necessary to control the entire system (DC motor/ buck-converter). A combination of DC motors with DC to DC power converters is reported by **Geçersiz kaynak belirtildi.**. In specific, the composition of a DC motor driven by a buck converter is reported by (Linares-Flores &Sira-Ramirez, 2004b; Linares-Flores & Sira-Ramirez, 2004a).

In DC to DC step down (buck converter), tiny current ripple and smooth DC output voltages resulting from the presence of the buck converter on a capacitor and a coil as energy storing elements.
The circuit design of the buck converter is important for gaining a minimum-power losses rate at any time in tracking systems of the angular velocity.

In the designing of the proportional- integral (PI) control, the P-term gets a fixed proportion closer to the setpoint right off the bat, the I-term closes the gap from the proportional term over time. As a result, PI controllers are widely utilized to minimize the percentage error between the output value with the reference setpoint.

METHODS

Modeling Of Buck-Converter With DC Motor System

Due to MOSFET switching operation modem, the buck converter is an inherently nonlinear system. The regulation is achieved at fixed frequency by the PWM according to the duty cycle of the PWM. Input DC supply is regulated to get the desired output voltage in a range from zero up to the input voltage.
A simplified model for a DC motor driven by buck converter is illustrated in Figure 1.

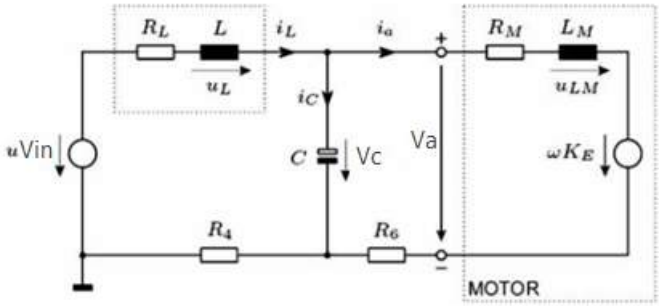

Figure 1. Simplified Model For A DC Motor Driven By A Buck-Converter

In a practical *switched* mode *power supply* (MOSFET) can be replaced by multiply the input voltage source with the variable $u \in \{0,1\}$, so the combination of input voltage source with the switch device is $V_{in} * u$.

In our scheme, the internal resistance of the coil windings was taken into account. The DC motor was modeled by ohmic resistance(R_M) with an inductance(L_M) and electromagnetic voltage supply($K_E\omega$). In summary: The consistency of the dynamic system (DC motor driven by a buck-converter), were taken in consideration and derived in the transfer function and the state space forms. the system of figure 1 is represented as:

$$u\,V_{in} = R_L I_L + L\frac{di_L}{dt} + V_c \tag{1}$$

$$V_C = R_m I_a + L_M\frac{di_a}{dt} + K_E\omega \tag{2}$$

$$i_L = C\frac{dV_C}{dt} + i_a \tag{3}$$

$$T = J\frac{d\omega}{dt} = K_M I_a \tag{4}$$

where the moment of inertia was considered as J and the tacho generator gain of the motor represented as K_M. In (1) and (2), for simplifying, the resistances R_4 and R_6 were dropped from the calculation because they had a very low measurement amplifier. The motor shaft dynamism (the model of the state space completed with the mechanical equation) was represented through equations (1) to (4), a linear fourth order system was described through

$$\dot{X} = Ax + Bu \tag{5}$$
$$Y = Cx + Du$$

With the vector $x = [i_L \quad V_C \quad i_a \quad \omega]^T$, u is the input, y is the output, the matrices A, B and C are given by

$$A = \begin{bmatrix} -\frac{R_L}{L} & -\frac{1}{L} & 0 & 0 \\ \frac{1}{C} & 0 & -\frac{1}{C} & 0 \\ 0 & \frac{1}{L_M} & -\frac{R_M}{L_M} & \frac{K_E}{L_M} \\ 0 & 0 & \frac{K_M}{J} & 0 \end{bmatrix} \tag{6}$$

$$B = \begin{bmatrix} \frac{V_{in}}{L} & 0 & 0 & 0 \end{bmatrix}^T, \quad C = [0 \quad 0 \quad 0 \quad 1] \text{ and } D=0$$

According to **Geçersiz kaynak belirtildi.**, the discrete switching variable input $u \in \{0,1\}$ can be superseded with the duty ratio $\delta \in [0,1]$. An analog input signal can

generate δ by the use of PWM-strategy, so the result may be referred to an averaged dynamic model, given by

$$\dot{X} = Ax + B\delta \tag{7}$$

Note that the validity of the linear system description occurs only when there is no saturation effect in the inductor. Otherwise the relation between the current i_L and the inductance L are non-linear.

In this study, the values of the parameters are defined as R_M= 6 ohm , L_M= 8.9 mH, $K_M = 0.0517$ N − m/A, K_E= 0.0517 V-s/rad, J = 7.95×10^{-6}kg-m^2 , U_e= 24 V, R_L= 0.2 , L = 1.33 mH , C = 470 µF and 45 kHz switching frequency has been used for the triggering the buck converter.

Since our system is a single-input, single-output and represented in state space by the form

$$\dot{X} = Ax + B\delta \tag{8}$$

$$Y = Cx$$

So, we can derivate relation between the state-space equation and the transfer function, let's assume

$$G(s) = \frac{output}{input} = \frac{\omega_{(s)}}{\delta_{(s)}} \tag{9}$$

we can take the Laplace transform for equation (8) to get

$$sX_{(s)} - x_{(0)} = AX_{(s)} + B\delta_{(s)} \tag{10}$$

$$\omega_{(S)} = CX_{(s)} \tag{11}$$

when the initial condition is zero, that is make $x_{(0)} = 0$,So

$$sX_{(s)} - AX_{(s)} = B\delta_{(s)} \tag{12}$$

$$(sI - A)X_{(s)} = B\delta_{(s)}$$

by multiply $(sI - A)^{-1}$ for both side of previous equation, we obtain

$$X_{(s)} = (sI - A)^{-1}B\,\delta_{(s)} \tag{13}$$

where I is identity matrix, by substituting the eq (11) with the previous equation, we obtain

$$\frac{\omega_{(S)}}{C} = (sI - A)^{-1}B\,\delta_{(s)} \tag{14}$$

so

$$G_{(s)} = \frac{\omega_{(S)}}{\delta_{(s)}} = C(sI - A)^{-1}B \tag{15}$$

$$G_{(s)} = [0 \quad 0 \quad 0 \quad 1]\left(\begin{bmatrix} s & 0 & 0 & 0 \\ 0 & s & 0 & 0 \\ 0 & 0 & s & 0 \\ 0 & 0 & 0 & s \end{bmatrix} - \begin{bmatrix} -\frac{R_L}{L} & -\frac{1}{L} & 0 & 0 \\ \frac{1}{C} & 0 & -\frac{1}{C} & 0 \\ 0 & \frac{1}{L_M} & -\frac{R_M}{L_M} & \frac{K_E}{L_M} \\ 0 & 0 & \frac{K_M}{J} & 0 \end{bmatrix}\right)^{-1} * \begin{bmatrix} \frac{U_e}{L} \\ 0 \\ 0 \\ 0 \end{bmatrix}^T$$

(16)

$$G_{(s)} = \frac{\omega_{(S)}}{\delta_{(s)}} = \frac{k}{s^4 + a_3 s^3 + a_2 s^2 + a_1 s + a_0} \tag{17}$$

Solving equation (16)

$$k = \frac{K_M V_{in}}{J L L_M C}$$

$$a_3 = \frac{R_L}{L} + \frac{R_M}{L_M}$$
$$a_2 = \frac{R_L R_M}{L L_M} + \frac{1}{LC} + \frac{1}{L_M C} + \frac{K_E K_M}{J L_M}$$
$$a_1 = \frac{R_L + R_M}{L L_M C} + \frac{R_L K_E K_M}{J L L_M}$$
$$a_0 = \frac{K_E K_M}{J L L_M C}$$

where k=2,805*10^{13} , $a_3 = 824.5$, $a_2 = 1.978 * 10^6$, $a_1 = 1.12 * 10^9$ and $a_0 = 6.043 * 10^{10}$

$$\frac{\omega_{(S)}}{\delta_{(s)}} = \frac{2{,}805*10^{13}}{s^4+(824.5)s^3+(1.978*10^6)s^2+(1.12*10^9)s+6.043*10^{10}} \quad (18)$$

Controller Design

The consistency of PI in general is a closed loop feedback system as shown in figure 2. It is work in principle is that the error (the reference angular velocity $\omega_{r(s)}$ without the current angular velocity $\omega_{(s)}$), is regulated by a proportional – Integral controller (PI controller) for maintaining the speed of the DC motor (in time-domain) with limited control behavior of duty cycle, with taking into account the undesirable transient behavior for overall system that may occur.

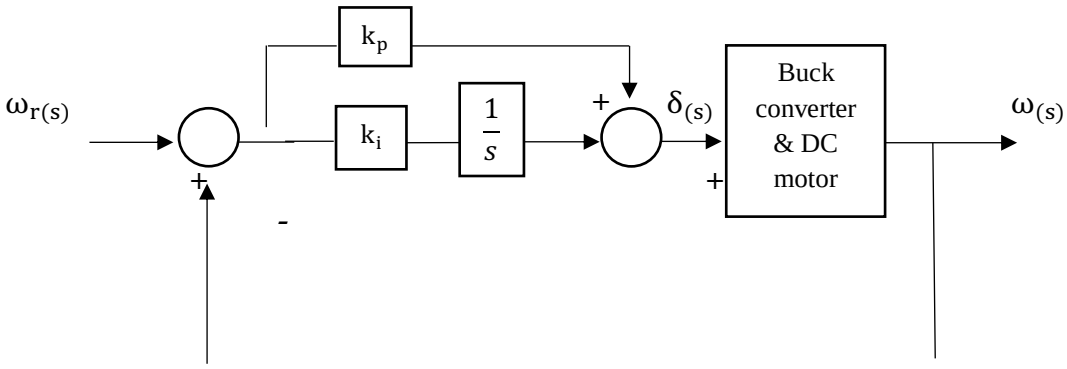

Figure 2. PI Controller Of A DC Motor Driven By Buck Converter

According to the above figure

$$\delta_{(s)} = [\omega_{r(s)} - \omega_{(s)}]\, G_{c(s)} \quad (19)$$

So, the transfer function of the closed loop was obtained as

$$\frac{\omega_{(s)}}{\omega_{r(s)}} = \frac{G_{c(s)} G_{(s)}}{1 + G_{c(s)} G_{(s)}} \quad (20)$$

The mathematical representation of PI control in the s- domain is:

$$G_{c(s)} = k_p + \frac{k_i}{s} \quad (21)$$

k_p is a proportional gain constant.

k_i is a integral gain constant.

The output signal (produced by a parallel connection of the two fixed value of PI) are driving the plant (buck converter and DC motor) after achieving mapping operation on that signal to convert it to square wave (with fixed frequency and variable duty cycle). The angular velocity of DC motor is measured (via encoder speed or tachometer) and compared with the reference velocity through a feedback. This error is used by PI to calculate the control signal again. This process is turned on continuously until the desired steady state-error is obtained. the effect of increasing PI parameter is illustrated table 1.

Table 1. Effects Of Increasing A Parameter Independently Geçersiz kaynak belirtildi.

parameter	Rise time	Overshoot	Settling time	Steady-state error	Stability
k_p	Decrease	Increase	Small change	Decrease	Degrade
k_i	Decrease	Increase	Increase	Eliminate	Degrade

Proportional Integral Tuning

When designing PI controller, most important part is how we tune the gains constant (k_p, k_i) in order to get optimum desired performance (more robust, less rise time, less overshoot, etc.). According to equation (18) a complex conjugate pole appears at $(-106 \mp J1340)$ which lead to (180 deg) phase delay at frequency $(2.49 * 10^3 \frac{rad}{sec})$. According to figure (3). The Bode plot of the overall system shows that it has gain margin (-31.10 dB) and phase margin (-159 deg) which denote that the system is unstable (because both of GM and PM are negative). So, to inhibit steady-state oscillation causes by unstable behavior, a PI controller was designed.

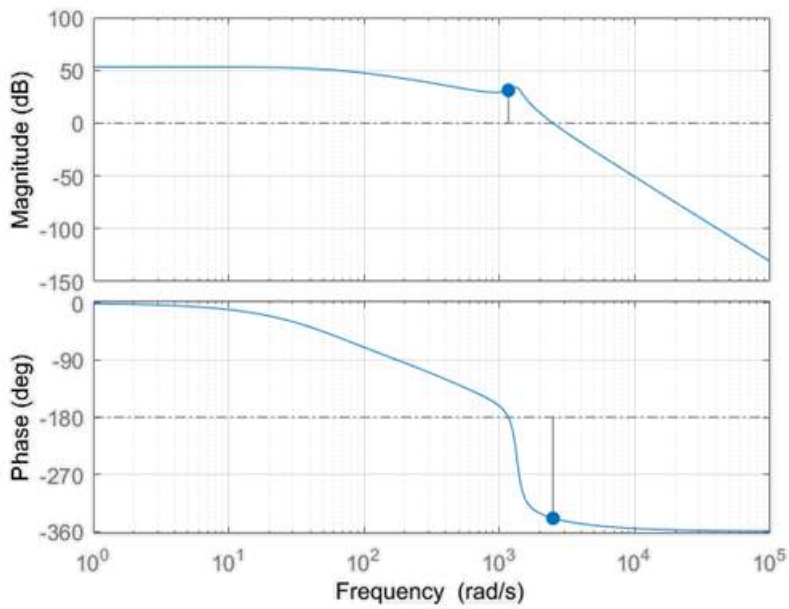

Figure 3. The Bode Plot For A DC Motor Fed From Buck Converter

The controller constants were tuned to obtain the desired phase and gain margins. The PI controller transfer function after tuning operation has been given as:

$$G_{c(s)} = 0.00691 + \frac{0.3968}{s} \quad (22)$$

The Bode plot of figure (4) shows us that the PI controller turns the system from unstable region to stable one with gain margin (12.40) dB and phase margin (70.90).

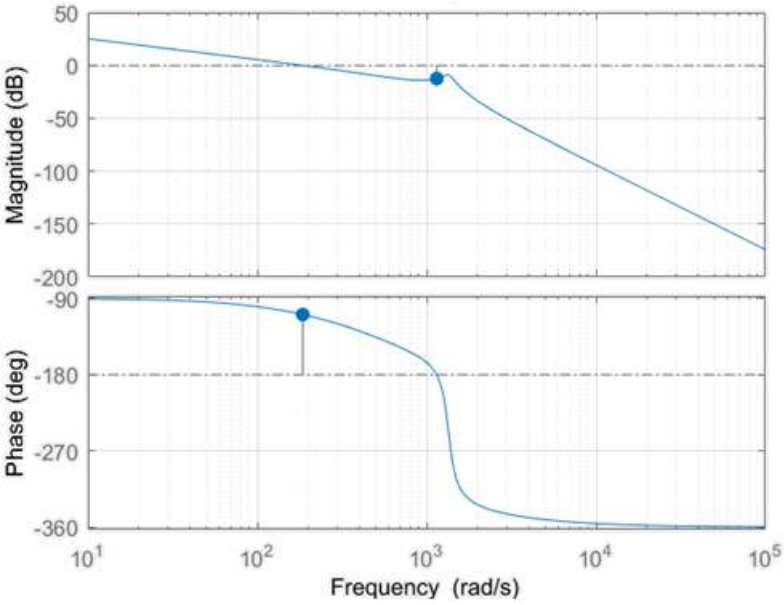

Figure 4. Bode Plot For PI Controller combination with the DC Motor driven by Buck Converter

EXPERIMENTAL STUDIES

The performance testing for the the DC motor driven by buck converter at the simulation environment are presented. The system performances are evaluated by terms of (duty cycle, output voltage of the buck converter and angular velocity). A computer simulation was designed for the control strategies with the aid of range-Kutta fourth order (4nd) integration method with 1 kHz sampling frequency.

Buck Converter Output

The microcontroller can produce pulses with a specific fixed frequency, which feeds the bootstraps circuit to provide a base to source voltage larger than the thresholding voltage of the transistor this make the transistor behave like a switch.
The motor output voltage depends on the transistor on-time amount. So, more voltage is feeding to the motor as increasing the duty cycle of the square wave produced from

the microcontroller. Now, according to $V_o = DV_{in}$ when 100% duty cycle has been applied on the buck converter lead to $V_o = V_{in}$.

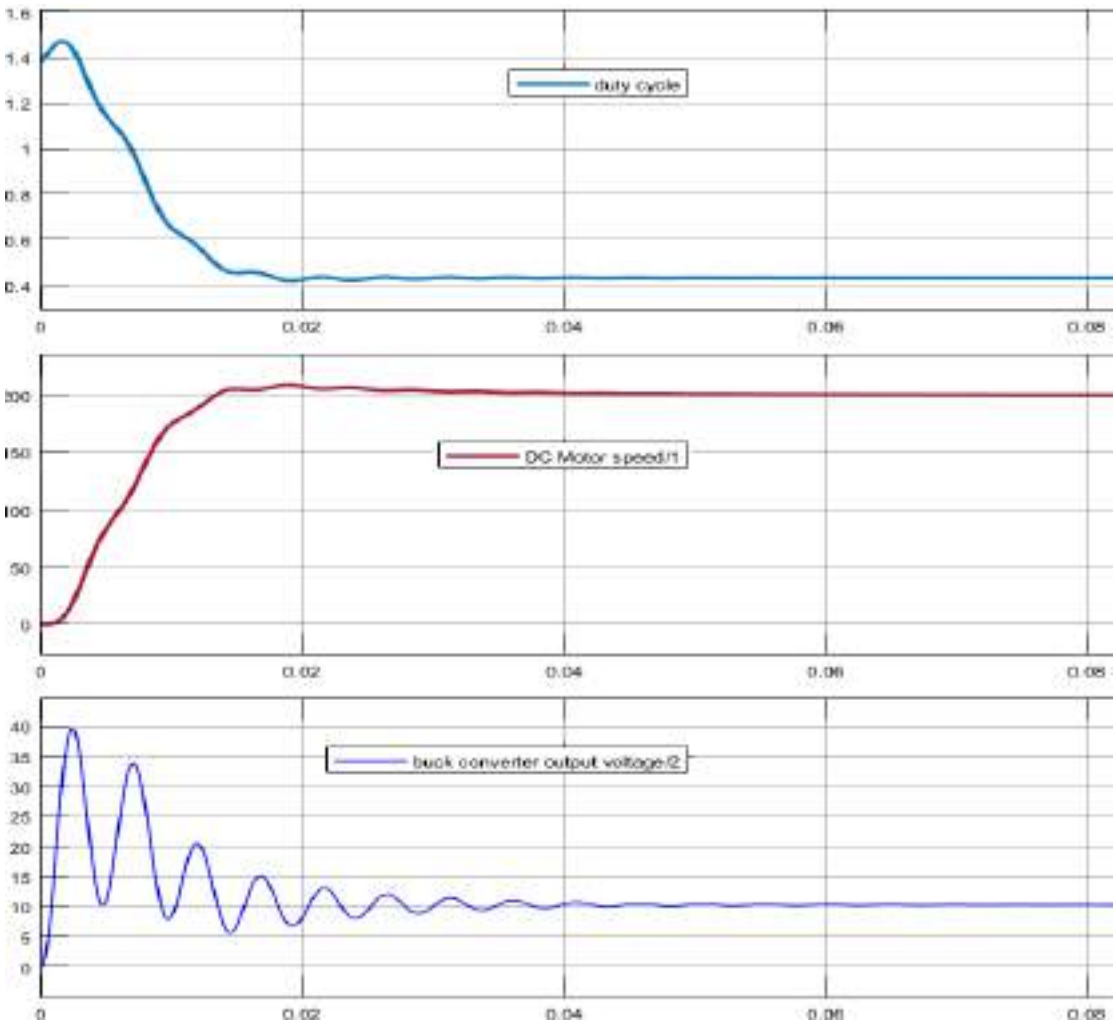

Figure 5. Duty Cycle, Output Voltage For 200 rad/sec Motor Speed

Figure.5 shows us that the system takes about 0.02 sec until it passes the transient period which is considered as an acceptable duration. At steady state, the duty cycle reaches 0.4308 while the output voltage is approximately about 10.3 volts for the case of 200 rad/sec reference input speed.

DC Motor

Appling the final value theorem on equation (18) to find the maximum speed measured by the tachometer at steady state when applying 100% duty cycle.

$$\omega_{max(Steady\ state)} = Lim_{s\to 0} S * \delta_{(s)} * \frac{k}{s^4+a_3s^3+a_2s^2+a_1s+a_0} \quad (23)$$

$$\omega_{max(Steady\ state)} = Lim_{s\to 0} S * \frac{1}{S} * \frac{k}{s^4+a_3s^3+a_2s^2+a_1s+a_0} = \frac{k}{a_0} = 464.173 rad/sec$$

(24)

figure 6 shows us at 0.03 sec an external torque has been applied on the DC motor. So, the tachometer reading value regulates the duty cycle by the use of the microcontroller

through elevating to trigger the DC motor for returning to the 200 rad/sec reference desired speed.

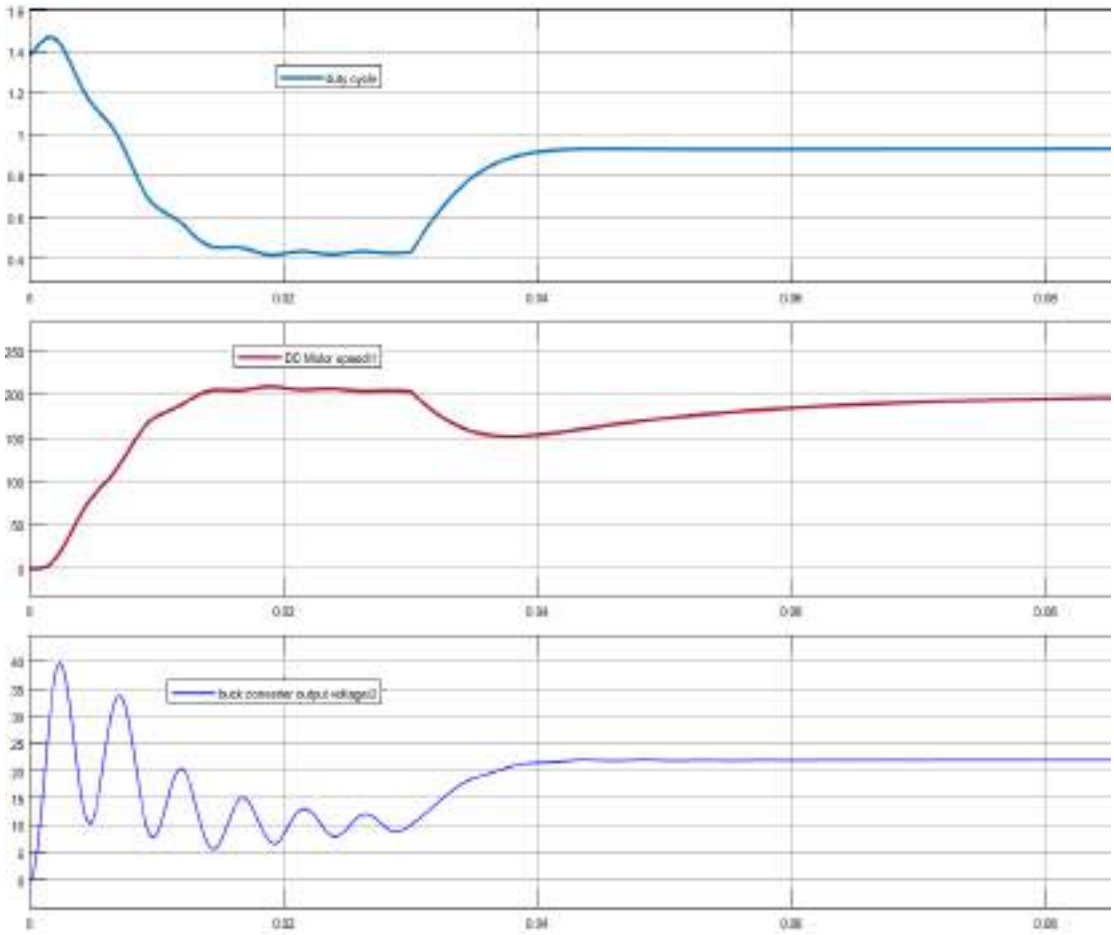

Figure 6. Appling An External Disturbance Torque On The DC Motor At 0.03 sec

CONCLUSION

At the first, the investigations and the modeling for plant (DC motor driven from buck converter) have been presented with the PI controller. The angular velocity was taken as a feedback to form a closed loop control system.

Modifying the gain and phase margins have been done using PI controller with pushing the system to be more robust Meanwhile, with better performance in transient time.

Simulation results show us a Smooth Start up for a DC motor and possibility of designing tracking control system for the angular velocity with an excellent disturbance torque rejection in the PI controller.

UTILIZATION OF WASTE PLASTIC IN MANUFACTURING OF BRICK

Jannatul MAOWA
Department of Civil Engineering, KUET, Khulna, Bangladesh
e-mail: jannatulmaowaaune@gmail.com

Muhammad Harunur RASHID
Department of Civil Engineering, KUET, Khulna, Bangladesh
e-mail: hafin02@gmail.com

ABSTRACT: The using of plastic made product has increased in the recent century. And in most country a big amount of waste plastic is thrown or dumped in open places and creates an environment challenge due to its non-degradable nature. As the plastic does not decompose in nature, the waste plastics remain unchanged and increase in quantity. In this research an attempt is made to manufacture brick block using plastic bottle, sand and bitumen in different mixing proportion. This is one of the way to manage the waste plastics effectively. The availability of used plastic bottle is very high which helps to cut the cost of making brick block. Energy consumed to produce plastic brick is much less than that for regular brick. Bitumen is added in certain percentages to improve the bonding capacity among all ingredients of brick. In this thesis, an attempt is made to study regard the properties of the brick which is manufactured using plastic wastes, sand and bitumen. The properties of brick block having different percentage of plastic, sand and bitumen were tested for compressive strength, water absorption and unit weight. It shows that a good bonding and strength has been achieved by introducing plastic waste in brick blocks. From study it is found that adding 5% of bitumen can lead to an increase of 39% of strength of brick block having no bitumen. The water absorption however showed excellent performance for these brick blocks.

Keywords: Plastic waste, Compressive strength, Bitumen, Permeability.

INTRODUCTION

Plastic waste is a global phenomenon and its side effects are felt throughout the universe. In day to day work a substantial amount of plastic is used in everywhere in the world. These plastics are inexpensive, lightweight and durable. As the plastic made products are cheap most of them are thrown here and there inappropriately. It makes up much of the street side litter in urban and rural areas. It is rapidly filling up landfills as choking water bodies and causing serious environmental consequences. According to ENSO Bottles, plastic bottle production has been negligible in the 1960's but over the years the picture is drastically changed but the rate of recycling is still very low. Plastic has the insolvability about 300 years in the nature, it is considered as a non-degradable waste and environmental pollutant. So recycling of plastics can be useful in mitigation of environmental impacts involving to it. Some researchers argues about the use of waste plastic to produce building block can be a suitable solution for replacement of conventional building materials. Information on Municipal solid waste

in Bangladesh disclosed by Waste Concern in 2009 and conclude the the solid waste contains plastic, rubber and leather waste is about 5.1% by weight. MoEE (2010) reported that most of them are plastic material near about 3.2%. Rate of recycling of plastic waste in Bangladesh is the highest (83%) in the world as compared to other countries, ie. India 60%, China 20%, Europe 20-40%, Japan 39%, South Africa 16%, England 17.7% and USA 28% (Suraiya and Rahman, 2017).

According to Mojtaba and Azin (2013) the plastic bottles as the building materials can have substantial effects on saving the building embodied energy by reducing the percentage of cement used and finally drop the CO_2 emission in environment from cement manufacturing industry. Thermal comfort in living houses is reported by Shilpi and Monika in 2013 by utilizing PET bottles in low cost housing construction in rural areas. Plastic is non-biodegradable, toxic, highly resistant to heat and electricity (best insulator) and not recyclable in true sense, plastic PET bottles used by some researchers to produce bottle- brick and used in rural housing (Ramadevi, 2012) . Puttaraj and Shanmukha (2014) argued that the uses of waste plastic in manufacturing of plastic-soil bricks can solve the problem of safe disposal of plastics.
Pratima and Akash in 2014, studied that building wall manufactured by plastic bottles have been less costly as compare to bricks. Arulmalar and Jothilakshmy in 2014, studied that the initial perception on the use of PET bottles in construction is changing day by day. Vikram examined in 2014 that the Eco-brick is a viable resource for construction purposes with a number of possible applications.

Recycling of waste plastic has some advantages since it is widely used and has a considerable service life. Moreover it does not require any type of maintenance. Plastic brick is easy to process and install. Normally in room temperature it is chemically inert. It reacts when the temperature is high. The composition of the plastic waste can vary in places. There are mainly two types of plastics in waste Polyethylene terephthalate and Polystyrene. Plastic bottles are made of Polyethylene terephthalate and polyethylene bags are made of polystyrene. Using waste plastic and sand brick can be made. These brick will consume less heat while processing. Moreover it will reduce the amount of waste plastic. Moreover high density plastic serves as a thermal insulator. This type of brick does not require extra binding material. Construction using this brick, consumes far less than normal brick construction. It also provides sound insulation. Making cost of this brick is less than soil made brick. The making process takes less time to complete than that of normal brick.

The uses of bituminous materials were initially limited to road construction. Most of the bituminous are colloidal in nature. Bituminous is thermoplastics. It is insoluble in water and highly impermeable to the passage on water. It is chemically inert. This property is mainly used to make plastic brick block. It also used for its binding properly. Maneeth et al. in 2014 studied that using 2% of bitumen gives the same compressive strength for plastic- soil bricks. But 5% bitumen content brick gives highest strength and increasing these percentage leads to the decrement of strength. Depankar and Manish in 2016 studied that mixing of more percentage of plastic in bitumen can lead to decrease in stability as there is a chance of formation of cavity. If

Poly Propylene is used instead of PET strength develops more. But the abundance of PP is not enough for such work.

Plastic brick can be used for low rise building where low cost in mandatory. Plastic brick reduce the overall cost of structure. Some countries like Colombia, India use brick that is made from waste plastic and sand for low rise building. This practice is becoming more popular day by day. These bricks give better appearance and smooth texture and surface. Plastic bricks are sufficiently strong to withstand the load of low rise building.

MATERIALS USED

Waste Plastic

In this research used plastic bottles are used. The plastic bottles use to hold potable water and other drinks, shampoo, detergent are made of polyethylene terephthalate (PET), because the material is both strong and light. PET consists of polymerized units of the monomer ethylene terephthalate, with repeating ($C_{10}H_8O_4$) units. These plastic bottles are shredded into pieces so that it can pass 4.75mm sieve. The shred are washed and cleaned properly so that any other chemicals or dirt cannot get mixed with the brick block. Melting temperature of these plastics is 146±5°C.

Sand

The sand that is used, is fine grained. Both fine grained and coarse grained sand is used. The coarse grain sand bonded weakly. But the fine grain bonded properly and strongly. The fineness modulus of the sand is 1.62. The sand was silver in color.

Bitumen

To check the bonding properties of bitumen, it is added in small percentage of total weight in brick block. Softening point of used bitumen was 49±5°C. Bitumen adds some blackish look to the brick block.

Mixing proportions

Mixing either two or three of them leads to plastic brick. Brick block containing only plastic and sand gives dark color but adding bitumen leads to blackish color. In order to find the change in compressive strength, water absorption and unit weight of brick block with different mixing ratio. The mix proportion of plastic and sand are 1:2, 1:4, 1:6. Bitumen is added in percentage of total; weight of total weight of sand and plastic. Two types of percentages are used 2.5% & 5%.

PROCEDURE

At the first stage plastic bottles mostly same type, are collected. Then it is shredded into pieces so that it can pass 4.75mm sieve. The shred is washed, cleaned and dried. On the other hand sand is cleaned and dried. According to ratio taken by weight sand

and plastic is mixed. This mixture is heated on a pan by a heater. Plastic starts melting after 146±5°C temperature. It takes 7-10minutes to melt all the plastic. Continuous staring is done. The mixture has a very short setting hence mixing process must not consume more time on the other hand the process should be complete.

This mixture is then poured in to the brick mold and they are compacted using steel rod and surface is finished using trowel. Before placing the mixture into the mold the sides of the mold are oiled to easy removal of bricks. After hardening, the mold is removed. About adding bitumen, bitumen is weighted according to the percentage of total weight of sand and plastic. Then bitumen is mixed with the sand and plastic. This mixture is heated then and mixed properly with the steel rod. When bitumen is added heating should be done carefully. If it is heated with high volume heat ignition may occur.

While putting the liquid mixing in the mold care should be taken. It should not be poured while it is too much hot. After removing heat it should put 1-2 min to reduce the temperature. Otherwise it will contain voids. This void will reduce the capability of the bricks. With the increase of bitumen brick block turns to be more blackish. Brick block having no bitumen show black color. But the color of brick block can be controlled by adding some additives. Size of the brick is 76.2mm ×25.4mm ×3.81mm.

Figure 1: Plastic Brick Block

Figure 2: Mold of the Brick

Table 1: Ratio of Sand and Plastic and Percentage of Bitumen

ID of brick block	Ratio (plastic: sand)	Bitumen,%
A	1:2	
B	1:4	0
C	1:6	
D	1:2	
E	1:4	2.5
F	1:6	
G	1:2	

H	1:4	5
I	1:6	

Testing Procedure

To check the performances of brick block following tests are done. Tests are done maintaining a fixed time gap between the time of processing and testing. Plastic bricks take time to get cool down and hardened. Without giving proper time to cool down it will not be capable of carrying of load as it is designed for. Tests are done in the laboratory of Civil Engineering Department of KUET.

Compressive Strength

Compressive strength test on bricks are carried out to determine the load carrying capacity of bricks under compression. This test is carried out with the help of compression testing machine. The procedure as mentioned Active Standard ASTM C1314 is used to determine the compressive strength of brick work. Generally three specimens of bricks are taken to laboratory for testing and tested one by one. In this test a brick specimen is put on crushing machine and applied pressure till it breaks.

Table 2: Compressive Strength of Bricks

ID of brick block	Compressive strength, (N/mm^2)
A	9.3
B	11.7
C	14.8
D	9.2
E	14.4
F	16
G	10.8
H	16.3
I	17.8

Water Absorption

This test is done according to the Standard ASTM C20. The testing system is partially shown in Figure 3 and results are presented in Table 3.

Figure 3: Soaking of Bricks

Table 3: Water Absorption of Brick Block

ID of the brick block	Water absorption, %
A	2.21
B	2.59
C	2.76
D	2.32
E	3.36
F	4.67
G	1.42
H	3.16
I	3.9

Unit Weight

This test is done according to Active Standard ASTM C20.

Table 4: Unit Weight Of Plastic Brick

ID of the brick block	A	B	C	D	E	F	G	H	I
Unit weight, kg/m^3	1640	1869	2128	1750	1942	2098	1926	2010	2130

RESULT

In this study, the results show a clear remark that with the change of the amount of sand, bitumen and plastic, the quality of the brick changes. Bitumen has a strong effect in bonding is seen throughout the result in every test. Strength, water absorption and unit weight change due to increment of bitumen is noteworthy. Test result shows the effectivity of according to their percentage and ratio.

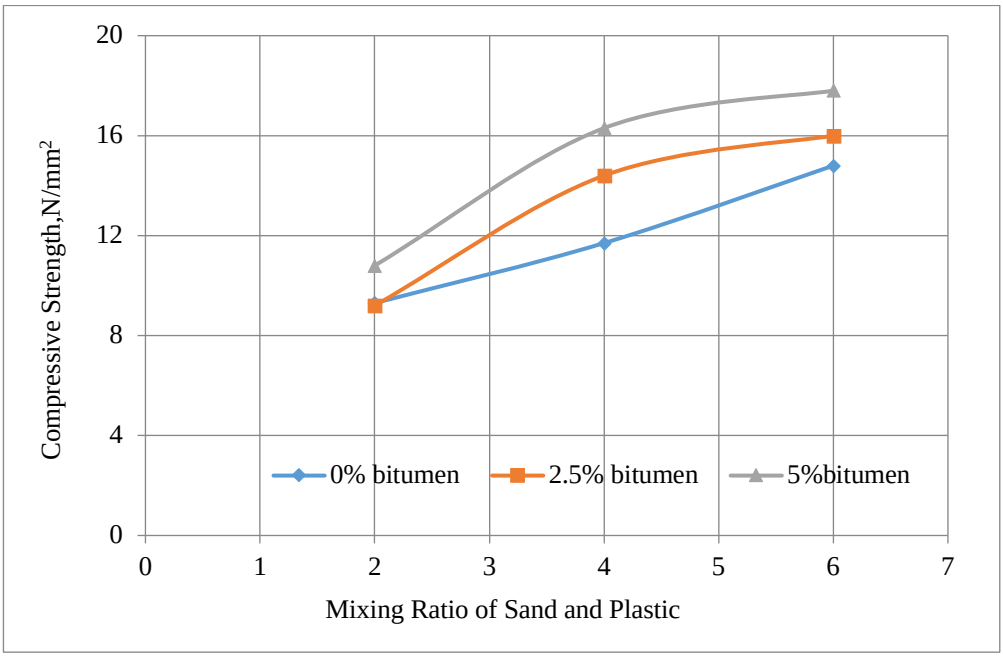

Figure 4 : Comparison of Compressive Strength for Different Bitumen Content

The graph shows the variation of strength changing in brick blocks plastic and sand ratio and again changing for its amount of bitumen. For the first curve for 0%bitumen content the strength goes up as the amount of sand increases. This is valid for 0%, 2.5%, 5% bitumen content.

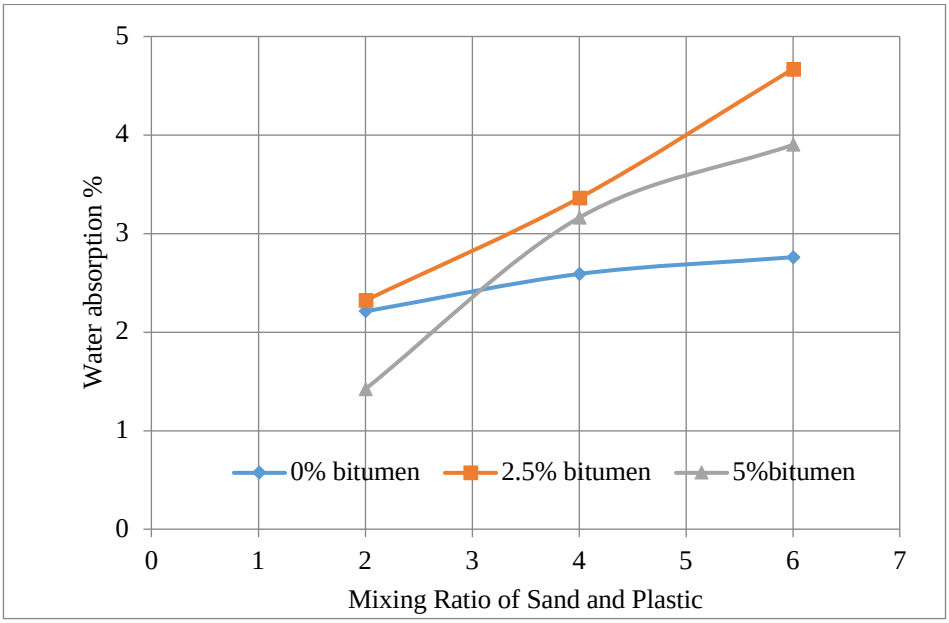

Figure 5: Comparison of Water Absorption for Different Bitumen Content

All the curves for water absorption show similar properties as for compressive strength curve. Increment in the amount of sand leads to more water absorption. Water absorption changes happen abruptly for 5% bitumen content.

These three line show act differently. At the beginning when there is no bitumen, the absorption increases slowly. For 2.5% bitumen content, slope of the line increases. Water absorption is higher for 2.5% is higher than that for no bitumen content. Again the water absorption for 5% bitumen content is lower than that for 2.5% bitumen content. This indicates that 5% bitumen adding will decrease the water absorption rate.

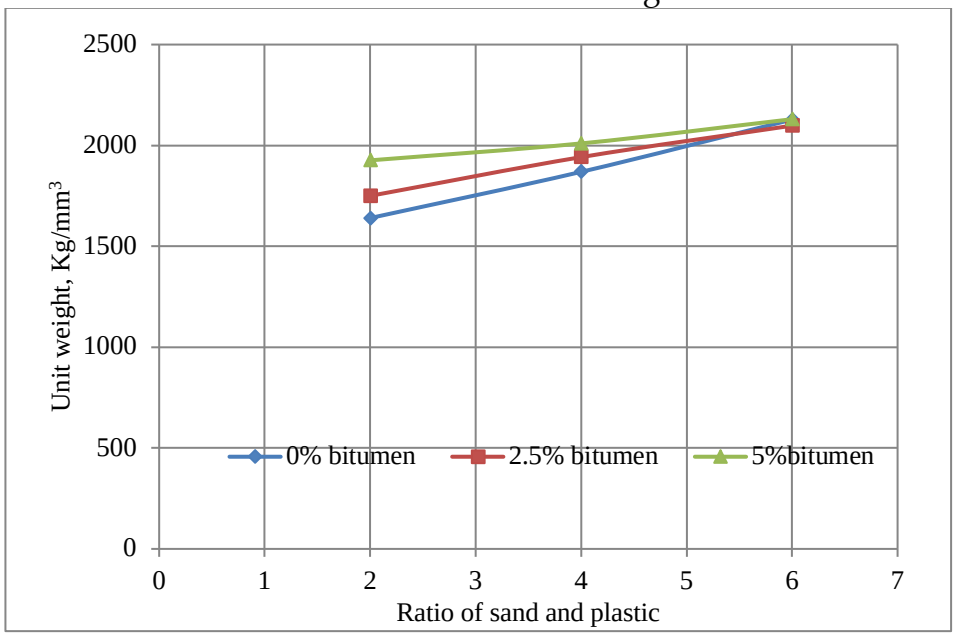

Figure 6: Comparison of Unit Weight for Different Bitumen Content

The change in unit weight caused by adding bitumen is less responsive.

Based on the findings of this study, the following results are summarized.
Bitumen improves the compressive strength of brick block
In this study, compressive strength varies from 9.3 to 18.6 N/mm^2, water absorption varies from 1.42 to 5.84% Unit weight varies from 1640 to 2130 kg/m^3.
According to IS, first class and second class brick's strength are 10.7 & 7N/mm^2 respectively. From the brick type B,C,E,F,G,H,I satisfy the first class brick's and the rest of them are second class brick according to strength. Water absorption of first class brick is less than 15% according to IS, which satisfy all the bricks.

CONCLUSIONS

From the research work bitumen makes a great impact on brick block .this changes are positive to make a brick more capable. Addition of bitumen provides more bonding to the brick. Hence it causes more strength which enables it to carry more load. But with the increase of bitumen it increases the water absorption. As the value of water absorption is low it is almost negligible. Again the unit weight also increases as bitumen is added. Bitumen improves the quality of brick block.

As the weight of the brick is pretty high, this brick can not be used as light weight component of structure. This brick block does not float in water.

The strength of plastic brick containing bitumen is high. As a result it can be used in the field as an alternate to clay brick.it may not be used in countries where temperature is high. But for cold based country this brick will give a better performance. Another disadvantage of plastic brick is, it cannot be used in places where fire protection is mandatory. This brick will not protect the structure from fire, as it will melt down. Firing process can lead to ignition of bitumen in the brick block.

REFERENCES

Arulmalar Ramaraj, Jothilakshmy Nagammal (2014). 30th International Plea Conference 16-18 December 2014, CEPT University, Ahmedabad, India.
Dipankar S, Manish P (2016). A laboratory study involving use of brick aggregate along with plastic modified bitumen in preparation of bituminous concrete for the roads of Tripura" ARPN Journal of Engineering and Applied Sciences 11(1): 570 -570.
Maneeth P D, Pramodh K, Krishor K, Shanmukha S. (2014). Utilisation of waste plastic in manufacturing of plastic soil brick" , journal of IJERT, 3: 529-536.
MoEF. National 3 R Strategy for Waste Management, Ministry of Environment and Forests, Government of the People's Republic of Bangladesh. 2010.
Mojtaba Valinejad S., Azin Shakiba B. (2013). Investigating the Application of Plastic Bottle as a Sustainable Material in the Building Construction. International Journal of Science, Engineering and Technology Research (IJSETR) 2(1): 2278 -7798.
Pratima P, Akash Shah, (2014) Sub stainable development using waste PET bottles as construction element'www. wastebottleconstruction.com.
Puttaraj Mallikarjun H., Shanmukha shettya (2014). Utilization Of Waste Plastic In Manufacturing of Plastic-Soil Bricks, International journal of technology enhancements and emerging engineering research 2(4):

Ramadevi K (2012). Experimental Investigation on the Properties of Concrete With Plastic PET (Bottle) Fibers as Fine Aggregates' International Journal of Emerging Technology and Advanced Engineering 2(6): 1-5.

Shilpi Saxena, Monika Singh (2013) Eco-Architecture: PET Bottle Houses. International Journal of Scientific Engineering and Technology 2(12): 1243-1246.

Suraiya Yasmin, Imranur Rahman, (2017). A review of solid waste management practice in Dhaka city, Bangladesh", International Journal of Environmental Protection and Policy, 5(2): 19-25.

Vikram Pakrashi (2014). Experimental Characterization of Polyethylene Terephthalate 1 (PET) Bottle Eco-Bricks 60: 50-56.

Waste Concern, (2009). Municipal solid waste (MSW) management in Dhaka, Bangladesh. . Waste Data Base of Bangladesh.http://www.wasteconcern.org/documents/waste%20Data%20Base_2009.pdf.

ASSESSMENT OF SEISMIC PERFORMANCE OF REINFORCED CONCRETE HIGH RISE BUILDINGS VIA TIME HISTORY ANALYSIS

Abdulgani ERSAYAN
ersayangani@gmail.com

Mehmet Eren GÜLŞAN
University of Gaziantep, Civil Engineering Department
gulsan@gantep.edu.tr

ABSTRACT: This study aims to investigate the seismic behavior of a typical reinforced concrete high-rise building via time-history analysis. 4 different structural systems are considered in the study to analyze the effect of existence and numbers of shear walls on lateral response of the buildings. Moreover, effects of number of storey and storey heights on the seismic performance of high-rise buildings are investigated. 6 storey number (15, 20, 25, 30, 35, 40) and 3 storey heights (3, 3.5 and 4 m) are selected for the study. All analyses are carried out by expert structural analysis software, named as SAP2000. The ground motion which was recorded during İzmit earthquake (1999) is used as time history function for the analyses. Totally, 144 analyses are performed within the study. Analysis results show that high-rise buildings without shear walls are not safe because of exceeding drift ratio limits even they contain columns with large cross sections. As expected, increase of shear walls decreases the maximum roof displacements of the buildings. However, increase of shear wall after a certain limit does not make a noticeable contribution even though it increases the construction cost significantly. Furthermore, analysis results show that periods of the buildings having more shear wall are lower. Increase in the number of storey and storey heights increases the period for the same structural system.

Key words: High rise buildings, shear walls, seismic analysis, drift ratio, period.

INTRODUCTION

The need for construction of high rise buildings has increased due to large increase in population and limitations regarding horizontal expansion of cities. Therefore, behavior of these structures against earthquake essentially requires investigation. Recent researches have shown that earthquakes with high frequency have remarkable effects on seismic response of buildings. In terms of structural elements, tall structures require appropriate structural solutions in order to provide adequate stability and rigidity. As a matter of fact, although effects of dead and live loads are main factors for design of short buildings, the focus of structural engineers is on controlling horizontal displacement as the height of the building increases. The shear wall is one of the most effective solutions to decrease the horizontal displacement. Several experimental studies have proven that properly designed shear walls show acceptable seismic performance against earthquake effects. (Thomsen, Thomsen & Wallace, 2004 and Dazio, Beyer & Bachman 2009). In addition to experimental studies, numerous

analytical studies have been carried out for shear walls by several researchers. (Lee & Kim, 2013; Sanchez-Alejandre & Alcocer, 2010 and Alarcon, Hube & Liera, 2014).

Due to the developments in the construction sector, the construction of high rise buildings has also increased in our country rapidly. Researches made in recent years have shown that these types of buildings have different behaviors as compared to low-rise buildings regarding response to horizontal loads.

The analysis of buildings under earthquake effect and the design of stable structural structure is one of the most important subjects of civil engineering. The devastating earthquakes that have taken place in recent years have led to a better understanding of this issue. Earthquake-resistant structural analysis and design is provided by earthquake regulations developed by each country in accordance with its local conditions. These regulations are continuously renewed by taking developments in science and technology into consideration. For instance, the Turkish Earthquake Regulation (2018) has been rearranged and the period of natural vibration, which enables us to observe the effect of the earthquake as more detailed, is of great importance in this regulation.

For high-rise buildings, it is important that the building should have sufficient bending stiffness around the vertical axis in addition to the flexural rigidity in two directions. In order to obtain sufficient stiffness, three major terms should be considered. Existence of bending stiffness in two directions in addition to torsional stiffness around the vertical axis is significant for high rise buildings. In a suitable stiffness arrangement, the first two vibration periods are flexural vibrations and third one is torsional vibration. Moreover, torsional effects can make contribution to flexural vibrations and flexural effects can make contribution to torsional vibrations in non-symmetrical structures. A significant amount of the earthquake and wind forces is resisted by shear walls in addition to columns in high rise buildings (Celep, 2017). Therefore, it is important to determine the amount and place of shear walls in the structural system during design of a high rise building.

The aim of this study is to investigate the effect of the several parameters including structural system type, storey number and storey height on seismic performance of reinforced concrete high rise buildings via time history analysis. 4 different structural system types were considered to research the effect of existence and location of shear wall on the seismic behavior. Moreover, 6 different number of storey (15, 20, 25, 30, 35, 40) and 3 different storey heights (3, 3.5 and 4 m) were considered for each structural system in the investigation. The analyses of the study are performed by an expert structural analysis software, named as SAP2000.

METHODS

2. Time History Analysis

Time history analysis is a step-by-step analysis of the dynamic response of a structure to a specified loading that may vary with time. Time history analysis is used to determine the seismic response of a structure under dynamic loading of a representative earthquake (Wilkinson and Hiley, 2006). Time history analysis provides for linear or nonlinear evaluation of dynamic structural response under loading which may vary according to the specified time functions. For time history analysis the equation of motion, which is specified in Eq. 1, is solved in the time (/frequency) domain by the use of either modal or direct-integration methods.

$$M\frac{d^2U(t)}{dt}+C\frac{dU(t)}{dt}+KU(t)=P(t)$$

Equation 1.Time History Formula

In this equation, *M*, *C*, *K*, *U* and *P* represent mass of the structure, damping coefficient, structure stiffness, nodal displacement and total load, respectively. Moreover *t* is time for the duration of earthquake.

Although response spectrum function and statically equivalent lateral load methods, which are other techniques for the evaluation of seismic performance, are effective for earthquake resistant structural design, time history analysis is better technique for the seismic analysis of structures. Since, structures respond to earthquake effects dynamically and dynamic response of structures can be obtained via time history analysis.

2.1. Earthquake Records

Because the Marmara earthquake is the largest and **longest peak acceleration magnitude** earthquake in Turkey's earthquake history; the Marmara earthquake has been chosen to be used in nonlinear dynamic analysis in this study. Station id and other records of Izmit Earthquake was recorded by Kocaeli Gebze Tubitak Marmara Araştırma Merkezi and these datas obtained from Earthquake Research Department General Directorate of Disaster Affairs . The earthquake stationis 4106 and earthquake depth is 15.9 km.

Table 1. Earthquake Data

Izmit Earthquake				
Eartquake Date	Center of Earthquake	**Magnitude**	**Records Time(s)**	Peak Acceleration (cm/s^2)
17/09/1999	**İzmit/Turkey**	**7.4**	**50**	264

Below are graphs of acceleration times in the x and y directions of Marmara earthquake taken from the Kandilli Observatory. Accelerations of x and y direction are shown in Fig 1.

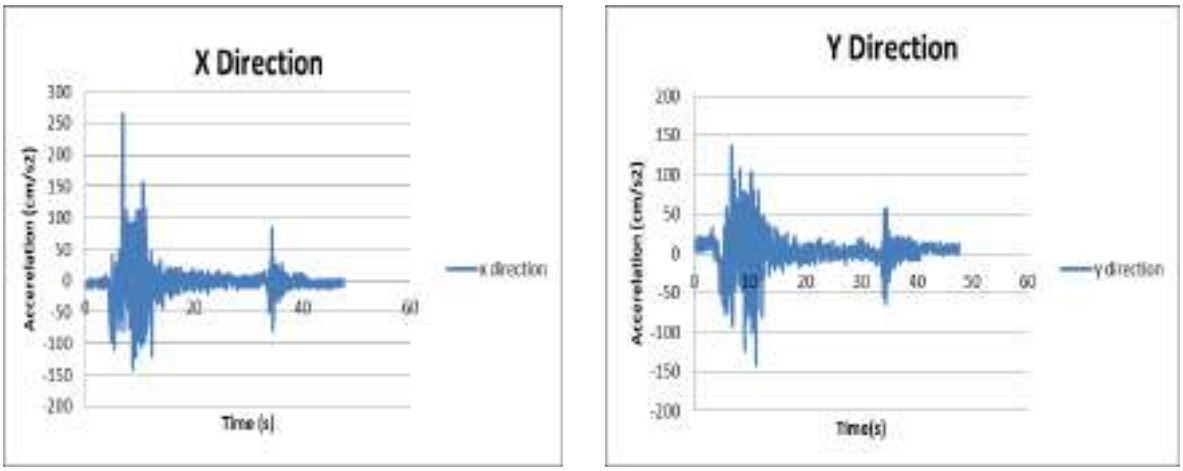

Figure 1. X and Y Direction Earthquake Acceleration

2.2 Description of the Structural Systems

A typical reinforced concrete office building, whose plan dimensions are 48 m x 48 m, was considered within the study. The building has totally 8 spans in each direction and length of each span is 6 m. It is assumed that the foundation of the building is rigid enough so that the building is fix supported on the ground. 4 different structural system was considered for time history analyses. Plan views of all of the systems are shown in Fig. 2. The first system only consists of beams and columns. The second system has tubular shaped shear wall in the center of the structure in addition to beams and columns. The third system has shear walls both in the center and along the most outer side of the structure. Lastly, the fourth system is very similar to the third system, except the forth one has also shear wall between the most outer side and center of the structure. As can be noted from Fig. 2 that the least rigid system is the first one and the most rigid system is the fourth one.

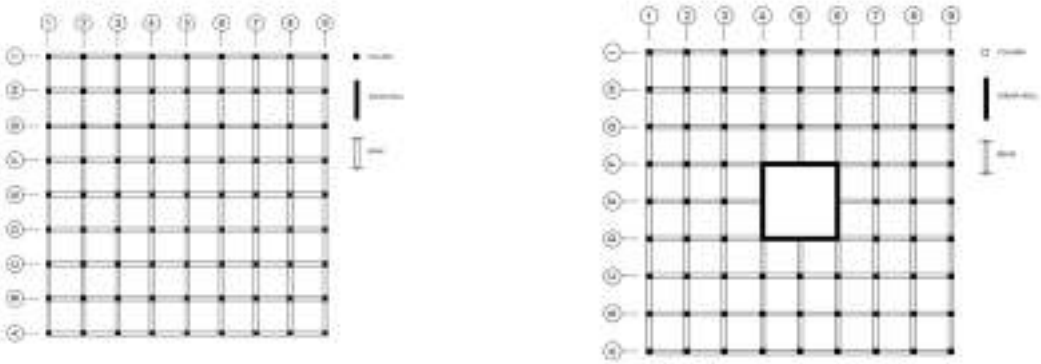

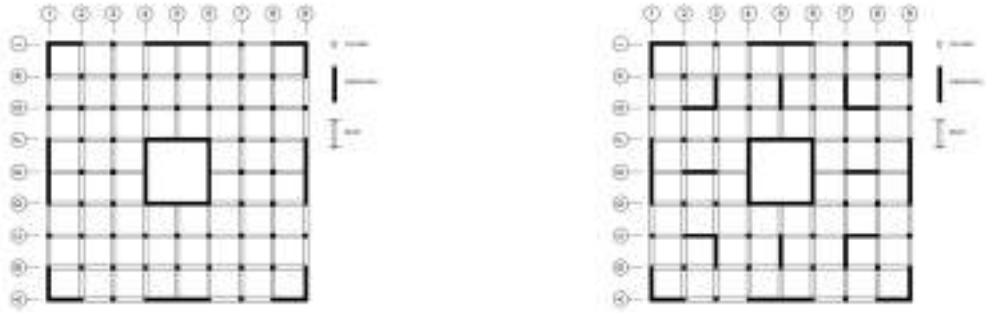

Figure 2. Type of Frame Systems

Width and height of all of the beams are 70 cm and 90 cm, respectively. All columns in structures have square cross-sections and their dimensions are 90 cm x 90 cm. Since the structure is high rise building, the slab thickness was selected as 20 cm. Plan dimensions of shear wall in the center are 5 m x 0.7 m and the dimensions of other shear walls are 6.7 m x 0.7 m. Concrete and steel reinforcement classes were selected as C30 and S420, respectively. Diameter of longitudinal and shear reinforcements was selected as 20 mm and 12 mm, respectively. Reinforcement configuration of columns and beams was arranged by taking regulations of Turkish structural design code (TS500) into consideration.

In this study, total 144 analyses were carried out by the consideration of 4 structural forms, 3 storey heights, 6 numbers of storey and 2 directions (x and y directions). All analyses were made via SAP2000, which is the one of the most effective structural analysis software. All information regarding with structures which were analyzed are given in Table 3.

Table 2. Information Regarding the Considered Structure

Frame Type	Height of Storeys (m)	Numbers of Storeys
Type 1	3m, 3.5m, 4m	15,20, 25, 30, 35, 40
Type 2	3m, 3.5m, 4m	15,20, 25, 30, 35, 40
Type 3	3m, 3.5m, 4m	15,20, 25, 30, 35, 40
Type 4	3m, 3.5m, 4m	15,20, 25, 30, 35, 40

RESULTS AND FINDINGS

Since it was found that the ground motion acting in x direction had much more effect on the structures numerically and general findings for the ground motion acting in y direction was found to be similar to the findings of the motion in x direction, the results are given for the ground motion acting in x direction in the following sections.

4.1 Results According to Storey Heights

4.1.1 Period

Change of periods according to different number of storey is shown in Fig 3. for different storey heights. It can be noted from the figure that as the numbers of storey increase, the period of the corresponding structure also increases. Moreover, as the

storey height increases, the period increases for the same structures (same type and same story number). Therefore, the highest periods are observed in all structures whose storey heights are 4 m.

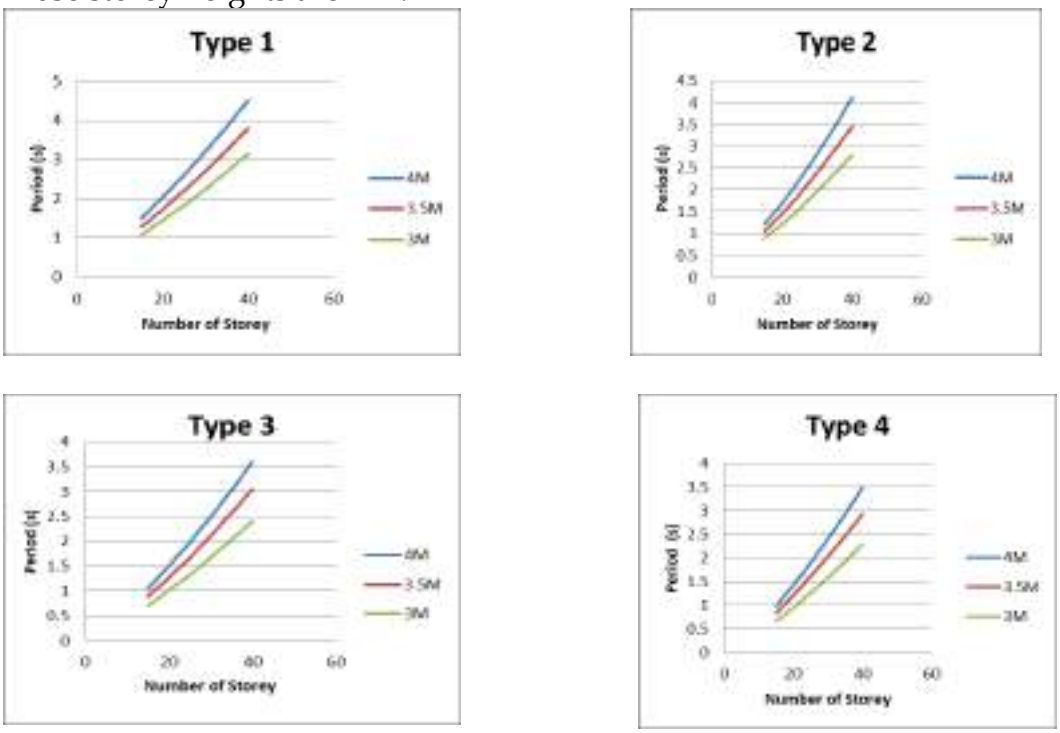

Figure 3. Period Results for Different Types of Frame

According to the results, it can be said that as the storey height of the structure increases, the rigidity of it decreases and correspondingly, the eartquake force decreases. However, in addition to earthquake forces, maximum roof displacement and drift ratio should be taken into consideration in order to make a comprehensive sesismic evaluation of the structures.

4.1.2 Maximum Roof Displacement

Maximum roof displacement versus numbers of storey graphs are shown in Fig 4. It can be noted from the figure that higher storey heights increse the maximum displacement. It is noticeable to note that the difference between the maximum displacements of the structures having storey heights of 3 m and 3.5- 4 m is larger in high storey numbers. This means that the storey height of 3m is safer for the high-rise constructions whose storey number is high regarding maximum roof displacement. Moreover, as the amount of shear wall increases, higher numbers of storeys can be selected for the construction of higher storey heigts. It can be concluded that for high rise buildings whose storey number is low (for instance 15-20), there is no much more differences between maximum displacement results of 3 m and 3.5-4 m storey heights. Therefore, higher storey numbers can be preferred for these types of high-rise buildings.

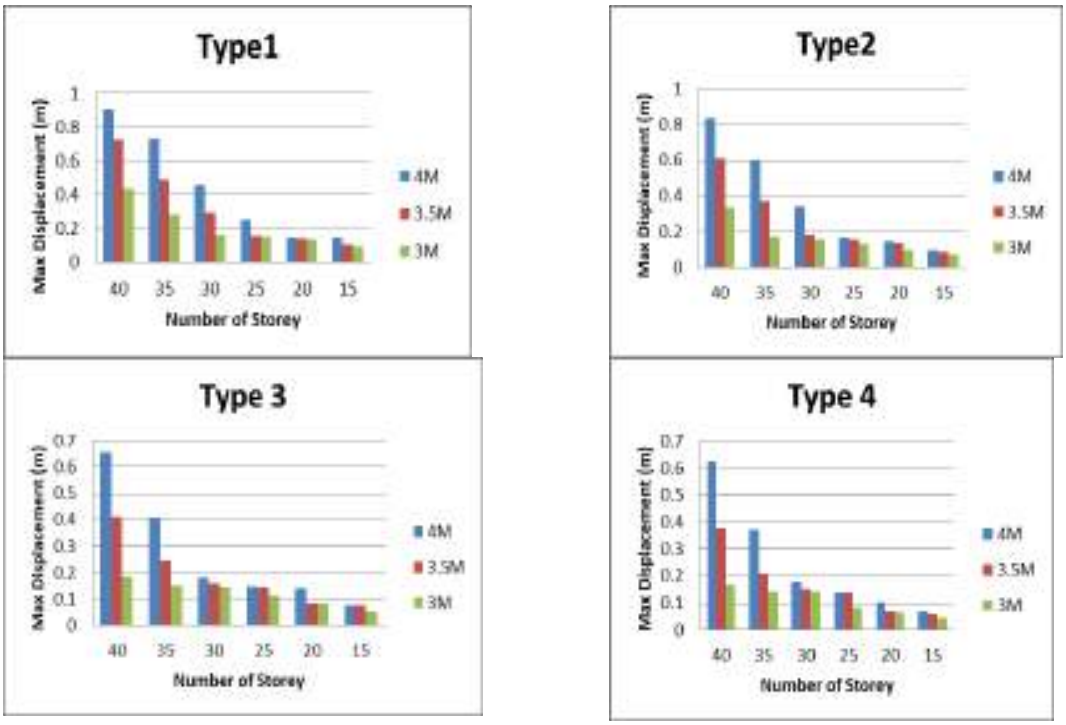

Figure 4. Maximum Displacement Results in Terms of Different Types of Frame for Different Storey Heights

4.1.3 Drift Ratio

Change of drift ratio values of all structures according to storey heights are shown in Fig 5. These graphs represent drift ratio values for the structures whose number of storey is 40. As expected, highest drift ratios are obtained in the structures having 4 m storey heights. According to the results, it can be said that the structures which consist of only beams and columns are not suitable for high-rise structures even large cross-section are preferred for the columns. Since, difference between drift ratio values in lower stroreys is very large for this type of structures.

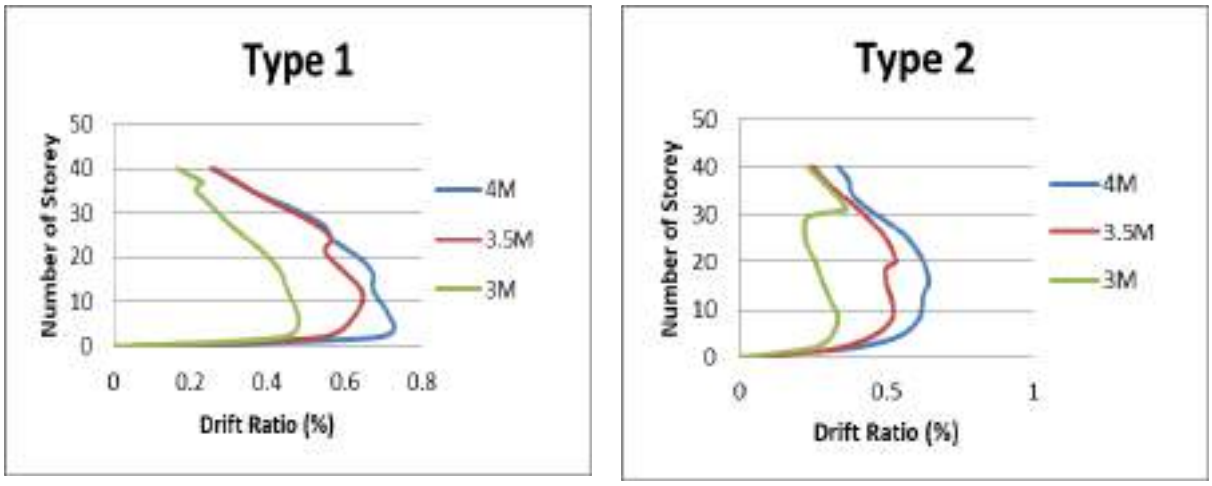

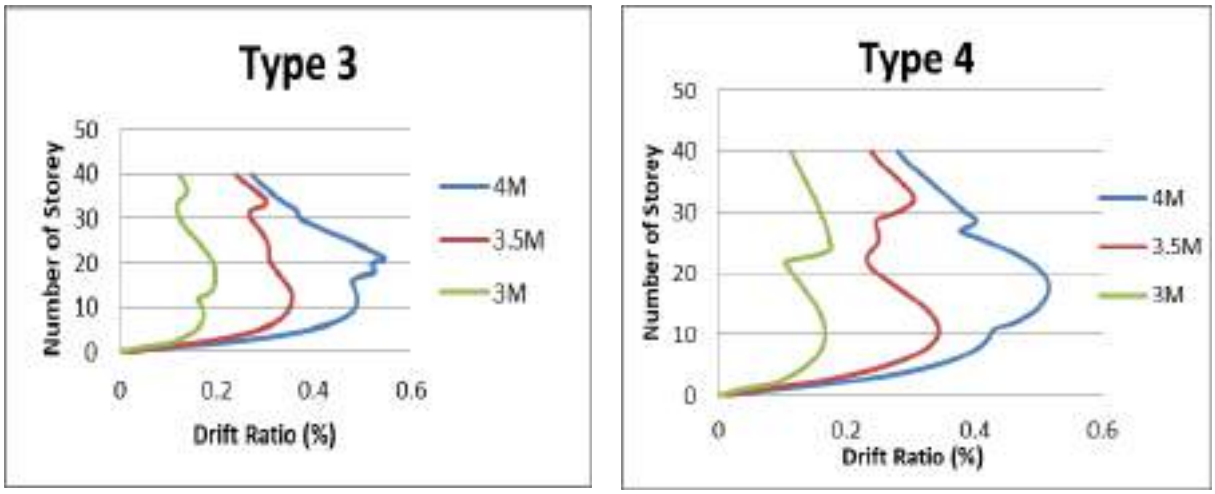

Figure 5. Drift Ratio Results for 40 Storey Structures

Provided that the shear wall is used sufficiently, the selection of 3 m and 3.5 m storey heights is suitable regarding drift ratio results. However, columns in the lower and middle floors should be stronger as compared to other columns for the buildings having much more numbers of storey.

4.2 Results According to Numbers of Storey

4.2.1 Results in Terms of Period

Period results according to number of storeys for each construction type are given in Fig 6. As can be observed from the figure that change of period values according to number of storey and storey heights is very similar. This can be explained with the fact that period is mostly related with total mass and rigidity of a structure.

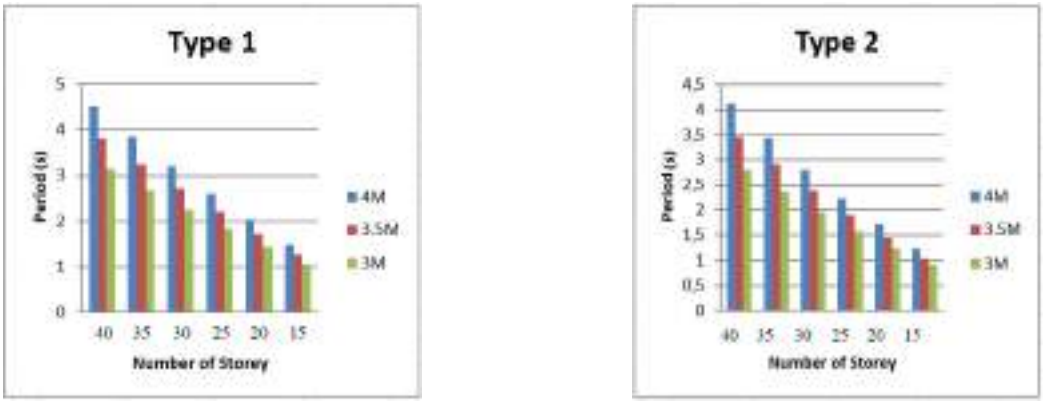

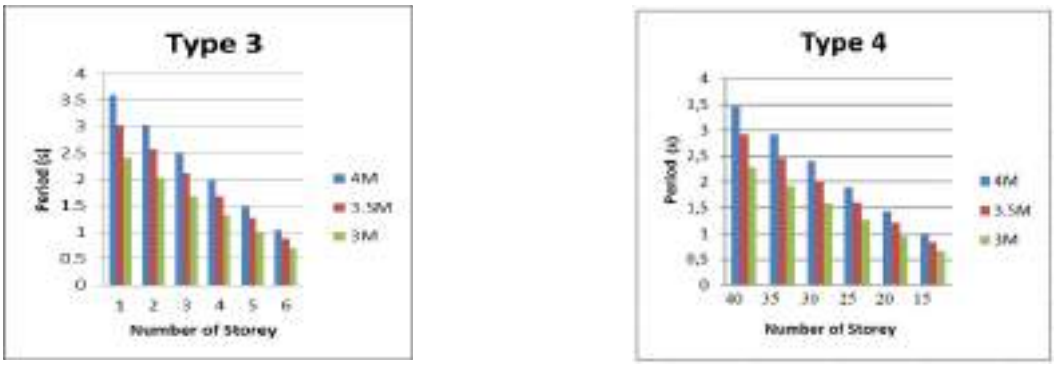

Figure 6. Period Results in Terms of Diffrent Types of Frame for Different Storey Numbers

4.2.2 Results in Terms of Maximum Roof Displacement

Maximum displacements of structures according to nember of storey are shown in Fig 7. It is worth to note that the maximum displacement increases abruptly after storey numbers of 30 for all type of structures. This increase is much more for storey heights of 4m. Therefore, it can be concluded that the designer should be very careful by taking storey height into consideration after certain numbers of storey.

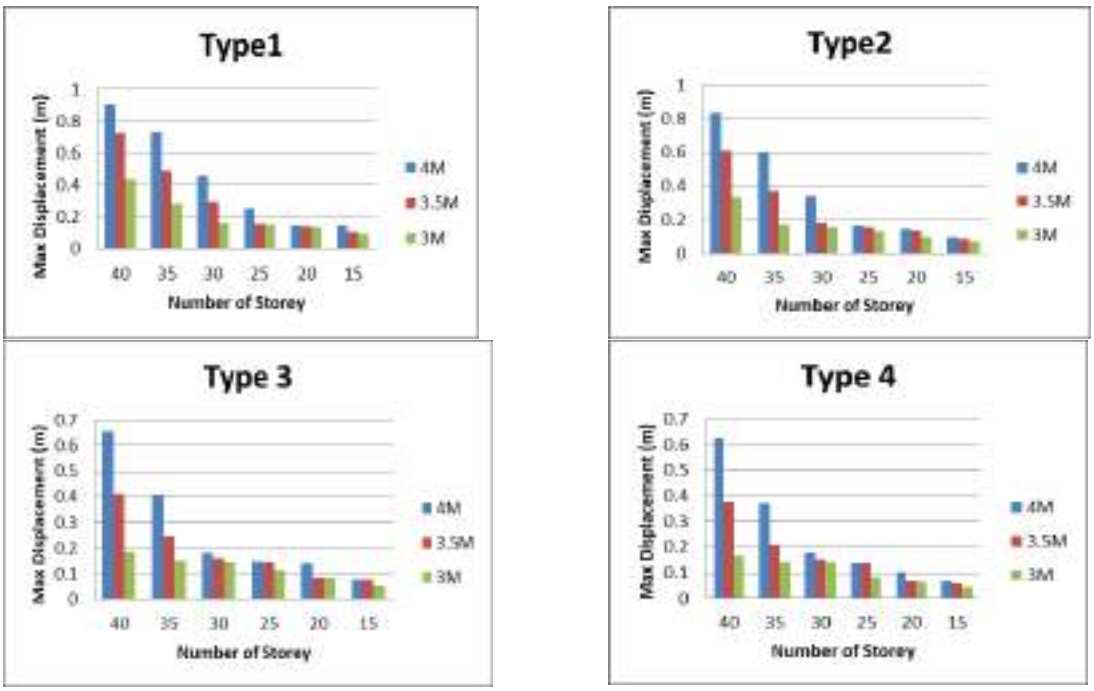

Figure 7. Max Displacement Results in Terms of Different Types of Frame for Different Storey Numbers

4.2.3 Results in Terms of Drift Ratio

Drift ratio values according to number of storey are given in Fig 8. for the structure systems having 4 m storey heights. These results also prove that the structures consisting of only beams and columns (Type 1) are not suitable for very high structures. Moreover, when the drift ratio values are observed for type 3 and 4, it can be observed that change of drift ratios of 35 and 40 numbers of storey are much more different from others. This situation also proves that rigidity and dominant mode of the structures change abruptly after 30 number of storey.

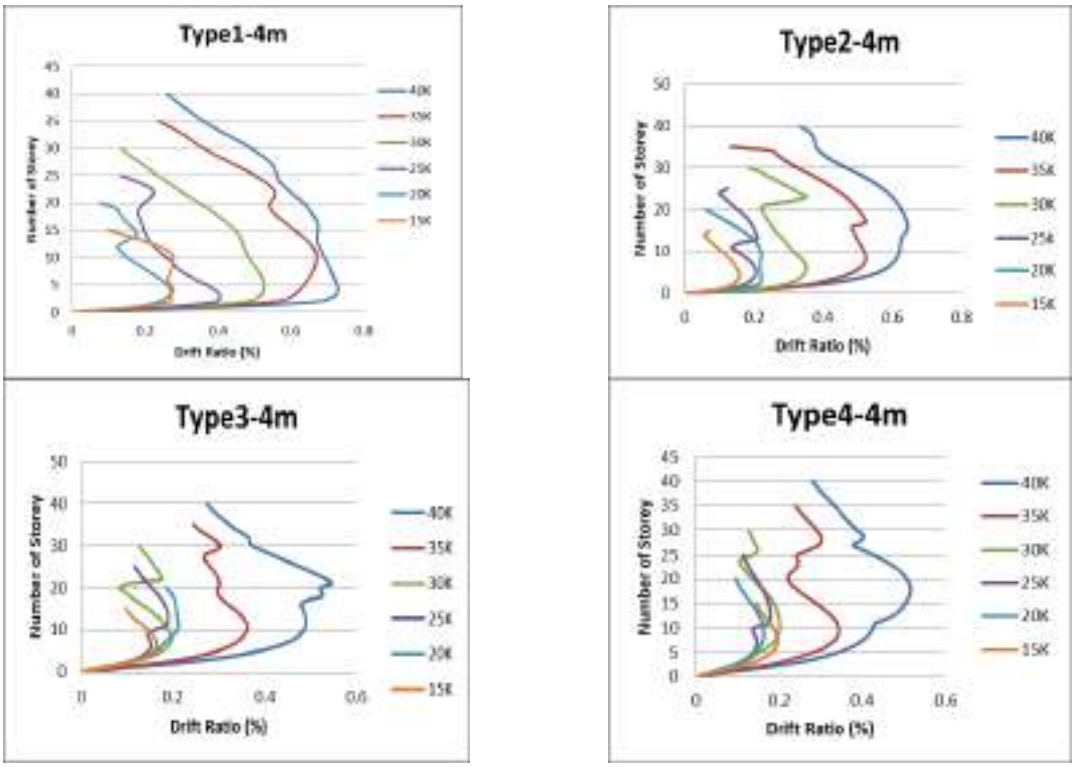

Figure 8. Drift Ratio Results in Terms of 4m Storey Height for Different Storey Numbers

4.3 Results as The Frame Type Changes

4.3.1 Results in Terms of Period

Resulting period values versus numbers of storey according to structural system types are given in Fig 9. for different storey height values. According to the figure it can be concluded that there is no much more difference between type 3 and type 4 regarding periods. Therefore, it can be said that their seismic performances are very similar to each other. However, construction cost of type 4 is higher that the cost of type 3. Therefore, there is no need to increase the amount of shear wall after a certain limit. Moreover, a well-designed outer and central shear walls are sufficient to achieve earthquake resistance.

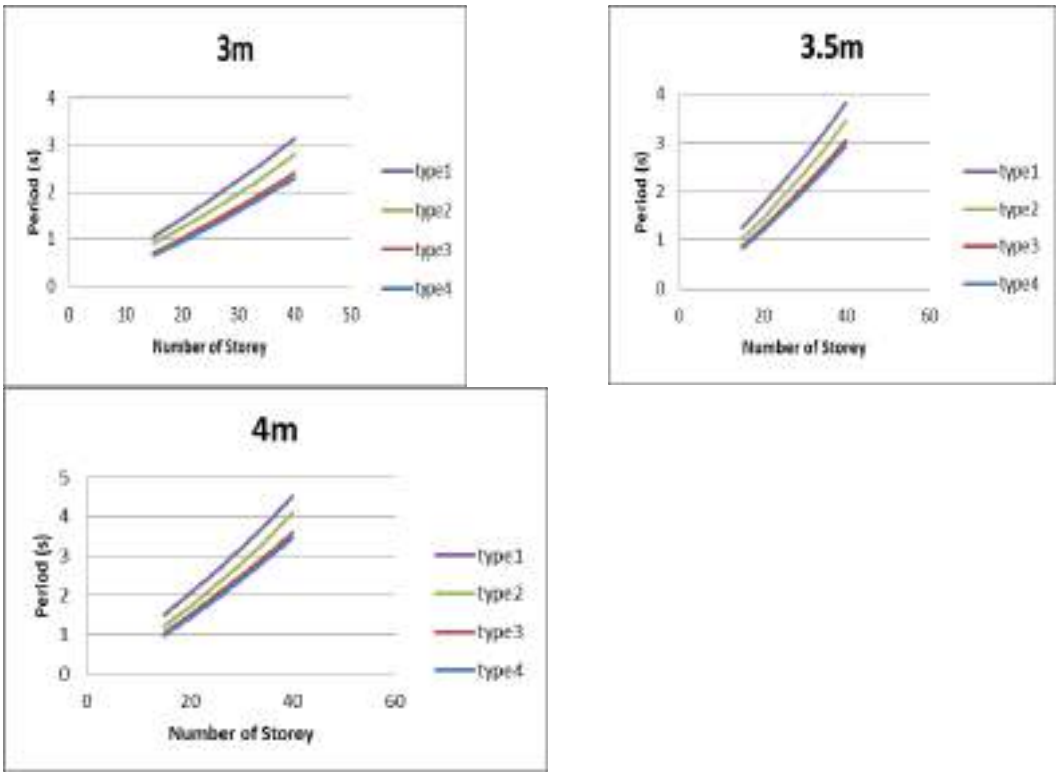

Figure 9. Period Results in Terms of Different Storey Heights for Different Types of Frame

4.3.2 Results in Terms of Maximum Roof Displacement

Maximum displacements of structures with respect to numbers of storey and structure types are shown in Fig 10. It can be concluded from the figure that differences between maximum displacement values become much more apparent for higher numbers of storey. For maximum displacements of type 3 and 4, higher storey heights change the maximum displacements abruptly. Therefore it can be concluded that 4 m storey height should not be preferred for high number of storeys (for instance, numbers greater than 30 for this study) even there are shear walls in the structural system.

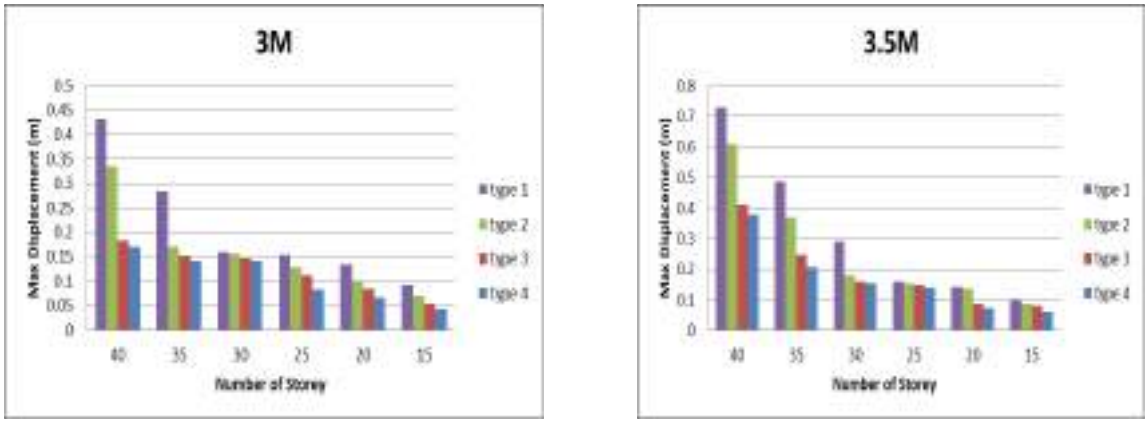

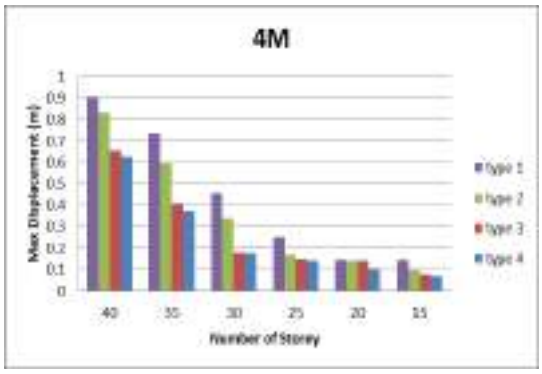

Figure 10. Maximum Displacement in Terms of Different Storey Heights for Different Types of Frame

4.3.3 Results in Terms of Drift Ratio

Drift ratio values of structures whose number of storey is 40 are shown in Fig 11. according to structural system type and storey heights. It can be observed from the figure that drift ratio values of type 3 and type 4 is very similar for all considered storey heights. Moreover, it can be concluded also that only central shear wall is not sufficient in order to achieve seismic resistance for the structures whose storey number is very high.

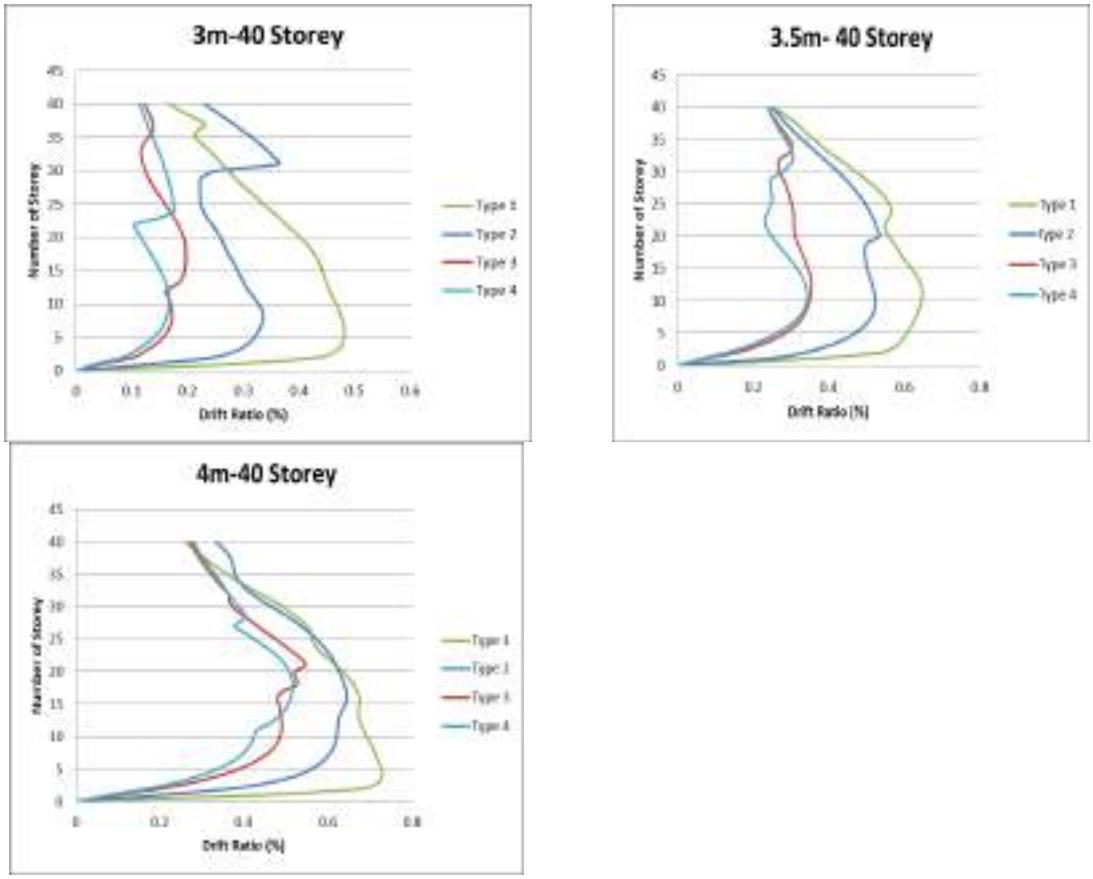

Figure 11. Drift Ratio Results in Terms of 40m Storey Number for Different Types of Frame

CONCLUSION

In this study, seismic performance of typical high-rise reinforced concrete office buildings was investigated via time history analysis by the consideration of different structural systems, numbers of storey and storey heights. The seismic record of İzmit earthquake (1999) was used for the analysis. All analyses were carried out by SAP2000 software.

Analysis results show that structures consisting of only beams and columns are not sufficient for the structures whose number of storey is very high. Especially, after 15 numbers of storey, these types of structures can not be preferred as structural system. The structural system containing shear walls in the center of the building can be preferred for higher numbers of storey, for instance 20-25 storey, provided that required design measures are taken. However, it is not sufficient for more numbers of storey when drift ratio, period and maximum roof displacement values are assessed.

It is concluded according to analysis results that 4 m storey height decreases the seismic performance of high-rise buildings even there are shear walls in the structural system. However, 3.5 m storey height can be used until 35 numbers of storey provided that sufficient amount of shear walls are used in the structural system.

Another important conclusion is that after a certain limit, there is no need to increase amount of shear wall. Moreover, existence of shear wall between central shear walls and most outer shear wall does not affect the seismic performance of the structure significantly. Moreover, shear walls generally increase the total construction cost of the structure. Therefore, it can be said that well-designed shear walls are sufficient in the outer sides and centers of high-rise buildings to achieve the required seismic performance.

RECOMMENDATIONS

This study can be extended by the consideration of other devastating earthquake records. A detailed cost analysis can be carried out to propose the optimized structural system. The similar study also can implemented by the consideration of higher numbers of storey, higher storey heights and different structural systems.

REFERENCES

Alarcon, C., Hube, M.A. & Liera, J. c. (2014). Engineering Structures. *Effect of axial loads in the seismic behavior of reinforced concrete walls with unconfined wall boundaries, 73*, 13-23.

Celep, Z. (2017). TMMOB İnşaat Mühendisleri Odası Bursa Şubesi Yayın Organı. *Yüksek Binaların Yapısal Tasarımı,70*,8-12

Dazio, A., Beyer, K., Bachman, H. (2009). Engineering Structures. *Quasi-static Cyclic Tests and Plastic Hinge Analysis of RC structural walls*, *31*, 1556-1571.

Lee, J. and Kim, J. (2013). Magazine of Concrete Research. *Seismic performance evaluation of staggered wall structures using Fema P695 procedure*, *65*, 1023-1033.

Sanchez-Alejandre, A., & Alcocer, S.M. (2010). Engineering Structures. *Shear strength of squat reinforced concrete walls subjected to earthquake loading-trends and models*, *32*, 2466-2476.

Thomsen, I. V., J. H., and Wallace, W.J. (2004). Journal of structural Engineering. *Displacement-Based Design of Slender Reinforced Concrete Structural WallsExperimental Verification*, *130*, 618-630.

PRODUCTION OF SUSTAINABLE ENERGY VIA INTEGRATION OF DIRECT BOROHYDRIDE

Afsin Y. CETINKAYA,
Department of Environmental Protection Technologies, Technical Sciences Vocational School, Aksaray University, Aksaray, Turkey
afsincetinkaya@gmail.com

ABSTRACT: Fuel cells offer a promising alternative to incumbent electrical power generation technologies (primarily based on fossil fuels), for medium-scale applications, such as remote or backup power, as well as small-scale applications, such as portable consumer electronics. Widespread adoption of the direct hydrogen-oxygen fuel cell, the most highly-developed fuel cell, is hindered by a number of problems related to the sourcing, storage and safe handling of hydrogen (particularly for mobile applications). A direct borohydride fuel cell (DBHFC) is a device that converts chemical energy stored in a borohydride ion (BH_4^-) and an oxidant directly into electricity by redox processes. Usually, a DBHFC employs an alkaline solution of sodium borohydride ($NaBH_4$) as fuel and oxygen or hydrogen peroxide as oxidant (Martins et al., 2017). DBHFC yields a high performance as a power source, there are several problems that need to be solved, such as hydrogen evolution and $NaBO_2$ accumulation at tha anode during operation. At the anode, the complete oxidation of borohydride ions to release $8e^-$ takes place, in theory. Key factor for the practical application of DBHFC is to prepare anode electrocatalysts that have high selectivity and high catalytic activity for improving the kinetic parameters of BH_4^- oxidation and inhibiting hydrolysis of BH_4^-. The precise mechanism of borohydride oxidation is still subject to speculation and, therefore, awaits further clarification (Santos et al., 2011). Two-dimensional (2D) nanomaterials have distinc properties owing to their extremely small size in one dimension. The common feature of 2d nanomaterials is that they usually contain only one or few atomic layers. 2D molybdenum disulfide (MoS_2) has attracted considerable amount of interest in recent years because of its unique properties such as direct bangap, high electron mobility, stable chemical properties and its graphene-like honeycomb lattice.

Key words: Borohyride, sustaianable energy, Fuel Cell

REFERENCES

Martins, J. I., Nunes, M. C., Koch, R., Martins, L., & Bazzaoui, M. (2007). Electrochemical oxidation of borohydride on platinum electrodes: The influence of thiourea in direct fuel cells. *Electrochimica acta*, *52*(23), 6443-6449. doi: 10.1016/j.electacta.2007.04.066

Santos, D. M. F., & Sequeira, C. A. C. (2011). Sodium borohydride as a fuel for the future. *Renewable and Sustainable Energy Reviews*, *15*(8), 3980-4001. doi: 10.1016/j.rser.2011.07.018.

EXPERIMENTALL STUDY OF THE EFFECT OF CONTRACTION RATIO ON BACKWATER BY USING BRIDGE PIER AS FLOW OBSTRUCTION

Assist. Prof. Mohammed S. Shamkhi
Wasit University
msewan@uowasit.edu.iq

MS.c. Student Mohammed Salim
Wasit University
muhammeds227@uowasit.edu.iq

ABSTRACT: The construction of bridge in any water course required to install the pier in the flow path. So, the study of backwater around bridge piers is very important for safe design of piers and other hydraulic structures. Backwater effected by different parameter and the contraction ratio is one of the important parameter. So, in this study the effect of contraction ratio on backwater has been studied by using laboratory flume having 12 m length and 0.5 m for each height and width. Different contractions ratio with 0.91, 0.82 and 0.73 have been used with single, double and triple pier has 4.5 cm thickness. Also, in this paper the subcritical flow in the flume was adopted for each run by using five different value of discharge range from 0.0075 m3/s to 0.035 m3/s. Generally, this research illustrated that the backwater rise upstream bridge piers is directly proportional with Froude number and contraction ratio. It was found that when using 0.91, 0.82 and 0.73 contraction ratio lead to increase the percentage ratio of backwater upstream bridge pier about 6.5% ,14% and 23.3% respectively. Also, in this paper the using of Artificial Neural network (ANN) to forecast the backwater rise give agreement result with correlation coefficient R equal to 0.998 and Mean Square Error (MSE) equal to $3.9*10^{-4}$.

Keywords: Backwater, ANN, Contraction ratio, Bridge pier, Froude number, Yarnell

INTRODUCTION

The construction of bridges over watercourses is very necessary to provide communication links between population areas **[1]**. Therefore it is important to study any cause may negatively impact on the bridge stability. Backwater represent a real problem caused by pier which is obstruct the flow because of it is location in the waterway and lead to increase the water level upstream bridge**[2]**. Also, in 1987, floods have been occurred in New England and New York were destroyed and damaged about 17 bridges **[3]**. Also, In a study of the cause of failure of 143 bridges worldwide, it was found that 70 failed due to flood events **[4]**. Therefore, the backwater upstream bridges considered the most important problem effect on hydraulic structure **[5]**. The amount of backwater caused by piers depends mainly on the Froude number and the contraction ratio. The increase and decrease in the contraction ratio effected by the number of piers in the water course. So, in this study the effect of three different contraction ratio on backwater will be presented as shown in Figure1. As well as development of ANN model to predict the backwater taking in consideration the effect of contraction ratio.

The objective of this study was to investigate the effect of contraction ratio on backwater curve using three models of bridge piers. Also, in this paper the performance of ANN for forecasting backwater rise due to bridge pier was studied.

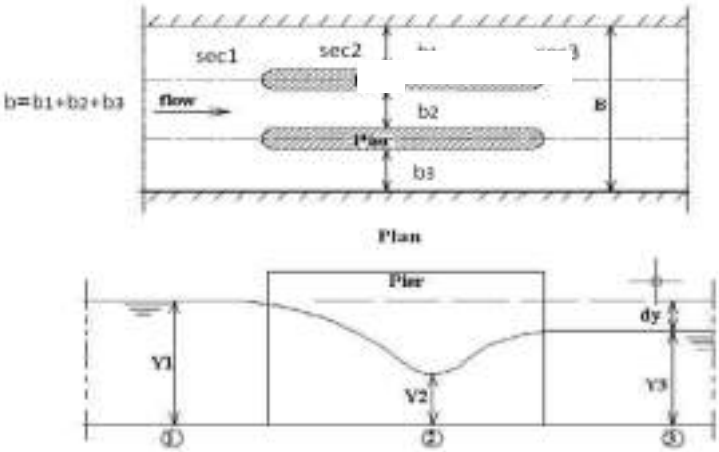

Figure1. Definition Sketch Of Simple Bridge Constriction

LETERATURE REVIEW

Contraction ratio is one of the most important parameter which has direct effect on the backwater rise, where many researchers have been studied the effect of contraction ratio on backwater curve. **Lane, 1920 [6]** carried out at Dayton, Ohio, a multi experiments on the flow of water through contractions in an open channel 6.8 feet(2.07m) wide. His tests were conduct with the following contractions: A 1-ft opening with rounded edges; a 1 feet (0.305) m and a 2 feet (0.61m) opening each with sharp edge contractions. These situation caused about 70.5 and 85.3 percent contraction. Lane calculated coefficients for use in the **D'Aubuisson and Weisbach[7]** formulas and pointed out certain conditions that somewhat limit the use of D'Aubuisson's formula . As stated by **Henderson, 1966[8]** ,the study of backwater rise upstream bridges was started by **Yarnel,1934 [9]**, in1934. He carried out several test to explain the effect of contraction ratio on backwater curve. He used long channel with 312 feet long (95.1 m), 10 feet (3.05m) wide. He used four series of tests, in the first series he used single pier with 14 inches(0.36m), in the second series he used double pier with same pier thickness in the first test, in the third and four series he used single pier with 3.5 feet (1.07m) and 5 feet(1.52m) thickness respectively. Consequently, four percents of contraction ratio, namely, 11.7, 23.3, 35, and 50. He found that the contraction ratio has a direct effect on backwater curve and drop in water level. Also, he found that the decrease in contraction ratio lead to increase in energy loses and decrease the flow area. Yarnell drive the following equation as a result of his work:

$$\frac{dy}{y_n} = k(k + 5Fr_n^2 - 0.6) * (\propto + 15 \propto^4)Fr_n^2 \qquad 1$$

dy backwater height;
yn normal flow depth
Fr_n normal Froude number
$\propto$ ratio of pier thickness to the distance between piers axis.
k pier-shape factor . 0.9 used for this study (semicircular pier nose)

Chow,1959[10] stated that the effect of backwater may extent to far distance of bridge pier in case of subcritical flow in the channel , while in case of supercritical flow the effect of backwater extent to short distance i.e. close to the bridge pier. Also, the backwater rise upstream bridges was studied by **Soliman et.et.1989 [11]**. **Henderson, 1966 [8]** employed the contraction ratio to distinguish between class A (unchoked flow or also known as subcritical) or class B (choked flow or also known as supercritical). He drive his formula by using energy and continuity equation as follow:
According to Figure 2.1, the energy equation between sec 2 and 3 can be written as:

$$r(y_2 + \frac{V_2{}^2}{2g}) = (y_3 + \frac{V_3{}^2}{2g}) \qquad 2$$

in which
y_2 depth of flow at section 2 (minimum flow depth)
y_3 downstream flow depth (section 3) in
V_2 flow velocity at section 2(between piers)
V_3 flow velocity at downstream (section 3)
r the residual ratio of energy between sections 2 and 3 range between 0.9 to1
Followed by continuity equation between section 2 and section 3 based on Figure1:
$Q_2 = Q_3$

$$y_2 b\, V_2 = y_3\, B\, V_3 \qquad 3$$

b the distance between pier axis
B the channel width
so contraction ratio;

$$\mathrm{Cr} = \frac{b}{B} \qquad 4$$

By rearranging the Equations 2,3 and 4, results the following equation

$$\mathrm{Cr}^2 = \frac{r^3 \mathrm{Fr}_3{}^2 (2+\mathrm{Fr}_2{}^2)^3}{\mathrm{Fr}_2{}^2 (2+\mathrm{Fr}_3{}^2)^3} \qquad 5$$

In which Fr_2 and Fr_3 are Froude numbers at sections 2 and 3, respectively. Hence, the critical value of downstream (Fr_3) is the value of Froude number corresponded to the value of Froude number at section 2 (Fr_2=1).
Henderson used the following equation to distinguishing between classes of flow (class A ,choked flow)and (class B, un choked flow) depending the equality of the momentums conservation in section 2 and 3, M2= M3 : leads to

$$\mathrm{Cr} = \frac{\left(2+\frac{1}{\mathrm{cr}}\right)^3 \mathrm{Fr}_3{}^4}{(1+2\mathrm{Fr}_3{}^2)^3} \qquad 6$$

in which
M2 momentum in section 2
M3 momentum in section 3.
Henderson stated that equation 6 is probably to be correct because it does not depend on any assumptions about energy conservation, and in any case it is more useful because its independent variables could be obtained from section 3, which are known initially. The main advantage of the momentum balance approach is that losses due to expansion or contraction are allowed for in the equation, while the energy equation approach requires appropriate coefficients to estimate the entry and exit losses. when the value of Froude number at section 2 equal to one (Fr_2=1), Froude number critical at downstream (Fr_{3c}) can be calculate using equation 5. The second level of headings

should be left justified, bold and first letters capitalized. The second level of headings should be left justified, bold and first letters capitalized.

$$Cr^2 = \frac{27r^3 {Fr_{3c}}^2}{\left(2+{Fr_{3c}}^2\right)^3} \qquad 7$$

When the value of Froude number in downstream (Fr_3) is less than the critical value of Froude number Fr_{3c}, then the flow between piers is subcritical (Figure 2 class-A or un choked flow), and when, the value of Froude number in downstream Fr_3 is greater than the critical value of Froude number Fr_{3c}, the flow between piers is supercritical (Figure 2 class- B or choked flow).

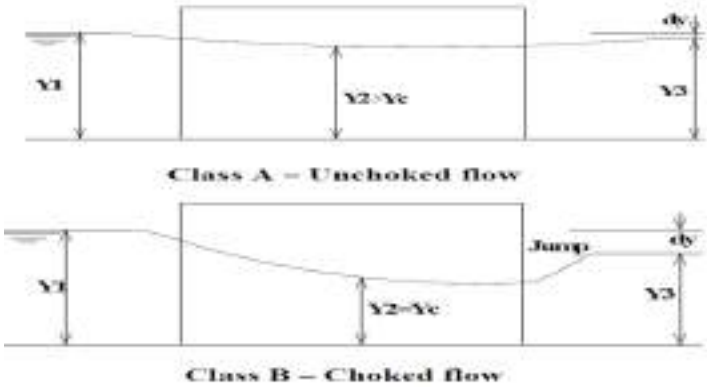

Figure 2. Type Of Flow Between Bridge Pier (Yarnell 1934)

It should be menetion that Yarnell formala used to find backwater rise in case of subcritical flow between bridge pier, while in case of supercritical flow the following Figure 3 bellow used to estamate the dimensioless backwater.

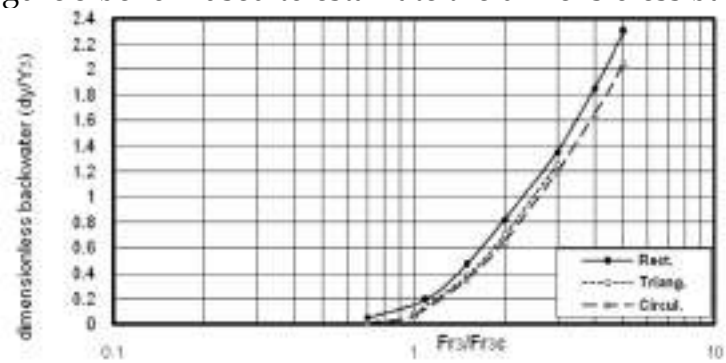

Figure 3. Dimensionless Backwater Rise At Supercritical Flow Between Pier Due To Yarnell (1934)

Hunt et.el,1999 [12] divided the bridge region into three zone: the contraction reach, the transition reach and the expansion reach. He tried to estimate the loses in energy in the transition reach (the region between bridge pier) by development a coefficient to estimate this losses. He found that the accurate prediction of energy losses depending on four parameters which are the expansion reach length, the contraction reach length, the expansion coefficient, and the contraction coefficient. He found that the expansion reach and contraction reach tended to increase with the decreased of channel slope, roughness and overbank. **Kai et.el,2006 [13]** investigate the effect of contraction ratio on the backwater and drop. He stat that the maximum backwater is affected by the ratio of the flow area obstructed by the piers to the total flow area downstream of the piers. **El-Alfy, 2009[14]** carried out an investigation to illustrate

the effect of contraction ratio. He used the application of energy principle to estimate the backwater level due to the obstruction by bridge piers in the stream. He found that backwater rise upstream bridge pie depend on the contraction ratio in the main degree, while the pier shape in the second degree. **Suribabu et al. ,2011[15]** used different shapes of bridge piers having equal projected area to study the backwater rise with two different contraction ratios of 0.33 and 0.40 under subcritical flow conditions. They found that the experimental results suggest that use of Yarnell's formula for backwater rise will over predict the rise in water level so they introduced a coefficient to modified the Yarnell equation. **Eid.et.al, 2016 [16]** using different three nose shapes of bridge piers were (rectangular, triangular and circular nose), under four different values of contraction ratio (C_r) of; 0.375, 0.3, 0.25 and 0.125. He found the backwater rise values decrease gradually with the increase of (Cr) values (expansion). Value of backwater rise decreases by a large rate at contraction ratio from 0.70 to 0.75. This means, it can be seen that any means of increasing the waterway area under a bridge can be effective in reducing the backwater.

DIMENSION ANALYSIS

As mention above to drive an equation assemblage the parameter effecting on backwater when using laboratory flume it should be use dimensional analysis. Previously, **[8,10,17,18 and 19]** explained some of the variables affecting the parameters that affect the backwater mechanism. The variable affecting the backwater depth (y_1) can be categorized as" follows:

1-Variables characterizing the fluid; viscosity (u) and density of water (ρ).

2-Variables characterizing the flow; normal flow depth (y), velocity (v) acceleration of gravity (g),Channel width (B) and channel bed slope (S_o).

3-Variables characterizing bridge piers; piers diameter or width (b) and pier length (L), and angle of approach flow to the pier axis (β).

The backwater depth is a function of all previous variables which can be written in the following formulas:

$$y_1 = f(\rho, u, y, v, g, B, S_o, b, L, \beta, K)$$

$$f(y_1, \rho, u, y, v, g, B, S_o, b, L, \beta, K) = 0$$

Then according to **PI[20]** theory the functional relationship describes backwater depth normalized with normal flow depth may be written as:

$$f\left(\frac{y_1}{y_n}, \frac{V*y_n}{u}, \frac{v^2}{y_n*g}, \frac{y_n}{B}, S_o, \frac{b}{y_n}, \frac{L}{y_n}, \beta, K\right) = 0$$

The influence of most of previous parameters is neglect as follow. The term 2, usually is insignificant parameter can be dropped from equation above if the flow around the pier is fully turbulent. Any combination of the dimensionless numbers involved in equation above is also dimensionless and may be used replace y_n/B and b/y_n by the contraction ratio Cr =b/B. The slope is constant for all runs so it is dropped. All used models have the same length and projected width for flow, so the ratio L/y_n is dropped. Also, the skewness angle β is constant in each run so it is dropped. Also, used the same shape in each run (I.e. constant shape factor K) lead to neglected this parameter. After determination and elimination process, the π-terms that influence and governed the backwater rise upstream pier can be rested the following form:

$$\frac{y_1}{y_n} = f(Fr_n, C_r) \; or \; \frac{y_2}{y_n} = f(Fr_n, C_r)$$

where $\frac{y_1}{y_n}$ is buildup ratio , C_r (contraction ratio) =b/B, Fr_n normal Froude number and $\frac{y_2}{y_n}$ is drop ratio

DEVELOPMENT OF ANN MODEL

More than that, in this study the artificial neural network **(ANN)** was employed to estimate backwater rise due to bridge pier by using MATLAP softweir. For this purpose 3-layer Feed forward neural network (FNN) used in this study contains only one intermediate (hidden) layer. It is important to mention that FNN can have multi hidden layer but the theoretical studies have shown that a single hidden layer is enough for ANN to estimated any complex nonlinear function **[21,22]**. In general, numerous experimental results seem to verify that one hidden layer may be sufficient for most forecasting problems **[23,24]**. The idea of ANN work is inspire from the human brain. Humans are able to rapidly recognize patterns and process data duo to the presence of billions of interconnected neurons. An ANN is a simplified mathematical representation of this biological neural network. It has the ability to learn from examples, recognize a pattern in the data, adapt solutions over time, and process information rapidly **[25]**. An ANN consists of a number of data processing elements called neurons or nodes, which are grouped in layers. The input layer neurons receive the input vector and transmit the values to the next layer of processing elements across connections. This process is continued until the output layer is reached. This type of network in which data flows in one direction (Forward) is known as a feed-forward network. The ANN theory has been described in many books, including the text by **[26]**. **Pinar,2010 [27]** tried to development a suitable model to estimate backwater through arch bridge. He used deferent Artificial neural networks and he stated that multi the linear preceptor (MLP) give agreement result.

EXPERMINTAL WORK

The experimental work was carried out in a re-circulating flume has diminution 12 length and 0.5 for each width and height in the Hydraulic Laboratory of the Middle Technical University, Kut Technical Institute, Iraq as shown in Figure 4. A baffles (screens) are placed at the flume inlet in order to damp any turbulence and smoother the flow. Water is supplied to the channel from a sump tank constructed below the floor level of the laboratory .The maximum discharge of the centrifugal pump is 40 lit/sec is installed beside the flume .The models of piers were made from timber and painted with a non permeable material to have a smooth surface. The experiments were achieved under five values of Froude number ranged between 0.5 and 0.64 by using different normal flow depth ranged from 4.5 cm to 10.7 cm. The discharge was calibrated for triangular V-notch at flume end. point gauges were used to measured Water depths with accuracy of ±0.1 mm. The flow velocity was measured by using mini-water velocity meter of accuracy ±2% as shown in Figure 5. In each run, the normal water depth associated to each discharge before putting the bridge pier (y_n) was measured .then After placing the bridge pier the following parameters were

measured: Upstream flow depth y_1,Flow depth through opening y_2, and Flow depth downstream y_3. Figure 6 show the the difference in cases using in this study.

Figure 4. The Flume Used In Present Study (Hydraulic Laboratory Of Technical Institute, Kut)

Figure 5. Velocity Measurement System: (a) Control Panel Box, and (b) Mini-Propeller.

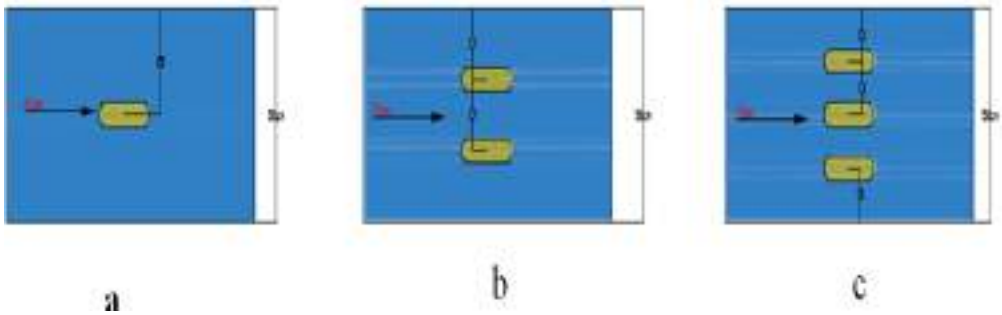

Figure 6. Pier Cases Using In This Study

RESULT AND FINDINGS

To investigate the effect of contraction ratio on backwater curve a fifteen runs were conduct to established the relationship between the buildup ratio and contraction ratio. A single, double and triple piers modeled of semicircle pier were installed in longitudinal direction of open channel. The installation of piers models were with equal spacing. Figures 7 demonstrate that the buildup ratio increase as the contraction ratio decrease. Table 1 show the buildup ratio percentage differences of single double

and triple model compare with the normal depth were approximately range from 2.2% to 23.3%. Also, Figure 7 show that that the increase in the value of Froude number led to increase in the backwater value. Theoretical explanation for it, the decrease of contraction ratio mean more lose in energy duo to increase the fraction between the flow and the surface area of the pier. Also the decrease of contraction ratio lead to decrease the flow area and increase the stagnation zone, in this zone the flow velocity become zero, this mean more loses in energy, as a result (according to the energy equation) with constant discharge the flow depth will increase to overcome this loses in energy. This fact has been proven by many researchers as mention in chapter two namely **[9,10,14,17and18]**. they proven that the increase in obstruction ratio lead to increase in energy loses as mean more backwater. Table 1 presented the values of contraction ratio with the buildup ratio y_1/y_n -1.

Table 1. The Buildup Ratio Percentage Differences For Semicircle Pier

Contraction ratio	Discharge m³/s	y_n cm	y_1 cm	$\frac{y_1}{y_n}-1$	$(\frac{y_1}{y_n}-1)\,100$
0.91	**0.035**	10.7	11.4	0.065	6.50
	0.025	8.8	9.3	0.057	5.70
	0.019	7.51	7.87	0.048	4.80
	0.012	5.89	6.1	0.036	3.60
	0.0075	4.5	4.6	0.022	2.20
0.82	**0.035**	10.7	12.2	0.140	14.0
	0.025	8.8	9.8	0.114	11.4
	0.019	7.51	8.2	0.092	9.20
	0.012	5.89	6.3	0.070	7.00
	0.0075	4.5	4.75	0.056	5.60
0.73	**0.035**	10.7	13.2	0.252	25.20
	0.025	8.8	10.55	0.199	19.90
	0.019	7.51	8.9	0.158	15.80
	0.012	5.89	6.6	0.121	12.10
	0.0075	4.5	4.9	0.089	8.90

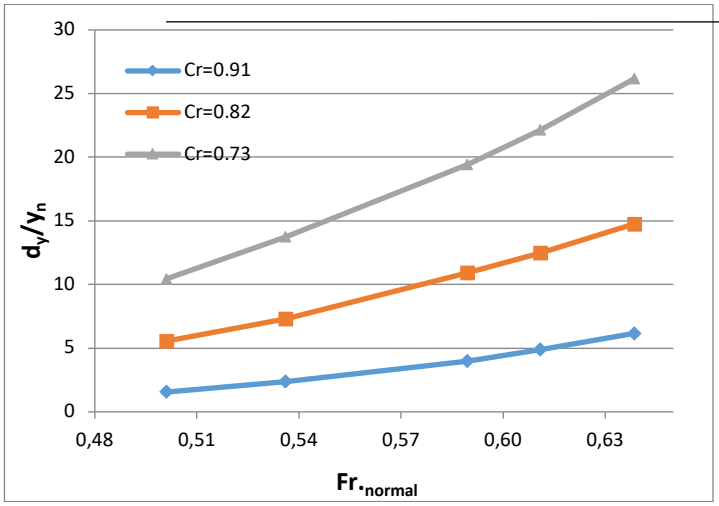

Figure 7. The Relationship Between Percentage Increase in Backwater Rise And Normal Fr. Number

Figures 8 show the backwater surface profile and drop for each contraction ratio in case of maximum discharge (0.035m^3/s). The figure show that the decrease in contraction ratio lead to increase in backwater curve. Also, the Figure show that the flow type is gradually varied flow for upstream and downstream bridge pier, but near the pier a sudden drop in water level due to the pier obstruction, consequently the hydraulic jump will accurse because of the changing in the flow type.

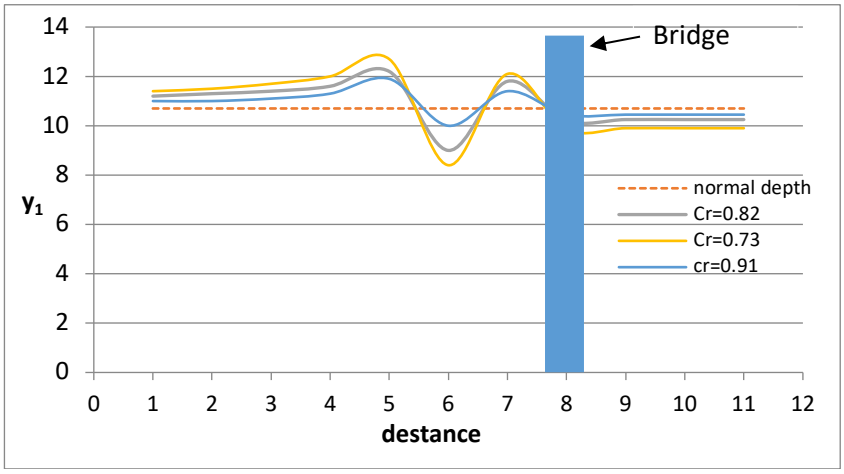

Figure 8. Backwater Surface Profile For Diffirent Contraction Ratio

Equation 6 state by [8] was use to distinguish between sub and supercritical flow between pier. The critical Froude number were 0.97,0.775 and 0.6 for contraction ratio 0.91, 0.82 and 0.73 respectively while the maximum downstream Froude number was 0.64. It is obviously that critical Froude number for 0.91 and 0.82 is higher than maximum downstream Froude number so type of flow will be subcritical. While in case 0.73 contraction ratio the flow was supercritical for the first two Froude number. The comparison between the experimental result and the result of Yarnell formula give a close result with average percentage error less than 10.4% as shown in the Figure 9 below.

According to **[21,22,23 and 24]** one hidden layer with Feed forward neural network (FNN) has been used in this study. Two input layers which are (Cr, Fr) have been used to predicate the output layer (y_1/y_n). Table 2 illustrate the characteristics of the ANN structures. Figure 10 show the relationship between the target (imported output) and output from the ANN, also the figure show that the number of samples are 15, which 30 % from the samples classified for validation and test which the correlation coefficient R is equal to 1, the remain samples (70%) using for training which the correlation coefficient R equal to 0.999. As a result, for all cases the correlation coefficient is equal to **R=0.998**. Figure 11 show the performance of ANN, which the green line for validation, the blue line for training and red line for testing. The figure show that the performance of ANN is very high as mean square error is very low which is equal to **3.9*10-5**. In general the result for ANN give a agreement result.

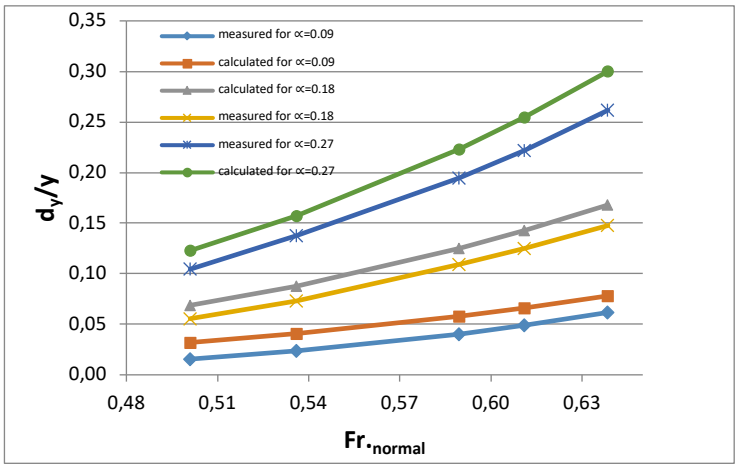

Figure 9. The Comparison Between The Experimental Result And The Result Of Yarnell Formula

Table 2. The Characteristics Of The ANN Used In This Study

No. of input layers	**2-layers**
No. of hidden layers	**1-layers**
Transform function	**TANSIG**
Learning rate	**LEARNGDM**
N. of neurons	**10 neurons**
Iteration	**Feed Forward Backprop**

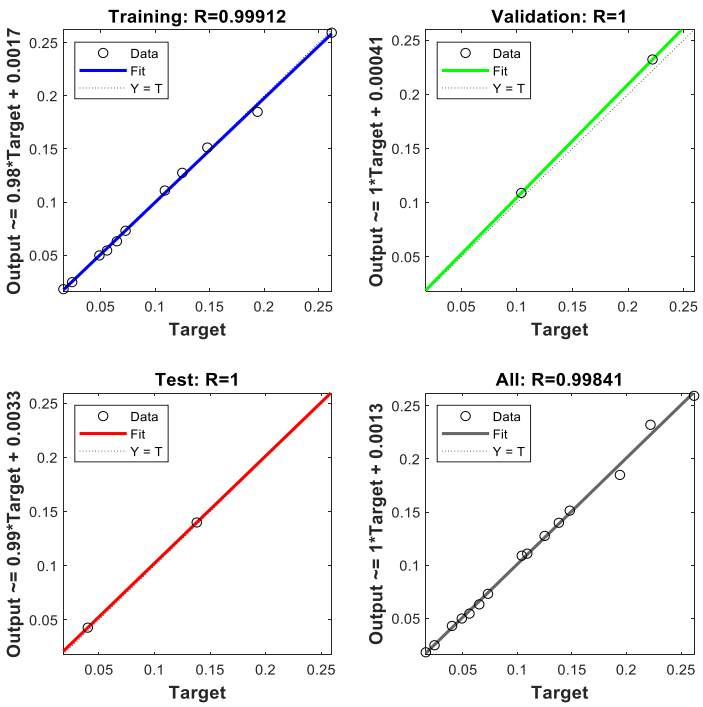

Figure 10. The Regression Between Date Using ANN

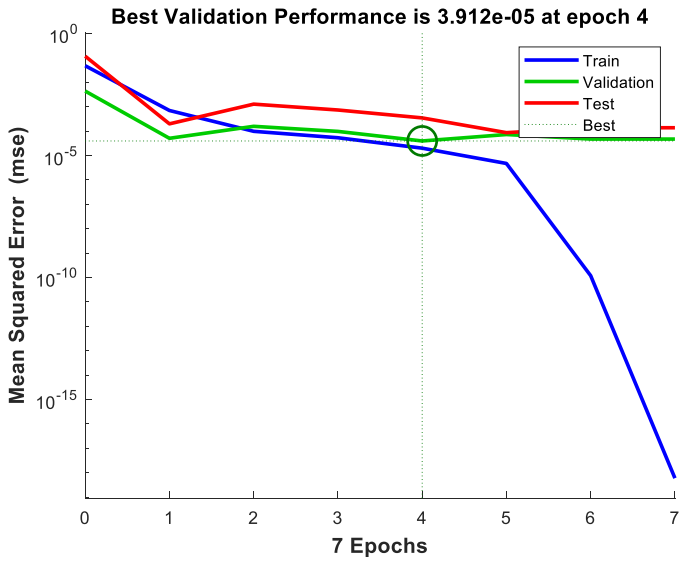

Figure 11. The Performance Of The Network Generated By ANN

CONCLUSION

The conclusions of this study are

For all types of piers the backwater rise upstream bridge is directly commensurate to the value of the Froude number (Fr).

The backwater curve depend mainly on the contraction ratio as the percentages increase was 6.54% ,14.13% and 23.6% when using single, double and triple models respectively (i.e. 0.91,0.82 and 0.73 contraction ratio).

The drop in water level between piers can be refer to a sudden change in the flow characteristics between upstream and down- stream. This changes depend mainly on the Froude number, contraction ratio and pier geometry. The increase in backwater is accompanied by an increase in drop between pier.

The comparision between the expermintal result and Yarnell formula give aclose result with percentge error less than 10.7. The variation between the backwater value resulted from experimental work and Yarnell equation could be referred to the difference in the condition of flow, pier geometry and the dimension of flume.

The using of ANN to estimate backwater rise due to bridge pier give acceptable result with correlation coefficient R equal to 0.998 and Mean Square Error RMSE equal to $3.9*10^{-5}$.

RECOMMENDATIONS

It must be kept in mind that the ANN model represent limited ranges of data gated from laboratory experiments. The additional laboratory data and field observations are required to verify the presented model.

The experimental work can be extended to study the effect of eccentricity, pier aspect ratio, flume geometry and pier shape on backwater rise.

References

Hamil L., 2000, "Bridge Hydraulics", 2nd Edition, Taylor & Francis Taylor e-Library.
G.V. Skogerboe, L.H. Austin K.Tao Chang 1970. Subcritical Flow at Open Channel Structures Bridge Constrictions. OWRR Project No. B-018-UTAH Matching Grant Agreement No. 14-01-0001-1952 Investigation Period - July 1, 1968 to June 30, 1970
Charbeneau, Randall J. and Holly, Edward R., "Backwater effects of bridge piers in subcritical flow", Center of Transportation Research, University of Texas, Project Summery Report 1805-S, 2001.
L.W. Zevenbergen, L.A. Arneson, J.H. Hunt, A.C. Miller,2012. Hydraulic Design Of Safe Bridges . FHWA-HIF-12-018 HDS 7
Martín Vide, 2002 Martín Vide, J.P. Ingeniería de Ríos. Ediciones UPC. 2002.
Lane, E. W.1920. Experiments On The Flow Of Water Through Contractions in an open channel. Amer. Soc. Civ. Engin. Trans. (1919—20) 83: 1149-1219, illus.
D'Aubuisson de Voisins, J.F. (1840) Traité d'hydraulique (Treatise on Hydraulics), 2nd edn, Piois, Levraut et Cie, Paris. Henderson, F.M. (1966)
Henderson, F.M. "Open channel flow", Macmillan Publishing Co., Inc., New York,1966.
Yarnell, D.L. "Bridge piers as channel obstructions", U.S. Department of Agriculture, Tech. Bull. No. 442, November 1934b.
Te Chow, V. (1959). Open-channel hydraulics (Vol. 1). New York: McGraw-Hill.
Soliman, M.A. "Design of irrigation structures and works", Al-Azhar University, Cairo, Egypt, 1989.
Hunt J, Brunner GW, Larock BE (1999). Flow transitions in bridge back- water analysis. ASCE Journal of Hydraulic Engineeringb125:981–983
Wang, KAI, FU, X. D., & Wang, G. Q. (2006). Comparison of existing backwater models for bridge piers in subcritical flows [J]. South-to-North Water Transfers and Water Science & Technology, 6, 014
El-Alfy 2009. Backwater Rise Due To Flow Constriction By Bridge Piers. Thirteenth International Water Technology Conference, IWTC 13 2009, Hurghada, Egypt
Suribabu, C.R., Sabarish, R.M., Narasimhan, R.E. and Chandhru, A.R. "Backwater rise and drag characteristics of bridge piers under subcritical flow conditions", European Water, Vol. 36, pp. 27-35, 2011.
Mohammed, M. I. I., & Eid, M. A. A. H. (2016). Effect of Erodible Bed on Backwater Rise Due to Bridge Piers Only In Case of Subcritical Flow. American Journal of Engineering and Technology Research Vol, 16(2).
Nagler, A. 1918. Obstruction of bridge piers to the flow of water. Trans., ASCE, Vol. 82, pp. 344-395.
Rehbock, T. (1919): "Zur Frage des Bruckenstanes," Zentrolblatt des Bauverwattung, Berlin, Germany, vol. 39, no. 37.
Kindsvater, C.E., and Carter, R.W., Tranquil flow through open channel constrictions, Trans. ASCE, Vo. 120, 1955, p.955.
Hanche-Olsen, H. (2004). Buckingham's pi-theorem. NTNU: http://www. math. ntnu. no/~ hanche/notes/buckingham/buckingham-a4. pdf.
Cybenko, G., \Approximation by superposition of a sigmoidal function", Math. Control Signals Syst., 2, 303{314, 1989.
Hornik, K., Stinchcombe, M. and White, H., \Multilayer Feed for ward Networks Are Universal Approximators", Neural Networks 2, 359{366, 1989.

Zhang, G., Patuwo, B.E. and Hu, M.Y., \Forecasting With Arti_cial Neural Networks: The State of the Art. Int. J. Forecasting, 14, 35{62, 1998.
Coulibaly, P., Anctil, F. and Bobe'e, B., \Pre'vision hydrologique par re'seaux de neurones arti_ciels: e'tat de l'art" Can. J. Civil Eng., 26, 293{304, 1999.
Leahy, P., Kiely, G., & Corcoran, G. (2008). Structural optimisation and input selection of an artificial neural network for river level prediction. Journal of Hydrology, 355(1-4), 192-201.
Rumelhart, D.E., Hinton, G.E. and Williams, R.J., \Learning internal representation by error propagation", In: Rumelhart, D.E. and McClelland, J.L. (Eds.), Parallel Distributed Processing: Explorations in the Microstructure of Cognition, 1. MIT Press, Cambridge, MA, 318{362, 1986.
Pinar, E., Paydas, K., Seckin, G., Akilli, H., Sahin, B., Cobaner, M., ... & Akar, M. A. (2010). Artificial neural network approaches for prediction of backwater through arched bridge constrictions. Advances in Engineering Software, 41(4), 627-635.

MONITORING OF ARSENIC FROM SPECIFIC POLLUTANTS IN DOWNSTREAM OF UZUNÇAYIR DAM LAKE (TUNCELİ)

Murat TOPAL
Munzur University, Faculty of Engineering, Department of Environmental Engineering, Tunceli, Turkey
murattopal@munzur.edu.tr

E. Işıl ARSLAN TOPAL
Fırat University, Faculty of Engineering, Department of Environmental Engineering, Elazığ, Turkey
eiarslan@firat.edu.tr

ABSTRACT: In this study, the concentration of arsenic from certain pollutants on the downstream side of Uzunçayır Dam Lake, which was built on the Munzur River, was monitored during the spring and summer seasons. Above ground water samples were collected in 2017 in March, April, May, June, July and August from the downstream of Uzunçayır Dam Lake. Arsenic concentrations in water samples were determined by ICP-MS. According to the data obtained, the highest arsenic concentration was 3.61 ± 0.18 µg/L in August and the lowest arsenic concentration was 0.84 ± 0.04 µg/L in May. Arsenic concentrations did not change much in spring. Arsenic concentrations increased in summer. As a result, arsenic concentrations in the waters from downstream of Uzunçayır Dam were determined to be smaller than the arsenic concentrations given by the regulations.

Key words: arsenic, lake, Munzur, water quality, Tunceli.

BELİRLİ KİRLETİCİLERDEN ARSENİĞİN UZUNÇAYIR BARAJ GÖLÜ (TUNCELİ) MANSAP TARAFINDA İZLENMESİ

ÖZET: Bu çalışmada, Munzur Nehri üzerine kurulmuş olan Uzunçayır Baraj Gölü mansap tarafında belirli kirleticilerden arseniğin konsantrasyonları ilkbahar ve yaz sezonu boyunca izlendi. Yerüstü su örnekleri Uzunçayır Baraj Gölü'nün mansabından 2017 yılında Mart, Nisan, Mayıs, Haziran, Temmuz ve Ağustos aylarında alındı. Su örneklerinde arsenik konsantrasyonları ICP-MS ile belirlendi. Elde edilen verilere göre en yüksek arsenik konsantrasyonu yaz mevsiminde Ağustos ayında 3,61±0,18 µg/L olarak, en düşük arsenik konsantrasyonu ise Mayıs ayında 0,84±0,04 µg/L olarak tespit edildi. İlkbahar mevsiminde arsenik konsantrasyonları çok fazla değişmezken Yaz mevsiminde arsenik konsantrasyonları artış göstermiştir. Sonuç olarak, Uzunçayır Barajından mansaplanan sulardaki arsenik konsantrasyonlarının yönetmeliklerle belirlenen arsenik konsantrasyonlarından daha küçük değerler aldığı belirlendi.

Anahtar sözcükler: arsenik, göl, Munzur, su kalitesi, Tunceli.

GİRİŞ

Arsenik (As); toprak, tatlı su ve deniz ortamlarında yaygın olarak bulunan zehirli bir elementtir (Wang ve diğ., 2015). Arseniğin çevrede bulunuşu, pirit cevherlerine adsorblanan arsenik bileşiklerinin jeokimyasal faktörler ile su içinde çözünmesi gibi doğal kaynaklı olabilir. Bunun yanısıra arseniğin çevrede bulunuşu; pestisitlerin ve fosfat gübrelerinin uygulanması, madencilik, endüstriyel prosesler, kömür yanması, kereste koruyucuları gibi yapay kaynaklı olabilir. Çevredeki arseniğin asıl kaynağı, As-zenginleştirilmiş minerallerden arseniğin salınmasıdır (Jaishankar ve diğ., 2014). Arseniğin bilinen herhangi bir biyolojik rolü bulunmamaktadır (Wang ve diğ., 2015). Arsenik her canlı türü için oldukça zehirlidir (Singh ve diğ., 2015). Arseniğe uzun süre maruz kalma; cilt bozukluklarına, kangrene, böbrek ve mesane kanserine yol açan kronik bir hastalık olan arsenicoza neden olabilir. Yüksek arsenik seviyelerine maruz kalmak öldürücüdür (Kaiser, 1998). Bu nedenlerle arsenik kirliliği, temel çevre problemlerinden birisidir (Zhang, 2004).

Kirlenmiş nehirlerin sularındaki arsenik konsantrasyonları; kirletici kaynağı, temel akış ve ana kaya yapısına bağlı olarak ortalama 0,1-2,1 µg/L aralığında değişir. Jeotermal girdiler, buharlaşma ve yeraltı suyu kirliliği, nehirlerdeki yüksek As konsantrasyonlarının ana sebebidir. Madencilik aktiviteleri de, nehir sularında yüksek As konsantrasyonlarının ortaya çıkmasına katkıda bulunabilir. Bu nedenlerle, arsenik yerüstü, yeraltı ve içme sularında sürekli izlenmesi gerekmektedir.

Dünya Sağlık Örgütü (WHO) yönergelerine göre, içme suyunda arsenik sınırı 0.01 mg/L dir. Kirletilmemiş yüzey ve yeraltı sularındaki arsenik seviyesi 1-10 µg/ L arasında değişir. Tatlı su sistemlerinde (nehirler ve göller), As konsantrasyonu; havzaların kaynağına ve jeokimyalarına bağlı olarak 0.15–0.45 µg/ L aralığındadır. Sulama sularında izin verilen arsenik sınır değeri WHO' nun sulama amaçlı su kullanım kılavuzuna göre 0.10 mg/L dir (Singh ve diğ., 2015).

Bu çalışmada, Tunceli ilinin önemli su kaynaklarından biri olan Munzur Nehri'nde arsenik konsantrasyonları ilkbahar ve yaz mevsimi boyunca izlendi. Munzur Nehri Munzur dağlarının eteklerinde bulunan doğal kaynaklardan doğmakta ve kuzeyde bulunan Mercan deresi ile birleşmektedir. Sonra, Tunceli ili içerisinde bulunan Pülümür çayı ile birleşek 25 km sonra Keban Baraj Gölü'ne ulaşmaktadır. Munzur Nehri'nin yüzey alanı 793 ha, yıllık ortalama akım 1629 hm^3'tür (TR, 2012). Fırat-Dicle Havzasında bulunan Uzunçayır Baraj Gölü ise Munzur Nehri üzerinde kurulmuş olan bir barajdır. Uzunçayır Barajının genel özellikleri incelendiğinde gövde hacmi 2,25 hm^3, yıllık ortalama akım 2847 hm^3, yağış alanı 3353 km^2'dir (TR, 2012). Uzunçayır Baraj Gölü alabalık yetiştiriciliğinde, tarımsal amaçlı sulamada kullanılan bir göldür.

YÖNTEM

Bu çalışmada, Munzur Nehri üzerine kurulmuş olan Uzunçayır Baraj Gölü mansap tarafında belirli kirleticilerden arseniğin konsantrasyonları ilkbahar ve yaz sezonu boyunca izlendi. İzleme çalışmaları kapsamında yerüstü su örnekleri 2017 yılında 10 gün arayla Mart, Nisan, Mayıs, Haziran, Temmuz ve Ağustos aylarında alındı. İlkbahar ve yaz aylarının seçilme nedeni Uzunçayır Barajından mansaplanan suların

sulama ve/veya içme suyu amaçla kullanılmasıdır. Çalışma alanı ve numune alma noktasını gösterir harita Şekil 1'de verilmiştir.

Şekil 1: Çalışma alanı ve numune alma noktası

Uzunçayır Barajından mansaplanan yerüstü su numuneleri belirlenen numune alma noktasının farklı noktalarından (5 ayrı nokta) yaklaşık 20 cm derinlikten 1 L olacak şekilde numune kaplarına alındı ve 0.01 N HCl ile pH'sı 2'nin altında olacak şekilde asitlendirildi. Hazırlanan su numunelerinde arsenik konsantrasyonları ICP/MS cihazı ile akredite olan bir laboratuvarda tespit edildi.

BULGULAR

Munzur Nehri Tunceli ilinin önemli bir su kaynağı olmakla beraber aynı zamanda Keban Baraj Gölü'nüde besleyen önemli nehirlerden birisidir. Çalışmamızda Uzunçayır Barajından mansaplanan yerüstü sularında İlkbahar mevsiminde tespit edilen arsenik konsantrasyonları Şekil 2'de verilmiştir.

İlkbahar mevsiminde arsenik konsantrasyonlarının aylara göre çok fazla değişmediği genellikle 0,84 ila 1,08 µg/L aralığında olduğu belirlendi. En yüksek arsenik konsantrasyonu Nisan ayında 1,08±0,05 µg/L olarak, en düşük arsenik konsantrasyonu ise Mayıs ayında 0,84±0,04 µg/L olarak tespit edildi. İlkbahar mevsiminde Mart ayında arsenik konsantrasyonları 0,94-0,98 µg/L aralığında değişirken bu değerler Nisan ayında artmış Mayıs ayında ise Mart ayına oranla bir azalma göstermiştir. Mart ayında arsenik konsantrasyonları incelendiğinde ortalama arsenik konsantrasyonu 0,96±0,04 µg/L olarak, Nisan ayında ortalama arsenik konsantrasyonu 1,04±0,05 µg/L olarak, Mayıs ayında ortalama arsenik konsantrasyonu 0,85±0,04 µg/L olarak tespit edildi. Uzunçayır Barajından mansaplanan yerüstü sularında Yaz mevsminde tespit edilen arsenik konsantrasyonları Şekil 3'de verilmiştir.

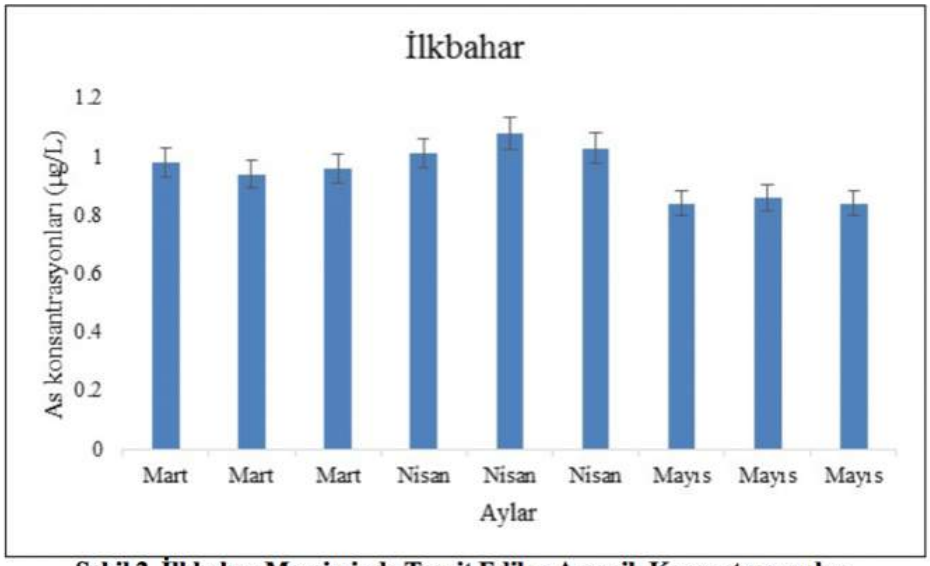

Şekil 2. İlkbahar Mevsiminde Tespit Edilen Arsenik Konsantrasyonları

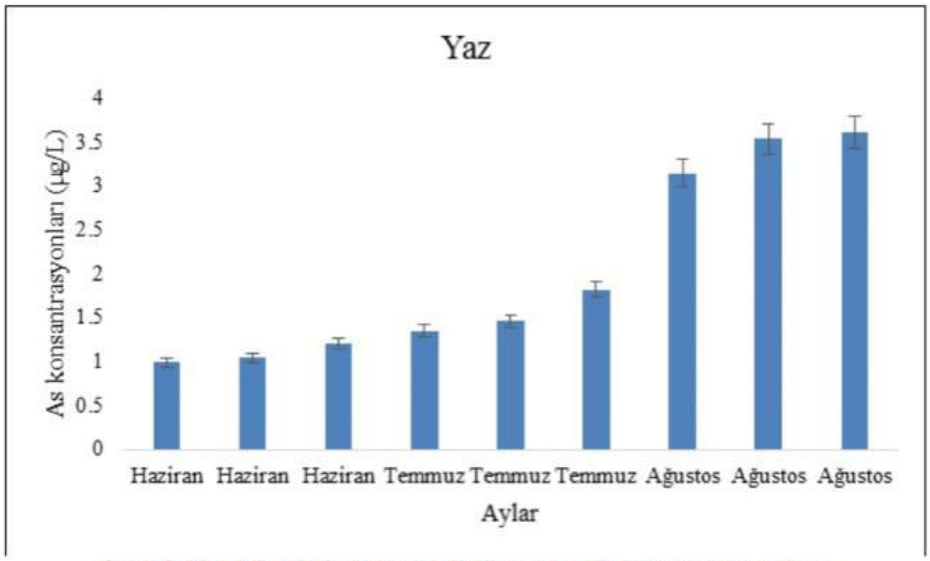

Şekil 3. Yaz Mevsiminde Tespit Edilen Arsenik Konsantrasyonları

Şekil 3 değerlendirildiğinde yaz mevsiminde arsenik konsantrasyonları sürekli bir artış göstermiştir. Haziran ayı başlangıcında 0,99±0,05 µg/L olarak tespit edilen arsenik konsantrasyonu Ağustos ayı sonunda 3,61±0,18 µg/L değerine ulaşmıştır. Bu artışın muhtemel sebebi madencilik ve antropojenik faaliyetler gibi etkilerden dolayıdır. Yaz mevsimi incelendiğinde Uzunçayır Barajından mansaplanan sularda en yüksek arsenik konsantrasyonu Ağustos ayında 3,61±0,18 µg/L olarak, en düşük arsenik konsantrasyonu ise Haziran ayında 0,99±0,05 µg/L olarak tespit edildi. Haziran ayında ortalama arsenik konsantrasyonu 1,08±0,05 µg/L olarak, Temmuz ayında ortalama arsenik konsantrasyonu 1,54±0,07 µg/L olarak, Ağustos ayında ise ortalama arsenik konsantrasyonu 3,43±0,17 µg/L olarak tespit edildi.

SONUÇ ve ÖNERİLER

Bu çalışma kapsamında Uzunçayır Barajından mansaplanan yerüstü sularında arsenik konsantrasyonları suların fazla kullanıldığı ilkbahar ve yaz mevsimi boyunca izlendi. Elde edilen veriler bazı yönetmeliklerde verilen değerlerle karşılaştırıldı. Elde edilen sonuçlar Tablo 1'de özetlenmiştir.

Tablo 1. Elde Edilen Sonuçların Standartlarla Karşılaştırılması

Standartlar	Değer (µg/L)
YSKY	**53**
TS266	**10**
İTASHY	**10**
WHO	**10**
Bu çalışma	**3,61**

30.11.2012 Tarih ve 28483 Sayılı Resmi Gazete'de yayınlanarak yürürlüğe giren Yerüstü Su Kalitesi Yönetmeliği Tablo 4'te arsenik konsantrasyonlarının Nehirler ve Göller için 53 µg/L değerini aşmaması gerektiği belirtilmiştir (YSKY, 2012). Türkiye için kabul edilen içme suyu standartı TS-266, 17.02.2005 Tarih ve 25730 Sayılı Resmi Gazete'de yayınlanarak yürürlüğe giren İnsani Tüketim Amaçlı Sular Hakkında Yönetmelik (İTASHY, 2005) ve WHO'ya göre arsenik konsantrasyonlarının kabul edilebilir maksimum sınır değeri 10 µg/L olarak belirtilmiştir. Çalışmamızda, arsenik konsantrasyonları Tablo 1'den de görüldüğü gibi maksimum 3,61±0,18 µg/L olarak tespit edildiğinden, Uzunçayır Baraj Gölü mansap sularının arsenik konsantrasyonları açısından kullanma, sulama veya içme suyu olarak kullanılmasında herhangi bir sakınca bulunmadığı belirlenmiştir.

KAYNAKLAR

İTASHY, İnsani Tüketim Amaçlı Sular Hakkında Yönetmelik (2005), 17.02.2005 Tarih ve 25730 Sayılı Resmi Gazete.

Jaishankar, M., Tseten, T., Anbalagan, N., Mathew, B.B., & Beeregowda, K.N. (2014). Toxicity, mechanism and health effects of some heavy metals. *Interdiscip Toxicol. 7* (2): 60-72.

Kaiser, J. (1998). Toxicologists shed new light on old poisons. *Science*, *279*, 1850-1851.

Singh, R., Singh, S., Parihar, P., Singh, V.P., & Prasad, S.M. (2015). Arsenic contamination, consequences and remediation techniques: A review, *Ecotoxicology and Environmental Safety*, *112,* 247-270

TR, Takdim Raporu (2012), DSİ 9. Bölge Müdürlüğü, 2013 Yılı Program-Bütçe Toplantısı Takdim Raporu, Nisan 2012, s376, Elazığ.

Wang, Y., Wang, S., Xu, P., Liu, C., Liu, M., Wang, Y., Wang, C., Zhang, C., & Ge, Y. (2015), Review of arsenic speciation, toxicity and metabolism in microalgae, *Reviews In Environmental Science and Bio/Technology, 14*, 427–451.

YSKY, Yerüstü Su Kalitesi Yönetmeliği (2012), 30.11.2012 Tarih ve 28483 Sayılı Resmi Gazete.

Zhang, H. (2004). Heavy-metal Pollution and Arseniasis in Hetao Region, China. *AMBIO: A Journal of the Human Environment, 33*, 138-140.

DIGITAL MODULATION RECOGNITION BASED ON ANNS APPROACH

Ahmed K.Ali
Gaziantep University, Department of Electrical and Electronics Engineering, Gaziantep, 27010, Turkey
Engineer.ahmed.ali25@gmail.com

Sattar B. Sadkhan, SMIEEE
University of Babylon - College of Information Technology
drengsattar@ieee.org

ABSTRACT: This concise paper does not provide a final solution, but highlights to the most promising lines of research from the recent literature in common directions for the automatic modulation classification project. The most common algorithm chosen on recent researches in the field of digital modulation recognition theory is based on artificial neural networks (ANNs) to recognize digital modulation signals. Here, the digital modulation recognition algorithm based on ANN have tested to recognize a set of modulation types; 2ASK, QASK, 2FSK, QFSK, 2PSK, QPSK, this approach can automatically choose the threshold for each feature. Also, it not only makes classifier intelligent but even to that improves the success rate of classification.

Keywords: modulation recognition, digital modulation, artificial neural networks

INTRODUCTION

Recently digital modulation techniques are more widely used in modern communication systems compare with analog modulation technology, therefore, the identification of digital modulated signals are one of hot topic for the researchers in the field of communication systems.

However, the identification methods of modulated signals can be divided into two categories: one is the decision theory method, and the other is the statistical model. Recognition method.(Han, Y., & Lee et al. 2016)(Dobre, Bar-Ness, and Wei Su 2003) The decision theory method uses hypothesis testing theory to solve the signal classification problem, usually based on the statistical characteristics of the signal, based on

The cost function minimization principle is derived, and the statistical test quantity is derived to form a decision criterion. This type of method is suitable for specific identification of certain types of modulated signals. Also, the range is narrow the various methods of modulation classification are documented in (Dobre, Bar-Ness, and Wei Su 2003),(Swami and Sadler 2000),(Han, Y., & Lee et al. 2016)

This paper proposes modulation recognition algorithm based on ANN MLP to recognize signals types; ASK2, ASK4, PSK 2, PSK4, FSK2, FSK4 which is commonly used digital modulated signals. The network identification method belongs to the statistical pattern recognition method, which is derived from the feature extraction

concept of classical pattern recognition theory. The neural network identification system is divided into two parts: feature extraction and signal recognition. Features extraction is based on analysis of various modulated signals, from signal Characteristic parameters that can distinguish various signals are extracted from information such as amplitude, phase, frequency, and power spectrum.(Wong and Nandi 2004) This type of identification abandons traditional big data. The statistical classification identification method uses the artificial neural network as the classifier, which makes the calculation amount small, the recognition speed is fast, and the detection is greatly improved. With the correct recognition rate, real-time processing of signal recognition can be realized if the parallel operation characteristics of the neural network can be utilized.

Features extraction

The identification features are based on the mathematical analysis of the signals, from the aspects of the amplitude, phase, frequency and power spectrum of the modulated signal. According to E. E. Azzouz and A. K.(Azzouz and Nandi 1997) proposed similar four characteristic parameters in order to make full use of the signal.

The various aspects of the information make the features parameters more differentiated, and the characteristic parameters proposed by Azzouz and Nandi are improved and expanded in (Ramkumar 2009)

Five key features are used to distinguish between modulation schemes and they are derived from the instantaneous phase $\varphi(t)$ instantaneous amplitude a(t) also the instantaneous frequency $f(t)$ of the signal. The key features are explained below

Gamma Max (γ max) ; $\boldsymbol{\gamma}_{max}$; **The maximum of the power spectral density of the normalized centered instantaneous amplitude, given by**

$$\boldsymbol{\gamma_{max} = Max(\frac{|DFT(a_{cn}(i)|^2}{N_s})} \quad (1)$$

Where$\mathbf{N}_s$: Number of samples per segment, and $\mathbf{a}_{cn}(i)$: is the normalized centered amplitude defined by

$$\boldsymbol{a_{cn}(i) = a_n(i) - 1}$$

And $\mathbf{a}_n(i) = \frac{a(i)}{m_a}$ $\mathbf{m}_a = \frac{1}{N_s}\sum_{i=1}^{N} a(i)$

Where

$\mathbf{m}_a$: Average value of the amplitude per one segment

N ; Number of symbols.

Sigma- AP (σ_{ap}); $\boldsymbol{\sigma}_{ap}$; **The standard deviation of the absolute instantaneous phase, given by**

$$\boldsymbol{\sigma}_{ap} = \sqrt{\frac{1}{N_c}\left[\sum_{a_n(i)>at_c} \varphi_{Nl}(i)^2\right] - \left[\frac{1}{N_c}\sum_{a_n(i)>at_c} |\varphi_{Nl}(i)|\right]^2} \quad (2)$$

Where
$\boldsymbol{\varphi_{Nl}(i)}$; Value of the normalized centered component of the instantaneous phase.
N_c; Number of samples in $\boldsymbol{\varphi_{Nl}(i)}$ which is $\boldsymbol{\varphi_{Nl}(i) > at_c}$.
$\boldsymbol{at_c}$; Threshold for $a(i)$ in case of below this value the evaluation of instantaneous phase becomes very difficult due to noise or in other words, we can say it becomes noise sensitive
Sigma- dp (σ_{dp}); $\boldsymbol{\sigma_{dp}}$; **Standard deviation of the direct instantaneous phase, defended as**

$$\boldsymbol{\sigma_{dp}} = \sqrt{\frac{\mathbf{1}}{\boldsymbol{N_c}}\left[\sum_{a_n(i)>at_c} \boldsymbol{\varphi_{Nl}(i)^2}\right] - \left[\frac{\mathbf{1}}{\boldsymbol{N_c}} \sum_{a_n(i)>at_c} \boldsymbol{\varphi_{Nl}(i)}\right]^2} \quad (3)$$

It can be see the standard deviation of the direct phase and non-absolute phase, calculated over the non-weak intervals of the signals.
Sigma- aa (σ_{aa}); $\boldsymbol{\sigma_{aa}}$; Standard deviation of the normalized centered absolute amplitude given as

$$\boldsymbol{\sigma_{aa}} = \sqrt{\frac{\mathbf{1}}{\boldsymbol{N_c}}\left[\sum_{a_n(i)>at_c} \boldsymbol{a_{cn}(i)^2}\right] - \left[\frac{\mathbf{1}}{\boldsymbol{N_c}} \sum_{a_n(i)>at_c} \boldsymbol{|a_{cn}(i)|}\right]^2} \quad (4)$$

It can be noted that $\mathbf{a}_{cn}$absolute standard deviation is being evaluated and not of acn Directly.
Sigma- af (σ_{af}) ;σ_{af}; **the standard deviation of the normalized centered absolute frequency given by**

$$\boldsymbol{\sigma_{af}} = \sqrt{\frac{\mathbf{1}}{\boldsymbol{N_c}}\left[\sum_{a_n(i)>at_c} \boldsymbol{f_N(i)^2}\right] - \left[\frac{\mathbf{1}}{\boldsymbol{N_c}} \sum_{a_n(i)>at_c} \boldsymbol{|f_N(i)|}\right]^2} \quad (5)$$

Now it must be noted that normalization of the frequency can be done in many ways but the method of normalization chosen is given below
And

$$\boldsymbol{f_n}(\mathbf{i}) = \frac{\mathbf{f_{m(i)}}}{\mathbf{r_s}}$$

$$\mathbf{m}_f = \frac{1}{N_s}\sum_{i=1}^{N} f(i)$$

$$f_m(\mathrm{i}) = \mathrm{f(i)} - m_f$$

Gamma Max_f (γ max f)

$$\boldsymbol{\gamma_{max\,f}} = \boldsymbol{Max}|\mathbf{FFT}(\boldsymbol{f_n(i)}|^2 \quad (6)$$

In their previous works, Azzouz and Nandi proposed the first five features. Here's a sixth feature proposed in a recent paper (Wang et al. 2010)has been taken into account as well. $\boldsymbol{\gamma_{maxf}}$ The maximum value of the power spectral density of the normalized centered instantaneous frequency. In this reports six digital modulation signals namely 2ASK, QASK, 2PSK, 4PSK, 2FSK and QFSK are written by 'Ultra Edit Text/Hex Editor Version 24.20.0.51. It possible to reads a m-file in MATLAB .A

random number generator has been used to generate the signals (Wang et al. 2010)As mentioned earlier, the features differentiate between different signals.
The feature parameter" $\boldsymbol{\gamma}_{\boldsymbol{max}}$ "divides the signals into two categories {2FSK, QFSK} and {2ASK, QASK, 2PSK, QPSK}. Since {2FSK, QFSK} signals have no amplitude information so their spectral power densities are zeroγ_{max}can be used to differentiate between signals that have amplitude information from those which don't have. (E. E. Azzouz and A. K. Nandi 1995)
$\boldsymbol{\sigma}_{\boldsymbol{ap}}$ Divides the signals in two subsets, 2ASK, QASK and 2PSK as the first and QPSK as the second. The first subset has no absolute phase information and the second one has. So,"σ_{ap}" discriminates between signals having absolute phase information from those having no absolute phase information.
$\sigma_{dp}$is used to differentiate between 2ASK and QASK as one subset and 2PSK as other subset. σ_{dp}Can discriminate between signals having direct pahase (2PSK) from the signals having no direct phase information (2ASK, QASK). (E. E. Azzouz and A. K. Nandi 1995)
2ASK and QASK can be differentiated by "σ_{aa}". 2ASK has no absolute amplitude information while QASK has both absolute and direct amplitude information. So "σ_{aa}" can be used to discriminate these two signals.
$\boldsymbol{\sigma}_{\boldsymbol{af}}$ Differentiates between FSK signals. 2FSK has no absolute frequency information while QFSK has both absolute and direct frequency information. (E. E. Azzouz and A. K. Nandi 1995)

STRUCTURE OF NEURAL NETWORK

The artificial neural network can automatically set various recognition thresholds to compare with decision tree algorithm, this gives a more realize intelligent recognition of modulated signals, also improved the speed of signals recognition with high accuracy of the recognition rate. The training of neural networks requires a certain number of training samples, thus, features that extracted from the known modulated signals are formatted as a row vector of data. Next, train process of the neural network, then the trained network can be employed to identify of modulation signals {2ASK, 4ASK, 2PSK, 4PSK, 2FSK, 4FSK}.In this work multi-layer feed-forward, neural network is used, and the network learning algorithm uses the back propagation algorithm. Due to the slow convergence of traditional back-propagation algorithms(Wong and Nandi 2004)
Suppose the network has a M number of layer, P layer is the input layer, T_j is the ideal output, and X_j is the input learning mode.

The net input for each node of the network is

$$\boldsymbol{S^l}_i = \sum_j \boldsymbol{W^l}_j \boldsymbol{P_j}^{(l-1)} - \boldsymbol{\theta^l} \quad \boldsymbol{l = 1, 2, 3 \ldots M} \tag{7}$$

The output is:

$$y^l{}_i = F\left(S^l{}_J\right) = \frac{1}{2} + \frac{1}{1 + e^{\frac{S^l{}_J}{K_1}}} \tag{8}$$

If $l = 1$, $P_j^{(1-l)} = X_J$, the network input learning mode, and other cases $P_j^{(1-l)}$are the output of each node $y_j{}^M$ Is the actual output of the network. Where K_1 is a nonlinear excitation function parameter, generally taken as + 0. 9. The output layer weight error of the network can be derived as.

$$\delta^M{}_i = 2\left[K_2 + \frac{\frac{1}{4} - y_j{}^2}{K_1}\right][T_j - y_j{}^M] \tag{9}$$

The weight error of the hidden layer can be derived in the same way.

$$\delta^l{}_i = 2\left[K_2 + \frac{\frac{1}{4} - P_j{}^2}{K_1}\right]\sum_j \delta_j{}^{(l+1)} W_j{}^{(l+1)}, l = 1, 2, 3 \dots M \tag{10}$$

Where K_2 is the error function adjustment factor, using a smaller positive number. The weight adjustments for each layer of the network are:

$$\Delta \mathbf{W}_\mathbf{j}{}^l(k) = \alpha(k)\delta^l y_j{}^{(l-1)} + \beta \Delta \mathbf{W}^l(k-1), l = 1, 2, 3 \dots M \tag{11}$$

Where β is the inertia coefficient, $\alpha(k)$ is the adaptive change step size, and the step adjustment amount is:

$$\Delta\alpha(k) = \begin{cases} +k_3 \; if \Delta E(i) < P(i = k - n + 1, \dots k) \\ -K_4 \; if \Delta E(i) > P(i = k - m + 1, \dots k) \end{cases} \tag{12}$$

Where ΔE is judged by the square of the output error $\Delta E = \sum_j [T_j - y_j]^2$ then the step size is

$$\alpha(k) = \alpha(k-1) + \Delta\alpha(k) \tag{13}$$

Finally, the adjustment of the weights of each layer is:

$$\mathbf{W_j(k)^l = W_j^l(k-1) + \Delta W_j(k)^l} \tag{14}$$

The threshold θ^lcan be regarded as an additional weighting factor, and the same formula is used to adjust the variation with the weighting factor

PERFORMANCE EVALUATION AND SIMULATION RESULTS

The simulation computer software used a carrier frequency of 200 kHz and a sampling frequency of 1200 kHz, which is four times higher than the carrier frequency. While the number of samples is 512 and symbol rate is 125 bps The neural network model MLP recognizer with a three-layer forward network has used as a classification of 6 types of modulation signals, the input layer included 5 neurons, the hidden layer is 10 neurons and the output layer is 6 neurons.

The number of neurons in the input layer is determined according to identifying the feature parameters, while in the output layer is identifying based on a number of class or modulation types. The number of neurons in the hidden layer is based on the principle of minimum mean square error and the best correct recognition rate of the network output. The simulation results show that for the identification of digital modulation signals when use number of 15 neurons in the hidden layer is superior to the use of 10 or 20 or 25 neurons. According to Figure 1, the Performance of BP MLP classifier with {10, 15, 20, 25} hidden layer neurons at different SNR values, for the modulation types {2 ASK.2FSK.2 PSK, 4ASK, 4FSK, 4PSK}.

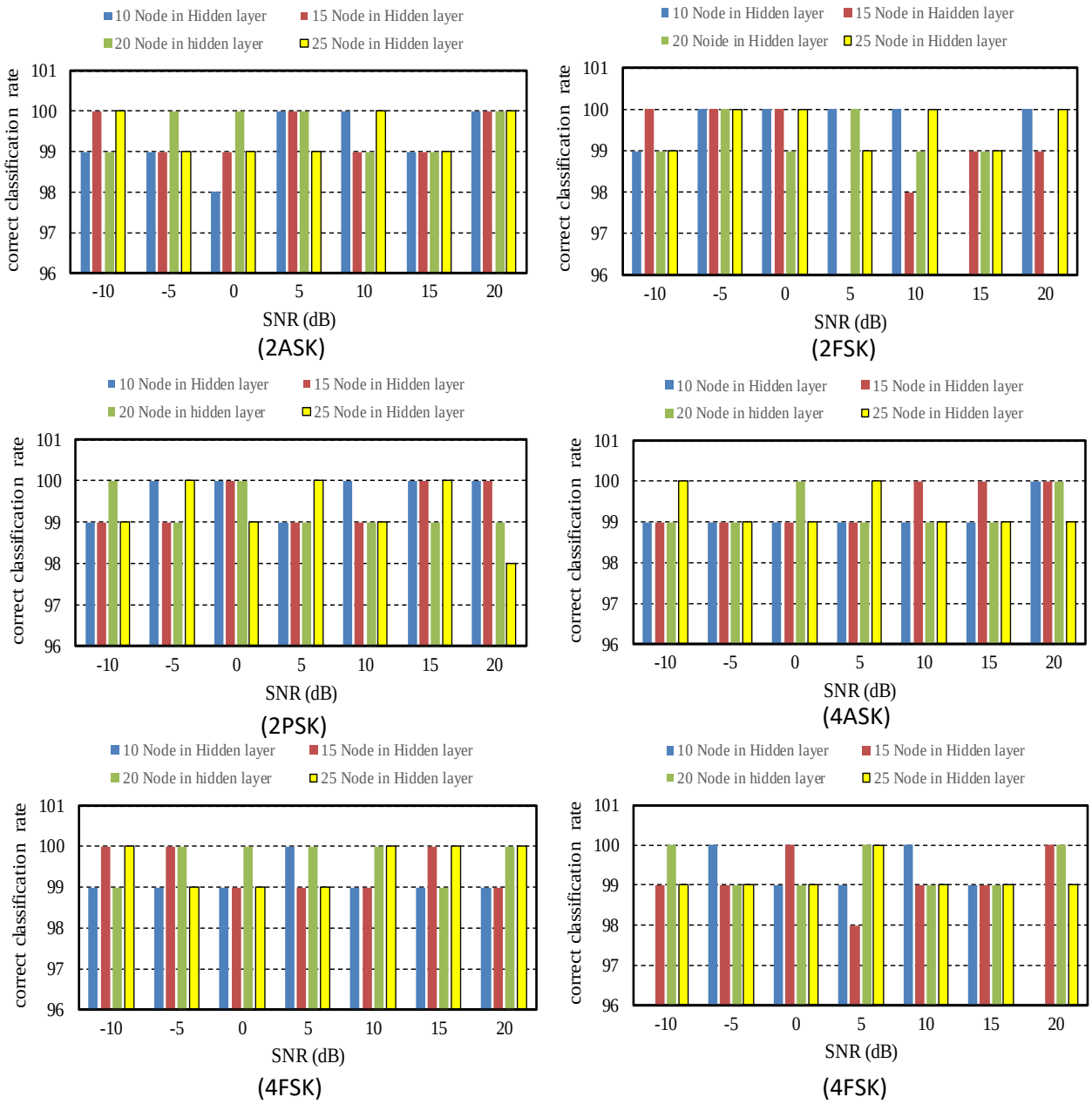

Figure 1. Performance of BP MLP classifier with {10, 15, 20, 25} hidden layer neurons at different SNR values, for the modulation types {2 ASK.2FSK.2 PSK, 4ASK, 4FSK, 4PSK}

CONCLUSION

Automatic modulation recognition is an important issue in communication intelligence and electronic support measure systems. The results of the ANN classifier has been encouraging but with a limited type of Modulations types; {2ASK, 4ASk, 2FSK z, 4FSK, 2PSK, 4PSK} are included. The simulation results show that the neural network classifier not only recognizes many types of signals but also can achieve a reliable recognition rate even at a lower signal-to-noise ratio SNR less than zero.

RECOMMENDATIONS

At present, some other statistical pattern recognition methods are proposed, but the effect is not satisfactory. A current statistical pattern recognition method the researches worked is mainly on two aspects: the analysis of the signal characteristics by extracted features, on the one hand, extracting the identification features that better reflect the signal difference, which can adopt some new theories and methods, such as time-frequency analysis methods, wavelet theory, Fourier transformer and other mathematical analysis methods. On the other hand, it is to improve the automation and intelligence of recognition, which can be combined with a large number of new methods and new theories in the field of signal processing, such as Support Vector Machine (SVM) theory, fuzzy logic theory, Neural networks, genetic algorithms, clustering algorithms, Kalman filtering, and various other adaptive signal classification methods. In pursuit of the simplicity of the algorithm, the recognition speed is fast, the recognition range is wide, the correct recognition rate is high, and more and better research and discovery are needed.

REFERENCES

Azzouz, E. E., and A. K. Nandi. 1997. "Automatic Modulation Recognition - II." *Journal of the Franklin Institute* 334(2): 275–305.

Dobre, O.A., Y. Bar-Ness, and Wei Su. 2003. "Higher-Order Cyclic Cumulants for High Order Modulation Classification." *IEEE Military Communications Conference, 2003. MILCOM 2003.* 1(C): 112–17. http://ieeexplore.ieee.org/document/1290087/.

E. E. Azzouz and A. K. Nandi. 1995. *Modulation, Automatic Of, Recognition Signals, Communication*. Kluwer Academic Publishers.

Han, Y., & Lee, J. (2016). Uplink Pilot Design for Multi-Cell Massive MIMO Networks. IEEE Communications Letters. https://doi.org/10.1109/LCOMM.2016.2571697 et al. 2016. "Hybrid Maximum Likelihood Modulation Classification for Continuous Phase Modulations." *IEEE Communications Letters* 20(3): 450–53.

Ramkumar, Barathram. 2009. "Automatic Modulation Classification for Cognitive Radios Using Cyclic Feature Detection." *IEEE CIRCUITS AND SYSTEMS MAGAZINE*: 27–45.

Swami, Ananthram, and Brian M Sadler. 2000. "Hierarchical Digital Modulation Classification Using Cumulants." *IEEE Transactions on communications* 48(3): 416–29.

Wang, Hua-kui et al. 2010. "A Research on Automatic Modulation Recognition with the Combination of the Rough Sets and Neural Network." In *A Research on Automatic Modulation Recognition with the Combination of the Rough Sets and Neural Network*, , 2–5.

Wong, M. L.D., and A. K. Nandi. 2004. "Automatic Digital Modulation Recognition Using Artificial Neural Network and Genetic Algorithm." *Signal Processing* 84(2): 351–65.

SMART GRID SYSTEMS in WIND ENERGY

Şakir BİNGÖL
Marmara University, Faculty of Engineering, Department of Electrical and Electronic Engineering,
sakir.bingol@marmara.edu.tr

İlkan H. AKPINAR
Marmara University, Faculty of Engineering Faculty, Department of Mechanical Engineering
ilkanhasan@hotmail.com

Ramazan LİKOĞLU
Marmara University, Faculty of Engineering Faculty, Department of Mechanical Engineering
rlikoglu61@gmail.com

Berkay BIDIK
Marmara University, Faculty of Engineering Faculty, Department of Mechanical Engineering
bbidik_14@hotmail.com

Muhammadali YUSUFİZADE
Marmara University, Faculty of Engineering Faculty, Department of Mechanical Engineering
yusufyali313@gmail.com

Eda YILMAZ
Marmara University, Faculty of Engineering Faculty, Department of Mechanical Engineering
eday172@gmail.com

B. Gültekin ÇETİNER
Marmara University, Faculty of Engineering Faculty, Department of Industrial Engineering
gultekin.cetiner@marmara.edu.tr

ABSTRACT: Power generated by renewable energy sources is highly aperiodic due to its probabilistic nature. This, in turn, may affect the quality of power obtained and the planning of power systems as well. In order to improve power-supply reliability and quality, the use of distributed energy resources has been increasingly developed as an alternative to large central power stations. This paper tracks new trends for the

grid integration and also its application to the field of renewable energy sources. A review of the appropriate storage-system technology used for the integration of intermittent renewable energy sources is also introduced.

Key words: Wind Energy, Smart Grid, Energy, Internet, Renewable Energy, Sources

INTRODUCTION

Fossil fuels remain the main sources in the global energy mix and are associated with the increase of carbon dioxide (CO2) emissions. The deployment of renewable energy sources (RES) can play a crucial role to reduce both (CO2) emissions and fossil fuel dependency (Lind et all., 2013). There are different factors affecting the increasing use of renewable energy sources. The use of renewable energy increased greatly just after the first big oil crisis in the late seventies. Although in many power generating systems, the main source of energy (the fuel) can manipulate, this is not true for solar, water, and wind energies (Samad & Annaswamy, 2011). In addition to renewable energy, the importance of the integration of the renewable energy to electrical grid also increased in recent years. Smart grids promise to facilitate the integration of renewable energy and will provide other benefits as well (Siona, 2014).

There are several concepts that forms a smart grid, but the common point is incorporated in the European Technology Platform. The definition is that "an electricity network that can intelligently integrate the actions of all users connected to it generators, consumers and those that do both - in order to efficiently deliver sustainable, economic and secure electricity supplies" (Mehmeti et all., 2016). Smart energy systems concentrate on many aspects of the energy chain to provide multiple benefits without compromising from the environmental protection, financial constraints, or societal wellbeing. Thus, it is essential to switch from traditional systems to smart grid systems. During the transition from traditional to smart energy systems, it is mainly expected to design, analyze, develop, and utilize transitional solutions to enhance their energetic, exegetic and environmental performance for better sustainability (Dincer & Acar, 2016). Thus, globally, billions of dollars are spent each year developing existing energy infrastructure to generate smarter grids (Hossain et all., 2016).
The breakthrough in renewable energy is expected in research area because of its availability, applicability and environmentally friendly nature, and the application of smart grid in renewable energy makes it substantial and more promising (Acemoglu et all., 2012).

Fossil Energy Sources

There is a trend towards renewable energy sources from energy-producing fossil fuels, as today's negative effects of fossil fuel consumption are felt too much. Although renewable energy can provide a clean source of electricity, fossil fuels account for the large part of the world's current energy production (International Energy Agency, 2017). In Figure 2.1, global energy consumption by fossil fuel source is presented as graph. However, there is a bright future for renewables. Renewables capture two-thirds of global investment in power plants to 2040 as they become, for many countries,

the minimum cost source of new energy generation. For instance, in the European Union, renewables make up 80% of new capacity and wind power becomes the significant source of electricity soon after 2030, because of booming growth both onshore and offshore wind turbines (Kyoto protocol, 1998).

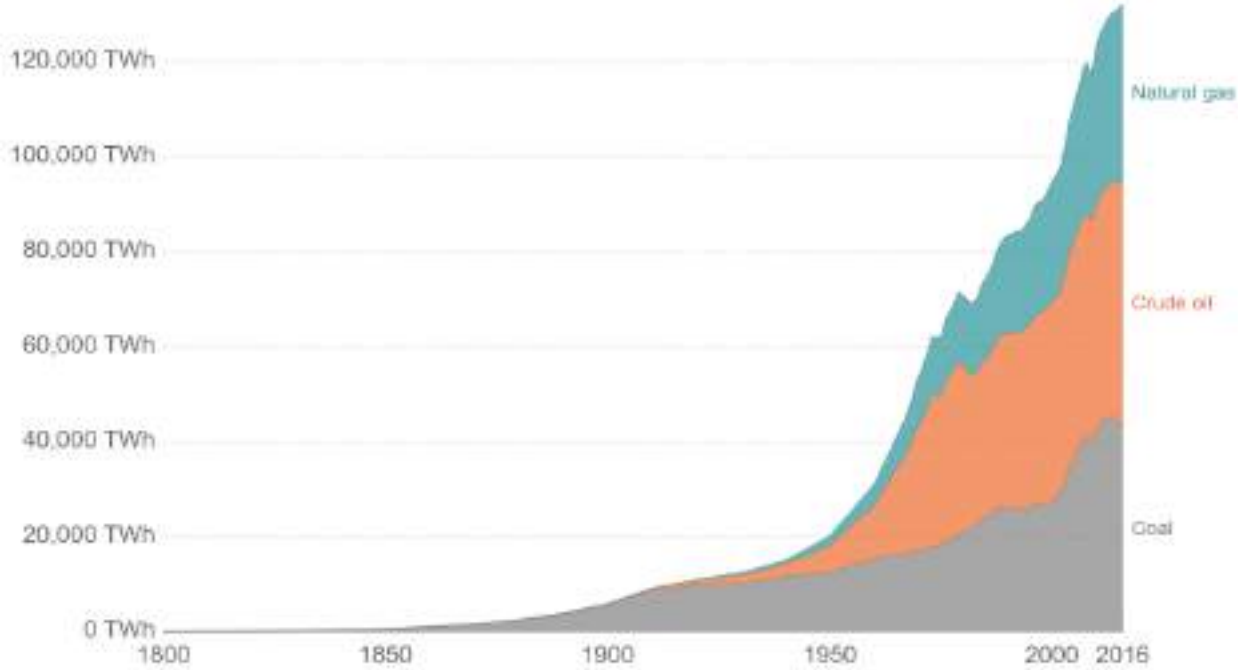

Figure 2.1 Global Primary Energy Consumption by Fossil Fuel Source, Measured in Terawatt-hours (TWh). (Sources: https://ourworldindata.org/fossil-fuels)

The adoption of renewable energy sources (RES) by European countries has been assured in international agreements and is also embodied and charged by the European Legislation and the various European member states themselves. The Kyoto Protocol assigned countries to a 5% reduction in greenhouse gases (Doha Amendment, 2012), and the "Doha Amendment to Kyoto Protocol" to the United Nations Framework Convention to Climate Change enforces countries to 18% reduction (from 1990 levels) of greenhouse gases by 2020 (Barbir et all., 1990). According to these agreements, states are supposed to reduce fossil fuel consumption to an appropriate level in favor of the environment. However, it will be not enough because not only the consumption of fossil fuels but also the negative effects of fossil fuels on the environment can be seen at all stages. For instance, excavation of coal ravages the land, which has to be regenerated and results in being of no use for several years. During the extraction, transportation, and storage of oil and gas, spills and leakages can happen, which cause water and air pollution. Refining processes also have an environmental effect (Tan et all.,2016). Inspite of carbon capture technologies which aims to prevent the greenhouse gas emissions from being released into the atmosphere, fossil fuels are not preferable in smart grid systems due to their emissions and nonrenewability (Al-Fattah & Startzman, 2000).

Al-Fattah and Startzman (Bentley, 2008), employed a "multicyclic Hubbert" approach to accurately model the gas-production history of each country producing gas. Models were then used to predict future production of natural gas worldwide. Results indicated that gas resources in most developed countries deplete at much faster rate than developing countries. Bentley (Bowden, 1985), reviewed global gas and oil

depletion as well as non-conventional gas and oil production. Bentley concluded that world gas supply is halfway to its peak on conventional gas which will be followed by a rapid decline in production.

Peak Oil is the point when the global energy output comes to its highest level and followed by a decrease in flow rates (Waisman et all., 2010). (Chapman, 2014) employed a general equilibrium model to review Peak Oil profiles and their macroeconomic effects. Their sensitivity test showed that date of Peak Oil depends on short-term oil prices only in the presence of high reserves. Chapman (Tsatskin & Balaban, 2008) collected opinions on Peak Oil dates and analyzed reasons for different predictions, early and late peak advocates, and reserve variations. Chapman suggested that Peak Oil should be acknowledged and new investments should be made on other energy sources. Tsatskin and Balaban (Mohr & Evans, 2009) investigated the biogenic and the abiogenic theories of oil formation.

Mohr and Evans (Patzek & Croft, 2010) developed a model that shows mineral resources production by considering supply and demand. They apply this model to coal production and concluded that the notion of coal abundancy is unjustified by estimating a production peak between 2011 and 2047 on energy basis. (Patzek & Croft, 2010) (Sorrell et all., 2010) employed multi-Hubbert cycle analysis to predict coal production. They argued that peak of global coal production is impending. More researches about fossil resource usage are shown in Table 2.1.

Table 2.1 List of Researches about Fossil Resources Usage for Energy Production.

Study Source	Research Area	Method/Data Used	Conclusion
(Bentley, 2008)	Future of the conventional natural gas supply to year 2050 by region and organization/group.		Faster depletion of gas resources in industrialized countries
(Bowden, 1985)	Rapid decline in conventional oil production, peak on conventional gas production, non-conventional oil production.		World gas supply is halfway to its peak on conventional gas
(Chapman, 2014)	Research on oil price dynamics, oil production profiles and growth trends using general equilibrium		Peak Oil depends on short- term oil prices only in the presence of high reserves
(Tsatskin & Balaban, 2008).	Evaluation on the criticality of oil peak		Peak Oil should be acknowledged/new investments should be made on other energy

(Mohr & Evans, 2009)	Peak oil from the perspective of the biogenic and abiogenic oil formation theories		
(Sorrel et all., 2010)	Global coal production based on the physical multi-cycle Hubbert analysis of historical production data (case-based).		peak of global coal production is impending
(Aguilera & Ripple, 2012)	Summary of the main findings of the UK Energy Research Centre (UKERC) study, a review about the physical depletion of conventional oil until 2030		
(Huber,2009)	Evaluation supply cost curves to assess the availability of conventional gas and oil in Europe	Variable Shape Distribution (VSD) model	Possibility of more gas and oil resources in Europe/Further decrease of production costs
(Kijima et all., 2010)	Relation between capitalist production and shift from biological to fossil energy	Investigating the capitalist production and circulation and historical background	Necessity of fossil fuel energy to capitalist social relations
(EIA,2017)	Research on theoretical models explaining environmental Kuznets curves (EKC)	Overview	Insufficient economic models to understand environment- income relationship

Importance of Renewable Energy

Unlike fossil fuels, renewable energy can regenerate and are infinite. There are five basic renewable energy sources in the world, namely biofuels, hydropower, geothermal, solar, and wind (Sherlock, 2015).

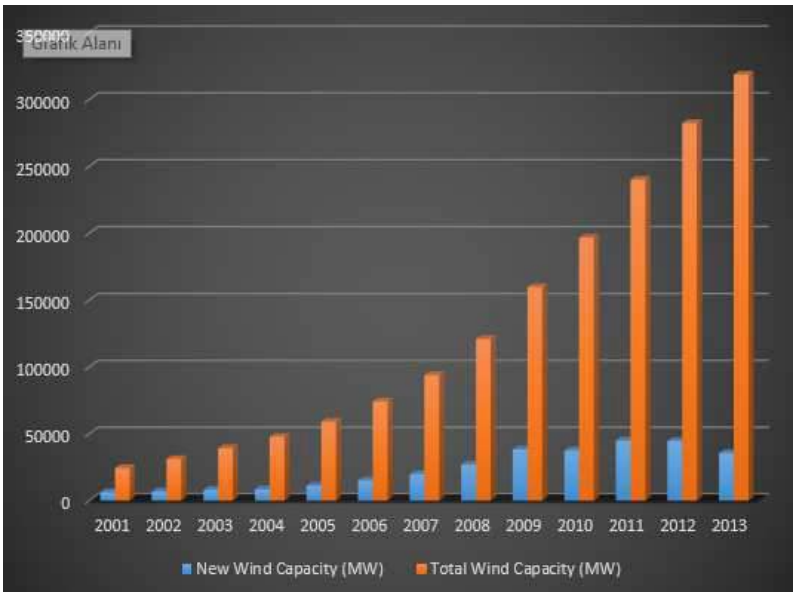

Figure 3.1 The Penetration Level of Wind Power into The Power System Over the World Has Been Increasing Very Fast. (Sources:www.wwindea.org)

Renewable energy sources play an important role in reducing greenhouse gas emissions. During the last two decades, many state governments have carried out various policies in order to reduce the amount of CO2 in the electricity sector by enhancing the access to renewable energy technologies. These policies consist of a wide variety of forms from direct subsidies, such as production tax credits which paid for each kilowatt-hour of renewable electricity produced and indirect financial incentives such as favorable tax accounting (EIA, 2018). The researchers also more concentrate on renewable energy production in recent years. Number of researches done about renewable energy in Science Direct database is plotted as in Figure 3.2.

Because wind is projected to become the predominant renewable electricity generation source in 2019, wind energy will be discussed extensively (Kaldellis et all., 2016). With the spread of the offshore type of wind turbine, the significance of the wind energy has increased because offshore types lower the environmental impact on land usage and have higher energy production due to the greater wind speed values (Andersen, 1999). In future, there is no reason why wind energy is not as the important source of energy as nuclear is (Petersen et all., 1997).

Due to the stochastic nature of the wind, the sciences of wind power prediction such as meteorology and climatology have a significant role in power generation (Li & Li, 2005). To get a stabile energy at a convenient cost in a location, the wind characteristics are examined in detail and an assessment of the wind energy have to be performed (Dıncer & Acar, 2016).

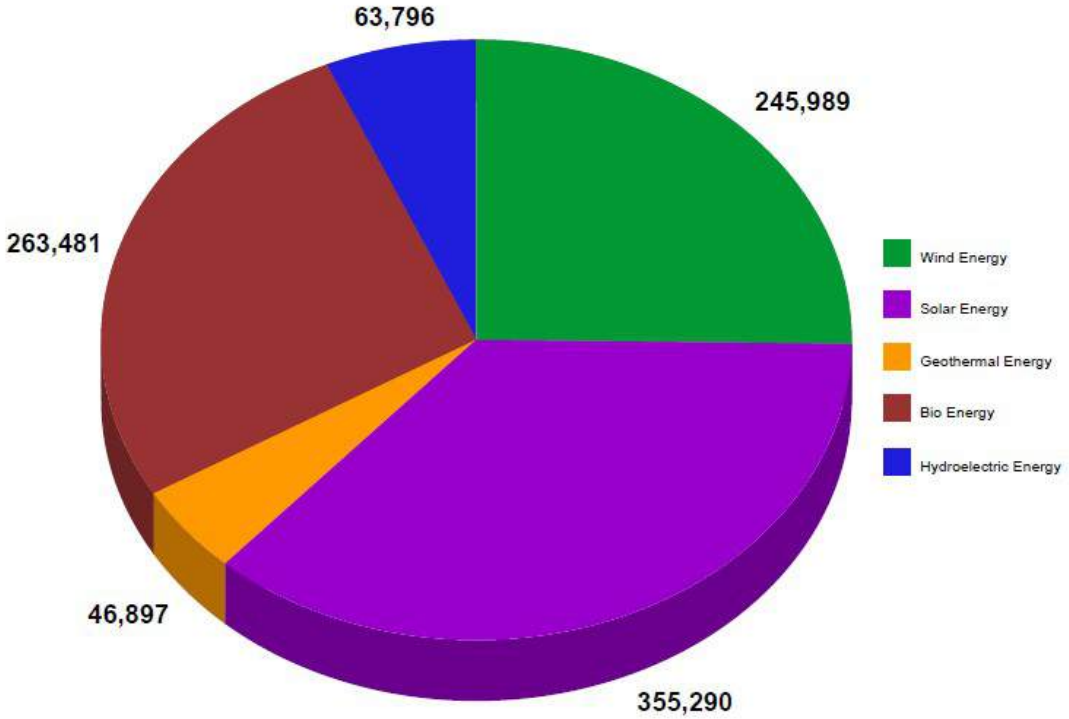

Figure 3.2 Number of Researches Done about Different Kind of Renewable Energy. (Sources:www.sciencedirect.com)

Smart Grid Technologies

The development of smart energy systems is directly related to the development of cleaner technologies and proper relationships(integration) established between traditional and smart energy systems (Dincer, 2016). In smart energy systems, it is essential to provide novel, integrated, and affordable energy storage systems for up-to-date energy carriers. This is the most basic and complex situation that should be considered (Ilhami et all., 2015).

A conventional grid consists of five major components: electricity generation plants, transmission grid, distribution grid, control center, and end-users. A detailed outlook of a smart grid infrastructure is showed in Figure 4.1. The great values of smart grid are bidirectional data communication, distributed generation, interaction through the exchange of information gathered from many sensors, interactive power electronics, and enhanced control abilities that conventional grid systems do not have (VCharge energy).

The network that transports energy frequently reaches maximum capacity. It means that green energy production is supposed to be halted for a time, so large amount of energy is being wasted. As an example of new smart grid systems, an intelligent system that is compatible with grid systems to increase the flexibility of the energy system with the help of the thermal storage devices (electric vehicles, home batteries, storage heaters). The thermal storage units are loaded at night, and they discharge the energy during the day. It makes the shifting of the energy demand from the peak periods much easier (Blumsack & Fernandez, 2012).

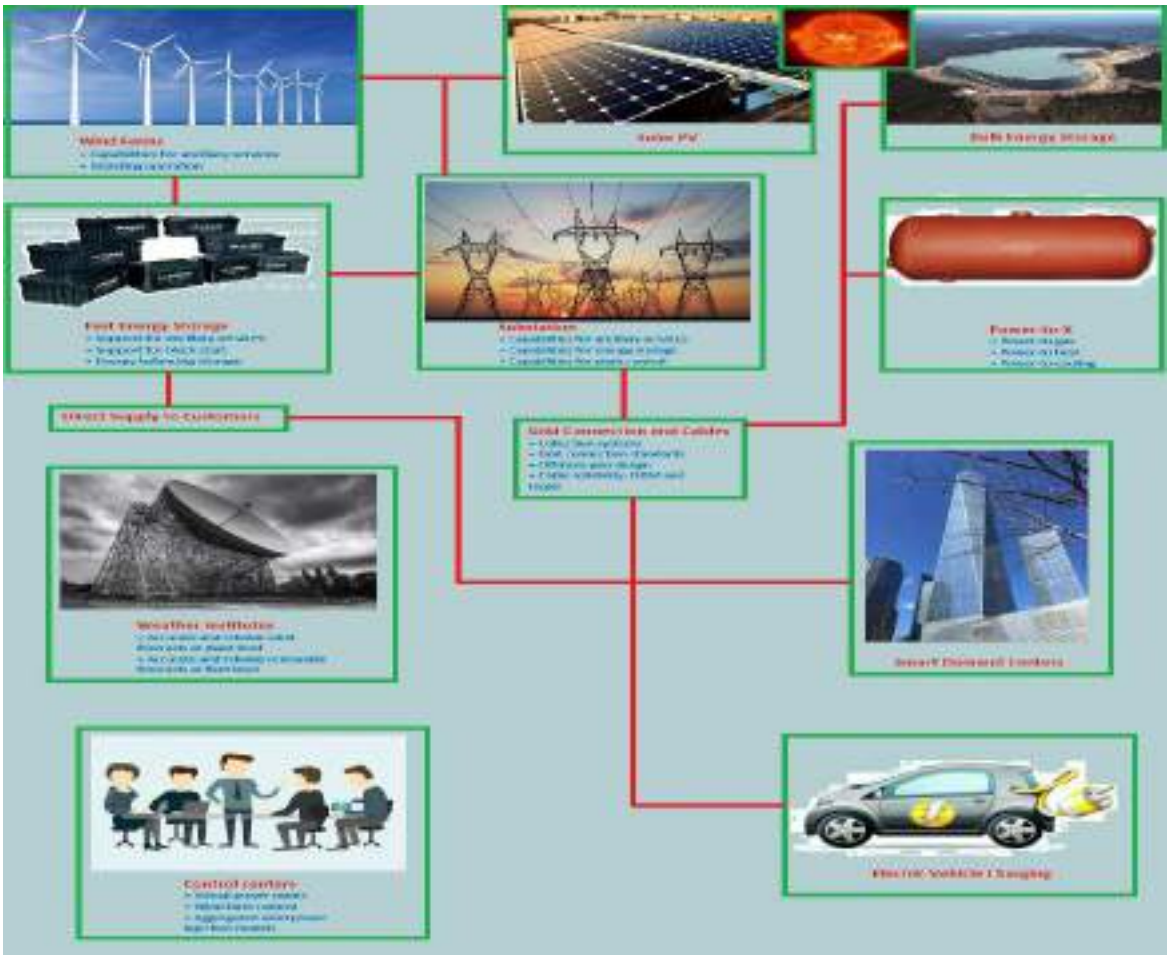

Figure 4.1 Schema of Energy Grid

One of the most well-known smart grid systems is the customer-side "smart meter." The smart meter is roughly a digital device that has the ability of recording the electric energy and providing communication between the utility and the customer. Thanks to the smart meter devices, customers will be able to see how prices change and then, reduce or shift their electricity usage (Spees & Lave, 2008). In this way, electric consumption will decrease seriously when the demand is a peak value. Further, substantial customer expense savings from load shifting could be obtained by shifting electric usage in small quantities to another time of day (Apt et all., 2007).

Another phenomenon for production or delivery of the electric power is distributed generation (DG). DG is defined as small scale production or storage that is located close to the place where the consumption takes place. In terms of efficiency, DG has superiority over the other systems with the elimination of the transportation. Large industrial establishments have been taking advantage of the system for a long time, and report considerable cost savings (S. Paul et all., 2014).

Integration of Wind Energy in Smart Grid

Wind energy play an important role in renewable energy production industry and many researchers study on. Number of studies have been done about wind energy generation is shown as graph in Figure 5.1. The integration of wind energy into the

grid for increased efficiency can increase the power output of Smart Grid Technology and we can also separate the entire system into three main divisions (Chun-Hao & Ansari, 2012). In addition to the wind turbine:
Turbine and Speed Control Box
The Wind Interface Box and
Network Connection and AC Network Transmission (Wei, 2010).
Turbine and Speed Control Box consist of Power and Speed Control devices for example; gear boxes, generator, turbine control unit, and network switches (Hashmi et all., 2011). The Wind Interface Box consists of AC and DC turbines, because the electricity generated from the wind turbine is AC. This rectified DC electricity is delivered over the DC transmission line and then supplied to the Battery Bank as a backup system for electricity use (Rebennack et all., 2009). The DC transmission line is then routed from the DC to the AC inverter to convert AC power (Kaldellis & Zafirakis, 2011). There is a check of battery charge and communication control to prevent the battery overcharge problem affecting the battery life and at the same time to prevent the overcharge first charge limit (Renewable Energy). These types of communication are made by optical fibers. The Grid Connectivity unit serves mainly inverted AC power that is directed to the three-phase power line and to the filter. This is how AC electricity generated from the wind turbine is connected to the grid (Shephard, 2014).

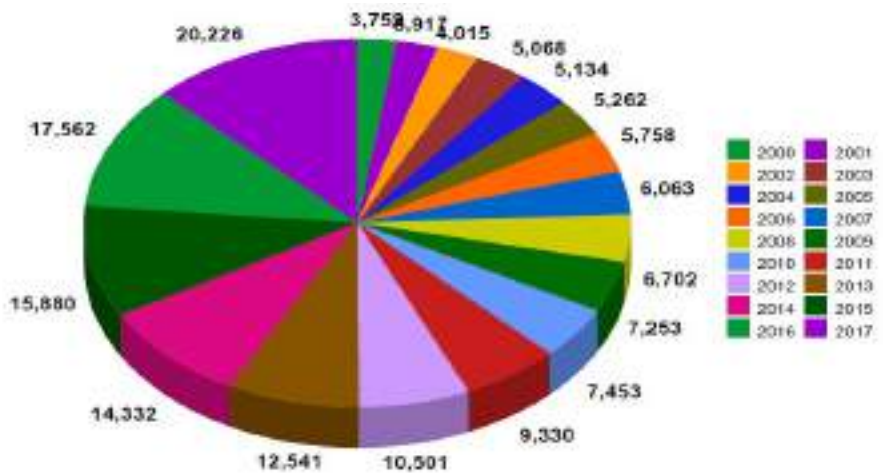

Figure 5.1 Number of researches about wind energy from 2000 to 2017 (Source:www.sciencedirect.com)

Demand for carbon-free electricity leads to a growing movement by adding renewable energy to the grid. The Renewable Portfolio Standards, authorized by the states, envisage a 20-30% penetration of renewable energy in the grid by 2020 or 2030, when considered by the federal government (Paul et all., 2014). Wind and solar energy exceed these renewable energy potential targets, indicating that renewable energy can ultimately grow beyond these initial targets. The grid faces two new and fundamental technological challenges in the renewal of renewable energy sources: location and variability. Renewable resources are concentrated in the remote center of population centers and require additional long distance, high-capacity transmission to meet

demand and supply (Gasch & Twele, 2012). Depending on the characteristics of the weather conditions, the variability of renewable materials is up to 70% for the daytime sun and up to 100% for the wind, which is now greater than the percentage of uncertainty at which the network is loaded with traditional resources as a student response.

CONCLUSION

Turkey, which have very limited primary energy sources, is largely dependent on primary energy imports. Half of Turkey's energy use is currently not oil, increased use of natural gas. While consumption of natural gas is expected to grow rapidly, 64 billion cubic meters of consumption is foreseen in 2020 (Schwartz et all., 1992). For this reason, the share of natural gas in total primary energy production is negligible. Moreover, Turkey's economic capacity of hydroelectric and thermal energy sources will be used entirely consumed until 2020 (WECTNC, 1997). Nuclear power plants are not available in Turkey. However, some new nuclear power plants are expected to be built in the five-year period . Turkey has a great potential of renewable energy sources. Solar and wind potential is especially important. Geothermal and solar energy production can be neglected when compared to biomass and hydropower. There is practically no application of wind energy. Wind energy has a great potential. In theory, Turkey has 160 TWh per year of wind potential, which is equivalent to twice the country's electricity generation in 1996. Wind energy should be emphasized and developed as a renewable energy source in the near future.

Since wind turbine technology was not able to utilize the source, significant wind energy potential has never been used before. However, during the past decade, increased knowledge of wind turbine behavior has led to more cost-effective wind turbines that are more efficient in generating electricity. It is estimated that the price of electricity generated from these wind turbines by these advanced turbines will compete with conventional power sources, including fossil fuels. Due to the increasing competitiveness of wind energy, wind energy assessment will be the basis for incorporating wind energy into the energy mix of the country. For example, in the 1992 study , maps of wind energy potential and windy areas were created for 48 adjacent states showing the distribution of these characteristics within Individual States. Wind power. The prominence of evaluating the right wind source is also recognized in other parts of the world. Detailed wind resource assessments have been considered or considered as part of a plan to increase the use of wind energy in Europe, Asia, Latin America, and other regions. The reduced cost of wind power and increased interest in renewable energy sources should ensure that the wind power becomes a viable energy source in the worldwide.

REFERENCES

Acemoglu, D., & Aghion, P.(Eds.) (2012). The environment and directed technical change. *American Economic Review 102* (1), 131–166.

Aguilera, R.F., & Ripple, R.D. (Eds.) (2012), Technological Progress and the Availability of European Oil and Gas Resources. *Application of Energy*, 96(0):387–92.

Al-Fattah, S.M., & Startzman, R.A. (2000). Forecasting World Natural Gas Supply. *J Petrol Technology*, 52; 62–72.

Andersen, P.D. (1999) Global Perspectives for Wind Power. Proceedings of the European Wind Energy Conference, 71 - 76.

Apt, J., & Blumsack, S. (Eds.) (2007) Competitive Energy Options for Pennsylvania, 95.

Barbir, F., & Veziroglu, T.N.(Eds.) (1990) Environmental Damage Due to Fossil Fuels Use. *Int. J. Hydrogen Energy*, 15(10):739–7.

Bentley, R.W. (2008). Global Oil & Gas Depletion: An Overview. *Energy Policy, 30*, 189-205.

Blumsack, S., & Fernandez, A. (2012) Energy: Ready or Not, Here Comes the Smart Grid!. *Energy, 37*; 61-68.

Bowden, G. (1985). The Social Construction of Validity in Estimates of US Crude Oil Reserves. *Social Studies of Science 15*, 207-240.

Chapman, I. (2014). The End of Peak Oil? Why This Topic is Still Relevant Despite Recent Denials. *Energy Policy, 64*, 93-101.

Chun-Hao, L., & Ansari, N. (2012) The Progressive Smart Grid System from Both Power and Communications Aspects, *IEEE Communications and Survey Tutorials*, 799-821.

Dincer, I. (2016) Greenization. *Int. J. Energy Res*, 40(15) 2035–7.

Dıncer, I., & Acar, C. (2016) Energy Smart energy systems for a sustainable future. *Applied Energy 194*;225-235.

Doha Amendment to the Kyoto Protocol, (2012). From https://unfccc.int/process/the-kyoto-protocol/the-doha-amendment

EIA, (2017) U.S. Energy Information Administration. Renewable energy explained. From https://www.eia.gov/energyexplained/?page=us_energy_home

EIA, (2018) U.S. Energy Information Administration., Electricity Generation from Fossil Fuels Declined in 2017 as Renewable Generation Rose. From https://www.eia.gov/todayinenergy/detail.php?id=35412

Fox, J., & Gohn, B. (Eds.) (2009) Smart grid technologies: Networking and Communications, Energy Management, Grid Automation, and Advanced Metering Infrastructure.

Gasch, R., & Twele, J. (2012) Wind *Power Plants; Fundamentals, Design, Construction and Operation*, Page -33

Hashmi, M., & Hanninen, S. (Eds.) (2011), Survey of Smart Grid Concepts, Architectures, and Technological Demonstrations Worldwide, ISGT Latin America

Hossain, M.S., &Madlool, N.A. (Eds.) (2016) *Role of smart grid in renewable energy* 1168-1184.

Huber, M.T. (2009) Energizing Historical Materialism: Fossil Fuels, Space and the Capitalist Mode of Production. Geoforum;40(1):105–15.

Ilhami, C., & Ersan, K. (Eds.) (2015) A Survey on the Contributions of Power Electronics to Smart Grid Systems. *Renewable and Sustainable Energy Reviews*, 47 562–579.

International Energy Agency, (2017) World Energy Outlook. Global Shifts in the energy system. From https://www.iea.org/weo2017/
Kaldellis, J.K., & Apostolou, D. (Eds.) (2016), E. Environmental and Social Footprint of Offshore Wind Energy. Comparison with Onshore Counterpart. Renew Energy;92:543–56.
Kaldellis, J. K. & Zafirakis, D., (2011) The wind energy (r) evolution: A short review of a long history. *Renevable Energy 36*, 1887-1901. from *http://citeseerx.ist.psu.edu/viewdoc/download?doi=10.1.1.472.8657&rep=rep1&type=pdf*
Kijima, M., & Nishide, K.(Eds.) (2010) Economic Models for the Environmental Kuznets Curve: A Survey J. Econ. Dyn. Control, 34(7):1187–201.
Kyoto protocol to the United Nations framework convention on climate change. (1998). From https://unfccc.int/resource/docs/convkp/kpeng.pdf
Li, M., & Li, X. (2005) Investigation of Wind Characteristics and Assessment of Wind Energy Potential for Waterloo Region, Canada. *Energy Convers Management*, 46:3014–33.
Lind, A., & Rosenberg, E. (Eds.) (2013) *Analysis of the EU Renewable Energy*, 364-377.
Mehmeti, A., & McPhail, S.J. (Eds.) (2016) *Life Cycle Sustainability of Solid Oxide Fuel Cells: From Methodological Aspects to System Implications*, 325:772–85.
Mohr, S.H., & Evans, G.M. (2009). Forecasting Coal Production Until 2100. *Fuel, 88*, 2059–2067
Patzek, T.W., & Croft, G.D. (2010). A Global Coal Production Forecast with Multi-Hubbert Cycle Analysis. *Energy 35*, 3109–22.
Paul, S., & Rabbani, Md. S. (Eds.) (2014), A Review of Smart Technology (Smart Grid) and its Features.
Paul, S., & Rahman, Md. S. (Eds.) (2014) Wind & Solar Power Systems. *International Journal of Scientific & Engineering Research*, Volume 5, Issue 11.
Petersen, E.L., & Mortensen, N.G. (Eds.) (1997) Wind Power Meteorology., Risø- I-1206(EN), 4-46.
Rebennack, S., & Iliadis, N.A.(Eds.) (2009), Electricity and CO2 Emissions System Price Modeling, IEEE Bucharest PowerTech.
Samad, T., & Annaswamy, A.M.(2011) The Impact of Control Technology. *Control for Renewable Energy and SmartGrids*, 2320 – 3765 .
Schwartz, M. N., & Elliott, D. L, (Eds.) (1992) Grldded State Maps of Wind Electric Potential.' *In Proceedings Windpower 92*, 50-58.
Shephard, D. G. (2014) *Historical Development of the Wind Mill*.
Sherlock, M. F. (2015), The Renewable Electricity Production Tax Credit, In brief; Tech. rep., Congressional Research Service.
Siano, P. (2014). Demand response and smartgrids a survey. *Renewable and Sustainable Energy Reviews*;30(0), 461– 78.
Sorrell, S., & Speirs, J. (Eds.) (2010). Global Oil Depletion: A Review of the Evidence. *Energy Policy, 38*, 5290-5295
Spees, K., & Lave, L.B. (2008) Impacts of Responsive Load in PJM: Load Shifting and Real Time Pricing. *Energy Journal*, 29:2.
Tan, Y., & Nookuea, W. (Eds.) (2016) Property Impacts on Carbon Capture and Storage (CCS) Processes, A review. *Energy Convers Manage*, 118:204–22
Tsatskin, A., & Balaban, O. (2008). Peak Oil in the Light of Oil Formation Theories. *Energy Policy, 36*, 1826-1828.

VCharge energy, Welcome to the Future of the Electric Grid. From https://www.vcharge-energy.com/

Waisman, H., & Rozenberg, J. (Eds.) (2010). Peak Oil Profiles Through the Lens of a General Equilibrium Assessment. *Energy Policy 48*, 744–753.

WECTNC, (1997) Seventh energy congress of Turkey, Energy statistics, World energy council; Turkish national committee.State planning organization (DPT) (2000), Eighth five year plan 2001–2005, Republic of Turkey, Ankara.

Wei, C. (2010) A Conceptual Framework for Smart Grid, Asia Pacific Power and Energy Engineering Conference (APPEEC). From *https://ieeexplore.ieee.org/xpl/mostRecentIssue.jsp?punumber=5447158*.

SUSTAINABILITY ASSESSMENT OF ENERGY STORAGE ALTERNATIVES THROUGH AN INTEGRATED FUZZY-BASED MCDM METHODOLOGY

Murat ÇOLAK
Kocaeli University, Department çof Industrial Engineering
colak.murat@kocaeli.edu.tr

İhsan KAYA
Yildiz Technical University, Department of Industrial Engineering
ihkaya@yildiz.edu.tr

ABSTRACT: Energy storage alternatives have been considered as critical technologies due to increasing importance of renewable energy in recent years. These technologies enable to store excess energy and to use when it is needed. On the other hand, sustainability is a significant concept for energy and energy storage technologies can be evaluated in terms of sustainability criteria defined as economic, environmental and social. At this point, fuzzy multi-criteria decision making (MCDM) methodologies can be effectively utilized to determine the most sustainable alternative among several technologies. In this paper, an integrated fuzzy MCDM methodology based on type-2 fuzzy sets and hesitant fuzzy sets (HFSs) has been proposed in order to evaluate energy storage alternatives. Not only the importance levels of criteria have been determined for energy storage, but also the alternatives including pumped hydro, compressed air, flywheel and battery have been ranked by using the proposed fuzzy-based methodology. As a result, the alternatives "compressed air" and "flywheel" have determined as the most and the least sustainable energy storage alternatives, respectively.

Key words: Energy storage, hesitant fuzzy sets, interval type-2 fuzzy sets, multi-criteria decision making, sustainability.

INTRODUCTION

Energy storage can be defined as an installation or method which is used to store energy generated in the power system and to use this energy when it is needed. Multi-criteria decision making (MCDM) is an important area of operations research and it is defined as the most common sub-section of decision making. MCDM methods are effectively utilized to evaluate many decision making problems in order to obtain useful and pragmatic solutions for these problems and they are substantially dependent to preferences of decision makers'. MCDM considers each of evaluation criteria and use analytic methods in order to realize a multi-criteria decision analysis. Alternatives are evaluated in terms of each criteria and the best one is selected by means of MCDM methods in the decision making process. MCDM methods are utilized to solve decision making problems in different fields such as energy planning, manufacturing, technology investments, and economics and management (Pohekar and Ramachandran, 2004; Hsu and Wang, 2011; Vahdani et al., 2013; Kousksou et al., 2014; Ozkan et al., 2015). Therefore, sustainability assessment of energy storage alternatives can be considered as a MCDM problem. Energy storage technologies can

be evaluated in terms of economic, environmental and social criteria and the most sustainable one among them can be selected.

The fuzzy set theory (FST) is utilized in MCDM problems as an effective tool in order to cope with uncertainties in the human decision making process. In general, there are both of qualitative and quantitative criteria which use imprecise data and human opinions in MCDM problems and therefore, fuzzy set theory developed by Zadeh in 1965 is effectively used to solve these problems. Since the classic MCDM methods are not adequate so as to handle such vagueness, fuzzy MCDM methods are more suitable tools to express imprecise data and human judgements (Ozkan et al., 2015). So, we suggested to utilize fuzzy set theory with MCDM methods in our methodology.

In this paper, a hybrid fuzzy MCDM methodology that consists of interval type-2 fuzzy AHP and hesitant fuzzy TOPSIS has been proposed to determine the most sustainable one among several energy storage alternatives. The criteria weights have been calculated via type-2 fuzzy AHP and four energy storage alternatives have been ranked through hesitant fuzzy TOPSIS method.

ENERGY STORAGE ALTERNATIVES

There are many energy storage alternatives which have different features. These technologies enable to store excess energy and to utilize when it is needed. The energy storage alternatives handling in the scope of this study have been briefly explained as follows (Schoenung, 2001; Chen et al., 2009; Chatzivasileiadi et al., 2013; Ferreira et al., 2013; Karellas and Tzouganatos, 2014; Kousksou et al., 2014; Özkan et al., 2015; Ren, 2018):

Pumped hydro energy storage (PHES)

Pumped hydro energy storage (PHES) technology is based on two water reservoirs as lower and upper. In charging position, the water is pumped from the lower reservoir to the upper reservoir. In discharging position, the water flows from the upper reservoir to the lower reservoir and rotates the turbines. By the way, mechanical energy is obtained and this energy is converted to electricity via generators. The service life of PHES technology changes between 30-50 years. Besides, while the efficiency of this technology is 65-70%, capital cost is 500-1500 Euros/kW.

Compressed air energy storage (CAES)

Compressed air energy storage (CAES) is a significant energy storage technology because of its high efficiency. This system is based on conventional gas turbine technology. The energy is stored as compressed air in an underground storage cavern. Compressed air is transformed to kinetic energy by using a set of high and low pressure turbines. Capital cost of this technology is depend on underground storage conditions and changes between $400-$800 per kW.

Battery energy storage (BES)

There are 4 main parts in a battery cell as the anode (negative electrode), the cathode (positive electrode), the electrolyte and the separators. While the anode provides electrons, the cathode accepts electrons. On the other hand, the electrolyte enables to transfer electrons between the anode and the cathode. The separators provide electrical insulation between positive and negative electrodes. As a result, the batteries store electricity as electrochemical energy.

Flywheel energy storage (FES)

Flywheel technology which is an electromechanical system enable to store kinetic energy in a rotating mass. The flywheel provides long life service opportunity as a major advantage and the efficiency of this technology is quite high with 90-95%. While limited energy storage is the main disadvantage of low speed flywheels, cost is the main disadvantage of high speed flywheels.
It is possible to handle evaluation of energy storage technologies as a MCDM problem. When the literature is analyzed it is seen that there are many MCDM studies related to this problem. Some of these studies have been briefly summarized as follows:

Barin et al. (2009), realized a MCDM study including AHP and fuzzy logic for selection among energy storage alternatives. They selected flywheel as the best alternative at the end of the study. Ak and Ağlan (2011), compared energy storage alternatives through fuzzy TOPSIS method. They evaluated pumped hydro, compressed air, flywheel, superconducting magnetic energy and battery technologies in terms of several criteria and they selected pumped hydro as the best alternative. Daim et al. (2012), suggested a MCDM methodology combining fuzzy Delphi method, analytic hierarchy process and fuzzy consistent matrix in order to evaluate energy storage technologies and they determined compressed air storage as the most suitable alternative. Özkan et al. (2015), evaluated 6 energy storage alternatives by using an integrated fuzzy MCDM model that consists of interval type-2 fuzzy AHP and interval type-2 fuzzy TOPSIS methods. They utilized type-2 fuzzy AHP so as to determine criteria weights and they applied type-2 fuzzy TOPSIS in order to rank alternative technologies. At the end of the study, they selected compressed air storage as the best alternative. Ren (2018), utilized a MCDM methodology integrating interval analytic hierarchy process (IAHP) and intuitionistic fuzzy combinative distance-based assessment (IFCODAS) methods in order to rank energy storage alternatives. In this paper, pumped hydro, compressed air, lithium-ion and flywheel technologies have been evaluated in terms of environmental, economic, technological and social criteria and their sub-criteria. Ren and Ren (2018), proposed a MCDM model in order to evaluate sustainability of energy storage technologies. They ranked pumped hydro, compressed air, lead-acid, lithium-ion and flywheel technologies by using economic, technological, environmental and performance main criteria.

THE PROPOSED FUZZY-BASED METHODOLOGY

In this section, the proposed MCDM methodology based on interval type-2 fuzzy sets and hesitant fuzzy sets (HFSs) has been briefly explained. In this context, firstly interval type-2 fuzzy sets and HFSs have been briefly introduced.

Interval type-2 fuzzy sets

Type-2 fuzzy sets were introduced by Zadeh (1975) as an extension of type-1 fuzzy sets. The membership functions of type-2 fuzzy sets are also fuzzy and this provides advantage to cope with uncertainties in the decision making process. Some basic definitions related to interval type-2 fuzzy sets which are the special form of type-2 fuzzy sets are presented as follows (Chen and Lee, 2010):

Definition 1: A type-2 fuzzy set $\tilde{\tilde{A}}$ in the universe of discourse X can be represented by a type-2 membership function $\mu_{\tilde{\tilde{A}}}$, presented as follows:

$$\tilde{\tilde{A}} = ((x,u), \mu_{\tilde{\tilde{A}}}(x,u)) \,\Big|\, \forall x \in X,\ \forall u \in J_x \subseteq 0,1\ , 0 \le \mu_{\tilde{\tilde{A}}}(x,u) \le 1 \tag{1}$$

Where Jx denotes an interval in [0, 1]. Moreover, the type-2 fuzzy set $\tilde{\tilde{A}}$ also can be represented as follows:

$$\tilde{\tilde{A}} = \int_{x \in X} \int_{u \in J_x} \mu_{\tilde{\tilde{A}}}(x,u)/(x,u) \tag{2}$$

where $J_x \subseteq [0,1]$ and $\iint$ denotes union over all admissible x and u.

Definition 2: Let $\tilde{\tilde{A}}$ be a type-2 fuzzy set in the universe of discourse X represented by a type-2 membership function $\mu_{\tilde{\tilde{A}}}$. If all $\mu_{\tilde{\tilde{A}}}(x,u) = 1$, then $\tilde{\tilde{A}}$ is called as an interval type-2 fuzzy set. An interval type-2 fuzzy set $\tilde{\tilde{A}}$ can be considered as a special case of a type-2 fuzzy set, represented as follows:

$$\tilde{\tilde{A}} = \int_{x \in X} \int_{u \in J_x} \frac{1}{(x,u)} \tag{3}$$

where $J_x \subseteq [0,1]$.

Hesitant Fuzzy Sets

Hesitant fuzzy sets (HFSs) which enable to have different membership values for membership of an element were developed by Torra (2010) as an extension of ordinary fuzzy sets. Some basic definitions with respect to HFSs have been given in the following (Torra, 2010; Xia and Xu, 2011; Liao and Xu, 2013):

Definition 1: Let X be a reference set, a hesitant fuzzy set on X is in terms of a function represented as h that when applied to X returns a subset of [0,1]. Besides, HFSs are indicated by using mathematical expression presented as follows:

$$E = \{\langle x, h_E(x)\rangle | x \in X\}$$

In this mathematical expression, hE(x) is a group of values in [0, 1] interval denoting suitable membership degrees of the element x ϵ X to the set E and hE(x) is called as a hesitant fuzzy element (HFE) (Xu and Xia, 2011).

Definition 2: Some basic operations (lower bound, upper bound, addition, multiplication, union, intersection and complement) for three HFEs h, h1 and h2 are presented in the following:

$$\text{Lower bound: } h^{-}(x) = \min h(x) \tag{4}$$

$$\text{Upper bound: } h^{+}(x) = \max h(x) \tag{5}$$

$$h_1 \oplus h_2 = \cup_{\gamma_1 \in h_1, \gamma_2 \in h_2} \{\gamma_1 + \gamma_2 - \gamma_1\gamma_2\} \tag{6}$$

$$h_1 \otimes h_2 = \cup_{\gamma_1 \in h_1, \gamma_2 \in h_2} \{\gamma_1\gamma_2\} \tag{7}$$

$$h_1 \cup h_2 = \{h \in h_1 \cup h_2 \,|\, h \geq \max(h_1^-, h_2^-)\} \tag{8}$$

$$h_1 \cap h_2 = \{h \in h_1 \cup h_2 \,|\, h \leq \min(h_1^+, h_2^+)\} \tag{9}$$

$$h^c = \cup_{\gamma \in h} \{1 - \gamma\} \tag{10}$$

Definition 3: Hesitant normalized Hamming and Euclidean distances have been presented respectively in the following equations (Xu and Xia, 2011).

$$d(h_1, h_2) = \frac{1}{l}\sum_{j=1}^{l} |h_{1\sigma(j)} - h_{2\sigma(j)}| \tag{11}$$

$$d(h_1, h_2) = \sqrt{\frac{1}{l}\sum_{j=1}^{l}\left|h_{1\sigma(j)} - h_{2\sigma(j)}\right|^2} \tag{12}$$

where l(h) represents the number of elements in the h and it is indicated as length of HFE. Generally, $l_{h_1} \neq l_{h_2}$ and the length of both HFEs is determined by means of $l = \max\{l(h_1), l(h_2)\}$ equation.

In this paper, a fuzzy-based MCDM methodology combining interval type-2 fuzzy AHP and hesitant fuzzy TOPSIS methods has been utilized in order to evaluate sustainability of energy storage technologies (Zhang and Wei, 2013; Cevik Onar et al., 2014; Kilic and Kaya, 2015; Colak and Kaya, 2017). A flowchart for the suggested methodology has been presented in Figure 1.

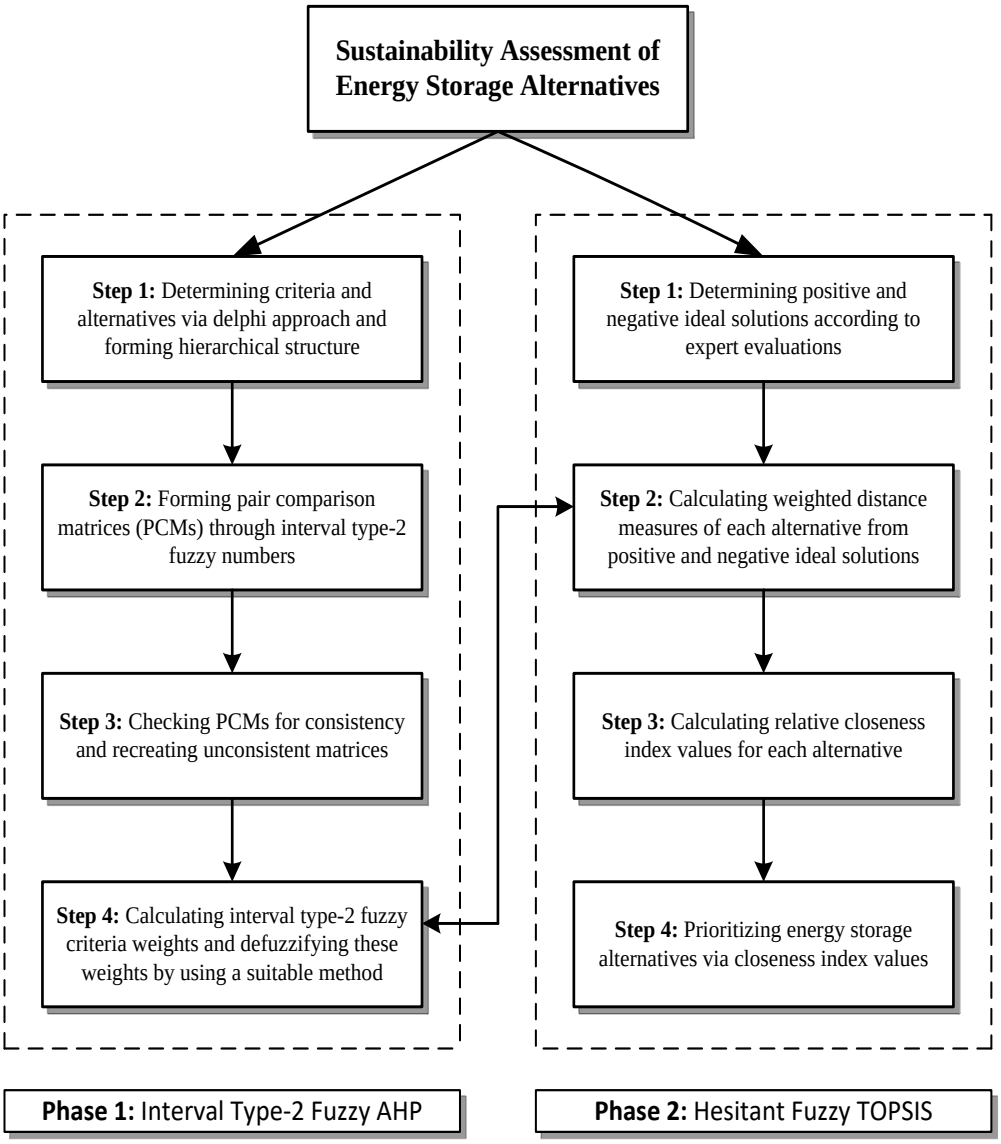

Figure 1. The Flowchart for the Proposed Methodology

CASE STUDY

In this paper, an application has been realized for sustainability assessment of energy storage technologies by using a hybrid MCDM methodology which consists of interval type-2 fuzzy AHP and hesitant fuzzy TOPSIS methods. While interval type-2 fuzzy AHP method has been utilized in order to calculate weights of criteria, hesitant fuzzy TOPSIS method has been applied for ranking alternative technologies. Initially, evaluation criteria and alternatives have been determined by means of Delphi approach, experts' ideas, and literature review. The hierarchical structure for criteria and alternatives is presented in Figure 2.

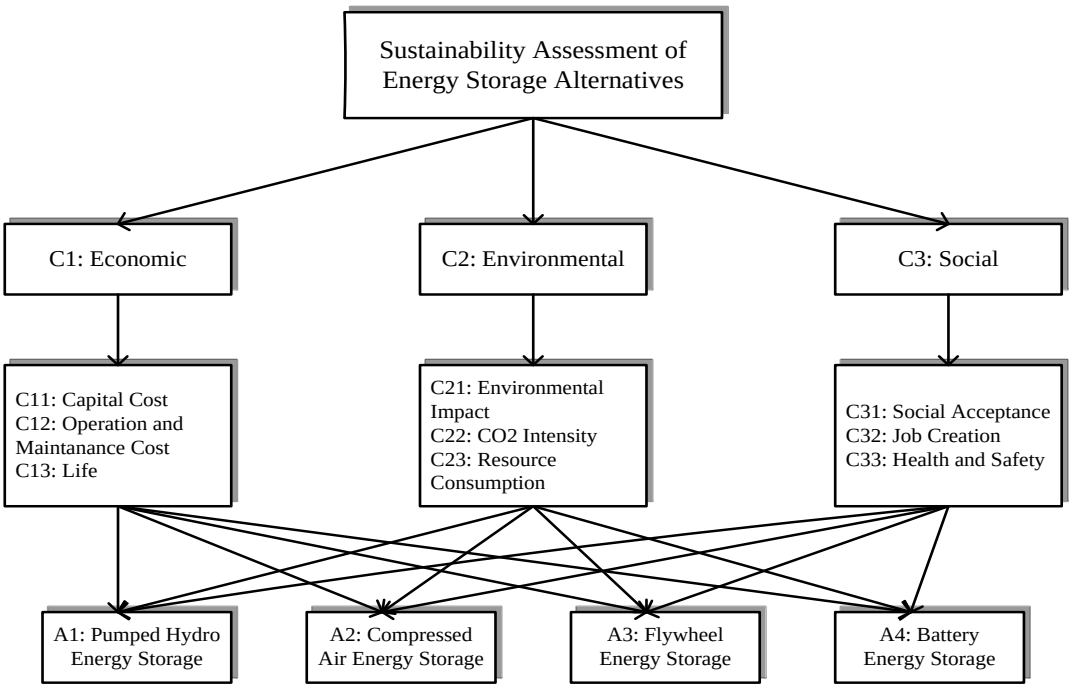

Figure 2. The Hierarchical Structure for Criteria and Alternatives

As seen in Figure 1, the weights of main criteria and sub-criteria have been calculated by using interval type-2 fuzzy AHP method. For this aim, pair comparison matrices have been formed by using evaluations of 3 decision makers. After checking consistency, the interval type-2 fuzzy weights have been calculated and crisp weights have been obtained via Center of Area (COA) method. The interval type-2 fuzzy, crisp and normalized weights for main and sub-criteria have been presented in Table 1.

Table 1. The Weights of Main and Sub-criteria

Criteria	Interval Type-2 Fuzzy Weights	Crisp Weights	Normalized Weights
C1	(0.25,0.28,0.35,0.39;1,1) (0.26,0.30,0.36,0.36;0.85,0.85)	0.318	0.3657
C11	(0.08,0.10,0.15,0.18;1,1) (0.09,0.11,0.16,0.17;0.85,0.85)	0.132	0.1718
C12	(0.05,0.06,0.08,0.10;1,1) (0.05,0.06,0.09,0.09;0.85,0.85)	0.072	0.0934
C13	(0.04,0.06,0.09,0.11;1,1) (0.05,0.06,0.09,0.10;0.85,0.85)	0.075	0.0981
C2	(0.31,0.33,0.37,0.39;1,1) (0.33,0.35,0.39,0.41;0.85,0.85)	0.360	0.4145

C21	(0.13,0.15,0.20,0.22;1,1)	(0.14,0.16,0.21,0.23;0.85,0.85)	0.179	0.2334
C22	(0.07,0.09,0.11,0.12;1,1)	(0.08,0.09,0.12,0.13;0.85,0.85)	0.102	0.1328
C23	(0.02,0.03,0.04,0.05;1,1)	(0.03,0.03,0.04,0.04;0.85,0.85)	0.035	0.0451
C3	(0.16,0.17,0.20,0.22;1,1)	(0.16,0.18,0.21,0.23;0.85,0.85)	0.191	0.2198
C31	(0.03,0.04,0.06,0.07;1,1)	(0.04,0.05,0.06,0.07;0.85,0.85)	0.052	0.0686
C32	(0.02,0.02,0.03,0.04;1,1)	(0.02,0.03,0.04,0.05;0.85,0.85)	0.032	0.0420
C33	(0.06,0.07,0.10,0.11;1,1)	(0.07,0.08,0.11,0.11;0.85,0.85)	0.088	0.1148

As seen in Table 1, the criteria "environmental" and "social" have been determined as the most and the least important main criteria with the weight of 0.4145 and 0.2198, respectively. Similarly, "environmental impact" and "job creation" have been determined as the most and the least important sub-criteria with the weight of 0.2334 and 0.0420, respectively. These criteria weights have been used to calculate weighted Euclidean distance measures in hesitant TOPSIS method. The hesitant fuzzy decision matrix has been presented in Table 2.

Table 2. Hesitant Fuzzy Decision Matrix

Alternatives	**C11**	**C12**	**C13**	**C21**	**C22**
A1	{0.6,0.7}	{0.5,0.6,0.7}	{0.5,0.6,0.9}	{0.5,0.7,0.8}	{0.4,0.5,0.7}
A2	{0.5,0.8,0.9}	{0.4,0.8}	{0.7,0.8}	{0.4,0.8}	{0.6,0.7,0.8}
A3	{0.3,0.5}	{0.5,0.6,0.7}	{0.5,0.6}	{0.5,0.6,0.7}	{0.5,0.7}
A4	{0.5,0.6,0.7}	{0.6,0.7,0.8}	{0.4,0.5}	{0.4,0.6,0.7}	{0.4,0.6}
Alternatives	**C23**	**C31**	**C32**	**C33**	
A1	{0.3,0.5,0.7}	{0.4,0.5,0.6}	{0.5,0.6}	{0.4,0.5}	
A2	{0.3,0.5,0.8}	{0.5,0.6,0.7}	{0.5,0.6,0.7}	{0.5,0.6}	
A3	{0.5,0.6,0.7}	{0.4,0.5,0.6}	{0.3,0.5,0.7}	{0.3,0.4,0.5}	
A4	{0.4,0.6,0.8}	{0.5,0.6}	{0.4,0.5,0.6}	{0.2,0.3,0.4}	

According to hesitant fuzzy decision matrix the closeness index values of each alternative have been calculated via hesitant fuzzy TOPSIS method and the energy storage alternatives have been ranked by using these values. The closeness index values for each alternative and ranking of alternatives have been presented in Table 3.

Table 3. The Closeness Index Values for Energy Storage Alternatives

Energy Storage Alternatives	**D+**	**D-**	**Ci**	**Rank**
A2: Compressed Air Energy Storage	0.204	0.331	0.619	1
A1: Pumped Hydro Energy Storage	0.229	0.265	0.537	2
A4: Battery Energy Storage	0.281	0.207	0.424	3
A3: Flywheel Energy Storage	0.283	0.199	0.413	4

As seen in Table 3, the alternatives "compressed air" and "flywheel" have been selected as the best and the worst alternatives in terms of economic, environmental and social criteria according to proposed methodology.

CONCLUSIONS

It is necessary to evaluate energy storage technologies in terms of economic, environmental and social criteria for sustainability assessment. Therefore, determination of the most sustainable energy storage alternative is exactly a MCDM problem and fuzzy MCDM methods can be effectively utilized to solve this problem. In this paper, it is aimed to determine the most sustainable one among four different energy storage alternatives by using an integrated fuzzy MCDM methodology that consists of interval type-2 fuzzy AHP and hesitant fuzzy TOPSIS methods. While the weights of evaluation criteria have been calculated via interval type-2 fuzzy AHP, four energy storage alternatives have been prioritized by means of hesitant fuzzy TOPSIS. As a result of this study, alternatives have been ranked as "compressed air", "pumped hydro", "battery" and "flywheel", respectively. As a future research suggestion, it can be said that different integrated fuzzy based MCDM methodologies based on different types of fuzzy sets can be utilized to solve this problem and the obtained results can be compared with the results of this study. On the other hand, the problem can be extended by adding new criteria and alternatives and a more comprehensive MCDM study can be realized in order to determine the most suitable energy storage alternative.

REFERENCES

Ak, R. & Aglan, C. (2011). Comparison of Energy Storage Alternatives Using Fuzzy TOPSIS Method. *World Congress on Engineering,* 6-8 July, London, U.K.

Barin, A., Canha, L. N., Rosa Abaide, A. & Magnago, K. F. (2009). Selection of Storage Energy technologies in a Power Quality Scenario – The AHP and The Fuzzy Logic. *35th annual Conference of IEEE Industrial Electronics*, 3-5 November, Porto, Portugal.

Cevik Onar, S., Oztaysi, B. & Kahraman, C. (2014). Strategic Decision Selection Using Hesitant fuzzy TOPSIS and Interval Type-2 Fuzzy AHP: A case study. *International Journal of Computational Intelligence Systems, 7,* 1002-1021.

Chatzivasileiadi, A., Ampatzi, E. & Knight, I. (2013). Characteristics of electrical energy storage technologies and their applications in buildings. *Renewable and Sustainable Energy Reviews, 25,* 814-830.

Chen, H., Cong, T. N., Yang, W., Tan, C., Li, Y. & Ding, Y. (2009). Progress in electrical energy storage system: A critical review. *Progress in Natural Science, 19(3),* 291-312.

Chen, SM. & Lee, LW. (2010). Fuzzy multi attributes group decision-making based on the interval type-2 TOPSIS method. *Expert Systems with Applications, 37,* 2790-2798.

Colak, M. & Kaya, I. (2017). Prioritization of renewable energy alternatives by using an integrated fuzzy MCDM model: A real case application for Turkey. *Renewable and Sustainable Energy Reviews, 80,* 840-853.

Daim, T. U., Li, X., Kim, J. & Simms, S. (2012). Evaluation of energy storage technologies for integration with renewable electricity: Quantifying expert opinions. *Environmental Innovation and Societal Transitions, 3,* 29-49.

Ferreira, H. L., Garde, R. & Fulli, G., Kling, W. & Lopes, J. P. (2013). Characterisation of electrical energy storage technologies. *Energy, 53,* 288-298.

Hsu, SC. & Wang, TC. (2011). Solving multi-criteria decision making with incomplete linguistic preference relations. *Expert Systems with Applications, 38(9),* 10882-10888.
Karellas, S. & Tzouganatos, N. (2014). Comparison of the performance of compressed-air and hydrogen energy storage systems: Karpathos island case study. *Renewable and Sustainable Energy Reviews, 29,* 865-882.
Kilic, M & Kaya, I. (2015). Investment project evaluation by a decision making methodology based on type-2 fuzzy sets. *Applied Soft Computing, 27,* 399-410.
Kousksou, T., Bruel, P., Jamil, A., El Rhafiki, T. & Zeraouli, Y. (2014). Energy storage: Applications and challenges. *Solar Energy Materials and Solar Cells, 120,* 59-80.
Liao, H. & Xu, Z. (2013). A VIKOR-based method for hesitant fuzzy multi-criteria decision making. *Fuzzy Optimization and Decision Making, 12,* 373-392.
Ozkan, B., Kaya, I., Cebeci, U. & Baslıgil, H. (2015). A Hybrid Multicriteria Decision Making Methodology Based on Type-2 Fuzzy Sets for Selection Among Energy Storage Alternatives. *International Journal of Computational Intelligence Systems, 8(5),* 914-927.
Pohekar, S. D. & Ramachandran, M. (2004). Application of multi-criteria decision making to sustainable energy planning - A review. *Renewable and Sustainable Energy Reviews, 8(4),* 365-381.
Ren, J. & Ren, X. (2018). Sustainability ranking of energy storage technologies under uncertainties. *Journal of Cleaner Production, 170,* 1387-1398.
Ren, J. (2018). Sustainability prioritization of energy storage technologies for promoting the development of renewable energy: A novel intuitionistic fuzzy combinative distance-based assessment approach. *Renewable Energy, 121,* 666-676.
Schoenung, S. M. (2001). Characteristics and Technologies for Long-vs. Short-Term Energy Storage, A Study by the DOE Energy Storage Systems Program, SANDIA REPORT, Unlimited Release Printed March 2001.
Torra, V. (2010). Hesitant fuzzy sets. *International Journal of Intelligent Systems, 25,* 529-539.
Vahdani, B., Tavakkoli-Moghaddam, R., Meysam Mousavi, S. & Ghodratnama, A. (2013). Soft computing based on new interval-valued fuzzy modified multi-criteria decision-making method. *Applied Soft Computing, 13(1),* 165-172.
Xia, M. & Xu, Z. (2011). Hesitant fuzzy information aggregation in decision making. *International Journal of Approximate Reasoning, 52,* 395-407.
Xu, Z. & Xia, M. (2011). Distance and similarity measures for hesitant fuzzy sets. *Information Sciences, 181,* 2128-2138.
Zadeh, L. A. (1975). The concept of a linguistic variable and its application to approximate reasoning - I, Information Sciences, 8(3), 199–249.
Zhang, N. & Wei, G. (2013). Extension of VIKOR method for decision making problem based on hesitant fuzzy set. *Applied Mathematical Modelling, 37,* 4938-4947.

PEANUT PRODUCTS USED in the FOOD INDUSTRY

Halef DİZLEK
Osmaniye Korkut Ata University, Faculty of Engineering, Department of Food Engineering, Osmaniye, Turkey
hdizlek@osmaniye.edu.tr

ABSTRACT: Peanut is an important summer plant that leguminous family, single-year and enriches the nitrogen content of soil. In the composition of peanuts; 45-55% fat, 20-25% protein, 16-18% carbohydrate, 6-8% moisture, 4-6% mineral matter, B (140-240 mg/kg) and vitamin E (83-220 mg/kg) and small amounts of vitamin C and D are also available. Peanut is a functional foodstuff and is used successfully alone or for the production of many foodstuffs. As a part of the peanut produced in our country is exported and separated as seed, almost the entire remaining portion is consumed as a snack (nut), and a very small portion is used in the production of peanut butter, in the oil industry, chocolate, confectionery and pastry. In recent years, the rise in the prices of other nuts, especially pistachio and hazelnut, in contrast, the price of peanut remains the same, has led to a significant increase in use of peanut-based products in the manufacturing industry (chocolate, confectionery and pastry). It is thought that peanut can be a good alternative to chocolate hazelnut creams for breakfast as peanut butter, it can be used with success in particularly bakery products, chocolate and confectionery sector and in the whole food industry in higher levels by processing it as semi-finished; roasted şak, flake, puree, flour, sesame and rice peanuts. It is foreseen that the added value of the by-products (flour and sesame peanut) which are low in price according to the firm (whole) peanut with a ratio of up to a quarter and therefore considered as unwanted and peanut fabrication waste, can be contributed to the national economy by increasing the added value with evaluation in different areas. In this study; peanut products used in the food industry are emphasized.

Key words: peanut, peanut products, food industry

GIDA ENDÜSTRİSİNDE KULLANILAN YERFISTIĞI ÜRÜNLERİ

ÖZET: Yerfıstığı; baklagiller familyasından yazlık, tek yıllık ve toprağın azot yönünden zenginleşmesini sağlayan önemli bir bitkidir. Yerfıstığının bileşiminde; %45-55 yağ, %20-25 protein, %16-18 karbonhidrat, %6-8 nem, %4-6 mineral madde bulunur, ayrıca B (140-240 mg/kg) ve E vitaminleri (83-220 mg/kg) ile az miktarda C ve D vitaminleri de mevcuttur. Yerfıstığı fonksiyonel bir gıda maddesi olup yalın olarak ya da birçok gıda maddesinin üretiminde başarı ile kullanılmaktadır. Ülkemizde üretilen yerfıstığının bir bölümü ihraç edildikten ve tohumluk olarak ayrıldıktan sonra kalan kısmın hemen tamamı çerez olarak tüketilir, çok az bir bölümü ise fıstık ezmesi üretiminde, yağ sanayisinde, çikolata, şekerleme ve pastacılıkta kullanılır. Son yıllarda başta antepfıstığı ve fındık olmak üzere diğer kuruyemişlerin fiyatının yükselmesi, buna karşılık yerfıstığı fiyatının aynı seyretmesi, yerfıstığı bazlı ürünlerin imalat (çikolata, şekerleme ve pastacılık) sanayinde kullanımında belirgin bir artışa yol açmıştır. Yerfıstığının ezme olarak kahvaltılarda

çikolatalı fındık kremalarına iyi bir alternatif olabileceği, yarı mamul şeklinde; kavrulmuş şak, file, püre, un, susam ve pirinç yerfıstığı olarak işlenmek suretiyle özelde unlu mamuller, çikolata ve şekerleme sektöründe, genelde ise tüm gıda sanayinde başarı ile daha yüksek düzeylerde kullanılabileceği düşünülmektedir. Fiyatı sağlam (bütün) yerfıstığına göre dörtte bire varan oranlarda düşük olan, bu nedenle fabrikasyonda istenmeyen ve yerfıstığı fabrikasyon atığı olarak kabul edilen yan ürünlerin (un ve susam yerfıstığı) farklı alanlarda değerlendirilmesi ile katma değerleri yükseltilerek ülke ekonomisine katkı sağlanabileceği öngörülmektedir. Bu çalışmada; gıda endüstrisinde kullanılan yerfıstığı ürünleri üzerinde durulmuştur.

Anahtar sözcükler: yerfıstığı, yerfıstığı ürünleri, gıda sanayi

GİRİŞ

"Fonksiyonel Gıdalar", vücudun temel besin öğeleri gereksinimini karşılamanın ötesinde insan fizyolojisi ve metabolik fonksiyonları üzerinde ilave faydalar sağlayan, böylelikle hastalıklardan korunmada ve daha sağlıklı bir yaşama kavuşmada etkinlik gösteren gıdalar veya gıda bileşenleridir (Bigliardi ve Galati, 2013; Dayısoylu ve ark., 2014). Yerfıstığı (YF) fonksiyonel bir gıda maddesi olup yalın olarak ya da birçok gıda maddesinin üretiminde başarı ile kullanılmaktadır.

Yerfıstığı; *Rosales* takımından, *Leguminosae* familyasından ve *Arachis* cinsinden tek yıllık bir bitkidir. Kültürü yapılan YF çeşitleri *Arachis hypogaea* L. türü içerisinde yer almıştır. YF; meyve kabuğu, tohum kabuğu (testa) ve tohum olmak üzere üç ana kısımdan oluşur. Yerfıstığı; baklagiller familyasından yazlık, tek yıllık ve toprağın azot yönünden zenginleşmesini sağlayan önemli bir bitkidir. Dünyada yetiştirilen başlıca yerfıstığı çeşitleri Virginia, Runner, Spanish ve Valencia'dır. Ülkemizde hemen tamamı Virginia kökenli olan (özellikle NC–7 çeşidi) yarı yatık formlu YF'ler yetiştirilmektedir. Genellikle ülkemizde üreticiler tohumlarını kendi ürünlerinden seçerek ayırdıkları için henüz standartlara uygun YF tohumu üretilememiştir. YF, içerdiği yağ oranına göre; yağlık (yağ oranı %45–60) ve çerezlik (yağ oranı %35-40) olarak tasnif edilmektedir. YF'nin bileşiminde; %45-55 yağ, %20-25 protein, %16-18 karbonhidrat, %6-8 nem, %4-6 mineral madde bulunur, ayrıca B (140-240 mg/kg) ve E vitaminleri (83-220 mg/kg) ile az miktarda C ve D vitaminleri de mevcuttur. (Arıoğlu, 1999; Gül ve ark., 2001; Dizlek ve ark., 2012). YF'nin kimyasal kompozisyonunun yaklaşık yarısının yağ olması (Fenercioğlu, 2010; Tülücü, 2010), bu ürünün yağlı tohumlar grubuna girmesinde temel etmendir.

YF'nin ülkemizde ilk defa Trakya Bölgesinde yetiştirilmeye başlandığı, daha sonra ise Ege, Akdeniz ve Güney Doğu Anadolu Bölgelerine yayıldığı tahmin edilmektedir. Türkiye'de ilk defa 1908'de Halkalı Ziraat Mektebi'nde ve 1935'de Antalya Sıcak İklim Nebatları Islah İstasyonu'nda (BATEM) denenmiştir (Kadirlioğlu, 2008). Ülkemizde YF üretimi Akdeniz Bölgesinde Adana, Osmaniye, Antalya ve Kahramanmaraş illerinde yoğunluk kazanmıştır (Çizelge 1.). Türkiye üretiminin yaklaşık %93'ünü gerçekleştiren özelde Çukurova genelde Akdeniz Bölgesinde YF, ekim nöbetine girmesi, kendinden sonra gelen bitkiye işlenmiş ve azotça zengin bir tarla bırakması

ve buğdaydan sonra ikinci ürün olarak yetiştirilebilmesi dolayısıyla büyük öneme sahiptir (Gürgen, 2004).

Çizelge 1. Ülkemizde İller Bazında Yerfıstığı Üretim Miktarı (TÜİK, 2016) (1)

	Üretim Yılı				
İller	2010	2011	2012	2013	2014
Adana	39715	34736	60764	68375	71045
Osmaniye	38996	36075	44718	42113	35164
Aydın	6120	6131	5666	5236	4847
Antalya	3269	3301	3285	3346	3496
Kahramanmaraş	5546	6684	3593	3327	3485
Şırnak	40	40	1191	2000	2000
Mersin	2073	1673	1622	1.3	0
Hatay	250	250	596	1150	925
Gaziantep	142	216	335	520	400
Muğla	623	600	421	300	331
Diğer	359	253	138	225	285
Toplam	97310	90416	122780	128265	123600

(1) Çizelgedeki değerler ton cinsinden verilmiştir.

Dünya 2014 yılı YF üretim rakamlarına göre (FAO, 2017), %37.8'lik pay ve 16.6 milyon ton üretim marjı ile Çin ilk sırada gelmektedir. Bunu 6.6 milyon ton ile Hindistan, 3.4 milyon ton ile Nijerya, 2.4 milyon ton ile Amerika Birleşik Devletleri (ABD) ve 1.8 milyon ton ile Sudan izlemektedir. Söz konusu yıla ait ülkemiz YF üretim miktarı ise sadece 123.600 tondur (Çizelge 1). Dolayısıyla mevcut durumda ülkemizin dünya YF üretim ve dış ticaretindeki payı oldukça düşüktür.

2005 yılı değerlerine göre dünyada üretilen bitkisel yağlı tohumların yaklaşık %10'unu (%9.3'ünü) YF oluşturmaktadır. 1965 ile 2005 yılları arasındaki 40 senede dünya YF üretiminde %131'lik bir artış (15.8 milyon tondan 36.5 milyon tona) kaydedilmiştir. Bu nedenle YF gelişmeye, üretim hacmi artmaya yatkın bir gıda (ham)maddesidir. İklim ve toprak özellikleri dikkate alındığında, yağlı tohumlu bitkilerin üretimi bakımından ülkemizde büyük bir potansiyelin mevcut olduğu, ancak, üretimin istenilen düzeylere çıkarılamadığı bildirilmektedir (Arıoğlu, 2007). Bu çalışmanın dolaylı olarak YF tarımının yaygınlaşmasına katkı sunacağı ve bu alanda potansiyeli mevcut olan ancak bir bakıma önemli düzeyde atıl kapasite ile çalışan ülkemizdeki boşluğun kısmen de olsa doldurulmasına yardımcı olacağı düşünülmektedir.

Osmaniye, 2010'lu yıllarda yıllık ortalama 1. ve 2. ürün toplamı olarak yaklaşık 40.000 ton üretimle, ilgili yıllarda Türkiye YF üretiminin %45'ini, veriminin %56'sını, ülkemizde üretilen YF'nin değerlendirilmesi ve pazarlanmasının ise %90'ını gerçekleştirmektedir. Osmaniye'de YF ticareti yapan 13 adedi büyük olmak üzere toplam 350 işletme bulunmaktadır. Bu işletmelerin her birinde ortalama 10 kişi istihdam edilmekte ve il genelinde bu sektörde yaklaşık 3.500 aile geçimini sağlamaktadır. Bu rakamlar göz önüne alındığında, YF üretimi ve ticareti Osmaniye'de işsizliği azaltıcı önemli bir istihdam sahası olarak önem taşımaktadır (Anonim, 2008; Dizlek ve ark., 2012).

2014 yılı verilerine göre ülkemizde YF üretimi yaklaşık 124.000 ton olup (TÜİK, 2016), bunun önemli bir bölümü çerezlik olarak tüketilmektedir (Emeksiz, 1994; Arıoğlu, 2007). Çerezlik olarak piyasaya sürülen kavrulmuş YF'nin atmosfer oksijeni ile temas etmesi durumunda ürün nemlenir ve çerezlik kalitesi önemli ölçüde sekteye uğrar. Dolayısı ile ürün albenisini yitirir. Ayrıca, ülkemizde üretilen YF'nin iç pazarda tekdüze bir tüketim alışkanlığı ile çerezlik olarak tüketilmesi (Arıoğlu, 2007), besleyici değeri (lipid [yağ], protein, mineral madde ve vitaminler bakımından zengin olan) yüksek olan bu ürünün tüketimini sınırlamaktadır. Nitekim günümüzde bireyler, aynı ürünleri sürekli olarak rutin bir biçimde tüketmemekte, farklı ürünlere yönelim göstermektedirler.

Gıda Endüstrisinde Kullanılan Yerfıstığı Ürünleri

Ülkemizde YF üretimi başlıca Adana ve Osmaniye illeriyle sınırlı kalmıştır. Üretimi yapılan YF'nin önemli bir bölümü ise çerezlik olarak tüketilmekte, gıda sanayisinde ve sanayinin diğer alanlarında yeterince kullanım alanı bulamamaktadır. Bu nedenle Türkiye, dünya YF üretiminde oldukça arka sıralarda yer almaktadır. YF'nin tarımının ve işlenmesinin genellikle aile işletmecileri tarafından küçük ölçekte yapılması bu durumu açıklamaktadır. Yine YF'nin ekiminde, hasadında ve kurutulmasında teknolojik tarım makinelerinin yeterince kullanılmaması ve hiçbir masraf gerektirmemesi nedeniyle genellikle açık alanda kurutmanın tercih edilmesine bağlı olarak ortaya çıkan aflatoksin sorunu diğer önemli nedenler olarak gösterilebilir (Eser, 2012).

Ülkemizde üretilen YF'nin bir bölümü ihraç edildikten ve tohumluk olarak ayrıldıktan sonra kalan kısmın hemen tamamı çerez (kuruyemiş) olarak tüketilir, çok az bir bölümü ise fıstık ezmesi üretiminde, yağ sanayisinde, çikolata, şekerleme ve pasta yapımında kullanılır (Emeksiz, 1994; Anonim, 2008; Fenercioğlu, 2010; Tülücü, 2010). Şekli uygun olmayan, hasat ve depolama sırasında zarar görmüş, uygun olmayan depolama koşullarında küflenmiş, doğrudan tüketime uygun olmayan YF'ler ise YF yağına işlenir. Şekil 1'de YF'nin gıda sanayisinde kullanım alanına göre sınıflandırılması gösterilmiştir. YF'nin çikolata sektöründe yaygın olarak kullanılmasının temel nedenlerinden bir tanesi, bunun fındık ve antepfıstığı ürünlerine göre fiyatlarının çok düşük olmasıdır. Fındık ve antepfıstığı işleyen çikolata ve şekerleme sanayi, 2004 yılından itibaren söz konusu hammaddelerin fiyatının çok yüksek olmasından dolayı YF'nin imalat sektöründe kullanılmasına dair AR-GE çalışmalarına başlamıştır. Bunun doğal bir yansıması olarak günümüzde YF'nin bileşiminde yer aldığı şeker ve çikolata esaslı ürün sayısının hızla arttığı gözlenmiştir.

Gıda sanayi dışında YF'nin sap ve yaprakları doğrudan hayvan yemi olarak, besin değeri bakımından zengin olan kepeği (kabuğun öğütülmüş hali) karma yem yapımında dolgu maddesi olarak ve soyulan YF zarı ise besicilikte kullanılır.

Bilindiği üzere, bitkisel yağ kaynakları içerisinde zeytinyağı diğer yağlara göre daha iyi (besleyici) bir kompozisyona sahiptir. YF yağının bitkisel yağlar içerisinde zeytinyağına en benzer yağ olduğu bildirilmiştir (Fenercioğlu, 2010). Zeytinyağı;

kendine özgü tat, koku ve aroması ile unlu mamullerde genellikle tasvip edilmeyen ağır bir lezzete sebebiyet vermesinden dolayı sınırlı bir kullanım alanına sahip iken, YF yağı daha hafif bir aromaya sahiptir. Bu nedenle YF yağının unlu mamullerin üretiminde kullanılması hem zengin bir bileşime (YF'deki doymamış yağ asitlerinin %45 ve %35'ini sırasıyla oleik ve linoleik asidin oluşturması, YF'nin elzem yağ asitlerinin önemli bir bölümünü bileşiminde bol miktarda bulundurması) sahip olmasından, hem de mamul ürün kalitesini duyusal anlamda olumsuz etkilememesinden dolayı daha pratik görülmektedir. YF yağının tadı güzel, rengi açık, görünüşü berrak olup, yüksek sıcaklık derecelerine karşı dayanıklı olduğu (dumanlanma noktasının yüksek olduğu), bileşiminde doğal halde bulunan antioksidan (tokoferol) maddelerden dolayı kızartıldıktan sonra bir süre muhafaza edilecek olan gıda maddelerinin üretiminde özellikle tercih edildiği bildirilmektedir (Fenercioğlu, 2010; Song ve ark., 2011). Ülkemizde sınırlı bir üretim ve tüketim düzeyine sahip olan YF yağının, yaklaşık 112 milyon ton olan dünya bitkisel yağ üretim pazarında önemli bir potansiyeli oluşturduğu (5.5 milyon ton) ve bitkisel yağlar içerisindeki oransal payının yaklaşık %5 düzeyinde olduğu bildirilmektedir. Dünya piyasasında YF yağının kullanım alanları şu şekilde özetlenebilir: Sıvı olarak kızartmalarda, sıvı veya margarin olarak yemeklerde, bisküvi yapımında, pastacılıkta, balık konservelerinde; düşük kaliteli YF yağları sabun vb. sanayi kollarında ve biyodizel üretiminde kullanılır (Arıoğlu, 2007).

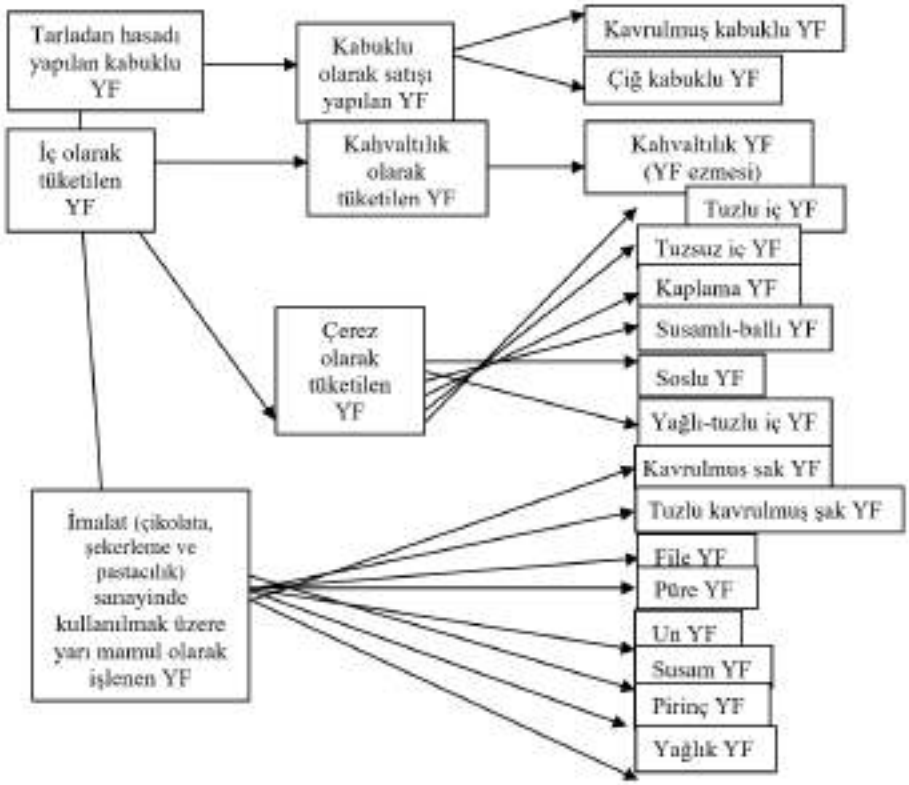

Şekil 1. Yerfıstığının Gıda Sanayinde Kullanım Alanına Göre Sınıflandırılması (İpek, 2017)

ABD'de üretilen YF'nin yaklaşık %21'i yağ sanayisinde değerlendirilmekte (Arıoğlu, 2007), önemli bir bölümü fıstık ezmesine işlenmekte (Fenercioğlu, 2010), şekerlemecilikte ve atıştırmalık gıda ürünlerinde kullanılarak (Tate ve ark., 1990) geniş bir yelpazede tüketilmektedir. Bu durum, YF'nin ülkemizdeki kullanım alanı (çerezlik) ile tezat bir yapı sergilemektedir. Bu çalışmanın planlanmasında ve ele alınmasındaki en önemli dayanaklardan birisi de budur: Maliyeti diğer yağlı tohumlara ve kuruyemişlere göre daha ucuz olan, protein, lipid, mineral madde ve vitamin gibi besin öğelerince zengin olan YF'nin farklı ürünlere işlenmesine kapı aralayarak ABD'de olduğu gibi kullanım potansiyelini artırmak ve günlük diyetlerde yer almasına katkı sunmak hedeflenmiştir. Böylece besleyici bir gıda olan YF, ülkemiz insanlarının günlük diyetlerinde daha fazla yer bulacak ve insanımızın hızlı yaşam tarzıyla birlikte tüketimi her geçen gün artan unlu mamulleri tüketirken doğal ve besleyici ürünleri de bünyelerine almalarına destek sağlanacaktır. Bu suretle ülkemizde bu alanda var olan boşluğun doldurulacağı tahmin edilmektedir. Unlu mamuller sektöründe son yıllarda başta un, susam ve pirinç YF olmak üzere püre YF'nin kullanım limiti artmıştır. Bundan dolayı söz konusu ürünlerin nasıl üretildikleri ve bünyelerinde herhangi bir katkı maddesi içermedikleri aşağıda verilen bilgiler ışığında sunulmuştur.

Püre, Un, Susam ve Pirinç Yerfıstığı Ürünlerinin Üretimi

Tohum kabuğu kırılarak elde edilen iç YF öncelikle çerezlik amaçla kullanılmaktadır. Ancak çerezlik olarak değerlendirilemeyen iç YF farklı kalibrelerde isimlendirilir: *1)* 7-10 mm arasında iriliğe sahip olan numara altı iç YF, *2)* ikiye ayrılmış olan Şak iç YF, *3)* buruşuk olan Pastalık iç YF ve *4)* hasarlı, çürük ve oksidasyondan dolayı rengi bozulan yağlık iç YF. Yukarıda belirtilen ilk 3 YF grubu, gıda sanayisinde muhtelif formlarda (şak, püre, un, susam, pirinç, yağ vb.) kullanılırken, *4)* madde imli YF biyodizel üretiminde kullanılır ve aflatoksin riskinden dolayı bunun gıda sanayisinde kullanılma potansiyeli yoktur. Çerezlik olarak kullanılamayan ve yukarıda *1)*, *2)* ve *3)* madde imleriyle belirtilen YF'ler fırınlanarak kavurma işlemine tabi tutulur. Bu işlem, 160-175 ^{o}C sıcaklıkta 30–60 d süre ile kontinü (sürekli) bir sistemde yapılır. Kavurma işlemi, 2.5 m yüksekliğinde, 1.2 m eninde ve tamamı yaklaşık 15 m uzunluğunda olan, birbiri ardına dizilmiş 3 ayrı bölümde yapılır. Her bir bölmesi yaklaşık 5 m uzunluğunda olan bu bölmelerin ilkine cehennemlik (fırının cehennemlik bölmesi) ismi verilmektedir. YF iriliğine ve içerdiği nem miktarına göre bu bölmede 5-10 d arasında (iriliği az olan YF'ler 5-6 d, iri YF'ler ise 9-10 d) bırakılır. Cehennemlikte ısıl işleme tabi tutulan YF'ler sonra dinlendirme bölmesine alınır ve burada kendi halinde bir süre bırakılır. Bu kısımda son olarak soğutma bölmesine alınan YF'ler, aspiratör desteğiyle sağlanan hava yardımı ile soğutulur. Böylece YF sıcak halde iken iç fıstıktan zor ayrılan YF zarı, soğutma işlemi ile iç fıstıktan daha kolay bir biçimde ayrılır. Kavrulan YF'ler daha sonra bir havuza tahliye edilerek burada toplanır. Sonra soyma işlemine tabi tutulur. Soyma işleminde iki kısım oluşur: tohum (bizir-tadı acıdır) ve kavrulmuş YF. Bizir, acı olduğu için gıda sanayisinde kullanılmaz. Kavrulmuş YF ise bütün halde ya da ikiye bölünmüş bir biçimde (şak fıstık) vals yüzeyi dişli olmayan, düz olan değirmenden (ezme, kırma makinesinden) geçirilerek boyutu küçültülür ve daha sonra eleme işlemine tabi tutulur. Burada amaç Pirinç iç YF elde etmektir. Çünkü Pirinç iç YF bazı pastalarda, çikolatalarda ve dondurma türlerinde süsleyici bileşen olarak kullanılır. Pirinç iç YF elde edilirken istenilmeyen fabrikasyon ürünleri de (Un ve Susam YF'ler) oluşur. Un iç YF'nin parçacık büyüklüğü 0-1 mm arasındadır. Susam iç YF'nin parçacık büyüklüğü 1-3 mm arasındadır. Pirinç iç YF ise piyasadan gelen talep doğrultusunda 3-5 mm, 3-6 mm, 4-6 mm, 4-7 mm irilikte hazırlanır. En ideal Pirinç YF boyutunun 3-5 mm olduğu bildirilmekte ve bu boyutun diğer iri boyutlara (6-7 mm) göre unlu mamullerin üretiminde kullanılmasının daha uygun olacağı düşünülmektedir. YF işleme teknolojisinde şak fıstık elde olunduktan sonra tüm bu işlemlerin yapılmasındaki esas amaç, az önce de belirtildiği gibi Pirinç YF elde etmek ve bunu şekerlemecilikte, çikolata ve pastacılıkta kullanıma arz etmektir. Ancak örneğin 3-5 mm Pirinç YF üretilirken 3 mm'den daha düşük iriliğe sahip olan kısım fire olarak değerlendirilmektedir. Benzer biçimde 4-6 mm irilikteki Pirinç YF'de ise 4 mm'den daha düşük iriliğe sahip olan kısım fire olarak ele alınmaktadır. Kalibrasyon arttıkça fire miktarının arttığı ve fire ismi ile anılan YF'lerin (Un ve Susam YF) çok ucuz bir fiyata satıldığı, YF işletmecilerinin üretim sırasında bu ürünlerin oluşmasını istemedikleri bildirilmektedir. Söz konusu YF ürünlerinin, sağlam iç YF'ye göre önemli ölçüde ekonomik değer kaybına uğradığı bilinmektedir. Püre YF ise, iç YF'nin 160-175 ^{0}C sıcaklıkta, 5-10 d süre ile kavurma işlemine tabi tutulması, takiben zarının soyulması ve püre makinesine beslenmesi suretiyle elde edilmektedir.

Konu üzerinde yapılan bir çalışmada (İpek, 2017; İpek ve Dizlek, 2018), kek üretiminde YF 4 farklı formda (Püre YF [YF tahini], Un YF [YF unu; parçacık boyutu 0-1 mm

arasında], Susam YF [susam iç YF; parçacık boyutu 1-3 mm arasında] ve Pirinç YF [pirinç iç YF; parçacık boyutu 3-5 mm arasında]) kullanılmıştır (Şekil 2.). Araştırıcılar, ilk olarak kullanılan YF formlarının (püre, un, susam ve pirinç) ve oranlarının (kek hamur ağırlığına göre %0, %7.5, %15, %22.5 ve %30) pandispanya nitelikleri üzerine, elde edilen veriler ışığında uygun YF formları (püre ve susam) ve oranları (%7.5, %15 ve %22.5) tercih edilerek bu etmenlerin sanayi tipi kek (top kek) nitelikleri üzerine etkilerini araştırmışlardır. Böylece katkı maddesiz ve doğal YF formlarını içeren kek üretimini gerçekleştirmeye çalışmışlar, üretilen keklerin yapısal ve tekstürel özelliklerini de kapsayan analitik nitelikleri ve duyusal özelliklerini saptamışlardır. Araştırma sonucunda; farklı formlarda ve oranlarda YF kullanımının pandispanya ve top kek niteliklerini etkilediği, pandispanya üretiminde mamul ürün nitelikleri bakımından en ideal ve en olumsuz YF formlarının sırası ile püre ve pirinç YF olduğu, YF parçacık büyüklüğünün artmasına koşut olarak pandispanya niteliklerinin genellikle gerilediği tespit edilmiştir. Pandispanya üretiminde belirli bir düzeye (%15) kadar YF kullanımının kek niteliklerinde sınırlı ölçüde, %22.5 ve üzerinde YF kullanılması durumunda ise ürün niteliklerinde belirgin gerilemelerin ortaya çıktığı, %7.5 ve %15 düzeylerinde püre ve susam YF kullanılarak beğenilir nitelikte, üstün kalitede top kek üretilebileceği ve bu ürünlerin gıda sanayisine sunulabileceği kanısına varılmıştır. Araştırmanın pandispanya ve top kek ayağından elde edilen veriler bir arada incelendiğinde, YF türevlerinin kek formülüne başarı ile adapte edilebildiği ve bunların duyusal olarak kek niteliklerini geriletmediği hatta kekte hoşa giden güzel bir lezzet ve aroma oluşturdukları ve YF'li keklerin çeşnili kek olarak piyasaya arz edilebilecekleri kanısına varılmıştır.

Püre YF Un YF Susam YF Pirinç YF

Püre YF Un YF Susam YF Pirinç YF

Şekil 2. Çikolata, Şekerlemecilik ve Pastacılıkta Kullanılan Farklı Yerfıstığı Formları (İpek, 2017; İpek ve Dizlek, 2018)

Araştırıcılar, çalışmalarında, besleyici özelliği yüksek olan doğal YF ürünlerini kek formülüne monte ederek yeni bir kek formülünün optimize edilmesini hedeflemiş, böylece bu alanda sektörde yer alan ürün çeşitliliğine bir halka ekleyerek yeni ürün geliştirilebileceğini öngörmüşlerdir. Ayrıca, aşağıdaki kanılara varmışlardır: "Ülkemizde daha çok çerezlik amaçla kullanılan ve salt bu nedenle pazarlanmasında zaman zaman darboğazların oluştuğu YF'ye, çerezlik dışında alternatif kullanım alanları oluşturulmuştur. Bu konuda YF'nin pilot uygulama sahası olarak kek, ana uygulama sahası olarak ise unlu mamuller alanında daha geniş düzeylerde kullanılmasının önü açılmıştır. Böylece genelde tarıma özelde ise YF'ye dayalı sanayi ile geçimini sağlayan Osmaniye çiftçisi ve tüccarına ürünlerini pazarlama konusunda yeni bir saha açılmıştır. Yürütülen çalışma ile Osmaniye'nin başlıca tarımsal ürünü olan YF'nin farklı kulvarlarda işlenmesine kapı aralanmış, uzun vadede ilin ekonomisine katkı sağlanmış, ürünün pazarlanmasında karşılaşılan sorunların kısmen de olsa aşılmasına destek sunulmuştur. YF'li kekin endüstriyel olarak üretimine ışık tutacak araştırma bulgularının, ürün üzerinden Osmaniye'nin tanıtımına katkı sunacağı, ayrıca yeni bir lezzet-damak tadının ortaya çıkmasına doğrudan etki edeceği düşünülmektedir. Yine YF sektöründe, Susam ve Un YF'ler Pirinç YF üretiminde istenmeyen ara ürünler olarak ortaya çıkmakta ve gıda sanayisinde sınırlı bir kullanım alanı bulmaktadır. Söz konusu YF'ler, sağlam iç YF'ye göre daha düşük ekonomik değere sahiptir. Böylece, bir taraftan fabrikasyonda istenmeyen ve YF fabrikasyon atığı olarak kabul edilen yan ürünlerin (Un ve Susam YF) farklı bir alanda değerlendirilmesi ile katma değerleri yükseltilerek ülke ekonomisine katkı sağlanmıştır. Unlu mamuller sektöründe sadece süsleme amacıyla bazı unlu mamullerin üst yüzeylerine eklenerek kullanılan Pirinç YF, süsleme-dolgu maddesi olmaktan öte kek formülünde miktar olarak da önemli düzeyde yer alan bir bileşen olarak kullanılabilecektir. Çünkü YF'nin yağ içeriğinin yüksek olması, kek formülünde kullanılacak nebati yağın diğer bitkisel kaynaklardan karşılanması yerine kısmen ya da tamamen YF'den tahsis edilmesi ile karşılanacak, bu açıdan YF'li kekte YF lezzet ve çeşni sağlamasının yanı sıra kitle oluşturucu bileşen olarak da görev yapacaktır. Bu durum YF'nin daha yüksek düzeylerde kullanımına olanak sağlayacaktır. Benzeri durum denemede kullanılan diğer YF ürünleri (Püre, Un ve Susam YF) için de geçerli olacaktır. Özellikle küçük yaştaki çocukların kek vb. ürünleri yaygın bir biçimde tükettikleri göz önüne alındığında, onlara katkı maddesi içermeyen sağlıklı ve daha besleyici bir ürün alternatifi sunulmuştur. Yapısında kanser vb. hastalıkları kronik yolla tetikleyici bir katkı maddesi içermediğinden sağlık dostu bir ürün geliştirilmiştir."

SONUÇ VE ÖNERİLER

Yerfıstığı bitkisi; ekim nöbetine girmesi, kendinden sonra gelen bitkiye işlenmiş ve azotça zengin bir tarla bırakması ve buğdaydan sonra ikinci ürün olarak yetiştirilebilmesi dolayısıyla büyük öneme sahiptir. Zengin ve besleyici bir kimyasal kompozisyona sahip olan YF, gıda sanayinde muhtelif amaçlarla kullanılabilme potansiyeline sahiptir. Bununla beraber ülkemizde daha çok çerez olarak tüketilir, çok az bir bölümü ise fıstık ezmesi üretiminde, yağ sanayisinde, çikolata, şekerleme ve

pasta yapımında kullanılır. Şekli uygun olmayan, hasat ve depolama sırasında zarar görmüş, uygun olmayan depolama koşullarında küflenmiş, doğrudan tüketime uygun olmayan YF'ler ise yağa işlenir.

YF'nin ezme olarak kahvaltılarda çikolatalı fındık kremalarına iyi bir alternatif olabileceği, yarı mamul şeklinde; kavrulmuş şak YF, file YF, püre YF, un YF, susam YF ve pirinç YF olarak işlenmek suretiyle özelde unlu mamuller, çikolata ve şekerleme sektöründe, genelde ise tüm gıda sanayinde başarı ile daha yüksek düzeylerde kullanılabileceği düşünülmektedir. Nitekim YF, fındık ve antepfıstığı gibi ürünlere iyi bir alternatif olup, anılan ürünlere göre birim maliyeti çok daha düşüktür. Fiyatı sağlam (bütün) YF'ye göre dörtte bire varan oranlarda düşük olan, bu nedenle fabrikasyonda istenmeyen ve YF fabrikasyon atığı olarak kabul edilen yan ürünlerin (un ve susam YF) farklı alanlarda değerlendirilmesi ile katma değerleri yükseltilerek ülke ekonomisine katkı sağlanabileceği öngörülmektedir.

Başta Adana ve bunu takiben Osmaniye'de önemli bir potansiyele sahip olan (bu iki il ülkemiz YF üretiminin sırasıyla %57 ve %29'unu, toplamda ise yaklaşık %86'sını gerçekleştirmektedir, TÜİK, 2016) ve daha çok çerezlik olarak tüketilen YF'nin, özelde unlu mamullerin genelde ise diğer tüm gıdaların formülasyonunda daha fazla kullanılarak kullanım sahasının genişletilmesi, böylece tüketim yelpazesinin genişletilememesinden ötürü zaman zaman piyasaya arz/talebinde ciddi sıkıntılar yaşanan YF'nin daha farklı şekilde kullanılmasına olanak tanınmasının yararlı olacağı düşünülmektedir.

KAYNAKLAR

Anonim. (2008). *Osmaniye kaleler şehri*. Seçil Ofset, Osmaniye.
Arıoğlu, H. (1999). *Yer fıstığı, yağ bitkileri yetiştirme ve ıslahı*. Çukurova Üniversitesi Basımevi, Adana.
Arıoğlu, H. (2007). *Yer fıstığının Türkiye ve Osmaniye ekonomisi açısından önemi ve yerfıstığı üretimini artırabilmek için alınması gerekli önlemler.* Osmaniye Ticaret Borsası Yayını, Osmaniye.
Bigliardi, B., & Galati, F. (2013). Innovation trends in the food industry: the case of functional foods. *Trends in Food Science and Technology*, *31*(2), 118-129.
Dayısoylu, K. S., Gezginç, Y., & Cingöz, A. (2014). Fonksiyonel gıda mı, fonksiyonel bileşen mi? gıdalarda fonksiyonellik. *Gıda Dergisi, 39*(1), 57-62.
Dizlek, H., Duman, A. D., & Tenekeci, O. (2012). Yerfıstığı ve Osmaniye'nin yerfıstığı potansiyeli. Türkiye 11. Gıda Kongresi. Bildiri Kitabı: 134. 10-12 Ekim 2012, Hatay.
Emeksiz, F. (1994). Adana ilinde yerfıstığı üretilen işletmelerin üretimle ilgili bazı yapısal özellikleri. *Çukurova Üniversitesi Ziraat Fakültesi Dergisi, 9*(2), 17-32.
Eser, E. (2012). Uzak infrared (fır) ışınlarının işlenmemiş iç yer fıstığının fiziksel, kimyasal ve mikrobiyolojik kalitesine etkisi. Mersin Üniversitesi Fen Bilimleri Enstitüsü Gıda Mühendisliği Anabilim Dalı Yüksek Lisans Tezi, Mersin.
FAO. (2017). Statistical databases. http://www.fao.org/faostat/en/#data/QC (Erişim Tarihi: 27.07.2017).
Fenercioğlu, H. (2010). *Yer fıstığının beslenme ve gıda endüstrisindeki önemi*. Osmaniye Ticaret Borsası, Osmaniye.

Gül, A., Arıoğlu, H., Tülücü, K., Biçici, M., Özgür, F., & Fenercioğlu, H. (2001). Osmaniye'nin simgesi: yerfıstığı ekonomisi, üretim tekniği, hastalık ve zararlıları, gıda sanayi açısından önemi. 1. Osmaniye Fıstık Festivali Etkinlikleri, Osmaniye Gazeteciler Cemiyeti Kültür Yayını, Sayı 1.

Gürgen, Y. (2004). *Tarımsal yayım, haberleşme araştırma ve uygulama merkezi çiftçi broşürü*.

İpek, E. (2017). Farklı form ve oranlarda yerfıstığı ürünleri kullanılarak ev ve sanayi tipi kek üretiminin optimizasyonu. Osmaniye Korkut Ata Üniversitesi Fen Bilimleri Enstitüsü Gıda Mühendisliği Anabilim Dalı Yüksek Lisans Tezi, Osmaniye.

İpek, T., & Dizlek, H. (2018). Farklı form ve oranlarda yerfıstığı ürünleri kullanılmasının top kek kalitesine etkisi. *Gıda Dergisi*, *43*(4), 591-604. doi: 10.15237/gida.GD18027

Kadiroğlu, A. (2008). *Yerfıstığı yetiştiriciliği*. Batı Akdeniz Tarımsal Araştırma Enstitüsü Müdürlüğü, Antalya.

Song, Y., Du, B., Zhou, T., Han, B., Yu, F., Yang, R., Hu, X., Ni, Y., & Li, Q. (2011). Optimization of extraction process by response surface methodology and preliminary structural analysis of polysaccharides from defatted peanut (*Arachis hypogaea*) cakes. *Carbohydrate Research, 346*, 305-310.

Tate, P. V., Chavan, J. K., Patil, P. B., & Kadam, S. S. (1990). Processing of commercial peanut cake into food-grade meal and its utilization in preparation of cookies. *Plant Foods and Human Nutrition, 40*, 115-121.

TÜİK. (2016). Türkiye İstatistik Kurumu, 2005-2014 yılları imalat sanayi üretim, satış, miktar, değer ve girişim sayıları. http://www.tuik.gov.tr/PreIstatistikTablo.do?istab_id=773 (Erişim Tarihi: 15.10.2016).

Tülücü, K. (2010). *Yerfıstığı üretimi*. Osmaniye Ticaret Borsası Yayını, Osmaniye.

IMAGE PROCESSING METHODS AND POROSITY MEASUREMENTS IN REEF-ROCKS

Mehmet OĞUZCAN
Iskenderun Technical University, Institute of Engineering and Science, 31200, Iskenderun-Hatay, Turkey mehmetoguzcan01@hotmail.com

Meryem YEŞİLOT KAPLAN
Iskenderun Technical University, Faculty of Engineering and Natural Science, Dept. of Petroleum&Natural Gas Engineering 31200-Iskenderun-Hatay-TURKIYE
meryemkaplan@gmail.com

ABSTRACT: The porosity is the most important parameter in oil exploration and production phases. Porosity occurs in reef and clastic rocks containing fluid and porosity values are the primary parameter measured in reservoir rock definitions. Porosity is observed in two types as primary and secondary. The primary porosity occurs during diagenesisand the secondary porosity occurs after diagenesis.

Although the porosity types vary depending on forming, the porosity in the rocks with high permeability can contain enough oil. Porosity measurements can be made by logging during laboratory experiments. Two dimensional porosity measurements can be made by petrographic imaging. Images obtained by optical microscopy and SEM (Scanning Electron Microscopy) are obtained from two dimensional porosity images and numerical results can be calculated with various imaging processing methods.

3D imaging can be performed with Micro-CT method in recent years. This method can be used in porosity measurements of reservoir rocks and give information about micro porosity. It is important to calculate the porosity values of the Horu formation around İskenderun (HATAY) in determining the quality of petroleum reservoir rock. There are four main reef groups in Horu formation **Geçersiz kaynak belirtildi.**.These are: (1) Massive reef cores, (2) Reef blocks, rubbles and breccias, (3) Bedded reef flanks and (4) Coral carpets and patches**Geçersiz kaynak belirtildi.**. The porosity values in the reef region were measured at an average of 15%.

Keywords: porosity, SEM, Micro-CT, 3D imaging

INTRODUCTION

Porosity is known as the ratio of the pore volume of a rock to the total rock volume. Porosity measurements in rocks are estimated by laboratory and logging methods. Porosity calculations can be made from images that petrographically obtained in recently. Petrographic data can be obtained by microscope images or SEM (Scanning Electron Microscope) images. In the microscope images, the porosity calculations can be used in sandstones and limestones and In the SEM images micro cracks and micro porosities can be observedin the SEM images . Data obtainment of images are called image processing methods. Image processing methods with porosity calculations give accurate as results and provide data in a cheaper and shorter time than other methods.

Porosity measurement can be performed with many imaging methods. Image analysis can be estimated with Micro-CT and image processing and SEM in previous studies.

MATERIAL AND METHODS

Reef rocks, which are of great importance in petroleum exploration are composed of algae, coral organisms, such as spongy organisms. Reef rocks, that develop in shallow waters, form a large amount of hydrocarbon because of the sedimentation of microorganisms. The majority of the reef rocks occur during the period of the Mesozoic, and these formations in Turkey occur in a shallow marine environment, Petrographic images of Horu formation (İskenderun-Osmaniye/HATAY) as reef rock were used for porosity measurements. (Figure 1).

Micro-CT methods, SEM (Scanning Electron Microscopy), and image processing can be used as estimating methods with logging in reef rocks. These images evaluated porosity in three dimensions or two dimensions to determine the petrographic properties of the rock.

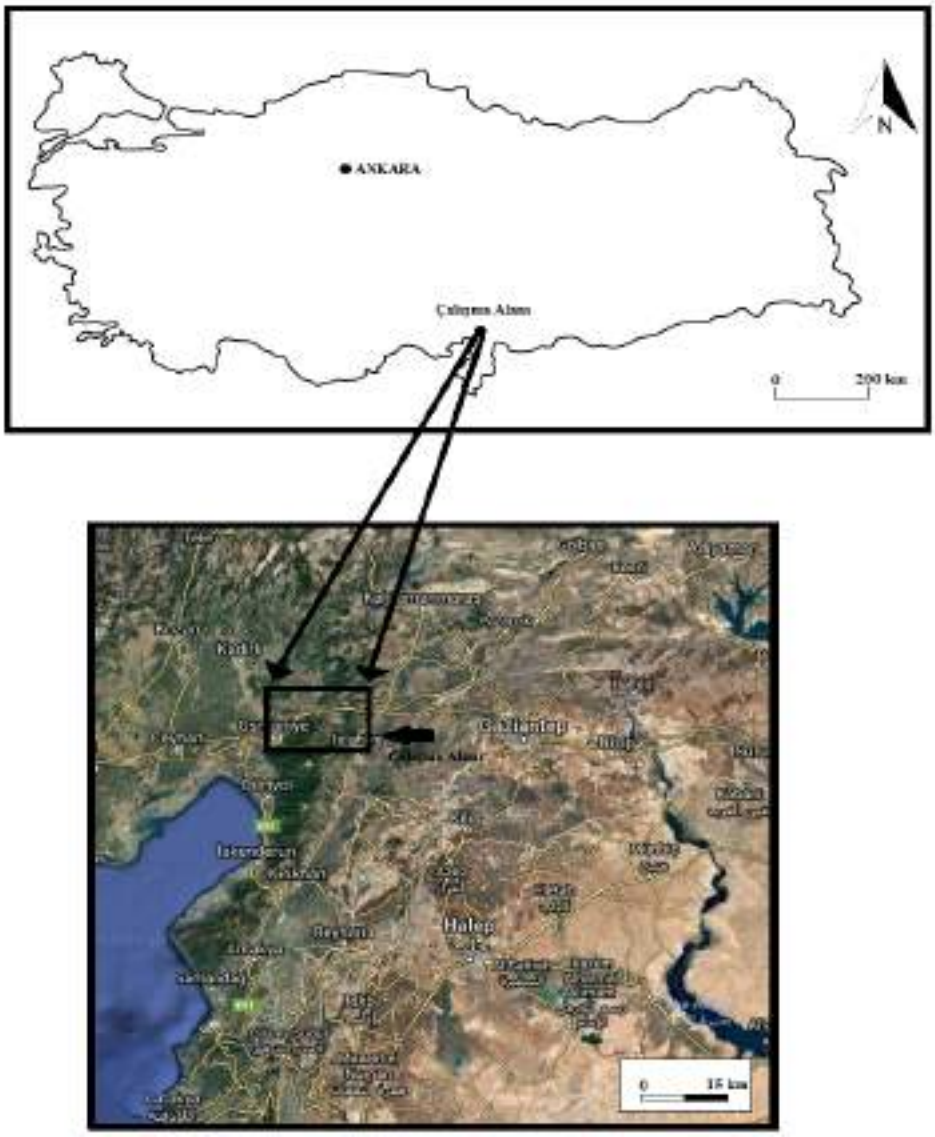

Figure 1. Location map of study area

IMAGE PROCESSING METHODS

Preparation of the image algorithm with the computer requires professional experience. There are different computer programs and algorithms used for this purpose and one of them is “ImageJ” program . This program offers calculating the morphology and texture properties on the image via using each parameter of the systematic command system. Calculations of the ImageJ program are calibrated and results are accepted. "ImageJ" program may be useful different branches of science.

SEM (Scanning Electron Microscope)

SEM microscope is defined as the method of obtaining images by scanning the surface of the sample with electron beam.. SEM imaging method that black and white image is usually obtained, is a efficient method to measure the average pore size and it can

be described as a perfect method for determining the porosity of porous silicon (PSi) layers containing image processing of the top view SEM micrographs. The processing program can measure the total area of the pores and calculate its proportion to the total scanned area. In cases where the pores are longitudinal, uniform and non-branched, as evident from crosssection images, it is assumed that it represents also the ratio between the total volume of the pores to the volume of the entire layer, which defines the porosity of the layer. Our results are in good agreement with the literature values that were obtained by two physical methods.

Porosity is a variable parameter with the presence of fine grained rocks such as shale and the shale has very low permeability that controls fluid flow and migration. Therefore, if digital imaging is performed under SEM microscope, the determination of the connected and closed pore network, the porosity and permeability of the rocks and the calculations required for their evaluation is necessary. . Using the Scanning Electron Microscope (SEM), the rock is screened pore, throat and mineral particles And morphological operators and a specialized disc structure element are combined to scan the rock and efficiently disassemble porosity and porosity passes and predict the porosity of shales. This shows that SEM can also work efficiently in shales.

Micro-CT Method

Computerized micro-CT imaging with X-ray is a technique that analyzes the internal structure of the objects by the difference in density. This is a non-destructive test, reef rock ensures that samples are evaluated while maintaining their integrity. The biggest advantage of micro-CT compared to other destructive techniques is that it performs three-dimensional imaging and produces numerical results. Although the chemical composition of the rock is not directly accessible, image acquisition is based on the absorption coefficient of the X-ray passing through the sample, depending on the energy, density and atomic number value. Micro-CT reconstruction separates data into two-dimensional sections. It produces three-dimensional gray level imaging by allowing access to any area of the object.

The presence of flow simulation of a porous structure depends largely on the modeling of petrographic characterization and the modeling of reservoir rocks. Mineral phase segmentation and pore network modeling are very important steps in Micro-CT based rock modeling. The success of pore network model (PNM) predicting petrophysical properties is based on image segmentation, image resolution and most importantly on rock structure (homogeneous, complex or micro porous) properties. Pore network modeling has achieved extensive research and development over the past decade, but the application of these models to various heterogeneous reservoir rocks is still a challenging task.

The internal structure of the rock sample taken with this type of tomography method can be observed non-destructive without any damage. The Rock has preserved its integrity. Because the object is drawn from a single plane, the data at hand is drawn in two dimensions. Scans taken from different angles can be observed in three dimensions.

Received data may present different data, such as the porosity of the rock, as well as its petrophysical structure. (Teles and Lopes, 2016) the analysed sample provides information on hydrocarbon retention, capacity and suitability for oil exploration. In addition, Micro-CT is a technology that uses computer-generated X-rays to produce tomography images (virtual slices) of certain areas of the object scanned by X-ray and enables the user to receive insider information. Completes the process without interrupting the object. Compared to conventional methods such as optical or scanning electron (SEM) microscopy, Micro CT Scan is used in continuous and uninterrupted scanning and crack development studies.

X-ray tomography has been used in different areas for over 40 years and has reached an even more advanced level in the last 10 years. The image processing method, such as porosity on rocks has recently been used.

POROSITY MEASUREMENTS

Porosity measurements of Horu formation was calculated on petrographic image of the core of the reef (Figure 2a). The stages in the calculation of the porosity distirubition on the images are as follows.

Image/Adjust/Brightness/Contrast command, is used making the image to 8-bit format (Image/Type/8-bit; Figure 2b). Image consists of different grayscale values in 8-bit grayscale images. Grey value ranges are expressed as G = {0, 1, 2, ... 255}. The Image/Adjust/ Threshold usually used to create a binary image from a grayscale image (Figure 2c). This command can also be used with color images. Image from gray colour to binary form, while brightness values of above the threshold value is 255, brightness values of below the threshold value is 0. Thus, the image brightness value consists of only two values

The Analyze/Set Measurements command can then be opened, which will open a list of possible measurement criteria. For measurement porosity distiribution percentance, "Area Fraction" must be selected.

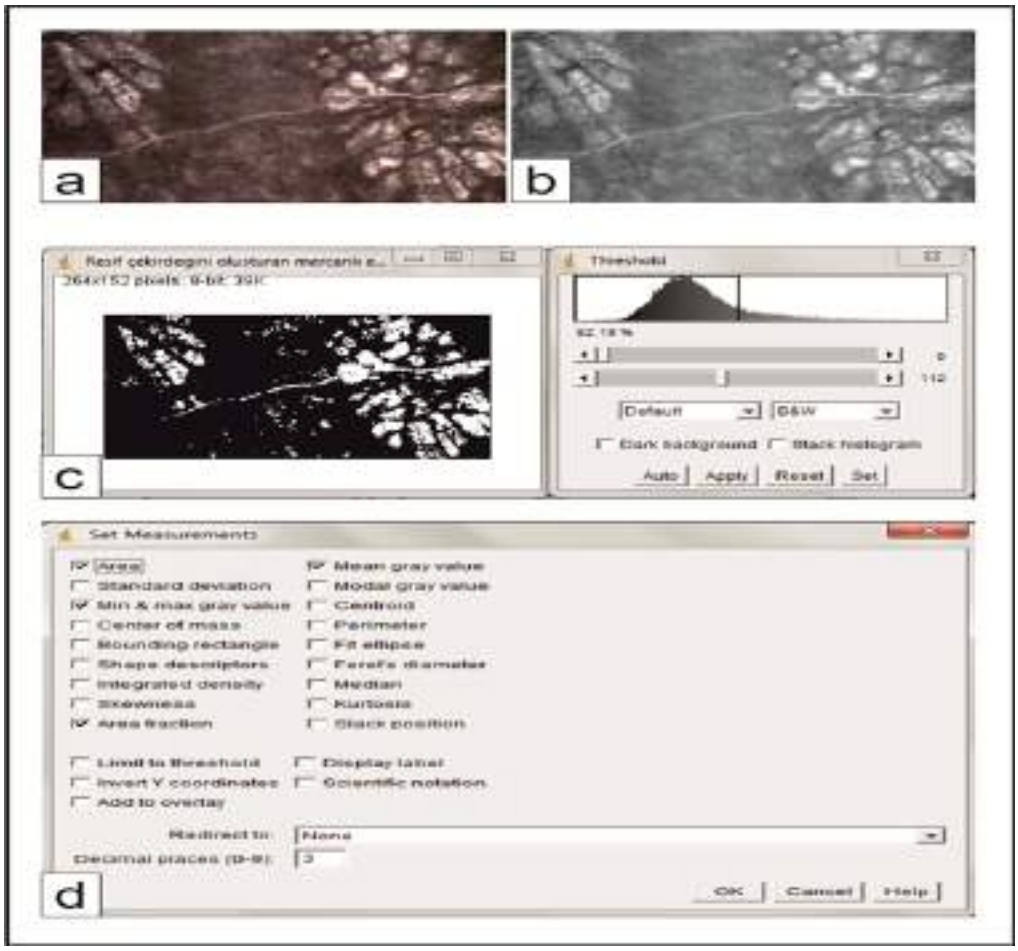

Figure 2. The process of porosity measurements by ImageJ. (a) Image of Horu formation (b) 8-bit format image, (c) binary image and thereshold comand, (d) set measurements command in the ImageJ.

Horu formation considered petroleum reservoir rock around Iskenderun (HATAY) and porosity values of Horu formation is important in determining the quality of the reservoir. There are four main zones on different reefs in the Horu formation. These are: (1) Massive reef cores, (2) Reef blocks, rubbles and breccias, (3) Bedded reef flanks and (4) Coral carpets and patches. The porosity values in the Reef region are 15% on average and can be considered as "Middle Reserve Rock".

RESULTS

The pore type should also be examined in reservoir rocks in addition to porosity and minerals,. Porosity has an important role in the permeability heterogeneity of carbonate reservoirs. Imaging models, which do not take into account the pore type variation in carbonate reservoirs, cannot fully explain the relationship between rock acoustic properties and reservoir parameter. For this reason, it is very important to use a screening method based on pore type and porosity. SEM, Micro-CT and imaging

methods are advantageous because porosity computation provides measurements without damaging the sample.

In the modeling of reefs, porosity values of imaging methods can be measured And among them, determination of petrographic properties of the reef, ability to migrate, transitions between porosities, effective porosity, applicability of three-dimensional imaging to artificial neural network systems, creation of porosity map in software languages such as Matlab, extraction of porosity with the reef map, determination of the accuracy rate of the previous data, imaging to be used methods of porosity calculation, accuracy of the imaging methods in terms of use, can be had knowledge in many issues.

Horu formation considered petroleum reservoir rock around Iskenderun (HATAY) and porosity values of Horu formation is important in determining the quality of the reservoir. There are four main zones on different reefs in the Horu formation. These are: (1) Massive reef cores, (2) Reef blocks, rubbles and breccias, (3) Bedded reef flanks and (4) Coral carpets and patches. The porosity values in the Reef region are 15% on average and can be considered as "Middle Reserve Rock".

REFERENCES

Abramoff, M., Magalhaes, P., & Ram, S. (2004). Image Processing with ImageJ Biophotonics International. 36-42.

Barrett, S., & Webster, J. (2017). Reef Sedimentary Accretion Model (ReefSAM): Understanding coral reef evolution on Holocene time scales using 3D stratigraphic forward modelling. Marine Geology. 108-126.

Choquette, P., & Pray, L. (1970). Geological nomenclature and classification of porosity in sedimentary carbonates, AAPG Bulletin. 207-250.

Elia, P., Nativ-Roth, E., Zeiri, Y., & Porat, Z. (2016). Determination of the average pore-size and total porosity in porous silicon layers by image processing of SEM micrographs. Microporous and Mesoporous Materials. 465-471.

Grove, C., & Jerram, D. (2011). an ImageJ macro to quantify total optical porosity from blue-stained thin sections. Comput. Geosci. 37.

Ikram, M. (2009). Sedimentology of Miocene Reef in the Surroundings of Osmaniye-Iskenderun, Eastern Mediterranean, SE Turkey, PhD Thesis. 26-110.

Iturraran-Viyeros, U., & Parra, J. (2014). Artificial Neural Networks applied to estimate permeability, porosity and intrinsic attenuation using seismic attributes and well-log data. 45-54.

Jin, X., Dou, Q., Hou, J., Huang, Q., Sun, Y., Jiang, Y., et al. (2017). Rock-physics-model-based pore type characterization and its implication for porosity and permeability qualification in a deeply-buried carbonate reservoir, Changxing formation, Lower Permian, Sichuan Bain, China. Journal of Petroleum Science and Engineeri. 223-233.

Levorson, A. (2001). Geology of Petroleum, The AAPG Foundation. 724.

Liu, R., & Sancaktar, E. (2018). Identification of crack progression in filled rubber by micro X-ray CT-scan. International Journal of Fatigue. 144-150.

Munawar, M., Lin, C., Cnudde, V., Bultreys, T., Dong, C., Zhang, X., et al. (2018). Petrographic characterization to build an accurate rock model using micro-CT: Case study on low-permeable to tight turbidite sandstone from Eocene Shahejie Formation. Micron. 22-33.

Sarkar, P., Kumar, A., Singh, K., Ghosh, R., & Singh, T. (2018). Pore system, microstructure and porosity characterization of Gondwana shale of Eastern India using laboratory experiment and watershed image segmentation algorithm. Marine and Petroleum Geology. 246-260.

Shen, X., Li, L., Cui, W., & Feng, Y. (2018).). Improvement of fractal model for porosity and permeability in porous materials. International Journal of Heat and Mass Transfer. 121.

Smal, P., Gouze, P., & Rodriguez, O. (2018). An automatic segmentation algorithm for retrieving sub-resolution porosity from X-ray tomography images. Journal of Petroleum Science and Engineering. 198-207.

Spinelli, F., Valente, S., Foroni, L., & Orrico, C. (2007). . Common Tasks in Microscopic and Ultrastructural Image Analysis Using ImageJ. Ultrastructural Pathology. 401-407.

Taylor, H., O'Sullivan, C., & Sim, W. (2015). A new method to identify void constrictions in micro-CT images of sand. Computers and Geotechnics. 279-290.

Teles, A., Lima, I., & Lopes, R. (2016). Rock porosity quantification by dual-energy X-ray computed microtomography. Micron. 72-78.

Tuzcu, S., & Karabıydıoğlu, M. (1991). Resifler: Genel Karakterleri, Fasiyeslerî, Evrimi ve Ekonomik Önemi, Jeoloji Mühendisliği Dergisi. 5-38.

Yeniay, G. (1983). XIII. Biostratigraphy of the Regional Wells Stratigraphic Section, Report of TPAO.

SINGLE BATHING DYEABILITY OF CATIONIC COTTON-WOOL MIXTURE

Özdemir Hüseyin
Technical Sciences Vocational Higher School, Textile Department, Gaziantep University, Gaziantep, Turkey
Corresponding author. Tel.: +90 5326905616, E-mail address: hozdemir@gantep.edu.tr.

ABSTRACT: The use of cationic cotton, whose production and usage area is increasing rapidly, is becoming widespread. The ionic charge of light cotton with various reactive agents in the light anionic structure becomes cationic and this gives new advantages to cotton. Today, the process of dyeing normal cotton fabrics with direct and reactive dyes is a process that produces a lot of energy, water use and pollution. This is mainly because commercially produced reactive and direct dyestuffs have only moderate affinity for cotton. Normal cotton fibers are composed of negative surface loads in the water and these loads act by pushing slow dyestuff consumption and anionic dyes. The inadequacy of affinity is eliminated by increasing the staining time and staining temperature using high concentrations of the electrolytes in the dye bath (eg sodium chloride, sodium sulfate). These disadvantages were prevented by cationic cotton.
Wool fibers have a cationic structure formed by ammonium conversion of the amino group. For this reason, anionic dyestuffs such as acid and metal complex are used in dyeing. Thus, the interaction of fiber-dyestuff with different ionic load is activated in electrostatic shooting and affinity increases.
In this study, the dyeability of cotton and wool in one bath has been proved experimentally. Thus, energy, water and time loss caused by dyeing in two separate baths are prevented. This gives a significant advantage in terms of cost.

Key Words: Cationic cotton, wool, ionic load, dyeability in a single bath.

KATYONİK PAMUK-YÜN KARIŞIMININ TEK BANYODA BOYANABİLİRLİĞİ

ÖZET: Günümüzde üretimi ve kullanım alanı hızla artmakta olan katyonik pamuğun karışımlarda da kullanımı yaygınlaşmaktadır. Hafif anyonik yapıdaki normal pamuğun çeşitli reaktif ajanlarla iyonik yükü katyonik hale gelmekte bu da pamuğa yeni avantajlar sağlamaktadır. Günümüzde direkt ve reaktif boyalarla normal pamuk kumaşların boyanması işlemi çok enerji, çok su kullanımı ve kirlilik üreten bir prosestir. Bunun nedeni daha çok ticari olarak üretilen mevcut reaktif ve direkt boyarmaddelerin pamuk için sadece orta afiniteye sahip olmalarından kaynaklanmaktadır. Normal pamuk lifleri sudaki negatif yüzey yüklerinden oluşur ve bu yükler yavaş boyarmadde tüketimi ve anyonik boyaları iterek hareket ederler. Afinitenin yetersizliği boya banyosundaki elektrolitleri yüksek konsantrasyonlarda kullanarak (örneğin sodyum klorür, sodyum sülfat) boyama süresini ve boyama sıcaklığını yükselterek giderilmektedir. Katyonik pamuk ile bu dezavantajların önüne geçilmiştir.
Yün lifleri amino grubunun amonyum dönüşümü ile oluşan bir katyonik yapıya sahiptir. Bu nedenle boyamada asit ve metal kompleks gibi anyonik yüklü

boyarmaddeler kullanılır. Böylece farklı iyonik yüke sahip lif-boyarmadde etkileşiminde elektrostatik çekimde devreye girer ve afinite artar.
Bu çalışmada iyonik yükleri aynı şekle dönüşen ve normalde tek banyoda boyanması mümkün olmayan pamuk ile yünün tek banyoda boyanabilirliği deneysel olarak ispatlanmıştır. Böylece iki ayrı banyoda boyama ile oluşan enerji, su ve zaman kaybının önüne geçilmiş olmaktadır. Bu da maliyet bakımdan önemli bir avantaj sağlamaktadır.

Anahtar Kelimeler: Katyonik pamuk, yün, iyonik yük, tek banyoda boyanabilirlik.

1.GİRİŞ

Günümüzde normal pamuğun yün ile tek adımda aynı banyoda boyanması kimyasal yapıları ve pH uyumu bakımından mümkün değildir. Pamuk bazik ortamda ve tuz-soda kullanılarak boyanabilirken, yün asidik ortamda boyanmaktadır. Yine pamuk hafif anyonik iyonik yükte ve boyamada direkt ve reaktif boyarmaddeler kullanılırken, yün katyonik iyonik yükte ve boyamada asit ve metal kompleks boyarmaddeler kullanılmaktadır. Bu iki farklı yapıdaki liflerden pamuğun katyonik hale getirilmesiyle aynı banyoda tek adımda boyamak mümkündür (tablo 1 ve 2).

Tablo 1. Tekstil Lifleri ve İyonik Yükleri (Yurdakul, 2006)

İYONİK YÜKÜ	LİF CİNSİ
Non-iyonik	Poliester, Asetat
Katyonik	Yün, İpek ve Poliamid
Anyonik	Poliakrilnitril (Akrilik)
Hafif Anyonik	Pamuk

Tablo 2. Boyarmaddeler ve İyonik Yükleri (Yurdakul, 2006)

İYONİK YÜKÜ	BOYARMADDE CİNSİ
Non-iyonik	Pigment, Dispersiyon
Katyonik	Bazik
Anyonik	Direkt, Reaktif, Asit, Metal Kompleks

Katyonize işlemi, katyonik reaktiflerle, pamuklu kumaşların sulu ortamda, hafif anyonik olan yüzeyi katyonik hale dönüştürülmekte böylece anyonik boyarmaddelere afinitesi ve subsantivitesi artırılmaktadır (Peter ve Adham, 2001).
Normal pamuk boyamada meydana gelen çevresel negatif etkileri azaltmak için boya banyolarının tekrar kullanımı, arıtma tesisleri, boyama işleminin optimizasyonu, üretimde kullanılan cihazların değiştirilmesi, uygun kimyasal madde seçimi ve yeni nesil uygun boyarmadde seçimi gibi uygulamalar önerilmiştir. Ancak bu öneriler çok yüksek bir parasal gideri de beraberinde getirmektedir (Schlaeppi, 1998).
Daha az maliyetle boya-lif etkileşimini artırmak mevcut ticari boyaların pamuğa olan affinite azlığının üstesinden gelmek için bazı araştırmacılar pamuk lifindeki katyonik

yükleri desteklemek için kullanılabilecek birçok kimyasal madde kullanmışlardır. Bu katyonik reaktifler ve selüloz etkileşimi şekil 1 ve 2'de verilmiştir. Direkt ve reaktif boyalar anyonik yükler taşıdıklarından katyonize pamuk bünyesindeki katyon gruplarından dolayı boyalar için yüksek affiniteye sahip özellik taşımasını sağlar. Ayrıca lif-boya arasındaki bağlara elektrostatik çekim de eklenerek boya tüketiminde ve sabitlemesinde olumlu gelişmeler meydana getirir (Lewis ve Lei, 1989).

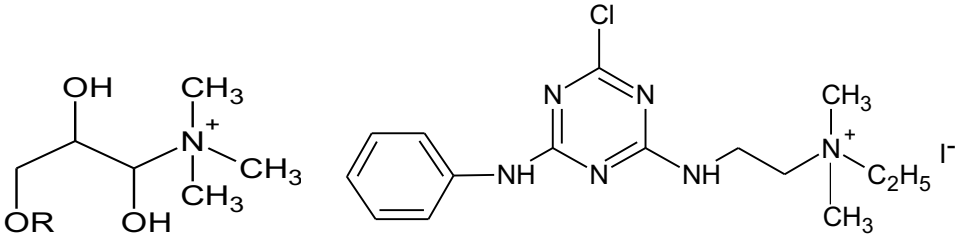

Şekil 1. Katyonik Reaktifler.

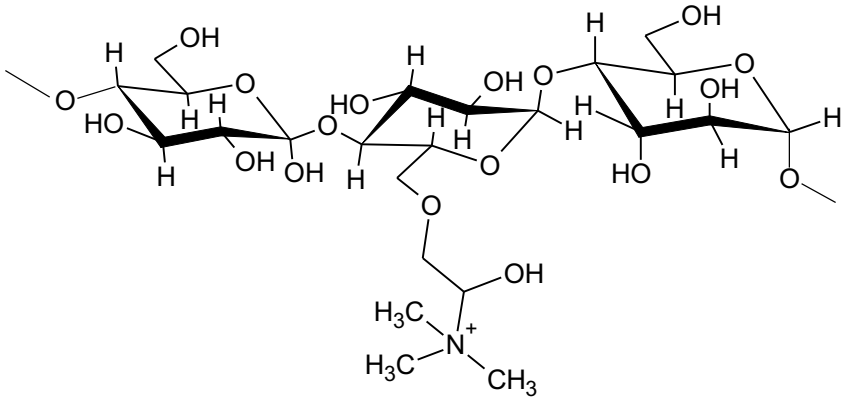

Şekil 2. Katyonik Reaktif-Selüloz Etkileşimi.

Bu çalışmanın avantajları çevresel etkilerin, enerji tüketiminin azaltılmasını ve boyahanelerin üretimlerinin artmasını sağlamaktadır. Bu çalışma ile yünün direkt ve reaktif boyalarla boyanabilirliği düşünülebilir.

2.MATERYAL

Çalışmalarda Gyrowash boyama makinesi, Roaches boyama makinesi, etüv, ışık kabini, Comeureg tentolab cihazları ve yıkama haslığı değerlendirmek için gri skala kullanılmıştır. Deneylerde kasarlı normal pamuk olarak GAP bölgesinde yetiştirilen, katyonize pamuk olarak ise İtalyan De Martini firmasının üretmiş olduğu ithal pamuk kullanılmıştır. Boyarmadde olarak ticari olarak kullanılan çeşitli reaktif, direkt ve asit boyarmaddeler kullanılmıştır. Boyamalarda kimyasal madde olarak yine ticari olarak üretilen ıslatıcı, kostik, hidrojen peroksit, stabilizatör, iyon tutucu, kırık önleyici, yağ sökücü, antiperoksit enzim, asetik asit, tuz, soda ve sabun kullanılmıştır. Boyamalar elyaf formunda yapılmıştır. Boyama öncesi ve sonrası resimler dijital fotoğraf makinesi kullanılarak görüntülenmiştir.

3.YÖNTEM

Katyonik pamuk ile yünün aynı banyoda boyanması pratikte pek uygulama alanı bulan bir boyama yöntemi değildir. Bu çalışmada katyonik pamuk-yün karışımını reaktif, direkt ve asit boyarmaddeler ile boyaması yapılmıştır. Boyama asidik ve nötre yakın ortamlarda, sıcaklık reaktif boyalar için 80°C, direkt boyalarda 100°C ve asit boyalarda 98°C'de olacak şekil ayarlanmıştır.

3.1. Katyonik pamuk – yün karışımının reaktif boyarmaddelerle pH 4 ve pH 6'da boyanması

Boyama için ticari olarak üretilmiş reaktif boyalar kullanılmıştır. Boyamada katyonik pamuk ile merinos yünü karışımı kullanılmıştır. Flotte oranı 1:50 olacak şekilde ayarlanan boyama banyosunda yumuşak su ile çalışılmıştır. Asidik ortam pH=4 için %80'lik asetik asit kullanılmış ve sürede 180 dakika olarak belirlenmiştir. Boyama şartları tablo 3'te verilmiştir.

Tablo 3. Katyonik Pamuk-Yün Karışımının Reaktif Boyalarla Boyama Şartları.

Boyarmadde Cinsi ve Miktarı	**pH**	**T (°C)**	**t(dk)**
%1 Reaktif Boyarmadde (Red C-RL)	4	80	180

Boyama sonrası banyodaki atık boya yükü ve boyama sonrası yün ve katyonik pamuğun boya tüketimi şekil 3'te görülmektedir.

Şekil 3. Boyama Sonrası Mamül Ve Atık Banyo Yükü.

pH = 6'da yapılan boyamada herhangi bir kimyasal kullanılmamıştır. Boyama şartları tablo 4'te verilmiştir.

Tablo 4. Katyonik Pamuk-Yün Karışımının Reaktif Boyalarla Boyama Şartları.

Boyarmadde Cinsi ve Miktarı	**pH**	**T (°C)**	**t(dk)**
%1 Reaktif Boyarmadde (Red C-RL)	6	80	180

Boyama sonrası banyodaki atık boya yükü ve boyama sonrası yün ve katyonik pamuğun boya tüketimi şekil 4'te görülmektedir.

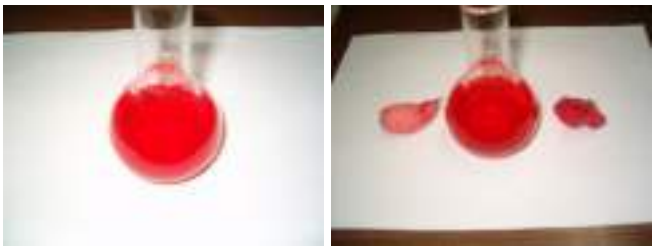

Şekil 4. Boyama Sonrası Mamül Ve Atık Banyo Yükü.

3.2. Katyonik pamuk – yün karışımının direkt boyarmaddelerle pH 4 ve pH 6'da boyanması

Boyama için ticari olarak üretilmiş direkt boyalar kullanılmıştır. Boyamada katyonik pamuk ile merinos yünü karışımı kullanılmıştır. Flotte oranı 1:50 olacak şekilde ayarlanan boyama banyosunda yumuşak su ile çalışılmıştır. Asidik ortam pH=4 için %80'lik asetik asit kullanılmış ve sürede 180 dakika olarak belirlenmiştir. Boyama şartları tablo 5'te verilmiştir.

Tablo 5. Katyonik Pamuk-Yün Karışımının Direkt Boyalarla Boyama Şartları.

Boyarmadde Cinsi ve Miktarı	**pH**	**T (°C)**	**t(dk)**
%1 Sirius RedF4BL (Dystar)	4	100	180

Boyama sonrası banyodaki atık boya yükü ve boyama sonrası yün ve katyonik pamuğun boya tüketimi şekil 5'te görülmektedir.

Şekil 5. Boyama Sonrası Mamül Ve Atık Banyo Yükü.

pH = 6'da yapılan boyamada herhangi bir kimyasal kullanılmamıştır. Boyama şartları tablo 6'da verilmiştir.

Tablo 6. Katyonik Pamuk-Yün Karışımının Direkt Boyalarla Boyama Şartları.

Boyarmadde Cinsi ve Miktarı	**pH**	**T (°C)**	**t(dk)**
%1 Sirius RedF4BL (Dystar)	6	100	180

Boyama sonrası banyodaki atık boya yükü ve boyama sonrası yün ve katyonik pamuğun boya tüketimi şekil 6'da görülmektedir.

Şekil 6. Boyama Sonrası Mamül Ve Atık Banyo Yükü.

3.3. Katyonik pamuk – yün karışımının asit boyarmaddelerle pH 4 ve pH 6'da boyanması

Boyama için ticari olarak üretilmiş asit boyalar kullanılmıştır. Boyamada katyonik pamuk ile merinos yünü karışımı kullanılmıştır. Flotte oranı 1:50 olacak şekilde ayarlanan boyama banyosunda yumuşak su ile çalışılmıştır. Asidik ortam pH 4 için %80'lik asetik asit kullanılmıştır. Boyama şartları tablo 7'de verilmiştir.

Tablo 7. Katyonik Pamuk-Yün Karışımının Asit Boyalarla Boyama Şartları.

Boyarmadde Cinsi ve Miktarı	**pH**	**T (°C)**	**t(dk)**
%1 Asit Boyarmadde (Yellow BR-S-2RL)	4	98	180

Boyama sonrası banyodaki atık boya yükü ve boyama sonrası yün ve katyonik pamuğun boya tüketimi şekil 7'de görülmektedir.

Şekil 7. Boyama Sonrası Mamül Ve Atık Banyo Yükü.

pH = 6'da yapılan boyamada herhangi bir kimyasal kullanılmamıştır. Boyama şartları tablo 8'de verilmiştir.

Tablo 8. Katyonik Pamuk-Yün Karışımının Asit Boyalarla Boyama Şartları.

Boyarmadde Cinsi ve Miktarı	**pH**	**T (°C)**	**t(dk)**
%1 Asit Boyarmadde (Yellow BR-S-2RL)	6	98	180

Boyama sonrası banyodaki atık boya yükü ve boyama sonrası yün ve katyonik pamuğun boya tüketimi şekil 8'de görülmektedir.

Şekil 8. Boyama Sonrası Mamül Ve Atık Banyo Yükü.

BULGULAR

Reaktif boyalarla pH = 4 (asidik ortamda) hem yün hem de katyonik pamuğun aynı banyoda boya tüketimi ve sabitlemesinin üst düzeyde olduğu görülmüştür. Asidik ortamda berrak boya atık suyu elde edilmiştir. Reaktif boyalarla pH 6'da özellikle yün kısmının boya tüketimi ve sabitlenmesinin yetersiz olduğu katyonik pamuk kısmının ise boya tüketim ve sabitlemenin istenilen düzeyde olduğu görülmüştür. Nötr ortamda boyama atık yükünün istenen düzeyde olmadığı da not edilmiştir.

Katyonik pamuk yün karışımının pH=4'de direkt boyalarla yapılan boyamalarında her iki elyaf türününde çok iyi düzeyde boya tüketimi ve sabitlemesi yaptığı görülmüştür. Asidik ortamda berrak boya atık suyu elde edilmiştir. pH =6'da direkt boyalarla yapılan boyamada yün kısmının boya tüketim ve sabitlenmesinin çok az olduğu katyonik pamuk kısmında ise boya tüketimi ve sabitlenmesinin yüksek düzeyde gerçekleştiği görülmüştür. Nötr ortamda boyama atık yükünün istenen düzeyde olmadığı da not edilmiştir.

Katyonik pamuk-yün karışımı asit boyalarla hem asidik hem de nötr ortamda boyanmıştır. Her iki ortamda da boya tüketimi ve sabitlemesi orta düzeyde gerçekleşmiştir.

SONUÇ

Normal pamuğun asidik ortamda terbiyesi nadiren yapılan bir uygulama iken katyonik pamuğun asidik ortamda da boyanabilmesinin yaygınlaştırılabileceği gerçeği ortaya konmuştur. Asidik ortamda sodyum klorit ağartması mevcut durumda hala yapılmakta ve ortamın asidik karakteri pamuğa zarar vermemektedir.

Pamukta kullanılan boyarmaddelerin lif ile yapmış olduğu çeşitli çekim kuvvetleri ve bağlara, katyonik pamukta bir de elektrostatik çekim kuvveti eklenmiştir. Çünkü mevcut pamuk boyalarının çoğunluğu anyonik yapıdadır. Bu da bu boyarmaddelerin katyonik yapıdaki katyonize pamuk ile elektrostatik çekim kuvveti ilave yardımıyla birbirine bağlanmasını sağlamıştır.

Kullanılan boyalardan asit boyarmaddeler yün, ipek ve poliamidde kullanıldığı için katyonik pamuk-yün, katyonik pamuk-ipek ve katyonik pamuk-poliamid karışımlarının daha kolay boyanabilmesinin mümkün olduğu, daha da geliştirilebileceği gerçeği ortaya konmuştur. Özellikle günümüzde tek cins elyaftan ziyade çok karışımlı elyaf çalışılması bu avantajın önemini daha da artırmaktadır. Bu çalışmada katyonik pamuk-yün karışımının tek banyoda boyanabilirliği önemlidir. Bu sayede bu iki lifin tek banyoda boyanması; sudan, kimyasal maddeden, zamandan ve enerjiden tasarruf sağlamada fayda sağlamıştır.

ÖNERİLER

Büyük çevresel sorunlara yol açan tekstil boyama proseslerinde atık yükü ne kadar azaltılırsa avantajdır. Hem katyonik pamuk hem de yünün asidik ortamda boyanması atık boyama yükünü azaltmıştır. Kimyasal olarak benzerlik gösteren katyonik pamuk-ipek ve katyonik pamuk-poliamid karışımlarının da tek banyoda boyanmasının mümkün olduğu konusunda bu çalışma öncülük sağlayabilir.

KAYNAKLAR

D. M. Lewis, S. Lei.,(1989). Improved cellulose dyeability by chemical modification of the fibre , *Text. Chem. Colorist.*, , 21-23.
DM. Lewis, KA Mcllroy., (1997). The Chemical Modification of Cellulosic Fibres to Enhance Dyeability. *Review of Progress in Coloration and Related Topics*, *27*, 5-17.
R.J. Harper, R.L. Stone. , (1986). Cationic cotton plus easy care, *Textile Chemist and Colorist, 11*, 33-35.
J. A. Clipson. , (1989). G. A. F. Roberts. , Differential dyeing cotton.1–Preparation and evaluation of differential dyeing cotton yarn, *J.S.D.C. , 105*, 158-162.
E. J. Blanchardt. , R. M. Reinhardt. , (1992). Dyeing of Crosslinked Cotton Containing Glycol Additives , *Textile Chemist and Colorist*, *24*, 1-13.
YA. Youssef, (2000). Direct dyeing of cotton fabrics pre¬heated with cationising agents. *Journal of Society Dyers and Colourists,10*, 316-322.
PJ. Hauser, AH Tabba., (2001). Improving the environmental and economic aspects of cotton dyeing using a cationised cotton. *Coloration Technology, 5*, 282-288.
DP. Chattopadhyay. (2001). Cationization of cotton for low-salt or salt-free dyeing, *Indian Journal of Fibre and Textile Research., 26*, 108-115.
K Srikulkit, P Larpsuriyakul., (2002). Process of dyeability modification and bleaching of cotton in a single bath. *Coloration Technology*., 2, 79-84.
Ponsa L, Salva J., (2003). Improving the ecological aspects of cotton dyeing. *Revista de la Industria Textil, 409*, 24-29.
Simeonov N. Petkova M., (2005). Spinning of viscose fibers from cationized viscose solution. *Man-Made Textiles in India., 4*, 132-135.
Bilgen M., (2005). Wrinkle Recovory for Cellulosic Fabric by Means of Ionic Crosslinking. *Msc Thesis, Raleigh; North Carolina State University*.

EXPERIMENTAL ANALYSIS OF MOISTURE ABSORPTION BEHAVIOR OF POLYPROPYLENE WOVEN FABRICS

Özdemir Hüseyin[1*]
[1] Technical Sciences Vocational Higher School, Textile Department, Gaziantep University, Gaziantep, Turkey
* Corresponding author. Tel.: +90 5326905616, E-mail address: hozdemir@gantep.edu.tr.
Çelik Emrah [2]
[2] Textile Engineering Department, Erciyes University, Kayseri, Turkey
E-mail address: emrahclk@hotmail.com

ABSTRACT: The developing technology has offered great advantages to the human being in textile field as it is in every field. These advantages are the emergence of the largest synthetic fibers. Today synthetic fibers are used extensively despite the disadvantages of natural fibers. Polypropylene fiber, one of the synthetic fibers, is not used as much as in the production of ready-to-wear and daily-use fabrics. Given the performance characteristics it has, it causes question marks that can not be used. For this reason, in this study, polypropylene fibers were used in woven fabrics and tried to reach the quantities of physical properties they showed.
In this study, fabrics were produced using 100% polypropylene raw material in 2 different woven constructions. The obtained polypropylene fabrics were tested on the same conditions with the cotton and viscose fabrics most used today in the garment industry. Moisture absorption behavior of polypropylene, cotton and viscose woven fabrics was compared with the tests. These tests reveal the advantages and disadvantages of polypropylene fiber.

Key words: Polypropylene woven fabric, moisture absorption, water repellency.

POLİPROPİLEN DOKUMA KUMAŞLARIN NEM ÇEKME DAVRANIŞLARININ DENEYSEL ANALİZİ

ÖZET: Gelişen teknoloji, her alanda olduğu gibi tekstil alanında da insanoğluna büyük avantajlar sunmuştur. Bu avantajların en büyüğü sentetik liflerin ortaya çıkmasıdır. Günümüzde doğal lifler ile sağlanamayan birçok özellik sentetik lifler ile sağlanabilmektedir. Sentetik liflerden birisi olan polipropilen lifi ise hazır giyim ve teknik olmayan alanlarda kullanıma yönelik kumaşların üretiminde yeteri kadar kullanılmamaktadır. Sahip olduğu performans özelliklerine bakıldığında neden kullanılamadığı soru işaretlerine sebep olmaktadır. Bu nedenle bu çalışmada polipropilen lifinin dokuma kumaşlarda kullanılabilirliğine, gösterdiği fiziksel özelliklerin niceliğine ulaşmaya çalışılmıştır.
Bu çalışmada birbirinden farklı 2 dokuma konstrüksiyonda %100 polipropilen hammadde kullanılarak kumaşlar üretilmiştir. Elde edilen polipropilen kumaşlar, bugün hazır giyim sektöründe en fazla kullanılan pamuk ve viskondan üretilmiş kumaşlar ile eşit şartlarda teste tabi tutulmuştur. Polipropilen, pamuk ve viskon dokuma kumaşların nem çekme davranışları yapılan testler ile kıyaslanmıştır. Bu testlerle polipropilen elyafın avantaj ve dezavantajları ortaya çıkarılmıştır.

Anahtar Kelimeler: Polipropilen dokuma kumaş, nem çekme, su geçirmezlik.

GİRİŞ

Dünya üzerinde yaşayan insan nüfusu arttıkça ve toplumların ekonomik yapısı geliştikçe arz-talep çıtaları her alanda yükselmiştir. Tekstil alanında da artan ihtiyaçları karşılamak doğal elyaflar ile mümkün olamaz hale gelmiştir. İnsanoğlu gelişen teknolojiyi kullanarak bu ihtiyacını sentetik lifleri kullanarak karşılamaya başlamıştır. Sentetik liflerden biri olan polipropilen de bu sayede birçok alanda kullanılmaya başlanmıştır. Polipropilen tüketici istek ve beklentilerini rahatça karşılayabilecek teknik özelliklere sahiptir. Bu nedenle de giderek artan kullanım alanı ve oranına sahiptir. Polipropilen; düşük yoğunluk, iyi mekanik özellikler, kimyasallara karşı yüksek direnç ve düşük maliyet özellikleri ile öne çıkan bir elyaf türü olmasına rağmen günümüzde daha çok çuval yapımı, halı endüstrisinde kullanmaktadır.
Tekstil sektöründe yapay liflerin kullanım alanları oldukça geniş olmasına rağmen polipropilen elyafının kullanım alanı sınırlı kalmıştır. Yapılan çalışmalar genellikle polipropilen elyafların boyanması ya da polimer yapısının geliştirilmesi üzerine gerçekleştirilmiştir. Polipropilen elyafının hazır giyim endüstrisindeki yeri ve uygunluğu yeteri kadar değerlendirilmemiştir. Polipropilen elyafı da sektörde ve endüstride hak ettiği önemi bulamamıştır. Günümüz dünyasında moda trendleri hızla değişmekte ve kıyafetlerin giyilme süreleri de gün ve gün azalmaktadır. İşte bu noktada tüketiciye modayı uygun fiyata sunmak bir zorunluluk haline gelmiştir. Hazır giyim endüstrisinde kullanılan diğer yapay liflere göre daha iyi fiziksel performans özelliklerine sahip olmasına rağmen kullanımının kısıtlı olması düşündürücü bir durumdur.

Polipropilen elyafının hazır giyim endüstrisinde, dokuma kumaş formunda göstereceği performansları inceleyeceğimiz bu çalışma ile polipropilen elyafın endüstriye kazandırılması amaçlanmıştır. Ayrıca yapılacak incelemeler ve izlenecek deneysel yollar ile elde edilen analitik sonuçlar doğrultusunda polipropilen elyafının kullanım alanlarının yaygınlaştırılması amaçlanmıştır.

MATERYAL

Yapılan bu çalışmada, 2 farklı konstrüksiyon ve 3 ayrı elyaf türünden dokunmuş kumaşlara nem çekme testi uygulanmıştır. Her kumaş türü için, her test metodu aynı standartlar altında geçekleştirilmiş ve kıyaslanabilir veriler elde edilmeye çalışılmıştır. Ayrıca bir elyaf türünden üretilmiş farklı konstrüksiyondaki yapıların özellikleri de gözlemlenmiştir. Polipropilen dokumalardaki polipropilen iplikler Gaziantep bölgesinde ticari olarak faaliyet gösteren General Non-woven işletmesinden temin edilmiş olup, Premium Tekstil firmasında dokunmuştur. Pamuk dokuma kumaşlar Uşak dokunmuş olup Akbey Mensucat aracılığı ile temin edilmiştir. Viskon dokuma kumaşlar ise Bursa bölgesinde dokunmuş olup Taha Giyim A.Ş.'den tedarik edilmiştir. Bu çalışmada kullanılan dokuma yapıları, özellikleri ve kumaş birim ağırlıkları tablo 2.1'de verilmiştir.

Tablo 2.1. İncelenen dokuma kumaşlar.

Örgü Yapısı	Bez Ayağı			Dimi		
Numune	1/1 Polip	1/1Pamuk	1/1 Viskon	2/1 Polip	2/1 Pamuk	2/1 Viskon
Numune Kodu	PPB	COB	CVB	PPD	COD	CVD
Elyaf Kompozisyonu	%100 Polipropilen	%100 Pamuk	%100 Viskon	%100 Polipropilen	%100 Pamuk	%100 Viskon
İplik numarası	170 Denye	Ne 30	Ne 30	170 Denye	Ne 30	Ne 30
İplik kat sayısı	Tek	Tek	Tek	Tek	Tek	Tek
Çözgü sıklığı	30	30	30	43	43	43
Atkı Sıklığı	24	24	24	26	26	26
Gramaj	120,5	113,3	115,8	156,6	143,6	149,8
Kumaş eni(cm)	150	150	150	150	150	150
Kumaş Maliyet (TL/m²)	5,65	5,7	5,8	6,5	6,2	6,4

YÖNTEM

Dokunmuş Kumaşlarda Nem Çekme Davranışlarının Belirlenmesi

Bu testlerin yapılmasında Taha Giyim A.Ş.'ye ait fiziksel test laboratuvarları kullanılmıştır. Bu laboratuvar akredite olup, test sonuçlarının doğruluğu açısından da çalışmaya güvenilirlik kazandırmaktadır. Çalışmada dokuma kumaşların fiziksel özelliklerini belirlemeye yönelik aşağıdaki testler uygulanmıştır.
Higroskopik (Nem Çekme) ve Su Geçirmezlik Özelliklerinin Belirlenmesi (Gost 3816-81 / ISO 811-81)
Kumaşların higroskopik özelliklerinin belirlenmesinde, Kumaşların Higroskopik (Nem Çekme) ve Su Geçirmezlik Özelliklerinin Belirlenmesi (Gost 3816-81/ISO 811-81/TSE 257 EN 20811) standardı uygulanmıştır.
Kumaşların nem çekme özellikleri, bulundukları ortamdan bünyelerine aldıkları su moleküllerinin tayini ile belirlenir. En basit tanımıyla nemli ağırlığın, nem uzaklaştırıldıktan sonraki ağırlığına farkı, ortamdan ne kadar nem aldığının göstergesidir. Ağırlıkça %98 nem içeren havadan kumaşın emdiği nem oranı, kumaşların nem çekme özelliklerini verir.
Numune hazırlama ve testin uygulanması
Her test için 50*200mm ölçülerinde 3 adet numune alınır. Her test numunesi ayrı tartı kaplarına yerleştirilir. Tartı kaplarına koyulan numuneler, önceden %98+/-1 özgül nem oranına ayarlanmış olan nemlendirme kabininde 4 saat süre ile bekletilirler. 4 saat süre ile bekletilen numuneler dikkatlice tartılırlar. Yapılan ölçümler nemli ağırlar olup kaydedilir. Daha sonra önceden ayarlanmış etüvde 107°C sıcaklıkta nem tamamen uzaklaşıncaya kadar kurutulurlar. Etüvden alınan numuneler, $CaCl_2$ içeren

desikatörlerde soğumaya bırakılırlar. Kurutulması ve soğutulması tamamlanan numuneler tekrar tartılırlar ve kaydedilir. Nemli ağırlık ile kuru ağırlıkları arasındaki kütle farkları bulunarak % nem çekme özellikleri belirlenir. Şekil 3.1 ve 3.2'de higroskopik özellik testinden görseller paylaşılmıştır.

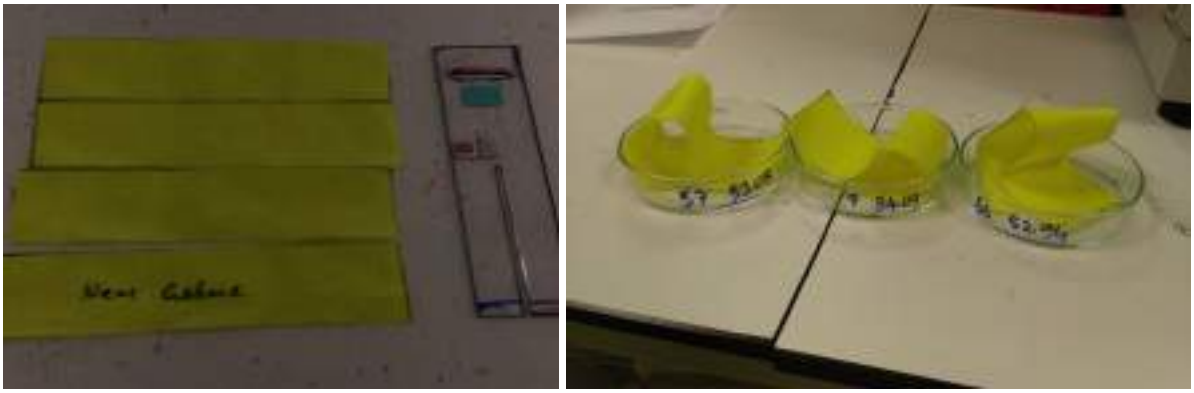

Şekil 3. 1. Higroskopik özellik test numuneleri

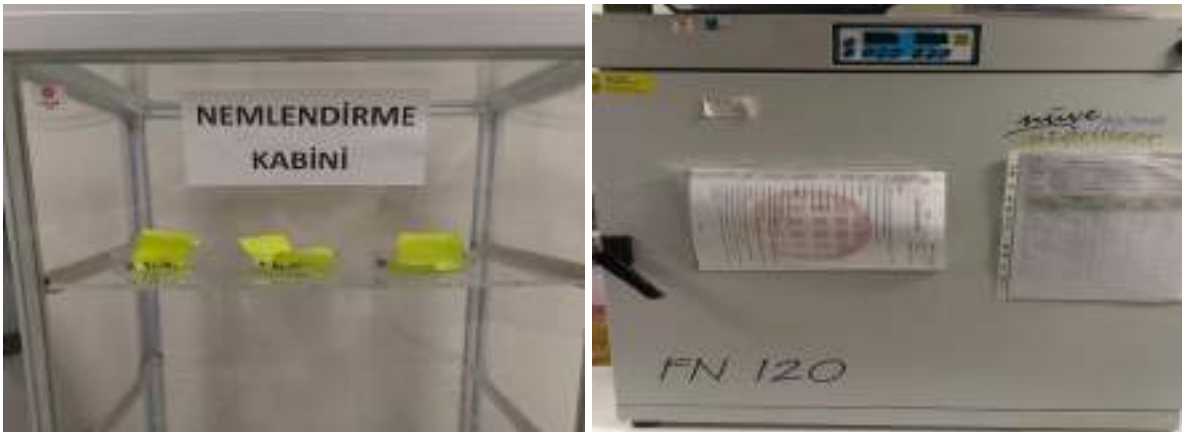

Şekil 3. 2. Higroskopik özellik testinde kullanılan nemlendirme kabini ve etüv.

3.2. Kumaşların Nem Çekme Özelliklerinin Belirlenmesi

Kumaşların nem çekme değerlerinin belirlendiği higroskopik özellik testinin sonuçları aşağıdaki gibidir. Higroskopik özellik, kumaşların nemli ve nemi uzaklaştırıldıktan sonraki ağırlıklarının ölçümü ile tayin edilerek hesaplanır. Testin uygulanması sırasında uygulama alanı 20 cm^2 ve hava basıncı 100 Pa'dır. Sonuçlar numunelerden 3'er tekrarlı ve 5'er test uygulanarak elde edilmiştir.

BULGULAR

Deneysel analizlerde çalışmamıza konu olan 2 farklı dokuma konstrüksiyon yapısıyla oluşturulan, 3 farklı elyaf içerikli dokuma kumaşlarımız, nem çekme özelliği açısından incelenmiştir. Piyasada en fazla kullanım alanına sahip elyaflar olan pamuk ve viskon elyafları ile polipropilen elyaf içerikli kumaşlar aynı standartlarda ve eşit şartlar altında incelenmiştir. Yapılan testler ve elde edilen tüm sonuçların ortalama değerleri test bulguları olarak not edilmiştir. Burada verilen değerler, her bir numune için uygulanan tüm test analizlerinin ortalamalarıdır.

4.1. Dokunmuş Kumaşlarda Nem Çekme Bulguları

Dokunmuş kumaşların nem çekme ve su ile işlem sonucu meydana gelen değişimler değerlendirilmiştir. Pamuk ve viskon dokuma kumaşların su ile işlem sonucu değişimleri ve nem çekme özellikleri beklenen bulgulardı. Polipropilen kumaşlarda ise nem çekme davranışı daha çok yüzey suyu şeklinde gerçekleşmiştir.
Çalışmada kullanılan dokuma yapıların higroskopik özellikleri ve nem çekme eğilimlerine ait test sonuçları tablo 4.1'de gösterilmiştir.

Tablo 4. 1. Higroskopik özellik test değerleri.

Higroskopi Test Sonuçları						
% Nem Çekme Oranı Değerleri						
Kumaş	**PPB**	**COB**	**CVB**	**PPD**	**COD**	**CVD**
Sonuçlar	5,37	17,61	25,35	7,01	15,37	25,26
	5,31	18,12	28,78	6,42	15,65	23
	5,47	16,95	24,57	5,75	14,25	22,43
	6,56	17,12	27,75	5,28	13,04	23,5
	6,5	18,19	25,6	5,07	15,14	24,51
Ortalama	**5,84**	**17,60**	**26,41**	**5,91**	**14,69**	**23,74**
Cv	**0,32**	**0,25**	**2,52**	**0,52**	**0,90**	**1,04**
SS	**0,56**	**0,50**	**1,59**	**0,72**	**0,95**	**1,02**

Çalışmada kullanılan polipropilen, pamuk ve viskon dokuma, bez ayağı yapıların higroskopik özelliklerinin değerleri şekil 4.1'de karşılaştırmalı olarak görülmektedir.

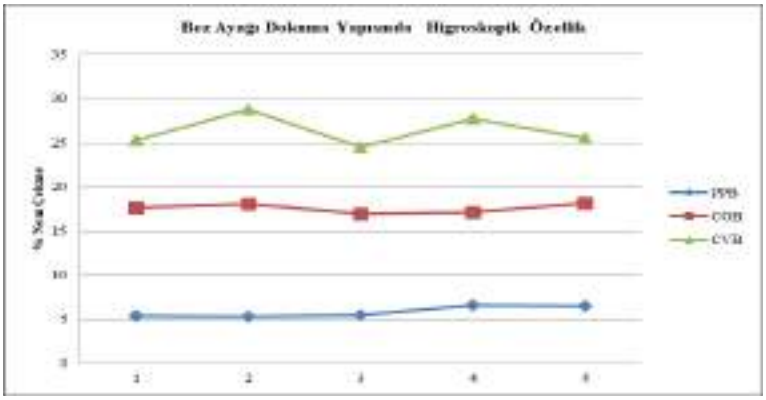

Şekil 4. 1. Bez ayağı kumaşların higroskopik özellik değerleri.

Çalışmada kullanılan polipropilen, pamuk ve viskon dokuma, dimi yapıların higroskopik özelliklerinin değerleri şekil 4.2'de karşılaştırmalı olarak görülmektedir.

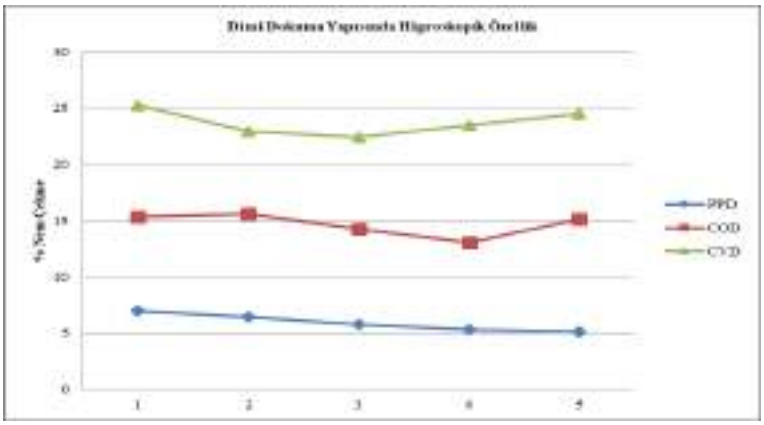

Şekil 4. 2. Dimi kumaşların higroskopik özellik değerleri

Çalışmada kullanılan dokuma kumaş yapılarının higroskopik özelliklerinin test sonuçlarının ortalama değerleri şekil 4. 3'de karşılaştırmalı olarak gösterilmiştir.

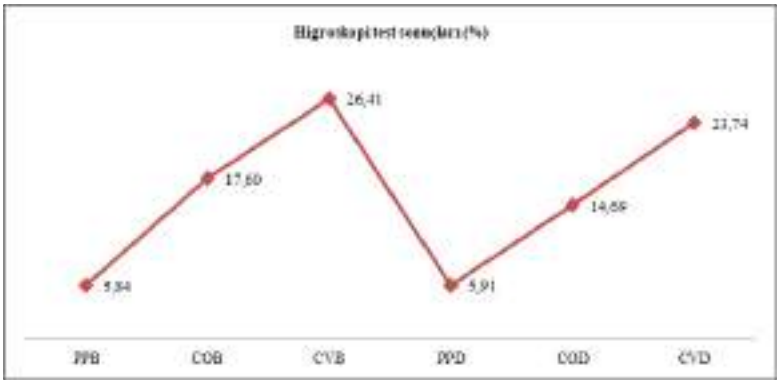

Şekil 4. 3. Higroskopik özellik test sonuçlarının ortalama değerleri.

SONUÇ

Bir tekstil hammaddesinde nem çekme özelliği lifin doğal yapısı ve amorf-kristalin bölge dağılımı ile ilgilidir. Lifin kimyasal yapısı, kimyasal yapısındaki hidrofil ve hidrofob grup sayısı nem çekme özelliğini etkiler. Bu hammaddeler içerisinde amorf bölgesi en çok olan viskon lifi yapısal olarak en hidrofil liftir. %60-70 amorf bölgeye sahip viskonun nem çekme özelliği pamuk ve polipropilenden üstündür. Polipropilenin ticari nem miktarı tüm poliolefin liflerinde olduğu gibi %0 olup, hidrofob bir liftir. Hidrofob olması yapının polimerizasyon reaksiyonu sonucu etrafını saran hidrofob karakterli H ve CH_3 gruplarıdır. Şekil 5.1 ve 5.2'de görüldüğü gibi lif yapısından kaynaklanan nem çekme özelliği dokuma yapılarda da kendini göstermiştir. Polipropilen dokumaların nem çekme özelliği hem pamuk hem de viskona nazaran oldukça düşük değerlerdedir.

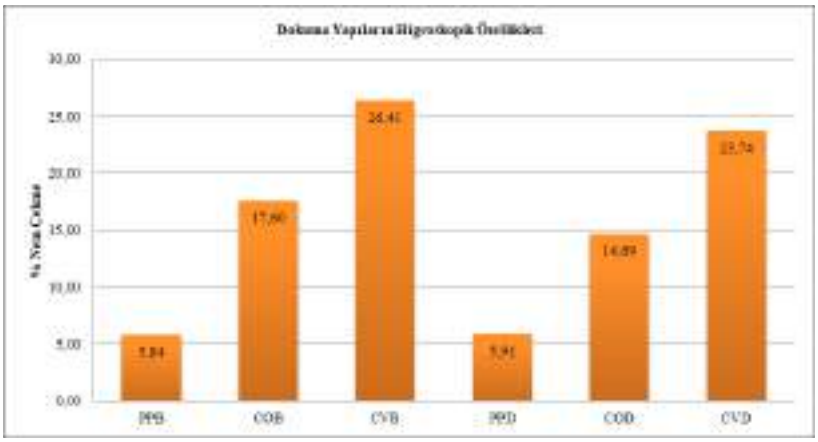

Şekil 5. 1. Bez ayağı ve dimi dokuma yapıların % nem çekme değerleri.

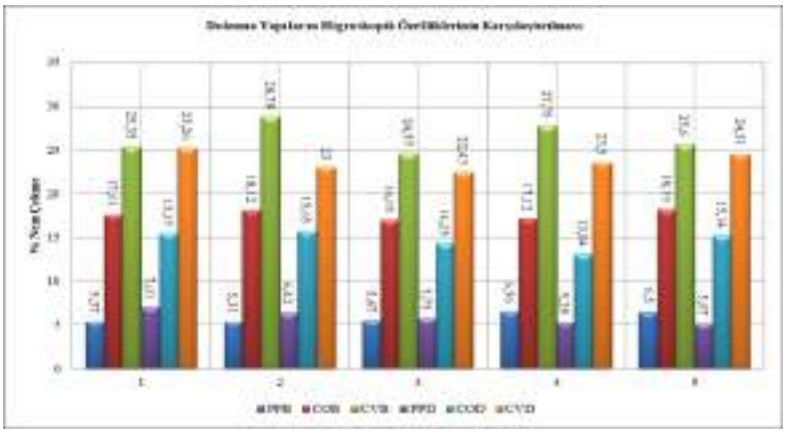

Şekil 5. 2. Bez ayağı ve dimi dokuma yapıların karşılaştırmalı olarak % nem çekme değerleri.

ÖNERİLER

Polipropilen kumaşların en belirgin ayırt edici özelliklerinden bir tanesi nem çekmedir. Polipropilen elyafın yapısal özelliği zaten nem çekmeye imkân vermemektedir. Polipropilen kumaşlar hidrofob özelliğinden dolayı çok düşük nem almıştır. Pamuk lifi ve rejenere selülozik elyaf olan viskon nem çekme değeri olarak polipropilenden çok daha iyi değerlere sahiptir. Çalışmadan elde edilen sonuçlar kullanılan hammadde özelliklerini doğrusal yansıtmıştır. Amorf-kristalin bölge oranları ve yapısal özellikleri çıkan sonuçlarla örtüşmektedir. Sonuçlardan hareketle polipropilenin hafif olması ve hidrofob karakteri bu yapıların deniz kıyafetlerin kullanılabilir olması açısından dikkate alınması gereken bir tespittir.

KAYNAKLAR

Atabek Yiğit E., (2009), Polipropilen Elyafının Boyanabilirliğinin İncelenmesi. T.C Sakarya Üniversitesi, Fen Bilimleri Enstitüsü, Kimya Mühendisliği A.B.D, Doktora Tezi, Sakarya.

Balcı O., (2003), Kumaş Oluşumu Yapı ve Özellikleri, T.C. Çukurova Üniversitesi, Fen Bilimleri Enstitüsü Tekstil Mühendisliği A.B.D, Yüksek Lisans Tezi, Adana.

Başer İ.;(2002); Elyaf Bilgisi, Marmara Üniversitesi, Teknik Eğitim Fakültesi, İstanbul,198s.

Büyükakıncı B.Yeşim., Özel Yöntemlerle Polipropilen Elyafın Boyanması T.C Marmara Üniversitesi, Fen Bilimleri Enstitüsü, Tekstil Eğitimi A.B.D, Yüksek Lisans Tezi,2005, İstanbul.

Cornelia, V., (2000), Handbook of Polyolefins. 2.Edition, Revised and Expanded, New York, NY, USA.

Çelik N., (2004), "Dokuma Kumaş Analizi" dersi notları, Çukurova Ünv. Tekstil Müh. Bölümü, Adana.

Çetin, C., (2007), "Dokuma Kumaş Özelliklerinin ve Görmüş Olduğu Mekanik Bitim İşlemlerinin Dokuma Kumaş Mukavemetine Etkisi" İ.T.Ü. Fen Bilimleri Enstitüsü,Yüksek Lisans Tezi.

Dayıoğlu, H, (1983), "Studies of the Incorporation of Basic Sites in-Polypropylene Fibres and of Their Aecesibility to Acid Dyes", Doktora tezi. Department of Textile Industries, Leeds University.

Güleryüz, Ö., (2011), Küresel Gelişmeler Işığında Türkiye'de Tekstil Sektörü ve Geleceği. T.C. Süleyman Demirel Üniversitesi, Sosyal Bilimler Enstitüsü, İşletme Anabilim Dalı, Tezsiz YüksekLisans Bitirme Projesi, Isparta.

İlter M., (2015), Tekstil Üretimi ve Yardımcı Kimyasallar Kitapçığı, TMMOB Kimya Mühendisleri Odası, İstanbul .

GOST 3816-81/ISO 811-81 standard (1982)-Tekstil kumaşları- Higroskopik (Nem Çekme) ve Su geçirmezlik Özelliklerini Belirleme Yöntemleri, Moskova

Karakas, Canbaz, H., (2005), "Polipropilen Lifleri" Tekstil ve Teknik.

Kiper, M., (1996), Polipropilen Liflerin Özellikleri ve Kullanım Olanakları. İMO İzmir Şubesi Haber Bülteni, İzmir, 64, 21-22.

Okur, A. (2002), Kumaşların Sürtünme Davranışları Üzerine Bir Araştırma Bölüm II: Viskon Kumaşlarda Bazı Yapısal Özelliklerin Sürtünme Özelliklerine Etkileri. Tekstil Maraton, 12(59): 58-62.

Özkürkçüler, Ö., (2005), Karaaslan, U., "Polipropilen Lif ve Özellikleri" Tekstil Maraton, 4, 23-25.

Öztürkmen, A., Gđrđsken, A., (2005), Polipropilenin Önlenemeyen Yükselisi, Tekstil Arastırma Dergisi, sayı 2.

Smirfitt, J.A., (1965), "Worsted 1x1 Rib Fabrics Part II Some Physical Properties" Journal of Textile Institute, 56(6): T298-T313.

Spruiell, J.E., Bond, E., (1999), Melt Spinning of Polypropylene. J.Karger-Kocsis, Ed., Polypropylene: An A-Z Reference, Kluwer Publishers, Dordrecht.

Uskaner, Y. A., Uskaner F., Aksoy M., (2000), "Conditioned Air Quench System for Polypropylene Carpet Yarn Spinning Machine" ULIBTK'99, 12. Ulusal Isı Bilimi ve Teknigi Kongresi, pp 265-270, 28-29, Sakarya.

Uskaner, Y. A., Uskaner F., Aksoy M., (1999), "Polipropilen _iplik Çekim Ünitesi Tasarımı, _malatı ve Performans Testleri" 9.Ulusal Makine Teorisi Sempozyumu, pp 35-45, 15-17, Gaziantep.

Wang, I.-C., (1994), Relationships Between Fibre Formation, Structure and Properties of Polypropylene FibresDepartment of Textile Industries, The University of Leeds.

MACHINE LEARNING BASED SENTIMENT ANALYSIS USING NAIVE BAYES ALGORITHM

Serkan OZBAY
Department of Electrical and Electronics Engineering, University of Gaziantep
sozbay@gantep.edu.tr

Ola Adnan AL-NISANI
Department of Electrical and Electronics Engineering, University of Gaziantep
engolaadnan@yahoo.com

ABSTRACT: Information technology has become an integral portion of our everyday life and it is very difficult to imagine it without the means of social media. The new communications and networks era are not only the entertainment tools but also modern tools for sharing important data, opinions, and ideas by users. Some of these data and information are so essential for analyzing and extracting important data that can be utilized later in decision support systems. In this work, sentiment polarity analysis is studied and a machine learning model is used to predict and analyze the data obtained from external sources. Naive Bayes approach is used as a classifier and it is known that Naive Bayes is one of the supervised machine learning techniques. The experimental results obtained from this work show that the Naive Bayes approach is one of the best and most efficient methods used in sentiment analysis techniques, which gives high accuracy results in the analysis of positive and negative polarity of the data. This method also yields high-quality results in a very short time.

Key words: Sentiment analysis, Positive and Negative polarity, Naive Bayes algorithm

INTRODUCTION

The term sentiment analysis stands for the processes of computationally analyzing, identifying, and categorizing people's opinions, sentiments, evaluations, appraisals, attitudes, and emotions expressed in a piece of text. Accoding to Liu (2012), the sentiment analysis is not a new research area, the studies has started in the early nineties. However the new application areas make this subject more attractive for the researchers. The trend of scientists to study this field is an indication of the importance of this issue in our lives where the sentiments analyses have become common techniques used for opinion mining purposes in the texts appearing in digital communications areas and networks (Medhat at al, 2014).

The recent studies have not only used techniques of the sentiment analysis but also combined the machine learning technology and artificial intelligence to analyze data obtained from several sources and begins to predict results through artificial intelligence and machine learning techniques (Go et al, 2009). Such models employ sentiment analysis techniques to analyze data and texts obtained from communication systems and the Internet and then they extract innovative data and texts with very

important information with the help of machine learning techniques. Emotional use of sentiment analysis techniques is the extraction of inner emotions in terms of positive and negative, such as anger, happiness, sadness, fear, and joy (Bütow at al).
Naive Bayes machine learning model is used in this work. It is known that Naive Bayes is a probabilistic classifier that uses supervised learning approach and that it is thought one of the most common methods in supervised machine learning models. Pak and Paroubek (2010) have stated that this technique has proven its ability to predict and distinguish data that carry the positive and negative characteristics.

NAIVE BAYES CLASSIFIER

It is known that supervised machine learning approaches are heavily used in decision making processes. The supervised machine methods assume the presence of some data that are utilized for the learning process. The data are labeled for classification to provide a learning scheme for future data analysis, identification, or categorization.
One of the most common and simple machine learning methods used in text mining is Naive Bayes classifier. In machine learning schemes, Naive Bayes classifier is a type of probabilistic classifiers and it is based on Bayes' theorem with strong (naive) assumptions between the features. The Bayes theorem is as follows.

$$P(H/x) = \frac{P(H)P(x/H)}{P(x)} \tag{1}$$

In this relation, $P(H/x)$ is the probability of hypothesis given predictor, $P(H)$ is the prior probability of hypothesis, $P(x/H)$ is the likelihood which is probability of predictor given hypothesis, and $P(x)$ is the prior probability of predictor.
Naive Bayes is very popular in the sentiment analysis areas for classifying texts because it is very simple and efficient procedure.

PROPOSED METHOD

In this study, a binary classification scheme is proposed for identifying the polarity of a given text as either positive or negative. Naive Bayes classifier is used to recognize the positive and negative emotions. The Naïve Bayes classifier predicts the positive and negative emotions using Bayes theorem. The proposed method uses some text pieces for learning process. Some of them are labelled as positive and the rest as negative. First step is preprocessing of those classes of texts and preparing them in suitable form for learning stage. Then the proposed classifier is trained using the dataset just prepared.

Next an input text to be analyzed is prepocessed and prepared for polarity classification. The classification relies on the computations of three types of probabilities: prior probabilities, conditional probabilities and posterior probabilities (Manning at al., 2009). The Naive Bayes based classification formula is based on the following formula:

$$P(label/features) = \frac{P(label) * P(features/label)}{P(features)} \quad (2)$$

The prior probabilites, $P(label)$, for two types of classes are computed using the database created for learning stage and the formulas are given as the followings:

$$P(positive) = \frac{total\ number\ of\ texts\ labelled\ as\ positive}{total\ number\ of\ texts\ in\ database} \quad (3)$$

$$P(negative) = \frac{total\ number\ of\ texts\ labelled\ as\ negative}{total\ number\ of\ texts\ in\ database} \quad (4)$$

$P(features)$ are also the prior probabilities of specific features in the input text.

$P(features/label)$ is the conditional probability that the specific fetaure appears given in a class.
The posterior probabilities, $P(label/features)$, are the probabilities of specific fetaures belonging to a class (positive or negative).
In our design, the features are words in the input text and involving the polarity information as negative or positive. Since input text may contain several features containing polarity information, the conditional probabilitiy is computed as the following:

$$P(features/label) = P(feature_1/label) * P(feature_2/label) * \ldots . * P(feature_n/label) \quad (5)$$

The classifier computes the posterior probabilities for each of the class as $P(positive/features)$ and $P(nagative/features)$ and finally compares the results. The proposed algorithm uses maximum a posteriori (MAP) estimation to decide the polaritiy of the input text. Since we have binary classification scheme, the bigger value denotes the label or class the features in input text belongs to.

DATA PREPARATION

In this work, the database is taken from the following Internet site: https://www.cs.uic.edu/~liub/FBS/sentiment-analysis.html#lexicon. The taking database package is containing a set of positive and negative polarity classes. The database is in the form of a unique package without partitioning into two parts positive and negative packages. The database preparing contains some steps. The first step is inserting the database included positive and negative classes into the system. The second step is reordering the positive and negative classes in one array. The third step is eliminating the special characters and numbers included the database such as: (#, $, %, &, ^, *, (,), -,:, 9, 5, 654). The fourth step has arranged the words of classes where each word takes one cell of the array. The last step is eliminating all empty cells of the array. All of these steps are explained in Figure 1.

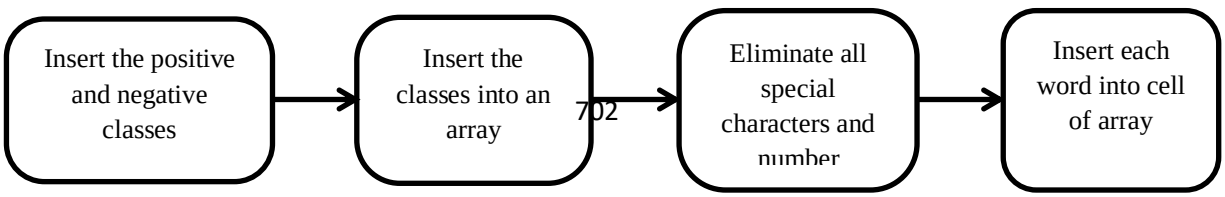

Figure 1. Structure of the Pre-processing

EXPERIMENTAL RESULTS AND DISCUSSION

In order to evaluate the performance of the proposed method, we have used MATLAB R2016b program. In this work, the sentiment analysis Lexicon database is used. We utilized 100 negative and 100 positive reviews. The minimum size of the negative class is 204 and the maximum size is 1644. Also the minimum size of the positive class is 219 and the maximum size is 1975. The process started by inserting these classes into the MATLAB environment and make pre-processing for these classes. The total words in the all classes are shown in the Table 1. Also the number of the negative words with repetition and without repetition is shown in Table 1. In addition, the number of the positive words with repetition and without repetition is also shown in the Table 1. The Naive Bayes classifier is used in this work as the machine learning algorithm. The size of the utilized dictionary in this project is 3004 words: 1502 words for the positive polarity and 1502 words for the negative polarity. The prior probability is calculated for all negative and positive polarity classes as in the Table 2.

Table 1. The Number of Words on the Classes, Negative and Positive Words with Repetition and without Repetition in Database

	Negative words		Positive words	
Total number of words in the classes	With repetition	Without repetition	With repetition	Without repetition
163322	78737	9090	84585	9470

Table 2. The Prior Probability Values of the Negative and Positive Classes

Total prior probability value	Negative prior probability value	Positive prior probability value
1	0.500	0.500

In the testing step, a text is given as the input. When we use a positive text like “I love the football game” the result of the system must be “It is a Positive Review”. The experimental values of the conditional and posterior probabilities for the defined sample text are given in Table 3. When we use a negative text like “I hate eating egg” the result we expect is “It is a Negative Review”. The result is the same as expectation and the corresponding probabilities are seen on Table 4.

Table 3. The conditional and posterior probabilities for the text "I love the football game"

Positive conditional probability	Negative conditional probability	Positive posterior probability	Negative posterior probability
0.000673601	6.11688e-05	0.000336800	3.05844e-05

Table 4. The conditional and posterior probabilities for the text "I hate eating egg"

Positive conditional probability	Negative conditional probability	Positive posterior probability	Negative posterior probability
4.5154e-05	7.2519e-05	2.2577e-05	3.6259e-05

For performance evaluation, we have used totally 100 texts, 50 texts are having positive polarity and 50 texts having negative polarity. Table 5 shows the results as follows.

Table 5. Performance of the Proposed Method

Number of texts	Accuracy (%)	Error (%)
50 positive labeled text samples	46 correct classification 92%	4 incorrect classification 8%
50 negative labeled text samples	48 correct classification 96%	2 incorrect classification 4%

As it is observed from the table above, the proposed method has classified 94 text samples out of 100 test text samples and thus it gives 94% accurate classification rate. The selected text samples for testing were not so long. The average number of words in text samples is 8. When a careful analysis is performed on incorrectly classified samples, it is seen that most of the sentences contain negation with a word "not". Thus it is observed that the proposed method has not performed well in these cases.

CONCLUSION

Sentiment analysis is still one of the hot topics to many researchers because of extensive application areas. In this paper, we proposed a binary classifier on this subject for text mining purpose. The system classifies and determines the polarity of the texts as two types of classes, positive and negative classes. The classifier uses as a database adopted in a machine learning structure. The Naive Bayes algorithm is used as a probabilistic classifier scheme. This method is chosen because of being simple and effective method. From the experimental results, it is seen that the Naive Bayes classifier gives very acceptable result and it needs a short time to reach decisions. On the other hand, it does not perform accurate classifications when the texts contain

negation. Hereafter, as a future study, higher accuracy rate is aimed even if the text contains negations. Moreover, the performance must be analyzed for longer text samples.

REFERENCES

Bütow, F., Schultze, F., & Strauch, L. Semantic search: sentiment analysis with machine learning algorithms on
German news articles

Go, A., Bhayani, R., & Huang, L. (2009). Twitter sentiment classification using distant supervision. *CS224N Project
Report, Stanford*, 1(12).

Liu, B. (2012). Sentiment analysis and opinion mining. *Synthesis Lectures on Human Language Technologies,* 5(1),
1-167.

Manning, C. D., Raghavan, P., & Schütze, H. (2008). Introduction to information retrieval (Vol. 1, No. 1, p. 496).
Cambridge: Cambridge university press.

Medhat, W., Hassan, A., & Korashy, H. (2014). Sentiment analysis algorithms and applications: A survey. *Ain
Shams Engineering Journal,* 5(4), 1093-1113.

Pak, A., & Paroubek, P. (2010). Twitter as a corpus for sentiment analysis and opinion mining. *Proceedings of the
Seventh conference on International Language Resources and Evaluation (LREC'10)* Vol. 10, No. 2010.

A TECHNICAL ANALYSIS ON THE EFFECT OF EXFOLIATED VERMICULITE AGGREGATE ON THERMAL COMFORT PARAMETERS OF COMPOSITE MORTARS FOR INSULATION PURPOSES

Lütfullah GÜNDÜZ
İzmir Katip Çelebi University
lutfullah.gunduz@ikc.edu.tr

Şevket Onur KALKAN
İzmir Katip Çelebi University
sevketonur.kalkan@ikc.edu.tr

A. Münir İSKER
Tepe Betopan Yapı Malzemeleri San. ve Tic. A.Ş.

ABSTRACT: In the world, with the increasing energy costs, the use of energy efficient products is becoming widespread in buildings, which are one of the reasons that cause the most energy consumption. In energy efficient constructon materials, a number of technical parameters and evaluation approaches have been developed as thermal comfort and thermal performance. Thermal comfort and thermal performance parameters are evaluated as specific heat value, heat capacity value, heat diffusion coefficient, thermal conductivity and heat storage. However, these parametric values do not provide detailed and sufficient technical information on the values that may be valid for aggregate components and building material derivatives used in the construction sector. In this paper, thermal comfort aspects and technical performances of exfoliated vermiculite aggregated composite mortar were experimentally analyzed in detail to be used in construction materials as raw materials. A comparative discussion for exfoliated aggregates based on the parameters such as thermal conductivity, specific heat value, heat storage capability, heat diffusion coefficient and heat storage efficiency will be given as numerical evaluations in the paper. According to the test results, when exfoliated vermiculite aggregate ratio increases, thermal comfort values are improved.

Key words: exfoliated vermiculite, composite mortar, heat storage, heat diffusion, specific heat

INTRODUCTION

Until recently, cement-bonded mortars obtained by fine-grained aggregates have generally been used as plaster mortar for grouting of the masonry elements of the masonry mortar or the inner and/or outer surfaces of the walls built with these masonry elements. However, in parallel with the technological developments in the use of mortar combinations, the use of special additive materials with natural content, the use of natural materials in nano-sized mortars as additive components or the use of reinforcing elements of the polymeric components obtained by chemical processes,

such as reinforcement elements etc., the new generation of innovative mortar combinations show development. In these mortars, cement-free component derivatives can be developed, as well as cement. They may also be produced in powder or wet mortar forms. These applications have started to create a new field in construction sector unlike traditional mortar usage. These mortars are generally named as new generation composite mortars due to their structural and technological features.

New generation composite mortars differ from traditional mortars due to their technological properties. For example, the unit weight of the units is lower than the normal mortars and they form lighter mortar combinations. Under the concept of insulation, thermal comfort, noise loss ability and acoustic comfort, resistance to water, resistance to fire and high temperature environments, water vapor diffusion capability and resistance to radiation environments such as the types of special developed species etc. show values of awareness. Composite mortars, especially in recent years as a natural result of global warming in buildings that provide significant added value to energy efficiency in the form of building components can be seen as a transformation. Today, one of the most important challenges the society facing is climate change. One of the biggest causes of climate change is the emission of greenhouse gases released into the environment. Taking the energy consumption to the minimum is an important way to minimize greenhouse gas emissions (Wu et al., 2016). In recent years, energy efficient buildings have started to carry a great importance both economic and environmental factors in the world. Countries increasingly focus on energy efficient buildings since one third of the energy consumption spent by buildings (Koksal et al., 2015). A green building is an environmentally sustainable and energy efficient building, designed, constructed and operated to minimize the total environmental impacts (Kibert, 2003). The concept of sustainable building incorporates and integrates a variety of strategies during the design, construction and operation of building projects. Minor energy saving can be achieved with measures to be taken during use in buildings, while the real energy saving in buildings can be provided by the measures in the design stage (Wu et al., 2016). Considering the economic and environmental point of view, when buildings are designed with high-energy efficiency, this reduce heating and cooling costs in the long term and thus fuel consumption will be reduced to minimum and prevent the environmental damage (Al-Jabri et al., 2005). Currently, the most widely used building materials are ceramic, natural stone, wood-resin composites, aluminum-resin composites and fiber-cements. Each of these materials have their own advantages, while durability, hardness, strength, unsuitability, cost of usage, etc. are also their disadvantages. For this reason, materials provide these features, developed from environmentally friendly and cost-effective raw materials and processing are important (Claramunt et al., 2016). One of the increasingly important types of materials for green building materials is also construction materials produced by composite mortars.

A number of technical parameters and evaluation approaches have been developed in construction sector in order to better define the impact levels of buildings' thermal comfort and to characterize thermal performance more meaningfully. Among these

parameters, parameters such as specific heat value, heat capacity value, heat diffusion coefficient, thermal conductivity and heat storage have to be defined numerically in relation to heat dissipation and heat storage capabilities. However, these parametric values do not provide detailed and sufficient technical information on the values that may be valid for aggregate components and building material derivatives used in the construction sector.

In this paper, thermal comfort aspects and technical performances of exfoliated vermiculite aggregated composite mortar were experimentally analyzed in detail to be used in construction materials as raw materials. All the experimental testing studies were carried out at construction materials innovation laboratory in İzmir Katip Çelebi University. A comparative discussion for exfoliated aggregates based on the parameters such as thermal conductivity, specific heat value, heat storage capability, heat diffusion coefficient and heat storage efficiency will be given as numerical evaluations in the paper. These parameter values are compared with the advantages and disadvantages of the material context as well as the performance effects that these types of aggregates will provide when used in any construction material.

MATERIALS AND METHODS

Materials Used

Cement

White cement used in this study was obtained from the local market that is comparable to EN 197-1 CEM 1 52.5R (52.5 N/mm^2) for all composite mortar samples.

Exfoliated Vermiculite

Vermiculite is a natural mineral, hydrated magnesium aluminum silicate with a highly variable and complicated chemical compound. It crystallizes in a monoclinic crystal system, in most of cases in a form of plate clutches. It is usually yellowish, Brown and olive color. It is a product of mica (phlogopite or biotite) erosion. A specific property of vermiculite is volume increase (even 30 times) during high temperature treatment, and in this process, expanded vermiculite is produced. It takes shape as the accordion. This form of vermiculite is exfoliated vermiculite. Vermiculite in exfoliated (expanded/expanded) form is light, inflammable, compressive, highly absorbable, inert and may have high positive ions exchange ability. Expanded vermiculite is a good sound and heat insulator (inflammable) suitable for temperatures from below -200°C to +1200°C. The exfoliated vermiculate is an inexpensive, environmentally friendly and non-toxic material. When considering those, exfoliated is an important raw material for energy efficient and sustainable buildings (Shoukry et al. 2016, Koksal et al., 2015, Binici et al., 2015, Abidi et al., 2015, Gencel et al., 2014, Chung et al., 2015, Demirçivi and Saygılı, 2014). Some physical properties of exfoliated vermiculite are given in Table 1.

Table 1. The Physical Properties of the Exfoliated Vermiculite.

Color	**Golden**

Shape	**Accordion shaped granule**
Water holding capacity	**> 160% by weight**
pH (in water)	**6 to 9**
Thermal conductivity (W/mK)	**0.035 – 0.065**
Bulk density (Kg/m³)	**90 - 220**

The exfoliated vermiculite used in this study was commercially first obtained from the local market in crude form. Then, in the laboratory environment, this crude form of vermiculite temperature was subjected to three different rates of exfoliation. These were 50%, 70% and 90% respectively, and different density values of vermiculite aggregates were obtained. The lower the density, the higher the rate of exfoliation in the temperature effect.

Volcanic Ash and Sliked Lime

Volcanic ash is powdery rock, minerals and volcanic glass fragments, which are less than 2 millimeters in diameter during volcanic eruptions. The term volcanic ash is generally used to include all explosives, including particles greater than 2 mm. In today's construction industry, volcanic ash is used to produce different building materials and to obtain low density composite mortar. Volcanic ash is also used as an abrasive in mechanics paste soap, abrasive hand soaps, and rubber erasers. Very fine ash is used in some toothpaste and powder, and minus-200-mesh ash has been used for polishing plate glass. Volcanic ash could be used instead of powdered pumice whenever the latter material is suitable. The Volcanic ash used in this study was commercially obtained from the local market in 1 mm sized fraction form.

Calcium hydroxide (traditionally called slaked lime) is an inorganic compound with the chemical formula $Ca(OH)_2$. It is a colorless crystal or white powder and is obtained when calcium oxide (called lime or quicklime) is mixed, or slaked with water. Slaked lime used in this study was commercially obtained from the local market as CL80 form.

Polymer Materials

Very low amount of cellulose was added to the mixtures in order to provide workability of the mortar. To improve the consistency of mortar combinations a powder form of commercial plasticizer was used. Because exfoliated vermiculate and volcanic ash have very high water absorption capacity, sodium oleate was added as a water reducer material and also the filler material, too.

Mixing Design

In order to evaluate the effect of exfoliated vermiculite aggregate on thermal comfort parameters of composite mortar samples for insulation purposes, one standard control mixture without using the exfoliated vermiculite aggregate was decided and an experimental study was performed. This standard control mixture used through this

research was obtained only mixing white cement (WCEM), sliked lime, volcanic ash and polymer additives. The mixture proportion of the control mixture for each batch are 30% of WCEM by weight, 6.5% of powder sliked lime by weight, 62.9% of volcanic ash by weight and 0.58% of total polymer mixture by weight, respectively. This mixture combination was used as constant for all the composite mortar sample preparations. Then, in order to analyze the effect of exfoliated vermiculite aggregate on thermal comfort parameters of composite mortar samples for insulation purposes, three different batches were decided as alternative lightweight composite mortar samples with 50%, 70% and 90% exfoliated vermiculite aggregates. For each exfoliation ratio, also three exfoliated vermiculite using ratios were used in sampling the composite mortars. Mixtures were based on proportions by weight and exfoliated vermiculite ratios were changed place with volcanic ash, the cement ratio was kept as constant as 30% by weight. Exfoliated vermiculite was used at the ratios of 22%, 32% and 42%, respectively for each batch. For testing to each series, a control series was prepared without exfoliated vermiculite. The rest of the mixture materials like sliked lime and polymer admixture were kept as constant 6.5% and 0.58% by weight respectively. For each series of exfoliated vermiculite aggregated mixture, twelve samples were cast, and thus, a total of 120 mortar specimens were investigated. The mixture proportions of the series are given in Table 2.

Table 2. Mixture proportions.

Mixture	WCEM (%)	Vermiculite VC (%)	Sliked Lime SL (%)	Volcanic Ash VA (%)	Polymer POL (%)	VC/WCEM
A0	**30**	**0**	**6.5**	**62.9**	**0.58**	**0.00**
A1	**30**	**22**	**6.5**	**40.9**	**0.58**	**0.73**
A2	**30**	**32**	**6.5**	**30.9**	**0.58**	**1.07**
A3	**30**	**42**	**6.5**	**20.9**	**0.58**	**1.40**
B0	**30**	**0**	**6.5**	**62.9**	**0.58**	**0.00**
B1	**30**	**22**	**6.5**	**40.9**	**0.58**	**0.73**
B2	**30**	**32**	**6.5**	**30.9**	**0.58**	**1.07**
B3	**30**	**42**	**6.5**	**20.9**	**0.58**	**1.40**
C0	**30**	**0**	**6.5**	**62.9**	**0.58**	**0.00**
C1	**30**	**22**	**6.5**	**40.9**	**0.58**	**0.73**
C2	**30**	**32**	**6.5**	**30.9**	**0.58**	**1.07**
C3	**30**	**42**	**6.5**	**20.9**	**0.58**	**1.40**

Twelve cubic test samples in 5x5x5 cm size were cast for each mixture to make sure from the coherence of the experiments. Samples were then removed from the molds after one day. They were cured for 28 days time. Any heat treatment was not applied to the samples and allowed to dry at room temperature. All test samples were analysed to determine compressive strength at 28 days curing time. Furthermore, the technical properties of unit weight, thermal conductivity and specific heat values of each sample

were also experimentally determined and the research findings were discussed in detail.

Test Methods

To measure the consistency of the mortars, flow table test was carried out. This test has been completed as required by the standard ASTM C230 (standard specification for flow table for use in tests of hydraulic cement) standard. According to this standard, the top of the flow table apparatus is cleaned and then truncate cone shaped mold is placed in the middle of the plate. The mortar is put into the mold. Mold is pulled up vertically and separated from the mortar. Finally, plate is fell down from 1.27 cm height for 25 times and the diameter of the spread mortar on the plate is measured for four times. The average of the measurement gives the flow value, which is the consistency.

The compressive strength tests were conducted according to EN 1015-11 standard. For the compressive strength testing, 5x5x5 cm cubic samples were used for each batch. The samples, after removal from the molds and cured at 3 days and then dried at room temperature until the testing time, were taken directly on the pressure test without any further action. All samples were tested by a compression testing device having a maximum loading force capacity of 303 kN. Compression loading speed for breaking the samples was maintained at a constant value of 0.1 kN/s during the entire experiments for all samples.

Thermal conductivity of test samples was experimentally determined by using a Hot Box Apparatus. The apparatus consists of basically 3 parts, which are hot room, sample room and cold room. The test device detects the temperature difference between hot room and cold room, when a material placed to the sample room. This operation is performed by thermocouples in the hot and cold rooms. Specific heat value of test samples was also experimentally determined in the laboratory as J/kgK unit.

RESULTS AND FINDINGS

The physical and some techno mechanical properties of exfoliated vermiculite aggregated composite mortar (EVACM) samples, fresh mortar volume weight, dry unit volume weight, compressive strength, consistency, thermal conductivity and specific heat performances were experimentally investigated. The research findings of these properties for EVACM samples are given in Table 3.

Table 3. Physical and techno mechanical properties of EVACM samples.

Mixture	**Fresh Mortar Volume Weight**	**Dry Unit Volume Weight**	**Consistency**	**Compressive Strength at 28 Days**	**Thermal Conductivity, λ**	**Specific Heat**

	(kg/m³)	(kg/m³)	(mm)	(N/mm²)	(W/mK)	(J/kgK)
A0	**979**	**758**	**142**	**2.64**	**0.148**	**880**
A1	**877**	**623**	**157**	**2.21**	**0.084**	**910**
A2	**876**	**592**	**143**	**1.91**	**0.080**	**935**
A3	**883**	**565**	**130**	**1.47**	**0.077**	**953**
B0	**979**	**758**	**142**	**2.64**	**0.148**	**880**
B1	**778**	**527**	**159**	**1.98**	**0.073**	**918**
B2	**747**	**476**	**147**	**1.52**	**0.067**	**941**
B3	**730**	**435**	**132**	**1.01**	**0.063**	**982**
C0	**979**	**758**	**142**	**2.64**	**0.148**	**880**
C1	**647**	**413**	**165**	**1.11**	**0.061**	**941**
C2	**591**	**352**	**151**	**0.76**	**0.056**	**964**
C3	**556**	**309**	**136**	**0.48**	**0.052**	**1045**

Consistency

Flow table test results for consistency analysis of fresh mortar are given in Table 3. When examining Table 3, it can be easily seen that the flow diameters was 142 mm for control samples, the values of flow diameters were also changed between 130-165 mm for exfoliated vermiculite aggregated mortars, too. Due to more water demand, the flow rate of EVACM samples with the using ratio 22% and 32% of exfoliated vermiculite aggregates is higher than the control mortar samples. Flow diameter for easy applicability of the insulating mortars is recommended to be approximately between 160 mm and 130 mm. If flow diameter is greater than 160 mm, it means that mixing water of fresh mortar is too much. All flow diameter values of tested mortars with exfoliated vermiculite aggregate were in the range of 160-130 mm. It means that consistency and workability of the EVACM is an acceptable level.

Unit Weight

Unit volume weight values of composites are given in Table 3. In control samples, dry unit volume weight of the hardened samples were determined as 758 kg/m^3. On the other hand, dry unit volume weight of EVACM mixtures with using exfoliated vermiculate aggregates were changed between 309 kg/m^3 and 623 kg/m^3. As the using ratio of exfoliated vermiculite aggregate increases in the mixture, the dry unit volume weight of the hardened mortar decreases. Therefore it was observed that increase in the rate of exfoliated vermiculite cause a decreasing trend in the unit volume weight values. Because, unit volume weight of exfoliated vermiculite is a very low value of 90-220 kg/m^3. Unit weight of the samples containing exfoliated vermiculite was observed up to approximately sixty percent of the control samples. This was also intended from the test results that lower unit weight means better thermal insulation.

Compressive Strength

Compressive strength values of control and EVACM samples were all tested at 7, 14 and 28 days curing as hardened structure. The 28 days curing compressive strength values of all the samples are given in Table 3. In 28 days curing compressive strength test stages, compressive strength values of all exfoliated vermiculite aggregated mortars remained under control mixture combinations. This can be explained by increasing the porosity of the matrix structure and decreasing the unit volume weight in the samples. As an exfoliated material is a porous material, it affects the strength of the material in a negative way.

Unit weight value and the compressive strength value are well known to be directly proportional. It was found that compressive strength value of 22% by weight exfoliated vermiculite series is 2.21 MPa and unit volume weight is 623 kg/m^3; compressive strength value of 32% by weight exfoliated vermiculite series is 1.91 MPa and unit volume weight is 592 kg/m^3. In addition, compressive strength value of 42% by weight exfoliated vermiculite series is 0.48 MPa and unit volume weight is 309 kg/m^3 on the basis of 90% exfoliation ratio of vermiculate aggregate. According to the results of experimental study, when exfoliated vermiculite ratio increased, the unit volume weight values of the samples decreased and unit weight of the samples decreased, and compressive strength also decreased. Besides, the decrease in compressive strength caused by the increase in the rate of vermiculite could be explained by porous and soft structure of exfoliated vermiculite aggregate. Still, all compressive strength values obtained from the experimental work found place for themselves in the TS EN 998-1 (Specification for mortar for masonry - Part 1: Rendering and plastering mortar) standard. According to this standard, thermal insulation mortars are required to take part in the CS-I or CS-II compression strength classes. According to 28 days compressive strength of all exfoliated vermiculite additive mortars are located in the range CS-I or CS-II classes. Compressive strength of EVACM varies in a range of 0.48-2.21 MPa. These values are suitable for interior and exterior plaster applications that are capable to satisfy mechanical requirements in TS EN 998-1 standard.

Thermal Comfort Parameters

The thermal comfort performance of the EVACM samples was mainly studied as two separate parameter groups: thermal comfort parameters obtained by experimental and thermal comfort parameters obtained by convergent calculations.

The thermal conductivity coefficient variation and specific heat changes of the samples were analyzed as the thermal comfort parameters obtained experimentally. The thermal conductivity coefficient of the materials is generally considered as a function of the density of the material. The lower the density, the lower the thermal conductivity coefficient of the material is expected.

Thermal conductivity of all hardened mortar samples were experimentally analyzed after 28 days of curing time. All research findings were statistically evaluated in a linear regression based on the material density and the thermal conductivity. This evaluation is given in Figure 1.

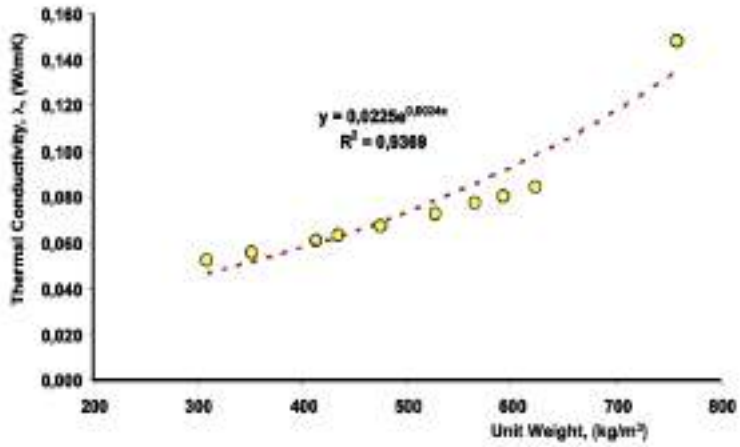

Figure 1. Density versus thermal conductivity of EVACM samples

The results show that thermal conductivity of control mixture without using exfoliated vermiculate aggregates was 0.148 W/mK. On the other hand, thermal conductivity of EVACM mixtures with using exfoliated vermiculate aggregates were changed between 0.052 W/mK and 0.084 W/mK. As the ratio of exfoliated vermiculite aggregate increases in the mixture, the thermal conductivity coefficient of the hardened mortar decreases. This also means that the hardened mortar acquires a more insulating form. Because the low thermal conductivity coefficient in materials generally represents that it is a more insulating material. For example, in the experimental series using vermiculite aggregate with an exfoliation ratio of 50%, while the thermal conductivity value of the samples using 22% wt. of vermiculite aggregate was determined as 0.084 W/mK, the thermal conductivity value of the samples decreased to 0.077 W/mK for the vermiculite using rate increased to 42%. A similar phenomenon was observed for other mixtures of mixtures.

Another point obtained in this experimental study is that as the rate of exfoliation in the production of vermiculite material increases, the thermal conductivity coefficient value decreases as a function of the decreasing unit weight. For example, the experimental series using 42% by weight of vermiculite aggregate showed that the thermal conductivity value of the samples with 50% exfoliation rate for vermiculite aggregate is 0.077 W/mK. Similarly it was also determined that the thermal conductivity value of the samples with 70% exfoliation rate for vermiculite aggregate is 0.063 W/mK and with 90% exfoliation rate for vermiculite aggregate is 0.052 W/mK. This phenomenon demonstrates that as the rate of exfoliation in the aggregate increases, the thermal conductivity decreases due to the increased porosity in the material and the material gains a more thermal insulating form.

As evaluating the experimental results for thermal conductivity values, it can be seen that reduction of exfoliated vermiculate aggregates ratio reduces the thermal conductivity. There was an acceptable linear relationship between the thermal conductivity and using rate of exfoliated vermiculate aggregates in the mixtures. Thermal conductivity of control mixtures was found to be in T2 category according to TS EN 998-1 standard. Using less than this ratio value excludes the out of scope for T2

category. On the other hand, there was an acceptable linear relationship between the thermal conductivity and exfoliated vermiculate/cement ratio, too. Thermal insulation category of all exfoliated vermiculate aggregated mortars tested was T1 class according to TS EN 998-1 standard. This represents that exfoliated vermiculate aggregated mortars are having particularly the better insulating properties than the control mortars.

The specific heat capacity value can be defined as the measure of the ability to absorb or absorb heat from the environment where a composite mortar formed in the composite structure is applied. In other words, it is an important parameter for the definition of heating and cooling phenomenon under the ambient conditions in which the composite mortar is used. The specific heat capacity of the composite mortar is the amount of heat required to increase the temperature of the unit mass by one degree in a certain temperature environment. This value is different from the point value because it is the average value in a given temperature zone. The energy of the molecules of a substance in relation to translation, rotation and vibration movements is called the internal energy of the object. The specific heat capacity value can also be called the specific heat value of the material. Specific heat is actually another physical property of matter. All matter has a temperature associated with it. The temperature of matter is a direct measure of the motion of the molecules: The greater the motion the higher the temperature. The specific heat capacity value can generally be defined as 2 different technical parameters for a material; It is called as heat capacity value and constant volume heat capacity value at constant pressure. The specific heat capacity value at constant pressure is usually symbolized by the parameter Cp, while the fixed volume specific heat capacity value is symbolized by the Cv parameter. The unit of both heat capacity values is defined as cal/g°C or J/kgK.

The specific heat of the materials could be optionally considered as a function of the density of the material. The higher the density, the lower the specific heat of the material might be expected. The specific heat of all hardened mortar samples were experimentally analyzed after 28 days of curing time. All research findings were statistically evaluated in a linear regression based on the material density and the specific heat. This evaluation is given in Figure 2. The results show that specific heat of control mixture without using exfoliated vermiculate aggregates was 880 J/kgK. On the other hand, specific heat of EVACM mixtures with using exfoliated vermiculate aggregates were changed between 910 J/kgK and 1045 J/kgK. As the ratio of exfoliated vermiculite aggregate increases in the mixture, the specific heat value of the hardened mortar increases. This also means that the hardened mortar absorbs heat from the environment making a more reliable insulating form. As evaluating the research results for the specific heat values, the experimental series using 42% by weight of vermiculite aggregate showed that the specific heat value of the samples with 50% exfoliation rate for vermiculite aggregate is 953 J/kgK. Similarly it was also determined that the specific heat value of the samples with 70% exfoliation rate for vermiculite aggregate is 982 J/kgK and with 90% exfoliation rate for vermiculite aggregate is 1045 J/kgK. This phenomenon demonstrates that as the rate of exfoliation in the aggregate increases, the specific heat increases due to the increased porosity in

the material and the material gains more ability to absorb heat from the environment where a composite mortar formed in the composite structure is applied.

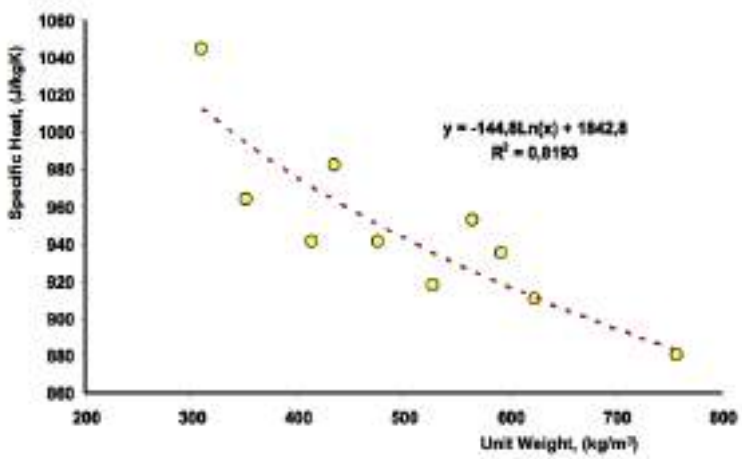

Figure 2. Density versus specific heat of EVACM samples

The heat storage capability and heat diffusion coefficient changes of the samples were analyzed as the thermal comfort parameters obtained by convergent calculations.

During the day, the effect of solar radiation and ambient temperature on the structure is constantly changing. All building materials have heat storage feature and store heat in certain amounts even during heating. This phenomenon depends on the specific heat, density, thickness and temperature difference of a component. Improvement of the heat insulation in a wall section can be achieved by low heat storage capacity of the building components forming this wall. In other words, it is desirable that all materials to be used as wall elements do not store heat in their bodies. As is known, during the warm-up, the building element stores the superficial heat. The heat storage capability of a structural element varies depending on the dry unit volume weight of the materials and the specific temperature value. In this context, the application of the new generation of composite mortars on the wall surfaces, and the criteria for the ability to store the heat in their bodies, gain a special importance in terms of characterizing the heat transfer from the mortar layer for insulation purposes.

When the heat transfer in the structural element in a building section is examined, multiplication of the density value of the structural element and the specific heat value is called the heat capacity of the material. This value also represents the heat storage capability of that material. The heat storage capability of all hardened mortar samples were given in Table 4.

Table 4. Thermal comfort properties of EVACM samples.

Mixture	Heat Storage Capability (J/m³K)	Heat Diffusion Coefficient (x10⁻⁶) (m²/sec)	Amount of heat required for 1°C temperature increase in 1 cm thickness application (cal)

A0	**0.667**	**0.222**	**1593**
A1	**0.567**	**0.148**	**1355**
A2	**0.553**	**0.145**	**1322**
A3	**0.538**	**0.143**	**1286**
B0	**0.667**	**0.222**	**1593**
B1	**0.484**	**0.150**	**1156**
B2	**0.447**	**0.150**	**1069**
B3	**0.428**	**0.148**	**1021**
C0	**0.667**	**0.222**	**1593**
C1	**0.389**	**0.157**	**929**
C2	**0.339**	**0.164**	**810**
C3	**0.323**	**0.162**	**771**

The heat storage capability of all hardened mortar samples were calculated according to the above approach for the 28 days of curing time. The results show that heat storage capability of control mixture without using exfoliated vermiculate aggregates was 0,667 J/m^{3}K. On the other hand, heat storage capability of EVACM mixtures with using exfoliated vermiculate aggregates were changed between 0.567 J/m^{3}K and 0.323 J/m^{3}K. As the using ratio of exfoliated vermiculite aggregate increases in the mixture, the heat storage capability of the hardened mortar decreases. This also means that the hardened mortar stores less heat in the element section where its used making a more reliable insulating form. To understand the effect of using exfoliated vermiculate aggregate in composite mortar structures based on the using ratio by weight and the exfoliation ratio during producing the aggregate obtained by heat treatment, a graphical analysis was made for the research findings. Graphical analysis of heat storage capability of all hardened mortar samples after 28 days of curing time is given in Figure 3.

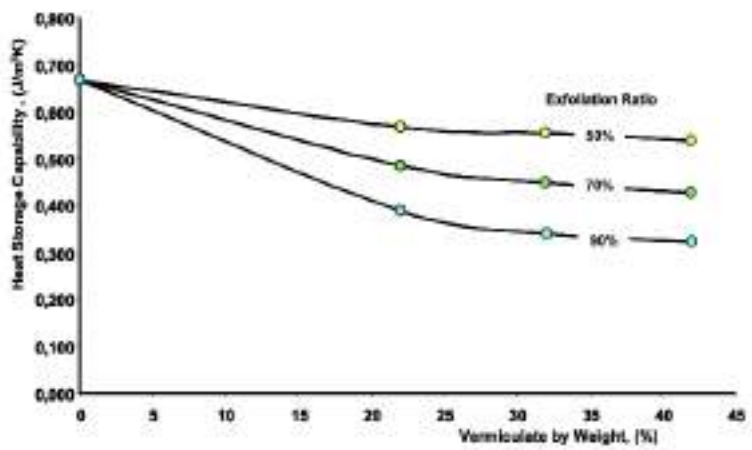

Figure 3. Using vermiculate aggregate ratio versus heat storage capability.

As evaluating the graphical analysis, it can be stated that increasing the vermiculate exfoliation ratio reduces the heat storage capability of the composite mortar structure. That means that the material stores less heat in the application area and this allows the

material to gain a more insulating character. The less heat stored, the higher the insulation property for heating or cooling purposes in a wall section.

Another convergent calculation is heat diffusion coefficient for the samples. Another material feature that is important in the time-dependent heat transfer is the heat diffusion coefficient. The heat diffusion coefficient indicates how fast the heat is spreading on and within a material surface. Unit of this parameter for a material is symbolized as m^2/sec. This coefficient can be defined as the ratio of the amount of heat transmitted in a material to the amount of heat stored within that material. The heat diffusion coefficient of all hardened mortar samples were also given in Table 3.

The heat diffusion coefficient of all hardened mortar samples were calculated according to the above approach for the 28 days of curing time. The results show that heat diffusion coefficient of control mixture without using exfoliated vermiculate aggregates was $0{,}222 \times 10^{-6}$ m^2/sec. On the other hand, heat diffusion coefficient of EVACM mixtures with using exfoliated vermiculate aggregates were changed between $0{,}148 \times 10^{-6}$ m^2/sec and $0{,}162 \times 10^{-6}$ m^2/sec. As the using ratio of exfoliated vermiculite aggregate increases in the mixture, the heat diffusion coefficient of the hardened mortar decreases. This also means that the heat will be transferred much more slowly through the material. To understand the effect of using exfoliated vermiculate aggregate in composite mortar structures on the material heat transfer characteristics, a graphical analysis was made for the research comparing with the control mixture findings. Graphical analysis of heat diffusion efficiency of hardened EVACM samples after 28 days of curing time is given in Figure 4.

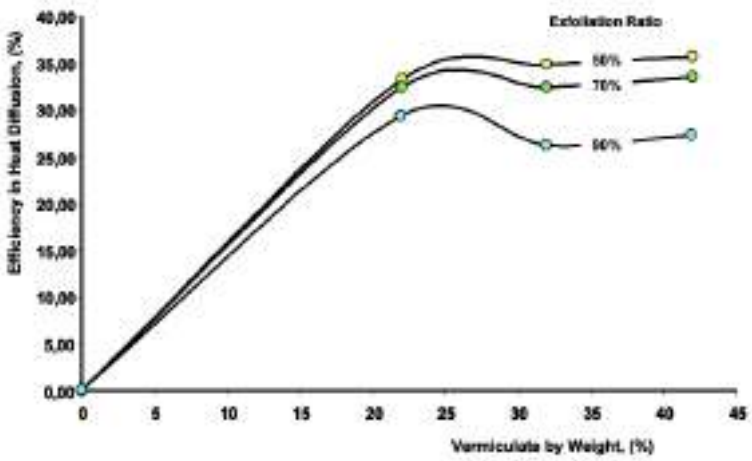

Figure 4. Using vermiculate aggregate ratio versus heat diffusion efficiency.

As evaluating the graphical analysis, it can be stated that increasing the vermiculate exfoliation ratio reduces the heat diffusion through the composite mortar structure. That means that heat is transferred much more slowly through the material in the application case and the material will exhibit a more resistant structure against heat passages. Therefore, the less heat diffused, the higher the insulation property for heating or cooling purposes in a material structure. If it is necessary to quantify this situation, in the EVACM samples, the rate of use of 32% vermiculite aggregates was found to provide 35% less heat dissipation than the control mixture. The materials with

high thermal conductivity coefficient or low heat capacity have high heat diffusion coefficients. The high heat diffusion coefficients represents the high heat dissipation from the material to the interior, and the low heat diffusion coefficient represents that the heat is absorbed and absorbed into heat energy in a large amount of material. In such materials, the amount of heat conduction is also low. In this context, it is desirable that the heat diffusion coefficients, that are the heat dissipation values, are low in the composite grout in terms of insulation performance. When formulating a composite mortar, it should be considered that the product is composed of components that will provide low heat diffusion. When the heat diffusion coefficient values of the vermiculite aggregates with different exfoliation values are examined, it can be seen that the heat capacity of the material is low while the heat diffusion coefficient of the same material can be higher. This may indicate that such materials will not absorb heat on the surface and body of the materials, but will make a relatively faster heat dissipation to the interior. If this approach will be dealt with in terms of amount of heat required for 1°C temperature increase in 1 cm thickness application, similar phenomenon is clearly seen. The action of all hardened mortar samples were also given in Table 4. Evaluating the table, it can be seen that the use of the increased vermiculite ratio indicates that the amount of heat required increasing the temperature of the material by 1oC decreases significantly. If it is necessary to quantify this situation, in the EVACM samples, the rate of using 32% vermiculite aggregates was found to require 49% less heat storage than the control mixture. To evaluate the effect of using exfoliated vermiculate aggregate in composite mortar structures on this comfort action, a graphical analysis was made for the research comparing with the control mixture findings as heat storage efficiency. Graphical analysis of heat storage efficiency of hardened EVACM samples after 28 days of curing time is given in Figure 5.

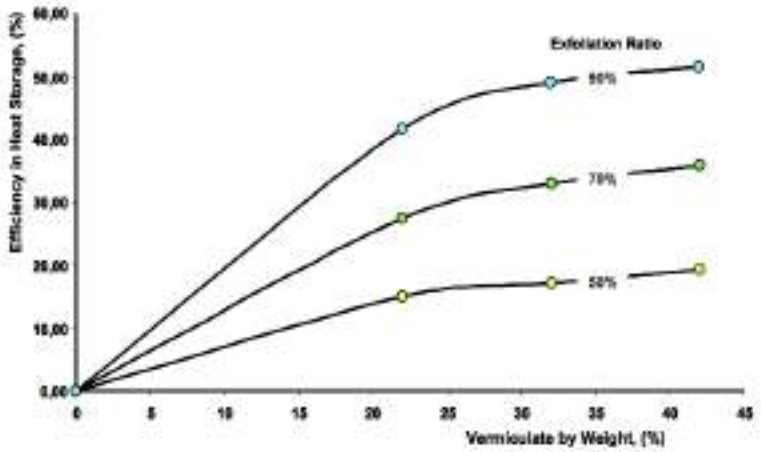

Figure 5. Using vermiculate aggregate ratio versus heat storage efficiency.

As evaluating the graphical analysis, it can be stated that increasing the vermiculate exfoliation ratio increases the efficiency in heat storage through the composite mortar structure. That means that less heat is stored in the material structure and the material will exhibit a more resistant structure against heat storage.

CONCLUSION

In this paper, thermal comfort aspects and technical performances of exfoliated vermiculite aggregated composite mortar were experimentally analyzed in detail to be used in construction materials as raw materials. All the experimental testing studies were carried out at construction materials innovation laboratory in İzmir Katip Çelebi University.

A comparative discussion for exfoliated aggregates based on the parameters such as thermal conductivity, specific heat value, heat storage capability, heat diffusion coefficient and heat storage efficiency will be given as numerical evaluations in the paper. These parameter values are compared with the advantages and disadvantages of the material context as well as the performance effects that these types of aggregates will provide when used in any construction material. According to the test results;

Consistency and workability of the EVACM is an acceptable level.
Unit weight of the samples containing exfoliated vermiculite was observed up to approximately sixty percent of the control samples. This was also intended from the test results that lower unit weight means better thermal insulation.
Compressive strength of EVACM varies in a range of 0.48-2.21 MPa. These values are suitable for interior and exterior plaster applications that are capable to satisfy mechanical requirements in TS EN 998-1 standard.

Thermal insulation category of all exfoliated vermiculate aggregated mortars tested was T1 class according to TS EN 998-1 standard. This represents that exfoliated vermiculate aggregated mortars are having particularly the better insulating properties than the control mortars.

As the ratio of exfoliated vermiculite aggregate increases in the mixture, the specific heat value of the hardened mortar increases. This also means that the hardened mortar absorbs heat from the environment making a more reliable insulating form.
It is desirable that all materials to be used as wall elements do not store heat in their bodies. As the using ratio of exfoliated vermiculite aggregate increases in the mixture, the heat storage capability of the hardened mortar decreases. This also means that the hardened mortar stores less heat in the element section where its used making a more reliable insulating form.

Increasing the vermiculate exfoliation ratio increases the efficiency in heat storage through the composite mortar structure. That means that less heat is stored in the material structure and the material will exhibit a more resistant structure against heat storage.

As the using ratio of exfoliated vermiculite aggregate increases in the mixture, the heat diffusion coefficient of the hardened mortar decreases. This also means that the heat will be transferred much more slowly through the material.

According to the test results, when exfoliated vermiculite aggregate ratio increases, thermal comfort values are improved. As a result of this study, it has could be concluded that the exfoliated vermiculite is a good energy efficient aggregate which can be used in heat-insulating materials that can be produced and appplied for energy efficient buildings.

REFERENCES

Abidi, S., Nait-Ali, B., Joliff, Y., Favotto, C. (2015). Impact of perlite, vermiculite and cement on the thermal conductivity of a plaster composite material: Experimental and numerical approaches. *Composites: Part B*, vol. 68, p. 392-400.

Al-Jabri, K.S., Hago, A.W., Al-Nuaimi, A.S., Al-Saidy, A.H. (2005). Concrete blocks for thermal insulation in hot climate. *Cement and concrete research*, vol. 35, p.1472-1479.

Binici, H., Sevinç, A.H., Efe, V. (2015). The production of insulation materials made with waste newsprint. *Çukurova University Journal of the Faculty of Engineering and Architecture*, vol. 30(2), p.13-23.

Chung, O., Jeong, S.G., Kim, S. (2015). Preparation of energy efficient paraffinic PCMs/expanded vermiculite and perlite composites for energy saving in buildings. *Solar Energy Materials & Solar Cells*, vol. 137, p. 107-112.

Claramunt, J., Fernandez-Carrasco, L.J., Ventura, H., Ardanuy, M. (2016). Natural fiber nonwoven reinforce cement composites as sustainable materials for building envelopes. *Construction and Building Materials*, vol. 115, p. 230-239.

Demirçivi, P., Saygılı G.N. (2014). Sorption isotherms and modeling studies of hdtma for adsorption onto vermiculite, perlite and zeolite clays. *Journal of Engineering and Natural Sciences*, vol. 32, p. 311-320.

Gencel, O., Diaz, J.J.D.C.D., Sutcu, M., Koksal, F., Rabanal, F.P.A., Martinez-Barrera, G., Brostow, W. (2014). Properties of gypsum composites containing vermiculite and polypropylene fibers: Numerical and experimental results. *Energy and Buildings*, vol. 70, p. 135-144.

Kibert C.J. (2003). Green buildings: an overview of progress. *Journal of land use and environmental law*, vol. 19(2), p.491–502.

Koksal, F., Gencel O., Kaya M. (2015). Combined effect of silica fume and expanded vermiculite on properties of lightweight mortars at ambient and elevated tempretures. *Construction and building materials*, vol. 88, p. 175-187.

Shoukry, H., Kotkata, M.F., Abo-El-Enein, S.A., Morsy, M.S., Shebl, S.S. (2016). Enhanced physical, mechanical and microstructural properties of lightweight

vermiculite cement composites modified with nano metakaolin. *Construction and Building Materials*, vol. 112, p. 276-283.

Wu, M.H., Ng, T.S., Skitmore, M.R. (2016). Sustainable building envelope design by considering energy cost and occupant satisfaction. *Energy for sustainable development*, vol. 31, p. 118-129.

FEATURE SELECTION FOR SMS SPAM FILTERING USING ROUGH SET THEORY

Rasim ÇEKİK
Department of Computer Engineering
Eskişehir Technical University
Eskisehir, 26555, Turkey
rasimcekik@anadolu.edu.tr

Alper Kürşat UYSAL
Department of Computer Engineering
Eskişehir Technical University
Eskisehir, 26555, Turkey
akuysal@anadolu.edu.tr

ABSTRACT: SMS spam problems show parallel growth with the rapid growth of technological development in the field of electronic communication among people. It is one of the short text classification problems. Many methods have been proposed to solve this problem in different studies using different feature extraction methods, feature selection methods, and analysis systems. Bag-of-words (BoW) and some other approaches can be used for feature extraction. While Gini index (GI) and chi-square (CHI2) are some examples to feature selection methods utilized in SMS spam filtering studies, Support Vector Machines (SVM) and k-nearest neighbor (k-NN) are some classification models used in the literature. In this paper, we propose a novel feature selection method based on rough set theory (RST) as an alternative and effective solution for this problem. The proposed method is tested on a SMS spam dataset using three different classifiers. Its performance is compared with four feature selection methods. It provides either a good or competitive performance according to the experimental results.

Key words: short text classification, sms spam, rough set, text mining

INTRODUCTION

With the rapid developments in information and communication technologies, short message service (SMS) has become one of the most popular and important communication methods. The growth in the usage of this technology has caused some problems such as SMS spam which needs effective solutions. SMS spam can be defined as SMS message containing advertisements, free services, promotions, awards, etc. which are sent to the users without a demand. There exist applications and studies for solving SMS spam problem such as many android apps (Choudhary, N. and Jain, A. K., 2017) and the filtering techniques (Puniškis, D. et al., 2006). Also, different solutions have been proposed in various studies. For example, (El-Alfy , E. S. M., and AlHasan, A.A, 2016) have proposed a model for filtering text messages. The model can be adapted for both SMS and e-mail. (Ma, J., et al., 2016) and (Chan, P. P., 2015) et al. have proposed a message topic model (MTM) and two methods for SMS spam filtering

i.e. feature reweighting method and good word attack for filtering spam messages, respectively.
Rough Set Theory (RST) has found its place in many areas due to its successful deductions on incomplete, vagueness and uncertainty data. Therefore, SMS spam filtering is a kind of problem where RST can be applied. The main idea of the RST is the notion of approximation space. Two advantages of RST for short text classification applications are follows: (i) it does not need any additional or preliminary information about dataset, and (ii) it is a tool for using in computer applications in circumstances including vagueness and uncertainty. In other words, the rough set theory approach can be stated as a formal framework to discover facts from imperfect data (Walczak & Massart, 1999). The results of the rough set approach can be indicated in the form of decision rules produces using a set of examples. In this study, rule-removing skill of rough sets approach has been used. For this process, LEM2 algorithm has been used. LEM2 algorithm is a rule induction algorithm to handle inconsistent data using rough set theory.

ROUGH SET THEORY

The rough set theory, proposed by Pawlak in 1985 (Pawlak, Z. (1982)., Pawlak, Z., & Skowron, A. (2007), Pawlak, Z. et al. (1995)) and it has become popular in many other disciplines (Ziarko, W., 1994). It is a new approach based on mathematics to imperfect knowledge. Vagueness is expressed by a boundary region of a set in this approach. This concept can be explained by means of topological operations, interior and closure, called approximations. Basic concepts of rough sets: information/decision systems, reducts and core, indiscernible relation set approximation, rough membership and dependency of attributes.

PROPOSED METHOD

The rough set approach can be considered as a framework to discover facts from imperfect data. In this study, rule-removing skill of rough sets approach has been used. For this process, LEM2 algorithm has been used. LEM2 algorithm is a rule induction algorithm to handle inconsistent data set using rough set theory.
The LEM2 algorithm has several methods such as basic minimal covering, extent minimal covering and satisfactory description. In this study, extent minimal covering method has been used. This method is utilized to generate a set of decision rules based on an extent minimal covering. The method is used for generating decision rules using extended LEM2. ModLEM is the modified LEM2. The ModLEM can deal with continuous values of attributes without the need of prior discretization and generates rules with extended syntax of conditions. So, ModLEM is able to generate tests in form: attribute ≤ value, attribute ≥ value or lower bound ≤ attribute ≤ upper bound, instead of simple tests in form attribute = value. ModLEM contains three different extensions: Interval extensions, Laplace measure and entropy measure. The architecture of the proposed method is presented in Figure 1.

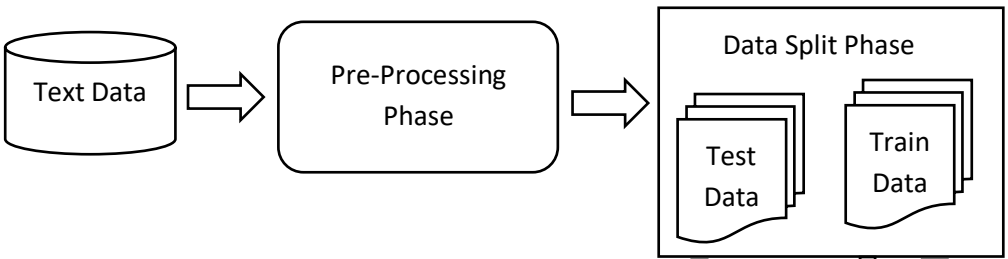

Figure 1: Architecture of proposed method

In the study, Laplace Measure extension of ModLEM is used. It is worth to mention that there are not any pre-processing operations done because of the pre-processing operations which have been performed on used data sets. Therefore, the pre-processing phase will not be discoursed. Processes handled in this study are given below respectively.

Selecting a subset data within the entire dataset: Since the used datasets are very large, they are divided into smaller subsets. The division operation has been made based on features using any feature selection method.

Divide subset data as train and test data: Subset data is divided as at randomly 66% train and 33 % test data.

Generation rules using train data: ROSE2 (Rough Set Data Explorer) has been used for generating rules on train data. ROSE2 is a software implementing basics of the rough set theory and rule discovery approaches. All computations are based on fundamentals of rough sets proposed by Z. Pawlak. One of implemented extensions uses the variable precision rough set model defined by W. Ziarko. Another extension applies the rough set approach based on a similarity relation, as proposed by R. Slowinski. The similarity relation is evaluated via inductive learning from data (Kryszkiewicz, M., 1998).

Generation features for new information system: In the phase, a new information system is generated. Features of new information system are selected according to the generated rules. All features and each feature in generated rules is included a set called F_{ALL} and F_{a_i}, respectively. Each feature of weight (W_{A_i}) is calculated the following formula:

$$W_{A_i} = \frac{F_{A_i}}{F_{ALL}} \quad \text{Where, } A_i \text{ shows } i^{th} \text{ feature.} \qquad (1)$$

Classification: In the phase, WEKA (Waikato Environment for Knowledge Analysis) has been used for classification and another features selection method. The WEKA (Hall et al., 2009) is name of one of the packages used in machine learning. It has been

developed as open source in JAVA language at Waikato University and it is distributed under GPL license. So, the WEKA is used for both classification and different features selection method.

An Example

Suppose that following Information System (IS) is given.

Table I: Information System

	A_1	A_2	A_3	**D**
D_1	1	0	1	1
D_2	0	0	0	1
D_3	1	0	0	1
D_4	0	1	0	1
D_5	0	1	1	2
D_6	1	0	1	2
D_7	1	0	1	2
D_8	1	0	0	2
D_9	0	0	1	2

The IS in Table-I is text document collection consisted nine document and three condition and one decision features.

Determine core and reduct of features: The reduct is the important part of an IS, which can discern all objects. The core is the common part of all reducts. The discernibility matrix is utilized to compute reducts and core. The below discernibility matrix is given for IS in Table I.

Table II: Discernibility Matrix

	D_1	D_2	D_3	D_4	D_5	D_6	D_7	D_8	D_9
D_1	λ								
D_2	λ	λ							
D_3	λ	λ	λ						
D_4	λ	λ	λ	λ					
D_5	A_1, A_2	A_2, A_3	A_1, A_2, A_3	A_3	λ				
D_6	λ	A_1, A_3	A_3	A_1, A_2, A_3	λ	λ			
D_7	λ	A_1, A_3	A_3	A_1, A_2, A_3	λ	λ	λ		
D_8	A_3	A_1	λ	A_1, A_2	λ	λ	λ	λ	
D_9	A_1	A_3	A_1, A_3	A_2, A_3	λ	λ	λ	λ	λ

For the discernibility matrix shown in Table II, the discernibility function has the following form:

$$F_C = (A_1 \vee A_2) \wedge (A_2 \vee A_3) \wedge (A_1 \vee A_2 \vee A_3) \wedge A_3 \wedge (A_1 \vee A_3) \wedge A_3 \wedge (A_1 \vee A_2 \vee A_3) \wedge (A_1 \vee A_3) \wedge A_3 \wedge (A_1 \vee A_2 \vee A_3) \wedge A_3 \wedge A_1 \wedge (A_1 \vee A_2) \wedge A_1 \wedge A_3 \wedge (A_1 \vee A_3) \wedge (A_2 \vee A_3)$$

$= (A_1 \wedge A_3)$

where, features A_1 and A_3 are core features and feature A_2 is reduct feature. So, feature A_2 is superfluous, whereas features A_1 and A_3 are indispensable. In this way, one reduct of the considered set of features is found. The representation is equivalent to

the one in Table I. Features A_1 and A_3 provide the same knowledge about the universe U, as the sets of features A_1, A_2 and A_3.

Table III: Reduced Information System (RIS)

	A_1	A_3	**D**
D_1	1	1	1
D_2	0	0	1
D_3	1	0	1
D_4	0	0	1
D_5	0	1	2
D_6	1	1	2
D_7	1	1	2
D_8	1	0	2
D_9	0	1	2

Determine core and reduct of features values: Simplification of the *RIS* can be achieved by dropping certain values of features, which are unnecessary for the system. Instead of one discernibility function, we have to construct as many discernibility functions, as there are documents in the *RIS*.

Table IV: Discernibility Matrix for RIS

	D_1	D_2	D_3	D_4	D_5	D_6	D_7	D_8	D_9
D_1	λ				A_1	λ	λ	A_3	A_1
D_2	λ	λ			A_3	A_1, A_3	A_1, A_3	A_1	A_3
D_3	λ	λ	λ		A_1, A_3	A_3	A_3	λ	A_1, A_3
D_4	λ	λ	λ	λ	A_3	A_1, A_3	A_1, A_3	A_1	A_3
D_5	A_1	A_3	A_1, A_3	A_3	λ	λ	λ	λ	λ
D_6	λ	A_1, A_3	A_3	A_1, A_3	λ	λ	λ	λ	λ
D_7	λ	A_1, A_3	A_3	A_1, A_3	λ	λ	λ	λ	λ
D_8	A_3	A_1	λ	A_1	λ	λ	λ	λ	λ
D_9	A_1	A_3	A_1, A_3	A_3	λ	λ	λ	λ	λ

To construct F_{D1}, one considers all documents of features from column 1 in Table IV; to construct F_{D2}, one takes into account all documents of features from column 2, etc.

$F_{D1} = A_1 \wedge A_3 \wedge A_3 = A_1 \wedge A_3$

$F_{D2} = A_3 \wedge (A_1 \vee A_3) \wedge (A_1 \vee A_3) \wedge A_1 \wedge A_3 = A_1 \wedge A_3$

$F_{D3} = (A_1 \vee A_3) \wedge A_3 \wedge A_3 \wedge (A_1 \vee A_3) = A_3$

$F_{D4} = A_3 \wedge (A_1 \vee A_3) \wedge (A_1 \vee A_3) \wedge A_1 \wedge A_3 = A_1 \wedge A_3$

$F_{D5} = A_1 \wedge A_3 \wedge (A_1 \vee A_3) \wedge A_3 = A_1 \wedge A_3$

$F_{D6} = (A_1 \vee A_3) \wedge A_3 \wedge (A_1 \vee A_3) = A_3$

$F_{D7} = (A_1 \vee A_3) \wedge A_3 \wedge (A_1 \vee A_3) = A_3$

$F_{D8} = A_3 \wedge A_1 \wedge A_1 = A_1 \wedge A_3$

$F_{D9} = A_1 \wedge A_3 \wedge (A_1 \vee A_3) \wedge A_3 = A_1 \wedge A_3$

Consequently, one can simplify Table-III in the following way in Table V.

Table V: * Denotes ' do not care'

	A_1	A_3	**D**
D_1	1	1	1
D_2	0	0	1

D_3	*	0	1
D_4	0	0	1
D_5	0	1	2
D_6	*	1	2
D_7	*	1	2
D_8	1	0	2
D_9	0	1	2

The above described decision table can also be considered as a set of decision (classification) rules of the form (as Laplace Measure extension of ModLEM):

$$A_k < i \implies D = j$$

where, A_k means that ' feature A_k has value i' and the symbol '$\Rightarrow$' denotes propositional implication and j describes class of document in D. Table-V can be regarded as a set of the following decision rules:

Rule-1: $(A_1 < 0.5)$ & $(A_3 < 0.5) \Rightarrow D = 1$ (2)
Rule-2: $(A_1 < 0.5)$ & $(A_3 \geq 0.5) \Rightarrow D = 2$ (2) where, (2) shows number of rule.
Approximate rule
Rule-3: $(A_1 \geq 0.5) \Rightarrow D = 1 \; or \; D = 2$
Each feature of weight is calculated with the formula (1). In the study, approximate rules has not been used because of it does not report exact result. So, each feature of weight (W_{A_i}) is as follows:
$F_{A_1} = \{A_1, A_1\}$ (There is one A_1 in both Rule-1 and Rule-2)
$F_{A_3} = \{A_3, A_3\}$ (There is one A_3 in both Rule-1 and Rule-2)
$F_{ALL} = \{A_1, A_1, A_3, A_3\}$ (Number of feature in all rules)
So, $W_{A_1} = \frac{2}{4} = 0{,}5$ and $W_{A_3} = \frac{2}{4} = 0{,}5$
$W_{A_2} is\ zero$ because of A_2 is not in any rule.
Each feature is ranked according to W_{A_i} and k features that have highest W_{A_i} are selected. In this way, k features are selected and those k features are features of new information system. Suppose that k =2 for given example, A_3 and A_3 are selected.

EXPERIMENTAL STUDY
In the study, an English SMS spam dataset is used. It is a publicly available SMS message collection in English (Nuruzzaman et al., 2011). This dataset consists of 425 spam and 450 legitimate messages. 612 instances are used for training and 263 instances are used for testing in the experiments.
In this paper, the proposed method is a feature selection method. After selecting features with the proposed method, classification operation is performed using Naïve Base, SMO, and BayesNet classifiers in WEKA. Those classifiers have been selected randomly. Also, Information Gain (IG), Gain Ratio (GR), Principal Components (PC), and OneR feature selection methods in WEKA are used for analyzing and comparing the performance of proposed method. In the experiments, all feature selection methods are tested with the same classifiers. Top-50, Top-100, Top-150, Top-200, Top-250 and Top-270 features are selected with each feature selection method. Later, the

success ratio of three classifiers on these feature subsets are given in Table VI, Table VII, and Table VIII, respectively.

Table VI: Accuracy of Naïve Bayes Classifier for Feature Selection Methods (%)

Selected Number of Features	Information Gain	Gain Ratio	Principal Components	OneR	RST
50	90,0152	92,7757	67,0608	93,5361	92,3954
100	94,6768	93,5361	65,3992	93,1559	92,3954
150	94,6768	93,5361	64,6388	93,1559	93,5361
200	**95,0570**	93,5361	65,3992	93,5361	93,9163
250	94,6768	93,9163	65,3992	93,5361	94,2966
270	94,6768	93,5610	65,7795	93,5361	94,2966

Table VII: Accuracy of SMO Classifier for Feature Selection Methods (%)

Selected Number of Features	Information Gain	Gain Ratio	Principal Components	OneR	RST
50	92,3954	93,1559	88,9734	92,7757	91,2548
100	91,2548	92,0152	88,9734	91,2548	91,6350
150	**93,5361**	91,6350	88,9734	92,7757	92,0152
200	92,3954	92,0152	88,2129	92,0152	92,7757
250	92,7757	92,3954	90,4943	91,6350	92,0152
270	93,1159	92,3954	91,2548	92,0152	92,3954

Table VIII: Accuracy of BayesNet Classifier for Feature Selection Methods (%)

Selected Number of Features	Information Gain	Gain Ratio	Principal Components	OneR	RST
50	90,8745	91,6350	90,4943	90,8745	93,1559
100	90,8745	92,0152	88,5932	90,8745	93,1559
150	90,8745	92,0152	88,9734	90,8745	93,5361
200	90,8745	92,0152	88,5932	90,8745	94,6768
250	90,8745	92,0152	88,5932	90,8745	94,6768
270	90,8745	90,8745	88,5932	90,8745	**94,6768**

As seen from Table VI, Table VII and Table VIII, it is clear that Naïve Bayes, SMO and BayesNet classifiers show the best result for Top-200 features with IG, Top-150 features with IG and Top-200 or Top-250 or Top-270 features with proposed feature selection method, respectively. Additionally, proposed method seems successful not only in Table VIII but also in other tables. This situation can be understood more easily on the graphics.

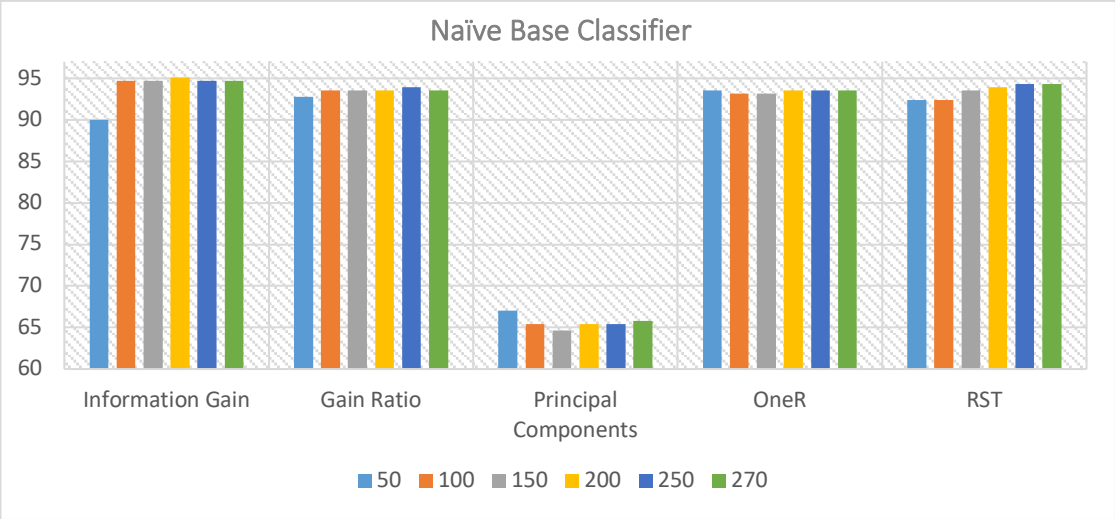

Figure 2: Classification with Naïve Bayes Classifier

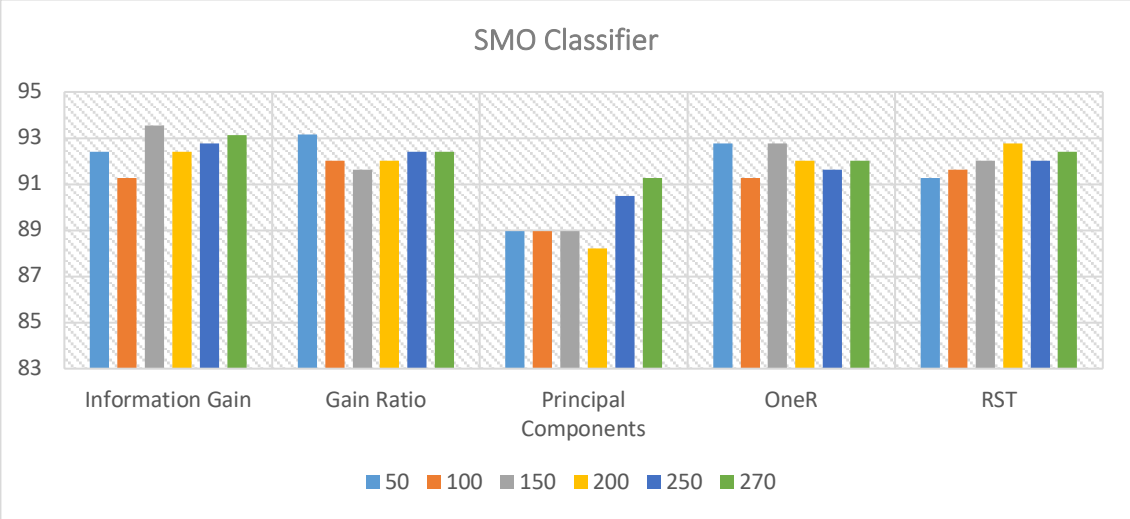

Figure 3: Classification with SMO Classifier

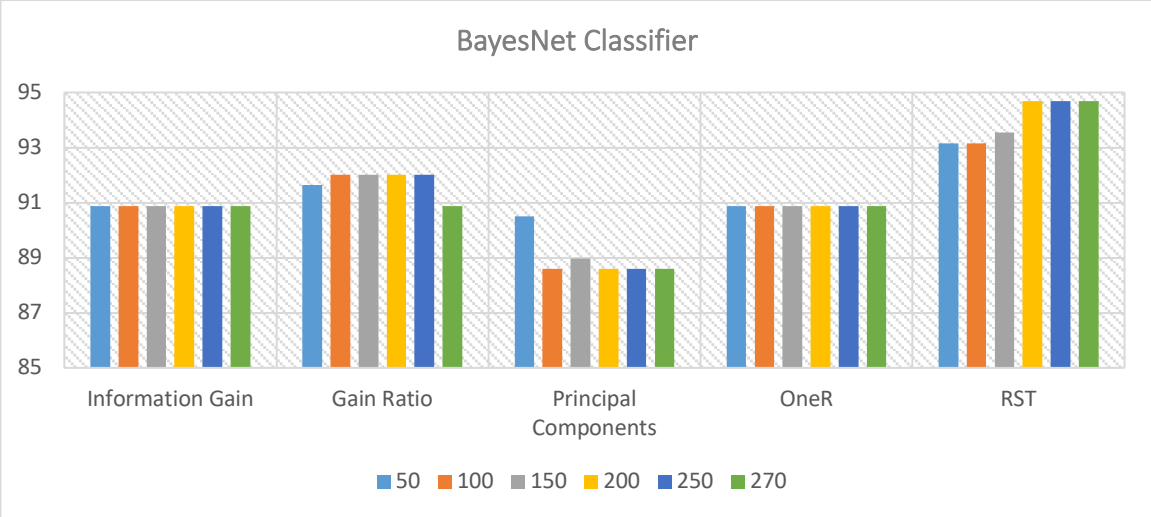

Figure 4: Classification with BayesNet Classifier

As seen from Figure 4, it is clear that proposed method achieves the best the result when BayesNet classifier is used. Also, as seen in Figure 2 and Figure 3, it achieves the second and the third higher performance, respectively. For example, for Naïve Bayes classifier, the best result is obtained with the Information Gain feature selection method with an accuracy value of 95,0570%. For the same classier, the proposed method produces the second highest classification score of 94,2966% (See Table VI). Additionally, for SMO classifier, proposed method produces one of the third highest classification score of 92,7757% (See Table VII). Finally, for BayesNet classifier, proposed method produces the highest classification score of 94,6768% (See Table VIII). Showing the success of all methods on a single table and a graphic can be useful to interpret the results as below (See Figure 5-6).

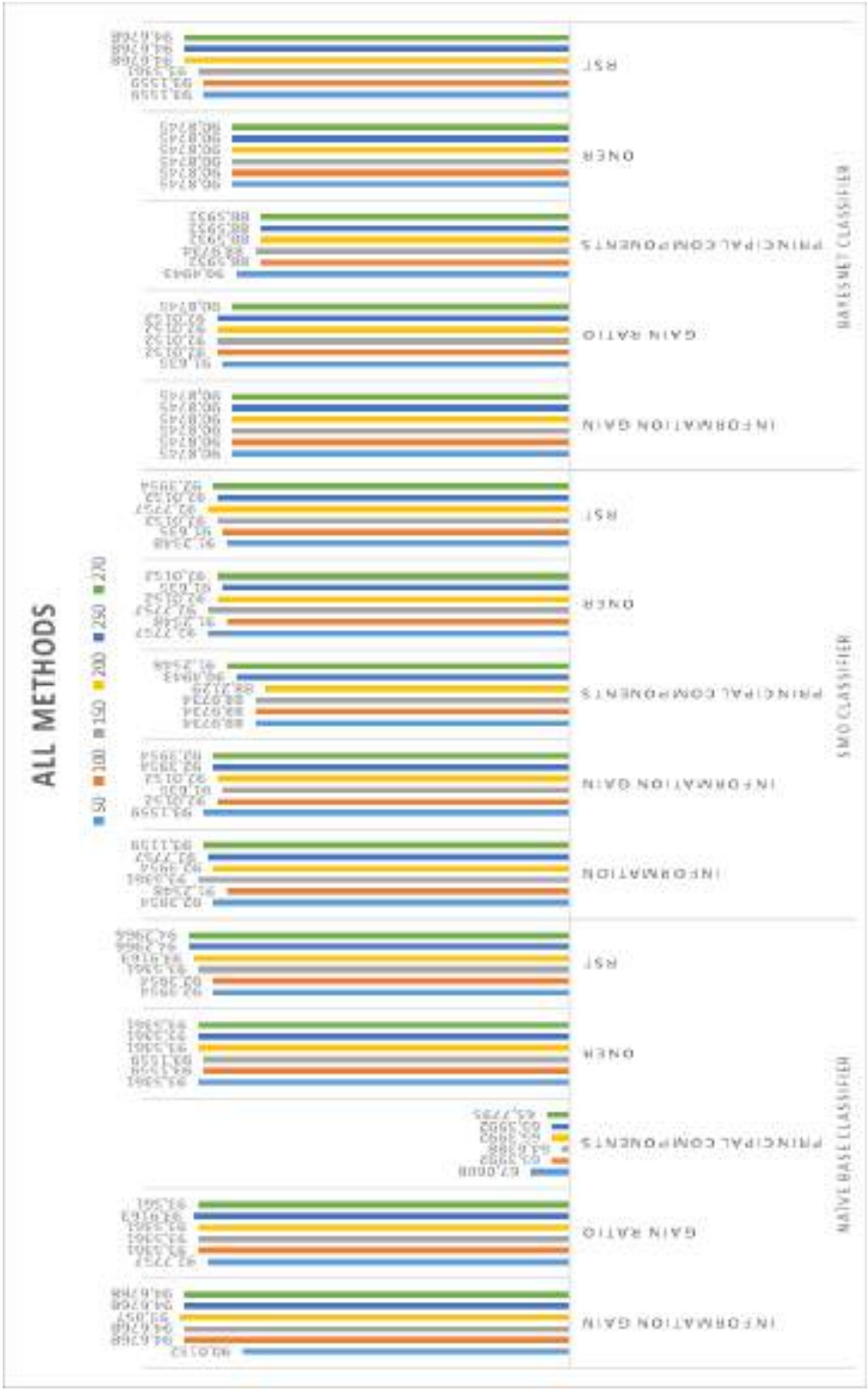

Figure 5: Summary of the Performances in a Table Structure

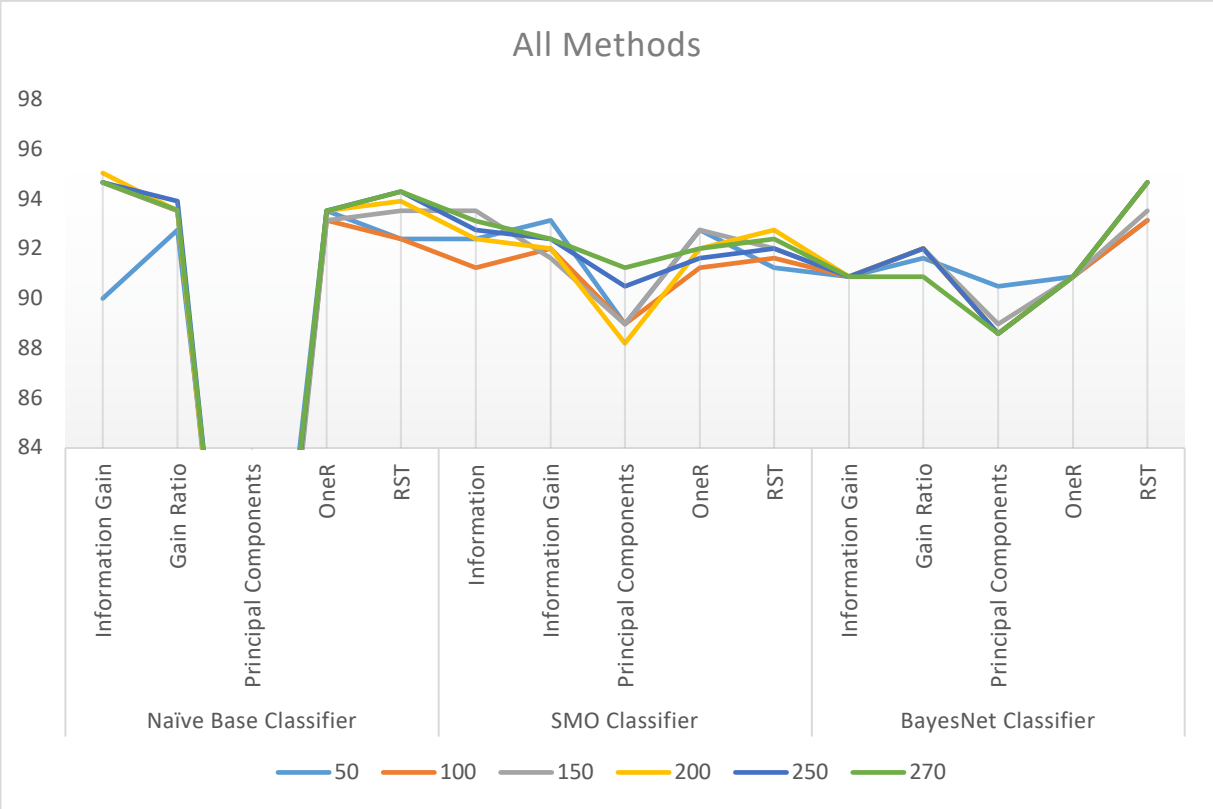

Figure 6: Summary of the Performances in a Graphic Structure

Consequently, the results of the experiment showed that the proposed feature selection method using RST influences the performance of the classifiers positively.

CONCLUSION AND FUTURE WORK

In this study, a new feature selection method is proposed to improve the performance of classification on SMS spam data. The most important advantage of proposed method is reduced complexity handling in consistency in dataset and taking care of hidden classification using rules created with RST. The RST finds core required features and reduce features. It provides either a good or competitive performance according to the experimental results. Therefore, the more efficient feature selection can be possible using the RST. In the future, proposed method will be tested on different datasets using different classifiers and it will be compared with different feature selection methods.

REFERENCES

Chan, P. P., Yang, C., Yeung, D. S., & Ng, W. W. (2015). Spam filtering for short messages in adversarial environment. Neurocomputing, 155, 167-176.
Choudhary, N., & Jain, A. K. (2017). Towards filtering of SMS spam messages using machine learning based technique. *In Advanced Informatics for Computing Research* (pp. 18-30). Springer, Singapore.

El-Alfy, E. S. M., & AlHasan, A. A. (2016). Spam filtering framework for multimodal mobile communication based on dendritic cell algorithm. *Future Generation Computer Systems*, 64, 98-107.

Hall, M., Frank, E., Holmes, G., Pfahringer, B., Reutemann, P., & Witten, I. H. (2009). The WEKA data mining software: an update. ACM SIGKDD explorations newsletter, 11(1), 10-18.

Kryszkiewicz, M. (1998). Rough set approach to incomplete information systems. *Information sciences*, 112(1-4), 39-49.

Ma, J., Zhang, Y., Liu, J., Yu, K., & Wang, X. (2016, September). Intelligent SMS spam filtering using topic model. *In Intelligent Networking and Collaborative Systems (INCoS), 2016 International Conference on* (pp. 380-383). IEEE.

Nuruzzaman, M. T., Lee, C., & Choi, D. (2011, August). Independent and personal SMS spam filtering. *In Computer and Information Technology (CIT), 2011 IEEE 11th International Conference on* (pp. 429-435). IEEE.

Pawlak, Z., Grzymala-Busse, J., Slowinski, R., & Ziarko, W. (1995). Rough sets. *Communications of the ACM*, 38(11), 88-95.

Pawlak, Z., & Skowron, A. (2007). Rough sets: some extensions. Information sciences, 177(1), 28-40.

Pawlak, Z. (1982). Rough sets. International journal of computer & information sciences, 11(5), 341-356.

Puniškis, D., Laurutis, R., & Dirmeikis, R. (2006). An artificial neural nets for spam e-mail recognition. *Elektronika ir Elektrotechnika*, 69(5), 73-76.

Ziarko, W. (1994). Rough sets and knowledge discovery: An overview. *In Rough sets, fuzzy sets and knowledge discovery (pp. 11-15)*. Springer, London.

Walczak, B. & Massart, D. L. Rough sets theory. *Chemometrics and intelligent laboratory systems*, 1999, 47.1: 1-16.

INVESTIGATION OF CHARGING AND DISCHARGING CHARACTERISTICS OF DIFFERENT TYPE BATTERIES ON HYBRID ELECTRIC VEHICLE MODEL

Yunus Emre EKİCİ
Inonu University, Engineering Faculty, Dept. of Electrical and Electronics Eng., 44280, Malatya, Turkey
emreekici@ogr.inonu.edu.tr

Nusret TAN
Inonu University, Engineering Faculty, Dept. of Electrical and Electronics Eng., 44280, Malatya, Turkey
nusret.tan@inonu.edu.tr

ABSTRACT: In this study, component-based modeling of a hybrid vehicle was performed. In order to model different battery types, a battery model has been created and then different types of batteries are modeled with different parameters. As a result, the charge and discharge characteristics of different battery types were analyzed on a hybrid vehicle model. In this analysis, two different driving scenarios are designed with equal starting conditions. These driving scenarios were carried out by analyzing the black boxes of the Trambus in Malatya and the charge discharge characteristics of the batteries were examined separately in these scenarios. The results are presented comparatively.

Key words: Batteries, hybrid electric vehicles, charging and discharging, traction system, trambus

HİBRİT ELEKTRİKLİ ARAÇ MODELİ ÜZERİNDE FARKLI TİP BATARYALARIN ŞARJ VE DEŞARJ KARAKTERİSTİKLERİNİN İNCELENMESİ

***ÖZET*:** Bu çalışmada önce hibrit bir aracın komponent bazında modellemesi yapılmıştır. Farklı batarya tiplerini modellemek için bir batarya modeli çıkartılmış takiben farklı parametreler ile farklı tipteki bataryaların modellemesi sağlanmıştır. Neticede hibrit bir araç modeli üzerinde farklı batarya tiplerinin şarj ve deşarj karakteristikleri analiz edilmiştir. Bu analizde eşit başlangıç koşullarına sahip, iki farklı sürüş senaryosu tasarlanmıştır. Bu sürüş senaryoları Malatya'da hizmet etmekte olan Trambüs'lerin kara kutularının analizi ile gerçekleşmiş ve bataryaların bu senaryolar dahilinde şarj deşarj karakteristikleri ayrı ayrı incelenmiştir. Elde edilen sonuçlar karşılaştırmalı olarak sunulmuştur.

Anahtar sözcükler: Bataryalar, hibrit elektrikli araç, şarj ve deşarj, çekiş sistemi, trambüs

GİRİŞ

Günümüzde fosil yakıtların giderek azalması ve çevre örgütleri tarafından çevresel duyarlılığın daha da artırılması yenilebilir enerji kaynaknaklarının önemini artırmıştır. Araştırmacılar yenilenebilir enerji kaynakları ile çalışan araçlar üzerinde çalışmalarını hızlandırmışlardır [1]. Otomotiv sanayinde yıllardır süregelen içten yanmalı motor teknolojisinden, elektrikli araç teknolojisine tamamen geçiş araç üreten firmalar için büyük bir risk oluşturmaktadır [2]. Buna ek olarak devletlerin fosil yakıtlardan bağımsız, yenilenebilir enerjiler ile çalışan araçlara tam olarak destek vermemesi tüketim toplumu tarafından bu araçlara yönelimi azaltmaktadır [3]. Bu olumsuzluklar karşısında araç üreticileri de ikilem ile karşı karşıya kalmaktadır [4].
Yukarıda sıralanan olumsuzluklara rağmen yenilenebilir enerjili araç üreten firmaların bataryalar konusunda dikkatli olması gerekmektedir. Bataryaların maliyet, güvenlik ve enerji depolama kapasitesinin doğru seçimi araç üretimi için kritik bir parametredir. Hibrit elektrikli araç konsepti üzerinde çalışan üreticiler için doğru batarya seçimi daha büyük bir öneme sahiptir. Günümüz elektrikli araç teknolojilerinde üç tür batarya kimyası otomotiv uygulamaları için başlıca adaylardır. Bu türler; Pb-asit, nikel metal hidrit ve lityum tabanlı bataryalardır. Kurşun asit bataryalar sıralı altı adet hücre içerir ve otomobillerde kullanılırlar. Bu tür bataryalarda her hücrenin anodu kurşundan yapılmıştır. Katot kısmı da bir metal levha üzerine oturtulmuş kurşundioksitten yapılmıştır. Katot ve anot,elektrolit görevi yapan sülfürik asit çözeltisine daldırılmıştır. Pb-asit bataryalar düşük maliyetli olmaları nedeniyle aydınlatma, marş ve ateşleme gibi sistemlerde kullanıldıkları gibi bu sistemler için üreticiler tarafından büyük oranda tercih edilmektedir. Golf arabaları ve tekerlekli sandalyeler gibi araçlarda yaygın olarak kullanılmaktadır.
Nikel Metal Hidrit bataryalar ise elektrikli araçlar için en çok kullanılan batarya çeşitlerinden biridir ve birçok elektrikli araç firması tarafından kullanılmaktadır. Örneğin General Motors'un EV1 gibi elektrikli araçlarında nikel metal hidrit bataryalar kullanılmıştır [5].
Son yıllarda, elektrikli araçlarda ve hibrit elektrikli araçlarda kullanımları için çeşitli Li-ion batarya teknolojileri incelenmiş ve geliştirilmiştir. Bunların arasında, lityum demir fosfat (LiFePO4) bataryaların, soğuktan az etkilenmeleri, yüksek sıcaklıklarda tam akım vermeleri, yüksek akım ile çok hızlı şarj olmaları bakımından elektrikli araç sektöründe önemli yer tutmaktadır. Yüksek güç gerektiren projelerde kullanılan lityum demir fosfat bataryaların normal yani şarj edilmemiş hali 3.3 volttur. Lityum iyon bataryalara göre depolamada daha yavaş bir kapasite kaybı vardır, raf ömrü uzundur. LiFePO4 bataryalar nominal gerilimlerini %10 - %90 SOC aralığında koruyabildikleri için otomobil üreticileri ve Ar-Ge toplumu arasında popülerlik kazanmaktadır [6-8].

Tablo 1'de yukarıda bahsedilen bu üç tip bataryanın parametreleri sunulmuştur. Görüldüğü üzere yüksek enerji yoğunluğu, uzun çalışma ömrü ve yüksek güvenliği ile elektrikli araçlarda kullanılmaya en uygun batarya tipi Lityum demir fosfattır [9-10].

Tablo 1. 21.yy'da Elektrikli Araçlarda Kullanılan Hücrelerin Üreticiler Tarafından Sağlanan Teknik Özellikleri

Özellikler	Pb-Asit	Nikel-Metal-Hidrit	Lityum İyon
Nominal Voltaj (V)	12	3.2	3.6 – 3.7
Şarj Limiti (V)	16	3.7	3.7
Ömür	2000	1500	3000
İşletme Sıcaklığı (T)	60	100	80
Güvenlik	Az	Orta	İyi
Enerji Yoğunluğu (Wh/kg)	40	70	150

Batarya tiplerinin farklı gerilim ve akım seviyelerinin olması batarya paketlerinin farklı değer aralıklarında çalışmasını sağlamaktadır. Bu çalışmada hibrit bir elektrikli araç modellenerek üzerinde mevcutta Malatya'da çalışan Trambüs araçlarının kara kutusundan alınan farklı gün ve saatlerdeki gaz pedalı sinyalleri 2 farklı senaryo olarak uygulanmıştır. Motaş A.Ş izni ile alınan bu veriler hibrit araç için uygulanarak günün farklı saatlerinde hibrit aracın reel bir sürüş senaryosunun ortaya çıkmasını sağlamıştır. Bir önceki çalışmamızda farklı batarya tiplerinin şarj ve deşarj karakteristiklerinin hibrit bir elektrikli araç modeli üzerinde incelemesi gerçekleştirilmiş ve ***"CIEA 2018 international conferance on innovative engineering applications"*** konferansında sunulmuştur. Yapılan bu çalışmada bir elektrikli araç üzerinden sürüş esnasında alınan gaz pedalı sinyalleri ile daha gerçekçi veriler elde edilmiştir ve bu uygulama esnasında aracın içten yanmalı motordan elektrikli motora geçişini tanımlamak için bir parametreye ihtiyaç duyulmuştur. Bu sebeple hibrit mod tanımlanmıştır. Dört farklı tip bataryaların şarj ve deşarj karakteristikleri bu model üzerinde incelenmiştir.

MATERYAL VE METOT

2.1 Hibrit Araç Modeli

Günümüzde kullanılan hibrit motorların neredeyse tamamı içten yanmalı bir benzin motorunun yanında batarya, elektrik motoru ve bir de jeneratörün sisteme dahil edilmesiyle oluşturulur. Bu teknoloji benzinli motorlara göre % 40-50 daha verimlidir. Çünkü hibrit motor teknolojisi daha akıllı bir sistemdir ve motora beş farklı işleyiş biçimi belirler. Hibrit elektrikli araçlar kablolu ve kablosuz olmak üzere iki farklı hibrit elektrikli araç modeli kullanılmaktadır. Kablolu hibrit elektrikli araç modelinde dizel motor, elektrik motoru ve batarya paketi bulunmaktadır. Sürüş esnasında dizel yakıt ve sürüş performansına göre bataryalar kullanılmaktadır. Bataryalar kullanıcı tarafından şarja takılır ve bir sonraki sürüş için şarjlanır [11].
İkinci modelde bataryaların şarj edilmesi için herhangi bir kabluya ihtiyaç bulunmamaktadır. Hibrit araç içerisinde bulunan dizel motor, generatörü çalıştırarak

bataryaların şarj olmasını sağlamaktadır. Bu çalışmada sürüş anında batarya karakteristiklerin incelenmesi üzerine çalışıldığında ikinci model elektrikli araç simulasyon konusu olarak seçilmiştir.

2.2 Batarya Modeli

Batarya modeli Şekil 1'de gösterilmiştir. Şarj ve deşarj eşitlikleri ise denklem 1 ve 2 de sunulmuştur.
Denklemlerde;
Ebatt doğrusal olmayan voltajdır. (V)
E0 sabit voltajdır. (V)
Exp(s) üstel bölge dinamiğidir. (V)
Sel(s) pil modunu ifade eder. Sel(s) = 0 batarya deşarjı, Sel(s) = 1 Batarya şarjı.
K polarizasyon sabitidir. (Ah^{-1})
i^* düşük frekanslı akım dinamiğidir.(A)
Q maksimum pil kapasitesidir. (Ah)
A eksponansiyel voltaj. (V)
B eksponansiyel kapasite. (Ah^{-1})

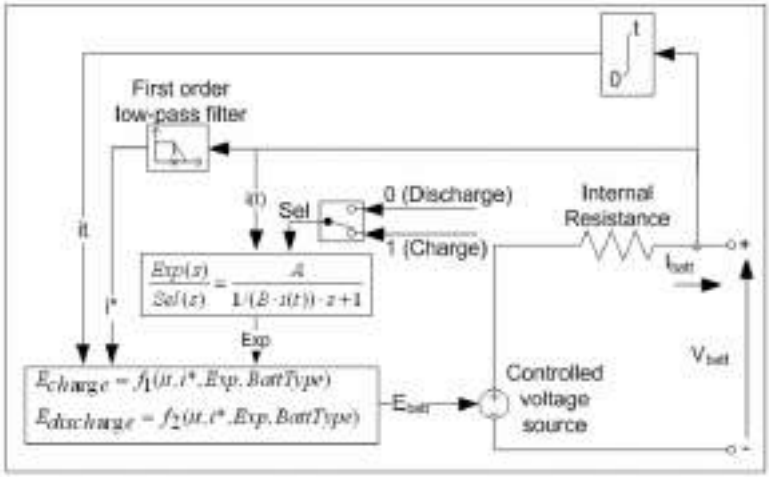

Şekil 1. Batarya Modeli

$$E_{Discharge}=E_0 - K\frac{Q}{Q-it}i^* - K\frac{Q}{Q-it}it + Ae^{-\beta it} \quad (1)$$

$$E_{Charge}= E_0 - K\frac{Q}{0.1Q+it}i^* - K\frac{Q}{Q-it}it + Ae^{-\beta it} \quad (2)$$

Bir lityum pilin şarj-deşarj özellikleri Şekil 2'de gösterilen detaylı modelden elde edilir.

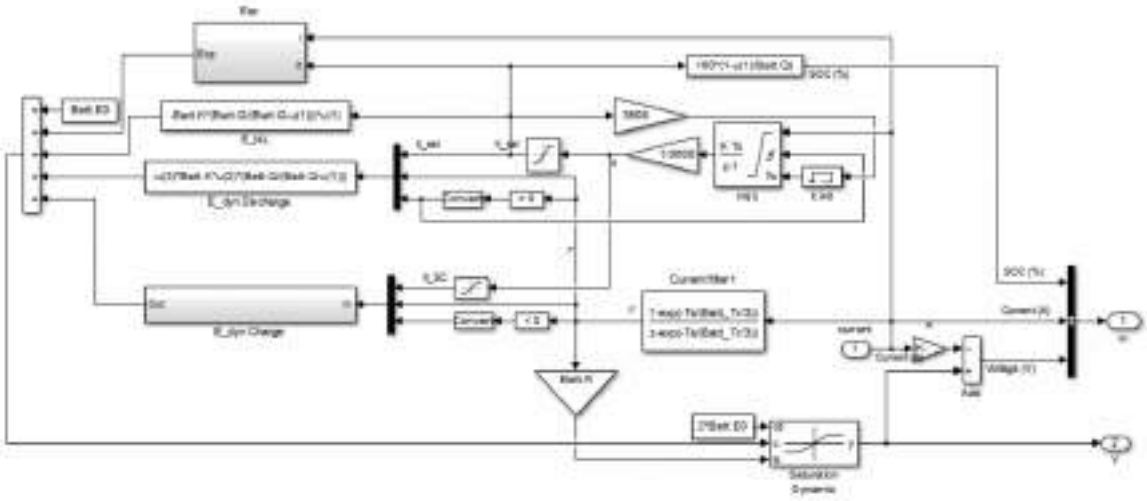

Şekil 2. Detaylı Batarya Modeli

SİMULASYON

Simülasyon, MATLAB® 2015a kapsamında SIMULINK'te hazırlanmıştır. Yapılan simulasyonun ideal örnekleme frekansı 1 kHz'dir. Çözücü olarak ode23tb kullanılmıştır. Simulasyonun genel görünümü Şekil 3'te gösterilmiştir. Ayrıca simülasyon için aşağıdaki varsayımlar ile yapılmaktadır.
Anahtarlar ve kontaklar idealdir.
Bataryalar tamamen sağlıklıdır.

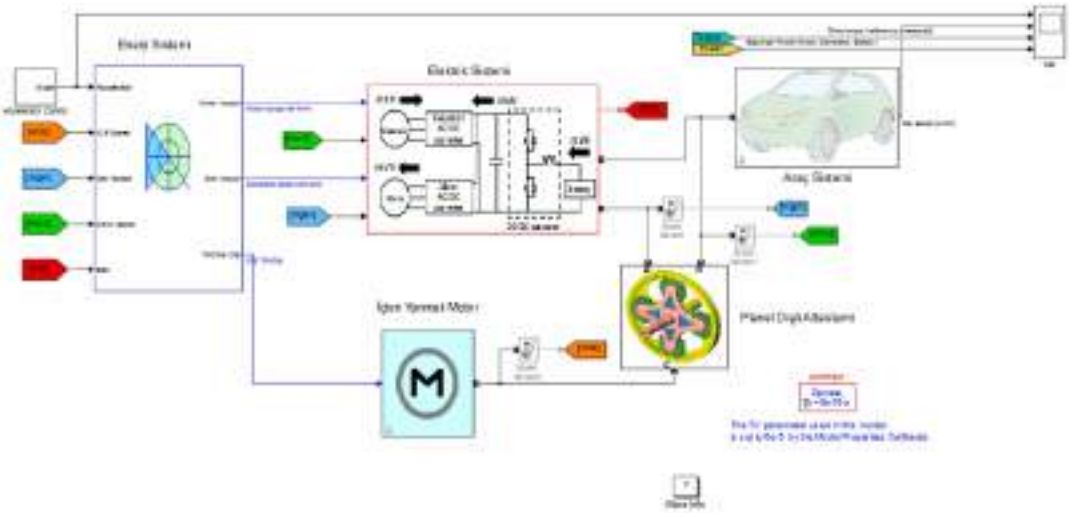

Şekil 3. Hibrit Elektrikli Araç Modeli

Mathworks üzerinden bir hibrit elektrikli araç modeli alınmış ve bu çalışma üzerine LiFePO4, Nikel-metal-hidrit, Kurşun-Asit ve Nikel Kadminyum tipi batarya grupları yerleştirilmiştir. Güçleri 14 kwh olacak şekilde farklı tipteki bataryalardan 4 adet

batarya paketi oluşturulmuştur. Tasarlanan hibrit elektrikli araç modeli üzerinde tüm batarya paketlerinin başlangıç State of Charge (SOC) değerleri %50 olarak belirlenmiştir. Ayrıca her batarya grubunun eşit güçte olmasına önem verilmiştir. Fakat pillerin nominal gerilimlerinin farklı olması dolayısıyla oluşturulan batarya paketleri farklı sayıda bataryadan meydana gelmiştir ve farklı toplam gerilim değerlerine sahiptir. Ayrıca Trambüs araçlarından alınan gaz pedalı verileri günün en yoğun ve en sakin zamanlarından alınmıştır.

Tablo 2. Farklı Dört Tip Batarya Parametreleri

Özellikler	LiFEPO4	Nikel Metal Hidrit	Kurşun-Asit	Nikel-Kadminyum
Nominal Voltaj (V)	3.2	3.2	2	1.25
Full Şarj Voltaj (V)	3.5	3.7	2.5	1.5
Akım Kapasitesi (Ah)	3	1.5	2.3	2.05
İç Direnç (R)	1.3	1.6	1.05	1.2

Trambüs araçları üzerinden alınan ilk sürüş senaryosunu oluşturan veri sabah 02.00 ile 04.00 arasından Şekil 4'teki gibi alınmış olup hibrit elektrikli aracın gaz pedal sinyali gibi düşünülmüştür. Alınan veriler içinden 1 dakikalık örneklem sinyal oluşturulmuş ve Şekil 5'te bu sinyal sunulmuştur.

Şekil 4. Senaryo 1 Trambüs Araçları Karakutu Gaz Pedalı Kullanım Oranı

Şekil 5. Senaryo 1 Hibrit Araca Uygulanan Örneklem Gaz Pedalı Sinyali

İkinci sürüş senaryosunda ise yolcuların yoğunlukta olduğu saat 11.00 ile 13.00 arasında oluşturulmuş oluş Şekil 6'da sunulmuştur. Yine 2 saatlik bir veri kaydı

yapılmış ve daha sonra hibrit araç simulasyonuna entegre edilebilecek 1 dakikalık örneklem sinyal oluşturulmuş ve Şekil 7'de sunulmuştur.

Şekil 6. Senaryo 2 Trambüs Araçları Karakutu Gaz Pedalı Kullanım Oranı

Şekil 7. Senaryo 2 Hibrit Araca Uygulanan Örneklem Gaz Pedalı Sinyali

Senaryo 1 ve 2 için Trambüs araçlarından alınan örneklem sinyalleri hibrit bir elektrikli araç modeli üzerinde uygulandığında Şekil 8 ve 9'daki gibi sinyaller meydana gelmiştir.

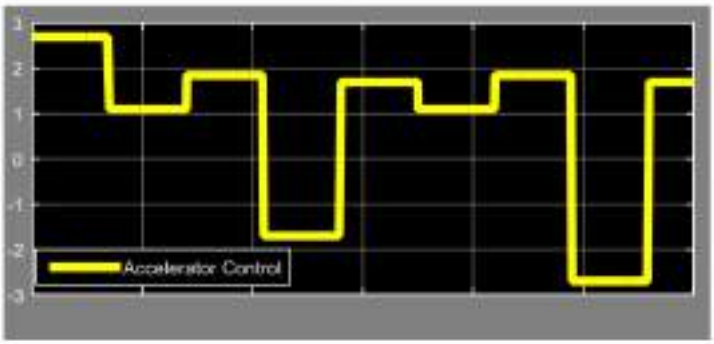

Şekil 8. Senaryo 1 için Hibrit Araç Gaz Pedalı Sinyali

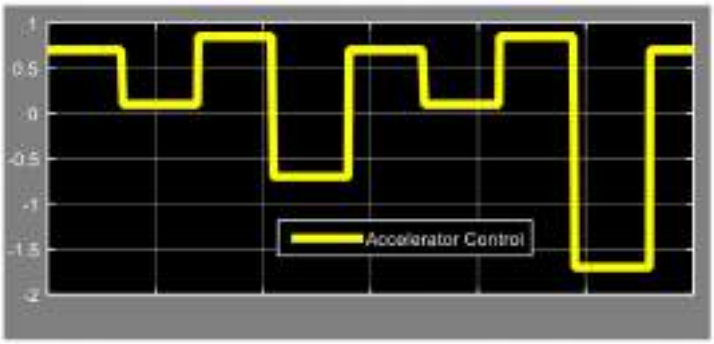

Şekil 9. Senaryo 2 için Hibrit Araç Gaz Pedalı Sinyali

Negatiften pozitife ve pozitiften negatife geçen gaz pedalı sinyalleri aynı zamanda ani değer düşümü ve yükselişi gösteren gaz pedalı sinyalleri hibrit mod değişimi üzerinde etkilidir.
Gaz pedalı sinyalleri pozitifte iken bataryalardan elektrik motoruna enerji akışı olmakta, negatifte ise motor jeneratör gibi çalışarak motordan bataryalara enerji akışı sağlanmaktadır. Bu sayede bataryaların şarj ve deşarj grafiklerinin ayrıntılı incelenmesi ve bataryalar arasında daha net yorumlar yapılmasına olanak sağlamıştır.

BULGULAR

Bataryaların şarj ve deşarj karakteristiklerinin incelenmesi için sistem üzerinde hibrit modun değişim göstermesi gerekmektedir. Hibrit mod aktif konumuna geçtiği zaman bataryaların deşarj işlemi başlamaktadır, hibrit mod pasif konumuna geçtiğinde ise sistem üzerinde generatör çalıştırılarak bataryaların şarj olması sağlanmaktadır. İlk senaryonun simulasyonda uygulanması neticesinde 5 noktada hibrit mod değişimi sağlanmıştır. Bu sayede simulasyon içerisinde batarya paketlerinin 5 defa şarjdan deşarja veya deşarjdan şarja geçiş karakteristikleri incelenmiştir.

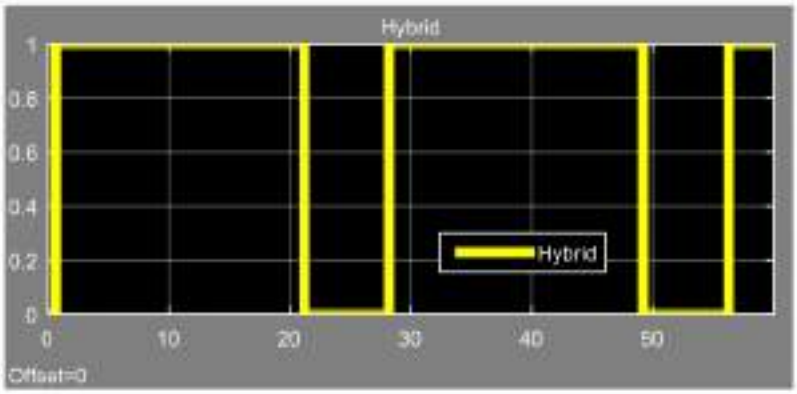

Şekil 10. Senaryo 1 için Hibrit Mod Değişimi

İkinci senaryoda ise 7 noktada hibrit mod değişimi sağlanmıştır. Birinci senaryodaki şarjdan deşarja geçişler daha yumuşak olmuştur. İkinci senaryo da ise daha sert geçişlerdeki tepkileri analiz edilmiştir.

Batarya paketlerinin birbirlerine göre performans kıyaslamasını yapmak için şarj ve deşarj min-max noktalarındaki doluluk oranları (SOC) parametre olarak seçilmiştir.

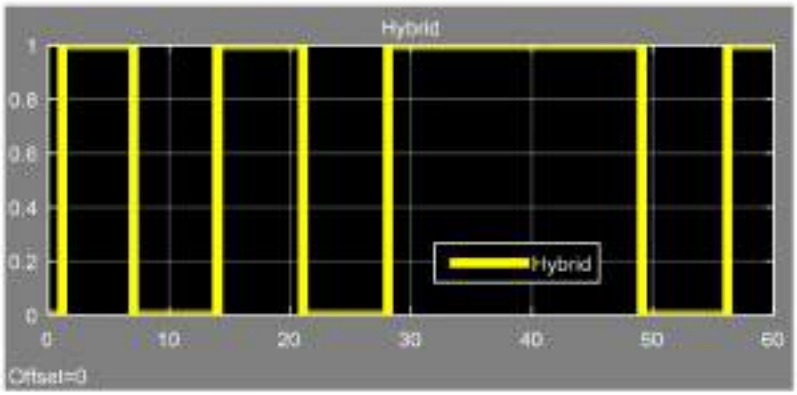

Şekil 11. Senaryo 2 için Hibrit Mod Değişimi

4.1 Senaryo 1

Birinci senaryoda LiFEPO4, Nikel-Metal-hydrid, Kurşun-Asit ve Nikel Kadminyum tipi bataryaların şarj-deşarj karakteristik analizi incelendiğinde 50.saniyesinde batarya paketlerinin enerjilerilerinin minumuma indiği ve şarja geçerek toparlandığı gözlemlenmektedir. Bu geçişler ve enerji değişimleri sırasında doluluk oranının en düşük seviyede azaltan batarya paketi LiFEPO4 olarak gözlemlenmiştir. Doluluk oranı bakımından en düşük performansı da Kurşun Asit batarya paketinin gösterdiği gözlemlenmiştir. Bu değişimler de Şekil 12,13,14 ve 15'te sunulmuştur.

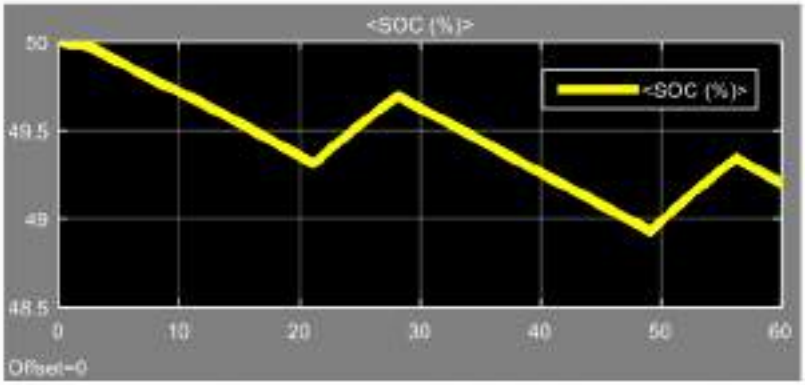

Şekil 12. LiFePO4 Şarj-Deşarj Karakteristiği

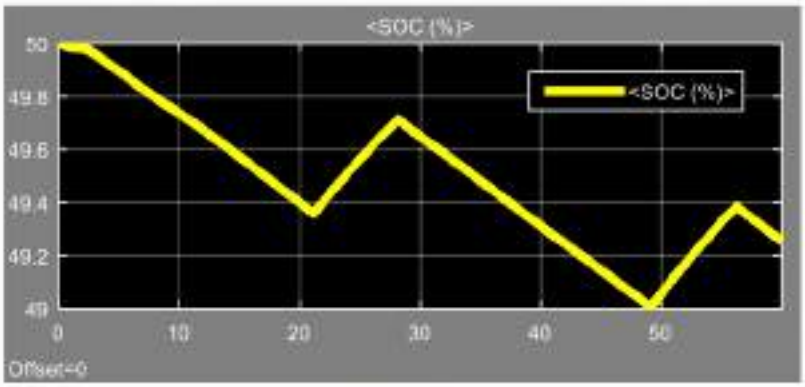

Şekil 13. Nikel-Metal-Hidrit Şarj-Deşarj Karakteristiği

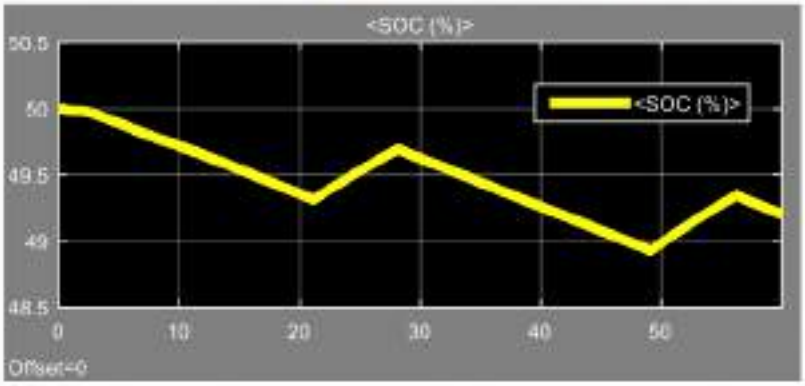

Şekil 14. Kurşun Asit Şarj-Deşarj Karakteristiği

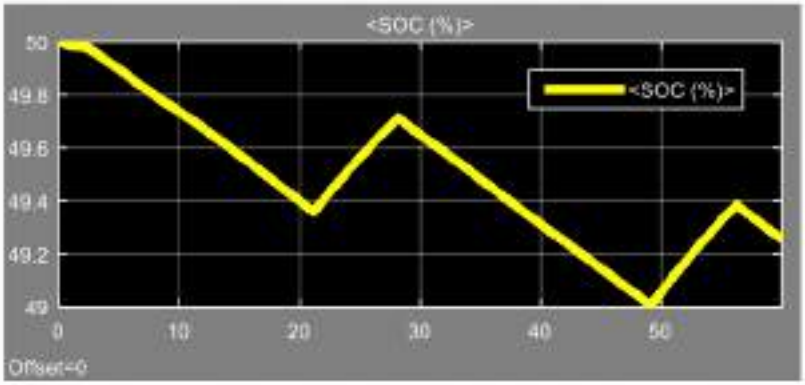

4.2 Senaryo 2

İkinci senaryoda LiFEPO4, Nikel-Metal-hydrid, Kurşun-Asit ve Nikel Kadminyum tipi bataryaların şarj-deşarj karakteristik analizi incelendiğinde 50.saniyesinde batarya paketlerinin enerjilerilerinin minumuma indiği ve şarja geçerek toparlandığı gözlemlenmektedir. Bu geçişler ve enerji değişimleri sırasında doluluk oranının en düşük seviyede azaltan batarya paketi LiFEPO4 olarak gözlemlenmiştir. Doluluk oranı bakıından en düşük performansı da Kurşun Asit batarya paketinin gösterdiği gözlemlenmiştir. Bu değişimler de Şekil 16,17,18 ve 19'da sunulmuştur.

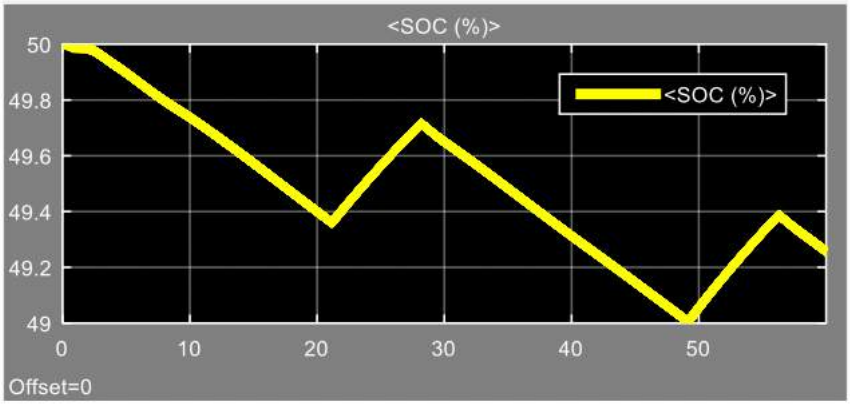

Şekil 16. LiFePO4 Şarj-Deşarj Karakteristiği

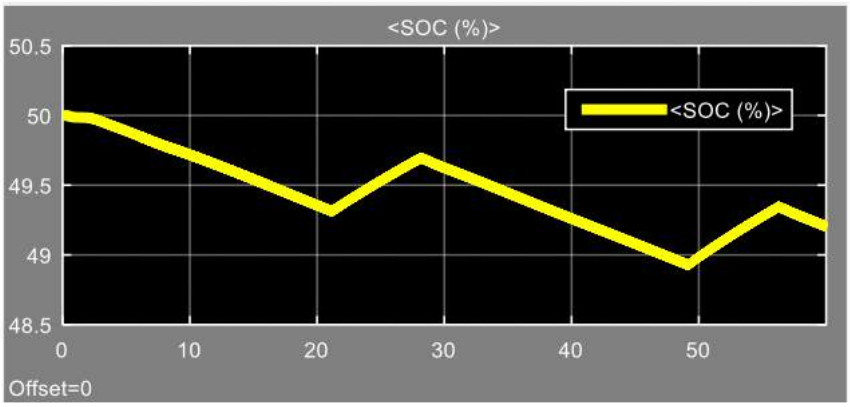

Şekil 17. Nikel Metal Hidrit Şarj-Deşarj Karakteristiği

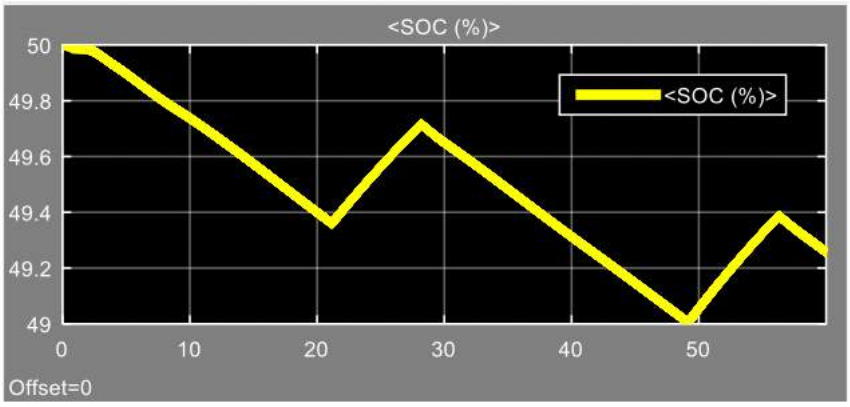

Şekil 18. Kurşun Asit Şarj-Deşarj Karakteristiği

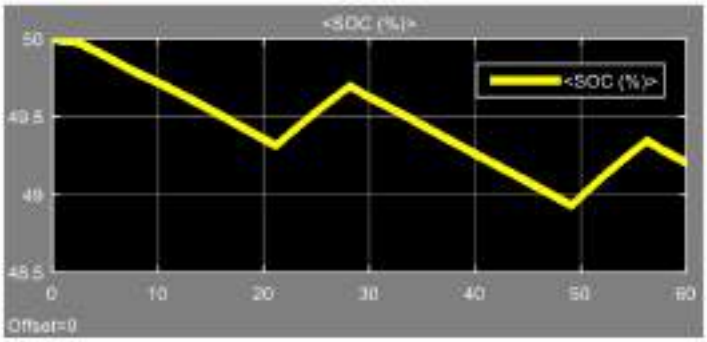

Şekil 19. Nikel Kadminyum Şarj-Deşarj Karakteristiği

SONUÇ

Hibrit araçlarda kullanılan batarya kimyalarının seçimi problemi bu çalışmada ele alınmıştır. Bu kapsamda modellenen dört farklı kimyaya sahip batarya paketlerinin şarj-deşarj karakteristikleri bir hibrit araç modeli üzerinde iki farklı senaryo dahilinde incelenmiştir. Elde edilen bulgular batarya paketlerinin şarj ve deşarj durumlarının en yüksek ve en düşük olduğu geçiş noktalarında doluluk oranları (SOC) kıyaslama parametresi olarak seçilerek incelenmiştir. Batarya paketlerinin performans parametreleri kullanılan senaryolara göre de tablo 3 ve 4'te sunulmuştur.

Tablo 3. Senaryo 1 Sonu Batarya Paketlerinin SOC Durumu

Batarya / Zaman	**LiFEPO4 (SOC)**	**Metal Nikel Hidrit (SOC)**	**Kurşun Asit (SOC)**	**Nikel Kadminyum (SOC)**
Başlangıç	%50	%50	%50	%50
T=21	%49.4	%49.45	%49.35	%49.4
T=28	%49.3	%49.6	%49.7	%49.55
T=50	%49	%48.95	%49	%48.9
T=55	%49.25	%49.2	%49.15	%49.2

Tablo 4. Senaryo 2 Sonu Batarya Paketlerinin SOC Durumu

Batarya / Zaman	**LiFEPO4 (SOC)**	**Metal Nikel Hidrit (SOC)**	**Kurşun Asit (SOC)**	**Nikel Kadminyum (SOC)**
Başlangıç	%50	%50	%50	%50
T=21	%49.5	%49.5	%49.55	%49.55
T=28	%49.7	%49.6	%49.8	%49.8
T=50	%49.2	%49.1	%49.4	%49.1
T=55	%49.5	%49.4	%49.2	%49.25

Buna göre her iki senaryoda da LiFEPO4 simulasyon sonunda en fazla doluluk oranına sahip olan batarya paketi olarak gözlemlenmiştir. Kurşun Asit ise en düşük doluluk oranına sahip batarya paketi olmuştur. Araçların tasarımsal kısıtlarının göz önünde alınmadığı bu çalışmada hibrit bir elektrikli araç için SOC performans parametresi olarak ele alındığında en yüksek performansı LiFEPO4 bataryaların sergilediği gözlemlenmiştir. Bu çalışmaya gelecekte sıcaklık parametresi, araçların tasarım kısıtları ve farklı batarya kimyaları dahil edilerek çalışmanın genişletilmesi planlanmaktadır.

KAYNAKLAR

Anseán, D., González, M., García, V. M., Viera, J. C., Antón, J. C., & Blanco, C. (2015). Evaluation of LiFePO4 Batteries for Electric Vehicle Applications. *IEEE TRANSACTIONS ON INDUSTRY APPLICATIONS*, 1855-1863.

Chen, X., Shen, W., Vo, T. T., Cao, Z., & Kapoor, A. (2012). An Overview of Lithium-ion Batteries for Electric Vehicles. *IPEC, 2012 Conference on Power & Energy*.

Garche, B. S. (2010). Lithium batteries: Status, prospects and future. *J. Power Sources*, 2419-2430.

Jonathan C. Ho, Y.-H. S. (2014). Evaluation of Electric Vehicle Power Technologies. *Proceedings of PICMET '14: Infrastructure and Service Integration.*

M. Hannan, M. L. (2017). A review of lithium-ion battery state of charge estimation and management system in electric vehicle applications: Challenges and recommendations. *Renewable and Sustainable Energy Reviews*, 834-854.

Moons, I. a. (2012). Emotions as determinants of electric car usage intention. *Journal of Marketing Management*, 195-237.

Pohl, H. a. (2010). Radical innovation in a small firm: a hybrid electric vehicle development project at Volvo Cars. *R&D Management*, 372-382.

Spotnitz, R. (2005). Battery Design LLC. *IEEE Vehicle Power and Propulsion Conference.*

tehad. (2017, mayıs 1). *Hibrid Otomobil Nedir, Nasıl Çalışır?* ağustos 13, 2018 tarihinde http://tehad.org/2017/05/01/hibrid-otomobil-nedir-nasil-calisir/ adresinden alındı

Voelcker, J. (2008). An Almost All-Electric Car? *IEEE Spectrum,*, 45(4) 9-9.

Zhang, W. (2011). Structure and performance of LiFePO4 cathode materials: A review. *J. Power Sources*, 2962-2970.

COMPARATIVE ANALYSIS OF SINGLE-SWITCH FORWARD CONVERTERS WITH PASSIVE SNUBBER

Prof. Dr. Hacı BODUR
Yildiz Technical University
bodur@yildiz.edu.tr

Mahir PINARBAŞI
Yildiz Technical University
mahirp@yildiz.edu.tr

Dr. Erdem AKBOY
Yildiz Technical University
eakboy@yildiz.edu.tr

ABSTRACT: In this paper, different five single-switch forward converters with passive snubber analyzed comparatively. In DC-DC converters, which are widely used for accumulator charging, electronic welding machines, insulated power supplies etc., the subjects of soft switching, stress reduction, efficiency improvement, etc. are studied intensively. In this study, application area of the circuit, voltage stress on the active power element, number of elements in the snubber cell, duty cycle, efficiency, etc. parameters of the circuits are taken into consideration and their advantages and disadvantages are emphasized.

Key words: forward converter, soft switching, snubber cell.

PASİF BASTIRMA HÜCRELİ TEK ANAHTARLI İLERİ YÖNLÜ DÖNÜŞTÜRÜCÜLERİN KARŞILAŞTIRMALI OLARAK İNCELENMESİ

ÖZET: Bu bildiride pasif bastırma hücreli beş farklı ileri yönlü DC-DC dönüştürücü yapısı karşılaştırmalı olarak incelenmiştir. Akümülatör şarjı, elektronik kaynak makineleri, izoleli güç kaynakları, vb. uygulamalarda yaygın olarak kullanılan ileri yönlü DC-DC dönüştürücüler üzerinde, yumuşak anahtarlama, stres azaltma, verim yükseltme, vb. konularda yoğun olarak çalışılmaktadır. Pasif bastırmalı ileri yönlü DC-DC dönüştürücülerin incelendiği bu çalışmada, devrenin uygulama alanı, aktif güç elemanı üzerinde oluşan gerilim stresi, bastırma hücresinde bulunan eleman sayısı, doluluk oranı, devrenin verimi, vb. parametreler göz önüne alınmış, devrelerin avantaj ve dezavantajları vurgulanmıştır.

Anahtar sözcükler: ileri yönlü dönüştürücü, yumuşak anahtarlama.

GİRİŞ

Gelişen teknolojiyle orantılı olarak elektrik enerjisine olan ihtiyaç ve talep de artmaktadır. Artan talep ile birlikte elektrik enerjisi değerlenmekte ve her geçen gün daha verimli kullanılması adına çalışmalar yapılmaktadır. Özellikle küçük boyutlu ve yüksek frekanslı güç kaynağı olarak kullanılmak üzere DC-DC dönüştürücülere olan ihtiyaç ön plana çıkmaktadır. DC-DC dönüştürücülerin daha verimli hale getirilmesi için yapılan çalışmalarda yumuşak anahtarlama teknikleri önemli bir yer tutmaktadır [1-5].

Yumuşak anahtarlama için kullanılan ve devrenin temel bir parçası olmayan ilave devreler bastırma hücreleri olarak adlandırılır [2]. Bastırma hücreleri aktif ve pasif bastırma hücreleri olarak ikiye ayrılırlar. İlave aktif eleman bulundurmayan hücrelere pasif, en az bir adet ilave aktif eleman bulunduranlara ise aktif bastırma hücreleri denilmektedir. Klasik bastırma yöntemlerinde anahtarlama enerjisi ilave dirençler üzerinde harcanırken, modern kontrol yöntemlerinde ise anahtar üzerinde stres yaratan enerjinin mümkün olan en az kayıp ile tekrar kaynağa veya yüke aktarılması amaçlanmaktadır. Özellikle yüksek frekansla çalışan devrelerde anahtarlama kayıplarının tekrar geri kazanılması devrenin verimi açısından oldukça önemlidir [1, 3-5].

Birkaç 100 W güç değerlerine kadar olan düşürücü dönüştürücü uygulamalarında ileri yönlü dönüştürücüler yüksek oranda tercih edilmektedir. Bu dönüştürücünün çok farklı yapılarda örnekleri bulunmaktadır. İleri yönlü dönüştürücülerin önemli dezavantajları, transformatörün kaçak ve mıknatıslama endüktanslarında biriken enerjilerin sıfırlanması gerekliliği, anahtar üzerinde yüksek gerilim stresi oluşması, sert anahtarlama ile verimin düşmesi olarak sıralanabilir. Düşük güçlerde, bu problemlerin çözümü için RC bastırma hücreleri kullanılmaktadır, ancak bu yöntemde kaçak endüktansta depolanan enerji direnç üzerinde harcanmakta ve frekans arttıkça devrenin kaybı artmakta ve verim düşmektedir [3].

Bu çalışmada, pasif bastırma hücreli beş farklı ileri yönlü DC-DC dönüştürücü yapısı karşılaştırmalı olarak incelenmiştir. Bu incelemelerde, devrenin uygulama alanı, aktif güç elemanı üzerinde oluşan gerilim stresi, bastırma hücresinde bulunan eleman sayısı, doluluk oranı, devrenin verimi vb. parametreler göz önüne alınmış, devrelerin avantaj ve dezavantajları sıralanmıştır.

TEMEL LCDD BASTIRMA HÜCRELİ İLERİ YÖNLÜ DÖNÜŞTÜRÜCÜ

Temel pasif LCDD bastırma hücreli ileri yönlü dönüştürücü yapısı [5] Şekil 1'de görülmektedir. Uygulanan bastırma hücresinde transformatörde yardımcı sargı bulunmamaktadır. LC bastırma hücresi mıknatıslanma enerjisini ekstra sargıya gerek kalmadan sönümleyebilmektedir. Ayrıca devrede anahtarlama elemanı olarak kullanılan transistörün anahtarlama kaybını minimize etmek amaçlanmıştır.

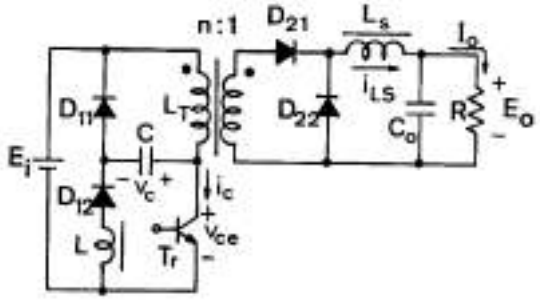

Şekil 1. Temel LCDD Bastırma Hücreli İleri Yönlü Dönüştürücü [5].

Devrenin bir anahtarlama periyodunda on farklı çalışma aralığı ve iki ayrı çalışma modu bulunmaktadır. Devre üzerindeki yarıiletken elemanların çalışma aralıklarına göre iletim ve kesim durumları Tablo 1'de özetlenmiştir.

Tablo 1. Temel LCDD Bastırma Hücresinin Durum Bilgisi ve Çalışma Modları

State	Tr.	D11	D12	D21	D22
1	OFF	ON	OFF	ON	OFF
2	OFF	ON	OFF	ON	ON
3	OFF	ON	OFF	OFF	ON
4	OFF	OFF	ON	OFF	ON
5	OFF	OFF	ON	ON	ON
6	OFF	OFF	OFF	ON	ON
7	OFF	OFF	OFF	OFF	ON
8	ON	OFF	ON	ON	ON
9	ON	OFF	ON	ON	OFF
10	ON	OFF	OFF	ON	OFF

Mod 1: 1-2-3-7-8-9-10
Mod 2: 1-2-3-4-5-6-8-9-10

V_{cep} transistör üzerindeki pik gerilim, V_c^* bastırma kapasitörü üzerindeki anlık gerilim, C bastırma kapasitörünün değeri, L_T transformatörün endüktans değeri, I_{LT} ve I_{Ls} sırasıyla mıknatıslanma akımı ve kesime girme anında transistörün çıkış akımı olmak üzere, aşağıdaki gibi hesaplanır.

$$V_{cep} \cong E_i + \sqrt{\frac{L_t}{C} I_{LT}^2 + \frac{l_{w1}+n^2 l_{w2}}{C} . \frac{I_{LS}^2}{n^2}} \quad (1)$$

Çalışma modu transistör üzerindeki pik gerilim ve giriş gerilimine bağlı olarak denklem (2)'deki gibi belirlenir,

$$V_{cep} < 2E_i \quad , \; Mode\ 1\ için.$$
$$V_{cep} \geq 2E_i \quad , \; Mode\ 2\ için. \quad (2)$$

Transistör üzerindeki pik gerilim bastırma kapasitörünün değeri ile ters orantılı olarak artar veya azalır. Böylece çalışma modunun bastırma kapasitörünün değeri ile

değiştiğini söyleyebiliriz. Şekil 2'de bastırma kondansatörünün pik gerilimine etkisi verilmiştir.

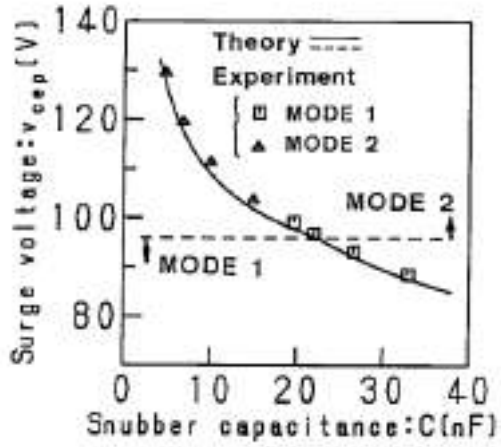

Şekil 2. Bastırma Kondansatörünün Anahtarın Pik Gerilimine Etkisi [5].

Şekil 3'te ise, kesime girme işleminde anahtar uçlarında oluşan gerilim piklerine bastırma kondansatörünün etkisi görülmektedir. Şekil 3'te görüldüğü gibi anahtarın kesime girme anında oluşan gerilim pikleri bastırma kapasitörü ile doğrudan ilişkilidir. Pik gerilim V_J iki çalışma modunun sınırında minimum değerini almaktadır.

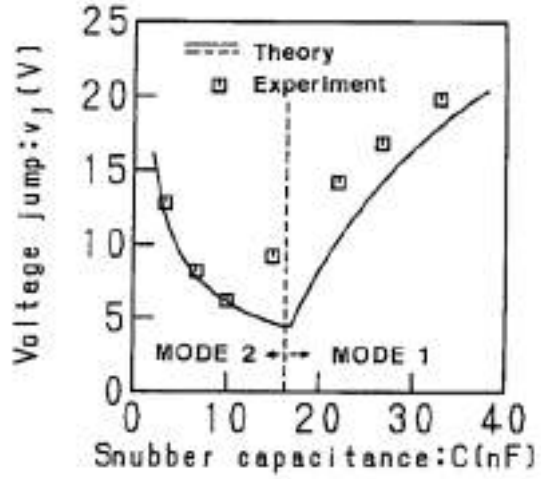

Şekil 3. Bastırma Kondansatörünün Kesim Anındaki Anahtar Gerilimine Etkisi [5].

Gerilim pikinin ve enerji kaybının çalışma modlarının sınırında minimum değerine ulaştığı görülmektedir. Çalışma sınır değeri de bastırma kapasitörü ve çıkış akımı ile değişmektedir. Buradan anlaşılmaktadır ki geniş aralıklı bir çıkış akımında sabit bir kondansatör değeri ile maksimum verimi sağlamak mümkün değildir. Ancak belirli bir çıkış akımında verimi yükseltecek bir kondansatör değeri seçilebilir. Bu kondansatör değerinden yola çıkarak da bastırma endüktansının değeri belirlenebilir.

Şekil 4'teki dalga şekillerinden görüldüğü gibi, anahtarlama elemanı üzerindeki gerilim stresi kapasitör gerilimi V_c ile doğru orantılı olarak artmaktadır. Ayrıca,

anahtarın hangi ölçüde bir ZVS altında kesime girdiği V_c geriliminin değerine bağlıdır ve V_c=E_i olduğunda tam ZVS sağlanır.

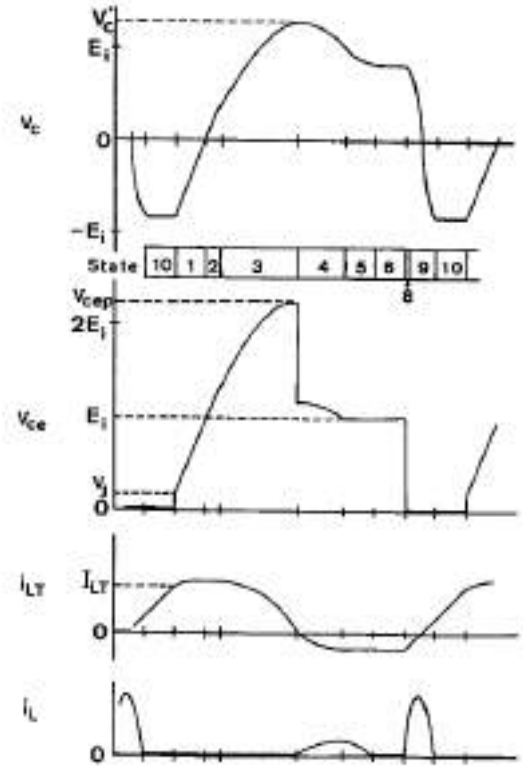

Şekil 4. Mod 2 için Gerilim ve Akım Dalga Şekilleri [5].

BASTIRMA ENDÜKTANSI L_S YERİNE KUPLAJLI SARGI BAĞLANAN İLERİ YÖNLÜ DÖNÜŞTÜRÜCÜ

Bastırma endüktansı L_s endüktansı yerine bir kuplajlı endüktansın kullanıldığı, tek anahtarlı, geri beslemeli ve pasif bastırma hücreli ileri yönlü dönüştürücü yapısı [1] Şekil 5'te verilmiştir. Dönüştürücüde üçüncü bir trafo sargısı kullanılır ve trafonun kaçak endüktansından faydalı bir şekilde yararlanılır. Sunulan dönüştürücü yapısının avantajları aşağıdaki gibidir.

Anahtarların sıfır gerilimde kesime girmesi sağlanır.
Transformatörün resetlenmesi sağlanır.
Kaçak endüktans enerjisi geri kazanılır.
Geri kazanılan enerji kaynak ve yük tarafına aktarılır.
Anahtarların sıfır akımda iletime girmesi sağlanır.

Şekil 5'te gösterilen L_s endüktansı yerine bir kuplajlı endüktansın kullanıldığı devrede, C_1 bastırma kapasitörü, n_3 transformatörün üçüncü sargısı, D_{s1} ve D_{s2} yardımcı diyotlardır.

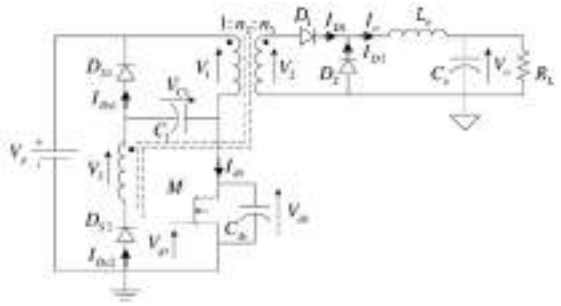

Şekil 5. Bastırma Endüktansı Ls Yerine Bir Kuplajlı Sargı Bağlanan İleri Yönlü Dönüştürücü [1].

Devrenin bir anahtarlama periyodu dokuz çalışma aralığıyla tamamlanmaktadır. L_{L1} ve L_{L2} kaçak endüktans değerleridir. Maksimum resetlenme süresi denklem (3)'te verilmiştir.

$$\Delta t_{off} \leq \Delta t_{offmax} \approx \pi\sqrt{L_p C_s} \quad (3)$$

$$L_p = L_m + L_{L1} \quad (4)$$

Anahtarlama elemanı üzerinde oluşan ekstra gerilim stresini göz ardı ederek uygulanabilecek maksimum bağıl iletim süresi denklem (5)'teki gibi elde edilmektedir.

$$D_{onmax} \approx 1 - \pi f_s\sqrt{L_p C_s} \quad (5)$$

Görüldüğü üzere maksimum bağıl iletim süresi primer endüktansına ve bastırma kondansatörüne ve anahtarlama frekansına bağlıdır. Maksimum bağıl iletim süresine göre anahtarın pik gerilim değişimi Şekil 6'daki gibidir.

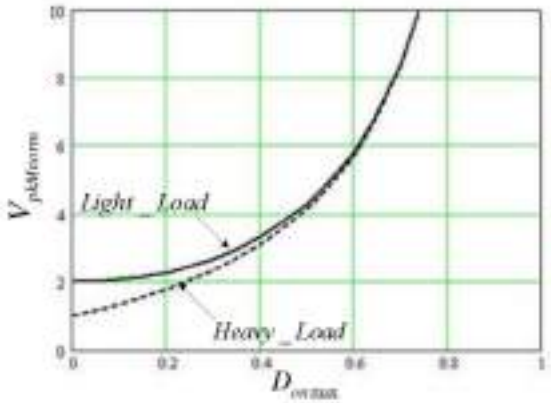

Şekil 6. Maksimum Bağıl İletim Süresine Göre Anahtar Üzerindeki Normalleştirilmiş Pik Gerilimin Değişimi [1].

Anahtarlama elemanı üzerine gelen maksimum gerilim stresi dönüştürücü maksimum bağıl iletim süresi ile hafif yüklerde çalışırken oluşmaktadır. Şekil 6'da sunulan grafikten anahtarların üzerine gelen gerilim stresinin bağıl iletim süresi ile üstel olarak arttığı ve hafif yüklerde anahtar üzerinde oluşan gerilim stresinin çok

daha fazla olduğu görülmektedir. (6) numaralı denklemden görüldüğü gibi, bağıl iletim süresinin artması ile anahtarlama elemanı üzerinde oluşan gerilim stresi katlanarak artmaktadır.

$$V_{pknorm} = \left(1 + \frac{\pi D_{on}}{1-D_{onmax}}\right).V_g \quad (6)$$

Anahtar üzerinde oluşan pik akım değeri ise denklem (7)'deki gibidir.

$$I_{pk} = n_2 I_o + (1+n_3)\left(n_3 V_g + V_{csmax}\right)\sqrt{\frac{C_1}{n_3^2(L_{L1}+L_{L3})}}$$
(7)

Şekil 7'deki grafikte görüldüğü gibi, 5 V çıkış gerilimi, 5 A çıkış akımı ve anahtarlama frekansı 200 kHz olan bir uygulaması yapılan devrenin verimi çıkış akımı değeri, dolayısıyla çıkış gücü ile değişmektedir. Hafif yüklerde verimin % 70'in altına düştüğü görülürken, devrenin maksimum verimi %80 civarındadır.

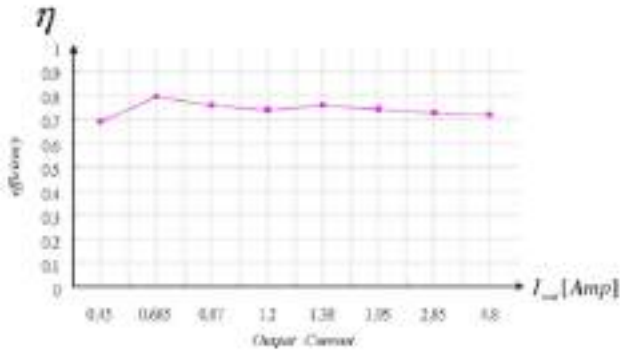

Şekil 7. Çıkış Akımına Bağlı Olarak Verimin Değişimi [1].

Bu devrede sunulan bastırma hücresi, yük ve giriş gerilimi değişimlerine karşılık devrenin çalışma modunun değişmemesini ve anahtarlama elemanı için geniş bir çalışma aralığında mükemmel bir ZVS sağlamaktadır. Bu üstünlüğünü üçüncü trafo sargısının sarım oranıyla sağlamaktadır. Devrenin en önemli avantajlarından birisi budur. Devrenin dezavantajları, üçüncü çalışma aralığı boyunca serbest dolaşım diyotu üzerinde yüksek gerilim piklerinin oluşması, iletimin ilk anında anahtarda oluşan akım pikinin yüksek olması ve dönüştürücü yapısının karmaşık olması söylenebilir.

PRİMER VE/VEYA SEKONDERE KUPLAJLI ENDÜKTANSLAR EKLENEN İLERİ YÖNLÜ DÖNÜŞTÜRÜCÜLER

Temel pasif LCDD bastırma hücreli dönüştürücüde primer ve/veya sekondere kuplajlı endüktanslar eklenen ileri yönlü dönüştürücü topolojileri [4] Şekil 8, 10 ve 11'de verilmiştir. Bu dönüştürücü yapıları üç farklı devreden oluşmaktadır. Şekil 8'de sunulan ilk devrede, primerde bir mıknatıslama endüktansı L_m sekonder tarafta ise bir kuplajlı endüktans L_w bulunmaktadır. Bu devreye I. devre yapısı denilmektedir. Şekil 8'deki devreden türetilen birinci devrede sadece primer tarafta L_m kuplajlı endüktansı

bulunmaktadır. Şekil 10'da sunulan bu devreye II. devre yapısı denilmektedir. Türetilen ikinci devrede ise sadece sekonder tarafta L_m kuplajlı endüktansı bulunmaktadır. Şekil 11'de sunulan bu devreye III. devre yapısı denilmektedir. Anahtarlama elemanı ZCS ile iletime girmekte ve ZVS ile kesime girmektedir.

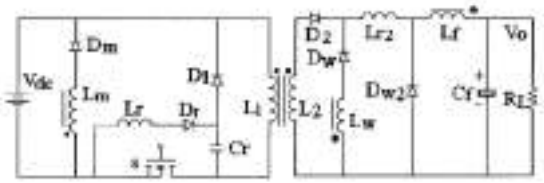

Şekil 8. Hem Primer Hem Sekondere Birer Kuplajlı Endüktans Eklenen Devre Yapısı [4].

C_r bastırma kondansatörü üzerinde oluşan V_{cr} geriliminin $+V_i$ ile $-V_i$ bandının dışına fazla çıkmayacağı Şekil 9'da görülmektedir. Böylece, bu devre yapısında aktif anahtarlama elemanı üzerinde oluşan gerilim stresinin giriş geriliminin iki katından çok daha fazla olmayacağı anlaşılmaktadır.

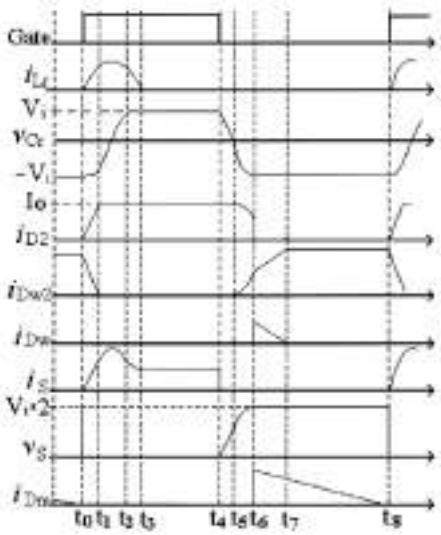

Şekil 9. Hem Primer Hem Sekonderde Kuplajlı Endüktans Bulunan Devre İçin Temel Dalga Şekilleri [4].

Bu dönüştürücünün bir anahtarlama periyodunda sekiz ayrı çalışma aralığı oluşmaktadır. Bir anahtarlama periyodu boyunca aktif anahtar ZCS ile iletime girmekte, ZVS ile kesime girmektedir. L_m mıknatıslama endüktansının sadece primere ve sadece sekondere konulduğu devre yapıları sırasıyla Şekil 10 ve Şekil 11'de görülmektedir.

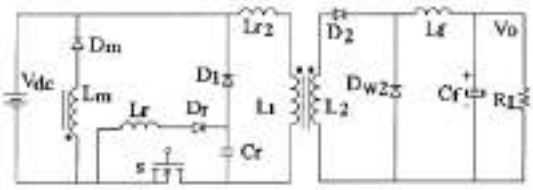

Şekil 10. Sadece Primere L_m Mıknatıslama Endüktansı Eklenen Devre Yapısı [4].

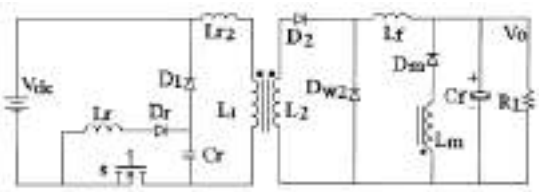

Şekil 11. Sadece Sekondere L_m Mıknatıslama Endüktansı Eklenen Devre Yapısı [4].

Şekil 12'de gösterilen temel akım ve gerilim dalga şekilleri Şekil 10 ve Şekil 11'de verilen devre yapıları için geçerlidir. İki devrenin de temel dalga şekilleri aynıdır. Şekil 12'den görüldüğü üzere bastırma kondansatörü C_r gerilimi V_{cr} giriş gerilimi $+V_i$ ile $-V_i$-ΔV gerilimi arasında değişmektedir. Kondansatörün ters gerilim tuttuğu aralıkta oluşan ekstra ΔV gerilimi L_{r2} endüktansının deşarj olmasıyla ortaya çıkan gerilimden kaynaklanmaktadır. Böylece Şekil 10 ve Şekil 11'de sunulan devrelerde aktif anahtarlama elemanı üzerinde oluşacak gerilim stresinin giriş geriliminin iki katından biraz daha yüksek olacağı görülmüştür.

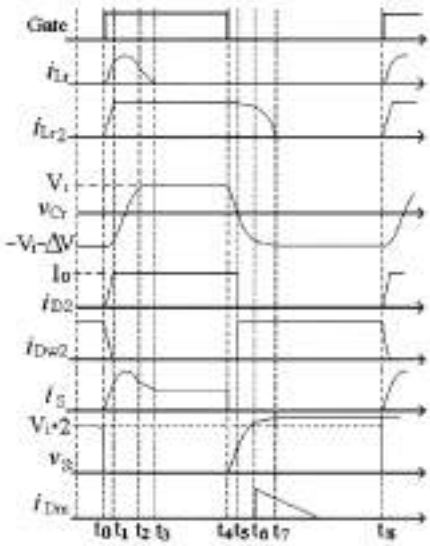

Şekil 12. Sadece Primerde ve Sadece Sekonderde Lm Mıknatıslama Endüktansı Bulunan Devre İçin Temel Dalga Şekilleri [4].

Şekil 9'da ZCS ile iletime giren D_{w2} diyodunun Şekil 12'de sert bir şekilde iletime girdiği görülmektedir.
Bastırma hücresi elemanları olan L_r ve C_r değerleri uygun şekilde seçilerek aktif anahtarlama elemanı üzerindeki akım stresi azaltılır.

$$\propto_2 = \frac{I_o}{V_{dc}}\sqrt{\frac{L_{r2}}{C_r}}$$
(7)

$$\omega_{02} = 2\pi f_0 = \frac{1}{\sqrt{L_{r2}C_r}} \quad (8)$$

Aşağıda elde edilen denklem (9)'dan yola çıkarak, dönüştürücünün statik kazancının bağıl iletim süresine (D), rezonans frekansına (w_{02}), normalize akıma (α_2) ve anahtarlama frekansına (f_s) bağlı olduğu görülmektedir. Gerilim kazancının beş farklı değişkene bağlı olması tasarım açısından zorluk oluşturmaktadır.

$$\frac{V_o}{V_{dc}} = D - \frac{f_s}{\omega_{02}}\left(\propto_2 - \frac{1}{2\propto_2}\right) \tag{9}$$

Doluluk oranının maksimum değeri aşağıdaki gibi bulunur.

$$D_{max} = \frac{N_1}{(N_1+N_m)} \tag{10}$$

$$N_{1m} = \sqrt{\frac{L_1}{L_m}} \tag{11}$$

Görüldüğü gibi D_{max} değeri primer endüktansı ile mıknatıslama endüktansının oranına bağlı olarak değişir. Şekil 13 ve Şekil 14'de sunulan verim değişimlerinde, Structure I ile gösterilen eğri, Şekil 8'de verilen primer ve sekonderde kuplajlı endüktans bulunan devreye aittir. Structure II ile gösterilen eğri, Şekil 10'da verilen primerinde L_m bulunan devreye aittir. Structure III ile gösterilen eğri ise, sekonderinde L_m mıknatıslama endüktansı bulunan devrenin değerlerini göstermektedir.

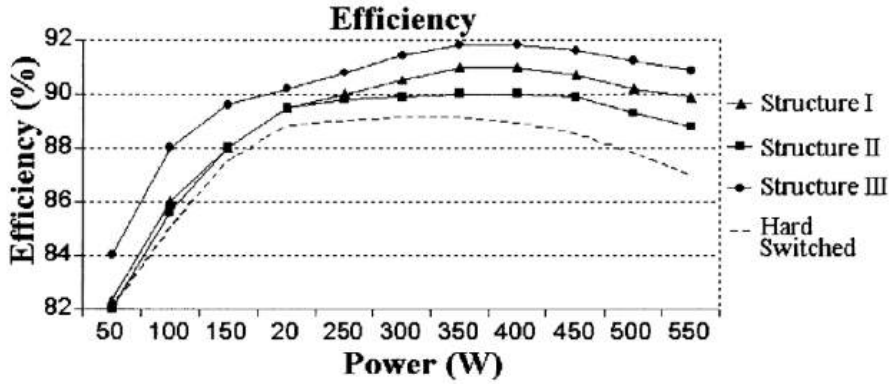

Şekil 13. Çıkış Gücüne Göre Verimin Değişimi [4].

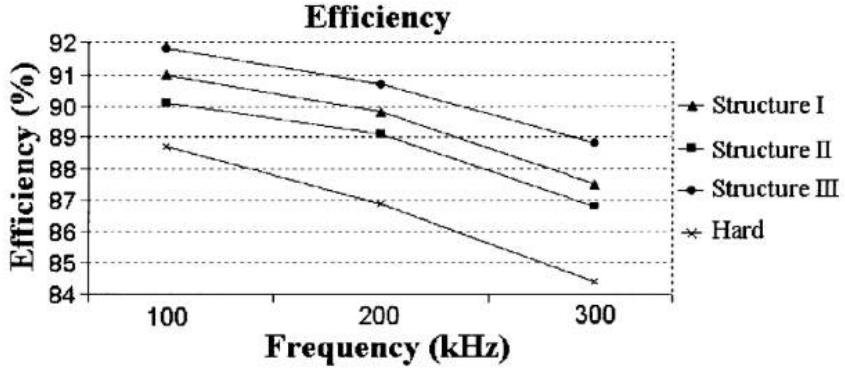

Şekil 14. Frekansa Göre Verimin Değişimi [4].

Şekil 13'teki grafikten görüldüğü üzere, L_m mıknatıslama endüktansı sekonderde bulunan devre topolojisi maksimum % 92 ile en yüksek verime sahiptir. Hem primerinde hem sekonderinde kuplajlı endüktans bulunan devre yapısında maksimum % 91 verim elde edilmiştir. L_m mıknatıslama endüktansı primerde bulunan yapıda ise maksimum % 90 olarak en düşük verim elde edilmiştir. Şekil 10 ve Şekil 11'de verilen yapıların teorik olarak temel dalga şekilleri aynı gözükse de elde edilen sonuçların farklı olduğu görülmüştür.

Sunulan son iki dönüştürücüde, fazladan bir kuplajlı endüktans bulunsa da, tek bir aktif anahtarlama elemanı ile iyi bir sonuç elde edildiği söylenebilir. Devrenin anahtarlama elemanı aşırı bir gerilim ve akım stresine maruz kalmaz ve yumuşak anahtarlama sağlanır. Devrenin dezavantajı olarak, hafif yüklerde anahtarlama elemanının kesime girmesinde ZVS'de bir zayıflığın oluşması gösterilebilir.

KARŞILAŞTIRMA

Üst bölümlerde kısaca incelenen literatürde mevcut olan ve iyi bilinen pasif bastırma hücreli tek anahtarlı ileri yönlü dönüştürücülerin etraflı bir karşılaştırması Tablo 1'de verilmiştir. Tabloda numaralandırılan bu topolojiler, kullanılan ilave elemanlar, devrenin basitliği, trafonun mıknatıslama ve kaçak endüktansı enerjilerinin aktarımı, anahtarın maruz kaldığı gerilim ve akım pikleri, doluluk oranı, iletime girmede ZCS ve kesime girmede ZVS sağlanması ve verim açılarından karşılaştırılmıştır.

Yapılan karşılaştırma sunucunda, (1) nolu temel LCDD bastırma hücreli devreye göre, sadece kesime girmede yüke bağlı olmaksızın tam ZVS sağlayan (2) nolu devrenin en kötü performans sergilediği söylenebilir. (3) nolu devrenin ise, özellikle (4) ve (5) nolu devrelere göre, sadece anahtarın maruz kaldığı pik gerilimi 2Vg'de sınırlamasına karşılık, oldukça karmaşık, pahalı ve zor uygulanabilir olduğu söylenebilir.

(4) ve (5) nolu devrelerin tek farkı, mıknatıslama endüktansı enerjisinin (4) nolu devrede giriş ve (5) nolu devrede çıkış kaynağına aktarılmasıdır. Bu durumda, doğal olarak verimi en yüksek olan devre (5) numaralı olan devre olmaktadır. Ancak, bu devre çok hafif yüklerde veya boşta çalışma özelliğini kaybeder. Bu özellik dikkate alındığında, en uygun ve uygulanabilir devrenin (5) numaralı devre olduğu söylenebilir. Aksi durumda, bu devrenin alternatifi (4) nolu devre olacaktır. Normal olarak, bu devrelerde doluluk oranının 0,5'in üzerine çıkarılması amacı yoktur.

Devrenin mümkün olduğunca sade ve basit olması ve doluluk oranının 0,5'in üzerine çıkarılması istendiğinde, en uygun ve uygulanabilir devrenin (1) nolu devre olduğu kolayca söylenebilir. Sadece hedeflenen maksimum anahtar pik gerilimi için bir kırpıcı eleman kullanmak yararlı olabilir.

Tablo 2. Karşılaştırma Tablosu

	(1) **Temel LCDD Bastırma Hücreli İleri Yönlü Dönüştürücü**	(2) **L_s Yerine Lm Mıknatıslama Endüktansı Bağlanan İleri Yönlü Dönüştürücü**	(3) **Hem Primer Hem de Sekondere Birer Kuplajlı Endüktans Bağlanan İleri Yönlü Dönüştürücü**	(4) **Sadece Primere Lm Mıknatıslama Endüktansı Bağlanan İleri Yönlü Dönüştürücü**	(5) **Sadece Sekondere Lm Mıknatıslama Endüktansı Bağlanan İleri Yönlü Dönüştürücü**
İlave Elemanlar	2 Diyot 1 Kondansatör 1 Endüktans	2 Diyot 1 Kondansatör 1 Kuplajlı Endüktans	2 Diyot 1 Kondansatör 1 Endüktans 2 Kuplajlı Endüktans	2 Diyot 1 Kondansatör 1 Endüktans 1 Kuplajlı Endüktans	2 Diyot 1 Kondansatör 1 Endüktans 1 Kuplajlı Endüktans
Devrenin Basitliği	Oldukça Sade ve Basit	Biraz Karmaşık	Çok Karmaşık	Biraz Karmaşık	Biraz Karmaşık
Mık.End. Enerjisi	Cs'ye Aktarılır	Cs'ye Aktarılır	Vg'ye Aktarılır	Vg'ye Aktarılır	Vç'ye Aktarılır
Kaç.End. Enerjisi	Cs'ye Aktarılır	Cs'ye Aktarılır	Vç'ye Aktarılır	Cs'ye Aktarılır	Cs'ye Aktarılır
Anahtarın Pik Gerilimi	2Vg'nin Üzerindedir. Yüke Bağlıdır. Üst Sınırı Sınırlamak Gerekebilir.	2Vg'nin Biraz Üzerindedir. Yüke Bağlıdır. Üst Sınırı Sınırlamak Gerekmez.	2Vg'de Sınırlanır. Üst Sınırı Sınırlamak Gerekmez.	2Vg'nin Biraz Üzerindedir. Yüke Bağlıdır. Üst Sınırı Sınırlamak Gerekmez.	2Vg'nin Biraz Üzerindedir. Yüke Bağlıdır. Üst Sınırı Sınırlamak Gerekmez.
Anahtarın Pik Akımı	Biraz Yüksek	Çok Yüksek	Biraz Düşük	Normal	Normal
İletim Bağıl Süresi	$D \geq 0.5$ 0,5'in Üzerine Çıkarılabilir. Ancak Gerilim Stresi de Artar.	$D \leq 0.5$ Prensip Olarak 0,5'in Altındadır.	$D \leq 0.5$ Prensip Olarak 0,5'in Altındadır.	$D \leq 0.5$ Prensip Olarak 0,5'in Altındadır.	$D \leq 0.5$ Prensip Olarak 0,5'in Altındadır.
İletime Girmede	Sağlanır	Sağlanır	Sağlanır	Sağlanır	Sağlanır

Kesime Girmede ZVS	Normalde Sağlanır. Hafif Yüklerde Kısmen Sağlanır.	Tam Sağlanır.	Normalde Sağlanır. Hafif Yüklerde Kısmen Sağlanır.	Normalde Sağlanır. Hafif Yüklerde Kısmen Sağlanır.	Normalde Sağlanır. Hafif Yüklerde Kısmen Sağlanır.
Devrenin Verimi	Biraz Düşük	Çok Düşük	Biraz Yüksek	Normal	Çok Yüksek

SONUÇLAR

Bu çalışmada, literatürde mevcut olan ve iyi bilinen, akümülatör şarjı, elektronik kaynak makineleri, izoleli güç kaynakları, vb. uygulamalarda yaygın olarak kullanılan pasif bastırma hücreli tek anahtarlı ileri yönlü dönüştürücüler, kısaca incelenmiş, ancak devrenin basitliği, mıknatıslama ve kaçak endüktans enerjilerinin resetlenmesi, anahtarın gerilim ve akım pikleri, doluluk oranı, yumuşak anahtarlama, verim, vb. açılarından etraflıca karşılaştırılmıştır.

Bir bütün ve sonuç olarak ele alındığında, en kötü toplam performansı (2) nolu devrenin sergilediği, maliyet ve uygulanabilirlik açısından (3) nolu devrenin oldukça kötü olduğu, anahtarın maruz kaldığı gerilim ve akım pikleri ile verim dikkate alındığında (5) nolu devrenin en iyi olduğu söylenebilir. Basitlik, maliyet, uygulanabilirlik ve 0,5'in üzerinde bir doluluk oranı istendiğinde ise, hala (1) numaralı temel LCDD bastırma hücreli devrenin en iyi performans sergilediği görülmektedir.

KAYNAKLAR

[1] Abramovitz, A., Cheng, T., & Smedley, K. (2010). Analysis and design of forward converter with energy regenerative snubber. *IEEE Transactions on Power Electronics, 25*(3), 667-676. https://ieeexplore.ieee.org/document/5272117/

[2] Bodur, H. (2014). *Güç Elektroniği.* İstanbul: Birsen Yayınevi.

[3] Bridge, C. D. (2000). Clamp voltage analysis for RCD forward converters. APEC 2000: *Fifteenth Annual IEEE Applied Power Electronics Conference and Exposition,* New Orleans, LA: IEEE

[4] Silva, E. S., Coelho, E.A.A., Freitas, L. C., Vieira, J. B., & Farias, V. J. (2004). A soft-single-switched forward converter with low stresses and two derived structures. *IEEE*

Transactions on Power Electronics, 19(2), 388-395. https://ieeexplore.ieee.org/document/1271322/

[5] Tanaka, T., Ninomiya, T., & Harada, K. (1988). Design of a nondissipative turn-off snubber in a forward converter. Proceedings from PESC '88: *19th Annual IEEE Power Electronics Specialists Conference.* Kyoto: IEEE.

INVESTIGATION OF COOLING PERFORMANCE IN CHAMBER DESIGNED FOR TORREFIED BIOMASS

Özben KUTLU
Ege University, Institute of Solar Energy, BESTMER
ozben.kutlu@ege.edu.tr

Günnur KOÇAR
Ege University, Institute of Solar Energy, BESTMER
gunnur.kocar@ege.edu.tr

ABSTRACT: Torrefied biomass is produced from biomass by using a thermal process carried out in the temperature range of 200-300°C and in inert atmosphere. Today, it is used as intermediate product for other thermal processes or an alternative fuel to lignite. In order to protect the properties of torrefied biomass, the hot product should be properly cooled before contacting with air and then stored. A cooling chamber should be used after the reactor in order to separate from liquid from torrefied biomass at the temperature of ~300°C, to avoid catching fire on contact with air, and to prevent absorbing moisture. In this study, a cooling and storage chamber was constructed to solve the problems in existing continuous torrefaction system. Broiler litter torrefied at the optimum torrefaction condition was used as a raw material to test the cooling performance. The effects of residence time, nitrogen flow rate, and frequency of mixing motor to moisture content and outlet temperature of product were analysed and optimised by using response surface methodology. The experimental set was prepared by Box-Behnken experimental design which is a type of response surface methodology. In this context, the optimum cooling condition was determined while the parameter playing a more prominent role was identified. The temperature and moisture content of torrefied litter were dropped below 50°C and 5%, respectively. Hence, the characterization of product has been upgraded to international standards, and the alternative fuel that can be safely stored in environmental condition has been produced.

This study was supported by Ege University Scientific Research Projects Coordination Unit (Project Number: 16GEE016).

Key words: Torrefied biomass, broiler litter, moisture content, cooling chamber, response surface methodology

RELATION BETWEEN HARDNESS PARAMETERS AND MATERIALS THICKNESS AT HEAT TREATMENT OF CARBURIZED STEEL

İdris KARAGÖZ
Yalova University
Idris.karagoz@yalova.edu.tr

Halil İbrahim KURT
Gaziantep University
hiakurt@gmail.com

Ramazan SAMUR
Marmara University
rsamur@marmara.edu.tr

ABSTRACT: Carburized steels with a carbon content of less than 0.20% cannot be cured by normal means. For the curing process, the amount of carbon material has to be increased. In this study; the carburization process was applied to the SAE 8620 (21NiCrMo2) carburized steel in a salt bath containing 10% cyanide (Potassium Cyanide KCN). Samples cut at two different sizes as 15x15x100 mm and 20x20x100 mm were milled to have a surface roughness value of Ra 0.8. The materials were heated gradually from room temperature to curing temperature of 930°C. At 930°C, the material was allowed to stand for six hours and then gradually decreased to 860°C. The materials were stored at 860°C for 40 minutes and then the materials were quenched with water in the oil cooling medium. After quenching, the materials were tempered at 180°C for two hours. Surface hardness and microhardness of the materials were measured and their microstructures were examined. The hardness depth for the materials was 1.6 mm and the effective hardness was 1.2 mm. Surface hardness values were measured as 810 HV for materials with a thickness of 15 mm and 810 HV for materials with a thickness of 20 mm. It was observed that the hardening was at a maximum level up to a depth of 0.2 mm, and the hardness values decreased as the core was approached. In microstructure investigations, it was observed that the martensitic layer was formed on the surface and this layer was lost as it penetrated inward. In addition to plain martensite forms, perlite particles were also seen in the microstructure. On the material hardness, the temperature and time of the roughing, the carbon potential of the material and the bath, the cooling rate and the hardenability of the steel were found to be important.

Key words: carburized steels, quenching, hardness, heat treatment, microstructure

SEMENTASYON ÇELİKLERİNİN ISIL İŞLEMİNDE MALZEME KALINLIĞINA BAĞLI OLARAK SERTLİĞE ETKİ EDEN PARAMETRELER

ÖZET: Karbon miktarı %0,20' nin altında olan sementasyon çelikleri normal yollarla sertleştirilemezler. Sertleştirme işlemi için malzemenin sahip olduğu karbon miktarının arttırılması gerekmektedir. Bu amaçla genellikle yüzeye karbon emdirme yapılan ve en eski yüzey sertleştirme metotlarından biri olan sementasyon işlemine tabi tutulurlar. Bu çalışmada; SAE 8620 (21NiCrMo2) sementasyon çeliğine %10 siyanür içeren (Potasyum Siyanür KCN) tuz banyosunda sementasyon işlemi uygulanmıştır. 15x15x100 mm ve 20x20x100 mm olarak iki farklı ölçüde kesilen numuneler, yüzey pürüzlülük değeri Ra 0,8 olacak şekilde frezelenmiştir. Malzemeler oda sıcaklığından sertleştirme sıcaklığı olan 930 °C' ye kadar kademeli şekilde ısıtılmıştır. 930 °C'de malzemeler altı saat süreyle bekletilmiş ve ardından kademeli bir şekilde sıcaklık 860 °C' ye düşürülmüştür. Malzemeler 860 °C'de 40 dakika bekletilmiş ve sonrasında malzemelere yağ soğutma ortamında su verilmiştir. Su verme sonrası malzemeler 180 °C'de iki saat süreyle temperlenmiştir. Mikroyapı incelemelerine uygun olarak malzemeler 1200 zımparaya kadar zımparalanmış, 3 µm ve 1 µm elmas pasta ile parlatması yapılarak asit çözeltisi ile yüzeyleri dağlanmıştır. Malzemelerin yüzey sertlikleri, mikrosertlik ölçümleri yapılmış ve mikroyapıları incelenmiştir. Malzemeler için sertlik derinliği 1,6 mm ve etkili sertlik derinliği ise 1,2 mm olarak tespit edilmiştir. Yüzey sertlik değerleri 15 mm kalınlığa sahip malzemeler için 832 HV ve 20 mm kalınlığa sahip malzemeler içinse 810 HV olarak ölçülmüştür. 0,2 mm derinliğe kadar sertleşmenin maksimum seviyede olduğu, çekirdeğe yaklaşıldıkça sertlik değerlerinin düştüğü görülmüştür. Mikro yapı incelemelerinde yüzeyde martenzitik tabakanın oluştuğu ve içeriye doğru penetre edildikçe bu tabakanın etkisini yitirdiği gözlemlenmiştir. Buna bağlı olarak iki numune arasında kalınlıkla birlikte sertlik değerlerinin bir miktar düştüğü gözlemlenmiştir. Mikroyapıda düz martenzit şekillerin yanında perlit taneciklerine de rastlanmıştır. Malzeme sertliği üzerinde, karbürüzasyon sıcaklığı ve zamanı, malzeme ve banyo karbon potansiyeli, soğutma hızı ve çeliğin sertleşebilirliğinin önemli olduğu görülmüştür.

Anahtar sözcükler: sementasyon çelikleri, su verme, sertlik ölçümü, ısıl işlem, mikroyapı

GİRİŞ

Isıl işlem, metallerin sertlik ve mukavemet gibi mekanik özelliklerini geliştirmek amacıyla uygulanan metalurjik bir işlemdir. Metal ve alaşımlara istenilen özellikleri kazandırmak amacıyla katı halde uygulanan kontrollü ısıtma ve soğutma işlemleri şeklinde de tanımlanmaktadır (Karagöz 2007). Çeliklere uygulanan ısıl işlemler genellikle üç grupta incelenir. Bunlar, 1- Tavlama, 2- Temperleme (Meneviş, gerilim giderme veya ıslah etme vb.), 3- Sertleştirme işlemi olarak sınıflandırılabilir. Sertleştirme işlemi, kritik bir sıcaklıkta veya üzerinde bir çeliğin ısıtılması ve daha sonra soğutma işleminin yapılması olarak açıklanabilir (Biçer & Karagöz 2017). Çeliklerin sertleştirilmesinde, çeliğin sahip olduğu karbon oranı oldukça önemlidir. Sementasyon çeliklerinin genel olarak karbon oranı % 0,20' nin altında, ancak bazı

türlerde % 0,25' e kadar çıkabilmektedir. Bu nedenle normal yollarla sertleştirilemezler (Topbaş 1998).

Malzemelerin karbon oranı düştükçe, çeliklerin işlemeye karşı dirençleri düştüğü için, talaşlı imalat yöntemleriyle işlenmeleri kolaydır. İşleme esnasında avantaj oluşturan bu durum, ürünlerin kullanımı esnasında malzeme yüzey sertliği ve sertlik derinliğine bağlı olarak çabuk aşınmakta ve deforme olarak bir dezavantaj oluşturmaktadır. Bu durumda yapılacak işlem, üretim esnasında sahip olduğu düşük sertlikten faydalanıp işlemek, sonrasında ise ısıl işlem yöntemleriyle sertliğini arttırmaktır (Karagöz 2007). Sementasyon çeliklerinde yüzeyde sert ve aşınmaya dayanıklı, çekirdekte ise daha yumuşak ve tok özellikler malzeme yüzeyine karbon emdirilmesi yöntemiyle gerçekleştirilmektedir.

Daha önce yapılan çalışmalarda Levy&Yan (1985) tarafından sertleştirilmiş AISI 8620 çeliğinin aşınma davranışı incelenerek ısıl işlemin aşınma davranışı üzerindeki etkisi belirlenmeye çalışılmıştır. Sharma ve ark. tarafından ısıl işlem uygulanmamış AISI 8620 çeliğinin CNC torna' da talaşlı imalat yöntemiyle şekillendirilmesindeki proses parametrelerinin optimizasyonun Taguchi ve Grey Taguchi Analizi kullanılarak incelenmiştir (Sharma et al 2014). Asi ve ark. (2007) tarafından gaz karbürüzasyon ile sertleştirilmiş SAE 8620 çeliğinin sementasyon derinliği ve yorulma özellikleri arasındaki ilişki incelenmiştir. Asi ve ark. (2009) tarafından yapılan benzer bir çalışmada da farklı sertleştirme sıcaklıkları ve süreleri kullanılarak gaz karbürüzasyonu ile sertleştirilmiş malzemenin yorulma performansı incelenmiştir. Çelik ve ark. (2001) süreç değişkenleri olarak zaman, sıcaklık ve farklı gaz karışımlarında çeliğin iyon nitrürleme davranışını incelemişlerdir.

Bu çalışmada; SAE 8620 (21NiCrMo2) sementasyon çeliğine %10 siyanür içeren (Potasyum Siyanür KCN) tuz banyosunda sementasyon işlemi uygulanmıştır. Su verme sonrası malzeme temperleme işlemine tabi tutulmuş, sonrasında sertlik ölçümleri ve mikroyapı incelemeleri gerçekleştirilerek malzeme kalınlığı, sertlik ve mikroyapı arasındaki ilişki belirlenmeye çalışılmıştır.

YÖNTEM

Çalışmalarda endüstrideki kullanım oranları dikkate alınarak daha çok dişli çarklar ve miller gibi makine parçaları ve kılavuz burç, kolon ve plaka gibi kalıp elemanlarının yapımında yaygın olarak kullanılan, TSE EN 10084 standardına uygun, malzeme no 1.6523 ve sembolü 21NiCrMo2 (SAE 8620) olan çelik kullanılmıştır. Malzemeler İMS Özel Çelik (İstanbul) firmasından sertifikalı ürün olarak temin edilmiştir. Malzemelere ait mekanik özellikler Tablo 1' de verilmiştir. GNR S7 marka (GNR/İtalya) kütle spektroskopi cihazı ile malzemelerin kimyasal bileşimi ölçülmüştür.

Tablo 1. 21NiCrMo2 Sementasyon çeliğine ait mekanik özellikler

Özellik	Değer

Çekme Mukavemeti	530 MPa
Akma Mukavemeti	385 MPa
Elastik Modül	190-210 GPa
Kayma Modülü	80 GPa
Poisson Oranı	0,27-0,30
Izod Darbe Dayanımı	115 J
Sertlik	149 HB
Kopma Uzaması	% 10

Hazırlanan numunelere %10 siyanür içeren (Potasyum Siyanür KCN) tuz banyosunda Şekil 1' de verilen ısıl işlem çevrimi ve süreçlere göre karbürüzasyon işlemi yapıldı. Malzeme kalınlığının sertlik üzerindeki etkisinin incelenmesi amacıyla 15x15x100 mm ve 20x20x100 mm ölçülerinde farklı kalınlıklarda numuneler hazırlanmış ve her iki numune grubu içinde Şekil 1' de verilen süreçler uygulanmıştır.

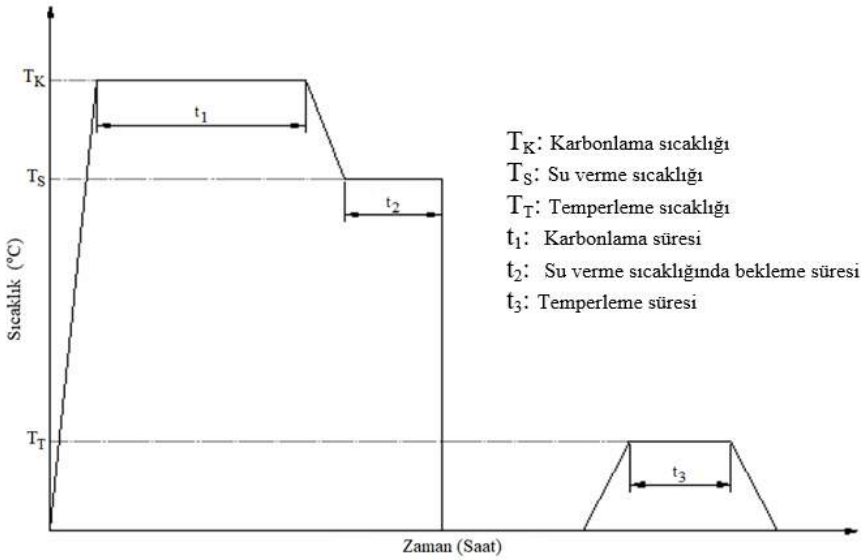

Deneme Kodu	Kalınlık (mm)	T_K (°C)	t_1 (Sa.)	T_S (°C)	t_2 (dk.)	TT (°C)	t_3 (Sa.)
1	15	930	6	860	40	180	2
2	20	930	6	860	40	180	2

Şekil 1. Isıl işlem çevrimi ve süreçler

Isıl işlem sonrası numuneler mikroyapı incelemelerine uygun olarak malzemeler 1200 zımparaya kadar zımparalanmış, 3 µm ve 1 µm elmas pasta ile parlatması yapılarak asit çözeltisi ile yüzeyleri dağlanmıştır. Numunelerin kesit yüzeyinden merkeze doğru MIKROSCAN marka sertlik ölçüm cihazı ile 1 kp yük ve 136° uç açısına sahip elmas

piramit uç kullanılarak HV cinsinden sertlikleri ölçülmüş ve optik mikroskop ile mikroyapı incelemeleri gerçekleştirilmiştir.

BULGULAR

Kütle spektroskopisi ölçüm sonuçlarına göre malzemenin kimyasal bileşimi Tablo 2' de verilen şekilde bulunmuştur. Sonuçlar incelendiğinde çalışmalarda kullanılan malzemelerin standarda uygun olduğu ve malzeme bileşiminin standartta belirtilen değerler arasında olduğu görülmüştür. Çeliğin kimyasal bileşimin standart değerlere uygun olması ısıl işlem proseslerinin doğru olarak uygulanabilmesi ve sonuçların güvenilirliği açısından önemlidir. Cidar sertliği olarak da isimlendirilen parçanın yüzeyindeki en yüksek sertlik değeri, çelikte bulunan karbon miktarına bağlı olarak değişiklik göstermektedir [2]. Kimyasal bileşimin uygun olmaması, mangan, silisyum, nikel gibi katı çözelti sertleşmesi ve krom, molibden gibi sertlik ve dayanım artışına sebep olan alaşım elementlerinin çeliğe etkisi göz önünde bulundurulduğunda, sertliğin kesitte dağılımı farklılaşacaktır. Bu durum parçanın kullanım amacının dışına çıkmasına, kolay aşınmasına ya da yüksek sertlik nedeniyle özellikle zorlamalı parçalarda malzemelerin deforme olmasına sebep olacaktır. Aynı şekilde parçanın yüzey sertliği ve çekirdek sertliği arasındaki fark hedeflenen ısıl işlemin başarısız olmasına ve ek bir proses gerektirmesine sebep olacaktır. Doğal olarak bu ikincil prosesler ısıl işlem ve parça üretim maliyetini arttıracaktır.

Tablo 2. 21NiCrMo2 çeliğinin kimyasal bileşim ölçüm sonuçları

Açıklama	**Kimyasal Bileşim (% ağırlık)**							
Element	**C**	**Si**	**Mn**	**$P_{maks.}$**	**$S_{maks.}$**	**Ni**	**Cr**	**Mo**
Standard	0,18-0,23	0,20-0,35	0,70-0,90	0,040	0,040	0,40-0,70	0,40-0,60	0,15-0,25
Bulunan	0,197	0,204	0,718	0,012	0,0076	0,439	0,415	0,158

Numunelerin sertlik ölçüm grafikleri Şekil 2' de verilmiştir. Malzemeler için sertlik derinliği 1,6 mm ve etkili sertlik derinliği ise 1,2 mm olarak tespit edilmiştir. Yüzey sertlik değerleri 15 mm kalınlığa sahip malzemeler için 832 HV ve 20 mm kalınlığa sahip malzemeler içinse 810 HV olarak ölçülmüştür. 0,2 mm derinliğe kadar sertleşmenin maksimum seviyede olduğu, çekirdeğe yaklaşıldıkça sertlik değerlerinin düştüğü görülmüştür.

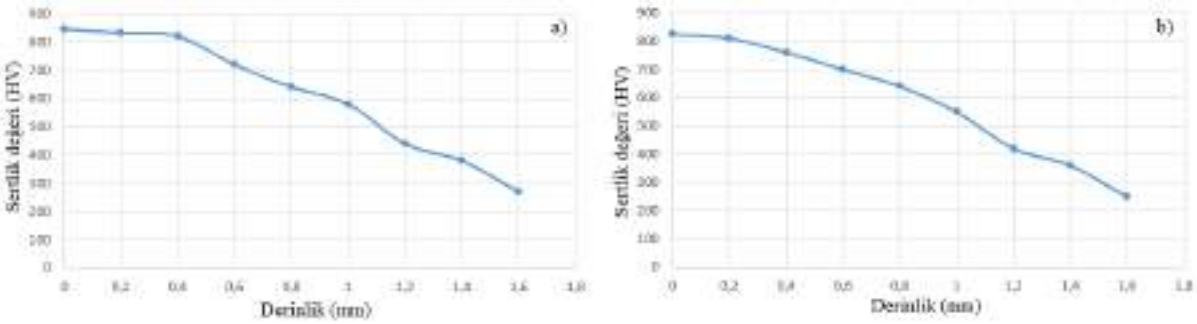

Şekil 2. Sertlik ölçüm grafikleri a) Kalınlık 15 mm, b) Kalınlık 20 mm

Şekil 3′ te mikroyapı incelemelerine ait resimler verilmiştir. Mikro yapı incelemelerinde yüzeyde martenzitik tabakanın oluştuğu ve içeriye doğru penetre edildikçe bu tabakanın etkisini yitirdiği gözlemlenmiştir. Buna bağlı olarak iki numune arasında kalınlıkla birlikte sertlik değerlerinin bir miktar düştüğü gözlemlenmiştir. Mikroyapıda düz martenzit şekillerin yanında perlit taneciklerine de rastlanmıştır.

Şekil 3. Mikroyapı fotografları a) Kalınlık 15 mm - 50x, b) Kalınlık 20 mm – 200x, c) Kalınlık 15 mm sertlik ölçümüne ait uç izi -500x

SONUÇ

Malzemeler prosese uygun olarak sertleştirilmiştir. Sementasyon sırasında çelik yüzeyden belli bir derinliğe kadar karbon emmiştir. Genel olarak her iki kalınlık içinde etkili sertlik derinliği 1,2 mm civarında olduğu ve çekirdeğe doğru sertliğin düştüğü görülmektedir. Sementasyon işlemi sonrasında istenen sertlik değerleri 0,8-1,6 mm arasında değişmektedir. Çalışmada elde edilen sertlik derinlikleri parçanın kullanım amacına göre uygun olarak gerçekleşmiştir. Dış kabukta ince bir martenzit tabakasının oluştuğu tespit edilmiştir. Karbürüzasyon süresiyle birlikte bu tabaka kalınlığının iç yüzeye doğru artacağı düşünülmektedir. Su verme sonrası martenzit fazının arttığı, temperleme ile birlikte martenzit fazının dairesel forma dönüştüğü ve bununda ürüne kullanım ömrü açısından avantaj oluşturacağı düşünülmektedir.

KAYNAKLAR

Asi, O., Can, A. Ç., Pineault, J., & Blassel, M. (2007). The relationship between case depth and bending fatigue strength of gas carburized SAE 8620 steel. *Surface & Coatings Technology*, *201,* 5979–5987.

Asi, O., Can, A. Ç., Pineault, J., & Blassel, M. (2009). The effect of high temperature gas carburizing on bending fatigue strength of SAE 8620 steel. *Materials and Design, 30,* 1792–1797.

Biçer, E., Karagöz, İ. (2017). Su Verme Sertleştirmesi Soğutma Ortamında Isıl İşlem Polimerlerinin Kullanımı. *2. Uluslararası Mühendislik Ve Tasarım Kongresi*, Kocaeli, Türkiye.

Çelik, A., Efeoğlu, İ., Sakar, G. (2001). Microstructure and structural behavior of ion-nitrided AISI 8620 steel. *Materials Characterization 46*, 39 – 44.

Karagöz, İ. (2007). Sementasyon Çeliklerinde Difüzyon Ve Sertlik Derinliğini Arttıracak Isıl İşlem Koşullarının İncelenmesi. Yüksek Lisans Tezi, Marmara Üniversitesi, Fen Bilimleri Enstitüsü, İstanbul, Türkiye.

Sharma, S. K., Rizvi, S. A., & Kori, R. P. (2014). Optimization of Process Parameters in Turning of AISI 8620 Steel Using Taguchi and Grey Taguchi Analysis. *Journal of Engineering Research and Application, 4(3)*, 51-57.

Topbaş, M. A. (1998). *Çelik ve Isıl İşlem El Kitabı*. İstanbul, Türkiye: Ekim Ofset.